V. Kafarov

Fundamentals of Mass Transfer

Gas-Liquid, Vapour-Liquid and Liquid-Liquid Systems

Mir Publishers
Moscow

V. Kafarov

Fundamentals of Mass Transfer

В. В. Кафаров

Основы массопередачи

Системы газ-жидкость, пар-жидкость, жидкость-жидкость

Издательство «Высшая школа»
Москва

V. Kafarov

Fundamentals of Mass Transfer

Gas-Liquid, Vapour-Liquid and Liquid-Liquid Systems

Translated from Russian
by Ram Wadhwa and Natasha Deineko

Mir Publishers · Moscow

First published 1975
Second edition 1985
Revised from the 1979 Russian edition

На английском языке

© Издательство «Высшая школа», 1979
© English translation, Mir Publishers, 1985

Preface

Since the publication of the second edition of this book in Russian (which has also been translated into English and German), the main ideas put forth in the analysis of mass-transfer processes have been developed further. In the first place, this applies to the analysis of turbulent transport phenomena in two-phase gas-liquid, vapour-liquid, and liquid-liquid systems. Turbulent transport phenomena, the related effects of axial and radial dispersion of liquids and gases, and the interaction of flows in two-phase systems have recently drawn the attention of all researchers engaged in the investigation of processes in chemical technology. The ideas of eddy transport of substance in liquids and gases have been developed and form the basis for the investigation of flow structure.

The application of computers has enhanced the possibilities of calculating the processes involving the separation of mixtures and stimulated the use of numerical simulation as the basic method for analyzing diffusion processes.

The present edition is intended for use as a textbook which contains the basic principles of one of the most important parts of the course *Processes and Apparatus in Chemical Industry*. This part is important by itself and is taught at present as a special course.

The author has striven to retain the structure of the book and the sequence of presentation of the material on the basis of system analysis. The basic ideas behind such an analysis are described in the Introduction.

It has now become possible to consider diffusion processes from the point of view of system analysis. This has made it possible to reveal more clearly the interrelation between parameters and their influence on the behaviour of the system as a whole.

The first part of the book is supplemented with calculations of equilibrium on the basis of Wilson and NRTL equations. The algorithm for such calculations is also given. Formulas for calculating physical and chemical properties of multicomponent vapour-liquid mixtures are presented. The methods for calculating the equilibrium state in

multicomponent liquid-liquid systems have been extended. The section concerning the algorithm for calculating batch rectification has been entirely rewritten. The method of calculating cyclic mass-transfer processes has been described.

The second and third parts of the book have not undergone significant alterations, but the system-analysis approach has been used in this edition.

The fourth part of the book is governed by the ideas of system analysis and has been supplemented by refined mathematical models. Besides, the same approach has been used for calculating the separation processes in multicomponent fractionation columns. We have endeavoured to stick to the main objective of calculating the diffusion apparatus, its output and separation ability, as well as its efficiency.

The author is grateful to I.M. Zhernova, Cand. Sc. (Eng.) who took an active part in the preparation of the revised manuscript. He is also deeply indebted to P.G. Romankov, Corresponding Member of the USSR Academy of Sciences and Reader N.V. Ozerova for reviewing the book and making valuable suggestions. The author will welcome any comments and suggestions for further improving the book.

Contents

Preface 5

Introduction 10

Part One
Equilibrium and Balance Equations in Mass-Transfer Processes

Chapter 1. Equilibrium Relations in Binary and Multicomponent Systems 14

1.1. Equilibrium Relations in Gas-Liquid and Vapour-Liquid Systems 14
1.1.1. Basic Concepts and Definitions 14
1.1.2. Ideal Systems 16
1.1.3 Non-Ideal Systems 19
1.2. Equilibrium Relations in Liquid-Liquid Systems. Basic Concepts and Definitions 35

Chapter 2. Material and Heat Balance Equations for Systems in Equilibrium 39

2.1. Determination of the Number of Theoretical Plates and Basic Laws 39
2.1.1. Batch Fractionation 55
2.1.2. Determination of the Number of Theoretical Plates for Low and High Concentrations of the Volatile Component 65
2.1.3. Separation Processes in Multicomponent Systems . . . 68
2.2. Extraction Processes 72
2.2.1. Extraction Through Single-Stage Contact 72
2.2.2. Multiple Contact Involving the Introduction of Fresh Solvent at Each Stage 74
2.2.3. Countercurrent Extraction 76
2.2.4. Extraction with Two Solvents 79
2.3. Cyclic Mass-Transfer Processes 80

Part Two
Hydrodynamic Principles of Mass-Transfer Processes

Chapter 3. Hydrodynamics of Single-Phase Flows 92

3.1. Basic Concepts of the Hydrodynamics of Single-Phase Flows 92
3.1.1. Continuity Equation for Flow (Constant-Flow Rate Equation) 95
3.1.2. Differential Fluid-Flow Equation 97
3.1.3. Onset of Vortex Motion in a Fluid 101

3.1.4. Differential Fluid-Flow Equations Taking the Rotation of Particles into Account. Basic Laws of Vortex Motion 105
3.1.5. Zhukovskii's Theorem on Lift Force and Direction of Vortex Motion 114
3.1.6 On the Relation Between Vortex Motion and Turbulence 117
3.1.7. Free Turbulence. Evolution of Turbulence 121
3.1.8. Similarity Principle as the Basis for Physical Modelling of Single-Phase Systems 125
3.1.9. Resistance Law for a Single-Phase Flow 133
3.2. Model Concepts about the Flow Structure (Distribution of Flow Particles in Space and Time) 135

Chapter 4. Hydrodynamics of Two-Phase Flows 141

4.1. Basic Concepts and Definitions 141
4.2. Interfacial Turbulence 150
4.3. Resistance in Two-Phase Flows. Hydrodynamic State Factor 160
4.4. Linear Velocity of Flow in a Two-Phase System 164
4.5. Unidirectional Flows in Two-Phase Systems 165
4.6. Hydrodynamic Parameters of a Bubbling Layer 169

Part Three
Fundamentals of Kinetics of Mass-Transfer Processes

Chapter 5. Mechanism of Mass Transport and Diffusion Laws 176

5.1. Basic Concepts and Definitions 176
5.2. Diffusion in a Single-Phase Stagnant Medium 181
5.3. Steady-State Diffusion in Moving Media 182
5.4. Mass Transfer in a Single-Phase Flow 186
5.5. Mass Transfer in Multicomponent Gas Systems 190
5.5.1. Diffusion in Multicomponent Systems 190
5.5.2. Diffusion in Multicomponent Liquid Systems 194
5.5.3. Mass Transport in Multicomponent Vapour-Liquid Systems 195

Chapter 6. Kinetics of Interphase Transport 198

6.1. Two-Film Model of Mass Transfer 198
6.2. The Model of Boundary Diffusion Layer 201
6.3. Penetration and Surface Renewal Model 203
6.4. Mass-Transfer Model Involving Adsorption 205
6.5. Mass-Transfer Model Based on the Concept of Interfacial Turbulence 207

Chapter 7. Methods of Expressing the Driving Force and Kinetics of Mass Transfer 212

7.1. Expression of Driving Force in Terms of Difference in Concentrations, and Kinetics in Terms of Mass-Transfer Coefficients 213
7.2. Expression of Driving Force in Terms of the Number of Transport Units and Parameter λ 215
7.3. Expression of Driving Force in Terms of the Number of Theoretical Contact Stages 220
7.4. Relations Between Efficiency, Mass-Transfer Coefficient, and Number of Transport Units 222
7.5. Relations Between Mass-Transfer Coefficient, Equivalent Packing Height, and Height of Transport Unit 224

Part Four

Modelling and Calculation of Diffusion Apparatus

Classification of Apparatus and Estimation of Efficiency . . . 229

Chapter 8. Apparatus with a Fixed Phase-Contact Surface 232
8.1. Film-Type Columns with Wetted Walls 232
8.2. Columns with Vertical Sheet Packing 236
8.3. Spray Columns 238

Chapter 9. Apparatus with Interfacial Area Formed in Flow 240

9.1. Plate Columns 240
9.1.1. Structural Features of Bubble-Cap Plate Columns and Their Hydraulics 240
9.1.2. Sieve-Plate Columns 260
9.1.3. Sieve-Plate Columns for Liquid-Liquid Systems . . . 271
9.1.4. Plates with a Unidirectional Phase Flow 273
9.1.5. Valve Plates 285
9.1.6. Regularly Rotating Two-Phase Flow in Contact Apparatus 290
9.1.7. Flow Sectionalization in Contact Apparatus 291
9.1.8. Plates without Downcomers (Columns with Grid Plates) 293
9.2. Packed Columns 299
9.2.1. Pressure Drop Through Dry Packings 299
9.2.2. Hydrodynamics of Two-Phase Systems in Packed Columns 301
9.2.3. Axial Dispersion in a Packing 317
9.2.4. Scaling of Packed Columns 319
9.2.5. Columns with Flooded Packing (Emulsifying Columns) 320

Chapter 10. Modelling and Design Calculations of Apparatus with Interfacial Surface Formed in Flows 330

10.1. Principles of Modelling the Processes of Separation of Multicomponent Systems 330
10.2. Modelling Algorithms and Mathematical Models of Rectifying Columns 337
10.3. Effect of the Flow Structure on Efficiency of Plate Columns 353
10.4. Estimation of the Efficiency of Mass Transfer on Plates for Separating Multicomponent Mixtures 372
10.5. Modelling and Calculation of Packed Columns 379
10.5.1. Mass Transfer in Packed Columns 379
10.5.2. Modelling and Calculation of Packed Absorption Columns 385
10.5.3. Modelling and Calculation of Packed Extraction Columns 391

Chapter 11. Apparatus with External Energy Supply 407

11.1. Apparatus with Mechanical Stirrers (Rabbles) 407
11.1.1. Modelling of Apparatus with Rabbles 407
11.1.2. Mixing in Gas-Liquid Systems 417
11.1.3. Mixing in Liquid-Liquid Systems 422
11.1.4. Extraction Columns with Stirrers 425
11.2. Pulsed Columns 428
11.3. Columns with Flow Vibrations 440
11.4. Rotational Apparatus 441

Subject Index 452

Introduction

Mass-transfer processes are characterized by the transport of substance. Since this transport is usually accomplished from one phase to another, mass-transfer processes involve several phases and several components. The driving force in such processes is the difference between a given concentration of the system components and the equilibrium concentration at which the process terminates.* Consequently, the limiting state of a process is reached when the system attains equilibrium. The following three aspects are considered while calculating and analyzing the mass-transfer processes:

(1) the necessary and sufficient conditions for the existence of a given number of phases and the laws of distribution of components in them. These conditions are determined by the phase rule and the laws of equilibrium.

(2) The necessary and sufficient conditions created for realizing a process. These conditions, called the operating conditions, are determined by specifying the initial and final concentrations of the treated products and their amounts. The relation between the given amounts and concentrations is established by material balance equations which in their final form lead to the operating lines of the process.

(3) The necessary and sufficient conditions determining the rates of mass transfer from one phase to another and depending on the difference between the equilibrium and operating concentrations (i.e. on the driving force of the process), physical properties of the systems and the hydrodynamic conditions of the process. The relation between these factors is established with the help of equations of diffusion kinetics.

A rational choice of construction of a diffusion apparatus and an estimate of its size can be made by simultaneously taking into account the above conditions. In turn, the hydrodynamic conditions under which a diffusion process occurs depend on the structural features of the apparatus. Hence, if the equilibrium equations and the

---

* According to thermodynamics, the driving force in mass-transfer processes can also be characterized by the difference in the chemical potentials of the system components.

given conditions for the process can be considered independently of the design features of the diffusion apparatus, the kinetics must be directly correlated with the actual design of the apparatus in which mass transfer takes place.

While analyzing mass-transfer processes in diffusion apparatus, the entire complex of processes occurring in them can be conditionally divided into two levels: the microscopic level (microkinetics of the process) and the macroscopic level (macrokinetics of the process). The microkinetic factors include the physical and chemical effects determining the rate of physical processes on a molecular (atomic) level and in the local volume of the apparatus. The macrokinetics of the process involves an investigation of the behaviour of physicochemical systems on the scale of the apparatus as a whole. In this case, the microscopic-level effects are superimposed by large-scale hydrodynamic, thermal, and diffusion phenomena. The nature of these phenomena is determined by the design characteristics of industrial apparatus, the mode of supply of external energy to the apparatus, the type of mixers, etc.

An analysis of mass-transfer processes makes it possible to study the effect of various conditions under which this process occurs on the properties of end products of separation. Besides, it permits an investigation of internal characteristics of the process such as the temperature and concentration over the column height, the location of the reference point corresponding to the maximum change of the temperature or other measurable parameters upon a change in the operating conditions, the optimal position for introducing the feed, removing the fractions, etc. This enables us to solve the problem of controlling the process. These problems can be solved by using simulation methods. At present, the methods of computational mathematics and the advances in computer technology have led to a wide application of mathematical modelling. This method paves the way for forecasting. The results of predictions can be used at the design stage, as well as during the operation of the existing setups.

The mathematical modelling of mass-transfer processes frequently employs the block principle according to which a model is constructed by combining its individual components. Having obtained the information on equilibrium values and constructing the material and heat balance equations of the process, we can use the hydrodynamic model of the process as the basis of its mathematical description. The kinetics of the mass-transfer processes is then investigated by taking into account the hydrodynamic conditions for the obtained model. The mathematical description of these processes takes into consideration the material and heat balance equilibrium equations and the boundary conditions. At the final stage of modelling, the mathematical description of all aspects of the process is combined to form the complete mathematical model.

The representation of a mathematical model of a process as a combination of subsystems (blocks) in turn allows us to represent the construction procedure for the given model as a combination of operations which consists of mathematical models of individual subsystems, i.e. to apply the block principle for constructing a mathematical model. The general structure of the mathematical model for mass-transfer processes has the following form:

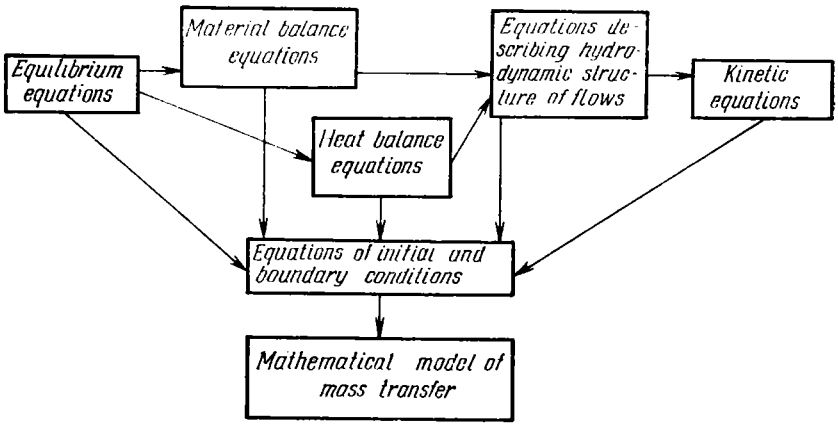

The application of the block principle for constructing mathematical models of the processes under consideration, which is based on the system approach, also permits us to outline, in principle, the solutions of the practically important problem of scaling the diffusion processes. From the point of view of mathematical modelling, scaling operation is just the deformation of the mathematical model upon a change in the geometric dimensions characterizing the structural features of the apparatus. When the block principle is employed for constructing a mathematical model, the influence of the geometrical dimensions on the properties of the process is reflected only in one subsystem, viz. "Hydrodynamics". Hence, the scaling operation can be carried out if we have a fairly accurate qualitative and quantitative description of this subsystem.

Each block of the mathematical model can, in principle, have a different level of mathematical description. The only important thing is that input and output variables of all the blocks of the model should be matched in order to obtain a closed system of equations for the mathematical model of the process as a whole. As for the internal variables of the blocks, they can be chosen from a sufficiently wide range. In the ideal case, the mathematical description of each block must contain equations whose parameters are only the physical and chemical properties of the components of the mixture being separat-

ed, as well as the geometrical features of the equipment and the factors determining the given external influences. At present, however, it is not always possible to obtain a detailed description of individual blocks. As a rule, this is associated with an extremely complicated mathematical description of a block, which itself leads to a highly intricate mathematical model of the process as a whole and, besides, may lead to certain computational difficulties. Hence, when the block principle is actually used for a mathematical description of each block, empirical relations have to be used at some stage of its detailed description.

The presentation of the material contained in this book is based on the ideas of system analysis and the realization of the block principle. The blocks "Equilibrium" and "Material and Heat Balance" are considered in the first part of the book, the block "Hydrodynamics" in the second part, and the block "Kinetics" in the third part. In the fourth part of the book, the blocks are combined into complete mathematical models which can be used to calculate and evaluate the design of various diffusion equipments.

Part One

Equilibrium and Balance Equations in Mass-Transfer Processes

Chapter One

Equilibrium Relations in Binary and Multicomponent Systems

1.1. Equilibrium Relations in Gas-Liquid and Vapour-Liquid Systems

1.1.1. Basic Concepts and Definitions

The equilibrium relations in gas-liquid systems are characterized by the distribution of a soluble gas between an inert gas and a solvent liquid. According to the phase rule, the equilibrium state of a system with three components $K = 3$ (inert gas, the gas being absorbed, and the absorbent) and two phases $\Phi = 2$ (gas-liquid) is determined by the values of three parameters ($N = K + 2 - \Phi = 3 + 2 - 2 = 3$). Usually, the concentration x in the liquid, the partial pressure p above the liquid, and the temperature T are taken as these parameters. The equilibrium distribution of the component being absorbed between the two phases depends on these parameters. At low concentrations of the component being distributed, the relation between the parameters p and x at a given temperature is expressed by Henry's law:

$$p = mx, \tag{1.1}$$

where m is the Henry constant.

The value of the Henry constant depends on the properties of the gas and the liquid, as well as the temperature. The linear nature of Eq. (1.1) is violated at high concentrations of the component being distributed. It is possible to obtain an analytical dependence of the type (1.1), i.e. to predict the value of m for any system, only for low concentrations (less than 1 mol %). The concentrations of the component being distributed between a gas and a liquid can be expressed in different units. It is possible to mutually convert the various units with the help of Table 1.

According to the phase rule, the number of parameters determining the state of a two-phase system $\Phi = 2$ (vapour-liquid) with K components is equal to the number of components $K + 2 = 2 + N$, $N = K$.

In order to analyze the phase distribution of components of a two-component system, the following combinations are chosen as the parameters: composition x and pressure p, composition x and temperature T, concentration of the low-boiling component simultaneously in vapour (y) and in liquid (x), i.e. ($y - x$). In accordance with the chosen pairs of parameters, the equilibrium relations are expressed through the plots of the x vs. p, x vs. T, and y vs. x dependences.

Before considering the graphic representation of equilibrium states, let us introduce certain basic concepts.

The *volatile component* of a mixture is the component with the highest vapour pressure at a given temperature among all the components of the mixture. Accordingly, the volatile component has the lowest boiling point. The component having the lowest vapour pressure, and the highest boiling point is called the non-volatile component.

Relative volatility of components is defined as the ratio of the vapour pressure of the volatile component (component A) to the vapour pressure of the non-volatile component (component B), both values corresponding to the same temperature:

$$\alpha = \frac{P_A}{P_B}, \tag{1.2}$$

where P_A and P_B are the vapour pressures of the individual component A and B respectively, mm Hg.

For multicomponent systems A—B—C—D ... arranged in the increasing order of their boiling points, the relative volatility of the components is expressed as follows:

$$\alpha_{AD} = \frac{P_A}{P_D}, \quad \alpha_{BD} = \frac{P_B}{P_D}, \quad \alpha_{CD} = \frac{P_C}{P_D}. \tag{1.3}$$

The relative volatility α can be calculated with a sufficiently high degree of accuracy directly from the boiling points by using the Clapeyron and Trouton equations. According to the Clapeyron equation, we get

$$\ln \frac{P_A}{P_B} \cong \frac{r_B - r_A}{RT}, \tag{1.4}$$

where r_A and r_B are the latent heats of evaporation of the components and R is the molar gas constant.

According to the Trouton equation (for atmospheric pressure)

$$r_B - r_A \cong 20.5\,(T_B - T_A), \tag{1.5}$$

where T_A and T_B are the boiling points of the components in degrees Kelvin.

Solving Eqs. (1.4) and (1.5) simultaneously, we get

$$\ln \frac{P_A}{P_B} \cong 20.5 \frac{T_B - T_A}{RT} \cong 20.5 \frac{T_B - T_A}{T_B + T_A}.$$

Conversion Table for Binary-

	Molar composition x, kg-mole per kg-mole of mixture	Mass composition a, kg, per kg of mixture
Molar composition x, kg-mole, per kg-mole of mixture	—	$\dfrac{a/M_A}{\dfrac{a}{M_A}+\dfrac{b}{M_B}}$
Mass composition a, kg, per kg of mixture	$\dfrac{M_A x_A}{M_A x_A + M_B x_B}$	—
Relative molar composition X, kg-mole, per kg-mole of solvent	$\dfrac{x_A}{1-x_A}$	$\dfrac{M_B a}{M_A(1-a)}$
Relative mass composition A, kg, per kg of solvent	$\dfrac{M_A x_A}{M_B(1-x_A)}$	$\dfrac{a}{1-a}$
Molar concentration C, kg-mole/m³	$\dfrac{\rho M_A x_A}{M_A x_A + M_B(1-x_A)}$	$\dfrac{\rho a}{M_A}$
Mass concentration A_v, kg/m³	$\dfrac{\rho M_A x_A}{M_A x_A + M_B(1-x_A)}$	ρa

However, since $\alpha = P_A/P_B$, we obtain

$$\log \alpha = \log \frac{P_A}{P_B} = \frac{1}{2.3} \ln \frac{P_A}{P_B} \cong \frac{20.5}{2.3} \cdot \frac{T_B - T_A}{T_B + T_A}.$$

In the final form, we get

$$\log \alpha \cong 9 \frac{T_B - T_A}{T_B + T_A}. \tag{1.6}$$

The relative volatility coefficients calculated with the help of Eq. (1.6) are the more in agreement with the experimental data, the closer the boiling points of the components. Equation (1.6) can be used for determining the relative volatility of such systems for whose components there are no experimental dependences between the vapour pressure and temperature.

1.1.2. Ideal Systems

Ideal systems are systems which obey the Raoult law. The latter establishes a linear relation between the concentration of a volatile component in a liquid which is in equilibrium with its vapour, and

Table 1

Mixture Relations

Relative molar composition X, kg-mole, per kg-mole of solvent	Relative mass composition A, kg, per kg of solvent	Molar concentration C, kg-mole/m³	Mass concentration A_v, kg/m³
$\frac{X}{1+X}$	$\frac{A/M_A}{\frac{A}{M_A}+\frac{1}{M_B}}$	$\frac{CM_B}{\rho+C(M_B+M_A)}$	$\frac{A_v/M_A}{\frac{A_v}{M_A}+\frac{\rho-A_v}{M_B}}$
$\frac{M_AX}{M_B+M_AX}$	$\frac{A}{1+A}$	$\frac{M_AC}{\rho}$	$\frac{A_v}{\rho}$
—	$\frac{M_BA}{M_A}$	$\frac{CM_B}{\rho-M_AC}$	$\frac{A_vM_B}{M_A(\rho-A_v)}$
$\frac{M_AX}{M_B}$	—	$\frac{CM_A}{\rho-M_AC}$	$\frac{A_v}{\rho-A_v}$
$\frac{\rho X}{M_B+M_AX}$	$\frac{\rho A}{M_A(1+A)}$	—	$\frac{A_v}{M_A}$
$\frac{\rho M_AX}{M_B+M_AX}$	$\frac{\rho A}{1+A}$	M_AC	—

its partial pressure above the mixture:

$$p_A = x_A P_A, \tag{1.7}$$

where p_A is the partial pressure of component A over the mixture, mm Hg; x_A is the mole fraction of component A in the liquid; and P_A is the pressure of the vapours of the individual (pure) component A, mm Hg.

If P is the total pressure over the mixture, the concentration y_A of the volatile component in the vapour in equilibrium is given in accordance with Dalton's law:

$$y_A = \frac{p_A}{P} \tag{1.8}$$

Equations (1.7) and (1.8) can be used to establish the relation between the concentrations of a volatile component in vapour and in liquid. Substituting the value of p_A from Eq. (1.7) into (1.8), we get

$$y_A = \frac{x_A P_A}{P}. \tag{1.9}$$

For a two-component system, the total pressure P is equal to the sum of the partial pressures p_A and p_B of the components:

$$P = p_A + p_B. \tag{1.10}$$

Taking into account Eq. (1.7), we can write

$$P = p_A + p_B = x_A P_A + (1 - x_A) P_B, \tag{1.11}$$

since $x_B = 1 - x_A$.

Substituting the value of P obtained above into Eq. (1.9), we get

$$y_A = \frac{x_A P_A}{x_A P_A + (1 - x_A) P_B}. \tag{1.12}$$

Introducing relative volatility into (1.9), we obtain

$$y_A = \frac{\alpha x_A}{\alpha x_A + (1 - x_A)}. \tag{1.13}$$

As a result of simple transformations, this equation can be reduced to a more convenient form:

$$\frac{y_A}{1 - y_A} = \alpha \frac{x_A}{1 - x_A}. \tag{1.14}$$

The ratio $y_A/(1 - y_A)$ in this equation expresses the amount of the volatile component per unit mass of the non-volatile component in the vapour, while the ratio $x_A/(1 - x_A)$ characterizes the amount of the volatile component per unit mass of the non-volatile component in the liquid. It follows from Eq. (1.14) that the relative concentration of the volatile component in vapour is α times higher than its concentration in liquid. The higher the relative volatility α of a mixture, the larger the difference in the concentrations of the components in the liquid and vapour phases. For an ideal system with any number N of components, the following equations relate the concentrations of their components in the liquid and vapour phases:

$$y_A + y_B + y_C + \ldots + y_N = 1, \tag{1.15}$$

$$x_A + x_B + x_C + \ldots + x_N = 1, \tag{1.16}$$

$$p_A + p_B + p_C + \ldots + p_N = P, \tag{1.17}$$

$$y_A P + y_B P + y_C P + \ldots + y_N P = P, \tag{1.18}$$

$$x_A P_A + x_B P_B + x_C P_C + \ldots + x_N P_N = P, \tag{1.19}$$

$$y_A = \frac{x_A P_A}{x_A P_A + x_B P_B + x_C P_C + \ldots + x_N P_N} = \frac{p_A}{P}, \tag{1.20}$$

$$y_B = \frac{x_B P_B}{x_A P_A + x_B P_B + x_C P_C + \ldots + x_N P_N} = \frac{p_B}{P}, \tag{1.21}$$

$$x_A = \frac{y_A/P_A}{y_A/P_A + y_B/P_B + y_C/P_C + \ldots + y_N/P_N}, \quad (1.22)$$

$$x_B = \frac{y_B/P_B}{y_A/P_A + y_B/P_B + y_C/P_C + \ldots + y_N/P_N}, \quad (1.23)$$

$$y_A = \frac{\alpha_{AN}x_A}{\alpha_{AN}x_A + \alpha_{BN}x_B + \alpha_{CN}x_C + \ldots + \alpha_N x_N}. \quad (1.24)$$

Figure 1 graphically shows the two-component systems with the parameters (x_A, P), (x_A, T) and (y_A, x_A) as coordinates. The y vs. x curve, constructed in accordance with Eq. (1.14), is frequently

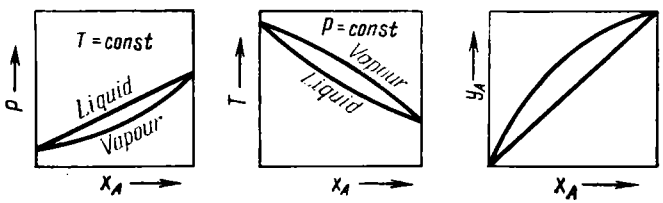

Fig. 1. Equilibrium diagrams of an ideal two-component system.

used for calculating the distillation processes in ideal systems. Figure 2 is the graphic representation of the equilibrium in a three-component system for a constant total pressure. Each vertex of the triangle describes the concentration of the corresponding individual component. The binary mixture of components A and B is represented by points on line AB, and that of components B and C—by points on line BC. Each composition of the three-component system is represented by a single point in the equilibrium triangle (point M). This composition is determined by the length of three perpendiculars on the side opposite to the given vertex. Thus, at the point M, the composition of the mixture will correspond to Ml for component A, Mk for component B, and Mm for component C. The equilibrium concentration of component A in liquid and vapour will be given by fl and el respectively.

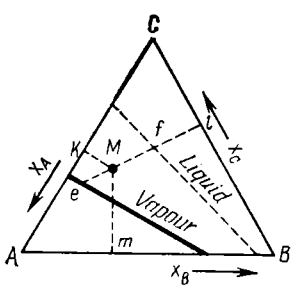

Fig. 2. Diagram of isothermal equilibrium composition of an ideal three-component system for P = const and T = const.

1.1.3. Non-Ideal Systems

The characteristic features of non-ideal systems are a deviation from the Raoult law and the ideal gas laws, the existence of heats of

mixing, and a change in the volume of the solution obtained as a result of mixing of individual components, etc. If the relative volatility in a non-ideal system passes through unity, the system is called *azeotropic.* Most of the liquid systems subjected to distillation are non-ideal.

In calculations of the distillation processes, the deviation of a system from the ideal behaviour is taken into account through the so-called activity coefficient which characterizes the activity of molecules in a solution as well as their interaction. The activity coefficient γ_A for component A is defined as the ratio

$$\gamma_A = \frac{p_A}{x_A P_A}, \tag{1.25}$$

while for component B we can write

$$\gamma_B = \frac{p_B}{x_B P_B}. \tag{1.26}$$

Since $p_A = x_A P_A$ and $p_B = x_B P_B$ for an ideal system, the activity coefficients for such a system are equal to unity, i.e. $\gamma_A = 1$ and $\gamma_B = 1$.

Depending on the intermolecular attraction, the activity coefficients in non-ideal systems can be greater or smaller than unity. The value of the activity coefficient is a function of all the remaining components in the solution and their concentrations. For example, γ_A for component A in a binary mixture will be equal to unity if $x_A = 1$, since pure liquids are treated as ideal systems. As the concentration x_A decreases, γ_A increases and attains its maximum value at $x_A = 0$. A similar dependence is also observed for other components. By introducing the concept of activity coefficient, we can express the quantitative relations between the components in vapour and liquid phases as follows:

$$\gamma_A = \frac{p_A}{x_A P_A} = \frac{y_A P}{x_A P_A}, \tag{1.27}$$

$$\gamma_B = \frac{p_B}{x_B P_B} = \frac{y_B P}{x_B P_B}, \tag{1.28}$$

$$\frac{x_A P_A \gamma_A}{y_A} = \frac{x_B P_B \gamma_B}{y_B} = \frac{x_C P_C \gamma_C}{y_C} = \ldots = \frac{x_N P_N \gamma_N}{y_N}, \tag{1.29}$$

$$\frac{x_A P_A \gamma_A}{P} + \frac{x_B P_B \gamma_B}{P} + \frac{x_C P_C \gamma_C}{P} + \ldots + \frac{x_N P_N \gamma_N}{P} = 1, \tag{1.30}$$

$$\frac{y_A P}{\gamma_A P_A} + \frac{y_B P}{\gamma_B P_B} + \frac{y_C P}{\gamma_C P_C} + \ldots + \frac{y_N P}{\gamma_N P_N} = 1, \tag{1.31}$$

$$\alpha_{AB} = \frac{\gamma_A P_A}{\gamma_B P_B}; \quad \alpha_{AC} = \frac{\gamma_A P_A}{\gamma_C P_C}; \quad \alpha_{AN} = \frac{\gamma_A P_A}{\gamma_N P_N}. \tag{1.32}$$

While calculating the distillation processes, we often represent the equilibrium data through the y vs. x graphs or triangular diagrams in the same way as for ideal systems. Figures 3 and 4 show typical equilibrium distribution diagrams for components of non-ideal systems. Corresponding graphs for azeotropic systems are shown in Figs. 5 and 6. In the absence of experimental equilibrium data, the

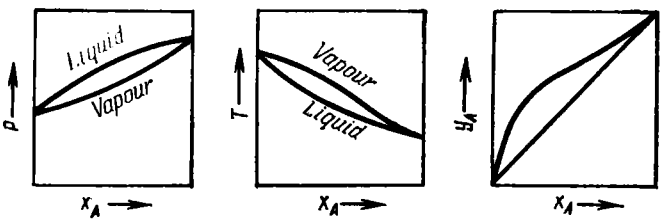

Fig. 3. Equilibrium diagrams of non-ideal two-component system.

equilibrium distribution of components can be calculated from Eqs. (1.25)-(1.32) if the activity coefficients of the components are known. The activity coefficients of the components depend on their concentrations. The calculations of the activity coefficients and volatility coefficients are fraught with certain difficulties, especially for multicomponent systems.

Gibbs introduced the concept of *chemical potential* for estimating the liquid-vapour (gas) equilibrium. A system will be in thermodynamic equilibrium if its phases are at the same temperature and if the chemical potentials of each component present in the liquid or vapour phase are identical. A more convenient parameter is the fugacity which is equivalent to the chemical potential and is uniquely connected with it. It is even more convenient from a physical point of view, since fugacity can be considered as the thermodynamic pressure. For ideal systems, fugacity is equal to the partial pressure of the component.

Thus, the equilibrium state of a two-phase system (liquid L-vapour (gas) G) can be represented in the following form by introducing fugacity:

$$f_i^G = f_i^L. \qquad (1.33)$$

This is the basic equation of state for a two-phase system. In this form, however, it is not very

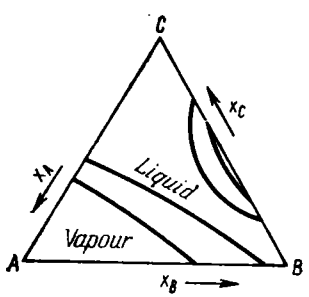

Fig. 4. Diagram of isothermal equilibrium composition of non-ideal three-component system for P = const and T = const.

useful for calculations. If we introduce the coefficients of volatility and activity, we can write the following expression for α:

$$\alpha_i = \frac{f_i^G}{y_i P}, \tag{1.34}$$

where y_i is the molar composition of the vapour phase, P is the total pressure of the system, and the following expression holds for γ:

$$\gamma_i = \frac{f_i^L}{x_i f_i^{OL}}, \tag{1.35}$$

x_i being the molar composition of the liquid, and f_i^{OL} the fugacity of the component in the standard state.

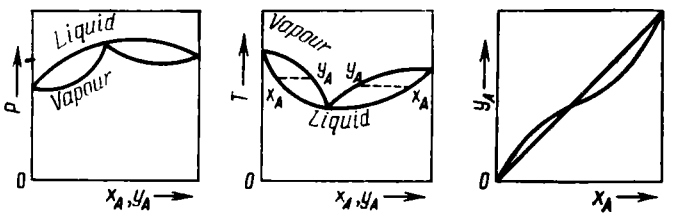

Fig. 5. Equilibrium diagrams of a two-component azeotropic system with a maximum pressure (lowest boiling point).

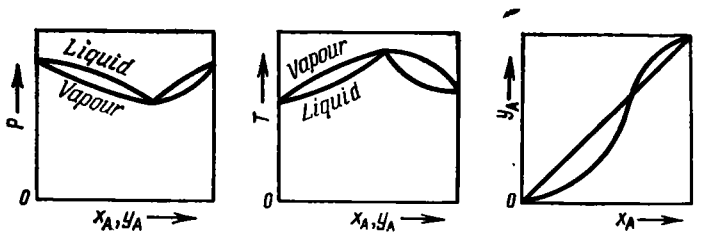

Fig. 6. Equilibrium diagrams of a two-component azeotropic system with a minimum pressure (highest boiling point).

Substituting (1.34) and (1.35) into (1.33), we obtain

$$\alpha_i y_i P = \gamma_i x_i f_i^{OL}. \tag{1.36}$$

This equation exactly reflects the equilibrium of multicomponent systems.

In calculations of the vapour-liquid equilibrium, the main attention is paid to the determination of the activity coefficients of the liquid phase. Under conditions far from the critical state, the density of the vapour phase is small in comparison with that of the liquid phase. Consequently, the intermolecular interaction in the vapour

phase is also weaker. Hence it is often assumed in calculations that the non-ideal behaviour of a system is due to the non-ideal nature of its liquid phase. Such an approach considerably simplifies the calculations of the parameters of the vapour phase: if the vapour phase obeys ideal gas laws, the fugacity will be equal to the partial pressure of the corresponding component of the mixture. Of course, such an assumption is not always true: for some component of the mixture the temperature or pressure of the system may be higher than the critical value.

In the general case, the volatility coefficient is a function of the temperature, pressure and the composition of the vapour phase. It can be calculated from the equations of state. One of the exact equations for calculating the volatility coefficient can be written in the form

$$\ln \alpha_i = \frac{1}{RT} \int_V^\infty \left[\left(\frac{\partial P}{\partial n_i} \right)_{T,\ V,\ n_j} - \frac{RT}{V} \right] dV - \ln Z; \quad j \neq i, \quad (1.37)$$

where n_i is the fraction of the ith component of the system, V is the volume of the vapour phase, and

$$Z = \frac{PV}{(n_1 + n_2 + \ldots)\, RT}. \quad (1.38)$$

If the vapour phase obeys the ideal gas laws, the integral is equal to zero and the coefficients α_i are equal to unity for all components. For calculating Z, we use the virial equation

$$Z = \frac{Pv}{RT} = 1 + \frac{B}{v} + \frac{C}{v^2} + \ldots, \quad (1.39)$$

where v is the molar volume of the gas, B is the second virial coefficient, C is the third virial coefficient, and so on.

Equation (1.39) expresses the relation between the volumetric parameters of a system and its composition. For pure components, the virial coefficients depend only on temperature while for a mixture they also depend on composition:

$$B_{\text{mix}} = \sum_i^N \sum_j^N y_i y_j B_{ij}, \quad (1.40)$$

$$C_{\text{mix}} = \sum_i^N \sum_j^N \sum_k^N y_i y_j y_k C_{ijk}, \quad (1.41)$$

where B_{ij} is the second virial coefficient for the mixture of components i and j, and C_{ijk} is the third virial coefficient for the mixture of components i, j and k.

Substituting (1.39), (1.40), and (1.41) into Eq. (1.37), we get

$$\ln \alpha_i = (2/v) \sum_j^N y_j B_{ij} + (3/2v^2) \sum_j^N \sum_k^N y_j y_k C_{ijk} + \ldots - \ln Z. \quad (1.42)$$

In actual calculations, the virial equation is used up to second term of expansion only and the pressure range for which it gives reliable results is limited by the quantity

$$P \leqslant \frac{T \sum_i^N y_i P_{\text{cr},\,i}}{2 \sum_i^N y_i T_{\text{cr},\,i}}, \quad (1.43)$$

where $P_{\text{cr},i}$ and $T_{\text{cr},i}$ are the critical pressure and the critical temperature of the ith component respectively. The volatility coefficient in this case is determined by the formulas

$$\ln \alpha_i = (2/v) \sum_j^N y_j B_{ij} - \ln Z, \quad (1.44)$$

and

$$Z = 1 + \frac{\sum_i^N \sum_j^N y_i y_j B_{ij}}{v} \quad (1.45)$$

The second virial coefficients B_{ii} and B_{jj} for pure components and the virial coefficients B_{ij} for the mixture of components i and j (which depend on volume) can be calculated from the experimental data. While these data can be obtained relatively easily for pure components, the problem is a lot more complicated for mixtures. Hence empirical relations are frequently used for calculating the virial coefficients. A change in the activity coefficients at normal pressure does not affect the equilibrium calculations significantly, and hence the low accuracy of the empirical relations for determining the virial coefficients introduces only a small error in the calculations. Nevertheless, it is better to use approximate formulas instead of assuming that the vapour phase behaves like an ideal gas. The following dependence, which has been proposed for non-polar gases, permits the calculation of the virial coefficients of pure components with a high degree of accuracy:

$$\frac{P_{\text{cr},\,i} B_{ij}}{RT_{\text{cr},\,i}} = f_B^{(0)}(T_R) + \omega_i f_B^{(1)}(T_R), \quad (1.46)$$

where $T_R = T/T_{\text{cr}}$ is the reduced temperature and

$$\omega_i = -\log\left(\frac{P_i^s}{P_{\text{cr},\,i}}\right) - 1.0,$$

P_i^s being the saturation pressure.

The following empirical relations have been proposed for determining the functions $f_B^{(0)}(T_R)$ and $f_B^{(1)}(T_R)$:

$$f_B^{(0)}(T_R) = 0.1445 - \frac{0.33}{T_R} - \frac{0.1385}{T_R^2} - \frac{0.0121}{T_R^3}, \quad (1.47)$$

$$f_B^{(1)}(T_R) = 0.073 + \frac{0.46}{T_R} - \frac{0.5}{T_R^2} - \frac{0.097}{T_R^3} - \frac{0.0073}{T_R^4}. \quad (1.48)$$

The second virial coefficients of polar gases are calculated with the help of the dependence

$$\frac{P_{cr,\,i} B_{ii}}{RT_{cr,\,i}} = f_B^{(0)}(T_R) + \omega_i f_B^{(1)}(T_R) + f_\mu(\mu_R T_R) + \eta_i f_a(T_R), \quad (1.49)$$

where $\mu_R = \frac{10^5 \mu_i^2 P_{cr,\,i}}{T_{cr,\,i}^2}$ is the reduced dipole moment, μ_i is the dipole moment of the ith component, and η_i is the equilibrium association constant. The functions $f_B^{(0)}(T_R)$ and $f_B^{(1)}(T_R)$ are determined from formulas (1.47) and (1.48), while $f_\mu(\mu_R T_R)$ and $f_a(T_R)$ are given by the formulas

$$f_\mu(\mu_R, T_R) = -5.237220 + 5.665807 \ln \mu_R - 2.133816 (\ln \mu_R)^2 + 0.25255773 (\ln \mu_R)^3 + \frac{1}{T_R} [5.769770 - 6.181427 \ln \mu_R + 2.28327 (\ln \mu_R)^2 - 0.264907 (\ln \mu_R)^3], \quad (1.50)$$

$$f_a(T_R) = \exp[6.6 (0.7 - T_R)]. \quad (1.51)$$

The second virial coefficients for a mixture of gases i and j are also determined from the reduced correlations by replacing certain parameters. Thus, calculations can be made for two non-polar gases with the help of Eqs. (1.47), (1.48), and (1.49), if the parameters $P_{cr,\,i}$, $T_{cr,\,i}$, and ω_i are replaced by the complexes:

$$T_{cr,\,ij} = (T_{cr,\,i} T_{cr,\,j})^{1/2}, \quad (1.52)$$

$$\omega_{ij} = \frac{1}{2}(\omega_i + \omega_j), \quad (1.53)$$

$$P_{cr,\,ij} = 4T_{cr,\,ij} \left[\frac{P_{cr,\,i} v_{cr,\,i}}{T_{cr,\,i}} + \frac{P_{cr,\,j} v_{cr,\,j}}{T_{cr,\,j}} \right] / (v_{cr,\,i}^{1/3} + v_{cr,\,j}^{1/3})^3. \quad (1.54)$$

For calculations involving two non-polar components, we can use Eq. (1.49) with the substitutions (1.53) and (1.54), the reduced dipole moment being given by the formula

$$\mu_R = \frac{10^5 \mu_i \mu_j P_{cr,\,ij}}{T_{cr,\,ij}^2}. \quad (1.55)$$

If the two components contain a polar and a non-polar gas, we can use Eqs. (1.46), (1.47), and (1.48) together with Eq. (1.53), while the following expression is used instead of parameter ω_i:

$$\omega_{ij} = \frac{1}{2}(\omega_i + \omega_j).$$

Thus, the non-ideal behaviour of the vapour phase is due to interaction between molecules. The relations considered above do not provide a complete picture of the change in parameters over a wide interval. Calculations of non-ideal systems show that the deviations of a system from ideal behaviour are manifested in the following: (a) at constant temperature and composition, an increase in pressure leads to a decrease in the volatility coefficient; (b) as the temperature increases at constant pressure and composition, the volatility coefficient tends to unity; (c) under constant temperature and pressure, the effect of the composition on the volatility coefficient is more pronounced at low concentrations of components.

Considerable difficulties are encountered in calculations for the liquid phase. In its present form, the theory of solutions permits us to predict the properties of only certain types of solutions. In general, the properties of solutions are studied experimentally with a view to obtain empirical dependences from the minimum amount of experimental results. These dependences are determined by correlating the activity coefficients with the physical properties of the system. The dependence of the activity coefficients on the properties of a system at constant temperature and pressure is obtained with the help of the Gibbs-Duhem equation

$$\sum x_i d \ln \gamma_i = 0, \tag{1.56}$$

where x_i is the molar composition of the liquid phase.

Using the concept of Gibbs' excess free energy ΔG^E (the difference between the change in free energy upon mixing of pure components and the change in the free energy of the ideal solution), individual activity coefficients may be expressed in terms of the mole fractions of the mixture components through the equation

$$RT \ln \gamma_i = \left(\frac{\partial n \Delta G^E}{\partial n_i} \right)_{p,\, T,\, n_j}. \tag{1.57}$$

If the excess free energy ΔG^E is expressed as a function of the liquid phase composition, we obtain Wohl's equation:

$$\frac{\Delta G^E}{2.303RT \sum_i q_i x_i} = \sum_{i,\, j} z_i z_j A_{ij} + \sum_{i,\, j,\, k} z_i z_j z_k A_{ijk} + \sum_{i,\, j,\, k,\, l} z_i z_j z_k z_l A_{ijkl} + \ldots, \tag{1.58}$$

where q_i, q_j, q_k are the effective molar volumes of the components i, j, k; A_{ij}, A_{ijk}, A_{ijkl} are the constants determined from the experimental data on binary, ternary, and quaternary systems respectively; and z_i, z_j, z_k ... are the effective volumetric fractions of the components i, j, k ... respectively. The effective volumetric fractions of the components are determined from the expression

$$z_i = \frac{q_i x_i}{\sum_i q_i x_i}. \tag{1.59}$$

Like the mole fractions, volumetric fractions are connected through the relation $\Sigma z_i = 1$.

The constants A_{ij}, A_{ijk}, and A_{ijkl} in Eq. (1.58) express the interaction of different groups of molecules ij, ijk, $ijkl$ in a multicomponent mixture. The larger the number of terms in this equation, the more accurately will it represent the behaviour of a given system. This, however, will involve a considerable increase in the number of experimental data required for determining the appropriate constants. Thus, for a ternary system, the third-order Wohl equation has the form

$$\begin{aligned}\frac{\Delta G^E}{2.303RT} = (x_1 + x_2 q_2/q_1 + x_3 q_3/q_1)\,[z_1 z_2 (A_{21} z_1 q_1/q_2 \\ + A_{12} z_2) + z_1 z_3 (A_{31} z_1 q_1/q_3 + A_{13} z_3) + z_2 z_3 (A_{32} z_2 q_1/q_3 \\ + A_{23} z_3 q_1/q_2) + z_1 z_2 z_3 (A_{21} q_1/q_2 + A_{13} + A_{32} q_1/q_3 - C)].\end{aligned} \tag{1.60}$$

The equations expressing the dependence of the activity coefficients of the components of a mixture on the composition are obtained through partial differentiation of Eq. (1.58) with respect to the number of the appropriate components. For example, for γ_1 we obtain the following equation:

$$\begin{aligned}\ln \gamma_1 = z_2^2 [A_{12} + 2z_1 (A_{21} q_1/q_2 - A_{12})] + z_3^2 [A_{13} + 2z_1 (A_{31} q_1/q_3 \\ - A_{13})] + z_2 z_3 [A_{21} q_1/q_2 + A_{13} - A_{32} q_1/q_3 + 2z_1 (A_{31} q_1/q_3 \\ - A_{13})] + 2z_3 (A_{32} q_1/q_3 - A_{23} q_1/q_2) - C(1 - 2z_1).\end{aligned} \tag{1.61}$$

The constants A_{ij} and C are determined from the experimental data for binary and ternary systems respectively. The following equations can be obtained from Eqs. (1.60) and (1.61): (a) Margules equation which assumes that the effective molar volumes of the components are equal; (b) van Laar equations which are obtained by replacing q_i/q_j by A_{ij}/A_{ji}; and (c) Scatchard-Hammer equations in which the effective molar volumes q_i are replaced by the molar volumes v_i of pure components.

Another widely used method describes the dependence of the activity coefficients on the solution composition in the form of the func-

tion Φ which is connected with the excess free energy as follows:

$$\Phi = \frac{\Delta G^E}{2.303RT} = x_1 \log \gamma_1 + x_2 \log \gamma_2 + \ldots + x_k \log \gamma_k. \quad (1.62)$$

Partial derivatives of this function with respect to the corresponding components lead to the activity coefficients:

$$\begin{aligned} \frac{\partial \Phi}{\partial x_1} &= \log \frac{\gamma_1}{\gamma_k} + x_1 \frac{\partial \log \gamma_1}{\partial x_1} + \ldots + x_k \frac{\partial \log \gamma_k}{\partial x_1}, \\ &\ldots\ldots\ldots\ldots\ldots\ldots\ldots\ldots \quad (1.63) \\ \frac{\partial \Phi}{\partial x_{k-1}} &= \log \frac{\gamma_{k-1}}{\gamma_k} + x_1 \frac{\partial \log \gamma_1}{\partial x_{k-1}} + \ldots + x_k \frac{\partial \log \gamma_k}{\partial x_{k-1}}. \end{aligned}$$

However, in accordance with Eq. (1.56), the sum of the last terms in Eq. (1.63) is equal to zero. This gives

$$\begin{aligned} &\frac{\partial \Phi}{\partial x_1} = \log \frac{\gamma_1}{\gamma_k}, \\ &\frac{\partial \Phi}{\partial x_{k-1}} = \log \frac{\gamma_{k-1}}{\gamma_k}; \quad \log \gamma = \Phi - x_1 \frac{\partial \Phi}{\partial x_1} - \ldots - x_k \frac{\partial \Phi}{\partial x_{k-1}}. \end{aligned} \quad (1.64)$$

For example, the function Φ for a ternary Redlich-Kister system is equal to

$$\Phi = \Phi_{12} + \Phi_{23} + \Phi_{31} + x_1 x_2 x_3 \ (C + D_1 x_1 + D_2 x_2), \quad (1.65)$$

where

$$\begin{aligned} \Phi_{12} &= x_1 x_2 [b_{12} + C_{12} (x_1 - x_2) + d_{12} (x_1 - x_2)^2 + \ldots], \\ \Phi_{23} &= x_2 x_3 [b_{23} + C_{23} (x_2 - x_3) + d_{23} (x_2 - x_3)^2 + \ldots], \\ \Phi_{13} &= x_1 x_3 [b_{13} + C_{13} (x_1 - x_3) + d_{13} (x_1 - x_3)^2 + \ldots]. \end{aligned}$$

Here, the constants b_{ij}, C_{ij}, and d_{ij} are determined from the data on binary systems, while the constants C and D_i are obtained from ternary systems. The dependences for the activity coefficients are obtained from Eqs. (1.64) and (1.65). Thus, for a ternary system, the third-order Redlich-Kister equations have the form

$$\begin{aligned} \log \frac{\gamma_1}{\gamma_2} &= b_{12} (x_2 - x_1) - C_{12} [(x_1 - x_2)^2 - 2x_1 x_2] \\ &+ x_3 [b_{13} + C_{13} (2x_1 - x_3) - b_{23} - C_{23} (2x_2 - x_3) + C (x_2 - x_1)], \quad (1.66) \\ \log \frac{\gamma_1}{\gamma_3} &= b_{13} (x_3 - x_1) - C_{13} [(x_1 - x_3)^2 - 2x_1 x_3] \\ &+ x_2 [b_{12} + C_{12} (2x_1 - x_2) - b_{23} - C_{23} (x_2 - 2x_3) + C (x_3 - x_1)]. \end{aligned}$$

For calculations of the equilibrium with the help of the above equations, we require experimental results on the equilibrium of ternary and higher-order systems which are obtained with considerable diffi-

culty. The only exception is the Wilson model which can describe the equilibrium state of multicomponent systems by simply using the data on binary systems appearing in the multicomponent system and the physical and chemical properties of pure components. This considerably simplifies the experimental work required for characterizing the multicomponent equilibrium. The Wilson model is also based on an expression for Gibb's excess free energy as a function of the liquid phase composition, although the form of this expression is somewhat different from that used for deriving Wohl's equation:

$$\frac{\Delta G^E}{RT} = -\sum_{i=1}^{N} x_i \ln\left[\sum_{j=1}^{N} x_j \Lambda_{ij}\right], \qquad (1.67)$$

where

$$\Lambda_{ij} \equiv \frac{v_j^L}{v_i^L} \exp -[(\lambda_{ij} - \lambda_{ii})/RT],$$

Here, v_i^L and v_j^L are the molar liquid volumes of pure components, and $(\lambda_{ij} - \lambda_{ii})$ is a parameter characterizing the difference in the coupling energies of i-i and i-j molecular pairs. To a fairly high degree of accuracy, we can assume that this parameter is independent of temperature in the medium pressure range. Substituting Eq. (1.67) into (1.57), we obtain Wilson's equation for calculating the activity coefficients:

$$\ln \gamma_k \equiv -\ln\left[\sum_{j=1}^{N} x_j \Lambda_{kj}\right] + 1 - \sum_{i=1}^{N} \frac{x_i \Lambda_{ik}}{\sum_{j=1}^{N} x_j \Lambda_{ij}} \qquad (1.68)$$

This equation contains parameters corresponding only to the binary pairs of different components. The parameters Λ_{ii}, Λ_{jj}, and Λ_{kk} are equal to zero. Experimental data on binary mixtures are sufficient for determining the parameters $(\lambda_{ij} - \lambda_{ii})$ and $(\lambda_{ji} - \lambda_{jj})$. A comparison of the experimental and theoretical results for binary and multicomponent systems shows that the agreement between the results is quite good. The best agreement is obtained when calculations are carried out with the help of a digital computer, since the solution requires a large number of iterations. In this respect, Wilson's model seems to be most promising for representing the equilibrium data in calculations involving computers. Wilson's equations are unsuitable for calculations involving partially miscible liquids.

The general algorithm for calculating the phase equilibrium in a multicomponent system (MCS) under a constant pressure in the system is shown in Fig. 7. The algorithm consists of two parts. The first

part (blocks *1-4*) involves a search for the parameters of the Wilson equation and calculations of the vapour phase composition y in binary systems under constant pressure. The second part (blocks *5-8*) deals with the computation of the temperatures and compositions y_k of the vapour phase in a multicomponent system under constant pressure.

Similar programmes have also been composed and worked out for calculating the equilibrium of multicomponent systems at constant

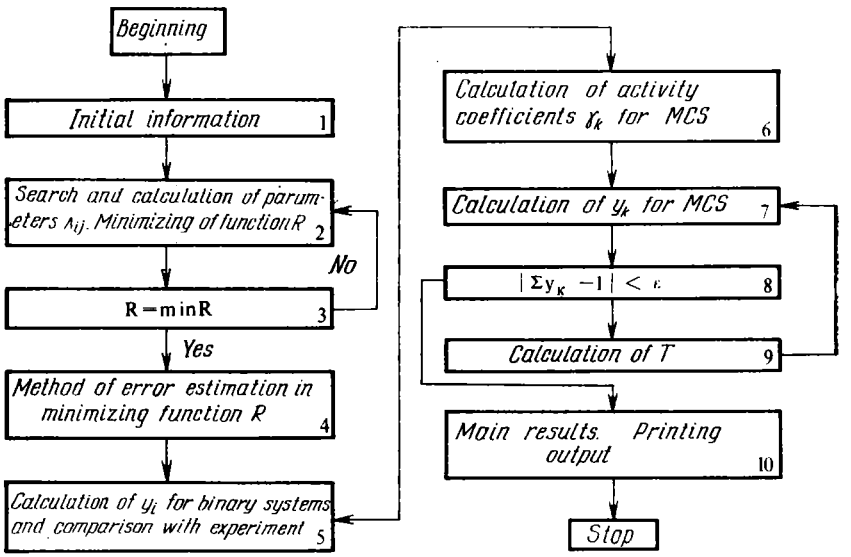
Beginning
Initial information 1
Search and calculation of parameters Λ_{ij}. Minimizing of function R 2
No
R = min R 3
Yes
Method of error estimation in minimizing function R 4
Calculation of y_i for binary systems and comparison with experiment 5
Calculation of activity coefficients γ_k for MCS 6
Calculation of y_k for MCS 7
$|\Sigma y_K - 1| < \varepsilon$ 8
Calculation of T 9
Main results. Printing output 10
Stop

Fig. 7. Block diagram of the algorithm for calculating the phase equilibrium of a multicomponent system.

temperature. The composition of the vapour phase of the ith component of the mixture is determined from the expression

$$y_i = \gamma_i x_i \frac{P_i^0}{P},$$

where y_i is the concentration of the ith component in vapour; γ_i is the activity coefficient of the ith component; x_i is the concentration of the ith component in liquid phase; P_i^0 is the pressure of the vapours of the pure ith component; and P is the total pressure in the system.

The activity coefficient for any component of a multicomponent system is determined from Eq. (1.67). The activity coefficients of bina-

ry systems are calculated with the help of the following equations:

$$\log \gamma_1 = -\ln(x_1 + \Lambda_{12}x_2) + x_2\left[\frac{\Lambda_{12}}{x_1+\Lambda_{12}x_2} - \frac{\Lambda_{21}}{\Lambda_{21}x_1+x_2}\right], \quad (1.67a)$$

$$\log \gamma_2 = -\ln(x_2 + \Lambda_{21}x_1) - x_1\left[\frac{\Lambda_{12}}{x_1+\Lambda_{12}x_2} - \frac{\Lambda_{21}}{\Lambda_{21}x_1+x_2}\right]. \quad (1.67b)$$

The functional dependence of the pressure of vapours of pure components on temperature is usually approximated by the equation

$$\ln P_i^0(T) = c_1 + \frac{c_2}{c_3+T} + c_4T + c_5T^2 + c_6 \ln T,$$

where T is the temperature in degrees Kelvin, and c_1, ..., c_6 are constant coefficients.

Sequence of calculations. The parameters $(\lambda_{ij} - \lambda_{ii})$ and $(\lambda_{jl} - \lambda_{jj})$ appearing in Λ_{ij} and Λ_{ji} are determined with the help of Eqs. (1.67a) and (1.67b) for all pairs of components constituting the multicomponent system from the experimental data on binary equilibrium. The solution is obtained by using the method of successive approximations, the degree of approximation depending on the sum of the squares of deviations of the equilibrium compositions of the vapour phase at certain points at which experimental and theoretical values are determined. The search for unknown parameters is carried out by following the minimizable function

$$R = \sum_{p=1}^{m}\left[y_{p(e)} - \frac{\exp\{x_{2p}[\Lambda_{12}/(x_{1p}+\Lambda_{12}x_{2p}) - \Lambda_{21}/(\Lambda_{21}x_{1p}+x_{2p})]\}\, x_{1p}P^0}{P(x_{1p}+\Lambda_{12}x_{2p})}\right]^2,$$

where $p = 1, 2, \ldots, m$ is the number of reference points; and $y_{p(e)}$ is the composition of the vapour phase at a reference point.

The search algorithm is composed in such a way that the values of the unknown parameters $(\lambda_{12} - \lambda_{11})$ and $(\lambda_{21} - \lambda_{22})$ obtained with its help satisfy the minimization condition $R = R_{\min}$ with a given degree of accuracy.

In the first stage of calculations, we calculate the optimal values of $(\lambda_{12} - \lambda_{11})$ and $(\lambda_{21} - \lambda_{22})$, the function R at the optimal point, the activity coefficients γ_p of the binary systems at the reference points, the composition y_p of the vapour phase for binary systems, and the relative error in the computation of the vapour phase composition.

In the second stage, the activity coefficients γ_k of the multicomponent system are calculated at the initial temperature by Eq. (1.68), followed by the composition of its vapour phase. After this, we calculate the temperature T_k of the multicomponent mixture at which the relation $\left|\sum_{k=1}^{N} y_k - 1\right| \leqslant \varepsilon$ corresponding to the thermodynamic equilibrium condition is satisfied with a given accuracy ε.

The initial information required for calculating the phase equilibrium of a multicomponent system with the help of the proposed algorithm includes data on the liquid-vapour equilibrium of the binary systems *x-y-T* or *x-y-P*, as well as the temperature dependence of the partial pressures of pure components.

Wilson's equation gives good results for calculating the equilibrium of mutually soluble multicomponent systems. If, however, mutually insoluble or partially soluble mixture components appear in multicomponent systems, it is better to use Hayle's NRTL (non-random two liquids) equation instead of Wilson's equation:

$$\ln \gamma_i = \frac{\sum_{j=1}^{N} r_{ji} G_{ji} x_j}{\sum_{k=1}^{N} G_{ki} x_k} + \sum_{j=1}^{N} \frac{x_j G_{ij}}{\sum_{k=1}^{N} G_{kj} x_k} \left(\tau_{ij} - \frac{\sum_{l=1}^{N} \tau_{lj} G_{lj} x_l}{\sum_{k=1}^{N} G_{kj} x_k} \right), \quad (1.69)$$

where

$$r_{ji} = (\lambda_{ji} - \lambda_{ii})/RT \text{ and } G_{ji} = \exp(-\alpha_{ji} r_{ji}).$$

Here, x_i is the content of the ith component in the liquid; γ_i is the activity coefficient of the ith component, v_i is the molar liquid volume of an individual substance; $\lambda_{ji} - \lambda_{ii}$ and α_{ji} are constants to be determined; R is the universal gas constant; T is the temperature; and N is the number of components.

The parameters appearing in Eq. (1.69) are calculated with the help of the well-known thermodynamic relation

$$Py_i = \gamma_i x_i P_i^0,$$

where y_i is the concentration of the ith component in the vapour phase, and P_i^0 is the vapour pressure of an individual substance. The parameters $\lambda_{21} - \lambda_{11}$, $\lambda_{12} - \lambda_{22}$ and α_{12} can be determined by using the experimental values of the total pressure P, the equilibrium phase compositions x and y, and the temperature T for binary systems, and by expressing the activity coefficients γ_1 and γ_2 by Eq. (1.69).

The block diagram of the algorithm for calculating the constants is shown in Fig. 8. It is based on the method of steepest descent with parabolic interpolation along the gradient. The search strategy is developed in such a way as to take into account the possibility of ravines, and consists in the following (Fig. 9). At first, a descent from an arbitrary point $\bar{x}_{in}$ along a gradient chosen beforehand and the parabolic interpolation are carried out. From the point corresponding to the minimum value of the optimality criterion F (point *1*) obtained in this way we take an orthogonal step (point *2'*) of magnitude h, after which the new minimum (point *2*) is determined by the method described above (descent along the gradient from point *2'* and parabolic interpolation). After this, points *1* and *2* are joined by a

straight line (in the direction *1-2*) along which a step is taken along decreasing the optimality criterion (point *3'*). The third minimum (point *3*) is then found in the same way as the previous two. If the value of the optimality criterion at this point is less than at point *2*, point *1* is rejected and another step is taken in the direction *2-3*

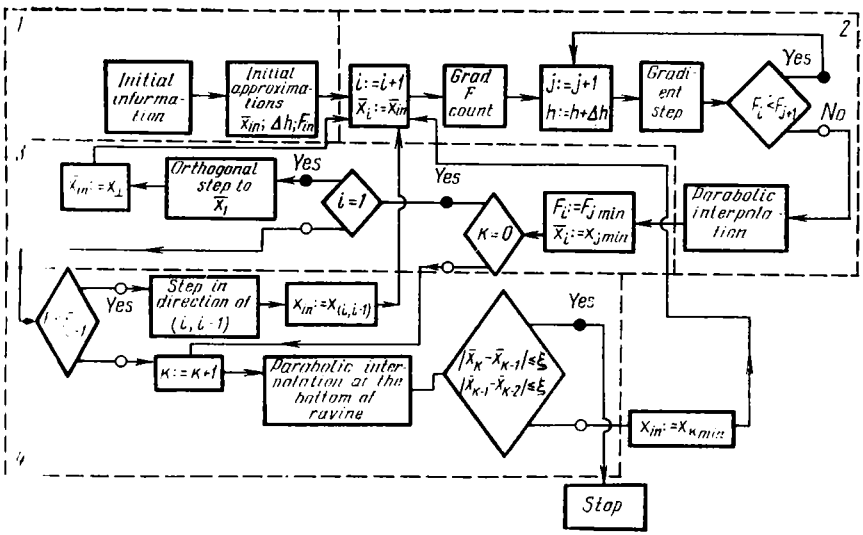

Fig. 8. Block diagram of the algorithm for calculating the constants in Eq. (1.69):

1—specification of the initial values; *2*—search of minimum in gradient and parabolic interpolation; *3*—search of minimum in the direction orthogonal to the initial direction; *4*—search of minimum in the directions of the ravine.

(point *4'*), followed by the determination of another minimum (point *4*). As soon as the value of a new optimality criterion becomes larger than the previous value, a parabola is constructed along the bottom of the ravine (index $k \neq 0$, see Fig. 8). From the minimum of this parabola, a descent along the gradient takes place and is followed by the parabolic interpolation. Three best points are chosen again and a parabola passing through these points is constructed. The whole cycle of calculations is then repeated. If the values of the arguments at the three points of the parabola constructed at the bottom of a ravine do not exceed a given value ε, the search is terminated.

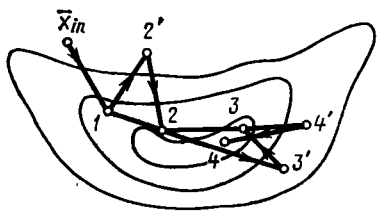

Fig. 9. Strategy for searching the constants in Eq. (1.69) in the presence of a ravine.

The optimality criterion has the form

$$F=\left[\sum_{i=1}^{m}(\varphi_{i\,\mathrm{exp}}-\varphi_{i\,\mathrm{theor}})^2/m\right]^{1/2}, \tag{1.70}$$

where m is the number of reference or equilibrium points, and φ are physical parameters (pressure, temperature, vapour composition, or the activity coefficient). For isobaric equilibrium data, a comparison between the experimental and theoretical values of pressure is most acceptable. In this case, the total pressure is calculated according to the formula

$$P = P_1^0\gamma_1 x_1 + P_2^0\gamma_2 x_2. \tag{1.71}$$

The following algorithm is used for calculating the normal boiling point of a mixture. It is assumed that the system obeys ideal gas laws. The relation between the vapour and liquid phases can then be expressed for each component through Henry's law:

$$y_i = \gamma_i x_i \frac{P_i^0}{P}, \quad (i=1,\ 2,\ \ldots,\ N), \tag{1.72}$$

where y_i is the composition of the vapour phase; x_i is the composition of the liquid phase; P_i^0 is the vapour pressure for a pure component; and P is the total pressure.

The ratio of the pressure of vapours of a pure component to the total pressure of the system k_i is a function of temperature in the simplest case:

$$\frac{P_i^0}{P} = k_i = \exp\left(A_{1,\,i} + A_{2,\,i}/T + A_{3,\,i}T + A_{4,\,i}\ln T\right), \tag{1.73}$$

where $A_{1,\,i} - A_{4,\,i}$ are constants to be determined from the experimental P-T results, and T is the temperature in degrees Kelvin.

Besides, the following relation is valid for any mixture:

$$\sum_{i=1}^{N} y_i = 1. \tag{1.74}$$

The system of equations (1.72)-(1.74) can be reduced to an equation in one unknown by summing the left- and right-hand sides of Eqs. (1.72). This gives

$$\sum_{i=1}^{N} k_i x_i \gamma_i = 1. \tag{1.75}$$

Introducing a new function, we can write this equation in an alternative form:

$$f(T) = \sum_{i=1}^{N} k_i x_i \gamma_i - 1 = 0. \tag{1.76}$$

The function $f(T)$ is a measure of the deviation of the sum of concentrations of the components in a gas from unity and is equal to zero at $T = T_{boil}$. It has one positive root which can be found with the help of the iterative secant method:

$$T_{k+1} = T_k - \frac{f(T_k)}{f(T_{k-1}) - f(T_k)} (T_{k-1} - T_k). \qquad (1.77)$$

1.2. Equilibrium Relations in Liquid-Liquid Systems. Basic Concepts and Definitions

Liquid-liquid systems usually contain two phases (two immiscible liquids) and three components. Hence, in accordance with the phase rule, the number of parameters determining the state of the system will be

$$3 + 2 = 2 + N_s \quad N = 3.$$

The equilibrium distribution of the third component between two liquid phases is fixed by the value of the concentrations in each phase and temperature.

A typical diagram of this kind is shown in Fig. 10. The system consists of three components A, B, and C at a constant temperature. Component C is soluble in A and B in all proportions, while components A and B have limited solubility in each other. The mixture of components A and B is shown by points along the side AB of the triangle, the mixture of A and C by points on the side AC, and the mixture of B and C by point on the side BC. Any point inside the triangle represents a mixture of three components. Since the triangle is equilateral, the composition of the mixture corresponding to a point inside it is determined by the lengths of the perpendiculars drawn from the given point to the side opposite to the given component. Thus, for the point M the composition of the mixture relative to the components A, B, and C will be given by the lengths of the perpendiculars Mx, My, and Mz respectively. This situation is a direct consequence of the principle according to which the diagram has been constructed. Thus, for example the concentration of component A at the point A is 100 percent, and at any other point this value will be less than 100 percent. Moreover, the farther a point from the point A, the lower the percentage of component A in the mixture and hence the shorter the perpendicular on the side BC of the triangle.

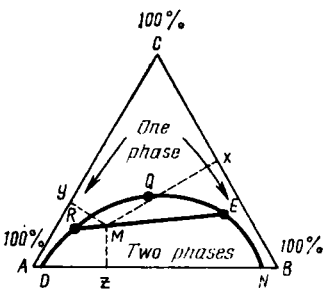

Fig. 10. Equilibrium diagram of a three-component liquid-liquid system.

The curve *DRQEN* demarcates the region of mutual solubility of the components and expresses the equilibrium distribution of component C in A and B. The points below the boundary curve *DRQEN* correspond to the region of separation of liquids A and B, while the points above this curve are in the region of complete mutual solubility of the components, where only one phase is present. For the point *M* below the boundary curve, the composition of the liquids being separated upon equilibrium saturation is characterized by the points *R* and *E*. All mixtures along the line *RE* form two liquid layers with concentration *R* and *E* respectively. The relative amounts

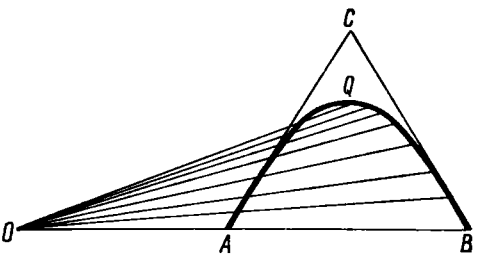

Fig. 11. Construction of a conode pole.

of each layer are inversely proportional to the segments formed along the line *RE*: $R/E = ME/RM$. Point *R* corresponds to the layer formed at the point *M* and rich in component A, while point *E* corresponds to the layer rich in the component B. The line *RE* joining the compositions of two equilibrium layers is called a *conode* (*tie line*). There is an infinite number of conodes within a boundary curve. If the conodes converge at one point (at the pole *O*, Fig. 11), the position of the focus *O* can be determined from two known conodes. This enables us to plot any other points without knowing the corresponding experimental data and to construct the equilibrium distribution curve. With increasing concentration of component C, the conodes within the boundary curve become smaller and are ultimately reduced to the point of inflection *Q*. At the point of inflection *Q*, the two liquid layers become identical in composition and density. This point can be determined in the same way as the critical point. The equilibrium distribution of the third component (for example, C) between the two phases (A and B) can be represented as the distribution coefficient while calculating the extraction processes.

The distribution coefficient in an extraction process is the ratio of the mass or mole fractions of the distributed component C in the phase rich in component B (x_{C-B}) if B is the solvent, to the mass or mole fraction of the component C in the phase rich in the component

Λ (x_{C-A}), i.e.

$$K = \frac{x_{C\text{-}B}}{x_{C\text{-}A}} = \text{const}, \tag{1.78}$$

where K is the distribution coefficient whose magnitude is greater than unity. This relation is valid for small concentrations of the distributed substance and in the absence of dissociation or association of molecules of the substance being distributed between phases. In the generel case, the following relation holds:

$$K = \frac{x^m_{C\text{-}B}}{x_{C\text{-}A}}, \tag{1.79}$$

where $m > 1$ is a variable quantity.

The suitability of a solvent for separating the components is best illustrated by graphs characterizing the selectivity of the solvent with respect to the component being separated. The selective action of a solvent (component B) during separation of a solution of A and C into individual components can be estimated by the relation

$$\beta = \frac{\dfrac{\%\ C}{\%\ C + \%\ A}\ \text{in phase B}}{\dfrac{\%\ C}{\%\ C + \%\ A}\ \text{in phase A}} = \frac{x_{C\text{-}B}/x_{A\text{-}B}}{x_{C\text{-}A}/x_{A\text{-}A}}, \tag{1.80}$$

where β is the selectivity coefficient; x_{C-B} and x_{A-B} are the concentrations of components C and A in the solvent layer; and x_{C-A}, x_{A-A} are the concentrations of the components in the residue.

In extraction processes, the solvent must always satisfy the condition $\beta > 1$. The higher the value of the selectivity coefficient, the more effective a solvent.

Considering that the activity of each component is constant in all phases in the equilibrium state, the selectivity coefficient can be calculated from the ratio of activity coefficients:

$$\beta = \frac{\gamma_{C\text{-}A}/\gamma_{A\text{-}A}}{\gamma_{C\text{-}B}/\gamma_{A\text{-}B}}. \tag{1.81}$$

Together with Eq. (1.69), this equation can be used to predict the equilibrium distribution in the liquid-liquid systems from the equilibrium data in the vapour-liquid systems. If the vapour-liquid data are used, the ultimate result will depend on the quality of the data and on the correct choice of α_{12}. For binary systems whose components are quite immiscible the value $\alpha_{12} = 0.20$ is found to be quite reliable. It is possible to predict the equilibrium in a ternary liquid-liquid system from binary system data if the most appropriate value of α_{12} has been chosen for each binary system.

On account of the significant effect of temperature on the equilibrium composition of the condensed phases (liquid phases), and also because of their considerable non-ideality, the methods described above for calculating the compositions of these phases give quite rough estimates. Hence one should resort to a theoretical determination of the composition of the equilibrium liquid phases only for obtaining approximate results. The experimental data contained in the handbooks should always be preferred.

Chapter Two

Material and Heat Balance Equations for Systems in Equilibrium

The steady-state conditions for processes involving mass transfer are usually characterized by the following parameters: specific flow rate of the absorbent or solution, i.e. the reflux ratio, and the number of theoretical contact stages (number of theoretical plates), which are obtained by jointly solving the material balance equations and the equilibrium equations.

The general form of the material balance equation is

$$G\,dy = -L\,dx, \tag{2.1}$$

where G is the rate of flow of the gas (vapour); L is the rate of flow of the liquid; y is the concentration of the component being distributed in the gas (vapour); and x is the concentration of the component being distributed in the liquid. The corresponding parameters for extraction are: L and G are the rates of extraction of pure liquid A and pure liquid B (solvent) respectively; x is the concentration of the component being extracted (C) in liquid A, and y is the concentration of the component being extracted (C) in the solvent. The minus sign indicates that the concentration of the component being distributed decreases in the given phase.

2.1. Determination of the Number of Theoretical Plates and Basic Laws

If the flow rates L and G are constant in an absorption process, integration of (2.1) within the given concentration limits leads to the equation of a straight line passing through two points (y_{1n}, x_{f1n}) and (x_{1n}, y_{f1n}):

$$\frac{L}{G} = \frac{y_{in} - y_{fin}}{x_{fin} - x_{in}}, \tag{2.2}$$

Figure 12 shows the straight line corresponding to Eq. (2.2), called the operating line for the process. Besides, the figure also shows the equilibrium curve which passes below the operating line, since

during absorption the concentration of the component being distributed is higher in the gas than in the liquid.

The slope of the operating line is the ratio L/G which is called the *specific flow rate of the absorbent* in absorption processes. The higher the specific flow rate of the absorbent, the farther the operating line from the equilibrium curve and the larger the difference between the flow rate and equilibrium concentration: $\Delta y = y - y^*$. In other words, the driving force of the process will increase with the flow rate. At the same time, the difference $\Delta x = x^* - x$ in the liquid-phase

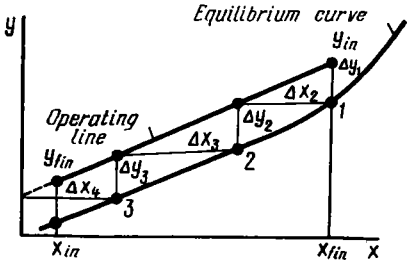

Fig. 12. Operating and equilibrium lines for an absorption process.

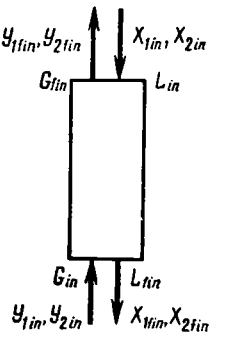

Fig. 13. Material fluxes in an absorption column.

concentrations will increase, i.e. the driving force of the process in the liquid phase will increase. The simultaneous variation of a given concentration up to the equilibrium concentration in the gaseous and liquid phases is called a *theoretical contact stage* or a *theoretical plate.*

The number of such contacts or the number of theoretical plates may be directly determined graphically in the given concentration range, or calculated analytically by simultaneously solving the equations for the operating line and the equilibrium curve. The most visual representation of the process is obtained through the graphic determination of the number of theoretical contacts (Fig. 12).

Starting from the given concentration y_{1n}, we drop a perpendicular on the equilibrium curve. From the point *1* corresponding to x_{fin} we draw a horizontal line till the point where it intersects the operating line. We again drop a perpendicular from this point to meet the equilibrium curve at the point *2* corresponding to the second theoretical contact. This process is repeated until the given values y_{fin} and x_{1n} are obtained. Thus the number of points of intersections with the equilibrium curve gives the number of theoretical contacts. In the case under consideration, there will be about four such points. With increasing specific flow rate of the absorbent at which the operating line deviates from the equilibrium curve, the driving force (Δy,

Δx) of the process increases while the number of required theoretical plates decreases. Upon a change in the thermal conditions of the system and consequently, upon a change in the pressure of the components the operating line becomes curved. In this case, it is necessary to compose a heat balance equation in addition to the material balance equation.

Let us consider the more general case for determining the number of theoretical plates for separating multicomponent systems when the operating line becomes curved. In accordance with Fig. 13, the amount of the ith absorbed component for a column will be

$$A_i = G_{in}\, y_{i,\,in}\Phi_i, \tag{2.3}$$

where Φ_i is the fraction of the absorbed (desorbed) ith component. The total amount absorbed will be

$$A = \sum A_i = G_{in}\,(y_{A,\,in}\Phi_A + y_{B,\,in}\Phi_B + y_{C,\,in}\Phi_B + y_{C,\,in}\Phi_C + \ldots). \tag{2.4}$$

The amount of the ith component leaving the absorber with the outgoing gas will be

$$a_i = G_{in}\, y_{i,\,in}\,(1 - \Phi_i). \tag{2.5}$$

The amount of the ith component leaving the absorber with the outgoing liquid is calculated from the equation

$$b_i = L_{in}x_{i,\,in} + G_{in}y_{i,\,in}\,\Phi_i. \tag{2.6}$$

From Eqs. (2.3) and (2.4), we get

$$G_{fin} = G_{in} - A = G_{in}\,[1 - (y_{A,\,in}\Phi_A + y_{B,\,in}\,\Phi_B + y_{C,\,in}\Phi_C + \ldots)], \tag{2.7}$$

$$L_{fin} = L_{in} + A = L_{in} + G_{in}\,(y_{A,\,in}\,\Phi_A + y_{B,\,in}\,\Phi_B + y_{C,\,in}\Phi_C + \ldots). \tag{2.8}$$

From Eqs. (2.5)-(2.8), we get

$$y_{i,\,fin} = \frac{a_i}{G_{fin}} = \frac{G_{in}y_{i,\,in}\,(1-\Phi_i)}{G_{in}-A} = \frac{y_{i,\,in}\,(1-\Phi_i)}{1-(y_{A,\,in}\Phi_A + y_{B,\,in}\Phi_B + y_{C,\,in}\Phi_C + \ldots)}. \tag{2.9}$$

$$x_{i,\,fin} = \frac{b_i}{L_{fin}} = \frac{L_{in}x_{i,\,in} + G_{in}y_{i,\,in}\Phi_i}{L_{in}+A}. \tag{2.10}$$

The total amount of heat in the absorber will be

$$Q = A_A q_A + A_B q_B + \ldots = \sum A_i q_i. \tag{2.11}$$

The heat carried away during the evaporation of a part of the solvent is equal to

$$Q_{ev} = \zeta L_{in} q_{ev}. \tag{2.12}$$

The heat spent in heating the liquid is equal to

$$Q_h = Q - Q_{ev} = \sum A_i q_i - \zeta L_{in} q_{ev}. \tag{2.13}$$

For a non-volatile solvent, $Q_{ev} = 0$ and $Q_h = Q$. Neglecting the change in the temperature of the gas flow, the temperature of the outflowing liquid can be expressed in the form

$$T_{fin} = T_{in} + \frac{Q_h}{L_{fin} C_{fin}}. \tag{2.14}$$

A similar calculation for desorption gives the following equations

$$A'_i = L'_{in} x'_{i,\,in} \Phi'_i, \tag{2.3a}$$

$$A' = A'_i = L'_{in} (x'_{A,\,in} \Phi'_A + x'_{B,\,in} \Phi'_B + x'_{C,\,in} \Phi'_C + \ldots), \tag{2.4a}$$

$$b'_i = L'_{in} x'_{i,\,in} (1 - \Phi'_i), \tag{2.5a}$$

$$a'_i = G'_{in} y'_{i,\,in} + L'_{in} x'_{i,\,in} \Phi'_i, \tag{2.6a}$$

$$G'_{fin} = G'_{in} + A', \tag{2.7a}$$

$$L'_{fin} = L_{in} - A', \tag{2.8a}$$

$$y'_{i,\,fin} = \frac{a_i}{G'_{fin}}, \tag{2.9a}$$

$$x'_{i,\,fin} = \frac{b_i}{L'_{fin}}, \tag{2.10a}$$

$$Q' = \sum A'_i q_i, \tag{2.11a}$$

$$Q_{ev} = \zeta L_{in} q_{ev}, \tag{2.12a}$$

$$Q'_h = Q' + Q_{ev}, \tag{2.13a}$$

$$T'_{fin} = T'_{in} - \frac{Q_h}{L'_{fin} C_{fin}}. \tag{2.14a}$$

These equations are solved by using the method of successive approximations.

1. Knowing the initial concentration of each component in the incoming gas and taking into account the difference in the absorptivity of each component, we can specify the fractions of the absorbed (desorbed) components. As a first approximation, we can write

$$\Phi_A : \Phi_B : \Phi_C : \ldots = 1/k_A : 1/k_B : 1/k_C : \ldots$$

and

$$\Phi'_A : \Phi'_B : \Phi'_C : \ldots = k_A : k_B : k_C : \ldots,$$

$$0 < \Phi_i \ (\Phi'_i) < 1.$$

2. Appropriate values of Φ_i (Φ'_i) are substituted into Eqs. (2.3)-(2.10) and (2.3a)-(2.10a), and the values of L_{fin}, $G_{fin}(L'_{fin}$, $G'_{fin})$, $y_{A,\,fin}$, $y_{B,\,fin}$, $y_{C,\,fin}$, . . ., $x_{A,\,fin}$, $x_{B,\,fin}$, $x_{C,\,fin}$, . . . ($y'_{A,\,fin}$, $y'_{B,\,fin}$, $y'_{C,\,fin}$, . . . , $x'_{A,\,fin}$, $x'_{B,\,fin}$, $x'_{C,\,fin}$, . . .) are calculated.

3. The value of $T_{fin}(T'_{fin})$ is calculated by substituting Φ (Φ') into Eqs. (2.11)-(2.14) and (2.11a)-(2.14a).

4. The terminal points $(x_{A,\,in}, y_{A,\,fin})$, $(x_{B,\,in}, y_{B,fin})$, $(x_{C,\,in}, y_{C,\,fin})$, . . . and $(x_{A,\,fin}, y_{A,\,in})$, $(x_{B,\,fin}, y_{B,\,in})$, $(x_{C,\,fin}, y_{C,\,in})$ of the operating lines are plotted in the x, y coordinates. The slope of the operating line at the terminal points in these two cases will be equal to

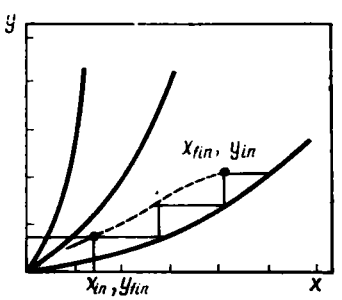

Fig. 14. Construction of equilibrium and operating lines:

—equilibrium curves; - - - - operating line.

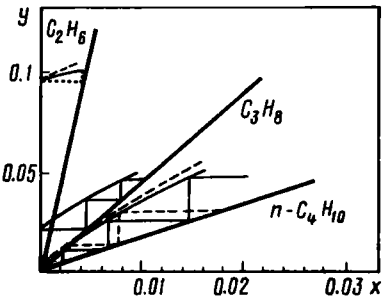

Fig. 15. To the example illustrating the calculation of absorption:

— first approximation; - - - - second approximation; . . . . third approximation.

L_{in}/G_{fin} and L_{fin}/G_{in} respectively. The operating lines are found to be curved and are plotted from $(x_{i,\,in}, y_{i,\,fin})$ with a slope L_{in}/G_{fin} to $(x_{i,\,fin}, y_{i,\,in})$ with a slope L_{fin}/G_{in} (Fig. 14). The slope of these curves varies uniformly between the two terminal slopes. Similar construction can also be carried out for desorption.

5. Equilibrium relations are plotted for each component for two terminal temperatures of the liquid T_{in} (T'_{in}) and T_{fin} (T'_{fin}). The equilibrium curve for each component is plotted from T_{in} (T'_{in}) at $x_{i,\,in}(x'_{i,\,in})$, terminating at the equilibrium relation corresponding to T_{fin} (T'_{fin}) at $x_{i,\,fin}$ ($x'_{i,\,fin}$).

6. The number n of theoretical plates is plotted graphically for each component. If the first values of absorbed (desorbed) fractions are chosen correctly, the number n_{act} of actual plates will be the same for all components:

$$n_{act} = n_A/\eta_A = n_B/\eta_B = n_C/\eta_C, \qquad (2.15)$$

where η_A, η_B, and η_C denote the efficiency of the plates with respect to the components A, B, and C. If $\eta_A = \eta_B = \eta_C$, we get

$$n_{act} = n_A = n_B = n_C. \qquad (2.16)$$

7. If Eqs. (2.15) and (2.16) are not satisfied, new values of Φ_i are chosen and the calculations are repeated.

Example. A mixture of gases with the percentage composition

$$CH_4\ 80,\quad C_2H_6\ 10,\quad C_3H_8\ 5,\quad n\text{-}C_4H_{10}\ 5$$

is absorbed at 24 °C by a non-volatile mixture of hydrocarbons. The overall pressure is 2 atm and the ratio of oil to gas L/G is equal to 3 moles per mole. It is necessary to extract 60 percent of C_3H_8. Find the number of theoretical plates and the composition of the gas leaving the absorber. The efficiency of a plate with respect to each component is assumed to be the same. The temperature variation inside the absorber is neglected.

Solution. The following basis is adopted for calculations. We assume that 100 moles of the incoming gas and 300 moles of the oil are present. The values of the distribution coefficients k are calculated from the vapour pressures of pure components in accordance with Raoult's law. The solubility of methane can be neglected. As a result, we obtain the following table:

Table 2a

Component	Vapour pressure P_i (atm) at 24°C	$k_i = P_i/P$	$y_{i,\,in}$ (mole fraction)
CH_4	—	—	0.80
C_2H_6	41.5	20.8	0.10
C_3H_8	8.84	4.42	0.05
$n\text{-}C_4H_{10}$	2.33	1.67	0.05

The equilibrium curves corresponding to the equation $y_i = kx_i$ with a slope equal to k_i are represented in Fig. 15. As the first approximation, we take

$$\Phi_{C_2} : 0.6 : \Phi_{C_4} = \frac{1}{20.8} : \frac{1}{4.42} : \frac{1}{1.67}$$

or

$$\Phi_{C_2} = 0.15 \text{ and } \Phi_{C_4} = 0.99.$$

The results of calculations on the basis of the first approximation are shown in the following table:

Table 2b

Component	Φ_i	A_i	a_i	b_i	G_{fin}	L_{fin}	$y_{i,\,fin}$	$x_{i,\,fin}$	n
C_2H_6	0.15	1.15	8.5	1.5	—	—	0.094	0.00485	—
C_3H_8	0.60	3.0	2.0	3.0	90055	309.45	0.0221	0.0097	2.7
$n\text{-}C_4H_{10}$	0.99	4.95	0.05	4.95	—	—	0.0055	0.016	3.15
		$\sum A = 9.10$							

It can be seen from the table that the number of theoretical plates is not the same for each component. Consequently, we must use the second approximation. This is chosen in the form $\Phi_{C_2} = 0.10$ and $\Phi_{C_4} = 0.95$.

The results of calculations based on the second approximation are presented in the following table:

Table 2c

Component	Φ_i	A_i	a_i	b_i	G_{fin}	L_{fin}	$y_{i,\text{ fin}}$	$x'_{i,\text{ fin}}$	n
C_2H_6	0.10	1.0	9.0	1.0	—	—	0.098	0.0026	0.6
C_3H_8	0.60	3.0	2.0	3.0	91.55	308.45	0.0219	0.0097	2.7
n-C_4H_{10}	0.95	4.45	0.55	4.45	—	—	0.006	0.0144	2.9
		$\sum A = 8.45$							

It can be seen from the table that the number of theoretical plates for ethane is smaller than for propane and butane. This means that the fraction of the absorbed ethane is very low. As the third approximation we take $\Phi_{C_2} = 0.145$ and $\Phi_{C_4} = 0.95$. The following results are obtained by using the third approximation:

Table 2d

Component	Φ_i	A_i	a_i	b_i	G_{fin}	L_{fin}	$y_{i,\text{ fin}}$	$x'_{i,\text{ fin}}$	n
C_2H_6	0.145	1.45	8.55	1.45	—	—	0.0938	0.0047	2.5
C_3H_8	0.60	3.0	2.0	3.0	91.0	308.9	0.022	0.0097	2.7
n-C_4H_{10}	0.95	4.45	0.55	4.45	—	—	0.00604	0.0144	2.7
		$\sum A = 8.9$							

It follows from the table that the number of theoretical plates for different components is practically the same. Hence the calculations are assumed to be over.

For graphical determination of the number of theoretical plates for distillation processes, as well as absorption processes, it is necessary to first calculate the equations of operating lines for the distillation process. These equations are derived under the following conditions:

1. The components being separated have nearly equal heats of evaporation. In other words, the amount of vapour condensed on a given plate is equal to the amount of vapour formed on it, but has a higher volatile content. This means that the same quantity of vapour passes per unit time through any cross section of the column.
2. The flows of liquids entering a column (initial mixture and reflux) are at the same temperature as the boiling point.
3. The composition of the liquid being returned from the fractionating column (condenser) to the top plate of the column is the same as

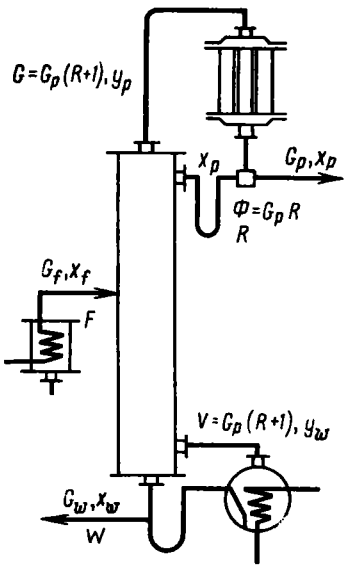

Fig. 16. Material flows in a fractionating column.

that of the vapour rising from this plate to the fractionating column. In other words, it is assumed that no separation takes place in the fractionating column.

4. The composition of the liquid flowing from the lowest plate of the column is the same as the composition of the vapour rising from the boiler or the still to this plate. In other words, it is assumed that separation does not take place in the still. In actual practice, the liquid flows into the still and the vapour obtained from it will be distinguished by a high content of the volatile component. This assumption enables us to have a spare theoretical plate.

The material flows in a continuous fractionating column are shown in Fig. 16. The following notation is used here: G_f, G_p, G_w, and Φ denote flow rate of the initial mixture, distillate, the still liquid and bottoms, kg·mole/hr, x_f, x_p, and x_w denote the composition of the initial mixture, distillate, and the still liquid with respect to the volatile component in mole fractions. From conditions 3 and 4 it follows that $x_p = y_p$ and $x_w = y_w$, where y_p and y_w represent the composition of the vapour with respect to the volatile component rising from the upper plate of the column and from the boiler.

Taking the flow rate of the distillate G_p as the basic quantity, we introduce the dimensionless ratios

$$G_f/G_p = F, \quad G_w/G_p = W, \quad \Phi/G_p = R,$$

where F is the feed number, W the still number, and R is the reflux ratio.

Equation of operating lines for a fractionating column. The material balance equation in the general form can be written as follows:

$$G\,dy = -L\,dx. \tag{2.17}$$

The flow rate G of vapour rising in the column is equal to the flow rate Φ of the condensed liquid used as reflux for the upper part of the column plus the flow rate G_p of the distillate:

$$G = \Phi + G_p. \tag{2.18}$$

Introducing the dimensionless ratios, we obtain

$$\frac{G}{G_p} = R + 1. \tag{2.19}$$

The flow rate of the liquid arriving at the upper part of the column (reflux) is equal to Φ. In the dimensionless form, we can write:

$$\frac{\Phi}{G_p} = R. \tag{2.20}$$

Thus, Eq. (2.17) assumes the form

$$(R + 1)\, dy = -R\, dx. \tag{2.21}$$

In a continuous fractionating column, the flow rates for the vapour and liquid remain constant. Hence the quantities $(R + 1)$ and R can be taken out of the integral. For any plate in the upper part of the column, from which vapour of composition y rises and on which the liquid has a composition x, we obtain (taking counter-currents into consideration)

$$(R+1) \int_{y}^{y_p} dy = -R \int_{x_p}^{x} dx, \tag{2.22}$$

whence

$$(R + 1)\,(y_p - y) = R\,(x_p - x). \tag{2.23}$$

After transformation and considering that $x_p = y_p$, we get

$$y = \frac{R}{R+1}\, x + \frac{x_p}{R+1}. \tag{2.24}$$

This equation establishes a relation between the compositions of the vapour and liquid in any cross section in the upper part of the column for given values of reflux ratio R and composition x_p of the distillate. It is called the *equation for the operating line of the upper part of a fractionating column.*

The equation for the operating line of the lower part of the column is obtained in the same way, the only difference being that in the lower part of the column (from the feed plate downward), the liquid flow rate increases by the feed number F:

$$(R+1) \int_{y_w}^{y} dy = -(R+F) \int_{x_w}^{x} dx, \tag{2.25}$$

whence

$$(R + 1)\,(y - y_w) = (R + F)\,(x - x_w). \tag{2.26}$$

After transformation and considering that $x_w = y_w$ and $F = W + 1$, we obtain

$$y = \frac{R+F}{R+1} x - W \frac{x_w}{R+1}. \tag{2.27}$$

Since the quantities

$$\frac{R}{R+1} = A, \quad \frac{x_p}{R+1} = B, \quad \frac{R+F}{R+1} = A_1, \quad W \frac{x_w}{R+1} = B_1$$

remain constant for a continuous column, Eqs. (2.24) and (2.27) are the equations of straight lines:

$$y = Ax + B, \tag{2.28}$$

$$y = A_1 x - B_1. \tag{2.29}$$

Figure 17 shows the equilibrium curve for fractionation in x, y coordinates, as well as the operating lines for the upper and lower

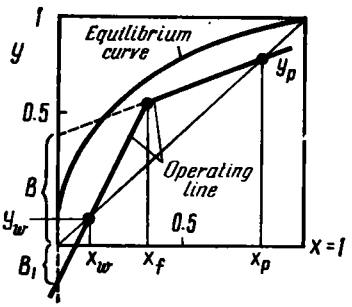

Fig. 17. Operating and equilibrium lines for a fractionation process.

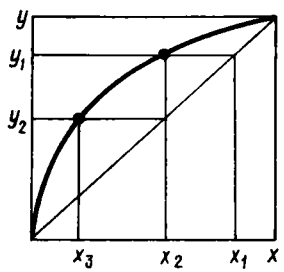

Fig. 18. To the derivation of the Fenske equation.

parts of the column, which intersect at a point corresponding to the composition x_f of the initial mixture (feed plate). The upper operating line starts at the point $x_p = y_p$ on the diagonal and cuts off an intercept

$$B = \frac{x_p}{R+1}$$

on the ordinate axis, its slope being equal to

$$A = \frac{R}{R+1}.$$

The lower operating line intersects the upper operating line, and the diagonal at the point $x_w = y_w$. It cuts off a segment

$$B_1 = \frac{W}{R+1} x_w$$

on the ordinate axis.

It remains for us to find the value of the ordinate corresponding to the composition x_f. The choice of this quantity is the determining factor in calculating a fractionation process. Two extreme positions can be chosen for the point of intersection of the operating lines: (1) the point of intersection lies on the diagonal, and (2) the point of intersection lies on the equilibrium curve.

Case (1) (the point of intersection of the operating lines lies on the diagonal). The slope of the operating line is the same as that of the diagonal, i.e. 45° and tan 45° = 1. This condition can be satisfied only when

$$\lim_{R\to\infty} \frac{R}{R+1} = 1. \tag{2.30}$$

Consequently, if the point of intersection of the operating lines lies on the diagonal and the operating lines themselves coincide with the diagonal, the reflux ratio $R = \infty$. This means that all the vapour condensing in the fractionating column completely returns to the column in the form of reflux, the column operates unproductively and no distillate is removed from it.

In this case, the driving force will have its maximum value if we express it as the difference between the operating and equilibrium concentrations ($\Delta y = y^* - y$ and $\Delta x = x - x^*$), the concentration will vary in large steps and the number of steps will be minimum. If the equilibrium curve is described by Raoult's equation, the minimum number of steps can be easily calculated by jointly solving Raoult's equation and the operating line equation. In order to illustrate such a solution, we use Fig. 18. For a point lying on the equilibrium line, we get

$$\frac{y_1}{1-y_1} = \alpha \frac{x_2}{1-x_2} \tag{2.31}$$

For a point on the operating line, we have

$$y_1 = x_1 \tag{2.32}$$

Solving these two equations jointly, we obtain

$$\frac{x_1}{1-x_1} = \alpha \frac{x_2}{1-x_2} \tag{2.33}$$

Similarly, for the second point, we get

$$\frac{y_2}{1-y_2} = \alpha \frac{x_3}{1-x_3}.$$

A joint solution of the equations gives

$$\frac{x_2}{1-x_2} = \alpha \frac{x_3}{1-x_3}$$

However, in accordance with Eq. (2.33), we have

$$\frac{x_2}{1-x_2} = \frac{1}{\alpha} \cdot \frac{x_1}{1-x_1}.$$

Consequently,

$$\frac{1}{\alpha} \cdot \frac{x_1}{1-x_1} = \alpha \frac{x_3}{1-x_3},$$

or

$$\frac{x_1}{1-x_1} = \alpha^2 \frac{x_3}{1-x_3}. \tag{2.34}$$

An examination of Fig. 18 where two theoretical plates are shown ($n = 2$), shows that the power of α is the same as this number. In the general case Eq. (2.34) can be written in the following form:

$$\frac{x_{fn}}{1-x_{fn}} = \alpha^n \frac{x_{in}}{1-x_{in}}. \tag{2.35}$$

Taking logarithms of both sides, we get

$$\log \frac{x_{fn}}{1+x_{fn}} = n \log \alpha + \log \frac{x_{in}}{1-x_{in}}.$$

Consequently, the number of theoretical plates is equal to

$$n = \frac{\log \dfrac{x_{fn}(1-x_{in})}{x_{in}(1-x_{fn})}}{\log \alpha}. \tag{2.36}$$

This equation is known in the distillation theory as the Fenske equation. It is used for determining the efficiency of plate-type fractionating columns. A nearly ideal mixture is separated in the column $R = \infty$ (the column is unproductive) and the concentrations x_{fn} of the upper part and x_{in} of the lower part is varied. The number of theoretical plates obtained with the help of Eq. (2.36) divided by the number of actual plates in the column gives the efficiency of the latter. The Fenske equation is also used for finding the efficiency of packed towers and other fractionating columns.

The Fenske equation is used for analysing the operation of active columns (for determining the efficiency and equivalent heights), and also is for obtaining preliminary estimates of the efficiency of separating a given mixture, i.e. for obtaining the approximate number of plates. For this purpose, it is expedient to reduce Eq. (2.36) to a form more convenient for analysis. Using the notation

$$\log \frac{x_{fn}(1-x_{in})}{x_{in}(1-x_{fn})} = \psi, \tag{2.37}$$

Eq. (2.36) can be reduced to the form

$$n = \frac{\psi}{\log \alpha}. \tag{2.38}$$

We use Eq. (2.37) for calculating the values of ψ for cases that are encountered most frequently in practice:

for $x_{1n} = 10$ percent and $x_{fn} = 90$ percent, $\psi \cong 2$, and the separation is coarse;

for $x_{1n} = 10$ percent and $x_{fn} = 99$ percent, $\psi = 3$, and the separation has a medium level of purity;

for $x_{1n} = 10$ percent and $x_{fn} = 99.9$ percent, $\psi \cong 4$, and the separation is fine.

Accordingly, we obtain the following equations for preliminarily calculating the number of plates necessary for an infinite reflux:

for coarse separation

$$n = 2/\log \alpha, \tag{2.39}$$

for medium separation

$$n = 3/\log \alpha, \tag{2.40}$$

for fine separation

$$n = 4/\log \alpha. \tag{2.41}$$

With the help of Eq. (1.6) we establish a relation between the number of plates necessary for the operation of an "unproductive" column and the boiling point of the components of the mixture:

$$n \cong \frac{\psi}{9}\left(\frac{T_A + T_B}{T_B - T_A}\right). \tag{2.42}$$

Table 3 gives a rough estimate of the number of plates necessary for separating a given mixture with a given relative volatility α and the difference ΔT in the boiling points of the components.

Table 3

Dependence of the Number of Theoretical Plates on Relative Volatility and the Difference in Boiling Points of Components

Relative volatility α	Difference in boiling points ΔT, °C	Number n of theoretical plates required	
		ordinary fractional distillation	fine fractional distillation
3.00	30	5	8
2.00	20	9	13
1.50	10	17	22
1.30	7	25	35
1.25	6	30	42
1.20	5	38	50
1.15	4	50	65
1.12	3	70	80
1.10	2.5	—	100
1.07	2	100	150

Case 2 (the point of intersection of the operating lines lies on the equilibrium curve). In this case, the driving force of the process (concentration difference) will be minimum, the steps in which the concentration varies will be small and their number will be infinite. This is so because an infinitely large number of steps can be inscribed

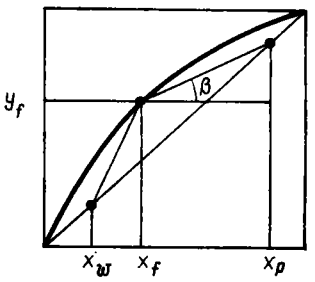

Fig. 19. To the derivation of the minimum reflux ratio.

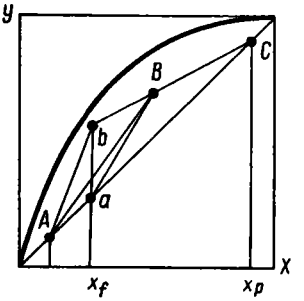

Fig. 20. The effect of the variation of the feed temperature.

in the angle as we approach the point (y_f, x_f) on the curve. This position of the point corresponds to the minimum reflux ratio which can be directly determined graphically (Fig. 19).

The minimum reflux ratio is determined from the slope of the operating line under the condition that the point of intersection of the operating lines lies on the equilibrium curve and its ordinate corresponds to the equilibrium composition y_{fp}. Then we get

$$\tan\beta = A = \frac{R_{\min}}{R_{\min}+1} = \frac{y_p - y_{fp}}{x_p - x_f}. \qquad (2.43)$$

Considering that $y_p = x_p$, we obtain as a result of transformation

$$R_{\min} = \frac{y_p - y_{fp}}{y_{fp} - x_f}. \qquad (2.44)$$

Under actual operating conditions for the fractionating column, the reflux ratio R, which is also called the operating reflux ratio, is set within the limits $R_\infty > R > R_{\min}$.

Thus the point of intersection of the operating lines may be displaced vertically between $y_f = x_f$ $(R = \infty)$ and $y_f = y_{fp}$ $(R = R_{\min})$. However, if the initial mixture is supplied to the column at a temperature other than the boiling point, the point will be displaced along the slope of the straight line described by the equation

$$y = \frac{q}{q-1}x - \frac{x_f}{q-1}, \qquad (2.45)$$

where q is the dimensionless ratio of the heat required to vaporize one mole of the feed to the heat of vapour formation.

If the liquid is supplied to the column at the boiling point $q = 1$ and $q/(q-1) = \infty$, i.e. the straight line becomes vertical (line *ab* in Fig. 20).

Thus, under fixed feeding conditions, the point of intersection of the operating lines (and hence the number of theoretical plates) will be completely determined by the reflux ratio. Conversely, for a fixed reflux ratio, the number of theoretical plates will be completely determined by the feeding conditions. Thus, for example, if feeding is carried out at a temperature below the boiling point of the liquid, the point of intersection of the operating lines will be dis-

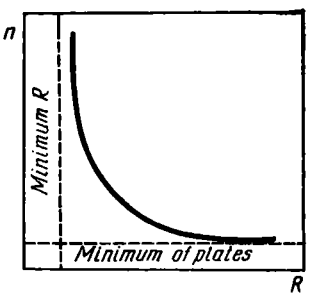

Fig. 21. To the determination of the operating reflux ratio.

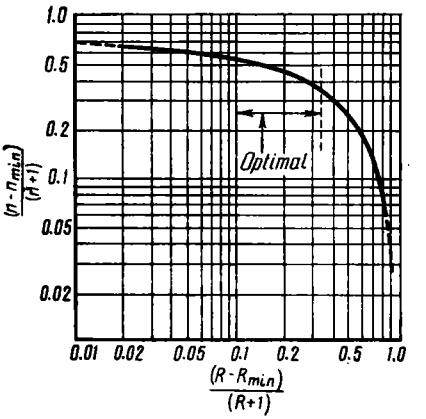

Fig. 22. Determination of the operating reflux ratio and the number of plates according to Gilliland.

placed from point *b* (corresponding to feeding at the boiling point) to point *B* (Fig. 20) and accordingly the operating lines for the upper and lower parts of the column will respectively be *CB* and BA_1 and the required number of plates will decrease.

The operating reflux ratio can be determined by constructing a graph showing variation of the number n of the theoretical plates as a function of the reflux ratio R (Fig. 21), as well as the graph proposed by Gilliland (Fig. 22). With the help of Eq. (2.44) the minimum reflux ratio R_{min} is first calculated and the minimum number of plates n_{min} is determined either by using Eq. (2.36) or graphically (from the y—x plot). After this, the ratio $(R - R_{min})/(R + 1)$ is determined for any value $R > R_{min}$ of the reflux ratio.

For the selected value of the ratio $(R - R_{min})/(R + 1)$, the value of $(n - n_{min})/(n + 1)$ is obtained with the help of the Gilliland plot (Fig. 22). This can be used, in turn, to calculate the required number n of theoretical plates corresponding to the reflux value R.

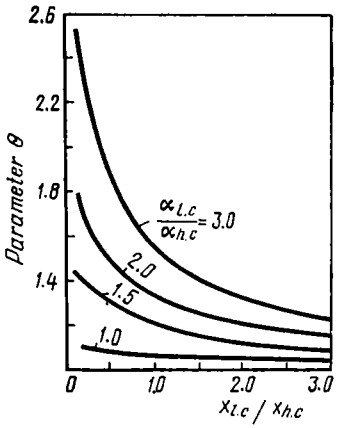

Fig. 23. Determination of the parameter θ in calculating R_{min} with the help of the Underwood method.

An analysis of the operation of active fractionating columns shows that the optimal economical value of $(R - R_{min})/(R + 1)$ lies in the interval 0.1-0.33. Taking 0.23 as the optimal value of this ratio we obtain the optimal reflux ratio, i.e. $R = 1.3 \times R_{min} + 0.3$.

The number of theoretical plates can also be obtained analytically. One of the widely used methods for calculating the minimum reflux ratio for multicomponent systems is based on the assumption that the relative volatility and the flow rate of vapours and liquids are constant over the height of the column. This method is called *Underwood's method.*

The Underwood equations have the following form:

$$\sum_{1}^{K} \frac{\alpha_i x_{i,p}}{\alpha_i - \theta} = R_{min} + 1; \quad \sum_{1}^{K} \frac{\alpha_i x_{i,f}}{\alpha_i - \theta} = 1 - q. \qquad (2.46)$$

The fraction q of the liquid in the feed is

$$q = \frac{b_{d_f} - b_f}{r_f}, \qquad (2.47)$$

where r_f is the specific heat of vaporization of the feed, b_{d_f} is the actual enthalpy of the feed, and b_f is the enthalpy of the feed at the dew point.

When liquid at the boiling point is used for feeding $1 - q = 0$.

If feeding is carried out by the vapour at the saturation temperature (dew point), $1 - q = 1$.

The value of θ lies within the values of α for the key components, and is determined either by trial with the help of Eq. (2.46) or graphically (Fig. 23), for $q = 1$, as a function of the ratio of mole fractions of the light and heavy key components in the feed for different values of their volatility ratio.

The values of the relative volatilities α of the components are taken at the mean temperature of the column $T_{mean} = (T_{upper} + T_{lower})/2$.

If the relative volatility varies with temperature, these quantities are calculated for a roughly estimated temperature at the feeding plate, ascribing the minimum calculated reflux value to this plate. The external reflux can then be obtained from the thermal balance.

2.1.1. Batch Fractionation

Figure 24 shows a batch fractionating column. The entire initial mixture is put into the still of the column, and fractional distillation is carried out in one of the following two ways: either a distillate of constant composition is removed, or the composition of the distillate continuously varies (fractional distillation).

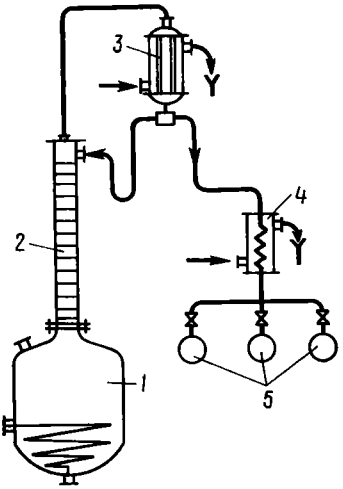

Fig. 24. Schematic diagram of a batch fractionating column:

1—still; *2*—column; *3*—condenser; *4*—cooler; *5*—fraction receivers.

If the distillate of a constant composition is removed, the volatile matter will be exhausted from the still during distillation. At the same time, the constant composition of the distillate must be maintained. This is possible only if the amount of reflux returning to the column continuously increases. Thus, for a given number of plates, calculations for the column must be carried out by using the dependence $R = f(\tau)$, where R is the reflux ratio and τ is the duration of the process in hours.

When distillate of varying concentration is being withdrawn, the quantity of reflux returning to the column may remain constant in the general case. In actual practice, however, the reflux is maintained at a constant level only during the removal of a given fraction (within the given temperature interval). The reflux ratio is usually increased while distilling a narrow fraction (in a narrow temperature range).

Batch fractionation has certain advantages over continuous distillation for separating multicomponent mixtures, since it involves only one apparatus as against a group of apparatus in the latter case. A typical example of batch fractionation is the separation of a mixture of components, say, A, B, C, etc., in the decreasing order of their volatility in the presence of insignificant amounts of light and heavy impurities. The products of separation are the components A, B, C, etc. of a certain purity. The sequence of operations for a set-up used for separating a three-component mixture can be represented by a flow chart with the following stages:

Stage 1 charging	The still containing the heavy remainder from the previous charge is filled with the mixture.
Stage 2 heating	Heat is supplied to the set-up and equilibrium is attained for a complete reflux.

	The more volatile components can be removed in this case if a certain operating pressure is maintained.
Stage 3 preconditioning	The lighter components are rejected until the distillate consists mainly of the component A.
Stage 4 light components	The mixture of the component A and lighter components is extracted at a high reflux ratio until the distillate contains component A with a given purity.
Stage 5 product A	The pure component A is extracted until its quality deteriorates due to contamination by the component B.
Stage 6 extraction of A and B	The mixture of components A and B is extracted at a high reflux ratio until the distillate is rich in component B with a given purity.
Stage 7 product B	The product B is extracted in the same way as described in stage 5.
Stage 8 extraction of B and C	Components B and C are extracted in the same way as in stage 6.
Stage 9 product C	The pure component C is extracted. The residue containing component C and heavier components is left behind until the next distillation. After a few distillations, the waste must be removed.

It follows from the above table that batch fractionation can be represented as the separation of two key components at each stage of the process.

The calculations for the fractional distillation process involve the determination of the amount of fractions being separated for given distillate and residue compositions, the number of plates and the reflux.

Extraction of a distillate of constant composition. Assuming that the liquid charge in the still considerably exceeds the quantity of the liquid in the column, the material balance equation with respect to the volatile component can be written in the following form:

$$G_f x_f = (G_f - G_{ev})\, x + G_{ev} x_p, \tag{2.48}$$

where G_f is the amount of the initial mixture, kg·mole; G_{ev} is the amount of the liquid evaporating at each instant of time, kg·mole; and x_f, x_p represent the concentration of the volatile component in the initial mixture and in the distillate. From Eq. (2.48), we get

$$G_{ev} = G_f \frac{x_f - x}{x_p - x}. \tag{2.49}$$

The extraction rate G_p of the product can be expressed as the derivative

$$G_p = \frac{dG_{ev}}{d\tau}. \tag{2.50}$$

Taking into account Eq. (2.49), Eq. (2.50) can be written in the following form:

$$G_p = \frac{d\left(G_f \frac{x_f - x}{x_p - x}\right)}{d\tau} = -G_f \frac{(x_p - x_f)}{(x_p - x)^2} \frac{dx}{d\tau}, \tag{2.51}$$

whence

$$G_p\, d\tau = -G_f \frac{(x_p - x_f)}{(x_p - x)^2}\, dx. \tag{2.52}$$

On the basis of the material balance, we write

$$G = G_p + G_p R = G_p (R + 1), \tag{2.53}$$

where G is the amount of the liquid evaporating per unit time, or the evaporation rate, kg·mole/hr, and R is the variable reflux ratio in kg·mole/kg·mole.

From Eq. (2.53), we get

$$G_p = \frac{G}{R+1} \tag{2.54}$$

Substituting the value of G_p from this equation into (2.51), we obtain

$$\frac{G}{R+1}\, d\tau = -G_f \frac{(x_p - x_f)}{(x_p - x)^2}\, dx. \tag{2.55}$$

Integrating this equation within the limits of variation of the liquid composition, i.e. between the initial charge composition x_f and the composition x_w of the still bottoms, we get the total distillation time τ (hr):

$$\tau = \int_0^{\tau} d\tau = \int_{x_f}^{x_w} \frac{-G_f (R+1)(x_p - x_f)\, dx}{G (x_p - x)^2}$$

$$= \frac{G_f (x_p - x_f)}{G} \int_{x_w}^{x_f} \frac{(R+1)\, dx}{(x_p - x)^2}, \tag{2.56}$$

or, for any instant of time τ and any composition x of the still liquid, and for the corresponding reflux ratio R, we have

$$\tau = \frac{G_f (x_p - x_f)}{G} \int_{x}^{x_f} \frac{(R+1)\, dx}{(x_p - x)^2}, \tag{2.57}$$

where x is the content of the volatile component in the still liquid for a given reflux ratio.

This equation was derived without taking into account the holding capacity of the column, hence it is valid only when the charge in the still considerably exceeds the liquid contained in the column. Since in actual practice, the charge in the still of industrial batch fractionation columns usually exceeds the quantity of the liquid held in the column, this equation can be used for obtaining rough estimates.

The main stage in calculations with the help of Eq. (2.57) is the determination of the reflux ratio R, which is necessary for maintaining a constant composition of the distillate as the composition of the still mixture changes. In practice, it is not difficult to carry out the calculations for a column by using the "plate to plate" method for a known composition of the vapour leaving the upper plate and a fixed value of the reflux ratio. The calculations are made from top to bottom. However, if the integral in Eq. (2.57) is evaluated numerically, formulas with equidistant nodal points are used as a rule. Hence the platewise calculations for a column must be carried out iteratively, when the appropriate values of the reflux ratio are determined for a fixed value of the concentration. Such an approach is not unique, since for some methods of computing a certain integral there is no need to break the function into equal intervals for the integration variable.

Starting from the quantity of the mixture G_f charged in the still (kg·mole), the composition x_f of the initial mixture (mole fractions), the composition x_p of the distillate (mole fractions), the composition x_w of still bottoms (mole fractions), and the rate of vaporization (or distillation) G (kg·mole/hr), the algorithm for calculating the process of batch fractionation in which a distillate of constant composition is extracted consists of the following stages:

1. The number of plates required for separation in the given interval from x_p to x_w is calculated. The required level of separation can be attained for different combinations of the number of plates and the reflux ratio R. Hence we must determine the optimal combination from the extremum of a certain criterion, for example, the minimum investment and maintenance costs of planning and execution of a process. If a mathematical model is available for fractionation, this problem can be solved by carrying out calculations for the column under different combinations of the parameters mentioned above and the most suitable choice of the variant.

The mathematical description of a column consists of the equations of overall material balance, the equations of componentwise material balance, and the liquid-vapour equilibrium equations. We assume that (a) the flow of the vapour and the liquid is constant over the height of the column; (b) the entire condenser is used; and (c)

the still is equivalent to a theoretical plate in its separation capacity. These assumptions, especially the first one, considerably simplify the problem without any loss of generality. For a fixed number n of the plates and a given efficiency η of a plate, the computational algorithm for a column consists of the following steps if the plates are counted from below:

(a) a certain initial value R of the reflux ratio is specified; (b) the equilibrium concentration of the highly volatile component is calculated from the equation $y_i^* = K_i x_i$ ($i = 1, 2, \ldots, n$), where K_i, the phase equilibrium constant, is a function of the temperature and the composition in the general case; (c) the composition of the vapour leaving the ith plate is calculated with the help of the equations

$$y_i = \begin{cases} y_i^*, & i = 0; \\ (1-\eta_i)\, y_{i-1} + \eta_i y_i^*, & i = 1, 2, \ldots, n; \end{cases}$$

and (d) the concentration of the component of the upper plate is calculated from the material balance equation for any cross section of the column.

The calculations are repeated for all plates of the column in accordance with the steps (b), (c), and (d).

After the composition of the distillate has been determined, the value of the reflux ratio obtained must be compared with the value required by the conditions of the problem. If the difference exceeds the value permitted by the accuracy of calculations, the value of the reflux ratio R should be changed somehow and the calculations must be repeated from step (b) onwards. In order to modify the reflux ratio, we can use any method for refining the roots of an equation in one unknown. In particular, satisfactory results on the convergence of solutions are obtained by using the secant method. Once the reflux ratio has been calculated, this variant must be evaluated and, if necessary, the calculations must be repeated by taking a different number of plates.

2. The value of the integral and the distillation time are calculated for different compositions of the residue in the still. The integral can be calculated with the help of Simpson's formula with a variable integration step. It can be seen from Eq. (2.57) that for each value of x_w we must have a corresponding value of the reflux ratio R. For a given composition of the still residue the reflux ratio can be calculated by the secant method, the domain of the possible solutions being outlined beforehand. For this purpose, it is expedient to calculate the integrals starting from the lowest attainable concentration of the highly volatile component in the still, since the reflux ratio obtained in this case will be the upper limit for the next value of concentration. The algorithm described in the first step can be used for calculating R. The block diagram for calculating the

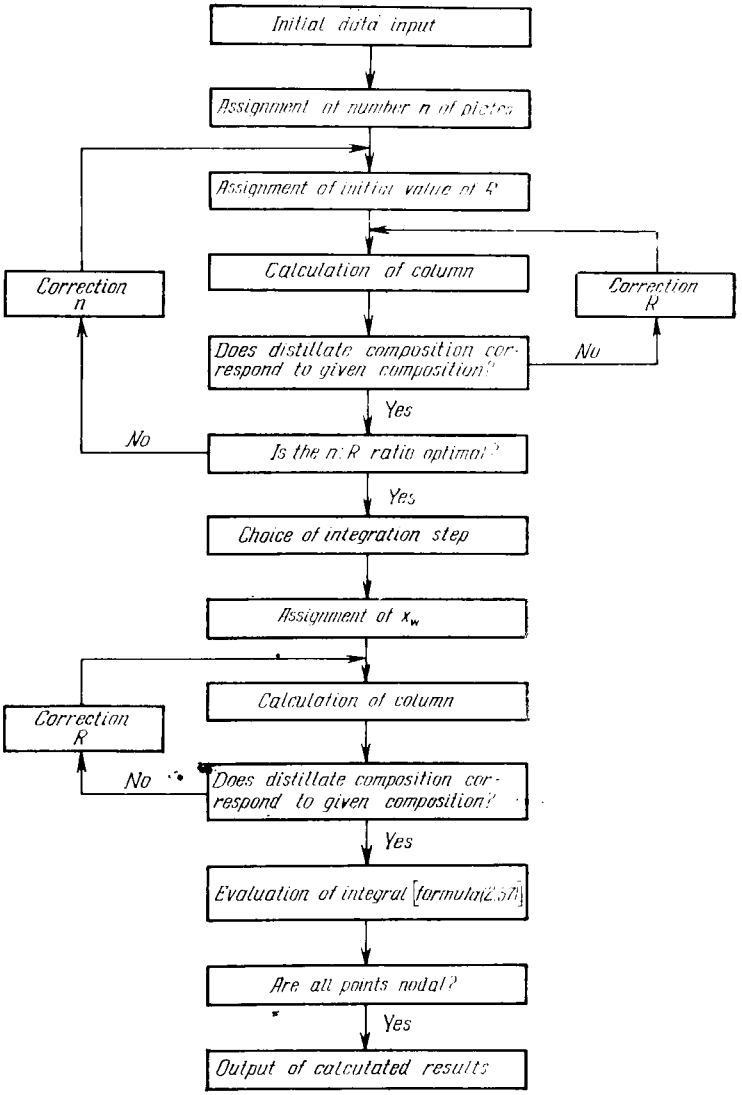

Fig. 25. Block diagram for the calculation of batch fractionation with the removal of constant-composition distillate.

distillation time for separating a distillate of constant composition is shown in Fig. 25.

Separation of distillate of variable composition. The main parameter of the process in this case is the amount of distilled product or the distillation time τ_R, which are calculated from the relations

$$\ln \frac{G_f}{G\tau} = \int_x^{x_f} \frac{dx}{x_p - x}, \tag{2.58}$$

$$\tau_R = \frac{R+1}{G_{ev}}(G_f - G_w) = \frac{R+1}{G_{ev}} G_p. \tag{2.59}$$

Before calculating the amount of the product or the distillation time, it is necessary to calculate the required reflux ratio for given technological parameters and number of plates. As in the case of separation of distillate of constant composition, this problem must be solved as an optimization problem for finding the optimal values of R and n.

The calculation of batch fractionation involving the separation of distillate of variable composition is carried out as follows:

1. The number of plates and the reflux ratio required for separating the distillate in the given composition range are determined. This step is carried out in the same way as for the corresponding process involving the separation of a distillate of constant composition.

2. The composition of the distillate is found with the help of Eq. (2.58) for fixed concentrations of the highly volatile component in the still. Since the slope of the operating line at the initial moment of time is not known, the calculations for the column must be carried out iteratively by a more precise determination of the distillate composition. Thus, for a fixed value of x_w, it is necessary to specify the distillate composition also in each case. The distillate composition is determined more precisely as a result of each iteration.

The algorithm considered earlier by us for modelling can also be used for calculating the composition of the distillate. The only difference is that instead of the reflux ratio in the present case the distillate composition is determined more precisely by iteration. The strategy for refinement remains unaltered in this case.

The integral in Eq. (2.58) can be determined with the help of Simpson's formula. Since the accuracy of integration depends on the number of nodal points, stringent restrictions concerning the speed are imposed on the algorithm for calculating the column parameters.

It is expedient to carry out the calculations starting with the maximum permissible concentration of the distillate. This quantity will serve as the upper limit for subsequent points. The block dia-

gram of the computational algorithm for fractionation involving separation of the distillate with varying composition is shown in Fig. 24. The only difference is that while calculating the integral for the column parameters with the help of Eq. (2.58), the distillate composition (and not the reflux ratio) is refined.

Optimal Strategy for Variation of the Reflux Ratio. In batch fractionation this strategy is defined as the problem of obtaining the required amount of the distillate of a given composition in the minimum possible time under preset initial conditions. Such problems are often referred to as the time optimization problems and can be considered on the basis of Pontryagin's maximal principle.

Suppose that we have a system of differential equations

$$\frac{dx_i}{d\tau} = f_i(x_1, x_2, \ldots, x_n, u_1, u_2, \ldots, u_n) \qquad (2.60)$$

$$i = 1, 2, \ldots, n$$

with given mixed boundary conditions

$$x_i(0) = x_i^0 \text{ and } x_i(T) = x_i^1; \quad i = 1, 2, \ldots, n. \qquad (2.61)$$

Of all the possible operations $u = u(\tau)$, $0 \leqslant \tau \leqslant T$, only those are to be selected which transform the system from state x^0 into state x^1 in the minimum possible time. For this purpose it is expedient to use the maximal principle which consists in the following: let $u(\tau)$, $0 \leqslant \tau \leqslant T$ be a permissible operation which transforms the system from state x^0 into state x^1, and let $x(\tau)$ be the corresponding trajectory such that $x(0) = x^0$ and $x(T) = x^1$. Then the necessary condition for the optimality of $u(\tau)$ and $x(\tau)$ in time is the existence of a non-zero continuous vector function $p(\tau)$ satisfying the following conditions:

(1) For all τ, $0 \leqslant \tau \leqslant T$, the Hamiltonian

$$H(p, x, u) = \sum_{j=1}^{n} p_j f_j(x, u) \qquad (2.62)$$

attains its maximum value at the point $u = u(\tau)$, i.e.

$$H(p(\tau), \quad x(\tau), u(\tau)) = \Omega[p(\tau), x(\tau)], \qquad (2.63)$$

(2) The following inequality is satisfied for a finite instant of time:

$$\Omega[p(\tau), x(\tau)] \gg 0. \qquad (2.64)$$

It can be shown that this condition is satisfied for all $0 \leqslant \tau \leqslant T$.

It should be noted that the following relation is valid for the auxiliary vector function $p = (p_1, p_2, \ldots, p_n)$:

$$\frac{dp_i}{d\tau} = \sum_{j=1}^{n} p_j \frac{\partial f_j}{\partial x_i}; \quad i = 1, 2, \ldots, n. \qquad (2.65)$$

Starting from the material balance equations for a fractionating column, we can write

$$G_w(\tau) + G_p(\tau) = G_f, \tag{2.66}$$

$$G_w(\tau)\, x_w(\tau) + G_p(\tau)\, x_p(\tau) = G_f x_f. \tag{2.67}$$

Assuming that the vapour leaving the upper plate is completely condensed, we can write for the condenser

$$G_u = (R+1)\frac{dG_p}{d\tau}. \tag{2.68}$$

Equations (2.66) and (2.67) contain four variables G_w, x_w, G_p, and x_p, of which two state variables are independent and are chosen arbitrarily. Combining (2.66) and (2.68), we can express one state variable as a function of time, i.e.

$$\frac{dG_w}{d\tau} = -\frac{G_u}{R+1} = -\frac{dG_p}{d\tau}. \tag{2.69}$$

Writing the balance equation for the upper plate of the column in the form

$$G_u y_N - L y_N = \frac{d}{d\tau}(G_p x_p) = -\frac{d}{d\tau}(G_w x_w) \tag{2.70}$$

and combining (2.68), (2.69) and (2.70), we get the following equation for the second state variable:

$$\frac{dx_w}{d\tau} = \frac{y_N - x_w}{G_w} \cdot \frac{G_u}{R+1}. \tag{2.71}$$

Equations (2.69) and (2.71) define two variables of state as functions of time. In order to determine the optimal time, we require that at the end of fractionation, we should obtain a given amount of the distillate of a certain composition at a certain instant of time. This is equivalent to specifying G_f and x_f at the instant T. Thus, the problem can be considered as that of finding a strategy for variation of the reflux so as to bring the system from the state (G_f, x_f) to the state $(G_w^{\text{fin}}, x_w^{\text{fin}})$ in the minimum time. Two admissible strategies of variation of the reflux, which allow such a transition (though not in the minimum time), correspond to the extraction at constant and variable composition respectively.

In order to solve the problem by the method of the maximal principle, we write the auxiliary vector p_i in the form

$$\frac{dp_1}{d\tau} = -p_2 \frac{G_u}{R+1} \frac{y_N - x_w}{G_w^2} \tag{2.72}$$

and

$$\frac{dp_2}{d\tau} = p_2 \frac{G_u}{R+1} \cdot \frac{1}{G_w}\left[\frac{dy_N}{dx_w} - 1\right] \tag{2.73}$$

as well as the Hamiltonian function

$$H(p_1, p_2, G_w, x_w, R) = p_1\left(-\frac{G_u}{R+1}\right) + p_2\left(-\frac{y_N - x_w}{G_w}\cdot\frac{G_u}{R+1}\right). \quad (2.74)$$

To find the optimal strategy of variation of reflux, we must find p_1, p_2, G_w and x_w as functions of time in the interval (0, T), and satisfying the following conditions:

(a) equations (2.69), (2.71), (2.72) and (2.74) are satisfied together with initial and final conditions for the variables of state G_w and x_w;

(b) the reflux ratio at each instant of time must correspond to the maximum value of the Hamiltonian for constant values of p_1, p_2, G_w and x_w;

(c) the maximum value of the Hamiltonian mentioned in (b) must be constant and positive over the entire interval (0, T).

The computation of the minimum flow time for a process begins with the specification of the initial values of the auxiliary variables p_1 and p_2 at the instant $\tau = 0$, and integration of Eqs. (2.69), (2.71), (2.72) and (2.73), ensuring that the condition (b) is satisfied at every step. The Hamiltonian is a homogeneous function of p_1 and p_2, so that it is necessary to specify just their ratio (p_1 is assumed to be equal to unity). Since $dx_w/d\tau$ is always negative, the concentration x_w must finally drop to the value x_w^{fin} at a certain instant T of time. Since G_w will not be equal to the final value G_w^{fin}, the initial ratio of the auxiliary variables must be refined again until these values coincide to the required degree of accuracy. In this case the optimal flow time of the process of batch rectification is equal to the value corresponding to such an approximation for $p_2(0)$ that $G_w = G_w^{\text{fin}}$, and $x_w = x_w^{\text{fin}}$.

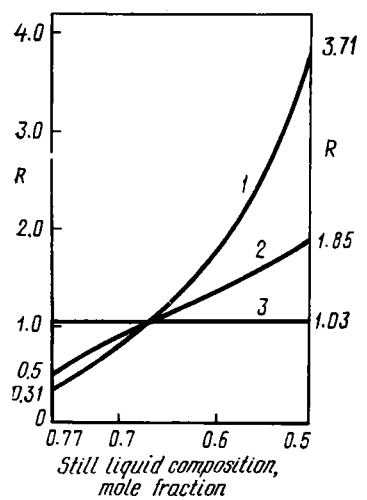

Fig. 26. The reflux ratio as a function of the mixture composition in the still for three operating regimes:

1—constant-composition distillate; *2*—optimal change in the reflux ratio; *3*—varying-composition distillate.

The program for computing the minimum time for a process basically contains three algorithms. The first algorithm is used for integrating the system of differential equations. The second one is required for calculating the distillate composition for given values of the reflux ratio and the

still mixture composition. The third algorithm is intended for maximizing the Hamiltonian.

The results of computations of the dependence of the reflux ratio on the composition of the still mixture, carried out on a digital computer for different regimes of distillate extraction, are shown in Fig. 26.

2.1.2. Determination of the Number of Theoretical Plates for Low and High Concentrations of the Volatile Component

For ideal binary systems we have the following equation:

$$y = \frac{\alpha x}{1+(\alpha-1)x}. \tag{2.75}$$

For small concentrations, when x tends to zero, this equation assumes the form

$$y = \alpha x. \tag{2.76}$$

In logarithmic coordinates, Eq. (2.76) is the equation of a straight line with slope α. Figure 27 depicts this equation in logarithmic coordinates. For small values of x, the equilibrium lines become straight lines and for different values of α, these straight lines are parallel and have a slope equal to unity.

For large concentrations, i.e. for $x \simeq 1$, the following relation holds (see Eq. (1.14)):

$$y = \alpha x \frac{1-y}{1-x}. \tag{2.77}$$

Comparing Eqs. (2.75) and (2.77), we get

$$(1-y) = \frac{1-x}{1+(\alpha-1)x}. \tag{2.78}$$

Since x tends to unity, the denominator of the right-hand side of this equation approaches the value α and the equation is reduced to the form

$$(1-y) = \frac{1-x}{\alpha}. \tag{2.79}$$

This equation can also be represented in the following form:

$$y = \frac{1}{\alpha}(x-1)+1. \tag{2.80}$$

Figure 28 depicts this equation in logarithmic coordinates.

Approximate Analytical Method. This method is based on the ratios of the slopes of the equilibrium curves and the operating lines.

For very high concentrations of the volatile fragment, the slope of the equilibrium curve, in accordance with Eq. (2.80), is equal to

$1/\alpha$. The slope of the upper operating line k is $R/(R+1)$. Then, starting from the top plate (with the distillate concentration x_p), we can write down a system of equations:

$$\Delta x_1 = x_p - x_1 = (1-x_p)(\alpha-1),$$
$$\Delta x_2 = x_1 - x_2 = k\alpha(x_p - x_1),$$
$$\Delta x_3 = x_2 - x_3 = k\alpha(x_1 - x_2) = k^2\alpha^2(x_p - 1),$$
$$\sum_1^n \Delta x = x_p - x_1 + k\alpha(x_p - x_1) + k^2\alpha^2(x_p - x_1) + \ldots$$
$$+ k^{n-1}\alpha^{n-1}(x_p - x_1) = x_p - x_A = \frac{k^n\alpha^n - 1}{k\alpha - 1}(x_p - x_1)$$
$$= (1-x_p)(\alpha-1)\frac{k^n\alpha^n - 1}{k\alpha - 1}. \qquad (2.81)$$

Taking logarithms and solving this equation, we get the number of theoretical plates

$$n = \frac{1}{\log k\alpha}\log\left[\frac{(x_p - x_a)(k\alpha - 1)}{(1-x_p)(\alpha-1)} + 1\right], \qquad (2.82)$$

where x_a is the composition of the liquid flowing from the plate for which the equilibrium composition varies linearly. If vapour com-

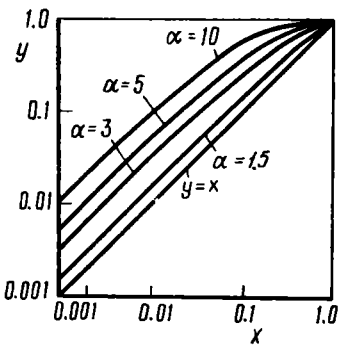

Fig. 27. Representation of equilibrium lines for $x \to 0$.

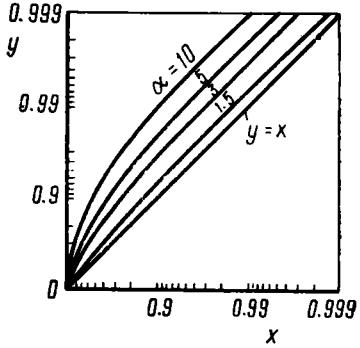

Fig. 28. Representation of equilibrium lines for $x \to 1$.

position is used instead of the liquid composition, the last equation is rewritten in the form

$$n = \frac{1}{\log k\alpha}\log\left[\frac{(y_p - y_a)(k\alpha - 1)}{k(1-y_p)(\alpha-1)} + 1\right]. \qquad (2.83)$$

Similarly, for very low concentrations of the volatile component in the still liquid for $k' = (R+F)/(R+1)$ and the composition x_{ak}

of the liquid in the lower part of the column, where the equilibrium composition varies linearly, we get

$$n' = \frac{1}{\log\left(\frac{\alpha}{k'}\right)} \log\left[\frac{k'(x_{a_k} - x_w)\left(\frac{\alpha}{k'} - 1\right)}{x_w(\alpha - 1)} + 1\right], \quad (2.84)$$

or

$$n' = \frac{1}{\log\left(\frac{\alpha}{k'}\right)} \log\left[\frac{(y_{a_k} - y_w)\left(\frac{\alpha}{k'} - 1\right)}{y_w(\alpha - 1)} + 1\right]. \quad (2.85)$$

Graphic Method. The number n of theoretical plates required for separating mixtures with very high or very low concentrations of the volatile component is determined graphically by plotting y-x diagram in logarithmic coordinates.

For very high concentrations, i.e. for values of x close to unity, the equilibrium curves plotted in logarithmic coordinates on the y-x diagram are straight lines with a slope equal to unity.

In the absence of a sufficient amount of experimental results, the equilibrium curve in logarithmic coordinates can be plotted by using only one experimental point through which a straight line with a slope equal to unity, i.e. at an angle of 45°, is drawn. If the concentration of the volatile component is less than 0.01 or greater than 0.95 mole fraction, the slope of the equilibrium line will be equal to unity.

For very low or very high concentrations, the number of theoretical plates is determined from the y-x diagram in logarithmic coordinates by proceeding in the following order:

1. Segments of the equilibrium curve for very high and very low concentrations are plotted by using Eqs. (2.79) and (2.76). Thus, for example, for a given overhead product composition equal to 99.95 mole percent, we plot the segment of the equilibrium curve between $x = 0.990$ and $x = 0.999$. From Eq. (2.79), we obtain $y = 0.998333$ and $y = 0.999833$ respectively (Fig. 29).

In accordance with Eq. (2.76), variation of x between the values $x = 0.010$ and $x = 0.0001$ for a given composition of the bottom product equal to 0.05 mole percent, we obtain $y = 0.60$ and $y = 0.0006$ respectively. The graph shown in Fig. 30 is plotted on the basis of these values.

2. The operating line for the top of the column is constructed on the basis of the equation

$$y = Ax + B$$

for given values of $A = R/(R + 1)$, $B = x_p/(R+1)$, and assuming different values for x, say, between 0.9995 and 0.9000, we obtain the corresponding values of y which are graphically plotted in Fig. 29.

The operating lines for the upper part of the column can be constructed by connecting the y-ordinate in the ordinary y-x diagram for

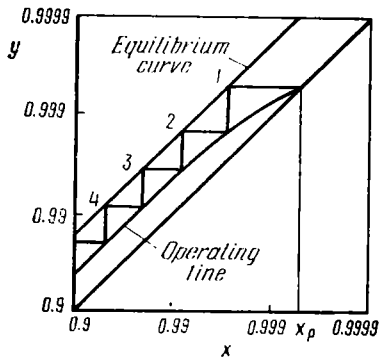

Fig. 29. To the determination of the number of theoretical plates for $x \to 1$.

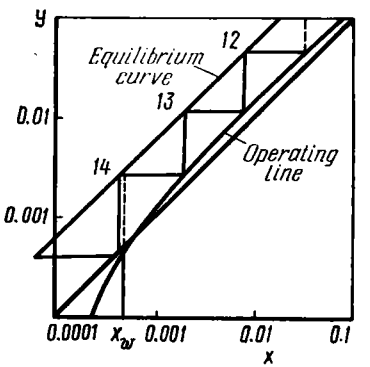

Fig. 30. To the determination of the number of theoretical plates for $x \to 0$.

the point of intersection of the upper and lower operating lines of the process, with the point $x = y = x_p$.

The operating line for the bottom part of the column is constructed with the help of Eq. (2.27)

$$y = A_1 x - B_1$$

for given values of $A_1 = (R + F)/(R+1)$ and $B_1 = Wx_w/(R + 1)$ and by assuming different values for x, say, between 0.0005 and 0.01. The corresponding values of y obtained in this way are plotted in Fig. 30.

3. The number of theoretical plates required for separating within a given range is obtained in a number of stages, beginning from the given value x_p of the distillate from the high-concentration diagram (see Fig. 29), followed by the mean concentration values from the ordinary y-x diagram, and finally, for low concentrations from the diagram shown in Fig. 30, until the given concentration x_w of the still liquid is attained.

2.1.3. Separation Processes in Multicomponent Systems

The presence of more than two components in a mixture considerably affects the calculations for the processes of separation in such systems. For binary systems, it is sufficient to specify, besides the pressure at which the process takes place, the concentration of the

volatile component in one of the phases, so that the state of an equilibrium system can be determined unambiguously. In a multicomponent system, on the other hand, it is necessary to fix $(k-1)$ other parameters in addition to the constant external pressure. Hence, the relation between the concentrations of a given component in liquid and vapour phases depends, besides pressure, on the concentrations of the other components in the liquid and vapour phases.

Unlike binary systems, when a multicomponent mixture is being separated, not all the components of the initial mixture are present in the top and bottom products. The lighter components are concentrated in the distillate, while the heavier components are left in the still bottoms. Only the components with intermediate volatility are distributed in a certain proportion between the two end products. Meanwhile, all the components of the initial mixture are present on the feed plate. Here, it becomes necessary to correlate the calculations for the distribution of concentrations in the top and bottom parts of the column with the position of the feed plate.

While considering the distillation of multicomponent systems, we introduce the arbitrary concept of key components which determine the evolution of the separation process. Conventionally, the key components define the boundary between two parts into which the mixture can be divided: all components of the initial mixture, which are more volatile than the light key component, appear only in the distillate, while all components which are less volatile than the heavy key component are left behind in the still liquid. On the scale of volatility, the light and heavy key components need not necessarily be adjacent to each other; other components of intermediate volatilities, distributed in different ways between the still bottoms and the distillate, may appear between these two. Thus, for example, when a multicomponent system of hydrocarbons (from methane to heptane) is being separated, and propane and *n*-butane are respectively chosen as the light and heavy key components, the mixture may also contain isobutane whose volatility lies between the volatilities of the key components. This component is combined with the key components nearest to it in volatility (*n*-butane in the present case). The composition of the heavy key component is determined by the difference between unity and the sum of the compositions of the light key component and other light components.

The minimum reflux in separating columns for two-component systems corresponds to the minimum driving force of the process or, accordingly, to the minimum change in the concentrations. *The region of minimum change in the concentrations or the region of conventionally constant concentrations* lies in the vicinity of the feed plate. Only one such region exists for a binary system. Two regions of constant concentrations exist for the separation of a multicomponent (containing more than three components) system.

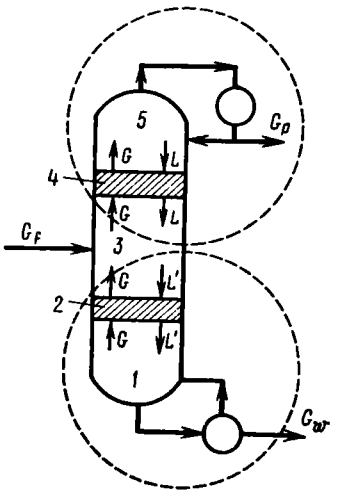

Fig. 31. Zones appearing in a column during the separation of multicomponent mixtures:

1—still zone; *2*—zone of constant concentration; *3*—intermediate zone; *4*—zone of constant concentration; *5*—zone of distillate; G is the vapour flow rate; L, L' are the liquid flow rates; G_f, G_D, and G_W are the flow rates of the initial mixture, distillate, and still liquid.

If a small number of plates are arranged above the feed plate, the concentration of the components whose volatility is less than that of the heavy key component is sharply reduced, and the upper constant concentration region is located at a higher position (Fig. 31). A small number of plates arranged below the feed plate drastically reduces the concentration of the components whose volatility exceeds that of the light key component, and the second constant concentration region is located at a lower level. Thus, for a multicomponent system with minimum reflux, the column is divided into five regions (Fig. 31):

1. The region adjoining the still. This region contains the heavy key component, whose concentration in the still liquid is given, and all less volatile components. The ratio of the concentration x_{lc} to the concentration x_{hc} and the concentrations of other less volatile fragments increases in the upward direction.

2. The region of constant concentration, where the concentrations x_{lc} and of less volatile components are constant.

3. The intermediate region, where the mixture is fed into the column and where the concentration of components less volatile than x_{hc} decreases to insignificant values, while the concentration of components more volatile than x_{lc} increases.

4. The second region of constant concentration, where the concentrations x_{hc} of the heavy component and of more volatile components are constant, is located above the third region.

5. The uppermost region, where the ratio of the concentration x_{hc} to the concentration of more volatile components decreases upward until the given composition of the distillate is attained.

If the mixture to be separated does not contain any components whose volatility is higher than the volatility of x_{lc}, all the components of the mixture will be present in the still liquid, and the lower region of constant concentration (region 2) will be adjacent to the feed plate. If components heavier than x_{hc} are absent, all the components will be present in the distillate, and the upper region of con-

stant concentration (region 4) will be adjacent to the feed plate.

The separation of a binary mixture under minimum reflux is a limiting case in which both the regions of constant concentration are adjacent to the feed plate.

A typical curve describing the distribution of components between plates during the separation of multicomponent systems is shown in Fig. 32. Thus, the separation of propane (C_3) and lighter components (C_2) from butane (C_4) and heavier components (C_5, C_6) is shown in Fig. 32, the top product being removed in the gaseous form. The concentration of components lighter than propane falls very rapidly below the feed plate, while the concentration of components heavier than butane falls rapidly above the feed plate. Consequently, the concentration of components lighter than propane will be insignificant in the bottom product, while in the top product the concentration of components heavier than butane will be negligible.

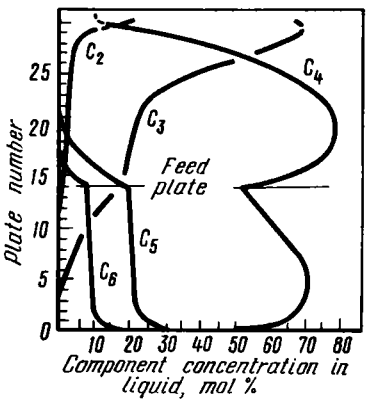

Fig. 32. Distribution of components over the plates during the separation of a multicomponent system.

Calculations are usually carried out from the top and bottom ends of the column toward the feed plate. If quite stringent requirements are imposed on the composition of the products, the compositions obtained at the feed plate from upward and downward calculations must be correlated. In order to obtain a more rapid convergence between the actual and calculated compositions, it is necessary to exactly specify the concentration of components which can be neglected in the top and bottom products before plate-to-plate calculations are started. For example, the concentration of any heavy component is calculated at some stage of fractionation in approximate proportion to the concentration assumed for this component in the top product. Thus, if we correct the concentration of a heavy component whose concentration in the top product is 10^{-6} mole fraction while the value 10^{-5} mole fraction was assumed in the calculations, all the calculated concentrations of this component in the upper part of the column must be multiplied by a factor of 10. A similar method must be applied for the stripping column also. Consequently, even slight errors in the concentrations of "negligible" components in the product may result in large deviations in the values of the compositions calculated near the feed plate where the actual concentrations of all the components may be substantial (see Fig. 31). Unfor-

tunately, there is no method which would allow us to predict exactly the distribution of the non-key components in the top and bottom products of the column in the general case. Hence the distribution assumed at the beginning of calculations is attained only after applying iterative procedures for "plate-to-plate" calculations.

In order to design fractionating columns for separating multicomponent mixtures, it is necessary to determine six design variables, viz. the number of plates, the feed plate number, reflux ratio, the distillate separation fraction, the fraction of the vapour flux in the feed, and the column pressure. These factors ensure that products of given quality are separated for the minimum value of the efficiency function.

The reflux ratio and the total number of plates are the two design parameters that are most difficult to determine.

At present, calculations for the separation processes for multicomponent mixtures are carried out with the help of computers by using the mathematical modelling method (see Chap. 10).

2.2. Extraction Processes

2.2.1. Extraction Through Single-Stage Contact

The process of extraction by a single-stage contact is shown in Fig. 33. If the liquids are immiscible, integration of the material balance equation (2.1) is carried out within the limits

$$-L\int_{x_0}^{x_1} dx = G\int_{0}^{y_1} dy,$$

whence

$$-L(x_1 - x_0) = Gy_1,$$

or

$$\frac{y_1}{x_1 - x_0} = -\frac{L}{G}, \tag{2.86}$$

where x_0 is the initial concentration in A of the component C being extracted; x_1 is the final concentration of C in A; and y_1 is the final concentration of the component in the solvent.

It follows from Eq. (2.86) that in y-x coordinates, the operating line is a straight line with a negative slope (Fig. 34*a*). If the equilibrium line has a slope m, i.e. if the linear distribution law holds, a joint solution of two equations (the equilibrium equation and the operating line equation) leads to the relation

$$Lx_0 = Lx_1 + mGx_1, \tag{2.87}$$

or

$$x_1 = \frac{L}{L + mG}\, x_0. \tag{2.88}$$

Equation (2.88) permits a direct calculation of the liquid composition after extraction (refined product composition).

The static parameters of single-stage extraction can be analyzed most comprehensively by using the ternary diagram for partially miscible or immiscible liquids. Figure 34*b* gives a graphic interpretation of the process provided that component B serves as the solvent, while the initial mixture (point *F*) contains component C dissolved in A. For low concentrations, components A and B are mutually soluble. Point *M* represents the composition obtained as a result of mixing solvent B with the initial mixture F (*BM* : *FB*) and gives the extract (point *E*) and the raffinate *R* (*MR* : *EM*). Lines *FB* and *RE* are the operating and equilibrium lines respectively for the

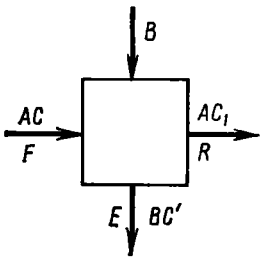

Fig. 33. Schematic diagram of a single-stage extraction:

A—liquid in which the substance being extracted is dissolved; *B*—solvent; *C*—the substance being extracted; *E*—extract, *R*—raffinate; *F*—initial mixture.

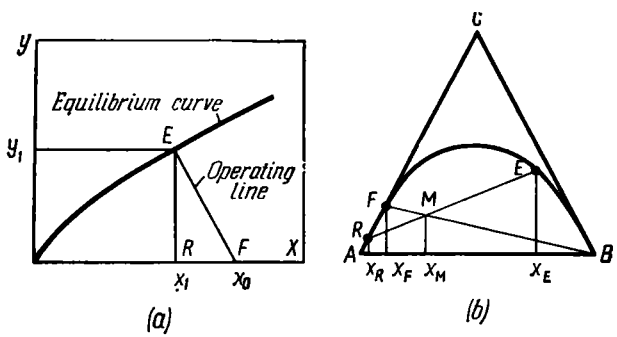

Fig. 34. Single-stage extraction:

a—position of the operating curve; *b*—calculation with the help of triangular diagram.

process. The quantity of the solvent necessary for extraction is determined by the corresponding position of point *M* on the straight line *FB* which does not extend beyond the boundary curve where the two-phase system is transformed into a single-phase system. Two layers are formed as a result of a single contact: the extract layer (on the branch of the boundary curve, lying on the side of solvent B), and the raffinate layer containing smaller quantity of the component C than the initial mixture F, and lying on the left branch of the boundary curve. If the raffinate is extracted and treated again with fresh solvent, the content of C in the raffinate will be further reduced. Thus

a multistage system will be realized, leading to a practically complete extraction of product C.

The amount of solvent in the extract and raffinate layers can be determined from the triangular diagram by using the ratio of the corresponding segments, or from the material balance of the component being extracted.

Considering the material balance shown in Fig. 34*b*, we arrive at the following relations:

$$F + B = M = R + E. \tag{2.89}$$

If x_F and x_M represent the concentration of the component C being extracted in the initial mixture and at the point M respectively, we obtain, in accordance with the material balance, the following relation:

$$Fx_F = Mx_M, \tag{2.90}$$

whence

$$x_M = \frac{Fx_F}{M} = \frac{Fx_F}{F+B}, \tag{2.91}$$

while the quantity of the solvent being consumed will be determined from the relation

$$B = \frac{F(x_F - x_M)}{x_M}. \tag{2.92}$$

If y denotes the content of the component being extracted in the extract, and x denotes the corresponding value in the raffinate, we can write

$$Ey + Rx = Fx_F, \tag{2.93}$$

whence we can obtain the quantity of the extract by taking into account Eq. (2.92):

$$E = \frac{Fx_F - (F+B)x}{y-x}. \tag{2.94}$$

The corresponding value for the raffinate is given by

$$R = F + B - E. \tag{2.95}$$

2.2.2. Multiple Contact Involving the Introduction of Fresh Solvent at Each Stage

The multistage process involving the introduction of fresh solvent at each stage is schematically shown in Fig. 35. Assuming that the amount G of the solvent introduced at each stage is constant and also assuming that the system obeys a linear distribution law, we ob-

tain on the basis of Eq. (2.88) the following equation for one stage:

$$x_1 = \frac{L}{L+mG}\, x_0.$$

Similarly, as the concentration varies from x_1 to x_2, we get for the second stage

$$x_2 = \frac{L}{L+mG}\, x_1 = \left(\frac{L}{L+mG}\right)^2 x_0,$$

and for any nth stage, we get

$$x_n = \left(\frac{L}{L+mG}\right)^n x_0. \tag{2.96}$$

Taking the logarithm of Eq. (2.96), we obtain the number n of

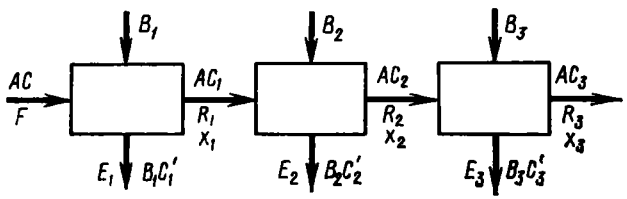

Fig. 35. Schematic diagram of a multistage contact with the feed of fresh solvent into each stage:

A—liquid in which the substance being extracted is dissolved; *B*—solvent; *C*—the substance being extracted; *E*—extract; *R*—raffinate; *F*—initial mixture.

contact theoretical stages required to change the concentration in the raffinate from x_0 to x_n:

$$n = \frac{\log\left(\frac{x_n}{x_0}\right)}{\log\left(\frac{L}{1+mG}\right)}. \tag{2.97}$$

This equation is graphically depicted in Fig. 36*a*.

Figure 36*b* shows graphically the process of extraction in a triangular diagram where fresh solvent is introduced at each stage (three stages). It can be seen from the figure that an insignificant concentration of the extractable component C is left in the raffinate R_3 at the end of a three-stage process. The highest degree of extraction is attained at the first stage, and the separation at subsequent stages is considerably reduced. Extraction at each stage can be carried out by using different amounts of the solvent. If the number of stages is large, we obtain practically pure component A and thus the three-component mixture ABC is separated into the component A and the mixture BC.

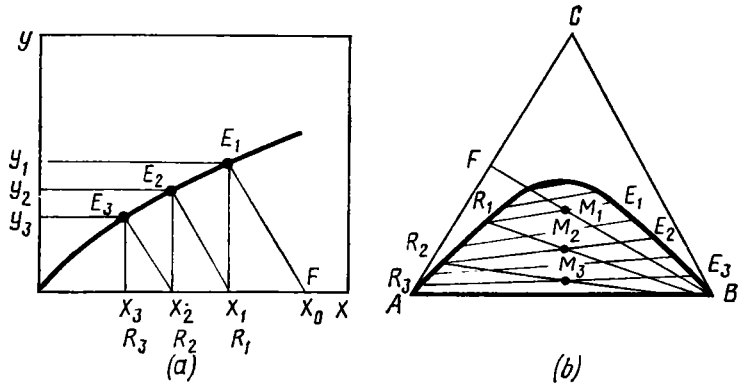

Fig. 36. Calculation of extraction for a multistage contact with fresh solvent fed into each stage:

a—calculation according to the y vs. x diagram; *b*—calculation with the help of triangular diagram.

A similar construction in the ternary diagram is valid for a system with any mutual solubility of liquids. Consequently, this is the most general method for calculations of an extraction process.

2.2.3. Countercurrent Extraction

Immiscible Liquids. The process of countercurrent extraction is schematically shown in Fig. 37*a*. The general differential equa-

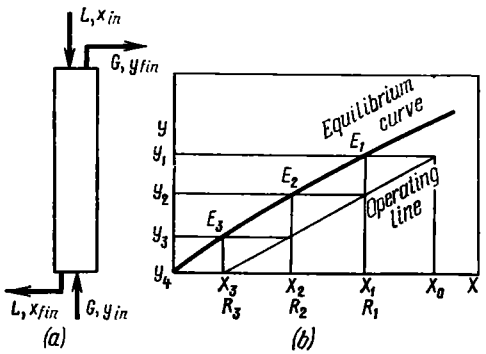

Fig. 37. Schematic diagram of countercurrent extraction (*a*) and determination of the number of contacts in countercurrent extraction (*b*).

tion (2.1) for material balance is applicable to immiscible liquids:

$$-L\,dx = +G\,dy.$$

The material balance equation can be obtained in the final form by substituting the integration limits corresponding to the countercurrent extraction:

$$-L\int_{x_{1n}}^{x_{fin}} dx = G\int_{y_{1n}}^{y_{fin}} dy,$$

whence

$$L(x_{1n}-x_{fin}) = G(y_{fin}-y_{1n}),$$

$$L/G = \frac{y_{fin}-y_{1n}}{x_{1n}-x_{fin}}. \qquad (2.98)$$

This equation is similar to the equation for the operating line of an absorption process. In rectangular coordinates, it represents a straight line passing through two points and having a slope equal

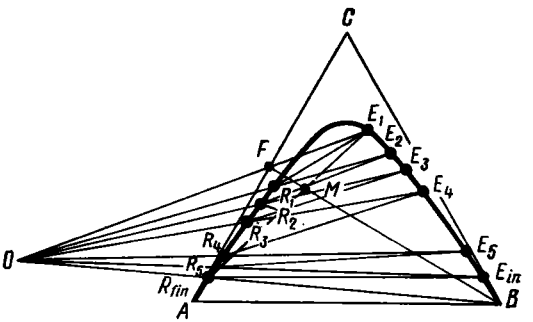

Fig. 38. Determination of the number of contacts in countercurrent extraction with the help of triangular diagram.

to L/G (Fig. 37*b*). In accordance with Eq. (2.98), the composition of the extract leaving any nth stage is a linear function of the composition of the raffinate flowing from the same stage. In other words, the change in concentration of each phase on each stage is linear, as represented by the corresponding segments of straight lines connecting the operating line with the equilibrium curve (contact stages).

The static parameters of the extraction process can be determined directly from the triangular diagram. For a given composition of the initial mixture (point F in Fig. 38), and a given composition of the final raffinate (point R_{fin}), the amount of the solvent consumed is determined by the position of the point M. Extending the straight line $R_{fin}M$ until it intersects the right branch of the boundary curve, we obtain the final composition of the extract (point E_1)*. Straight

* The construction can be carried out without finding the point M. For this purpose, we must know the composition E_1 of the extract.

lines E_1F and BR_{fin}, which limit the extraction process under given conditions, intersect outside the triangular diagram at a point O, called the pole of the diagram. Point E_1 also lies on the conjugate equilibrium line and has a corresponding equilibrium composition R_1. Connecting R_1 with the pole O of the diagram and extending the straight line until it intersects the right branch of the boundary curve, we obtain the composition E_2 of the extract after second theoretical stage of contact. The equilibrium composition of the raffinate corresponding to this composition of the extract is R_2.

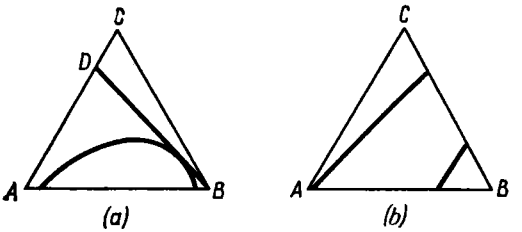

Fig. 39. Diagrams for systems separated with a reflux.

Joining point R_2 with the pole O and extending the straight line until it meets the right branch, we obtain point E_3 (third theoretical contact stage), to which corresponds the equilibrium composition R_3 of the raffinate. Connecting point R_3 with the pole O and extending the straight line until it intersects the boundary curve, we get the composition E_4 of the extract after the fourth contact stage. Point E_4 must lie on the equilibrium conjugate line corresponding to the composition R_4 of the raffinate. Similarly, we obtain points E_5 and R_5. Joining point R_5 with the pole at the intersection of the boundary curve, we obtain the composition E_{fin} to which corresponds the given final composition R_{fin} of the raffinate. If no such coincidence is observed, the calculation must be repeated for another given composition of the raffinate layer or, in other words, we must specify other values of R_{fin}.

If the lines originating from the pole O coincide with the equilibrium conjugate lines, an infinite number of contact stages will be required. Since the line $R_{fin}B$ does not coincide with the equilibrium conjugate line, the limiting position of the pole O can be determined from the point which is the most distant from the triangle and is the point of intersection of the equilibrium conjugate line with the extension of $R_{fin}B$. Points of intersection lying in the vicinity of the triangle correspond to the condition of infinite number of stages. If point O lies beyond the limiting position, a large amount of solvent will be required.

The physical and chemical properties of the systems under consideration determine the choice of the method of their separation. Thus, for instance, it follows from Fig. 39*a* that for the system represented in the diagram, it is possible to obtain only a raffinate layer of sufficiently high degree of purity (the straight line *DB* characterizes the maximum degree of purification). The second system represented in Fig. 39*b* ensures the production of purer raffinate and extract. In this case, it is expedient to introduce reflux for separating the mixture. The reflux can be introduced at both ends of the column, although the raffinate form is rarely used in practice.

2.2.4. Extraction with Two Solvents

When two solvents are used for extraction, the initial mixture containing components A and D is fed at about mid-height of the column in which the two solvents C (light) and B (heavy) flow in countercurrent. The distribution of components A and D between solvents B and C depends on the selective solubility of the components. If the activity coefficient of component A in solvent B is less than in solvent C, solvent B will have a greater affinity toward component A. Thus we obtain the following distribution between phases:

$$\frac{x_{A\text{-}B}}{x_{A\text{-}C}} = \frac{\gamma_{A\text{-}C}}{\gamma_{A\text{-}B}}, \qquad (2.99)$$

where $x_{A\text{-}B}$ is the concentration of component A in solvent B; $x_{A\text{-}C}$ is the concentration of component A in solvent C; $\gamma_{A\text{-}C}$ is the activity coefficient of component A in solvent C; and $\gamma_{A\text{-}B}$ is the activity coefficient of component A in solvent B. Similarly, we obtain the following relation for the distribution of component D:

$$\frac{x_{D\text{-}B}}{x_{D\text{-}C}} = \frac{\gamma_{D\text{-}C}}{\gamma_{D\text{-}B}}, \qquad (2.100)$$

where $x_{D\text{-}B}$ is the concentration of component D in solvent B; $x_{D\text{-}C}$ is the concentration of component D in solvent C; $\gamma_{D\text{-}B}$ is the activity coefficient of component D in solvent B; and $\gamma_{D\text{-}C}$ is the activity coefficient of component D in solvent C.

Consequently, if component A is predominantly soluble in solvent B, solvent C would be preferable for extracting D, i.e. the activity coefficient $\gamma_{D\text{-}B}$ must be higher than the activity coefficient $\gamma_{D\text{-}C}$ to the maximum possible extent. As mentioned earlier, the ratio of these coefficients is called the selectivity coefficient:

$$\beta = \frac{\gamma_{A\text{-}C}/\gamma_{A\text{-}B}}{\gamma_{D\text{-}C}/\gamma_{D\text{-}B}} = \frac{x_{A\text{-}B}/x_{A\text{-}C}}{x_{D\text{-}B}/x_{D\text{-}C}}, \qquad (2.101)$$

or

$$\beta = \frac{\gamma_{A\text{-}C}/\gamma_{D\text{-}C}}{\gamma_{A\text{-}B}/\gamma_{D\text{-}B}} = \frac{x_{A\text{-}B}/x_{D\text{-}B}}{x_{A\text{-}C}/x_{D\text{-}C}}. \qquad (2.102)$$

If substances A and D do not interact and hence their distribution in the solvents remains unchanged, and also, if the solvents are immiscible or their mutual solubility does not change due to the presence of the substances being treated, the number of theoretical stages is usually determined graphically. If these conditions are not satisfied, the calculations are carried out on a computer with the help of mathematical modelling.

2.3. Cyclic Mass-Transfer Processes

At the present time, the intensification of the mass-transfer processes is achieved by ensuring an intensive renewal of the surface of contact between phases, thus increasing the driving force of the process. In particular, this is attained by shifting the load alternately, from vapour (gas) to liquid and vice versa.

The operating cycle of a column working in the cyclic regime consists of two parts: the vapour feed period during which the vapour passes upwards through the column while the liquid remains at each plate, and the liquid feed period during which the vapour is not fed, and the reflux and the feed are introduced into the column while the liquid from each plate flows to the lower plate. The efficiency of plate columns in cyclic regime is considerably higher than for ordinary stationary columns.

The following assumptions are made while deriving equations for calculating ideal rectifying columns* operating in the cyclic regime: (1) the mass of the vapour in the column is small in comparison with the quantity of the liquid; (2) the flow rate of the vapour during the vapour period is constant; (3) the quantity of the liquid in the rectifying and stripping sections of the column is constant and equal; (4) a binary mixture is separated; (5) equilibrium is attained at the plates; (6) the equilibrium dependence is linear; and (7) during the liquid period, liquid flows from plate to plate in the displacement regime.

The first five of these assumptions are made for the sake of simplicity. The sixth condition is usually not fulfilled during rectification, although the entire equilibrium curve can be replaced by a few straight lines.

Let us consider the cyclic column shown in Fig. 40. Vapour is introduced into this column during the vapour period with an instantaneous rate G_i. During the liquid period, a fraction ε of the liquid

* See Rivas, O. R., An Analytical Solution of Cyclic Mass-Transfer Operations. *Ind. Eng. Chem. Process Des. Dev.*, 16, 3 (1977).

retained on plate φ flows down to the next plate where it mixes with the remaining fraction $(1-\varepsilon)$ of the liquid on this plate. The average flow rates L and G of liquid and vapour during one cycle are determined from the equations

$$L = \frac{\varphi\varepsilon}{t_c}, \qquad (2.103)$$

$$G = G_i\left(\frac{t_v}{t_c}\right), \qquad (2.104)$$

where t_c and t_v represent the total time of a cycle and the duration of the vapour period respectively, s.

During the vapour period, the liquid does not flow and the material balance equation for the part isolated in Fig. 40 has the form

$$G_i(y_0 - y_n) = \varphi\frac{dx_1}{dt} + \varphi\frac{dx_2}{dt} + \ldots + \varphi\frac{dx_n}{dt}, \qquad (2.105)$$

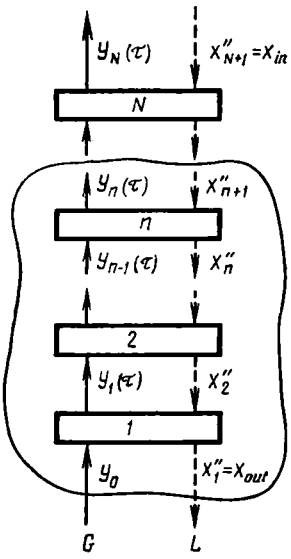

Fig. 40. Schematic diagram of material flows for a cyclic column operation.

where y_0 and y_n are the instantaneous concentrations of the highly volatile component in the vapour arriving from the still and leaving the nth plate, mol %, and x is the instantaneous concentration of the more volatile component, mol %.

We introduce the dimensionless time

$$\tau = t/t_v. \qquad (2.106)$$

During the vapour period, the value of τ changes from 0 to 1. Equation (2.105) can be rewritten in the following form:

$$G_i t_v (y_0 - y_n)\, d\tau = \varphi(dx_1 + dx_2 + \ldots + dx_n). \qquad (2.107)$$

Integrating both sides of this equation between $\tau = 0$ and $\tau = 1$ and taking into account that the average vapour composition during the vapour period is given by

$$\bar{y}_v = \int_0^1 y_n\, d\tau,$$

we obtain

$$G_i t_v (\bar{y}_0 - \bar{y}_n) = \varphi(x''_1 - x'_1 + x''_2 - x'_2 + \ldots + x''_n - x'_n), \qquad (2.108)$$

where x' and x'' are the compositions of the liquid, mol % at the beginning and the end of the vapour period respectively, and $\bar{y}_0$ is the average composition of the vapour arriving from the still, mol %.

The periodicity condition for a cyclic column has the form

$$x'_n = \varepsilon x''_{n+1} + (1 - \varepsilon)\, x''_n. \tag{2.109}$$

Substituting this equation into (2.108), we get

$$G_i t_v\, (\bar{y}_0 - \bar{y}_n) = \varphi\varepsilon\, (x''_1 - x''_{n+1}). \tag{2.110}$$

Proceeding from the average flow rates, we obtain from Eqs. (2.103) and (2.104)

$$\frac{G}{L}\, (\bar{y}_0 - \bar{y}_n) = (x'_1 - x''_{n+1}). \tag{2.111}$$

Considering that $x''_1 = x_{out}$, we get

$$\bar{y}_n = \frac{L}{G}\, (x''_{n+1} - x_{out}) + \bar{y}_0. \tag{2.112}$$

This is the equation of the operating line for a cyclic countercurrent plate column. If in this equation we replace $\bar{y}_n$ by y_n, x''_{n+1} and x'_1 (x_{out}) by x_{n+1} and x_1 respectively, we obtain an equation of the operating line for a stationary countercurrent plate column:

$$y_n = \left(\frac{L}{G}\right)(x_{n+1} - x_1) + y_0. \tag{2.113}$$

In the steady state, y_n and x_n are obtained under equilibrium conditions, while Eq. (2.113) can be used together with the equilibrium relation $y = f(x)$ for calculating the efficiency of a stationary column. In the cyclic regime, $\bar{y}_n$ and x''_n are not in equilibrium, and hence Eq. (2.112) and the equilibrium relation are insufficient for determining the efficiency of the column. It is necessary to know the flow of the process in the column for one period of the cycle.

The material balance equation for the nth stage of a cyclic column during the vapour period can be written in the following form:

$$\varphi \frac{dx_n}{dt} = G_i\, (y_{n-1} - y_n). \tag{2.114}$$

Going over to the average flow rates and dimensionless time, we get

$$\frac{dx_n}{d\tau} + \frac{G}{L}\, \varepsilon\, (y_n - y_{n-1}) = 0. \tag{2.115}$$

Since y_n and y_{n-1} are unknown functions of time, we obtain an analytical solution of Eq. (2.115) by making the following assumptions about the properties of the concentration profile:

1. During the vapour period, each plate is continuously depleted in the more volatile component whose concentration in the liquid phase decreases monotonically.

2. The differential equation for the first plate is solved for the constant vapour composition y_0 arriving at this plate. We assume that the equilibrium curve can be replaced by the straight line

$$y = mx + b \tag{2.116}$$

for a small concentration region. Thus we obtain the following differential equation for the first plate:

$$\frac{dx_1}{d\tau} + \varepsilon \frac{G}{L}(mx_1) = \text{const.} \tag{2.117}$$

The general solution of this equation has the form

$$x_1 = A_1 + C_1 e^{-\lambda\tau}, \tag{2.118}$$

where A and C are constants, and

$$\lambda = \frac{mG}{L}. \tag{2.119}$$

3. For a very large column ($n \to \infty$), the concentration profile on the last plates must tend to a straight line, since the liquid composition is almost the same at the beginning and the end of the vapour period. Hence,

$$x_\infty = A_\infty + B_\infty \tau. \tag{2.120}$$

In view of the assumptions 2 and 3, the profile at any stage can be represented by a general function of the type

$$x_n = A_n + B_n \tau + C_n e^{-\lambda\tau}. \tag{2.121}$$

This equation describes the boundary profiles established by assumptions 2 and 3 if $B_1 = C_\infty = 0$. For each plate, coefficients A_n, B_n and C_n are obtained from the condition that the function satisfies the following relations:

(a) the concentration at the beginning of the vapour feed period

$$x_n(0) = x_n'; \tag{2.122}$$

(b) the concentration at the end of the vapour period

$$x_n(1) = x_n''; \tag{2.123}$$

(c) the area under the average composition curve

$$\int_0^1 x_n \, d\tau = \bar{x}_n. \tag{2.124}$$

From these conditions, we obtain

$$A_n = x'_n\left(1+\frac{d}{2}\right)+\frac{d}{2}x''_n - d\bar{x}_n,$$

$$B_n = f\bar{x}_n + \left(1-\frac{f}{2}\right)x''_n - \left(1+\frac{f}{2}\right)x'_n, \tag{2.125}$$

$$C_n = d\bar{x}_n - \frac{d}{2}x''_n - \frac{d}{2}x'_n,$$

where

$$d = \frac{1}{\left(\frac{1}{2}+\frac{1}{\lambda}\right)(1-e^{-\lambda})-1}, \tag{2.126}$$

and

$$f = d\,(1-e^{-\lambda}). \tag{2.127}$$

Using the coefficients defined by Eq. (2.125), we find that Eq. (2.121) gives a monotonic decrease in the concentration x in the interval $0 \leqslant \tau \leqslant 1$. Hence this general function also satisfies assumption 1. Thus, Eq. (2.121) describes the concentration profile at any stage. From this equation, we get

$$\frac{dx_n}{d\tau} = B_n - \lambda C_n e^{-\lambda\tau}. \tag{2.128}$$

Substituting this equation into (2.115), we get

$$B_n - \lambda C_n e^{-\lambda\tau} + \frac{G}{L}\varepsilon y_n(\tau) = \frac{G}{L}\varepsilon y_{n-1}(\tau). \tag{2.129}$$

This equation is valid for the entire interval $0 \leqslant \tau \leqslant 1$. For $\tau = 0$, we get

$$B_n - \lambda C_n + \frac{G}{L}\varepsilon y'_n = \frac{G}{L}\varepsilon y_{n-1}. \tag{2.130}$$

But $y'_n = mx'_n + b$ and $y'_{n-1} = mx'_{n-1} + b$.

Consequently, Eq. (2.130) assumes the form

$$B_n - \lambda C_n + \lambda\varepsilon x'_n = \lambda\varepsilon x'_{n-1}. \tag{2.131}$$

Using relations (2.125) and (2.131), we get

$$(f-\lambda d)\,\bar{x}_n + \left(\lambda\frac{d}{2}+1-\frac{f}{2}\right)x''_n + \left(\lambda\varepsilon+\lambda\frac{d}{2}-\frac{f}{2}-1\right)x'_n = \lambda\varepsilon x'_{n-1}. \tag{2.132}$$

From the equilibrium condition, we obtain

$$\bar{x}_n = \frac{\bar{y}_n - b}{m}. \tag{2.133}$$

Eliminating $\bar{y}_n$ from this equation, we obtain with the help of Eq. (2.112):

$$\bar{x}_n = \frac{1}{\lambda}(x''_{n+1} - x_{\text{out}}) + \left(\frac{\bar{y}_0 - b}{m}\right). \tag{2.134}$$

Substituting this equation into Eq. (2.132), we get

$$\left(\frac{f-\lambda d}{\lambda}\right) x''_{n+1} + \left(\lambda\frac{d}{2} + 1 - \frac{f}{2}\right) x''_n + \left(\lambda\varepsilon + \lambda\frac{d}{2} - \frac{f}{2} - 1\right) x'_n$$
$$+ (f-\lambda d)\left[\frac{(\bar{y}_0 - b)}{m} - \frac{x_{\text{out}}}{\lambda}\right] = \lambda\varepsilon x'_{n-1}. \tag{2.135}$$

Let us introduce the periodicity condition (2.109) into this equation. We consider two cases, $\varepsilon = 1$ and $\varepsilon \neq 1$:

I. $\varepsilon = 1$. Then Eq. (2.109) gives

$$x''_n = x'_{n-1} \text{ or } x''_{n+1} = x'_n. \tag{2.136}$$

Substituting this relation into Eq. (2.135), we get

$$x'_n = P + Qx'_{n-1}, \tag{2.137}$$

where

$$P = \frac{(f-\lambda d)\left(\frac{x_{\text{out}}}{\lambda} - \frac{\bar{y}_0 - b}{m}\right)}{\left(\frac{\lambda}{2} - 1\right) d + \left(\frac{1}{\lambda} - \frac{1}{2}\right) f + (\lambda - 1)}, \tag{2.138}$$

$$Q = \frac{\left(1 - \frac{d}{2}\right)\lambda + \left(\frac{f}{2} - 1\right)}{\left(\frac{\lambda}{2} - 1\right) d + \left(\frac{1}{\lambda} - \frac{1}{2}\right) f + (\lambda - 1)}. \tag{2.139}$$

Using Eq. (2.137) for the plates 1, 2, 3, . . ., N, we get

$$x'_1 = P + Qx'_0,$$
$$x'_2 = P + Qx'_1 = P + PQ + Q^2x'_0,$$
$$\cdots\cdots\cdots\cdots\cdots\cdots$$
$$x'_N = P(1 + Q + Q^2 + \ldots + Q^{N-1}) + Q^N x'_0,$$

or

$$x'_N = P\sum_{i=0}^{N-1} Q^i + Q^N x'_0. \tag{2.140}$$

If $|Q| < 1$, the sum is equal to

$$\sum_{i=0}^{N-1} Q^i = \frac{1-Q^N}{1-Q}. \tag{2.141}$$

Here, Eq. (2.140) assumes the form

$$x'_N = \frac{P(1-Q^N)}{(1-Q)} + Q^N x'_0. \tag{2.142}$$

Considering that $x'_N = x''_{N+1} = x_{in}$, we finally obtain for $|Q| < 1$:

$$N = \frac{\ln[(1-Q)x_{in} - P] - \ln[(1-Q)x'_0 - P]}{\ln Q}. \tag{2.143}$$

Similarly, we get for $|Q| > 1$:

$$N = \frac{\ln[(Q-1)x_{in} + P] - \ln[(Q-1)x'_0 + P]}{\ln Q}. \tag{2.144}$$

For $Q = 1$, we get

$$N = \frac{x_{in} - x'_0}{P}. \tag{2.145}$$

In Eqs. (2.140)-(2.145), x'_0 is the fictitious concentration, since there is no zeroth plate and Eq. (2.137) is not applicable for the first plate. With the help of Eq. (2.132) for the first plate with $\varepsilon = 1$, we obtain the following expression for x'_0:

$$(f - \lambda d)\bar{x}_1 + \left(\lambda + \lambda\frac{d}{2} + \frac{f}{2} - 1\right)x'_1 = \left(\frac{f}{2} - \lambda\frac{d}{2} - 1\right)x''_1 + \lambda\bar{x}_0, \tag{2.146}$$

where $\bar{x}_0$ is the concentration of the liquid, which is in equilibrium with the concentration of the vapour entering the column, mol %.

Equation (2.146) is the real material balance equation for the first plate. Equation (2.137) is obtained by substituting the condition (2.109) into (2.135). For the first plate, this means that

$$x''_1 = x'_0 = \bar{x}_0. \tag{2.147}$$

This, however, is not true, since there is no zeroth plate. The value of $\bar{x}_0$ will be equal to x''_1 (x_{out}) if and only if the number of plates is infinite. Substituting (2.147) into (2.146), we get

$$(f - \lambda d)\bar{x}_1 + \left(\lambda + \lambda\frac{d}{2} - \frac{f}{2} - 1\right)x'_1 = \left(\lambda + \frac{f}{2} - \lambda\frac{d}{2} - 1\right)x'_0. \tag{2.148}$$

Let us now define x'_0 in such a way that Eq. (2.148) is valid for the first plate. Equating the right-hand sides of Eqs. (2.146) and (2.148), we get

$$\left(\frac{f}{2} - \lambda\frac{d}{2} - 1\right)x''_1 + \lambda\bar{x}_0 = \left(\lambda + \frac{f}{2} - \lambda\frac{d}{2} - 1\right)x'_0. \tag{2.149}$$

We solve this equation in x_0', taking into account that $x_1'' = x_{out}$:

$$x_0' = \frac{\left[\left(\frac{f}{2} - 1 - \lambda\frac{d}{2}\right) x_{out} + \lambda\bar{x}_0\right]}{\left[\left(1 - \frac{d}{2}\right)\lambda + \left(\frac{f}{2} - 1\right)\right]}. \qquad (2.150)$$

Equation (2.145), into which the value of x_0' given by Eq. (2.150) is substituted, is used for calculations when the degree of separation is given but the number of plates is not known.

II. $\varepsilon \neq 1$. The periodicity condition has the form

$$x_n' = \varepsilon x_{n+1}'' + (1 - \varepsilon)\, x_n'', \qquad (2.151)$$

$$x_{n-1}' = \varepsilon x_n'' + (1 - \varepsilon)\, x_{n-1}''.$$

Substituting this relation into Eq. (2.135), we get

$$P_2 x_{n+1}'' - P_1 x_n'' - P_0 x_{n-1}'' = Q, \qquad (2.152)$$

where

$$P_2 = \left[\left(\frac{1}{\lambda} - \frac{\varepsilon}{2}\right) f + \left(\lambda\frac{\varepsilon}{2} - 1\right) d + (\varepsilon\lambda - 1)\,\varepsilon\right],$$

$$P_1 = \left[\left(\frac{\lambda}{2}\varepsilon - \lambda\right) d + \left(1 - \frac{\varepsilon}{2}\right) f + (2\lambda\varepsilon - \lambda - 1)\,\varepsilon\right],$$

$$P_0 = \lambda\varepsilon\,(1 - \varepsilon), \qquad (2.153)$$

and

$$Q = (f - \lambda d)\left[\frac{x_{out}}{\lambda} - \frac{(\bar{y}_0 - b)}{m}\right].$$

The general solution of Eq. (2.152) has the form

$$x_n'' = C_1\beta_1^n + C_2\beta_2^n + \frac{Q}{(P_2 - P_1 - P_0)}, \qquad (2.154)$$

where

$$\beta_1 = \frac{P_1 + \sqrt{P_1^2 + 4P_2P_0}}{2P_2},$$

and

$$\beta_2 = \frac{P_1 - \sqrt{P_1^2 + 4P_2P_0}}{2P_2}. \qquad (2.155)$$

The constants C_1 and C_2 are obtained by writing down Eq. (2.154) for the zeroth and first plates:

$$C_1 = \frac{\beta_2 x_0''}{(\beta_2 - \beta_1)} - \frac{x_{out}}{(\beta_2 - \beta_1)} - \frac{(\beta_2 - 1)\,Q}{(\beta_2 - \beta_1)(P_2 - P_1 - P_0)}, \qquad (2.156)$$

$$C_2 = \frac{x_{out}}{(\beta_2 - \beta_1)} + \frac{(\beta_1 - 1)\,Q}{(\beta_2 - \beta_1)(P_2 - P_1 - P_0)} - \frac{\beta_1 x_0''}{(\beta_2 - \beta_1)}.$$

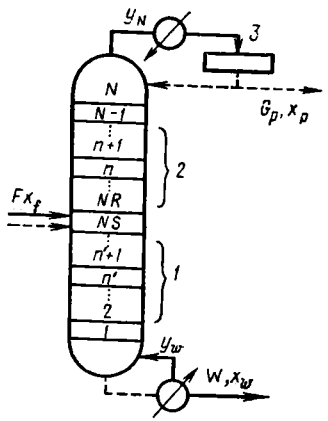

Fig. 41. Schematic diagram of a distilling column with a cyclic operation:

1—rectifying part, *2*—stripping part, *3*—collecting tank.

The concentration x_0'' is calculated from the periodicity condition:

$$x_0'' = \frac{\bar{x}_0 - \varepsilon x_{out}}{(1-\varepsilon)}. \quad (2.157)$$

Let us apply Eq. (2.154) to the Nth plate

$$x_{1n} = C_1\beta_1^{N+1} + C_2\beta_2^{N+1} + \frac{Q}{(P_2 - P_1 - P_0)}, \quad (2.158)$$

where x_{1n} is the concentration of the liquid fed to the column.

Equation (2.158) can be used for calculating the number N of plates by the trial-and-error method. However, considering that $\beta_2 \ll \beta_1$, the number N of plates can be calculated to a fairly high degree of accuracy from the equation

$$N = \frac{\left[\ln\left(x_{1n} + \frac{Q}{(P_0 + P_1 - P_2)}\right) - \ln C_1\right]}{\ln \beta_1} - 1. \quad (2.159)$$

Relations (2.158) and (2.159) are violated when $(P_2 - P_1 - P_0) = 0$, and for $\lambda = 1$, we get

$$x_{1n} = C_1 + C_2\beta_2^{N+1} + (N+1)\frac{Q}{(P_2 + P_0)}. \quad (2.160)$$

Since β_2 can be neglected, we get

$$N = \frac{(x_{1n} - C_1)(P_2 + P_0)}{Q} - 1. \quad (2.161)$$

Here

$$C_1 = \frac{\beta_2 x_0''}{(\beta_2 - 1)} - \frac{x_{out}}{(\beta_2 - 1)} + \frac{Q}{(\beta_2 - 1)(P_2 + P_0)}, \quad (2.162)$$

$$C_2 = \frac{(x_{out} - x_0'')}{(\beta_2 - 1)} - \frac{Q}{(\beta_2 - 1)(P_2 + P_0)}.$$

The above method of calculations is applicable to cyclic operations in countercurrent absorption and stripping columns. In the case of distillation, it is necessary to take into account the conditions at the top and bottom plates, as well as at the feed plate.

Let us consider the cyclic distillation column shown in Fig. 41. During the vapour period, the vapour from the still is fed to the

column, while the vapour from the Nth plate of the rectifying section is condensed and collected in the receiver. During the liquid period, a part of the condensate is removed in the form of the end product, and a part is returned to the Nth plate in the form of reflux. The feed is supplied to the column during the liquid period if it is in the liquid form, and during the vapour period if it is a mixture in the gaseous form.

I. $\varepsilon = 1$. *Rectifying section.* For this section the equations derived above can be used without any alterations if appropriate values of concentrations at the input and output, as well as the factor λ, are used.

The quantity $\bar{y}_0$ is determined from the material balance equation of the rectifying section of the column for one cycle. Assuming that $(\bar{y}_0)_{rec} = (\bar{y}_N)_{str}$, we get

$$(\bar{y}_0)_{rec} = (\bar{y}_N)_{str} = \left(\frac{L}{G}\right)_{rec} [(x_{out})_{rec} - x_p] + x_p. \quad (2.163)$$

For total condensation, $(x_{in})_{rec} = x_p$. It should also be noted that $(x_{out})_{rec} = (x'_0)_{rec} = (x''_N)_{rec}$.

Stripping section. For this section of the column, we use Eqs. (2.138), (2.139), (2.143)-(2.146). It is only necessary to replace $\bar{y}_0$ by y_w and x_{in} by $(x'_N)_{str}$, and to determine x_{out} by introducing the boundary condition for the bottom plate:

$$(x_{out})_{str} = \left(\frac{W}{L}\right)_{str} x_w + \left(\frac{G}{L}\right)_{str} y_w, \quad (2.164)$$

where x_w is the concentration of the still product, in mol %; w is the quantity of the still product, mole/s; and y_w is the vapour composition in equilibrium with x_w, mol %.

Feed plate. The feed is introduced in the form of liquid. The liquid enters the column during the liquid period and the concentration $(x'_N)_{str}$ at the feed plate is determined by the relation

$$(x'_N)_{str} = \frac{Fx_f + L_{rec}(x''_N)_{rec}}{(F + L_{rec})}, \quad (2.165)$$

where F is the quantity of the initial mixture, mole/s; and x_f is the concentration of the initial mixture, mol %.

During the liquid period, the initial mixture (of composition x_f) mixes with the liquid from the upper plate (with composition $(x'_N)_{rec}$), thus determining the composition of the mixture on the plate below the feed plate, namely $(x'_N)_{str}$. The optimal position of the feed plate corresponds to the stage at which flows with different compositions do not mix, i.e.

$$(x''_N)_{rec} = (x'_N)_{str} = x_f. \quad (2.166)$$

If the feed is in the form of a vapour mixture, it enters the column during the vapour period, the optimal position of the feed plate

corresponds to $(\bar{y}_N)_{str} = x_f$. The concentration $(x''_N)_{rec}$ is determined from the expression

$$(x''_N)_{rec} = \frac{(F/L_{rec})(x_f - m(x'_N)_{str})}{\left(\lambda_{rec} + \frac{f}{2} - \lambda_{rec}\frac{d}{2} - 1\right)} + (x'_N)_{str}. \qquad (2.167)$$

Since $(x'_N)_{str} = (x_{out})_{rec}$, we can find $(x'_N)_{str}$ from Eq. (2.163):

$$(x'_N)_{str} = (G/L)_{rec}(\bar{y}_N)_{str} + [1 - (G/L)_{rec}]\, x_p. \qquad (2.168)$$

II. $\varepsilon \neq 1$. Equations for this case can be easily obtained from Eq. (2.158) by using similar arguments.

Example. Find the number of theoretical plates during cyclic rectification of a mixture of benzene and toluene under following conditions: $\varepsilon = 1$, $x_p = 0.95$ (the concentrations are given in mole fractions of benzene), $x_w = 0.05$, $x_f = 0.50$, $(L/G_p)_{rec} = 1.57$, $(G/G_p)_{rec} = 2.57$, $(L/G_p)_{str} = 3.57$, and $(G/G_p)_{str} = 2.57$. The equilibrium curve is shown in Fig. 42.

It can be seen from Fig. 42 that the equilibrium curve can be replaced by four straight lines:

$y = 2.2x$ for $0 \leqslant x \leqslant 0.18$;

$y = 1.5x + 0.08$ for $0.18 \leqslant x \leqslant 0.35$;

$y = 0.85x + 0.30$ for $0.35 \leqslant x \leqslant 0.60$;

$y = 0.457x + 0.525$ for $0.60 \leqslant x \leqslant 1$.

The number of plates in the stripping distillation section N_{str} is determined by using three segments of the equilibrium curve, while the number N_{rec} of plates in the rectifying section is determined by using two segments.

Stripping section. Since $\varepsilon = 1$, we can use Eqs. (2.143)-(2.145). For the first segment, we have $m = 2.2$; $b = 0.0$; $(G/L)_{str} = (G/G_p)_{str}/(L/G_p)_{str} = 2.57/3.57 = 0.72$. From Eq. (2.119), we get $\lambda = m(G/L) = 2.2 \times 0.72 = 1.58$; $(\bar{y}_0)_1 = y_w = mx_w = 2.2 \times 0.05 = 0.11$; $(x_{in})_1 = 0.18$. The value of $(x_{out})_1$ is obtained from Eq. (2.164). Thus, $L_{str} = w + V_{str}$, and hence $(W/L)_{str} = 1 - (G/L)_{str} = 1 - 0.72 = 0.28$. Consequently, we get $(x_{out})_1 = 0.28 \times 0.05 + 0.72 \times 0.11 = 0.093$. From Eqs. (2.126) and (2.127), we get $d = -9.96$ and $f = -7.91$. From Eqs. (2.138) and (2.139), we calculate $P = 0.43$ and $Q = 2.77$. From Eq. (2.150), we get $x'_0 = 0.0779$. Since $|Q| > 1$, we get from (2.144) $(N_{str})_1 = 0.68$.

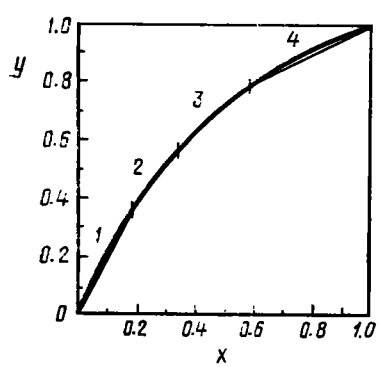

Fig. 42. Equilibrium curve for benzene-toluene mixture.

On the second segment, we get $m = 3/2$; $b = 0.08$; $\lambda = 0.72 \times 1.5 = 1.08$; $(x_{out})_2 = (x'_0)_2 = (x_{in})_1 = 0.18$ and $(x_{in})_2 = 0.35$. It should be noted that $(\bar{y}_0)_2 = (\bar{y}_n)_1$. The quantity $(\bar{y}_n)_1$ is determined from (2.112) under the condition that $(x''_{n+1})_1 = (x_{in})_1 =$

$= 0.18$. This gives $(\bar{y}_n)_1 = (\bar{y}_0)_2 = 0.231$. In analogy with the first segment, we get $(N_{str})_2 = 0.82$.

The feed plate is reached on the third segment. Since the initial mixture is boiling liquid, we obtain from Eq. (2.166) $(x_{in})_3 = (x'_N)_{str} = x_f = 0.50$. For this segment, we get $m = 0.85$; $b = 0.30$; $\lambda = 0.612$; $(x'_0)_3 = (x_{out})_3 = (x_{in})_2 = 0.35$; $(\bar{y}_0)_3 = (\bar{y}_n)_2 = 0.467$. Substituting these values into the corresponding equations, we calculate $(N_{str})_3 = 1.1$. The total number of plates in the distillation section is $N_{str} = (N_{str})_1 + (N_{str})_2 + (N_{str})_3 = 2.6$.

Rectifying section. On the first segment, we get $m = 0.85$; $b = 0.30$; $(G/L)_{rec} = (G/G_P)_{rec}/(L/G_P)_{rec} = 2.57/1.57 = 1.64$. Hence, we get $\lambda = 1.39$; $(x_{out})_1 = (x'_0)_1 = (x^*_N)_{rec} = 0.50$ and $(x_{in})_1 = 0.60$. From Eq. (2.163), we get $(\bar{y}_0)_1 = (0.50 - 0.95)/1.64 + 0.95 = 0.675$. Using the values obtained above, we get $(N_{rec})_1 = 0.54$.

On the second segment, we have $m = 0.475$; $b = 0.525$; $\lambda = 0.78$; $(x_{out})_2 = (x'_0)_2 = 0.60$; $(x_{in})_1 = x_P = 0.95$. From Eq. (2.163), we get $(\bar{y}_0)_2 = 0.736$. Substituting this value into the corresponding equation, we get $(N_{rec})_2 = 2.13$. Consequently, $N_{rec} = 0.54 + 2.13 = 2.67$.

The total number of theoretical plates is equal to $N = N_{rec} + N_{str} = 5.27$.

The total number of plates required for such separation in a stationary column is 11.5. This means that for a given mixture under specified conditions, the cyclic operation more than doubly increases the theoretical efficiency of separation.

Part Two

Hydrodynamic Principles of Mass-Transfer Processes

Chapter Three

Hydrodynamics of Single-Phase Flows

3.1. Basic Concepts of the Hydrodynamics of Single-Phase Flows

In the presence of free surfaces, mass-transfer processes involve the flow of gases and liquids. The substance must pass within the boundaries of the given phase right up to the interface, penetrate through it and propagate within the boundaries of the second phase.

A substance is transported in gas and liquid flows through a direct contact between molecules and as a result of interaction between them (*molecular transport governed by the laws of microkinetics*), as well as by the liquid particles, or conglomerates of molecules, which move from one point of the given medium to another (*vortex transport governed by the laws of macrokinetics*).

The predominant influence of any transport mechanism is determined by the hydrodynamic conditions of the process. The transport mechanism for a substance within each phase is directly associated with the hydrodynamics of a single-phase flow, while the two-phase flow hydrodynamics is applied when considering the transport mechanism through an interface. In the case of macroscopic transport of a substance, the vortex motion of the fluid becomes significant, since vortices are the carriers of energy and mass in a flow. An analysis of the vortex motion of a fluid explains the mechanism of displacement of particles and several other phenomena observed in mass-transfer processes.

The motion of a fluid is accompanied by a change in the values of some physical quantities. These changes can be used to evaluate the process of motion.

In general, a physical quantity can vary with time at a given point (*local variation*), or while passing from one point in space to another (*convective variation*). If the linear velocity of the fluid is chosen as the variable physical quantity and if we consider the velocity along the

x-axis, the local variation in velocity over time interval $d\tau$ will be $\frac{\partial w_x}{\partial \tau} d\tau$, while the convective variation will be $\frac{\partial w_x}{\partial x} dx$ as we cover the distance dx.

The time derivative of a given quantity, taking into account both the local variation and the convective variation in time, is called the *total* or *substantial derivative of this quantity*. From its definition follows the form of its notation:

$$\frac{Dw_x}{d\tau} = \frac{\partial w_x}{\partial \tau} \cdot \frac{d\tau}{d\tau} + \frac{\partial w_x}{\partial x} \cdot \frac{dx}{d\tau} + \frac{\partial w_x}{\partial y} \cdot \frac{dy}{d\tau} + \frac{\partial w_x}{\partial z} \cdot \frac{dz}{d\tau},$$

or, after transformation, considering that

$$\frac{dx}{d\tau} = w_x; \quad \frac{dy}{d\tau} = w_y; \quad \frac{dz}{d\tau} = w_z,$$

we get

$$\frac{Dw_x}{d\tau} = \frac{\partial w_x}{\partial \tau} + w_x \frac{\partial w_x}{\partial x} + w_y \frac{\partial w_x}{\partial y} + w_z \frac{\partial w_x}{\partial z}. \tag{3.1}$$

The first term on the right-hand side of this equation is the local derivative of velocity along the x-axis, while the sum of the remaining three terms expresses the convective derivative of velocity.

Equations similar to Eq. (3.1) can also be written for the other (y- and z-) coordinate axes. If a change in concentration takes place in the flow of a substance, the corresponding expression for the total derivative of concentration assumes the form

$$\frac{Dc}{d\tau} = \frac{\partial c}{\partial \tau} + w_x \frac{\partial c}{\partial x} + w_y \frac{\partial c}{\partial y} + w_z \frac{\partial c}{\partial z} \ldots . \tag{3.2}$$

Steady and Unsteady Motion. The definition of steady and unsteady motion follows directly from the concept of the total derivative. If a given physical quantity, which determines the flow of the fluid, does not change with time at a given point, i.e. if the local derivative is equal to zero, the motion is called steady. Thus, steady-state motion is characterized by the equality

$$\partial w/\partial \tau = 0. \tag{3.3}$$

If $\partial w/\partial \tau \neq 0$, the motion is called unsteady, and time will be one of the characteristic parameters of the flow. In the flow of liquids, the unknown quantities are the velocity and pressure, or their distribution in the flow. In accordance with Eq. (3.3), the velocity and pressure at any point in the steady-state motion of a fluid will be functions of only the coordinates of the point, i.e.

$$w = f_0(x, y, z), \qquad P = f(x, y, z). \tag{3.4.}$$

For the unsteady flow, the velocity and pressure at any point will depend on the coordinates as well as time.

Streamline. Let us consider an elementary particle at point A in the flow (Fig. 43*a*). We denote the flow velocity at point A by w (it is shown in the form of a vector in Fig. 43 *a*). In a certain period of time $\Delta\tau$, this particle will occupy a new position A' and will have a velocity w'. After equal intervals of time, the particle will successively occupy positions A', A'', A''', etc. Drawing tangents to the

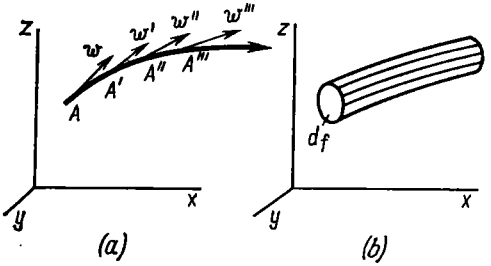

Fig. 43. Streamline (*a*) and stream tube (*b*) in a liquid.

velocity vectors at these points, we obtain in the limit a line enveloping the direction of the velocity. This line is called *streamline.*

Thus, the streamline can be defined as an imaginary line whose tangent at any point coincides with the velocity vector of the liquid at that point. The differential equation for a streamline can be written as

$$\frac{dx}{w_x} = \frac{dy}{w_y} = \frac{dz}{w_z}, \tag{3.5}$$

or, as two sets of equations:

$$w_y\,dx = w_x\,dy; \quad w_z\,dy = w_y\,dz. \tag{3.6}$$

In the steady-state motion, the streamlines coincide with the trajectories of fluid particles. Such a coincidence does not take place in unsteady motion.

A stream tube is a part of the fluid bounded by streamlines passing through all the points of any infinitely small closed contour in the region occupied by the fluid (Fig. 43*b*). For the steady-state motion, the stream tube will simultaneously be the trajectory tube also.

The fluid flowing inside a stream tube is called *stream filament.* The totality of all the moving stream filaments constitutes the *streamline flow.*

The area f of the cross section normal to the direction of the liquid flow is called the *free cross-sectional area.*

The perimeter of a free cross section in contact with the walls and confining the flow is called the *wetted perimeter* (Π).

The ratio of the free cross-sectional area f to the wetted perimeter Π is called the *hydraulic radius* r_h. This is one of the most important

characteristics of the flow. The quadrupled value of the hydraulic radius is called the equivalent diameter d_e. Thus,

$$r_h = \frac{f}{\Pi}, \tag{3.7}$$

$$d_e = 4r_h = \frac{4f}{\Pi}. \tag{3.8}$$

Rate of Flow. The rate of flow of a liquid is the amount of liquid passing through the free cross section per unit time. If a finite flow is considered as a set of infinite number of streamlines having cross section df and moving with different velocities, the flow rate V_s will be equal to

$$V_s = \int_f w_a \, df, \tag{3.9}$$

where w_a is the actual velocity at a given point, m/s.

The law of distribution of velocities over the flow cross section depends on a number of factors and is usually a complex function. Consequently, it was found practically convenient to introduce the concept of the mean flow velocity which is defined as the ratio of the actual volumetric flow rate of the liquid to the cross-sectional area, i.e.

$$w_m = \frac{V_s}{f} = \frac{\int_f w_a \, df}{f}. \tag{3.10}$$

Expressing the rate of flow in terms of the mean velocity, we get

$$V_s = w_m f. \tag{3.11}$$

The mass and volumetric flow rates are connected through the relation

$$V_s = \frac{L}{3600\rho} = w_m f, \tag{3.12}$$

where L is the flow rate of the liquid, kg/hr, and ρ is the density of the liquid, kg/m^3.

3.1.1. Continuity Equation for Flow (Constant-Flow Rate Equation)

Let us apply the law of conservation of mass to a moving flow of fluid. For this purpose, we consider an infinitely small volume of the fluid in the flow, bounded by a parallelepiped with sides dx, dy, dz (Fig. 44).

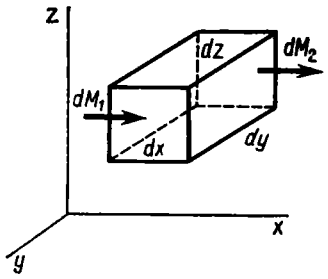

Fig. 44. To the derivation of the flow continuity equation.

Let us consider the mass of the fluid entering and leaving the parallelepiped during an infinitely small time interval $d\tau$, assuming that ρ is the density of the fluid. In order to simplify the dependence, let us consider the variation in the mass along the x-axis.

The mass of the fluid entering the parallelepiped through the face $dydz$ will be

$$dM_1 = \rho_x w_x \, dy \, dz \, d\tau. \quad (3.13)$$

The mass of the fluid leaving the parallelepiped through the opposite face due to a change in the density and velocity will be

$$dM_2 = \left(\rho_x + \frac{\partial \rho_x}{\partial x} dx\right)\left(w_x + \frac{\partial w_x}{\partial x} dx\right) dy \, dz \, d\tau. \quad (3.14)$$

The difference between the amounts of fluid entering and leaving the parallelepiped will be

$$\rho_x w_x \, dy \, dz \, d\tau - \left(\rho_x + \frac{\partial \rho_x}{\partial x} dx\right)\left(w_x + \frac{\partial w_x}{\partial x} dx\right) dy \, dz \, d\tau$$

$$= \rho_x w_x \, dy \, dz \, d\tau - \rho_x w_x \, dy \, dz \, d\tau - \rho_x \frac{\partial w_x}{\partial x} dx \, dy \, dz \, d\tau$$

$$- w_x \frac{\partial \rho_x}{\partial x} dx \, dy \, dz \, d\tau - \frac{\partial \rho_x}{\partial x} dx \frac{\partial w_x}{\partial x} dx \, dy \, dz \, d\tau. \quad (3.15)$$

Cancelling and neglecting the quantities of small order of magnitude, we get

$$-\left(\rho_x \frac{\partial w_x}{\partial x} + w_x \frac{\partial \rho_x}{\partial x}\right) dx \, dy \, dz \, d\tau. \quad (3.16)$$

Since the expression in the parentheses is the derivative of a product, we can write

$$-\frac{\partial (\rho_x w_x)}{\partial x} dx \, dy \, dz \, d\tau. \quad (3.17)$$

Accordingly, for all three coordinate axes, we get

$$-\left[\frac{\partial (\rho_x w_x)}{\partial x} + \frac{\partial (\rho_y w_y)}{\partial y} + \frac{\partial (\rho_z w_z)}{\partial z}\right] dx \, dy \, dz \, d\tau. \quad (3.18)$$

For a parallelepiped of constant dimensions, this excess mass is due to a change in the density of the elementary volume with time, which can be expressed in the form

$$\frac{\partial \rho}{\partial \tau} d\tau \, dx \, dy \, dz. \quad (3.19)$$

Equating Eqs. (3.18) and (3.19), we get

$$\frac{\partial \rho}{\partial \tau} + \frac{\partial (\rho_x w_x)}{\partial x} + \frac{\partial (\rho_y w_y)}{\partial y} + \frac{\partial (\rho_z w_z)}{\partial z} = 0. \tag{3.20}$$

This is the differential continuity equation for flow.

For steady-state motion, we have

$$\frac{\partial \rho}{\partial \tau} = 0 \tag{3.21}$$

Consequently, the differential continuity equation assumes the form

$$\frac{\partial (\rho_x w_x)}{\partial x} + \frac{\partial (\rho_y w_y)}{\partial y} + \frac{\partial (\rho_z w_z)}{\partial z} = 0. \tag{3.22}$$

Integration of this equation for each given cross section f_1, f_2, f_3, . . ., f_n leads to the dependence

$$\rho_1 w_1 f_1 = \rho_2 w_2 f_2 = \rho_3 w_3 f_3 = \ldots = \rho_n w_n f_n. \tag{3.23}$$

If the fluid is incompressible (dropping), i.e. if

$$\frac{\partial \rho_x}{\partial x} = \frac{\partial \rho_y}{\partial y} = \frac{\partial \rho_z}{\partial z} = 0, \tag{3.24}$$

the differential continuity equation for the steady-state flow assumes the form

$$\frac{\partial w_x}{\partial x} + \frac{\partial w_y}{\partial y} + \frac{\partial w_z}{\partial z} = 0. \tag{3.25}$$

Integration of this equation for each given cross section f_1, f_2, f_3, . . ., . . ., f_n leads to the dependence

$$w_1 f_1 = w_2 f_2 = w_3 f_3 = \ldots = w_n f_n. \tag{3.26}$$

However, since in accordance with Eq. (3.11) the product of the velocity of a liquid and the cross-sectional area is the flow rate, Eq. (3.26) can be called the *constant flow-rate equation.*

Thus, it follows from Eq. (3.26) that during the motion of an incompressible liquid, the volume occupied by any part of the liquid remains unchanged. In other words, it is completely filled by the liquid, without any voids or discontinuities between the particles of the liquid. That is why this equation is called the *continuity equation for flow.*

3.1.2. Differential Fluid-Flow Equation

The differential flow equation establishes the relation between the forces acting in a fluid.

First of all, let us establish this dependence for a fluid moving without friction (ideal fluid) and subjected to gravitational and pres-

sure forces. In order to derive the equation, we shall use a basic principle of mechanics, according to which a body is in a state of motion if the sum of the projections of all the forces acting on it is equal to the product of the mass of the moving body and its acceleration.

Let us consider an elementary parallelepiped with edges dx, dy, dz in a moving fluid (Fig. 45), and express the projections of forces

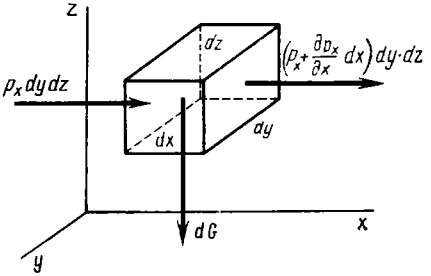

Fig. 45. To the derivation of the equation of motion.

acting on it, directing the gravitational force dG along the z-axis. For the x-, y- and z-axes respectively, we get

$$\begin{aligned} p_x\,dy\,dz-\left(p_x+\frac{\partial p_x}{\partial x}dx\right)dy\,dz&=\rho\,\frac{Dw_x}{d\tau}dx\,dy\,dz,\\ p_y\,dx\,dz-\left(p_y+\frac{\partial p_y}{\partial y}dy\right)dx\,dz&=\rho\,\frac{Dw_y}{d\tau}dx\,dy\,dz,\\ -dG+p_z\,dx\,dy-\left(p_z+\frac{\partial p_z}{\partial z}dz\right)dx\,dy&=\rho\,\frac{Dw_z}{d\tau}dx\,dy\,dz. \end{aligned} \tag{3.27}$$

Cancelling and reducing to a unit volume, we obtain

$$\begin{aligned} -\frac{\partial p_x}{\partial x}&=\rho\,\frac{Dw_x}{d\tau},\\ -\frac{\partial p_y}{\partial y}&=\rho\,\frac{Dw_y}{d\tau},\\ -\gamma-\frac{\partial p_z}{\partial z}&=\rho\,\frac{Dw_z}{d\tau}. \end{aligned} \tag{3.28}$$

Expansion of the total derivatives on the right-hand side of this equation gives

$$\begin{aligned} -\frac{\partial p_x}{\partial x}&=\rho\left(\frac{\partial w_x}{\partial\tau}+w_x\frac{\partial w_x}{\partial x}+w_y\frac{\partial w_x}{\partial y}+w_z\frac{\partial w_x}{\partial z}\right),\\ -\frac{\partial p_y}{\partial y}&=\rho\left(\frac{\partial w_y}{\partial\tau}+w_x\frac{\partial w_y}{\partial x}+w_y\frac{\partial w_y}{\partial y}+w_z\frac{\partial w_y}{\partial z}\right),\\ -\gamma-\frac{\partial p_z}{\partial z}&=\rho\left(\frac{\partial w_z}{\partial\tau}+w_x\frac{\partial w_z}{\partial x}+w_y\frac{\partial w_z}{\partial y}+w_z\frac{\partial w_z}{\partial z}\right). \end{aligned} \tag{3.29}$$

This system of differential equations is called *Euler's differential equations of motion.*

Integral of Euler's Equations of Motion. Bernoulli's Equation. For a steady-state fluid flow under the condition that the velocity components vary only in the direction of the corresponding axes, Eqs. (3.29) assume the form

$$\begin{aligned} -\frac{\partial p_x}{\partial x} &= \rho w_x \frac{\partial w_x}{\partial x}, \\ -\frac{\partial p_y}{\partial y} &= \rho w_y \frac{\partial w_y}{\partial y}, \\ -\gamma - \frac{\partial p_z}{\partial z} &= \rho w_z \frac{\partial w_z}{\partial z}. \end{aligned} \tag{3.30}$$

These equations express the action of forces at a point in the moving fluid. In order to express the action of forces along the entire face of the parallelepiped (Fig. 45), we must multiply the left- and right-hand sides of Eqs. (3.30) by the lengths of the corresponding faces. This gives

$$\begin{aligned} -\frac{\partial p_x}{\partial x}\,dx &= \rho w_x \frac{\partial w_x}{\partial x}\,dx, \\ -\frac{\partial p_y}{\partial y}\,dy &= \rho w_y \frac{\partial w_y}{\partial y}\,dy, \\ -\gamma\,dz - \frac{\partial p_z}{\partial z}\,dz &= \rho w_z \frac{\partial w_z}{\partial z}\,dz. \end{aligned} \tag{3.31}$$

Summing these equations, we obtain the total variation of the forces acting in the entire volume of the elementary parallelepiped:

$$\begin{aligned} &\gamma\,dz + \left(\frac{\partial p_x}{\partial x}\,dx + \frac{\partial p_y}{\partial y}\,dy + \frac{\partial p_z}{\partial z}\,dz\right) \\ &+ \rho\left(w_x \frac{\partial w_x}{\partial x}\,dx + w_y \frac{\partial w_y}{\partial y}\,dy + w_z \frac{\partial w_z}{\partial z}\,dz\right) = 0. \end{aligned} \tag{3.32}$$

The expressions in parentheses represent total differentials dP of the pressure and of squared velocity, since in the latter case any component can be expressed as follows:

$$w_x \frac{\partial w_x}{\partial x}\,dx = d\left(\frac{w_x^2}{2}\right). \tag{3.33}$$

Taking into consideration Eq. (3.33), we can write Eq. (3.32) as a sum of total differentials:

$$\gamma\,dz + dP + \rho d\left(\frac{w^2}{2}\right) = 0. \tag{3.34}$$

The integral of this equation will be

$$\gamma z + P + \rho \frac{w^2}{2} = \text{const} \tag{3.35}$$

or

$$z + \frac{P}{\gamma} + \frac{w^2}{2g} = \text{const}, \tag{3.36}$$

where z is the position of the point in the flowing fluid with respect to the reference level (level height, m); P/γ is the static head at the point under consideration, m; and $w^2/2g$ is the velocity, or dynamic, head at this point, m.

Equation (3.36), which is the final form of the equation of motion, is called *Bernoulli's equation.* For two points at different heights in the fluid, Bernoulli's equation is written in the following form:

$$z_1 + \frac{P_1}{\gamma} + \frac{w_1^2}{2g} = z_2 + \frac{P_2}{\gamma} + \frac{w_2^2}{2g}. \tag{3.37}$$

According to the Bernoulli equation, the law of motion of a fluid can be interpreted as follows:

(1) when an ideal fluid is in steady flow, the sum of static and dynamic heads is a constant quantity at any point on the flow;

(2) in the steady flow of an ideal fluid, the pressure is lower at the point where the velocity is higher;

(3) in the steady flow of an ideal fluid, the sum of potential energy ($z + P/\gamma$) and kinetic energy ($w^2/2g$) is constant.

Although the Bernoulli equation has been derived for restricted conditions (steady flow and frictionless fluid), it nevertheless provides a solution of the basic problems of the flow of a fluid by relating the velocity to pressure in the flow.

Differential Fluid-Flow Equations with Friction. Navier-Stokes Equation. In order to take friction into account, we must introduce an additional term into Euler's differential flow equation. This additional term is obtained from Newton's equation of motion, according to which the force τ_0 of internal friction per unit area in the case of unidimensional flow is written as

$$\tau_0 = \mu \frac{\partial w_x}{\partial z}, \tag{3.38}$$

where μ is the viscosity of the fluid (Newton's law).

Since Eqs. (3.27) contain the projections of the forces acting on a moving fluid onto the corresponding coordinate axes, we obtain the following expression for the force of friction with respect to z-axis:

$$-\tau_0 dx\, dy + \left(\tau_0 + \frac{\partial \tau_0}{\partial z} dz\right) dx\, dy. \tag{3.39}$$

Taking Eqs. (3.38) and (3.39) into account, the differential equations for unsteady flow of a viscous fluid involving a change in the velocity components in all directions assume the form

$$\begin{aligned}
-\frac{\partial p_x}{\partial x}+\mu\left(\frac{\partial^2 w_x}{\partial x^2}+\frac{\partial^2 w_x}{\partial y^2}+\frac{\partial^2 w_x}{\partial z^2}\right)&=\rho\frac{Dw_x}{d\tau},\\
-\frac{\partial p_y}{\partial y}+\mu\left(\frac{\partial^2 w_y}{\partial x^2}+\frac{\partial^2 w_y}{\partial y^2}+\frac{\partial^2 w_y}{\partial z^2}\right)&=\rho\frac{Dw_y}{d\tau},\\
-\gamma-\frac{\partial p_z}{\partial z}+\mu\left(\frac{\partial^2 w_z}{\partial x^2}+\frac{\partial^2 w_z}{\partial y^2}+\frac{\partial^2 w_z}{\partial z^2}\right)&=\rho\frac{Dw_z}{d\tau}.
\end{aligned} \tag{3.40}$$

These equations are called the Navier-Stokes equations for an incompressible fluid.

In the general form, Eqs. (3.40) cannot be solved analytically, since it is impossible to set the boundary conditions for a viscous fluid in an unsteady flow. However, these equations mathematically represent a whole class of fluid flow and serve as a mathematical model for this kind of motion.

The basic equation of hydrodynamics, viz. the equation of motion for a fluid, characterizes only the forces acting on the flowing fluid, but does not provide an answer to the question as to how the fluid particles move in this case. In other words, it does not reveal the mechanism of motion since, in accordance with the equations derived above, a particle in a moving fluid is subjected to rotational motion besides the translational motion, extension, or compression. The rotational motion of fluid particles is called the *vortex motion of the fluid.* Hence, the equations described above must be supplemented by the equations describing the rotary motion of a fluid.

3.1.3. Onset of Vortex Motion in a Fluid

The equilibrium condition for forces acting in the direction of the flow is obtained from the Bernoulli equation:

$$\frac{P}{\gamma}+\frac{w^2}{2g}=H,\quad \frac{dH}{dn}=0, \tag{3.41}$$

where H is the fluid head (the constant in Bernoulli's equation); and dn is the distance between two streamlines of the fluid along the vertical.

The condition $dH/dn = 0$ is the condition for vortex-free motion. However, when the fluid is in motion, forces perpendicular to the direction of the flow may appear and then the constant in the Bernoulli equation will not retain its value. These forces may cause the rotation of fluid particles and give rise to centrifugal forces.

Due to viscosity, one layer of a fluid may be displaced with respect to another over the cross section in a single-phase flow. This

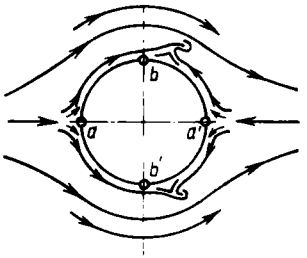

Fig. 46. Streamlining of a cylinder.

generates forces perpendicular to the flow and results in the vortex flow of the fluid. Thus, viscosity is the source of the vortex flow of a fluid. Consequently, vortex flow can appear only in a real viscous fluid.

For the emergence of such a motion, the existence of *separation surfaces*, which have different values of H, is essential. In other words, the gradient dH/dn must be non-zero.

Separation surfaces are often observed in actual practice. A random perturbation is sufficient to cause a rapid distortion of the separation surface, an increase in the velocity difference at some places and, conversely, a decrease in this value at some other places. This leads to a rapid chaotic destruction of the separation surface into a large number of vortices, i.e. to the formation of a vortex layer.

During the countercurrent flow of fluids, the interface formed is wavy in the beginning. According to the Bernoulli equation, the pressure is higher at the crests of waves of each individual flow and, on the contrary, is lower at the troughs. Such a distribution of pressure indicates that the surface is unstable: the fluid will begin to flow from pockets of higher pressure to places where the pressure is lower. This, however, means that the waves formed previously will begin to grow, thus causing the interface to split into individual vortices. In actual practice, the initial perturbations do not usually distort the separation surface in the form of a regular train of waves but rather in a completely random manner. Consequently, in the final stage of disintegration, a random sequence of large and small vortices is formed.

The motion of a fluid past a body of any shape leads to vortex formation due to the emergence of separation surfaces.

By way of an example, let us consider a uniform infinite flow of a fluid around a cylinder (Fig. 46). The fluid flowing upstream is divided into two parts which smoothly flow past the cylinder right up to the midsection bb' (maximum cross section perpendicular to the direction of the flow). The velocity of this flow increases from the point of separation until it reaches its maximum value at the midsection. According to the Bernoulli equation, the pressure will drop at places where the velocity increases. Consequently, the pressure at the points b and b' will be lower in comparison to the points a and a'.

If friction appears in the neighbourhood of the body around which the fluid flows, a *boundary layer* is formed. The thickness of this

layer depends on the viscosity of the fluid: the higher the viscosity, the thicker the boundary layer. The boundary layer serves as a sort of interlayer (separation surface) between the cylinder and the rest of the flow, and if there is a higher pressure at the points a and a', it is imparted to the body through the boundary layer. This pressure difference sort of "squeezes" the boundary layer to the points b and b', resulting in the appearance of streams from a to b and b', and from a' to b and b'. On the other hand, the main part of the flow is normal to the boundary layer region. These countercurrents are

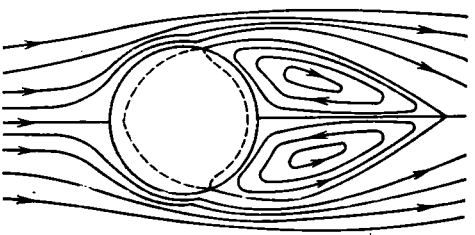

Fig. 47. Streamlining of a spherical soluble particle.

responsible for the appearance of vortices beyond points b and b'. These vortices are washed away by the flow, and new vortices, formed in the same way, replace them.

Figure 47 shows the flow past a soluble spherical droplet. The separation surfaces create inhomogeneous flows, leading to a nonuniform dissolution of the droplet over the entire surface. After a short interval of time, the sphere assumes the form shown by the dashed line. This indicates that the dissolution of spherical particles is not uniform.

When a liquid flows through a round hole with sharp edges in a plane wall (Fig. 48), the separation surface formed begins to curl and forms a vortex ring which is absorbed by the fluid stream. Vortices of this kind are formed in plate columns due to the flow of a gas or a liquid through the perforations in the plates.

The separation surfaces which are responsible for vortex flow may appear due to a change in pressure or density (or specific volume) of the flowing fluid since, in this case, the constant in the Bernoulli equation does not preserve its value. In the theory of vortex motion, this is known as Bjerknes' theorem, according to which the *intersection of isobaric* ($p = \text{const}$) *and isosteric* (specific volume $v = \text{const}$) *surfaces leads to a circulation of the fluid which varies with time*, i.e. *causes a vortex flow*. These surfaces intersect on account of the fact that the specific volume is not a function of pressure (otherwise the surfaces would superimpose without intersecting), but

depends on the varying concentrations C and temperature T. In other words, there exists a function $v = f_0(C, T)$. This is exceptionally important for heat- and mass-transfer processes, since the separation surfaces between moving phases are a typical case of intersection of isobaric and isosteric surfaces. To simplify the analysis of the vortex motion of the fluid, its main characteristics are

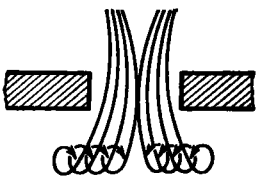

Fig. 48. Vortex formation in the fluid flowing through a hole.

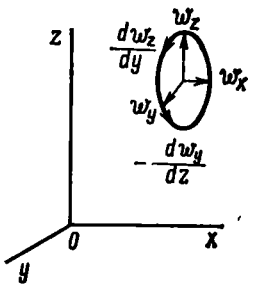

Fig. 49. Vortex components.

assumed to be the same as for an ideal fluid. If w_x, w_y, w_z are the components of flow velocity of a fluid (Fig. 49), the rotation of the fluid with respect to the corresponding coordinate axes will be achieved by varying only two components of the flow velocity w. In this case, the component corresponding to the axis around which the rotation is taking place is excluded. Thus, for example, in order to create rotational motion around the x-axis, it is necessary to vary the velocity component w_z in the positive direction of y-axis, i.e. to change $\partial w_z/\partial y$, while the component w_y should be varied in the negative direction of the z-axis, i.e. $(-\partial w_y/\partial z)$ should be varied. Thus, for rotation around the x-axis to take place, there must exist the difference

$$\left(\frac{\partial w_z}{\partial y} - \frac{\partial w_y}{\partial z}\right). \tag{3.42}$$

Similarly, for y- and z-axes, we get

$$\left(\frac{\partial w_x}{\partial z} - \frac{\partial w_z}{\partial x}\right), \tag{3.43}$$

$$\left(\frac{\partial w_y}{\partial x} - \frac{\partial w_x}{\partial y}\right). \tag{3.44}$$

Expressions (3.42)-(3.44) represent the rotation of the fluid around the corresponding axis and are therefore called *vortex components*.

3.1.4. Differential Fluid-Flow Equations Taking the Rotation of Particles into Account. Basic Laws of Vortex Motion

In order to take into account the rotation of particles of a flowing fluid, we use Euler's equation of motion for a fluid. We divide the right- and left-hand sides of Eq. (3.29) by the density ρ of the fluid. The equations then assume the following form:

$$\begin{aligned}
\frac{\partial w_x}{\partial \tau} + w_x \frac{\partial w_x}{\partial x} + w_y \frac{\partial w_x}{\partial y} + w_z \frac{\partial w_x}{\partial z} &= -\frac{1}{\rho}\frac{\partial p_x}{\partial x}, \\
\frac{\partial w_y}{\partial \tau} + w_x \frac{\partial w_y}{\partial x} + w_y \frac{\partial w_y}{\partial y} + w_z \frac{\partial w_y}{\partial z} &= -\frac{1}{\rho}\frac{\partial p_y}{\partial y}, \\
\frac{\partial w_z}{\partial \tau} + w_x \frac{\partial w_z}{\partial x} + w_y \frac{\partial w_z}{\partial y} + w_z \frac{\partial w_z}{\partial z} &= -g - \frac{1}{\rho}\frac{\partial p_z}{\partial z}.
\end{aligned} \tag{3.45}$$

The following transformations are introduced in order to take into account the rotation of the fluid in the equations of motion. The total velocity of a fluid particle is expressed in terms of its components as follows:

$$w^2 = w_x^2 + w_y^2 + w_z^2. \tag{3.46}$$

The partial derivatives of both sides of this equation with respect to x, y and z will be

$$\begin{aligned}
\frac{\partial}{\partial x}\left(\frac{1}{2}w^2\right) &= w_x \frac{\partial w_x}{\partial x} + w_y \frac{\partial w_y}{\partial x} + w_z \frac{\partial w_z}{\partial x}, \\
\frac{\partial}{\partial y}\left(\frac{1}{2}w^2\right) &= w_x \frac{\partial w_x}{\partial y} + w_y \frac{\partial w_y}{\partial y} + w_z \frac{\partial w_z}{\partial y}, \\
\frac{\partial}{\partial z}\left(\frac{1}{2}w^2\right) &= w_x \frac{\partial w_x}{\partial z} + w_y \frac{\partial w_y}{\partial z} + w_z \frac{\partial w_z}{\partial z}.
\end{aligned} \tag{3.47}$$

Subtracting Eqs. (3.47) from both sides of the Euler equation (3.45), we get

$$\begin{aligned}
\frac{\partial w_x}{\partial \tau} + w_y \frac{\partial w_x}{\partial y} + w_z \frac{\partial w_x}{\partial z} - w_y \frac{\partial w_y}{\partial x} - w_z \frac{\partial w_z}{\partial x} &= -\frac{1}{\rho}\frac{\partial p_x}{\partial x} - \frac{\partial}{\partial x}\left(\frac{1}{2}w^2\right), \\
\frac{\partial w_y}{\partial \tau} + w_x \frac{\partial w_y}{\partial x} + w_z \frac{\partial w_y}{\partial z} - w_x \frac{\partial w_x}{\partial y} - w_z \frac{\partial w_z}{\partial y} &= -\frac{1}{\rho}\frac{\partial p_y}{\partial y} - \frac{\partial}{\partial y}\left(\frac{1}{2}w^2\right), \\
\frac{\partial w_z}{\partial \tau} + w_x \frac{\partial w_z}{\partial x} + w_y \frac{\partial w_z}{\partial y} - w_x \frac{\partial w_x}{\partial z} - w_y \frac{\partial w_y}{\partial z} &= -g - \frac{1}{\rho}\frac{\partial p_z}{\partial z} - \frac{\partial}{\partial z}\left(\frac{1}{2}w^2\right).
\end{aligned} \tag{3.48}$$

The left-hand sides of these equations can be rewritten as follows by taking into account Eqs. (3.42)-(3.44):

$$\frac{\partial w_x}{\partial \tau} + 2\left[\frac{1}{2}\left(\frac{\partial w_x}{\partial z} - \frac{\partial w_z}{\partial x}\right) w_z - \frac{1}{2}\left(\frac{\partial w_y}{\partial x} - \frac{\partial w_x}{\partial y}\right) w_y\right] = -\frac{1}{\rho}\frac{\partial p_x}{\partial x} - \frac{\partial}{\partial x}\left(\frac{w^2}{2}\right),$$

$$\frac{\partial w_y}{\partial \tau} + 2\left[\frac{1}{2}\left(\frac{\partial w_y}{\partial x} - \frac{\partial w_x}{\partial y}\right) w_x - \frac{1}{2}\left(\frac{\partial w_z}{\partial y} - \frac{\partial w_y}{\partial z}\right) w_z\right] = -\frac{1}{\rho}\frac{\partial p_y}{\partial y} - \frac{\partial}{\partial y}\left(\frac{w^2}{2}\right), \quad (3.49)$$

$$\frac{\partial w_z}{\partial \tau} + 2\left[\frac{1}{2}\left(\frac{\partial w_z}{\partial y} - \frac{\partial w_y}{\partial z}\right) w_y - \frac{1}{2}\left(\frac{\partial w_z}{\partial z} - \frac{\partial w_z}{\partial x}\right) w_x\right] = -g - \frac{1}{\rho}\frac{\partial p_z}{\partial z} - \frac{\partial}{\partial z}\left(\frac{w^2}{2}\right).$$

In accordance with Eqs. (3.42)-(3.44) and (3.49), we introduce the following notation for the axial components of the angular velocity of rotation ω of the particle:

$$\omega_x = \frac{1}{2}\left(\frac{\partial w_z}{\partial y} - \frac{\partial w_y}{\partial z}\right), \quad (3.50)$$

$$\omega_y = \frac{1}{2}\left(\frac{\partial w_x}{\partial z} - \frac{\partial w_z}{\partial x}\right), \quad (3.51)$$

$$\omega_z = \frac{1}{2}\left(\frac{\partial w_y}{\partial x} - \frac{\partial w_x}{\partial y}\right). \quad (3.52)$$

In accordance with (3.42)-(3.44), the expressions (3.50)-(3.52) are called vortex components and are the projections of the angular velocity ω onto the coordinate axes.

The equations of motion of a fluid taking into account the rotation of its particles (equations of motion in terms of vortex components) assume the form

$$\begin{aligned}
\frac{\partial w_x}{\partial \tau} + 2(\omega_y w_z - \omega_z w_y) &= -\frac{1}{\rho}\frac{\partial p_x}{\partial x} - \frac{\partial}{\partial x}\left(\frac{1}{2}w^2\right),\\
\frac{\partial w_y}{\partial \tau} + 2(\omega_z w_x - \omega_x w_z) &= -\frac{1}{\rho}\frac{\partial p_y}{\partial y} - \frac{\partial}{\partial y}\left(\frac{1}{2}w^2\right), \quad (3.53)\\
\frac{\partial w_z}{\partial \tau} + 2(\omega_x w_y - \omega_y w_x) &= -g - \frac{1}{\rho}\frac{\partial p_z}{\partial z} - \frac{\partial}{\partial z}\left(\frac{1}{2}w^2\right).
\end{aligned}$$

It follows from Eqs. (3.53)* that for each given axis, the projection of the vortex onto this axis is missing. For example, in the equation of motion with respect to the x-axis, the fluid particle rotates around the other two axes, viz. y- and z-axes.

* Equations (3.53) were first introduced in 1882 by I.S. Gromeka, Prof. of the Kazan University, and are called Gromeka's equations of vortex motion.

The total magnitude and direction of rotation of a particle can be found as the diagonal ω of the rectangular parallelepiped with edges ω_x, ω_y, ω_z along the x-, y-, and z-axes (Fig. 50). For an observer

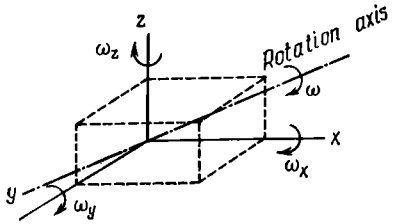

Fig. 50. Angular velocities of rotation of liquid particles.

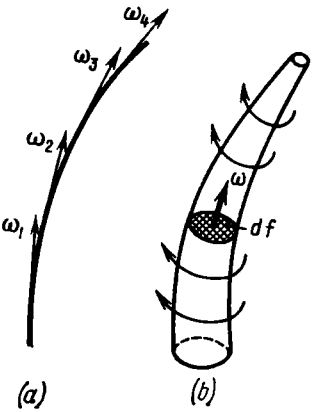

Fig. 51. Vortex line (*a*) and vortex tube (*b*).

standing at the origin and facing the rotational axis, the clockwise rotation corresponds to the positive direction of rotation. According to Fig. 50, the magnitude of total rotation is equal to

$$\omega^2 = \omega_x^2 + \omega_y^2 + \omega_z^2. \tag{3.54}$$

From the expressions (3.50)-(3.52) for the vortex components, it follows that

$$\frac{\partial \omega_x}{\partial x} + \frac{\partial \omega_y}{\partial y} + \frac{\partial \omega_z}{\partial z} = 0. \tag{3.55}$$

This equation is identical to the continuity equation for an incompressible (dropping) liquid with density $\rho = \text{const}$ [see Eq. (3.25)]. For dropping liquids, therefore, vortices can be identified with the components of the total velocity of the liquid particle and identical operations can be carried out over them.

Thus, the vortex motion of a fluid is determined by the field of vector quantities, which is a field of angular velocities of rotation of fluid particles lying in the part of space under consideration, filled by the fluid.

A vortex field is distinguished by vortex lines and vortex tubes, and the concept of a vortex line (Fig. 51*a*) is similar to that of a streamline in which the vectors ω are plotted along the tangents instead of the velocities w. The concept of a vortex tube (Fig. 51*b*) is similar to the concept of a stream tube.

The instantaneous angular velocity of an infinitely small fluid particle is called *vortex velocity.*

A vortex line is a line whose tangent at each point coincides with the vortex velocity vector of the fluid at the given instant of time (Fig. 51*a*).

The differential equation for vortex lines has the form

$$\frac{\partial x}{\omega_x} = \frac{\partial y}{\omega_y} = \frac{\partial z}{\omega_z} \tag{3.56}$$

or, in the form of two sets of equations, we can write

$$\omega_y \, \partial x = \omega_x \, \partial y; \quad \omega_z \, \partial y = \omega_y \, \partial z. \tag{3.57}$$

A vortex tube (vortex cord, vortex filament) is a part of the fluid bounded by vortex lines passing through all the points of an infinitely small closed contour in the region occupied by the fluid. The vortex tube is the circulation flux of the fluid of an infinitely small cross section df.

A vortex surface is the surface bounding a vortex tube.

The stress or *the strength* of vortex tubes is twice the product of the angular velocity and the cross-sectional area of the tube:

$$J = 2\omega \, df. \tag{3.58}$$

The most important property of a vortex tube is that the stress along the tube is constant. By analogy with the constancy of the flow rate, we have

$$\omega_1 \, df_1 = \omega_2 \, df_2 = \omega_3 \, df_3, \tag{3.59}$$

or

$$J_1 = J_2 = J_3. \tag{3.60}$$

According to Eq. (3.60), a large angular velocity appears at the smaller section of the tube. Consequently, a vortex tube cannot terminate in the fluid, since a decrease in the tube cross section to zero would mean an infinitely large angular velocity.

Vortex tubes in the limited volume of a fluid terminate at the vessel walls, or at the free surface of the fluid, or form closed vortex rings.

The strength of a vortex tube can also be determined from the velocity circulation. This is similar to the concept of work done by a force in classical mechanics.

Let us consider a point A belonging to a closed contour of length l in a fluid (Fig. 52). Let $\overline{w}$ be the velocity vector of the fluid at A, and K be the tangent to the contour. The angle between the velocity vector $\overline{w}$ and the tangent K is denoted by α. Taking the sum of the products of the projections of the velocity on the corresponding tangent at each point of the closed contour and the element dl of

the length of the contour, we obtain the circulation around a closed contour:

$$\Gamma = \oint_l \overline{w} \cos \alpha \, dl. \tag{3.61}$$

If the angles between the tangent and the coordinate axes are denoted by α_1, β_1, γ_1, and the angles between the direction of the

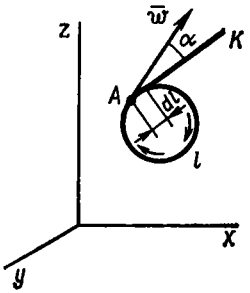

Fig. 52. Illustration of the concept of the velocity circulation.

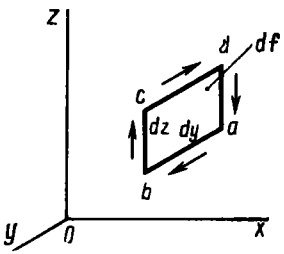

Fig. 53. Circulation around a contour.

velocity and the coordinate axes by α_2, β_2, γ_2, respectively, the following relation holds between these angles and the angle α:

$$\cos \alpha = \cos \alpha_1 \cdot \cos \alpha_2 + \cos \beta_1 \cdot \cos \beta_2 + \cos \gamma_1 \cdot \cos \gamma_2.$$

Let us express the cosines in terms of the velocity, elements of the arc, and their projections onto the coordinate axes:

$$\cos \alpha = \frac{w_x}{w} \cdot \frac{dx}{dl} + \frac{w_y}{w} \cdot \frac{dy}{dl} + \frac{w_z}{w} \cdot \frac{dz}{dl}. \tag{3.62}$$

Substituting this equation into the circulation equation, we get

$$\Gamma = \oint_l (w_x \, dx + w_y \, dy + w_z \, dz). \tag{3.63}$$

This equation is similar to the equation of the sum of elementary works in mechanics, the only difference being that the force is replaced by velocity in Eq. (3.63). Proceeding from this equation, the velocity circulation Γ can be defined as the work performed by the velocity over a closed contour:

$$\Gamma = \oint_l w \, dl. \tag{3.64}$$

In order to establish a relation between the circulation and the strength of a vortex tube, we consider an infinitely small closed contour *abcd* with sides *ab* and *cd* (*dy* and *dz*) inside the liquid (Fig. 53).

We assume that the velocities at the point a (x, y, z) of this contour are w_x, w_y, w_z respectively. The velocities acting on the sides ab and cd are w_y and $-\left(w_y + \frac{\partial w_y}{\partial z} dz\right)$ respectively, and their sum is equal to $\left(-\frac{\partial w_y}{\partial z} dz\right)$. The velocities acting on the sides bc and da are w_z and $-\left(w_z + \frac{\partial w_z}{\partial y} dy\right)$, and their sum is equal to $\left(-\frac{\partial w_z}{\partial y} dy\right)$. In order to obtain an expression for circulation over the total infinitely small contour $abcd$ in accordance with Eq. (3.63), we must sum the products of the velocities and the lengths of individual sides:

$$\Gamma = -\frac{\partial w_y}{\partial z} dz\, dy + \frac{\partial w_z}{\partial y} dy\, dz. \tag{3.65}$$

According to Eq. $(3.50)_3$

$$\frac{\partial w_z}{\partial y} - \frac{\partial w_y}{\partial z} = 2\omega_x.$$

Hence

$$\Gamma = 2\omega_x\, dy\, dz = 2\omega_x\, df. \tag{3.66}$$

But, in accordance with Eq. (3.58),

$$2\omega_x\, df = J.$$

Consequently,

$$\Gamma = J. \tag{3.67}$$

Thus, circulation around a closed contour is equal to the stress of the vortex tube passing through this contour.

A similar relation holds for the intensity and circulation for a contour of any finite dimensions. This is formulated as the Stokes theorem, according to which *the velocity circulation around a closed contour is equal to the sum of stresses of all vortex tubes passing through this contour.*

Since the stress along a tube is constant for a closed contour, the time derivative of circulation is equal to zero:

$$\frac{\partial \Gamma}{\partial \tau} = 0 \tag{3.68}$$

In other words, the circulation around a contour is independent of time (Thomson's theorem). The velocity and cross-sectional area of a vortex tube may change with time, but their product remains constant. In other words, the stress of a vortex tube remains constant during its motion.

The principle of conservation of vortices in an ideal fluid can be formulated as follows: *the fluid mass forming a vortex tube in an ideal fluid moves and continues to be a vortex tube whose strength is constant*

over the entire length, and does not change with time. According to the law of conservation of vortices, *if a vortex exists, it is conserved for ever.* This conclusion, however, is valid only for an ideal fluid. In a real viscous fluid, vortices emerge and die down under the influence of viscosity.

In real fluids, the principle of conservation of vortices turns into the principle of stability of the forms of vortex flow. In all practical cases, vortices have a considerable stability.

The presence of vortices in a fluid leads to the appearance of additional velocities in it, thus increasing the transfer of the substance

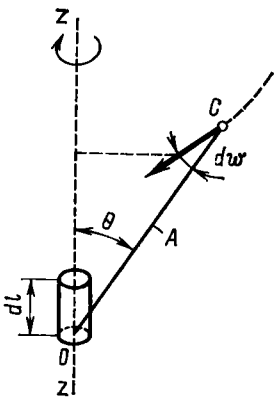

Fig. 54. To the determination of the velocity generated by a vortex.

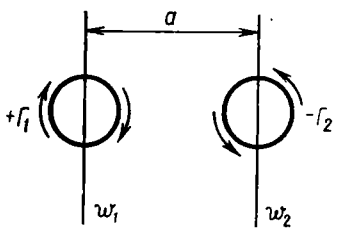

Fig. 55. Interaction of two vortices.

and considerably influencing the nature of mass-transfer processes. We denote by dw the velocity of a fluid at a point C (Fig. 54) due to the action of the elementary vortex segment dl, and by A the distance of this point C from the vortex. Let θ be the angle between the straight line OC and the rotational axis z-z. If the intensity of the vortex tube is equal to J and the velocity circulation is denoted by Γ, the velocities of the motion induced by vortices are calculated in the general case with the help of the equation

$$dw = \frac{\Gamma \sin \theta \, dl}{4\pi A^2}. \qquad (3.69)$$

If several vortices are present, they interact with each other and cause the vortex systems to move in space.

If a second vortex with opposite circulation Γ_2 is located at point C (Fig. 54), the interaction between the two vortices can be represented as in Fig. 55. Taking $dl = 2\pi a$ as the length of the elementary segments of the vortices and $A = a$ as the distance between two vortices for $\theta = 90°$, it can be seen on the basis of Eq. (3.68) that the

first vortex will induce the displacement of the second with a velocity

$$w_1 = \frac{\Gamma_2}{2\pi a}, \tag{3.70}$$

while the second vortex will induce the displacement of the first with a velocity

$$w_2 = \frac{\Gamma_1}{2\pi a}. \tag{3.71}$$

Here, the positive circulation Γ_1 corresponds to the motion in a circle in the clockwise direction.

In the vortex tube region, the entire liquid mass will obtain from the vortex a velocity (Fig. 56) which will have its maximum value

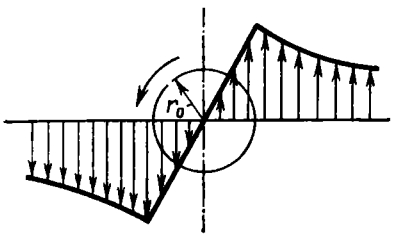

Fig. 56. Velocity field created by a vortex.

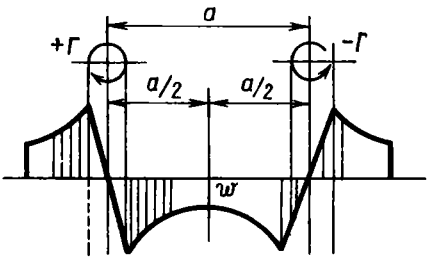

Fig. 57. Velocity field created by two vortices.

on the vortex tube surface of radius r_0, gradually decreasing with increasing distance from the velocity axis. If we have a vortex couple, the velocity distribution in the field of action of this couple will have the form shown in Fig. 57. Under the influence of the velocity

$$w = \frac{P}{2\pi a},$$

of motion caused by a vortex, the vortex couple will move translationally in space along the straight line perpendicular to the shortest segment a connecting the two vortices. If the vortices have different directions, they will move like planets with respect to the common centre. If, however, the vortex couple has the same direction of circulation, the centre of rotation of the couple will be located at the mid-point of the distance between the two.

Mass-transfer processes in industrial systems are often characterized by the flow of fluid past different elements of the apparatus. Hence the motion of vortices formed behind a body as a result of the flow is of practical interest.

For a certain velocity depending on the viscosity and the width of the body in flow, vortices begin to break away behind it alternately to the left and to the right. At a certain distance behind the body,

the vortices are separated by a definite distance between each other. Depending on the shape of the body in the path of the fluid flow, the vortices arrange themselves symmetrically or in staggered patterns (Fig. 58). Vortices in the two rows have opposite directions, i.e. $\Gamma_1 = -\Gamma_2$. The distance h between the rows of vortices (width of the vortex layer) is independent of velocity but depends on the width of the body. A row of vortices is called a vortex chain. The velocity of a vortex chain is:

for a symmetric pattern of vortices

$$w = \frac{\Gamma}{2a} \cot \frac{\pi h}{a}; \quad (3.72)$$

for a staggered pattern of vortices

$$w = \frac{\Gamma}{2a} \tan \frac{\pi h}{a}. \quad (3.73)$$

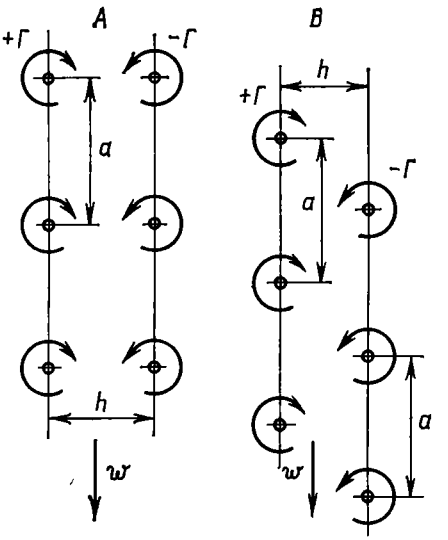

Fig. 58. Arrangement of vortices behind a streamlined body:

A—symmetric arrangement; *B*—staggered arrangement.

The stability condition for vortex chains can be written as follows:

$$\frac{h}{a} = 0.2806. \quad (3.74)$$

Since vortices lead to the appearance of additional velocities in the fluid, these velocities in turn impart a momentum to the fluid. This momentum is determined by the Zhukovskii equation:

$$M = \rho \Gamma a h, \quad (3.75)$$

where M is the momentum, equal to mw; m the mass of the fluid; w the velocity of the fluid; ρ the density of the fluid; Γ the circulation; a the distance between two neighbouring vortices in a chain; and h the width of vortex layers.

Equation (3.75) is the mathematical expression for the Zhukovskii theorem, which states that *the momentum transferred to an infinite layer of fluid by two parallel, rectilinear and continuous vortex layers having finite width, equal stress, and opposite rotation is equal to the product of the density of the fluid, the vortex circulation, separation between vortex layers, and their width.*

This momentum is transferred to the fluid only in the direction of the normal to the plane of vortex layers, or parallel to the layers,

or along their extension. It follows from this theorem that an isolated vortex layer of finite width imparts no momentum to the fluid and does not act on it as a force.

3.1.5. Zhukovskii's Theorem on Lift Force and Direction of Vortex Motion

Let us consider the flow of a fluid past a rotating cylinder. Let a cylinder, rotating in the clockwise direction, be placed in the path of the flow (Fig. 59). On the side of the cylinder where the circular velocity is added to the flow velocity, vortices are either not formed at all, or are very few in number. A region filled with vortices will be created on the diametrically opposite side.

Consequently, the process of fluid flow in this case will not be symmetric. Considering a section of the cylinder normal to the axis, we can see that the flow velocity will be higher above the cylinder than below it. In accordance with Bernoulli's theorem, a higher velocity means a lower pressure and consequently the pressure on top of the cylinder will be reduced while it will be increased underneath the cylinder. This difference in pressure gives rise to a lift force which tends to move the cylinder in a direction perpendicular to the flow. The rotation of the cylinder creates considerable forces perpendicular to the flow, the magnitude of the transverse force depending on the ratio of the flow velocity and the velocity of rotation of the cylinder.

The lift created in a circular cylinder rotating in a flow is a special case of Zhukovskii's theorem; the lift force owes its origin to the velocity circulation around the rotating cylinder.

Denoting the velocity circulation by Γ, the velocity of fluid flow by w, the density of the liquid by ρ, and the length of the cylinder by l, we can write an expression for the lift force:

$$R = \rho \Gamma w l. \qquad (3.76)$$

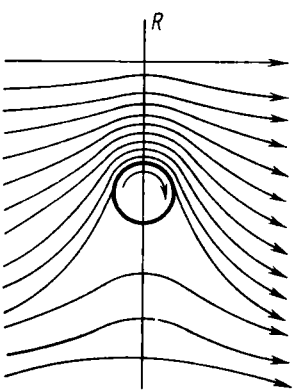

Fig. 59. Flow past a rotating cylinder.

This equation is the mathematical expression for the lift force: *the lift caused by the vortex circulation in a direction perpendicular to the axis of an infinite flow with a velocity w is equal to the product of fluid density, circulation, flow rate, and the length of the cylinder.*

This theorem can be used to determine the lift force of any objects moving in a fluid. Zhukov-

skii worked out the theory of adjoint vortices, the essence of which lies in that streamlined bodies can be replaced by vortices. Hence, it is possible to apply Zhukovskii's theorem to the motion of vortices. The vortex must be subjected to the same force which acted on the solid cylinder, i.e. the Zhukovskii force.

Thus, any vortex moving inside a fluid or subjected to a flow of the fluid past it is always acted upon by a force in the same direction as the Zhukovskii force, i.e. normal to the vortex axis and to the velocity of the flow past the vortex.

The kinetic energy of vortex particles is $mw^2/2$, where m is the mass of the particles and w is the velocity of the layer from which the vortex is formed. A part of this kinetic energy is converted into the kinetic energy of vortex rotation, equal to $I\omega^2/2$, where I is the moment of inertia of the vortex core and ω is the angular velocity of its rotation. If the kinetic energy of the vortex decreases by a certain fraction, the translational velocity of the vortex motion must also decrease, and the vortex must lag behind the layer from which it was formed. The displacement of a vortex relative to the fluid surrounding it must create a Zhukovskii force which will displace the vortices toward points where the velocity is higher, i.e. from the periphery toward the flow axis. If the motion is taking place in a tube, this force will be directed from the tube wall into the fluid. This situation entirely pertains to vortices breaking away from rough walls.

A vortex moving normally to the flow axis is also subjected to friction forces. Hence its path will not be a straight line, but an arc convex toward the flow. Besides, vortices interact and create a certain velocity field in the fluid. Consequently, fluid particles move in complex trajectories. Since vortices are formed in low-velocity layers (i.e. layers close to the wall), they will retard the motion of high-velocity layers upon coming in contact with them. Thus, vortices level out the velocities in the cross section of the flow. This is of paramount importance in mass-transfer processes where the equalization of velocities and concentrations across the flow is a decisive factor.

We can determine the relation between the lift force of a vortex and the drag force encountered by it during its flow. Replacing the velocity circulation (3.76) by the work done by the force on the surface of a vortex filament of diameter d, we get

$$R = C_a l\, d\rho \frac{w^2}{2}, \tag{3.77}$$

where C_a is the lift coefficient which is determined experimentally.

In order to lift or displace a vortex, we must overcome the drag force which is expressed as follows in the case of a fluid flowing

past objects placed in its way:

$$R_d = \zeta l\, d\rho \frac{w_v^2}{2}, \tag{3.78}$$

where ζ is the drag coefficient depending on the Reynolds number Re and ld is the midsectional area of the vortex. Equating the forces

$$C_a l\, d\rho \frac{w_v^2}{2} = \zeta l\, d\rho \frac{w_v^2}{2}, \tag{3.79}$$

we obtain the velocity of an ascending vortex:

$$w_v = \sqrt{\frac{C_a}{\zeta}}\, w \tag{3.80}$$

As a first approximation, we can assume that the smallest vortices will be formed when their inertia forces are balanced by the viscous forces, i.e. when their Reynolds number is equal to unity. For small vortices, when $\mathrm{Re} \leqslant 1$, we get in accordance with Stokes' law

$$\zeta = \frac{C}{\mathrm{Re}}. \tag{3.81}$$

Substituting the value of ζ thus obtained into Eq. (3.80), we get

$$w_v = \sqrt{\frac{C_a}{C}}\, \mathrm{Re}^{0.5}\, w. \tag{3.82}$$

For a quadratic variation of the drag, i.e. for large vortices, $\zeta = \mathrm{const} = C_0$, and the velocity of ascent of the vortex will be

$$w_v = \sqrt{\frac{C_a}{C_0}}\, w. \tag{3.83}$$

In the latter case, the order of magnitude of the ascent velocity can be estimated from the following comparison. The drag coefficient C_0 for a sphere is 0.10-0.30, and for a cylinder, $C_0 = 0.50$-0.60. Judging by Prandtl's experiments, we can state that the coefficient C_a is of the same order of magnitude as C_0. Hence it can be assumed that the velocity w_v will be comparable with the velocity w.

The power of a vortex can be determined from the equation

$$N_v = R_d w_v = C_a l\, d\rho \frac{w^2}{2} \sqrt{\frac{C_a}{C_0}}\, w = C_a \sqrt{\frac{C_a}{C_0}}\, l\, d\rho \frac{w^3}{2} \tag{3.84}$$

Hence the loss of head in the vortex flow of a fluid can be expressed as

$$H_v = \frac{N_v}{V_s \gamma} = \frac{C_a \sqrt{\frac{C_a}{C_0}}\, l\, dw^3}{2V_s g}, \tag{3.85}$$

where V_s is the flow rate of the fluid.

Energy losses in a flow occur each time a vortex rises. When applied to an entire vortex layer with number n of vortices and of surface area ld, located in a tube of length l_t and diameter d_t, the loss of head will be proportional to the area $F = nld_t$ and the ratio l_t/d_t. The loss of head in a vortex layer filling the tube will then be

$$H \approx \frac{C_a}{2}\sqrt{\frac{C_a}{C_0}}\cdot\frac{Fw^2}{V_{sg}}\cdot\frac{l_t}{d_t} \approx \frac{C_a}{2}\sqrt{\frac{C_a}{C_0}}\cdot\frac{w^2 l_t}{gd_t} \qquad (3.86)$$

or, in dimensionless form,

$$\frac{H}{l_t} \approx \frac{C_a}{2}\sqrt{\frac{C_a}{C_0}}\cdot\frac{w^2}{gd_t} \approx \frac{C_a}{2}\sqrt{\frac{C_a}{C_0}}\,\mathrm{Fr}. \qquad (3.87)$$

Equation (3.86) can be easily reduced to the equation for the loss of head:

$$H = \lambda\frac{w^2}{2g}\cdot\frac{l_t}{d_t}, \qquad (3.88)$$

where

$$\lambda = C_a\sqrt{\frac{C_a}{C_0}}.$$

3.1.6. On the Relation Between Vortex Motion and Turbulence

Vorticity Transport. Interaction between vortices may lead to turbulence. When vortices rotating in opposite directions approach each other, they get mutually attracted and coalesce. Merging of vortices results in the appearance of streams of different sizes moving in all directions along random curvilinear trajectories with different velocities. These streams then break up into small vortices and small streamlines which are continuously mixing with each other (turbulent mixing). Thus, when oppositely rotating vortices of different sizes and having different momenta coalesce, turbulence appears at the site of coalescence. The origin and growth of turbulence is shown in Fig. 60.

The length of the vortex coalescence path can be determined by using Taylor's turbulence model. The mixing length will be equal to the mean path covered by a moving vortex until it disappears and loses its identity. This vortex gives away its energy to the flow and transports substance in the mass-transfer process.

Taylor's physical model of turbulence is based on the assumption that the transverse transport of vortices gives rise to turbulent shear stresses in the flow. In the case of molecular transport (laminar flow), only longitudinal transport of mass and energy is observed. On the

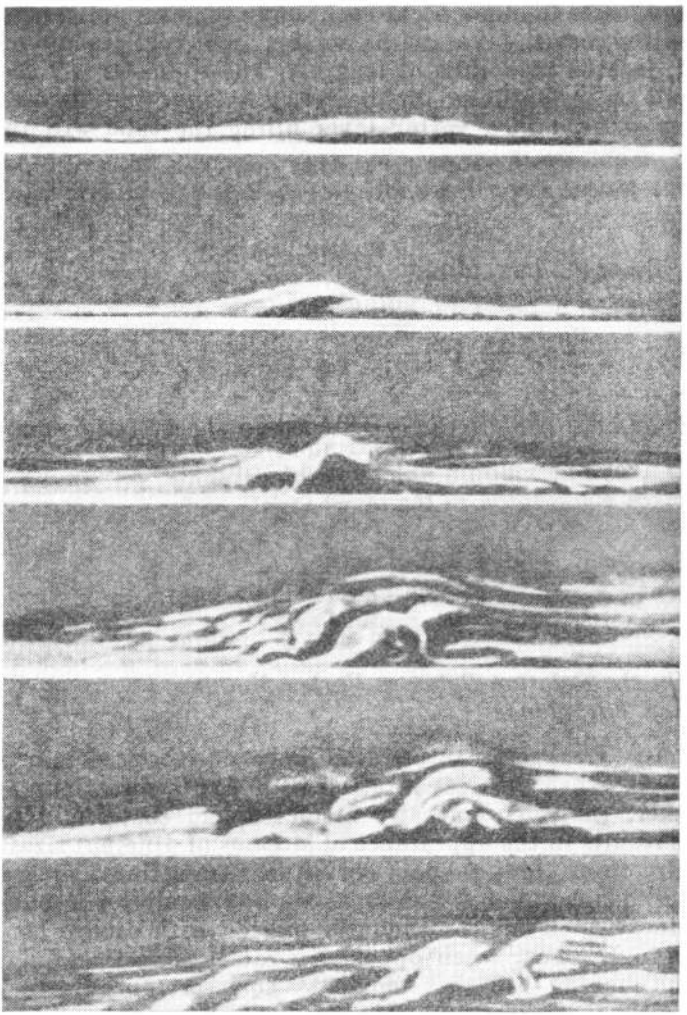

Fig. 60. Origination of turbulence.

other hand, the turbulent flow involves longitudinal as well as transverse transport, thus leading to the appearance of an additional shear stress and, accordingly, to an additional transport of mass (Fig. 61). Thus, for example, suppose that streams a and b move with longitudinal velocities w_{y_1} and w_{y_2} respectively. The difference

$$\Delta w_y = w_{y_1} - w_{y_2}$$

in the velocities results in the appearance of the usual Newtonian shear stress which is expressed by the equation

$$\tau_m = -\mu \frac{dw_y}{dx} = -\rho\nu \frac{dw_y}{dx}. \tag{3.89}$$

In turbulent motion, we have besides a longitudinal motion a transverse motion with velocity w_x. The latter motion is caused by vortices which lead to a tangential (shear) stress τ_t:

$$\tau_t = -\rho\varepsilon_p \frac{dw_y}{dx}, \tag{3.90}$$

where ε_p is the coefficient of vortex viscosity which is not a physical constant but depends on the hydrodynamic conditions of the process, and above all on the velocity of the fluid flow.

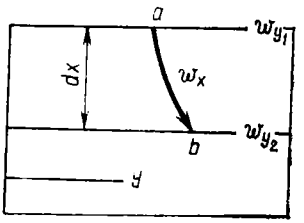

Fig. 61. To the derivation of the equation of vorticity transport.

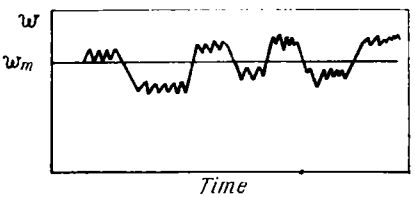

Fig. 62. Velocity fluctuation.

When the molecular and turbulent transports take place simultaneously, the shear stress τ is given by

$$\tau = \tau_m + \tau_t = -\rho(\nu + \varepsilon_p) \frac{dw_y}{dx}. \tag{3.91}$$

The turbulent shear stress can also be obtained from Gromeka's equations directly. For this purpose, we must establish a correlation between ω_x, ω_y, ω_z and the corresponding velocities w_x, w_y, w_z, or between transverse and longitudinal velocities. This correlation can be expressed in the form of the relation (for a single axis)

$$2\omega_z w_x = w_x l \frac{\partial^2 w_y}{\partial x^2}, \tag{3.92}$$

$$-\frac{1}{\rho} \cdot \frac{\partial p}{\partial y} = w_x l \frac{\partial^2 w_y}{\partial x^2}, \tag{3.93}$$

where l is the mixing length on which the vortex ω_z loses its identity by mixing with the liquid and imparting a transverse velocity w_x to its particles.

The turbulent flow results in the appearance of velocity fluctuations, i.e. the velocity oscillates about a certain mean value (Fig. 62).

The instantaneous fluctuation velocity is defined as the difference between the actual and mean velocities:

$$w_{ac} - w_m = \Delta w. \tag{3.94}$$

The instantaneous fluctuation velocity Δw can assume positive as well as negative values. Hence at any instant of time, the velocity w at any point in the turbulent flow is expressed by the relation

$$w = w_m \pm \Delta w. \tag{3.95}$$

The fluctuation is averaged over time and by the mean square law:

$$\overline{\Delta w} = \frac{\sqrt{\Sigma (\Delta w)^2}}{n}, \tag{3.96}$$

where n is the number of terms under the summation sign.

The ratio

$$\frac{\overline{\Delta w}}{w_m} = I_t \tag{3.97}$$

characterizes the turbulence intensity and is a measure of the fluctuations at a point in the flow. The turbulence intensity is usually expressed in percent. Thus, in the boundary turbulent layer, I_t = = 20-30 percent, while in atmospheric air it is just about 0.2 percent. If the velocity fluctuations are identical in all directions, the turbulence is called *isotropic turbulence.*

Besides intensity, turbulence is characterized by its *scale*, which can be expressed in terms of the mixing length.

The time averaging of the quantities appearing in Eq. (3.93) can be presented in the following form:

$$-\frac{1}{\rho} \cdot \frac{\partial P}{\partial y} = \overline{w}_x l \frac{\partial^2 \overline{w}_y}{\partial x^2} \tag{3.98}$$

The transverse fluctuation can be taken equal to

$$w_x = l_1 \frac{\partial w_y}{\partial x}. \tag{3.99}$$

The time-averaged value of $w_x l_1$ gives

$$\overline{w}_x l_1 = -\left| \overline{l l_1} \frac{\partial \overline{w}_y}{\partial x} \right|. \tag{3.100}$$

Introducing this value of $\overline{w}_x l_1$ into Eq. (3.94) and replacing $\overline{l l_1}$ by l_w^2, we get

$$\frac{1}{\rho} \cdot \frac{\partial P}{\partial y} = l_w^2 \left| \frac{\partial \overline{w}_y}{\partial x} \right| \frac{\partial^2 \overline{w}_y}{\partial x^2}. \tag{3.101}$$

Let us now introduce the turbulent shear stress. Considering the relation

$$-\frac{\partial P}{\partial y}+\frac{\partial \tau}{\partial x}=0, \tag{3.102}$$

we can replace the left-hand side of Eq. (3.101) by $(1/\rho)\,(\partial\tau/\partial y)$. This gives

$$\frac{\partial \tau}{\partial x}=\rho l_w^2\left|\frac{\partial \bar{w}_y}{\partial x}\right|\frac{\partial^2 \bar{w}_y}{\partial x^2}. \tag{3.103}$$

Assuming that l_w is independent of x, integration of (3.103) gives

$$\tau=\frac{1}{2}\rho l_w^2\left|\frac{\partial \bar{w}_y}{\partial x}\right|\frac{\partial \bar{w}_y}{\partial x}. \tag{3.104}$$

In order to reduce this equation to a form similar to (3.89), we represent $(1/2)\,l_w^2\,(\partial w_y/\partial x)$ in terms of the vortex viscosity coefficient ε_p. In this case, for a steady flow on the average, we get

$$\tau=\rho\varepsilon_p\frac{\partial w_y}{\partial x}.$$

If the mixing length l is assumed to be equal to the length through which momentum is transported instead of vorticity (Prandtl's turbulence model), the following relation can be established between l_w and l:

$$l_w=\sqrt{2}\,l \tag{3.105}$$

Taylor's model gives a better agreement between experimental and theoretical results for heat and mass transfer, as compared to Prandtl's model.

3.1.7. Free Turbulence. Evolution of Turbulence

Taylor's model proved to be most fruitful in analyzing the so-called free turbulence. Free turbulence corresponds to turbulent flows which are not confined by any walls and, hence, are not limited by any conditions that may appear in the case of rigid walls. The absence of rigid boundaries of the flow precludes the existence of a laminar sublayer. This allows us to ignore the effect of viscosity in all cases of free turbulence and explains the self-similarity of such flows.

The distribution of velocities, temperatures, and concentrations in the case of free turbulence is determined by the constancy of parameters which follows from the principle of corresponding states:

$$\left(\frac{\rho_0}{\rho}\right)^{1/2}\left(\frac{w}{w_0}\right)=\text{const};\quad \frac{\Delta t}{\Delta t_0}=\left(\frac{w_0}{w}\right)^{1/2};\quad \frac{\Delta C_m}{\Delta C_0}=\left(\frac{w_0}{w}\right)^{1/2}. \tag{3.106}$$

In this case, the boundaries of free streams do not suppress turbulent fluctuations, and the normal components of velocity, temperature, and concentrations differ from zero.

Free turbulence is observed during the outflow of streams into an immobile or moving fluid, in the wake of a moving body (or in the trace behind a fixed body streamlined by an infinite flow), and also under certain hydrodynamic conditions in two-phase flows when the molecular transport does not affect the mass-transfer process significantly.

In two-phase flows (gas-liquid, vapour-liquid, liquid-liquid), the hydrodynamic conditions on the free surface that always appears on the interface differ considerably from the hydrodynamic conditions at a rigid boundary (wall). In contrast to the wall, the free surface does not necessarily suppress the turbulent fluctuations. A fully developed free turbulence may appear near the free surface, when the turbulence evolution within each phase involves the free surface into turbulent fluctuations.

The theory of isotropic turbulence was developed by Kolmogorov. According to this theory, the "first-order fluctuations", consisting in random motion of individual volumes of fluid having a diameter of the order of $l' = l$ (where l is the mixing length) relative to each other, are superimposed on the averaged flow. The velocities of these random motions are of the order of $w^{(1)}$. In this case, the first-order fluctuations prove to be unstable at high velocities and are superimposed by the "second-order fluctuations" with the mixing length $l^{(2)} < l^{(1)}$ and the relative velocity $w^{(2)} < w^{(1)}$. This process of successive reduction of turbulent fluctuations continues till the Reynolds number Re

$$\mathrm{Re}^{(n)} = \frac{l^{(n)} w^{(n)}}{\nu} \tag{3.107}$$

characterizing the turbulence of a fluctuation of a sufficiently high order n, becomes sufficiently small. If the effect of viscosity on the nth order fluctuation becomes significant, the $(n + 1)$-order fluctuations will not be superimposed on them.

From the energy point of view, the process of turbulent mixing can be visualized as follows: the first-order fluctuations absorb the energy of a motion and transfer it successively to higher-order fluctuations, while the energy of the smallest fluctuations dissipates in the form of heat on account of viscosity.

Due to the random nature of motion transfer from lower-order to higher-order fluctuations, it is natural to assume that within small (in comparison with $l^{(1)}$) regions of space, small fluctuations of higher orders approximately obey a spatially isotropic statistical distribution. Within small time intervals, this distribution can naturally be treated as a nearly steady-state distribution even if the flow is not stationary as a whole.

At very large Reynolds numbers, the differences in the velocity components at close points are determined exclusively by higher-order fluctuations. This leads to the hypothesis of isotropic turbulence.

The sizes l_s of smallest vortices that constitute a turbulent flow in which the energy of turbulent motion is transformed (dissipates) into heat can be determined from Einstein's equation in the case of isotropic turbulence

$$l_s = \nu^{3/4}\varepsilon^{-1/4}, \tag{3.108}$$

where ν is the kinematic viscosity and ε is the rate of energy dissipation.

Proceeding from Kolmogorov's thesis on isotropic turbulence, we can apply Eq. (3.108) to non-isotropic turbulence as well.

The rate of energy dissipation is determined from the Kármán-Howarth equation

$$\varepsilon \approx 1.65\ (\Delta\bar{w})^3/L_t, \tag{3.109}$$

where $\Delta\bar{w}$ is the fluctuation rate and L_t is the turbulence scale obtained by measuring the correlation coefficient for similar velocities at two points. Combining Eqs. (3.108) and (3.109), we obtain

$$l_s = \left(\frac{L_t}{1.65}\right)^{1/4}\left(\frac{\nu}{\Delta\bar{w}}\right)^{3/4}. \tag{3.110}$$

As a first approximation, we can assume that the smallest vortices will exist when their inertial forces are balanced by viscous forces, i.e. when their Reynolds number is equal to unity:

$$\mathrm{Re} = \frac{\Delta\bar{w}l_s}{\nu} = 1 \tag{3.111}$$

$$l_s \approx \nu/\Delta\bar{w}. \tag{3.112}$$

It follows from the Einstein diffusion equation (3.108) that the time of mixing θ_{mix} of a vortex with the mass of a fluid is

$$\theta_{mix} = \frac{l_s^2}{2D_m}, \tag{3.113}$$

where l_s is the size of the vortex and D_m is the molecular diffusion coefficient.

Equations (3.110), (3.112), and (3.113) make it possible to estimate the minimum time of mixing, i.e. the time required for turbulent mixing to ultimately become molecular.

Table 4 contains the data on the turbulence scale, size of smallest vortices, and the minimum time of mixing for carbon dioxide diffusing into gases and liquids in a turbulent flow at 1 atm and 15 °C. It follows from the table that despite the difference in the values of the kinematic viscosities of gases and liquids, the smallest vortices

Table 4

Basic Mixing Parameters for CO_2 Diffusing into Various Media (15°C, 9.8×10^4 Pa (1 atm))

Medium	Kinematic viscosity ν, m^2/s	Molecular diffusion coefficient of CO_2 D_m, m^2/s	Turbulence scale L_t, m	Fluctuation rate $\Delta\overline{w}$, m/s	Smallest vortex size l_s, mm		Minimum mixing time for CO_2 θ_{mix}, s
					Eq. (3.110)	Eq. (3.112)	
Air	14.6×10^{-6}	0.14×10^{-4}	0.061 0.61	0.305 1.22 1.22 3.05	0.25 0.09 0.16 0.08	0.05 0.012 0.012 0.005	0.0020 0.0002 0.0008 0.0002
Hydrogen	102.5×10^{-6}	0.606×10^{-4}	0.061	0.305 1.22	1.10 0.30	0.34 0.08	0.0098 0.0012
Water	1.141×10^{-6}	1.59×10^{-8}	0.0305 0.061	0.0305 0.122 0.0305 0.122	0.16 0.06 0.19 0.07	0.03 0.008 0.03 0.008	7.67 0.96 10.85 1.36
Ethyl alcohol	1.625×10^{-6}	0.32×10^{-10}	0.0305	0.0305 0.122	0.24 0.08	0.05 0.014	17.17 2.12

in them are comparable in size. However, due to the lower values of molecular diffusion coefficients in liquids, the time of mixing in them is larger than in the case of diffusion in gases.

3.1.8. Similarity Principle as the Basis for Physical Modelling of Single-Phase Systems

The similarity principle makes it possible to single out a group of similar phenomena from the class of phenomena described by differential equations by reducing them to the dimensionless form.

Similarity of phenomena. The phenomena for which the ratios of their characteristic quantities remain constant at any point of space are called similar. In this case the similarity is called *complete.* If, however, the similarity is observed only for some quantities, it is called *partial.*

Since any process occurs within a certain geometrical contour, it is necessary to establish *the geometrical similarity* first, and then *the physical similarity* characterizing a given process.

Geometrical similarity. The simplest idea about the geometrical similarity of two figures is known from geometry. If the linear dimensions of a figure are considered not only as scalar quantities but also as quantities having a certain direction, similar figures must be arranged in space so that their corresponding elements be parallel to each other.

The ratio of corresponding dimensions of a model and a prototype is called *the scale of the model.* Having taken a linear dimension l_m of the model and dividing it by the corresponding dimension l_p of the prototype, we obtain the linear scale of the model:

$$a_l = \frac{l_m}{l_p}. \tag{3.114}$$

For example, if we consider two vessels with agitators, whose diameters are D_1 and D_2 respectively, the heights of the layers of mixed liquids are H_1 and H_2, and the diameters of agitator blades are d_{a_1} and d_{a_2}, their heights being h_{a_1} and h_{a_2}. For these apparatus to be similar, the following equalities must be observed:

$$a_D = \frac{D_1}{D_2}, \quad a_H = \frac{H_1}{H_2}, \quad a_d = \frac{d_{a_1}}{d_{a_2}}, \quad a_h = \frac{h_{a_1}}{h_{a_2}}. \tag{3.115}$$

For geometrical similarity, we have

$$a_D = a_H = a_d = a_h. \tag{3.116}$$

It is more convenient, however, to express the geometrical similarity of the apparatus by introducing a *characteristic geometrical dimension.* Thus, if in the model of the apparatus with an agitator under

consideration we take the diameter d_a of the agitator blade as the characteristic dimension and compare with it all the basic dimensions for the given model,

$$\frac{D_1}{d_{a_1}} = i_D, \quad \frac{H_1}{d_{a_1}} = i_H, \quad \frac{h_{a_1}}{d_{a_1}} = i_h, \tag{3.117}$$

the geometrical similarity will be observed if in any apparatus with the same characteristic dimension the values of the dimensionless ratios i_D, i_H, i_h are the same, i.e.

$$i_D = \frac{D_2}{d_{a_2}} = \frac{D_1}{d_{a_1}}, \quad \frac{H_2}{d_{a_2}} = \frac{H_1}{d_{a_1}} = i_H, \quad \frac{h_2}{h_{a_2}} = \frac{h_1}{d_{a_1}} = i_h. \tag{3.118}$$

The dimensionless ratios i_D, i_H, i_h, etc., which have the same values for the model and the prototype, are called *the invariants of geometrical similarity.*

Thus, geometrical similarity is observed when the geometrical similarity invariants have the same values, i.e.

$$i_D = \text{idem}, \quad i_H = \text{idem}, \quad i_h = \text{idem}. \tag{3.119}$$

The geometrical similarity invariants may numerically differ from one another. The fact that similarity invariants are dimensionless makes it possible to apply the conditions of geometrical similarity to apparatus of any size, provided that the ratio of a given dimension to the characteristic dimension satisfy equality (3.118). For flows in pipes, channels, or industrial apparatus, the equivalent diameter d_e is taken as the characteristic dimension (for round tubes, d_e coincides with the tube diameter).

Physical similarity. In analogy with geometrical similarity, physical similarity is observed when its invariants are the same in the systems being compared.

Just as the geometrical similarity invariants, the physical similarity invariants must be dimensionless quantities. But since a physical phenomenon is characterized by a number of physical quantities (velocity, density, viscosity, etc.), the main objective of the similarity method is to compose the dimensionless ratios of these quantities.

This problem can be solved in two ways: (1) by the similarity transformation of differential equations to the dimensionless form, and (2) by means of dimensional analysis.

Similarity transformation of differential equations to the dimensionless form. Using the equation of motion of a viscous fluid as an example, we can show how such a transformation of differential equations to the dimensionless form can be realized. For this purpose, we write the system of equations (3.40) for a one-dimensional steady-state flow relative to the z-axis:

$$-\gamma - \frac{\partial P_z}{\partial z} + \mu \frac{\partial^2 w_z}{\partial z^2} = \rho \frac{dw_z}{d\tau}. \tag{3.120}$$

We multiply all the terms of this equation by dz, which is equivalent to the change of all the parameters over the distance dz:

$$-\gamma\, dz - \frac{\partial P_z}{\partial z}\, dz + \mu\, \frac{\partial^2 w_z}{\partial z^2}\, dz = \rho\, \frac{dw_z}{d\tau}\, dz = \rho w_z\, dw_z. \quad (3.121)$$

This equation is a mathematical model of a flowing viscous fluid having the inertial force $\rho w_z\, dw_z$ and moving under the action of the gravity force $\gamma\, dz$, forces of pressure $(\partial P_z/\partial z)\, dz$, and forces of friction $\mu\, (\partial^2 w_z/\partial z^2)\, dz$. The forces in Eq. (3.121) are referred to unit volume and act over the distance dz.

In analogy with the concept of geometrical similarity invariants, we compare all the acting forces with the inertial force. The ratio of these forces to the inertial force (or vice versa) must lead to dimensionless ratios. Let us replace the differential expressions by finite ones:

inertial force $\rho w_z\, dw_z \sim \rho w^2$, (3.122)

gravity force $\gamma\, dz \sim \gamma l$, (3.123)

pressure force $\frac{\partial P_z}{\partial z}\, dz \sim \Delta P$, (3.124)

friction force $\mu \frac{\partial^2 w_z}{\partial z^2}\, dz \sim \mu\, \frac{w}{l^2}\, l \sim \mu\, \frac{w}{l}$. (3.125)

Taking the ratio of inertial forces to the force of gravity, we obtain

$$\frac{\text{inertial force}}{\text{gravity force}} = \frac{\rho w^2}{\gamma l} = \frac{w^2}{gl}. \quad (3.126)$$

If the dimensionless term (3.126) remains the same in the compared systems of flowing fluids, i.e. if

$$\frac{w_1^2}{gl_1} = \frac{w_2^2}{gl_2} = \frac{w_3^2}{gl_3} = \ldots = \frac{w^2}{gl} = \text{idem}, \quad (3.127)$$

this term is the physical similarity invariant with respect to the action of forces of gravity and is called the Froude number:

$$\frac{w^2}{gl} = \mathrm{Fr} = N_{\mathrm{Fr}}. \quad (3.128)$$

Taking the ratio of pressure forces to the inertial force, we obtain

$$\frac{\text{pressure force}}{\text{inertial force}} = \frac{\Delta P}{\rho w^2}. \quad (3.129)$$

If the dimensionless term (3.129) remains the same in the compared systems of flowing fluids, i.e. if

$$\frac{\Delta P_1}{\rho_1 w_1^2} = \frac{\Delta P_2}{\rho_2 w_2^2} = \frac{\Delta P_3}{\rho_3 w_3^2} = \ldots = \frac{\Delta P}{\rho w^2} = \text{idem}. \quad (3.130)$$

This term is called the physical similarity invariant with respect to the action of pressure forces, and is called the Euler number:

$$\frac{\Delta P}{\rho w^2} = \mathrm{Eu} = N_{\mathrm{Eu}}. \tag{3.131}$$

Finally, by taking the ratio of inertial force to the friction force, we obtain

$$\frac{\text{inertial force}}{\text{friction force}} = \frac{\rho w^2}{\mu w/l} = \frac{\rho w l}{\mu}. \tag{3.132}$$

If the dimensionless term (3.132) remains the same in the compared systems of flowing fluids, i.e. if

$$\frac{\rho_1 w_1 l_1}{\mu_1} = \frac{\rho_2 w_2 l_2}{\mu_2} = \frac{\rho_3 w_3 l_3}{\mu_3} = \ldots = \frac{\rho w l}{\mu} = \text{idem}, \tag{3.133}$$

this term is called the physical similarity invariant with respect to the action of the forces of internal friction or forces of molecular viscosity, and is called the Reynolds number:

$$\frac{\rho w l}{\mu} = \mathrm{Re} = N_{\mathrm{Re}}, \tag{3.134}$$

Since the ratio of the viscosity of a fluid to its density $\mu/\rho = \nu$ is the kinematic viscosity, the Reynolds number can be represented as follows:

$$N_{\mathrm{Re}} = \mathrm{Re} = \frac{wl}{\nu}. \tag{3.135}$$

Thus, the transformation performed permits the replacement of the differential equation of motion by the equation in terms of dimensionless numbers in the form of the function

$$f(\mathrm{Fr}, \mathrm{Eu}, \mathrm{Re}) = f(N_{\mathrm{Fr}}, N_{\mathrm{Eu}}, N_{\mathrm{Re}}). \tag{3.136}$$

The form of the functional dependence in (3.136) can only be established by experiment.*

The representation of equations connecting the parameters in the dimensionless form broadens the possibility of their application to a wide class of physical phenomena, i.e. makes it possible to use the basic mathematical principle of isomorphism. This principle con-

* Equations of the type (3.136) are also called "criterion" equations, while the dimensionless terms are called the "similarity criteria". In order that equations of the type (3.136) express the relation between similarity criteria, it is necessary to establish strict analytical dependences between the parameters of the process under investigation instead of simply reducing the equation to a dimensionless form. For this reason, dimensionless terms appearing in Eq. (3.136) should be called the corresponding dimensionless numbers rather than similarity criteria.

sists in the extension of functional dependences to a broad class of problems of mathematical description of the processes occurring in apparatus of various dimensions with various physical parameters while retaining the invariance of dimensionless groups. Thus, equations of the type (3.136) permit the scaling transformation of phenomena and processes under consideration and the realization of physical similarity or physical simulation.

Basic principles of dimensional analysis. The dimensional analysis of the physical quantities characterizing a given phenomenon makes it possible to construct dimensionless groups and obtain the equations in the form similar to (3.136). This method is used when the phenomenon is studied insufficiently and cannot be described by a differential equation.

Dimensional analysis permits the reduction of the most general functional dependence to a strictly definite number of dimensionless groups of physical quantities, and in the presence of similarity, to a strictly definite number of similarity invariants. This method is based on the concept of the dimensions of a physical quantity, which means the representation of this quantity as a function of basic units of measurement.

The basic units of measurement are the units of length L, units of time T, units of mass M, etc. Thus, the dimensions of the velocity w can be represented in the form of the dimensional formula

$$w = \left[\frac{L}{T}\right] = [LT^{-1}].$$

The concept of dimensions of physical quantities allows us to represent them in the form of exponential equations. If the principle of homogeneity is observed in equations relating the physical quantities, such equations can also be represented as exponential equations in the basic units of measurement, the form of the dependence remaining the same for different scales of the units involved.

The number of dimensionless groups which can be obtained from a given functional dependence is established with the help of the π-theorem: if n physical quantities characterizing the process and expressed through m basic units of measurement appear in the functional dependence of the most general form, this dependence can be reduced to $(n - m)$ dimensionless ratios, the so-called π-ratios.

The reduction of the initial functional relations of the most general form to a relation between dimensionless π-groups can be illustrated with the help of the following example. Suppose that on the basis of experimental measurements it is established that the drag force R of a body moving near the free surface of a viscous fluid depends on the quantities

$$R = f(l, w, \rho, \mu, g),$$

where R is the drag force, N; l the linear dimension of the body, m; w the velocity of the fluid, m/s; ρ the fluid density, kg/m^3; μ the viscosity, Pa·s; and g the acceleration due to gravity, m/s^2.

Let us write the dimensions of the quantities appearing in the initial dependence in the form of dimensional formulas:

$$[R] = [\mathrm{N}] = [LMT^{-2}], \qquad [l] = [\mathrm{m}] = [L],$$
$$[w] = [\mathrm{m/s}] = [LT^{-1}], \qquad [\rho] = [\mathrm{kg \cdot m^3}] = [ML^{-3}],$$
$$[\mu] = [\mathrm{Pa \cdot s}] = [L^{-1}MT^{-1}], \qquad [g] = [\mathrm{m/s^2}] = [LT^{-2}].$$

We substitute the dimensional formulas of the corresponding physical quantities into the initial dependence and express this dependence in the form of an exponential equation with a constant coefficient a and exponents:

$$[LMT^{-2}] = a\,[L]^x\,[LT^{-1}]^y\,[ML^{-3}]^z\,[L^{-1}MT^{-1}]^p\,[LT^{-2}]^q$$

whence

$$[LMT^{-2}] = aL^{x+y-3z-p+q}T^{-y-p-2q}M^{z+p}. \tag{3.137}$$

Comparing the exponents of like bases on the left- and right-hand sides of this equation, we obtain three equations in five variables:

$$x + y - 3z - p + q = 1,$$
$$y + p + 2q = 2,$$
$$z + p = 1.$$

On the basis of the π-theorem we find that for the number $n = 6$ of the physical quantities that can be expressed in terms of the three basic units of measurement (M, L, T), i.e. $m = 3$, the initial functional dependence can be reduced to three dimensionless relations. Accordingly, we solve the obtained system of three equations in the three variables x, y, z, assuming that p and q are given. This gives

$$z = 1 - p,$$
$$y = 2 - p - 2q,$$
$$x = 2 - p + q.$$

Substituting the exponents into the exponential equation, we get

$$R = al^{2-p+q}\,w^{2-p-2q}\rho^{1-p}\mu^p g^q.$$

Regrouping the factors, combining the quantities with like exponents and considering that $R/l^2 = \Delta P$, we obtain the formula for the drag force in the form of the dimensionless equation

$$\frac{\Delta P}{\rho w^2} = a\left(\frac{wl\rho}{\mu}\right)^{-p}\left(\frac{w^2}{gl}\right)^{-q}.$$

Considering that $\Delta P/\rho w^2$ is the Euler number, $wl\rho/\mu$ is the Reynolds number, w^2/gl is the Froude number and a is the dimensionless proportionality factor, we obtain

$$\mathrm{Eu} = a\,\mathrm{Re}^{-p}\,\mathrm{Fr}^{-q}.$$

Thus, in the case of similarity the dimensional analysis makes it possible to obtain exponential equations from dimensionless numbers which are identical to similarity invariants. Using the dimensionality principle, we can find the relations between physical quantities expressed through dimensionless groups only if we know all the quantities involved in this relation. For this reason, the dimensionality method alone may be insufficient for determining the relations between physical quantities, and a good understanding of the essence of the process is required.

Usually, the relations (3.136) between similarity invariants are represented in the form of exponential equations. In this case, the experimental points are plotted in logarithmic coordinates, which gives the plots of the dependences in the form of straight lines. The position of the straight line near which the experimental points are concentrated is determined by the least squares method. The slope of the obtained straight line expresses the exponent n of the characterizing dimensionless group, while the intercept represents the proportionality factor or coefficient A in the exponential equation

$$\lambda = A\mathrm{Re}^{-n} \tag{3.138}$$

The proportionality coefficient A, however, is usually determined not only by the intercept; a number of values of Re are preset for the obtained exponent n, and the corresponding values of Re^{-n} are calculated. The corresponding number of values of λ are taken from the plot for the given values of Re, and the exponential equation is solved for A:

$$A = \frac{\lambda}{\mathrm{Re}^{-n}} = \lambda\mathrm{Re}^{n} \tag{3.139}$$

If a vertical or horizontal region appears on the curve representing the relation between dimensionless groups, this indicates the appearance of the so-called self-similarity regime. For example, the self-similarity regime sets in in rough pipes for large Reynolds numbers, the drag coefficient becoming a constant (λ = const) independent of Re.

The self-similarity regime may appear in different processes. Self-similarity can be characterized by the independence of the process of any parameter, i.e. it can be self-similar in the sense of being independent of the linear dimensions of the system, of some physical properties of the system, and so on. For example, the emulsifying regime in packed columns is self-similar in the sense that it is independent of the molecular characteristics of the process such as

molecular viscosity or molecular diffusion. The distribution of the liquid over the cross section of the packed column in the emulsifying regime becomes self-similar since it is independent of the column diameter. The self-similarity conditions, i.e. the elimination of the effect of one or several parameters on the process, considerably simplify the task of modelling the process as a whole (for example, the modelling of rectification in packed emulsifying columns). The so-called flooding regime in diffusion apparatus is a self-similar regime of two-phase systems.

In physical modelling, a given phenomenon is investigated during its reproduction on different scales and by analyzing the effects of physical properties and linear dimensions. An experiment is carried out directly for the physical process under consideration. Experimental results are represented in the form of dimensionless groups obtained by combining different physical quantities and linear dimensions.

Physical modelling is reduced to the reproduction of constant characteristic dimensionless groups in the model and the prototype. Practically, this means that the physical process under investigation must be reproduced in several stages, i.e. we must go over from smaller scales of realization of a given physical process to larger scales. Thus, the physical model is deformed directly in the physical process itself. Such an approach requires the reproduction of the physical process on a larger and larger scale (up to industrial scale).

When applied to comparatively simple systems such as hydraulic or thermal systems with a single-phase flow, the similarity principle and physical modelling are justified since they operate with a limited number of parameters. For complex systems and processes described by a complex system of equations with a large set of dimensionless groups which become incompatible when used simultaneously, the application of physical modelling is associated with considerable difficulties. It becomes impossible to construct dimensionless groups which would take into account the large number of phases incorporated in the system. Therefore, equations of the type (3.136) give good results when applied for the treatment of experimental data only for single-phase systems. The attempts to replace the description of two-phase systems by introducing dimensionless groups obtained for each phase separately are not substantiated scientifically, since in this case the interaction between the phases is not taken into account.

At present, the methods of physical modelling have acquired a new quality: they can be used for determining the deformation limits for the coefficients appearing in the equations of a mathematical model and thus permit the scaling of the mathematically described process and establish the adequacy of the model for the object under investigation.

3.1.9. Resistance Law for a Single-Phase Flow

The resistance offered to the steady flow of a viscous fluid is investigated with the help of the equation

$$\mathrm{Eu} = f(\mathrm{Re}).$$

In order to analyze the resistance appearing in pipes and apparatus, the geometrical similarity invariant l/d_e is introduced in addition, where l is the length of the pipe (channel) and d_e is the characteristic dimension (equivalent diameter):

$$\mathrm{Eu} = f_0\left[(\mathrm{Re})\frac{l}{d_e}\right]. \tag{3.140}$$

This equation expresses the resistance law in pipes and apparatus, and can be reduced to a form convenient for calculations. For this purpose, we express the numbers Eu and Re in terms of corresponding physical quantities:

$$\frac{\Delta P}{\rho w^2} = f_0\left(\frac{wd}{\nu}\right)\frac{l}{d_e}, \tag{3.141}$$

or

$$\Delta P = 2f_0\left(\frac{wd}{\nu}\right)\frac{l}{d_e}\frac{w^2\rho}{2}. \tag{3.142}$$

Introducing the specific gravity instead of density ($\gamma = g\rho$) and the function $2f_0\,(wd/\nu) = f\,(wd/\nu)$ into Eq. (3.142), we can reduce it to the form

$$\Delta P = f\left(\frac{wd}{\nu}\right)\frac{l}{d_e}\cdot\frac{w^2\gamma}{2g}. \tag{3.143}$$

Denoting $f\,(wd/\nu) = \lambda$, we obtain

$$\Delta P = \lambda\frac{l}{d_e}\frac{w^2\gamma}{2g}. \tag{3.144}$$

The dimensionless quantity λ in this equation is called the coefficient of external friction. Combining the two dimensionless quantities λ and l/d_e into one (the so-called friction coefficient ζ), we obtain the pressure drop due to friction in terms of the velocity, or dynamic, head:

$$\Delta P = \zeta\frac{w^2\gamma}{2g}, \tag{3.145}$$

where

$$\zeta = \lambda\frac{l}{d_e}. \tag{3.146}$$

Equations of the form (3.145) or (3.146) were previously obtained on the basis of Zhukovskii's theorem (see p. 114).

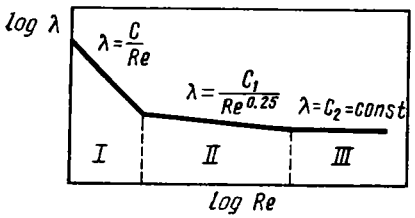

Fig. 63. The friction coefficient λ as a function of Re.

The resistance law in the form of Eqs. (3.145), (3.146) is widely used in engineering calculations. It is essential in calculations to determine the form of the dependence

$$\lambda = f(\mathrm{Re}). \qquad (3.147)$$

The form of this function depends on the nature of the fluid flow. For small flow velocities and a strong effect of molecular viscosity, the quantity λ strongly depends on the number Re, and the relation

$$\lambda = C/\mathrm{Re} \qquad (3.148)$$

remains valid.

If the exponent of the Reynolds number is equal to unity, this law governs the laminar flow of fluids in pipes and the motion of small-size bodies in the flow of fluids (Stokes' settling law). The weaker the effect of molecular viscosity on the pattern of the fluid flow, the smaller the exponent of Re; and the smaller the exponent of Re, the more intensive the turbulence. For example, for a turbulent flow in pipes, Eq. (3.147) becomes

$$\lambda = \frac{C_1}{\mathrm{Re}^{0.25}}. \qquad (3.149)$$

In the limiting case, the exponent of Re may turn out to become zero. In this case, the flow regime does not depend on Re, i.e. it is independent of the effect of molecular viscosity. Such a regime is called *self-similar*; it is the regime of developed turbulence. Self-similar regime sets in in rough pipes during the settling of bodies of a sufficiently large size and having high velocity (Newton's settling law), during a high-speed rotation of bodies (stirrers) in fluids, and so on.

Thus, the exponent of the Reynolds number may vary between 1 and 0 depending on hydrodynamic regime.

A graphic representation of this dependence (Fig. 63) shows that three hydrodynamic regimes* can be realized in principle in a single-phase flow: (1) regime I—laminar flow with the predominant influence of molecular viscosity; (2) regime II—turbulent flow with a relatively weak effect of molecular viscosity; and (3) regime III—the regime of fully developed turbulence (self-similar regime), where molecular viscosity has no effect. Accordingly, in compliance with

* An additional, intermediate regime may appear upon a transition from laminar to turbulent flow.

Eq. (3.144) and Fig. 63, the pressure drop in a single-phase flow depends on the flow velocity in the following way:

I—laminar regime $\Delta P \propto w$;
II—turbulent regime $\Delta P \propto w^{1.75}$;
III—regime of fully developed turbulence $\Delta P \propto w^2$.

3.2 Model Concepts about the Flow Structure (Distribution of Flow Particles in Space and Time)

In order to calculate the processes of mass transfer and the extent of their completion, we must know the time distribution of flow particles in an apparatus, since certain fractions of the flow may be settled in the apparatus, while some others may get through depending on the time of contact and diffusion.

The time distribution for flow particles in the apparatus is stochastic and can be estimated by a statistical distribution.

The most significant sources of non-uniformity in the time distribution of flow elements in industrial apparatus are (1) the non-uniformity in the velocity distribution of the system; (2) turbulization of flows; (3) molecular diffusion; (4) the presence of stagnant regions in the flow; (5) channel formation, by-passing and cross currents in the system; (6) temperature gradients of moving media; (7) heat- and mass exchange between phases; etc.

The enumerated reasons existing in industrial apparatus and operating in various combinations stipulate a specific nature of non-uniformities in each concrete case. In order to estimate flow non-uniformities, a number of the so-called distribution functions are introduced, each of which is a result of the establishment of the one-to-one correspondence between an arbitrary flow particle and a certain time interval typical of this particle.

It may turn out that the actual duration of stay of flow particles in the apparatus is insufficient for diffusion processes to be realized. This circumstance determines the effectiveness of diffusion process as a whole. For this reason, model concepts about the internal structure of flows are widely used at present for the mathematical description of intricate processes. On the one hand, this facilitates the formulation of the boundary conditions for the equation, and on the other, makes it possible to plan certain experimental investigations required for determining the parameters of the equation of motion.

The description of the flow structure is also essential for mass-transfer processes since it permits the establishment of the nature of motion and distribution of substances in these flows. Hence, all hydrodynamic flow models will be written normally in the form of equations describing the variation of concentration of a substance in the flow.

Mathematically, flow structure models are usually described in the form of differential equations. The coefficients of mathematical models are called the model parameters. Unknown model parameters are determined experimentally. An indicator (perturbation) is introduced into an apparatus at the flow entrance, and the response function of the flow is determined at the exit. Pulsed or step perturbations are the ones most frequently used, and the response functions are denoted by $C(\tau)$ and $F(\tau)$ respectively.

If the adopted model corresponds to the actual flow structure, the experimental response function may be considered as the plot of the solution of the model equation under appropriate initial and boundary conditions. By comparing the solution with the experimental response function for a typical perturbation, we can determine the unknown model parameters.

The variety of interacting diffusion and heat flows can be formalized, in view of the stay time distribution, in the form of typical mathematical models such as the model of ideal mixing, of ideal displacement, cell model, diffusion model, and hybrid model.

The model of ideal mixing. The conditions of physical realization of this model are satisfied if a complete (ideal) mixing of flow particles occurs in the entire flow or in its region under consideration. At the entrance into the region of an ideal mixing cell, the substance is instantaneously distributed over the entire volume of this cell. The equation describing the change in the concentration in the ideal mixing region has the form

$$V_a \frac{dC}{d\tau} = V(C_0 - C), \tag{3.150}$$

where V_a is the volume of the ideal mixing region; V is the volume velocity of the flow entering and leaving the region of ideal mixing; C_0, C are the substance concentrations at the exit and in the ideal mixing region; and τ is the time.

In chemical engineering, conditions close to ideal mixing are often created by introducing special stirrers, reflecting partitions, etc. into the apparatus.

The concentration in the ideal mixing region, and hence at the exit from this region, can be calculated for any instant of time with the help of the equation

$$C(\theta) = C/C_0 = e^{-\theta}, \tag{3.151}$$

where $\theta = \tau V/V_a$ is the dimensionless time.

The model of ideal displacement. The conditions of physical realization of this model are satisfied for a plug flow, when it is assumed that there is absolutely no mixing in the direction of the flow, while ideal mixing takes place in the transverse direction. The equation describing the change in the concentration in the region of ideal dis-

placement has the form

$$\frac{\partial C}{\partial \tau} = -w\frac{\partial C}{\partial x}, \qquad (3.152)$$

where $w = V/F$ is the linear flow velocity.

The ideal displacement model is employed in chemical engineering for describing the apparatus operating on the displacement principle, such as the columns with a large length-to-diameter ratio or packed columns in emulsifying regime. The advantages of this model are the relative simplicity of the solution of equation in the mathematical description and an acceptable accuracy of the reproduction of real hydrodynamic conditions in many cases.

Equation (3.152) contains two variables: time τ and the length l, i.e. $C = C(x, \tau)$. Its solution under the initial conditions

$$C(x, 0) = C_0, \quad 0 \leqslant x \leqslant l, \qquad (3.153)$$

and the boundary condition

$$C(0, \tau) = C_0(\tau), \ \tau > 0, \qquad (3.154)$$

has the form

$$C(x, \tau) = \begin{cases} C_0, & \tau < \frac{x}{w}, \\ C_0\left(\tau - \frac{l}{w}\right), & \tau > \frac{x}{w}, \end{cases} \qquad (3.155)$$

where l is the length of the ideal displacement region.

Any change in the concentration at the entrance of the ideal displacement region appears at its exit after a lapse of time

$$\tau = \frac{l}{w} = \frac{lF}{wF} = \frac{V_a}{V}. \qquad (3.156)$$

The cell model. The physical essence of the cell model consists in that the flow is split into a number of cells connected in series. It is assumed that ideal mixing of the flow occurs within each of these cells, while the mixing between the cells is absent. The number n of such ideal cells is a parameter characterizing the model of the actual flow. For $n = 1$, the model characterizes ideal mixing, while for $n = \infty$, it corresponds to ideal displacement.

Provided that the volumes of all cells are equal and their sum is equal to the volume of the apparatus, and the volume flow velocity is constant, the cell model is described by the system of equations

$$\frac{dC_i}{d\tau} = \frac{V}{V_a}(C_{i-1} - C_i), \quad i = 1, 2, 3, \ldots . \qquad (3.157)$$

The solution of this system of equations for different initial conditions and different types of perturbations applied at the entrance has the form:

pulsed perturbation

$$C(\theta) = \frac{C}{C_0} = \frac{n^n \theta^{n-1}}{(n-1)!} \exp(-n\theta), \qquad (3.158)$$

step perturbation

$$F(\theta) = \left[1 + n\theta + \frac{n^2\theta}{1\times 2} + \ldots + \frac{n^{n-1}\theta^{n-1}}{(n-1)!} \exp(-n\theta)\right]. \qquad (3.159)$$

The diffusion model. There exist one- and two-parametric diffusion models.

One-parametric model. This model is based on the displacement model complicated by reverse mixing obeying the formal diffusion law. The parameter characterizing the model is the turbulent diffusion coefficient, or the coefficient of longitudinal mixing D_L. While constructing a one-parametric diffusion model, the following assumptions are made: the change in the concentration of a substance is a continuous function of the coordinate (distance); the substance concentration is constant in a given cross section, and the volume flow velocity and the coefficient of longitudinal mixing are constant over the length and cross section of the flow.

Under these assumptions, the model is described by the equation

$$\frac{\partial C}{\partial \tau} = -w\frac{\partial C}{\partial x} + D_L \frac{\partial^2 C}{\partial x^2}. \qquad (3.160)$$

This equation differs from Eq. (3.152) in the additional term $D_L\, \partial^2 C/\partial x^2$ which takes into account turbulent diffusion and mixing. The quantity D_L is determined experimentally.

Two-parametric model. This model takes into account the mixing of a flow in the longitudinal and radial directions and is characterized by the coefficients of the longitudinal (D_L) and radial (D_R) mixing. It is assumed that the quantities D_L and D_R are invariable over the length and cross section of the apparatus, and the flow velocity is constant.

For the flow in a cylindrical apparatus of radius R with a constant velocity over the length and cross section, the equation of the two-parametric model has the form

$$\frac{\partial C}{\partial \tau} = -w\frac{\partial C}{\partial x} + D_L \frac{\partial^2 C}{\partial x^2} + \frac{D_R}{R}\frac{\partial}{\partial R}\left(R\frac{\partial C}{\partial R}\right). \qquad (3.161)$$

When the coefficients D_L and D_R of the longitudinal and radial mixing are determined experimentally, they are usually represented in the form of dimensionless groups, viz. the Peclet numbers: $Pe = wL/D_L$ or $Pe_R = wL/D_R$, where L is the characteristic linear dimension of the system. In this case, the equation of the diffusion model is also reduced to the dimensionless form. For this purpose, the dimensionless length $x/L = z$ and the time $\tau = L/w = V/V_v$

are introduced, where V is the volume of the system and V_v the volume velocity of the flow.

Considering that the volume velocity is assumed to be constant, Eq. (3.160) is reduced to the form

$$-\frac{dC}{dz}+\frac{D_L}{wL}\frac{d^2C}{dz^2}=0. \qquad (3.162)$$

If $D_L/wL = 0$ (Pe $= \infty$), the diffusion model is transformed to the ideal displacement model; if $D_L/wL = \infty$ (Pe $= 0$), the diffusion model is transformed into the ideal mixing model.

Hybrid models. While describing the motion of actual flows, it may happen that none of the above hydrodynamic models provides a sufficiently accurate reproduction of the flow properties. In such cases, complex hydrodynamic hybrid models are employed. Hybrid models are based on the simplest models to which stagnation regions are added, and by-passing and recirculation of individual sections of the flows are introduced. The mathematical description of the process becomes more complicated, but this is compensated by the possibility of reproducing the properties of the simulated process to a required accuracy.

The expression "stagnation region" is a conditional concept. These regions usually include the volumes of the system in which the mean duration of stay of a substance is 3-10 times more than the mean duration of stay for the main flow.

In processes of mass exchange in packed columns, such regions are the dead zones, i.e. idle volumes of the apparatus.

As there are no ideal stagnation regions in real systems, there can be no instantaneous by-passing in them, since the elements of the media pass through the vessel in a finite time. In actual practice, if the mean duration of stay for a certain part of the system is 0.1-0.3 of the stay time of the main flow, it is assumed that the system contains a by-passing flow.

These two types of non-uniformities are essentially based on the same physical phenomenon, viz. the motion of individual parts of the flow having different volume velocities. Consequently, a system with the same structure can be considered as a system with stagnation regions on the one hand and a system with by-passing on the other, depending on which region of the flow is taken as the main (working) region.

The following distribution functions for the stay time are the effective means for revealing different types of non-uniformities in flows:

(1) the differential distribution function $f(t)$;

(2) the integral distribution function $F(t)$:

$$F(t)=\int_0^t f(t)\,dt;$$

(3) the function of intensity $\lambda(t)$:

$$\lambda(t) = -\frac{d}{dt} \ln [\bar{\tau}_m (1 - F(t))].$$

The parameters of hybrid models are the volumes of individual cells (ideal mixing, ideal displacement, stagnation regions) and the ratios of the flows connecting these cells (the fraction of by-passing flow, the fraction of recirculating flow).

A cell model with backmixing between the cells is one of the most commonly used hybrid models in the analysis of mass-transfer processes realized in columns (towers). The amount of recirculating flow characterizes the intensity of the mass transferred in the direction opposite to that of the main flow. The practical application of the cell model with backmixing between cells involves the development of calculation methods for the time-response characteristics of this model, as well as the derivation of design formulas connecting the model parameters with the numerical characteristics of the distribution function.

Chapter Four

Hydrodynamics of Two-Phase Flows

4.1. Basic Concepts and Definitions

Two-phase flows are heterogeneous systems with an interface which is referred to as *the free surface* for gas-liquid, vapour-liquid, and liquid-liquid systems.

The forces acting in two-phase flows have been considered while analyzing hydrodynamic phenomena occurring in single-phase flows. However, the presence of two phases changes the pattern of flow in such systems as well as their nature, since *the interaction between phases* plays a decisive role. Hence it is impossible to describe the regimes in such systems by using the concepts like "laminar" or "turbulent" flow, which are common for single-phase flows. A two-phase system should be considered as a physico-chemical system that can be defined as a multiphase multicomponent continuous medium distributed in space and varying with time. At each point of this system, as well as on the interface, the transport of mass, energy, and momentum takes place in the presence of sources (sinks) of these quantities.

While considering the variety of physico-chemical effects and phenomena appearing in the course of constrained motion of an aggregate of drops in the liquid phase or bubbles in the gaseous phase, it is natural to single out five hierarchic steps for these effects: (1) the complex of effects on the atomic and molecular level; (2) the effects on the scale of super-molecular or globular structures; (3) the multitude of physico-chemical phenomena associated with the motion of a single inclusion of the disperse phase and the phenomena of energy and mass transport through the interface; (4) physico-chemical phenomena in the ensemble of inclusions performing a constrained motion in a continuous phase layer, and (5) the combination of processes determining the macrohydrodynamic situation in the apparatus.

1. The first hierarchic level of effects in a physico-chemical system is characterized by physico-chemical interactions on the molecular level. The system is assumed to be homogeneous, i.e. perfectly mixed on the level of individual atoms and molecules. The nature of evolution and the course of physico-chemical processes is determined

only by physical properties of these particles and the magnitudes of molecular viscosity, thermal conductivity, and molecular diffusion coefficients.

The environmental effects play an important role in the physico-chemical interaction among particles of the first hierarchy level. These effects are manifested in the form of kinetic, diffusive, thermodynamic, and topological effects of the variation of physico-chemical properties of the medium.

2. The second hierarchic level of a physico-chemical system is formed by physico-chemical effects on the level of molecular globules.

The structure of a chemically homogeneous system (i.e. the system from the first level) becomes more complicated from the point of view of hydrodynamics when supermolecular formations or globules appear in it. These are the aggregates of closely arranged molecules, which exhibit a relative thermodynamic stability (integrity) upon hydrodynamic perturbations. Each globule behaves as an "elementary" physico-chemical system in which the entire complex of thermal and diffusion phenomena is observed. The system completely split into separate aggregates of molecules which are uniformly distributed over the apparatus volume is called fully segregated. Segregation is typical both of the continuous and disperse phases.

Segregation and its influence on transport phenomena play a very important role in systems with a high viscosity.

The phenomena constituting the first and second hierarchic levels form a part of the effects from the higher structural levels of a physico-chemical system.

3. The third hierarchic level of a physico-chemical system contains the following phenomena. An element of the disperse phase (bubble or drop), in which mass transfer takes place both in the bulk and on the interface, moves within a continuous phase under the action of Archimedean force, inertial forces, and drag forces. While crossing an interface, this element experiences the action of mass-, energy-, and momentum-transport mechanisms. It is natural to take the non-equilibrium nature of the heterogeneous system as the initial cause of interfacial flows of a substance, which determine the multitude of phenomena constituting the transfer mechanism through the interface. This can be manifested in several ways: non-equilibrium composition, non-equilibrium temperature distribution, and non-equilibrium velocity distribution, i.e. the difference in the velocities of phases. Each of these types mainly causes the transport of the corresponding quantity and, at the same time, indirectly affects the transport of other quantities.

Mass- and energy flows cause a change in the enthalpy of the continuous and disperse phases, as well as in other physical and thermodynamic properties of phases, such as viscosity, density, heat capacity, composition, and temperature. The changes in the physico-

chemical properties of the phases determine the degree of departure of the heterogeneous system from equilibrium.

The mass and energy transport through the interface violates the balance of forces on the interface and causes local non-uniformities in its surface tension. These local changes in surface tension are the main reason behind interfacial spontaneous convection which can be ordered or disordered. The latter effect influences the mass transport between the phases and deforms the interface, i.e. changes its shape and curvature.

The momentum flux through the interface at each point of the surface is the vector sum of two components: the flux of the impulse of forces normal to the interface and the flux of the impulse of forces tangential to the interface, which are responsible for the generation of circular currents within an inclusion. The circular currents intensify the processes of mass- and heat transfer in the disperse phase element. The normal and tangential stresses on the interface reorient the inclusion in space, change the trajectory of its motion, and also deform the interfacial surface.

The difference in the dynamic head of turbulent vortices at different points of the interface makes a considerable contribution to the deformation of the interface. The strains may be so large that the interface breaks down, and the inclusion is split into smaller elements. The breaking may occur only under the action of relatively weak vortices. The probability of large strains and breaking decreases for large-scale vortices which remain unchanged over distances of the order of the inclusion diameter.

The non-uniformity in the velocities of phases leads to surface diffusion as a result of which a surface-active substance (surfactant) is "blown to the stern" of the flowing inclusion, thus creating the non-uniformity in the distribution of the surface-active substance over the surface of the inclusion. This effect plays an important role in creating a non-uniform surface tension of the interface and gives rise to additional drag forces (competing with the tangential stresses of the flow), which suppress the circulation currents within the inclusion.

The deformation of the interface is associated with a number of effects among which the most important are (a) the breaking of drops or bubbles and a subsequent change in the interfacial area; (b) development of interfacial turbulence, spontaneous emulsification, and surface elasticity; (c) the change in thermodynamic characteristics (saturation pressure, temperature, composition, deviation from chemical equilibrium, etc.) in the bulk of an inclusion. The effects associated with the deformation of the interface intensify the mass-, energy-, and momentum transport through the interface.

4. The fourth hierarchic level of the structure of a physico-chemical system includes the following effects. Each element of the disperse

phase performing a constraint motion in a limited volume of a continuous medium leaves a turbulent wake in it. Under the predominant action of Zhukovskii's forces, the vortices from individual wakes interact with each other thus causing the turbulization of the entire continuous phase. The surface of inclusions located in the region of interaction between the turbulent wakes is enveloped by the vortices of the continuous phase and drawn into the turbulent motion. This affects the entire complex of physico-chemical phenomena of the third hierarchic level. In particular, a change in the trajectory of motion of inclusions provides the opportunity for their collision, coalescence and, as a consequence, the redistribution of the fields of concentrations, temperatures, and pressure within the elements of the disperse phase. Simultaneously, turbulent fluctuations in the continuous phase are suppressed due to the dissipation of their energy into heat, which changes the heat content of the continuous phase.

As an individual inclusion moves in the infinite volume of a continuous medium, the corresponding tensor fields of concentration, temperature, velocity, pressure and other physico-chemical characteristics are induced in the continuous phase. In a real industrial apparatus the volume of the continuous phase is limited by the apparatus dimensions, and the motion of elements of the disperse phase is cooperative in nature. This leads to a deformation of the fields of concentration, temperature, and velocity. The complex of phenomena described above form the essence of an involved process which is called the straitening effect.

The phenomena of the fourth hierarchic level of a physico-chemical system determine the hydrodynamic situation in a local volume of the apparatus. For this reason, the term "local thermodynamics" appropriately describes these phenomena. Local hydrodynamics is manifested in a certain volume which is considered as unit volume due to its small size in comparison with the entire volume of the apparatus. The dimensions of this volume, however, are such that it contains a sufficient number of inclusions of the disperse medium. The basic quantitative characteristics of the physico-chemical system from this level are the normal and tangential stresses, the values of the strain and the strain rate, the coefficients of viscosity, diffusion, thermal conductivity, the rates of phase transformations, etc.

A semiempirical concept of locality is usually based on the determination of the ratio of the turbulent exchange coefficient to the kinematic viscosity. The methods of separation of the domain of integration and determination of the turbulent exchange coefficient at the interface determine the peculiarities of different theories of interphase transfer.

The effects of the first, second, third, and fourth hierarchic levels of the structure of a physico-chemical system are closely connected

with each other and form a complex of microhydrodynamic factors determining the transport of a substance in a heterophase multicomponent system.

5. The fifth hierarchic level of a physico-chemical system contains the complex of phenomena which determine the so-called hydrodynamic situation on macrolevel in an apparatus. This complex of phenomena characterizes the hydrodynamic structure of flows in the apparatus as a whole rather than in its isolated local volume.

The initial factors determining the specific properties of the effects from the fifth hierarchic level are structural features of the industrial apparatus. They include geometrical properties of the apparatus, the type of mixers and heat exchangers, the arrangement of inlet and outlet pipes, the presence and shape of reflecting partitions, diffusers, plates, distribution systems, and so on.

The structural features of an apparatus directly determine the supply of extraneous mechanical energy spent for creating the mechanical agitation in the system, the transport (supply or removal) of heat (determined by the structural properties of heat exchangers and the regime of the supply of heat-transfer agents), as well as the hydrodynamic, concentration, and thermal perturbations introduced with the inward flow of initial reagents.

The combined influence of the three factors of mechanical stirring, perturbations introduced with inward flows, and geometrical properties of the working volume of the apparatus form a certain topology of flows in the apparatus. This topology, or hydrodynamic structure of the flows in the apparatus, is determined by the nature and spatial arrangement in its working volume of macrohydrodynamic non-uniformities of the flows such as stagnation regions, by-passes, the regions of laminar and turbulent flow, and circulating currents.

As the hydrodynamic structure of the flows changes in the apparatus, its basic quantitative characteristics (the distribution of particles of the continuous and disperse phases over trajectories, over the duration of stay in the apparatus, the holding capacity of the apparatus with respect to the continuous and disperse phases, the distribution of disperse phase inclusions according to dimensions, and so on) also change. The peculiarities of the hydrodynamic structure of the flows and the apparatus geometry influence the formation of the concentration and temperature fields in the apparatus. Besides, perturbations from the inward flows and the conditions of heat supply to the apparatus also make a significant contribution.

Each hierarchic level of a physico-chemical system considered above is characterized by the corresponding form of the mathematical description. The first-level effects are basically described with the help of phenomenological and statistical methods of physico-chemical kinetics and chemical thermodynamics. The main problem for this level is the interpretation of the mechanisms of molecular

interactions and the calculation of kinetic constants or the molecular diffusion coefficients.

The information gained on the first level is enriched and modified on the second hierarchic level by taking into account the information of the degree of segregation of the system and the structure of supermolecular formations. The operating apparatus of this level involves the mathematical models of flow segregation, as well as various theories of heterophase processes.

The third level effects are mainly described by the methods of mechanics of small-scale flows in the vicinity of disperse phase inclusions, thermodynamics of surface phenomena, the methods for describing the equilibrium in multicomponent systems, and various theories of interphase transfer.

The phenomena belonging to the fourth hierarchic level of a physico-chemical system can be described with the help of the methods of statistical theory of continuous media, the methods of mechanics of disperse systems, the models constructed on the basis of mathematical methods of the kinetic theory of gases, and so on.

The equations for the first, second, third, and fourth levels of hierarchic structure of the effects in a physico-chemical system constitute a part of the mathematical description of the fifth-level phenomena as a mathematical description of the subsystems of the entire system on the apparatus scale. It was found that in practice this description must above all be simple and convenient. Consequently, the information gained from the lower levels must be condensed to the greatest possible extent and supplied to the upper level in a sufficiently simple and compact form. The information can be condensed by the order-of-magnitude estimation of the quantities involved in the description of the lower levels, by revealing the most important factors affecting the technological process, by using simpler model structures with a simplified form of mathematical description instead of exact relation, and so on.

In the motion of two-phase flows in industrial apparatus, the continuous and disperse phases are distinguished. The disperse phase is distributed in the continuous phase. The apparatus diameter is usually calculated from the linear velocity of the continuous phase. Consequently, the determination of the linear velocity of the continuous phase is the main problem in the engineering calculations of the hydrodynamics of heterophase systems.

The structural characteristic of the apparatus containing a two-phase flow considerably influences the state of the flow. For this reason, the hydrodynamic analysis of two-phase systems is inseparable from the construction of the apparatus.

In mass-transfer processes, the maximum difference in concentrations must be created in each cross section of the apparatus to ensure the most intense process. This can be attained with the help of

countercurrent flow of phases in industrial apparatus. A gas, vapour, or light liquid (extract) move upwards, and liquid (heavy liquid in the case of extraction) moves downwards. Cross current can be realized in the individual parts of the apparatus, for instance, on the plates of columns.

The distribution of a liquid and a gas in the flow is characterized by the holding capacity with respect to the disperse phase, i.e. the amount of substance in the disperse phase (m^3) contained at a given moment in unit volume (m^3) of the continuous phase. Thus, its dimensions are $\varphi = m^3/m^3$. The value of φ varies with hydrodynamic conditions, attaining the maximum at the so-called *inversion* point. After passing this point, the phases are reversed, i.e. the disperse phase becomes continuous.

The holding capacity is extremely important for mass-transfer processes, since it determines the area of the interface and the duration of contact. The variation of φ depending on the velocity of a gas or vapour in gas-liquid systems is similar to the variation of the pressure drop in such two-phase systems. For a given velocity of the gas (vapour), the pressure drop in gas-liquid or vapour-liquid systems is an unambiguous hydrodynamic characteristic of the two-phase system.

Using the principles of mathematical modelling and analyzing the mathematical models of the flow structure, it is possible to determine the distributions of velocity and pressure in a two-phase flow. In the case of two-phase flows, the basic quantitative characteristics of the system are the pressure drop, the resultant velocity of the continuous phase, and the holding capacity with respect to the disperse phase. In order to obtain quantitative characteristics of a two-phase flow, two principles can be used.

First, the principle of comparison of the difference between the amount of energy and mass transferred in a two-phase flow and the amount of energy and mass transferred in a one-phase flow in relation to the amount of energy and mass transferred in the one-phase flow with respect to the same characteristic quantity, for example, for the same linear velocity of the continuous phase. This principle proved to be helpful for obtaining quantitative hydrodynamic and diffusion characteristics of two-phase systems.

Second, the principle of corresponding states can be used by taking for comparison the inversion state of a two-phase system as a standard.

In a countercurrent flow, the vertical flows of phases experience the action of the forces of gravity of the liquid flowing down and of friction of the opposite gas (vapour) flow or the flow of a light liquid (extraction). The difference in the density of liquids constituting the phases is the driving force causing the relative motion of phases.

The limiting state involving a separate motion of flows is attained when the force of friction at the interface becomes equal to the force of gravity (or, in other words, when the force of gravity becomes equal to the force of pressure in the countercurrent flows). When this equality is reached, the holding capacity with respect to the disperse phase sharply increases, and the hydrodynamic situation of the process changes. If the force of pressure of the countercurrent gas flow exceeds the force of gravity of the flowing-down liquid, the liquid may be carried out of the apparatus, and the two-phase flow becomes unidirectional, or the so-called flooding of the apparatus is observed. Since in the inversion state the maximum amount of the disperse phase is contained in the continuous phase, the most uniform mutual distribution of the phases in the flow takes place in this case. This simplifies the obtaining of quantitative relations characterizing a two-phase flow. Comparing the quantitative characteristics of a two-phase flow (such as pressure drop, velocity, and holding capacity) in a given state with their values at the inversion points, it is possible to describe this state quantitatively.

In contrast to one-phase flows, quite new forces (in particular, the forces of *interfacial surface tension*) may appear at the interface in two-phase flows. These forces accomplish the work of formation of the surface of liquid at the interface. The work expended to form a unit surface is called *the surface tension.* The surface tension is a physical constant for a given liquid-gas or liquid-liquid system,* if no heat- or mass-transfer process takes place.

Surface tension σ can be calculated from the equation

$$\sigma = \left[\frac{[p](\rho_l - \rho_v)}{M}\right]^4, \tag{4.1}$$

where ρ_l, ρ_v are the densities of the liquid and vapour of a given substance; M is its molecular mass; $[p]$ is the parachor of the given substance. The parachor $[p]$ is an additive function of the composition and the molecular structure of the given substance, i.e.

$$[p] = \sum np_a, \tag{4.2}$$

where p_a are the parachor components for different types of atoms, bonds, or groups of molecules, and n is the number of the given type of atoms, bonds, or groups in a molecule.

Disregarding the vapour density in comparison with the density of the liquid, we can simplify formula (4.1):

$$\sigma = \left[\frac{[p]\rho_l}{M}\right]^4. \tag{4.3}$$

* The surface tension at the interface between two liquids is called the interfacial tension.

We can also recommend the approximate equation

$$\sigma \approx 1.085 T_b \left[\frac{\rho_l - \rho_v}{M}\right]^{2/3}, \tag{4.4}$$

where T_b is the boiling point of the given substance under normal conditions, K.

The change in the surface tension with temperature can be calculated with the help of the following empirical equation, which provides a good agreement with experiment at temperatures far from critical:

$$\frac{\sigma_2}{\sigma_1} = \left(\frac{T_{cr} - T_2}{T_{cr} - T_1}\right)^{1/2}, \tag{4.5}$$

where T_{cr} is the critical temperature of a given substance, K.

This formula can be applied to mixtures of liquids if instead of T_{cr} we substitute the pseudocritical temperature $T_{cr,m}$ which can be calculated from the equation

$$T_{cr,m} = T_{cr1}x_1 + T_{cr2}x_2 + \ldots, \tag{4.6}$$

where x_1, x_2 is the mole fraction of components in the mixture.

The surface tension for a mixture of liquids can also be calculated from the empirical relation

$$\sigma_m = \frac{\sigma_1\sigma_2}{\sigma_1 x_1 + \sigma_2 x_2}. \tag{4.7}$$

In a hydrodynamic analysis of two-phase flows, the surface tension is introduced in the form of the so-called Weber number We, which is equal to the ratio of the inertial force to the surface tension force:

$$N_{We} = We = \frac{\rho w^2 l}{\sigma}. \tag{4.8}$$

The form of the Weber number may change depending on the specific conditions under which a process occurs. For example, the Weber number for the process of mechanical mixing of two immiscible liquids has the form

$$We = \frac{\rho_m n_a^2 d_a^3}{\sigma}, \tag{4.9}$$

where n_a is the agitator rotational velocity, r.p.s.; d_a is the diameter of the agitator blade, m; and ρ_m is the density of the mixture.

When analyzing the motion of drops of the disperse phase in the continuous phase flow in hollow extraction columns, the Weber number is represented in a more complex form:

$$We = \frac{\rho_c \left(\frac{w_d}{\varphi} + \frac{w_c}{1-\varphi}\right)^2 d_{dr}}{\sigma}, \tag{4.10}$$

where ρ_c is the density of the continuous phase; w_d, w_c are the linear velocities of the disperse and continuous phase referred to the total cross section of the apparatus; φ is the disperse-phase holding capacity; and d_{dr} is the diameter of a disperse-phase drop.

The interfacial tension can also be introduced in the analysis in the form of the relative quantity

$$\frac{\sigma_{1-2}}{\sigma_{1-a}+\sigma_{2-a}} \tag{4.11}$$

where σ_{1-2} is the interfacial tension, σ_{1-a} is the surface tension at the first liquid-air interface, and σ_{2-a} is the surface tension at the second liquid-air interface.

For most organic liquids, the value of the surface tension σ at the air-liquid interface at room temperature ranges between 25×10^{-3} and 40×10^{-3} N/m, except fluorohydrocarbons ($15 \times 10^{-3} < \sigma < 25 \times 10^{-3}$ N/m) and polyhydrogenated alcohols ($\sigma \simeq 65 \times 10^{-3}$ N/m). For liquid metals, the surface tension varies between 0.3 to 0.6 N/m (for mercury, $\sigma = 0.476$ N/m at 20 °C). The surface tension for the water-air system at 20 °C is $\sigma = 0.07275$ N/m.

The interfacial tension varies over a wide range. For example, at the water-dipropylamine interface, $\sigma = 1.66 \times 10^{-3}$ N/m (20 °C), while at the water-*n*-hexane interface, $\sigma = 51.1 \times 10^{-3}$ N/m.

The surface tension decreases almost linearly with temperature, attaining the value zero at the critical temperature.

4.2. Interfacial Turbulence

The interfacial turbulence is caused by the vortices generated as a result of the instability of a free surface or interface. At present, we can formulate the necessary and sufficient conditions for the appearance of interfacial turbulence.

1. The velocities of the phases differ in magnitude and direction. A viscous liquid offers resistance to the countercurrent flow. Since opposite velocity vectors form couples of forces at the interface, the layers of the flows adjoining the interface begin to rotate (Fig. 64) with a subsequent washing out of these layers into vortices. The intensity of flow stagnation is proportional to the energy of the main disturbances causing stagnation. Thus, the friction between the flows results in that the boundary layers of the gas and liquid are pierced by vortices. The vortices appearing on the surfaces of the gas and liquid flows penetrate these flows under the action of Zhukovskii's force, thus increasing the intensity of the vortex field. The formation of vortices causes a sharp increase in the interfacial area per unit volume (Fig. 65).

In crossflows, for example, when the liquid flows in the horizontal direction and the gas (vapour) in the vertical direction (as in plate

columns), favourable conditions are created for the vortex formation at the interface. In this case, the resultant driving force acts at a certain angle to the horizontal in the direction of the liquid flow, generating considerable shear stresses at the interface. The angle of action of this force depends on the shape and type of plates and on the direction of the liquid and gas flows. Depending on the magnitude of this angle, the energy of the liquid supplied to the flow of the

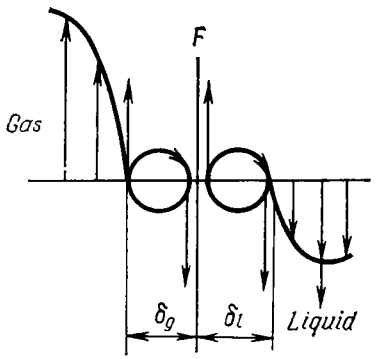

Fig. 64. Evolution of vortex layers at the interface.

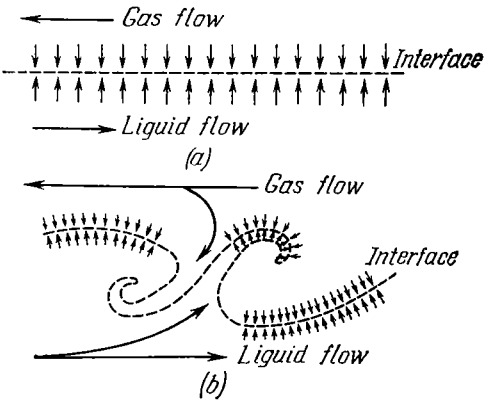

Fig. 65. Change in the interfacial surface during vortex formation:

a—interfacial surface without vortex formation; *b*—interfacial surface during vortex formation.

foam or vapour-liquid emulsion formed in this case, so that the height of the layer of foam or vapour distribution along the plate is a function of this angle.

The phenomena occurring on a free surface differ in principle from those taking place at a solid boundary (wall), where it is assumed that the velocity of the liquid drops to zero and turbulent fluctuations are suppressed. The evolution of vortices in two-phase systems leads to the mutual penetration of vortices into the two phases, accompanied as if by liquid "emulsification". Under these conditions, a two-phase system exhibits features peculiar to free turbulence: the absence of damping of turbulent fluctuations, the presence of nonzero normal velocity components, and finally, the absence of noticeable effect of molecular characteristics.

The turbulence which appears at the interface between moving phases (on free surfaces) and propagates into the phases in the form of continuously appearing and vanishing vortices can be defined as *fully developed free turbulence.* The hydrodynamic gas-liquid emul-

sion system formed in this case differs in principle from the so-called foams.*

A gas-liquid emulsion is a moving system of gas-liquid vortices. It originates in the bulk of liquid as a result of collisions between the bubbles and gas jets moving at a high velocity. The collision of bubbles and filling of a liquid with a gas is determined by the kinetic energy of the gas. Hence, for a sufficiently high velocity of the gas, the entire liquid may be transformed into a gas-liquid emulsion regardless of the presence of adsorption layers on the gas-liquid interface.

In a gas-liquid emulsion, vortex motion is superimposed onto the translational motion of the gas which flows at a high velocity exceeding several times the velocity of a rising bubble. As a result, mass collisions between bubbles and gas jets take place, accompanied by their coalescence and breaking up, transitions from bubbles to vortex flows and back to bubble formation. In this process, the liquid may stretch into thin films, then merge again into drops or layers, and so on.

Thus, in a gas-liquid emulsion layer, the interface is highly developed and rapidly renewed, which involves an especially intense mixing of the gas phase which has a considerably lower viscosity in comparison with the liquid phase. These factors strongly intensify the mass- and heat-exchange in comparison with a bubbling layer at the same liquid flow.

2. Since the flows have different densities, and the density, being a function of concentration and temperature (which is typical of mass-exchange processes), may change within each flow, the isobaric and isosteric surfaces interact at the interface of the two-phase flow, or alternatively, an interfacial area is created, leading to an intense vortex formation.

3. The change in the surface tension due to the variation of concentrations and temperatures leads to intense vortex formation at the interface. In the course of diffusion through the surface, the concentration of the substance being distributed at the interface may be nonuniform. This leads to a local change in the surface tension and, as a result, to surface instability.

The relation between the pressure P_1 on the inner surface of a drop and P_2 on the outer surface for the surface tension σ and the radius

---

* Foam is a stable crosslinked system of films of liquid and gas. It usually originates as gas bubbles leave a layer of liquid at a small velocity and is formed on account of the adsorption layers ensuring a certain mechanical strength and a corresponding lifetime of cells. Foam has a sufficiently strong cellular structure resembling a honeycomb. The gas bubbles rising to the surface at a low velocity cannot overcome the mechanical strength of the surface film since they have a low kinetic energy.

of curvature r can be represented as follows:

$$P_1 - P_2 = 2\sigma/r. \tag{4.12}$$

As a result of surface fluctuation of the concentration, the surface tension changes by $\Delta\sigma$. In this case, we obtain the following relation for the newly formed surface:

$$P_1 - P_2 = 2\,(\sigma - \Delta\sigma)/r, \tag{4.13}$$

or

$$P_1 + (2\Delta\sigma/r) - P_2 = 2\sigma/r. \tag{4.14}$$

It follows from this relation that a decrease in the surface tension is equivalent to an increase in pressure P_1. Since $\Delta\sigma$ arises almost

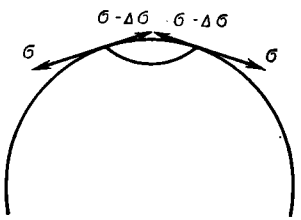

Fig. 66. Stresses appearing on the surface of a drop as a result of surface tension.

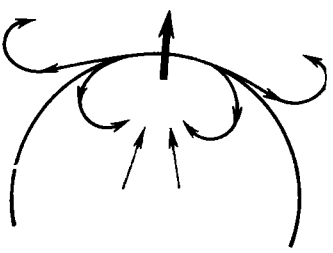

Fig. 67. Direction of forces resulting in disintegration of the drop.

instantaneously, the increase in P_1 is manifested as an impulse in the direction of higher concentrations of the substance being distributed. Figure 66 shows the emergence of forces as a result of the difference appearing in the surface tension forces on the surface of a drop. The viscosity forces of the liquid tend to decrease the intensity of flows caused by the difference $\Delta\sigma$. As a result, the surface of the drop breaks down (Fig. 67). Figure 68 illustrates the vortex formation on the surface of a drop of carbon tetrachloride in water, followed by its destruction in the course of extraction by acetic acid. Figure 69 shows the formation and washout of vortices. The sequence of droplet destruction with intense vortex formation is illustrated in Fig. 70.

Specially conducted studies of the interface between two immiscible phases during extraction revealed a considerable turbulence originating continuously at the interface. This can be explained by different values of surface tension at close points of the surface due to concentration and temperature gradients created on the surface. Intense interfacial turbulence is also observed in adsorption processes (Figs. 71, 72).

As the pressure increases, the surface tension on a gas-liquid interface decreases, since the difference in intermolecular interactions

becomes smaller as the molecules go over from one phase to the other. Thus, the dissolution of a gas leads to a decrease in the surface tension and intensifies the vortex formation if there is no change in the polarity of liquids.

The addition of surface-active substances (surfactants) to a liquid flowing down in the form of a thin film decreases the frequency and the amplitude of vortex formation. For diffusing molecules, surface-active substances play the role of a barrier: the resistance to mass

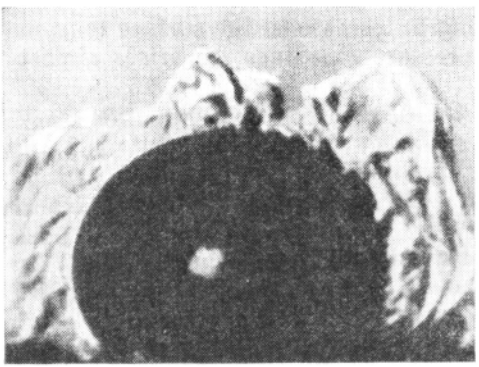

Fig. 68. Vortex formation at the surface of a drop during extraction (for a system consisting of 40 percent aqueous solution of acetic acid-carbon tetrachloride).

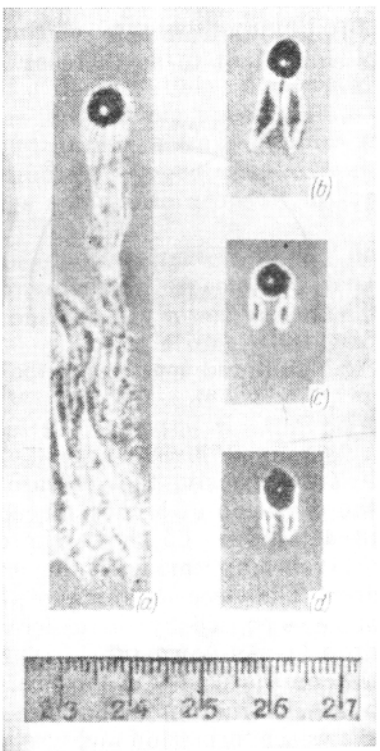

Fig. 69. Vortex formation observed during water extraction of acetic acid from benzene:

a—pure water; *b*—water containing 0.3 mg/l of polyethylene glycol (mol. mass 4000); *c*—water containing 15 mg/l of polyethylene glycol; *d*—water containing 500 mg/l of polyethylene glycol.

transfer increases with their concentration. In some cases, the resistance passes through a maximum. Sometimes, a further addition of surfactants after attaining the maximum again leads to vortex formation. The action of different surfactants has a specific nature.

Depending on whether the surface tension increases or decreases in the course of mass transfer, systems can be divided into three groups:

(1) systems with a positive value of the surface tension gradient $d\sigma/dx > 0$ (x is the concentration of the volatile component);

(2) systems with a negative value of the surface tension gradient $d\sigma/dx < 0$;

(3) neutral systems with $d\sigma/dx = 0$.

The hydrodynamic stability of a process varies depending on the sign of $d\sigma/dx$.

Let us consider a system in which $d\sigma/dx < 0$ is the case of rectification. The surface tension in the bulk of the liquid for such a system is smaller than at the interface. A vortex reaching the surface

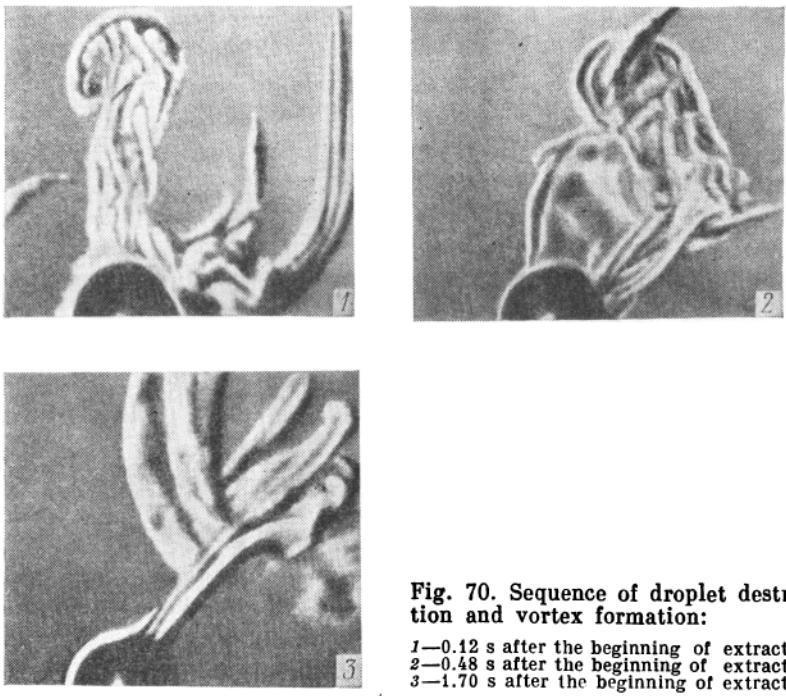

Fig. 70. Sequence of droplet destruction and vortex formation:

1—0.12 s after the beginning of extraction; *2*—0.48 s after the beginning of extraction; *3*—1.70 s after the beginning of extraction.

carries the liquid with a higher concentration of the volatile component (x) and accordingly, a lower temperature. However, a change in the concentration affects the surface tension to a greater extent than a change in the temperature. Consequently, the liquid coming from the bulk must have a lower surface tension than the liquid it replaces. Hence, the local change in concentration leads to an imbalance of forces of surface tension. As a result, the liquid with lower surface tension will dissipate at the interface and cause convective streams intensifying the normal mechanism of surface renewal and increasing the mass-transfer coefficient. If the surface tension varies almost linearly with the composition, the difference between the

surface tension at the surface and in the bulk will depend on the magnitude of the concentration driving force. Since the latter passes through a maximum at the same point where the composition varies within $0 < x < 1$, the value of the mass-transfer coefficient must also

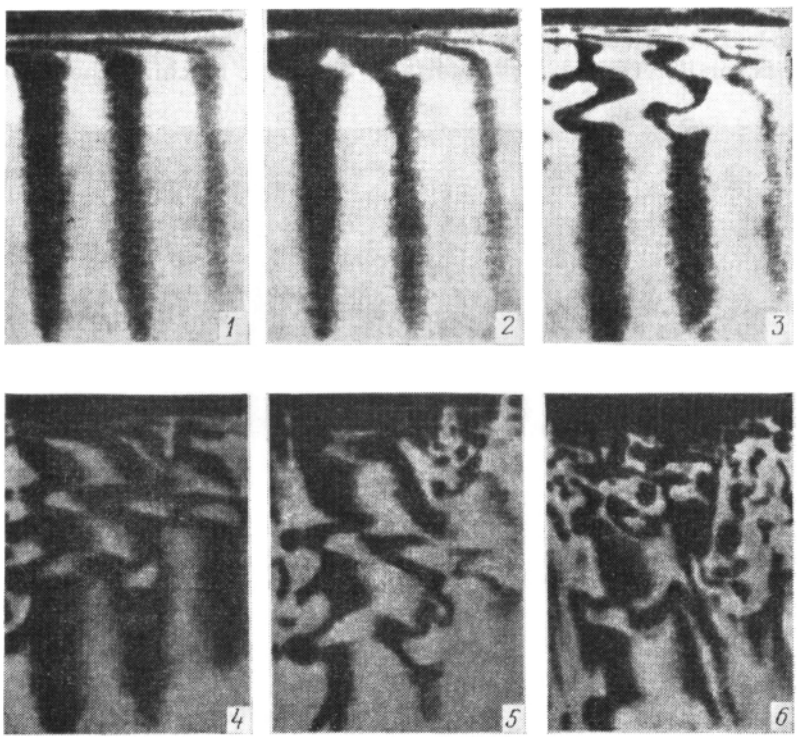

Fig. 71. Sequence of evolution of interfacial turbulence during absorption of carbon dioxide by monoethanolamine (0.046 g-mole/l). Duration of interaction: *1*—32.5 s; *2*—34 s; *3*—00 s; *4*—38 s; *5*—40 s; *6*—44 s.

pass through a maximum. However, within the limits of each phase, the development of turbulence is considerably affected by the ratio of kinematic viscosities.

A surface tension gradient may appear not only as a result of the difference in concentrations, but also as a result of heat transfer. This is observed, for example, during distillation. As heat is transferred from vapour to liquid, thin films have a higher temperature than the surface of the bulk of the liquid. Since the surface tension decreases with increasing temperature, the difference appears between the temperature in the bulk of the liquid and at the interface.

When two bubbles come into contact, the thin film separating the bubbles quite rapidly attains the state of equilibrium with vapour, and if the more volatile component has a lower surface tension, the tension in the film will increase in comparison with that in the bulk of the liquid. The resulting difference in the surface tension increases

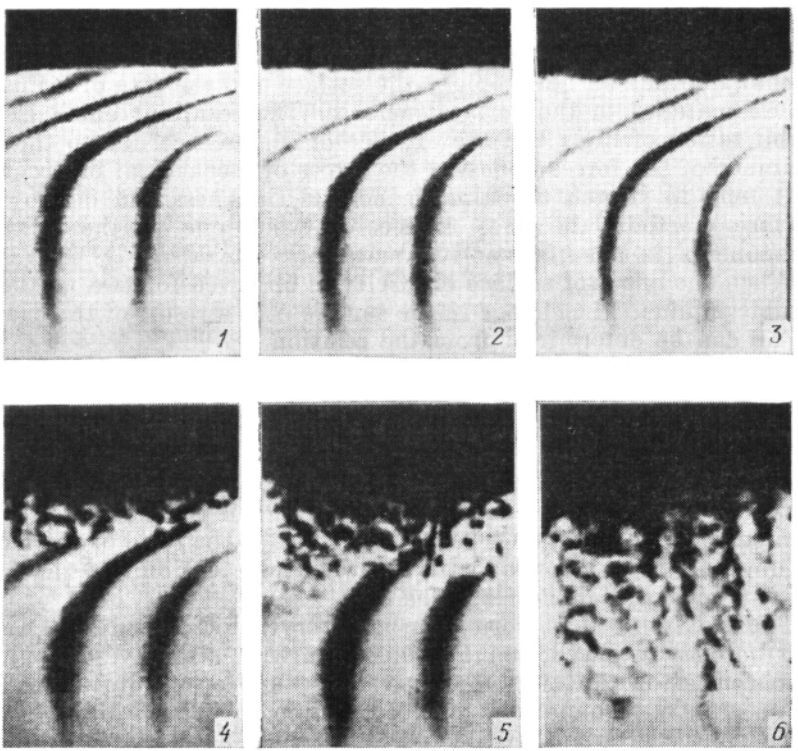

Fig. 72. Sequence of evolution of interfacial turbulence during absorption of carbon dioxide by monoethanolamine (1.01 g-mole/l). Duration of interaction: *1*—11 s; *2*—12 s; *3*—13 s; *4*—14 s; *5*—15 s; and *6*—16.5 s.

the imbalance of forces, thus causing a motion at the interface. A fresh mass of liquid is supplied at the points of contact between the film and the bulk of the liquid. The film thickness increases, coalescence decreases, and the foam is stabilized. On the contrary, if a more volatile component has a higher surface tension, the motion originating at the interface facilitates the drainage of the film, speeds up coalescence and hampers the foam formation.

In addition to the concentration and temperature difference, the two factors responsible for the surface tension gradient at the interface, the surface tension gradient may also be created on account of the so-called "surface elasticity". Surface elasticity is a result of the difference in the surface tension of the increased surface and the static surface. The substances which decrease the surface tension have the maximum concentration at the surface. If the surface increases, the concentration of these substances instantaneously drops, and the surface tension increases as a result. This increase in surface tension depends on how rapidly the surface and the rate of diffusion of the material to the surface increase. The resultant effect is the stabilization of films and the absence of coalescence due to the appearance of the forces opposing the forces of mechanical destruction that tend to stretch the film, reduce its thickness and destroy it. Surface elasticity becomes noticeable when one of the mixture components is a surface-active material.

When the effect of surface elasticity is observed for two mutually soluble liquids, the change in the surface S as a result of the change in $\Delta\sigma$ can be determined from the relation

$$\Delta\sigma = \frac{1}{\rho_m RT}\,\theta(x)\left(\frac{d\sigma}{dx}\right)^2\sqrt{\frac{\pi S}{2D_m}}, \qquad \theta(x) = \frac{x(1-x)}{1-x+bx}, \quad (4.15)$$

where x is the mole fraction of the component with a lower surface tension; ρ_m is the molar density of liquid; D_m is the molecular diffusion coefficient; R is the gas constant; and b is the ratio of the molar volumes of the component with a low surface tension and the component with a high surface tension.

The maximum foam formation is observed for mixtures in which $\theta(x)\,(d\sigma/dx)$ is maximum. For mixtures with strongly pronounced foam-formation capacity, the maximum foam formation takes place for $x < 0.05$. Pronounced foam formation is observed only when $\theta(x)\,(d\sigma/dx)^2$ attains the value 10^4 dyne^2/cm^2 and is noticeable when this factor is of the order of 10^3 dyne^2/cm^2. The turbulence on free surfaces increases under the following conditions: (1) the substance diffuses from the phase with a higher viscosity; (2) the substance diffuses into the phase with a lower surface tension; (3) the presence of a large difference in the kinematic viscosities of liquids constituting the phases and between the molecular diffusion coefficients; (4) the presence of a high concentration gradient at the surface; (5) the surface tension sharply changes with the concentration; (6) the liquids in both phases have low viscosities and surface tensions; (7) the absence of surfactants, and (8) the interfacial area is large.

The above conditions for vortex formation at the interface are observed simultaneously, interacting in an intricate manner. The hydrodynamic conditions created in a certain diffusion apparatus,

as well as the conditions for the flows, may play an exceptionally important role. For example, in an apparatus with a fixed surface of contact, the surface tension may affect the process in a different way in comparison with an apparatus where the interface is created in the course of the flow. Liquid films are stabilized when the surface tension of the reflux increases towards the bottom of the column, whereas liquid films are broken into streams and drops upon a decrease in the surface tension.

The interfacial area formed during the spraying of a liquid changes insignificantly with the surface tension. For a given liquid mixture, the destruction or stabilization of films may affect the mass exchange: this effect is determined by the surface tension gradient in the reflux along the column height.

In apparatus with a fixed area of phase contact (film type), the rate of mass transfer for mixtures in which the surface tension of the reflux increases, can be two or more times as high as for the mixtures in which the surface tension of the reflux decreases. In industrial apparatus, where the interface is created by the liquid dispersion, this effect is weaker.

In sieve-plate columns with a small open area and small perforations, a stable cellular foam may be formed, and the effect of surface tension becomes significant. On the other hand, in columns with a large open area and large perforations, where intense emulsification of liquids takes place, the effect of surface tension is less pronounced.

On the basis of the theory of vortex motion, we can assume that vortices of equal size with the same circulation velocity appear at comparable points of a turbulent flow unbounded by a solid wall. Since mass exchange takes place on the free surfaces of the phases, and turbulent nature of mass transfer is possible, the pressure drop, which characterizes the intensity of vortex formation in a two-phase system, must be taken by considering only that part of energy which is spent for the interaction between the flows. This energy is proportional to the difference in the resistance of a two-phase (ΔP_{g-l}) and single-phase (ΔP_g) flows for the same velocity of the single-phase flow. If there is a hydrostatic column of liquid in an apparatus the pressure of this column must be subtracted from the resultant difference.

The larger the difference in the resistances offered to the flow in apparatus with and without reflux for a given reflux ratio, the larger the amount of energy consumed for the interaction between the flows of phases, for the evolution of their turbulence, and hence for the amount of substance transported. The role of free turbulence accordingly becomes more important.

For small reflux ratios, the difference in the resistance of the apparatus with and without reflux is relatively small, and therefore an

insignificant amount of energy is spent for mass transfer. In this case, the resistance of the apparatus with reflux mainly depends on the skin friction drag appearing as the gas flows through the passage. Mass transfer will take place in a liquid film on a geometrically fixed surface.

For relatively high reflux ratios and high rates of the gas (vapour) flow, mass transfer occurs in the entire volume of the gas-liquid emulsion, on the highly developed interface rather than on a geometrically fixed surface, which corresponds to large values of the difference $\Delta P_{g-l} - \Delta P_g$.

Thus, the interfacial turbulence can be quantitatively taken into account with the help of the resultant dimensionless *factor of hydrodynamic state of a two-phase system.*

4.3. Resistance in Two-Phase Flows. Hydrodynamic State Factor

The pressure drop per unit height of the apparatus in a two-phase flow is determined not only by the resistance offered to the motion of the gas phase, but also by the head which can additionally be created in the gas flow in order to compensate for the friction of the liquid flow. Thus, we can write

$$\left(\frac{\Delta P}{l}\right)_{g\text{-}l} = \lambda_g \frac{w_g^2 \gamma_g}{2g d_{e,\,g}} + \lambda_l \frac{w_l^2 \gamma_l}{2g d_{e,\,l}}. \tag{4.16}$$

If we denote by ε the fraction of the cross section occupied by the liquid phase, the fraction occupied by the gas phase will be $1 - \varepsilon$. The velocity of the liquid-phase flow, expressed in terms of its mass flow rate L referred to the total cross section of the apparatus can be represented as

$$w_l = \frac{Z}{\varepsilon \rho_l \times 3600}, \tag{4.17}$$

where w_l is the linear velocity of the liquid flow, m/s; L is the mass flow rate, kg/hr·m^2; ρ_l the density of the liquid, kg/m^3. Correspondingly, the velocity of the gas phase is given by

$$w_g = \frac{G}{(1-\varepsilon)\,\rho_g \times 3600}, \tag{4.18}$$

where w_g is the linear velocity of the gas flow, m/s; G is the mass flow rate of the gas, kg/hr·m^2; and ρ_g is the density of the gas, kg/m^3. The equivalent diameter for the gas and liquid flows is

$$d_{e,\,g} = \frac{4(1-\varepsilon)}{s}, \tag{4.19}$$

$$d_{e,\,l} = \frac{4\varepsilon}{s}, \tag{4.20}$$

where s is the specific area of the phase contact, m^2/m^3.

If we divide the pressure drop in the two-phase flow by the pressure drop in the gas flow upon its passage through the cross section equal to $(1 - \varepsilon)$, Eq. (4.16) becomes

$$\frac{\left(\frac{\Delta P}{l}\right)_{g\text{-}l}}{\left(\frac{\Delta P}{l}\right)_g} = 1 + \frac{\lambda_l}{\lambda_g}\left(\frac{w_l}{w_g}\right)^2\left(\frac{\gamma_l}{\psi_g}\right)\left(\frac{1-\varepsilon}{\varepsilon}\right). \qquad (4.21)$$

In the conditions of the two-phase flow under consideration the Reynolds number for the liquid flow can be represented in the form

$$\mathrm{Re}_l = \frac{Ld_{e.l}}{3600\,\varepsilon\mu_l} = \frac{4L}{3600 s g \mu_l} \qquad (4.22)$$

and, respectively, for the gas flow in the form

$$\mathrm{Re}_g = \frac{4G}{3600 s g \mu_g}. \qquad (4.23)$$

The drag coefficients can be represented in the general form as follows:

$$\lambda_l = \frac{c}{\left(\frac{4L}{3600 s g \mu_l}\right)^m} \qquad (4.24)$$

for the liquid flow and

$$\lambda_g = \frac{c}{\left(\frac{4G}{3600 s g \mu_g}\right)^m} \qquad (4.25)$$

for the gas flow.

Substituting the values of the drag coefficients and velocities from Eqs. (4.17) and (4.18) into Eq. (4.21), we obtain

$$\frac{\left(\frac{\Delta P}{l}\right)_{g\text{-}l}}{\left(\frac{\Delta P}{l}\right)_g} = 1 + \left(\frac{L}{G}\right)^{2-m}\left(\frac{\gamma_g}{\gamma_l}\right)\left(\frac{\mu_l}{\mu_g}\right)^m\left(\frac{1-\varepsilon}{\varepsilon}\right)^3. \qquad (4.26)$$

The ratio $(1 - \varepsilon)/\varepsilon$ in this equation characterizes the relative value of the open area occupied by the gas in the apparatus cross section, relative to the cross-sectional area occupied by the liquid. However, the fractions $(1 - \varepsilon)$ and ε occupied by the flows are usually unknown. The problem on the pressure drop can be solved as follows. If we divide the pressure drop $(\Delta P/l)_{g-l}$ in the two-phase flow by the pressure drop $(\Delta P/l)_g$ in the single-phase flow as it passes through the total cross section of the apparatus for the same gas velocity w_g, and accordingly replace the dimensionless group on the right-hand side of Eq. (4.26) by the group

$$\left(\frac{L}{G}\right)^{2-m}\left(\frac{\gamma_g}{\gamma_l}\right)\left(\frac{\mu_l}{\mu_g}\right)^m \eta,$$

we can establish the following relation for the given experimental values of L/G, γ_g/γ_l, and μ_l/μ_g, corresponding to the experimental values of $(\Delta P/l)_{g-l}$:

$$\eta = f\left[\left(\frac{L}{G}\right)^{2-m}\left(\frac{\gamma_g}{\gamma_l}\right)\left(\frac{\mu_l}{\mu_g}\right)^m\right]. \tag{4.27}$$

or, denoting

$$\left(\frac{L}{G}\right)^{2-m}\left(\frac{\gamma_g}{\gamma_l}\right)\left(\frac{\mu_l}{\mu_g}\right)^m = \Phi, \tag{4.28}$$

we obtain

$$\eta = f(\Phi). \tag{4.29}$$

Equation (4.26) can be reduced to the form

$$\frac{\left(\frac{\Delta P}{l}\right)_{g-l}}{\left(\frac{\Delta P}{l}\right)_g} = 1 + \left(\frac{L}{G}\right)^{2-m}\left(\frac{\gamma_g}{\gamma_l}\right)\left(\frac{\mu_l}{\mu_g}\right)^m \eta, \tag{4.30}$$

or

$$\frac{\left(\frac{\Delta P}{l}\right)_{g-l}}{\left(\frac{\Delta P}{l}\right)_g} = 1 + \Phi\eta. \tag{4.31}$$

When solving Eq. (4.31), experimental data must be available for establishing relation (4.29). The data are treated in the following sequence.

For a given hydrodynamic regime of a single-phase flow, the exponent m of the Reynolds number is calculated from the relation

$$\lambda = \frac{c}{\mathrm{Re}^{m'}} \tag{4.32}$$

For a purely molecular transport the laminar flow $m = 1$, while for fully developed turbulence under self-similar conditions, $m = 0$.

For a turbulent flow in smooth pipes, $m = 0.25$, while for pipes with packing $m = 0.2$. When the value of m is chosen, the parameter

$$\Phi = \left(\frac{L}{G}\right)^{2-m}\left(\frac{\gamma_g}{\gamma_l}\right)\left(\frac{\mu_l}{\mu_g}\right)^m. \tag{4.33}$$

is calculated from the experimental values of L, G, γ_g, γ_l, μ_l, and μ_g.

For a given experimental value of L/G and the same linear velocity of the gas (or the same mass flow rate G of the gas for a given hydrodynamic regime), which corresponds to the resistance of the dry apparatus $(\Delta P/l)_g$, the resistance of the apparatus with reflux is measured, the value of the parameter η is determined with the help of Eq. (4.31), and dependence (4.29) is plotted in logarithmic coordinates.

The plot obtained in this way is used for establishing the relation connecting η and Φ:

$$\eta = B\Phi^{-z}. \tag{4.34}$$

The value of η is then substituted into Eq. (4.31):

$$\frac{\Delta P_{g\text{-}l}}{\Delta P_g} = 1 + \Phi\,(B\Phi^{-z}). \tag{4.35}$$

After substituting the value of Φ from Eq. (4.33) into (4.35), the equation for the pressure drop can be obtained in the following final form:

$$\left(\frac{\Delta P}{l}\right)_{g\text{-}l} = \left(\frac{\Delta P}{l}\right)_g \left[1 + \beta \left(\frac{L}{G}\right)^a \left(\frac{\gamma_g}{\gamma_l}\right)^b \left(\frac{\mu_l}{\mu_g}\right)^c\right]. \tag{4.36}$$

This equation can be used for calculating the so-called hydrodynamic state factor of a two-phase system:

$$f = \frac{\Delta P_{g\text{-}l} - \Delta P_g}{\Delta P_g} = \beta \left[\left(\frac{L}{G}\right)^a \left(\frac{\gamma_g}{\gamma_l}\right)^b \left(\frac{\mu_l}{\mu_g}\right)^c\right]. \tag{4.37}$$

It should be borne in mind that besides the ratio L/G, we must know the absolute values of the gas flow rate G or the liquid flow rate L, since different hydrodynamic states of the two-phase flow may exist for the same ratio L/G. Consequently, we must know in addition the equation connecting the flow rate of the gas (or liquid) with the parameter Φ.

The order of magnitude of L and G in Eq. (4.36) must be the same (i.e. $L/G \leqslant 10$), since for large values of L/G, the effect of the hydrostatic column of liquid on $\Delta P_{g\text{-}l}$ becomes significant.

On the basis of the principle of corresponding states, the hydrodynamic state of a two-phase system can be characterized by the ratio w/w_{inv}, where w is the resultant velocity of the gas in the given hydrodynamic regime and w_{inv} is the resultant velocity of the gas in the reduced regime (inversion point). The quantity β appearing in the factor f is a single-valued function of w/w_{inv}, and, therefore, the factor f characterizes the hydrodynamic state of a two-phase system.

If interfacial tension is present in a two-phase (liquid-liquid) flow, it must be introduced into the hydrodynamic state factor of the two-phase system, for example, in the form of relation (4.26). Then formula (4.37) can be reduced to

$$f = \beta \left(\frac{L}{G}\right)^a \left(\frac{\gamma_g}{\gamma_l}\right)^b \left(\frac{\mu_l}{\mu_g}\right)^c \left(\frac{\sigma_{1\text{-}2}}{\sigma_{1\text{-}a} + \sigma_{2\text{-}a}}\right)^d. \tag{4.38}$$

For liquid-gas and liquid-vapour systems, we have

$$\frac{\sigma_{1\text{-}2}}{\sigma_{1\text{-}a}+\sigma_{2\text{-}a}}=1.$$

The hydrodynamic state factor of a two-phase system can also be obtained on the basis of the theory of turbulent two-phase flows.

4.4. Linear Velocity of Flow in a Two-Phase System

The linear velocity of a gas, vapour and liquid as a result of interaction between phases must be determined from the relation between the same quantities that characterize the hydrodynamic state of a two-phase system, although the quantitative relations may be different. The resultant linear velocity of the flow, referred to the total apparatus cross section (with the equivalent diameter d_e taken as the characteristic dimension and in the presence of the driving force created by the force of gravity), can be represented in the dimensionless form as an analog of the Froude number: $w_0^2/(F_0^2 g d_e)$, where w_0 is the linear velocity of the flow referred to the total cross section of the apparatus, F_0 is the fraction of the apparatus open area, and d_e is the equivalent diameter.

In deriving the equation of drag in a two-phase flow, it was shown that the ratio of the cross sections of the two-phase flow, occupied by the gas and the liquid, is a function of the parameter Φ (see (4.33)):

$$\Phi=\left(\frac{L}{G}\right)^{2-m}\left(\frac{\gamma_g}{\gamma_l}\right)\left(\frac{\mu_l}{\mu_g}\right)^m,$$

and the interfacial tension $\sigma_{1\text{-}2}/(\sigma_{1\text{-}a}+\sigma_{2\text{-}a})$.

The resultant linear velocity of the gas must be a function of the same quantities:

$$w_0=f_0\left[\left(\frac{L}{G}\right)^{2-m}\left(\frac{\gamma_g}{\gamma_l}\right)\left(\frac{\mu_l}{\mu_g}\right)^m\left(\frac{\sigma_{1\text{-}2}}{\sigma_{1\text{-}a}+\sigma_{2\text{-}a}}\right)^z\right] \tag{4.39}$$

Introducing the analogue of the Froude number, the relation can be represented in the dimensionless form:

$$\frac{w_0^2}{F_0 g d_e}=f_1\left[\left(\frac{L}{G}\right)^{2-m}\left(\frac{\gamma_g}{\gamma_l}\right)\left(\frac{\mu_l}{\mu_g}\right)^m\left(\frac{\sigma_{1\text{-}2}}{\sigma_{1\text{-}a}+\sigma_{2\text{-}a}}\right)^z\right] \tag{4.40}$$

For $m = 0$, the parameter Φ of a two-phase flow for gas-liquid and vapour-liquid systems has the form

$$\Phi'=\left(\frac{L}{G}\right)^2\left(\frac{\gamma_g}{\gamma_l}\right) \tag{4.41}$$

The parameter Φ' is an analogue of the kinetic energy of the liquid and gas flows. Indeed, the kinetic energy is defined by the equation

$$K_e=\frac{mw^2}{2}. \tag{4.42}$$

Introducing the density ρ instead of mass m, we obtain

$$K_e = \rho \frac{w^2}{2}, \tag{4.43}$$

or

$$K_e = \frac{\gamma w^2}{2g}. \tag{4.44}$$

But since the linear velocity is proportional to the mass flow rate, we obtain, respectively, for the two flows

$$\begin{aligned} K_{e,\,g} &= \frac{G^2 \gamma_g}{2g}, \\ K_{e,\,l} &= \frac{L^2 \gamma_l}{2g}. \end{aligned} \tag{4.45}$$

The ratio of the kinetic energies of the flows is expressed by

$$\frac{K_{e,\,l}}{K_{e,\,g}} = \left(\frac{L}{G}\right)^2 \left(\frac{\gamma_l}{\gamma_g}\right). \tag{4.46}$$

This equation differs from (4.41) in the inverse ratio of specific gravities, which cannot affect these equations in terms of energy. Therefore, the parameter Φ' can be defined as an analogue of the kinetic energy of the liquid and gas flows in a two-phase system.

When calculating the velocity of vapour or gas in packed, plate, and other types of apparatus, the parameter Φ' in Eq. (4.41) can be given the form

$$\Phi'' = \left(\frac{L}{G}\right) \left(\frac{\gamma_g}{\gamma_l}\right)^{1/2}. \tag{4.47}$$

or

$$\Phi''' = \left(\frac{L}{G}\right)^{1/2} \left(\frac{\gamma_g}{\gamma_l}\right)^{1/4}. \tag{4.48}$$

4.5. Unidirectional Flows in Two-Phase Systems

The unidirectional motion of flows in vapour-liquid or gas-liquid two-phase systems is observed in some types of stills, condensers, absorption and rectifying columns, and chemical reactors.

The distinguishing feature of unidirectional motions in two-phase systems is that the flows move not as a single entity but each phase moves relative to the other, the phase with a larger specific gravity moving slower and decelerating the motion of the lighter phase. There are several types of motion in such systems depending on the mass flow rate of each phase (gas concentration) as well as on the vertical or horizontal direction of their motion. However, there may be similar kinds of motion for the vertical and horizontal directions.

Figure 73 represents the possible kinds of motion for the vertical and horizontal gas-liquid flows. The following regimes of flows are distinguished.

1. *Bubbling regime I.* In this regime, the gas moves in the liquid in the form of individual bubbles with a velocity exceeding the velocity of the liquid. Such a regime may appear, for instance, when

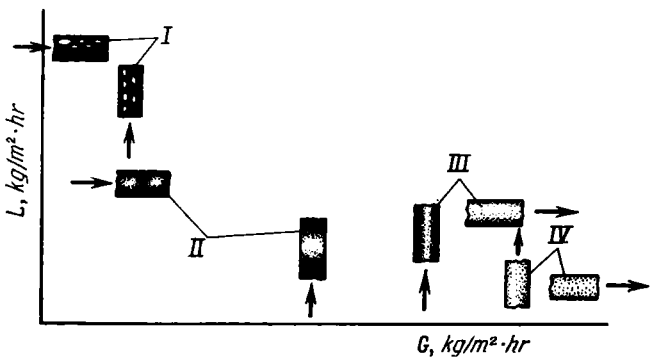

Fig. 73. Types of flows in unidirectional two-phase systems.

a relatively small amount of gas is introduced into a liquid flowing at a constant velocity. The gas breaks into small bubbles which remain discrete during the motion of the system.

2. *Plug regime II.* In this regime, the bubbles unite to form peculiar gas plugs resembling in shape the shells with heads of a parabolic outline. Thus, alternating gas and liquid plugs move through the pipe, the liquid plugs containing inclusions of gas bubbles.

3. *Annular regime III.* The gas moves in the middle, while the liquid pierced by gas bubbles moves along the walls of the pipe.

4. *Emulsifying regime IV.* As the flow rates of the vapour (gas) become sufficiently high, phase inversion takes place: the gas becomes a continuous phase, and the liquid becomes the disperse phase. In this case, the system moves as a continuous, homogeneous disperse mass of liquid and fine bubbles of gas, forming a gas-liquid emulsion.

This classification of regimes represents the most typical forms of flow of gas-liquid systems. However, the transient types of motion, such as *core-type*, *semi-annular*, *film-emulsion*, and *drop* flows are also encountered. In the case of comparatively low gas and liquid flow rates, the system in a horizontal pipe may separate into the liquid and gas moving along the pipe with or without wave formation, in the form of a core-type flow, etc.

Figure 74 shows the variation of the pressure drop in a two-phase system $(\Delta P/l)_{g-l}$ and in the holding capacity φ_R related by

$$\varphi_R = \frac{V_g(1-q)}{q}, \qquad (4.49)$$

where V_g is the volumetric rate of gas flow and q is the volume fraction of the gas for various regimes in a unidirectional vertical flow at a constant velocity of liquid ($\sim$0.62 m/s). It can be seen from the figure that only in the emulsifying regime (IV) the variation of different quantitative characteristics of a two-phase flow is the same or at least similar. This is in agreement with the properties of motion of two-phase systems considered above.

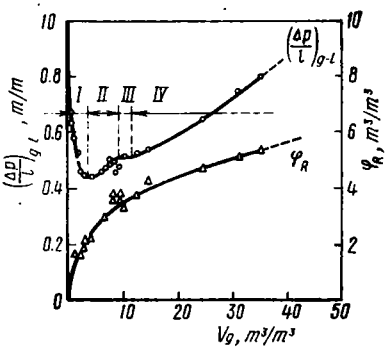

Fig. 74. Variation of $(\Delta P/l)_{g-l}$ and of holding capacity for different regimes for unidirectional vertical motion of a two-phase system:

I—bubbling flow; *II*—plug flow; *III*—annular flow; *IV*—emulsifying flow.

For vertical pipes, we may take the dimensionless group determining the transition from one flow regime to another in the form of the so-called Froude number for mixtures:

$$\mathrm{Fr}_{mix} = \frac{w_{mix}^2}{g d_p}, \qquad (4.50)$$

$$w_{mix} = \frac{v_l + v_g}{\pi d_p^2/4}, \qquad (4.51)$$

where v_l and v_g are the volumetric flow rates of liquid and gas, m³/s, and d_p is the inner diameter of the pipe, m.

The so-called volumetric gas concentration is a function of the Froude number:

$$\varphi_{v\cdot c} = \frac{v_g}{v_g + v_l}. \qquad (4.52)$$

It was found that the following relationship is observed for the boundary between the bubbling (I) and plug (II) regimes:

$$\varphi_{v\cdot c} = 0.05\ \mathrm{Fr}_{mix}^{0.2}. \qquad (4.53)$$

For the boundary between regimes (II) and (III), we have

$$\varphi_{v\cdot c} = (0.12 \text{ to } 0.5)\,\mathrm{Fr}_{mix}^{0.15-0.10}. \qquad (4.54)$$

For the boundary between (III) and (IV) regimes,

$$\varphi_{v.c} = (0.65 \text{ to } 0.85)\,\mathrm{Fr}_{mix}^{0.05-0.02}. \qquad (4.55)$$

Figure 75 represents the variation in the ratio of the pressure drop ΔP_{g-l} in a two-phase flow to the pressure drop in a one-phase flow

$$\psi_g = \left(\frac{\Delta P_{g\text{-}l}}{\Delta P_g}\right)^{1/2}$$

for the gas phase and

$$\psi_l = \left(\frac{\Delta P_{g\text{-}l}}{\Delta P_l}\right)^{1/2}$$

for the liquid phase, provided that the gas and the liquid move at the same velocity, temperature, and pressure as in a two-phase flow.

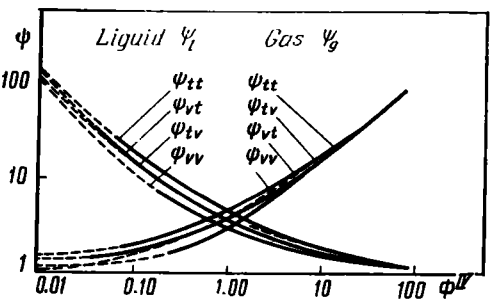

Fig. 75. ψ vs. Φ dependence:

ψ_{vv}—the two phases are in laminar flow; ψ_{tv}—gas is in turbulent flow while liquid is in laminar flow, or vice versa; ψ_{vt} and ψ_{tt}—gas and liquid are in turbulent flow.

The pressure drop in a two-phase unidirectional flow can be determined through the modified factor Φ which can be expressed as follows:

$$\Phi^{IV} = \left(\frac{\Delta P_l}{\Delta P_g}\right)^{1/2}, \tag{4.56}$$

or

$$\Phi^{IV} = \left[\left(\frac{w_l}{w_g}\right)^m \left(\frac{\gamma_g}{\gamma_l}\right)^n \left(\frac{\mu_l}{\mu_g}\right)^c\right]^{0.5}, \tag{4.57}$$

where the exponents m, n, and c are determined by the flow regime of the phase. First, the Reynolds numbers for each phase are calculated, then ΔP_g and ΔP_l are determined separately from the equation of drag for a single-phase flow. Having determined tha parameter Φ^{IV} from Eq. (4.56), we can find ψ for each phase with the help of Fig. 75, whence the pressure drop in a two-phase flow can be calculated:

$$\Delta P_{g\text{-}l} = \psi_g^2 \Delta P_g, \tag{4.58}$$

and

$$\Delta P_{g\text{-}l} = \psi_l^2 \Delta P_l. \tag{4.59}$$

In order to find the pressure drop in a unidirectional flow of air-water mixtures in rough horizontal pipes, we can use the equation

$$\frac{\Delta P_{g\text{-}l}}{\Delta P_l} = 1 + c\left(\frac{G}{L}\right)^{0.875m}\left(\frac{\mu_g}{\mu_l}\right)^{0.125m}\left(\frac{\gamma_l}{\gamma_g}\right)^{0.5m}, \qquad 4.60)$$

where ΔP_{g-l} is the pressure drop in a two-phase flow; ΔP_l is the pressure drop in the liquid flow; and c and m are constants determined experimentally.

The pressure drop in a two-phase flow at the inlet of a channel (vertical pipe) can be calculated from the equation

$$\frac{\Delta P_{g\text{-}l}}{\Delta P_g} = 1 + 5.4\left(\frac{L}{G}\right)^{0.7}\left(\frac{\gamma_g}{\gamma_l}\right)^{0.4}\left(\frac{\mu_l}{\mu_g}\right)^{0.1}. \qquad (4.61)$$

If the vertical pipe is arranged so that its bottom edge is in the immediate vicinity of the liquid surface, the region of a lower static pressure is formed under the pipe as the gas flows into it. This drop in the static pressure on the surface of the liquid causes the liquid to rise along the pipe axis. The column of liquid is entrained by the gas flow, accelerated in the region where the gas stream broadens to one or two diameters, and the liquid is intensely emulsified.

4.6. Hydrodynamic Parameters of a Bubbling Layer

A bubbling layer is one of the most typical two-phase systems employed in industrial equipment (various types of plate columns and bubbling apparatus).

A bubbling layer has an extremely intricate structure since it is nonhomogeneous, some of its physical parameters (e.g. viscosity) are not determined, there is no fixed interface (it continuously changes its size and shape), and gas bubbles rising to the surface, as well as gas streams, create high-intensity circulation currents of liquid. For this reason, till now there is no exact quantitative description of the bubbling layer. The parameters of the layer, which determine its structure, are the density and height of the gas-liquid layer, the size and velocity of bubbles, the area of interface, and the longitudinal mixing of the liquid and gas phase.

Although there is no precise classification of regimes of bubbling, we can definitely single out two regimes: the bubbling and spray regimes.

The bubbling regime has the following features: (a) at the bubbler outlet, the bubbles break away uniformly at regular intervals of time; (b) upon acceleration over a very short distance, the bubbles rise rectilinearly and uniformly, i.e. at a constant velocity, and the distance between them remains constant. Assuming the bubbles have spherical shape and there is no interaction between them, we

can obtain the formula for the bubble diameter on the basis of the balance of forces acting on a bubble at the moment it breaks away from the perforations of the bubbler:

$$d_b = \sqrt[3]{\frac{6d_p\sigma}{(\rho_l-\rho_g)g}}. \qquad (4.62)$$

where d_b is the bubble diameter; d_p is the diameter of a bubble perforation; σ is the surface tension of the liquid; ρ_l and ρ_g are the densities of the liquid and gas, respectively; and g is the acceleration due to gravity.

This equation is in good agreement with experimental data over a wide range of variation of physical properties of liquid, gas rates, and diameters of bubble perforations.

The spray regime has the following features: (a) the separation between bubbles becomes so small that they coalesce into a continuous jet; (b) the velocity of rising bubbles varies slightly and depends on the gas phase flow rate, while the trajectory may deviate from the vertical; (c) the bubble diameter depends on the gas flow rate, and the shape of the bubbles undergoes deformation.

When a chain of spherical bubbles is formed and they come into contact, we can assume that the formation of a bubble takes place at the same rate at which the previous bubble is detached. Then, using the balance of forces acting on a bubble, we can write the following expression for the bubble diameter d_b:

$$d_b = \sqrt[3]{\frac{6V_g}{\pi w_0}}, \qquad (4.63)$$

where V_g is the volumetric flow rate of the gas and w_0 is the velocity of an individual bubble. Using Eqs. (4.62) and (4.63), we can calculate the critical volumetric gas flow rate, determining the boundary between the bubbling and the spray regimes:

$$V_{g,\,cr} = \frac{\pi w_0}{6}\left[\frac{6d_p\sigma}{g(\rho_l-\rho_g)}\right]^{2/3} \qquad (4.64)$$

Equations (4.62)-(4.64) are approximate since they do not take into account the interaction between the bubbles and their interaction with the liquid. As the gas flow rate increases, the frequency of bubble formation becomes constant (17-40 s^{-1}). The influence of walls becomes noticeable when the apparatus diameter is smaller than 200 mm. The average diameter of bubbles decreases with increasing diameter of the apparatus at the same flow rate. The diameter of the bubbler perforation and its open area have practically no effect on the bubble diameter (a 100-fold increase in the perforation diameter only doubles the bubble diameter).

Upon dynamic interaction between liquid and gas, the bubbles break up and coalesce. As a result, more stable (from the point of

view of energy) bubbles are formed in the bubbling layer, and their dimensions are independent of the conditions under which the gas is introduced into the liquid. The mean bubble radius r is determined from the equation

$$r = \frac{\xi w_0^2}{2g}, \qquad (4.65)$$

where ξ is the coefficient of resistance offered to the relative motion of the bubble. This coefficient is determined graphically (Fig. 76).

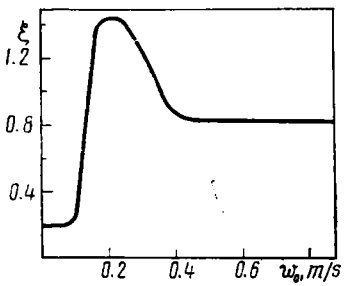

Fig. 76. Drag coefficient as a function of the gas velocity.

Figure 77 shows the change in the bubble diameter with the height of the layer of liquid in the apparatus for different gas velocities.

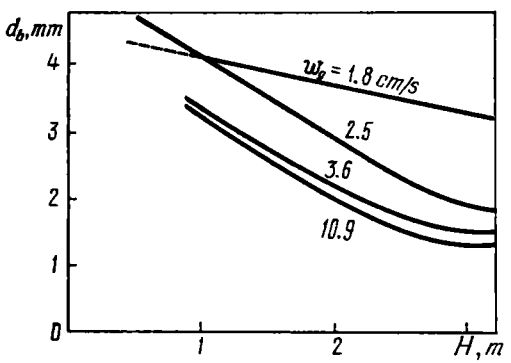

Fig. 77. Mean bubble diameter as a function of the bubbling column height for different gas velocities.

Figure 78 represents the dependence of the velocity w_0 of a rising bubble on its diameter.

The entire range of velocity of ascending bubbles can be tentatively divided into four regions:

(1) $d_b < 0.7$ mm. The bubbles behave as solid particles, and the velocity of their ascent is governed by Stokes' law;

(2) 0.7 mm $< d_b <$ 1.4 mm. The bubbles retain the spherical shape, but internal circulation appears, thus decreasing the stress on the interface. The velocity of ascent exceeds the value calculated by Stokes' law;

(3) 1.4 mm $< d_b <$ 6.0 mm. The bubbles are no longer spherical and ascend in a zig-zag manner. The resistance to their motion

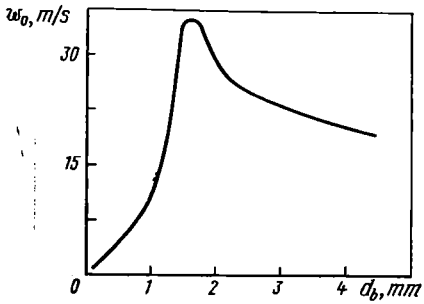

Fig. 78. Velocity w_0 of ascending bubble as a function of its diameter d_b.

somewhat increases due to the formation of a hydrodynamic trail. A change in the bubble diameter leads to an insignificant change in the velocity of ascent.

(4) $d_b > 0.006$ m. The bubbles are bowl-shaped. The limiting velocity of ascent increases with the bubble diameter.

In the case of mass bubbling, the bubbles have a shape of flattened ellipsoid whose minor axis is oriented in the direction of motion. The velocity of ascent for such bubbles can be calculated from the following equation:

$$w_0 = \left(\frac{\sigma^2 g}{3\pi\mu}\,\frac{1}{\rho_l}\right)^{1.5}. \qquad (4.67)$$

The interfacial area a in a bubbling apparatus increases with the gas flow rate: $a \propto w^{0.5\text{-}0.7}$. It was also established that the physical parameters of the phases influence the interfacial area. As the density ρ_l of the continuous phase increases, the interfacial area increases in proportion to $\rho^{0.2\text{-}0.5}$ and decreases in proportion to $\sigma^{-(0.6\text{-}1.0)}$.

Gas content of a bubbling layer. In the bubbling regime in which the bubbles do not interact, the motion of bubbles is similar to the precipitation of solid spherical particles. The dependence of the gas content on the gas velocity in the empty column is described by the following equation:

$$w = \alpha\varphi\,(1 - \varphi), \qquad (4.68)$$

where w is the gas velocity in the empty column, cm/s; α is the coefficient corresponding to the velocity of an individual bubble (which practically ranges between 30 and 32 cm/s), cm/s; and φ is the gas content of the layer.

The dependence of the gas content on the velocity of the gas phase and the densities of the liquid and gas phases is described by the following empirical formula

$$\varphi = 1 - \exp\left[-\frac{0.2w/w_0\left(\frac{\rho_g}{\rho_l}\right)^{0.2}}{1+0.00875\left(\frac{w}{w_0}\right)^{0.95}\left(\frac{\rho_g}{\rho_l}\right)^{0.75}}\right]. \qquad (4.69)$$

In small-diameter apparatus for which the ratio $D/d_b < 40$, the influence of the walls becomes significant. The height of the gas-liquid layer also affects the gas content, since the motion of bubbles is a nonstationary process over the layer height. At the bottom of the layer, the bubbles move at high velocities, but at the top of the

layer they are decelerated. Consequently, the gas content of an apparatus of a small height is considerably higher than the gas content in an apparatus of a large height.

The effect of the apparatus diameter and the layer height on the gas content φ of the bubbling layer is taken into account by the correction factors K_D and K_H:

$$\varphi = 1 - K_D K_H \varphi_0' \tag{4.70}$$

where

$$K_D = 1 - \exp\left[-1.1\left(\frac{w_g}{w_0}\right)^{0.5}\left(\frac{\sqrt{gD}}{w_g}\right)^{0.75}\right], \tag{4.71}$$

$$K_H = 1 - \exp\left[-0.405\left(\frac{w_g}{w_0}\right)^{0.7}\left(\frac{\sqrt{gH}}{w_g}\right)\right], \tag{4.72}$$

φ_0' is the gas content of the bubbling layer in an apparatus with a small diameter and a small height of the layer of liquid; D is the apparatus diameter, cm; and H is the height of the layer of clear liquid, cm. The influence of the apparatus diameter on the gas content becomes insignificant beginning from D = 15-20 cm, and the influence of height, from H = 0.6 m.

The values of the gas content for a system with continuous flow of liquid can be obtained from the values of the gas content φ_0'' for a batch-type system:

$$\varphi_w = (1 \pm 0.04 w_l)\,\varphi_0'', \tag{4.73}$$

where the plus sign corresponds to the liquid in counterflow, and the minus sign to the liquid in forward flow, and w_l is the empty-column velocity of liquid, cm/s.

Equation (4.73) is valid for velocities of liquid ranging from 0 to 20 cm/s for forward flow and from 0 to 10 cm/s for counterflow systems.

The sectioning of bubbling apparatus* essentially increases the gas content of the layer.

Longitudinal mixing of liquid phase. The structure of the liquid phase in a bubbling apparatus is described sufficiently well by the diffusion model worked out on the basis of the semi-empirical theory of longitudinal dispersion of a substance.

The longitudinal mixing coefficient does not depend on the height of the gas-liquid layer. An increase in the apparatus diameter enhances the transverse nonuniformity, thus inevitably increasing the longitudinal mixing coefficient which is directly proportional to the apparatus diameter (Fig. 79). The liquid-phase longitudinal mixing coefficient D_L depends on the diameter of the bubbler perforation: when the diameter d_p of perforation is small, small bubbles

* Bubbling apparatus is an installation containing a high layer of liquid and equipped with special distributors for supplying a gas

are formed, due to which D_L diminishes. Starting from $d_p = 1$ mm, the quantity D_L becomes independent of d_p. The velocity w_l of the liquid phase does not affect the value of D_L for velocities $w_l \leqslant$

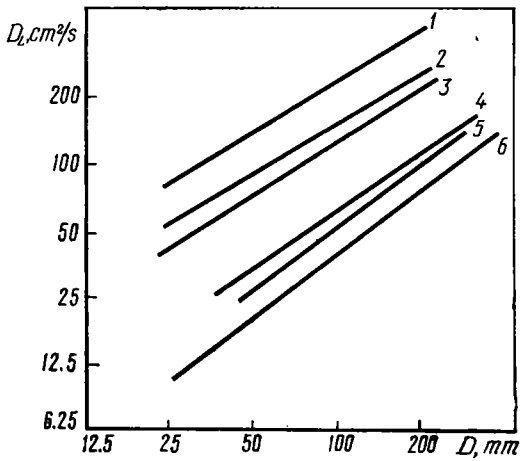

Fig. 79. The effect of the apparatus diameter on the axial dispersion of the liquid phase for different gas velocities:
1—10 cm/s; 2—8 cm/s; 3—6 cm/s; 4—3 cm/s; 5—2.2 cm/s; 6—1.5 cm/s.

$\leqslant w_{cr}(1 - \varphi)$. When the velocity $w_l > w_{cr}(1 - \varphi)$, the value of D_L increases linearly with w_l. The value of the critical velocity is determined by the relation

$$w_{cr} = \frac{w_l}{1 - \varphi}. \tag{4.74}$$

The degree of circulation of the liquid phase increases with its velocity, as a result of which the longitudinal mixing coefficient D_L grows. The value of this coefficient for the liquid phase is calculated from the empirical relations

$$D_L = Dw_{cr} + 1.67Dw_0 \left(\frac{w_g}{w_0}\right)^{2/3} \tag{4.75}$$

for $w_l \leqslant w_{cr}(1 - \varphi)$ and

$$D_L = Dw_{cr} + 12.1D\frac{w_{cr}}{1 - \varphi}\left(\frac{w_g}{w_0}\right)^{2/3}. \tag{4.76}$$

for $w_l > w_{cr}(1 - \varphi)$.

As the pressure increases, the value of D_L for moderate gas velocities ($w_g < 10$ cm/s) becomes lower, while for high velocities of the gas it is independent of pressure. With a rise in temperature, the

value of D_L considerably increases for all gas velocities. The value of D_L linearly increases with the viscosity of the liquid phase.

The sectioning of bubbling apparatus considerably reduces the longitudinal mixing of the liquid phase due to the suppression of the circulation of liquid inside the apparatus. As the open area of partitions decreases, the longitudinal mixing of the liquid is reduced. An increase in the number of partitions considerably decreases the value of D_L. The diameters of the holes in the partitions practically do not affect the longitudinal mixing coefficient.

Longitudinal mixing of gas phase. The structure of the gas-phase flow is close to ideal (perfect) mixing within the entire range of gas flow rates. For small flow rates of the gas ($w_g < 2.5$ cm/s), the structure of the gas-phase flow is described by 3-7 cells of ideal mixing, while at high gas rates, by ideal mixing.

It was found that when the concentration of a tracer-gas was measured more accurately with the help of a low-inertia infra-red adsorption gas analyzer, the structure of the gas-phase flow is described by 6-10 cells of perfect mixing over the entire range of gas flow rates. In apparatus with a small height of the gas-liquid layer, the gas-phase longitudinal mixing considerably increases due to a stronger influence of edge effects. An increase in the apparatus diameter practically does not affect the gas-phase longitudinal mixing. This is very important from a practical point of view, since it allows us to apply the experimental results on longitudinal mixing, obtained in experimental setups, to industrial installations. When the apparatus is sectioned with partitions, the longitudinal mixing in the gas phase increases due to the retention of a part of the bubbles near the partitions.

Part Three

Fundamentals of Kinetics of Mass-Transfer Processes

Chapter Five

Mechanism of Mass Transport and Diffusion Laws

5.1. Basic Concepts and Definitions

Mass transport is realized simultaneously in two ways: by molecular diffusion (microkinetics) and by eddy diffusion (macrokinetics).

Molecular diffusion. Molecular diffusion is the branch of microkinetics in which mass transport is accomplished by molecules. Gas molecules continuously move and collide with each other. The number of such collisions is very large owing to high velocities and large numbers of molecules. The molecules as if "push aside" each other, as a result of which the direction and magnitude of molecular velocities continuously change. The huge number of collisions among molecules makes them "joggle" at one place rather than move in a certain direction. This explains a permanent, spontaneous, and slow mixing of gas molecules and transport of energy and mass.

Let us consider the behaviour of solute molecules in a solution. Solute molecules continuously collide with solvent molecules. These collisions lead to a random motion of molecules. Although the mean path covered by a molecule in a given interval of time can be calculated, a method for predicting its actual path does not exist. The graphic representation of the probable position of the molecule with time would give a number of concentric circles around its original position.

The first attempt to establish the relationship between the random molecular motion and diffusion flow was made by Einstein in the analysis of the Brownian movement. Considering the motion only along the x-axis and assuming that the positive and negative displacements are equally probable, Einstein showed that the probability of the horizontal displacement from x to $x + dx$ is equal to

$$N_p = \frac{1}{\sqrt{2\pi\Delta_1^2}} \exp\left(-x^2/2\Delta_1^2\right) dx, \qquad (5.1)$$

where Δ_l is the root-mean-square value of the linear displacement.

There is a simple relation between Δ_l^2 and the molecular diffusion coefficient D_m [see Eq. (3.113)] which is equal to the number of molecules per unit cross-sectional area per unit time if the concentration gradient is equal to unity:

$$D_m = 1/2\ (\Delta_l^2)/\tau. \tag{5.2}$$

The number of particles crossing the surface is equal to $(1/2)\ (\Delta_l^2) \times \times (C_2 - C_1)$, and Eq. (5.1) can be written in the form

$$N_p = \frac{1}{\sqrt{4\pi D_m \tau}} \exp\left(-x^2/4D_m\tau\right) dx. \tag{5.3}$$

This equation is valid if the initial amount of the solute corresponds to the boundary conditions for $x = 0$ and $\tau = 0$. If we multiply the right-hand side of Eq. (5.3) by the amount of substances, we obtain the concentration of the solute during the entire period τ.

Fick's first law. Although the statistical interpretation of diffusion gives a visual picture of its nature, Fick's law is the first deterministic formulation of the diffusion rate. In analogy with the thermal flow, Fick established that the velocity of transport for a given temperature and pressure is proportional only to the concentration gradient. If q is the diffusion flow, i.e. the velocity of mass transport of a substance per unit area, and dC/dz is the concentration gradient, the following equation is valid for a unidirectional flow:

$$q = -D_m\ (dC/dz), \tag{5.4}$$

where D_m is the molecular diffusion coefficient for a given system, which is assumed constant and has the dimensions L^2T^{-1}. The minus sign indicates that the mass flow is directed oppositely to the concentration gradient. In accordance with the concept of diffusion flow, the substance Q (kg·mole) passing through the area F (m^2) during time τ (hrs) is

$$q = \frac{Q}{F\tau} = -D_m \frac{dC}{dz}. \tag{5.5}$$

Since the diffusion of both components of a binary system requires that the flow of one of the components be balanced by the opposite flow of the other component, we can write Eq. (5.5) for each of the components. Normally, only one equation is used for expressing diffusion in binary systems under given conditions, assuming that the coefficient remains the same for each of the components. The diffusion coefficients are identical only if the volumes of the components A and B remain unchanged during diffusion.

Let us write the diffusion coefficient for each of the substances:

$$q_A = -D_A\ (dC_A/dz), \tag{5.6}$$

$$q_B = -D_B\ (dC_B/dz). \tag{5.7}$$

Let V_A and V_B be the constant volumes taken as units of measurements for determining the concentrations of A and B. If the measurement of concentrations does not significantly affect the measurement of volume, V_A and V_B will be proportional to molar volumes. The volume of component A diffusing per unit time through a unit cross-sectional area amounts to $-D_A V_A (dC_A/dz)$, while for component B it is equal to $-D_B V_B (dC_B/dz)$. If the volume of the system remains unchanged, the difference in diffusing volumes in the cross section under consideration will be equal to zero, i.e.

$$-D_A V_A (dC_A/dz) + D_B V_B (dC_B/dz) = 0. \tag{5.8}$$

The volumes of components A and B per unit total volume of solution are $V_A C_A$ and $V_B C_B$ respectively. If only components A and B are present, we have

$$V_A C_A + V_B C_B = 1. \tag{5.9}$$

Differentiating this equation with respect to z, we get

$$V_A (dC_A/dz) + V_B (dC_B/dz) = 0. \tag{5.10}$$

It follows from Eqs. (5.8) and (5.10) that $D_A = D_B$, or $V_A = 0$, or $V_B = 0$. If V_A and V_B cannot be considered constant, $D_A \neq D_B$. For conventional organic systems D_A can be assumed equal to D_B, and the diffusion coefficient should be treated as the coefficient of mutual diffusion, i.e. $D_{AB} = D_m$. Fick's first law for unidirectional diffusion can be represented in the vector form:

$$q = -D_m \operatorname{grad} C = -D_m \nabla C. \tag{5.11}$$

Hydrodynamic derivation of Fick's first law. We can arrive at Fick's equation if we take the osmotic pressure as the driving force. The force acting on a solute particle in a dilute solution can be expressed by the following equation:

$$\vec{f} = -(m/C) \operatorname{grad} P_{os}, \tag{5.12}$$

where C is the concentration; m the particle mass; and P_{os} the osmotic pressure. Since $P = (CRT/mN_A)$, where N_A is the Avogadro number, we can represent this equation in the following form:

$$\vec{f} = -(RT/N_A) [(\operatorname{grad} C)/C]. \tag{5.13}$$

In a steady-state flow, where each particle has a constant velocity $\vec{v} = B\vec{f}$, where B is the "mobility" (a factor depending on the size and shape of the particle and the viscosity of the medium being distributed). Using the expression for $\vec{f}$, we obtain

$$\vec{v} = -(RT/N_A)(B) [(\operatorname{grad} C)/C]. \tag{5.14}$$

Introducing the flux $\vec{q}$, we get

$$\vec{q}=C\vec{v}=-(RT/N_A)(B)(\text{grad}\,C)=-D_m\,\text{grad}\,C, \qquad (5.15)$$

where $D_m = (RT/N_A)(B)$.

When the drag $1/B$ of the flow is equal to the Stokes resistance $6\pi\mu r$, expression (5.15) leads to the Stokes-Einstein equation

$$\frac{D_m\mu}{kT}=\frac{1}{6\pi r}, \qquad (5.16)$$

where D_m is the molecular diffusion coefficient; μ the solution viscosity; k the Boltzmann constant; and r the radius of solute molecules.

Eddy diffusion. This type of diffusion is associated with macrokinetic concepts according to which mass transport is accomplished by macroparticles of liquid and is determined by the turbulence of the flow and its hydrodynamic state. Eddy diffusion is also called *turbulent diffusion*. In eddy flow of liquids, an additional mass transport appears in the flow. In this case, the amount of substance being transported is determined in the same way as the quantity of energy additionally transferred in the flow [Eq. (3.90)], i.e. from the relation

$$q_B=-D_t\frac{dC}{dz}, \qquad (5.17)$$

where D_t is the eddy, or turbulent, diffusion coefficient. Like the eddy viscosity, it is not constant but depends on the hydrodynamic conditions of a process.

The evolution of eddy flow leads to an intense transport across the flow, appearance of turbulence, and hence to intense mixing in the flow. At the same time, mass transfer processes require the presence of a concentration gradient along the flow from the entrance to the exit from the apparatus. The concentrations must continuously change. Vigorous mixing in the turbulent flow leads to longitudinal mixing as well, which diminishes the longitudinal concentration gradient and deteriorates the separation. The higher the eddy diffusion coefficient D_t, the greater the influence of mixing effect. In this respect, the coefficient D_t is the characteristic of mixing intensity in diffusion processes.

Hence, the development of turbulence does not always lead to intensification of mass transfer. Consequently, mass transport in apparatus must be organized in such a way that the effect of longitudinal mixing associated with turbulence is reduced to minimum. In practice, this can be attained by using fine packing, by creating unidirectional gas and liquid flows in plate towers of special construction, and finally, by designing apparatus of jet-column type.

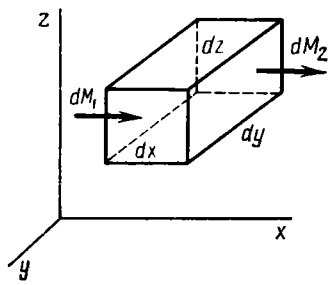

Fig. 80. To the derivation of Eq. 5.30).

Hence, the total mass transfer due to molecular and eddy diffusion is equal to

$$q = q_m + q_B = -(D_m + D_t)\frac{dC}{dz}. \quad (5.18)$$

In practical calculations of mass-transfer processes, the total mass transfer is usually expressed through the total diffusion equation

$$q = K\Delta C, \quad (5.19)$$

where K is the mass-transfer coefficient whose dimensions depend on the units in which concentration is measured, and ΔC is the difference in concentrations or the driving force of the process, which can be averaged by different methods. By expressing the concentration gradient of Eq. (5.18) in terms of finite differences, we obtain

$$q \cong (D_m + D_t)\frac{\Delta C}{\Delta z}. \quad (5.20)$$

Comparing Eqs. (5.19) and (5.20), we get

$$K \approx \frac{D_m + D_t}{\Delta z}. \quad (5.21)$$

It follows from this relation that the mass-transfer coefficient takes into account the molecular and turbulent mechanisms of mass transfer.

Fick's second law. Let us consider the total derivative of concentrations:

$$\frac{DC}{d\tau} = \frac{\partial C}{\partial \tau} + w_x\frac{\partial C}{\partial x} + w_y\frac{\partial C}{\partial y} + w_z\frac{\partial C}{\partial z}. \quad (5.22)$$

If we analyze the material balance equation for the substance supplied to and removed from an elementary parallelepiped with faces dx, dy, and dz (Fig. 80) in the liquid flow, we obtain the following relationships. Let us consider the mass transport along the x-axis and express the quantity of substance entering and leaving the parallelepiped owing to molecular diffusion. According to Eq. (5.5), we have at the entrance

$$dM_1 = D_m\frac{\partial C}{\partial x}\,dy\,dz\,d\tau, \quad (5.23)$$

while at the exit

$$dM_2 = -D_m\frac{\partial}{\partial x}\left(C + \frac{\partial C}{\partial x}\,dx\right)dy\,dz\,d\tau, \quad (5.24)$$

the difference being

$$D_m \frac{\partial^2 C}{\partial x^2} dx\, dy\, dz\, d\tau. \tag{5.25}$$

For all the faces of the parallelepiped in the directions of the three coordinate axes we obtain

$$D_m \left(\frac{\partial^2 C}{\partial x^2} + \frac{\partial^2 C}{\partial y^2} + \frac{\partial^2 C}{\partial z^2} \right) dx\, dy\, dz\, d\tau. \tag{5.26}$$

The excess quantity of substance will be carried away from the parallelepiped by the liquid flow in which the change of concentration is determined by Eq. (5.22). This flow through the parallelepiped of volume $dx\, dy\, dz$ will change the concentration during the time $d\tau$ by

$$dx\, dy\, dz\, d\tau \frac{DC}{d\tau}. \tag{5.27}$$

Substituting Eq. (5.27) into Eq. (5.26), we get

$$\frac{DC}{d\tau} = D_m \left(\frac{\partial^2 C}{\partial x^2} + \frac{\partial^2 C}{\partial y^2} + \frac{\partial^2 C}{\partial z^2} \right). \tag{5.28}$$

Replacing $DC/d\tau$ by its value from Eq. (5.22), we obtain

$$\frac{\partial C}{\partial \tau} + w_x \frac{\partial C}{\partial x} + w_y \frac{\partial C}{\partial y} + w_z \frac{\partial C}{\partial z} = D_m \left(\frac{\partial^2 C}{\partial x^2} + \frac{\partial^2 C}{\partial y^2} + \frac{\partial^2 C}{\partial z^2} \right). \tag{5.29}$$

The left-hand side of this equation contains the local and convective diffusion components, while the right-hand side describes the molecular diffusion.

For a steady-state diffusion process

$$\frac{\partial C}{\partial \tau} = 0. \tag{5.30}$$

Equation (5.29) is called *the Fick second law.*

Thus, if D_m is independent of concentration, Fick's second law can be represented in the form

$$\frac{DC}{d\tau} = D_m \nabla^2 C. \tag{5.31}$$

In the general case, D_m is a function of concentrations, and Fick's second law is expressed as follows:

$$\frac{DC}{d\tau} = \operatorname{div} (D_m \operatorname{grad} C) = \nabla (D_m \nabla C). \tag{5.32}$$

5.2. Diffusion in a Single-Phase Stagnant Medium

In a stationary state, we have the following expression for the equimolecular mass flux q along z-axis:

$$q = -D_{AB} \frac{dC}{dz}. \tag{5.33}$$

After the separation of variables, this equation assumes the form

$$qdz = -D_{AB}dC, \tag{5.34}$$

for the boundary conditions $z = z_1$, $C = C_{A_1}$, $z = z_2$, $C = C_{A_2}$, we obtain

$$q = D_{AB}\frac{C_{A_1} - C_{A_2}}{z_2 - z_1}. \tag{5.35}$$

This equation is valid for highly dilute systems at a constant temperature. For the diffusion of component A through the stagnant component B under a constant pressure P and temperature for an ideal gas system, we obtain

$$q = -\frac{D_{AB}(P/RT)}{1 - x_A}\frac{dC_A}{dz} = -\frac{D_{AB}(P/RT)}{P - p_A}\frac{dp_A}{dz}$$

$$= -D_{AB}(P/RT)\frac{d\ln p_B}{dz}, \tag{5.36}$$

where x_A is the mole fraction of component A.

For $q = \text{const}$, Eq. (5.36) assumes the following form after integration:

$$q = \frac{D_{AB}(P/RT)}{z_2 - z_1}\ln\frac{p_{B_2}}{p_{B_1}} = D_{AB}\frac{P/RT}{z_2 - z_1}\frac{p_{A_1} - p_{A_2}}{p_{B_m}}, \tag{5.37}$$

where p_{A_1} and p_{A_2} are the partial pressures of component A at two points separated by a distance $z_2 - z_1$ in the direction of diffusion, and $p_{B,m} = \frac{p_{B_2} - p_{B_1}}{\ln p_{B_2}/p_{B_1}}$ is the logarithmic mean of the partial pressure of non-diffusing gas.

Equation (5.37) is used for determining the diffusion coefficient in gases with the help of Stefan's method and is called the Stefan equation. If the partial pressure of component A is small in comparison with the partial pressure of component B, i.e. if the system is highly dilute, the value of p_{B_m} is virtually equal to P, and Eq. (5.37) is reduced to

$$q = \frac{D_{AB}}{RT(z_2 - z_1)}(p_{A_1} - p_{A_2}). \tag{5.38}$$

This equation can be obtained directly from Eq. (5.35) if instead of the concentration of component A we substitute its partial pressure $C_A = p_A/RT$.

5.3. Steady-State Diffusion in Moving Media

Diffusion through a falling film. There are several analytic solutions for diffusion of dissolved substance A through a liquid film of component B in a laminar flow. The accuracy of these solutions de-

pends on the assumptions under which they are obtained. In the simplest analytic solution, it is assumed that the contact time is very short and the following conditions are admissible: (a) the film moves with a flat velocity profile w_0 (Fig. 81), (b) the film has an infinite thickness, and (c) the concentration at the surface ($x = 0$) is equal to C_0.

We take the diffusion equation in the form

$$w_0 \frac{\partial C_A}{\partial z} = D_{AB} \frac{\partial^2 C_A}{\partial x^2}, \tag{5.39}$$

where the component $\partial^2 C_A/\partial z^2$ in the direction of the flow can be ignored. For the boundary conditions

(a) for $x = 0$, $C_A = C_{A_0}$ for all z,
(b) for $x = \infty$, $C_A = C_{A_\infty}$ for all z, and
(c) for $z = 0$, $C_A = C_{A_\infty}$ for all x,

the solution of Eq. (5.39) leads to the following dependence:

$$\left(\frac{C_A - C_{A_\infty}}{C_{A_0} - C_{A_\infty}}\right) = 1 - \operatorname{erf} \frac{x}{\sqrt{4 D_{AB} z / w_0}}. \tag{5.40}$$

This equation is also valid for non-stationary diffusion through the film for $\tau = z/w_0$. Equation (5.39) was solved for diffusion through a falling film with flat density profile for a finite thickness of the liquid film with the following boundary conditions:

(a) for $x = 0$, $C_A = C_{A_0}$ for all z,
(b) for $x = \delta$, $\partial C_A/\partial x = 0$ for all z, and (5.41)
(c) for $z = 0$, $C_A = C_{A_1}$ for all x.

This solution has the form

$$\frac{C_A - C_{A_1}}{C_{A_0} - C_{A_1}} = 1 - 2 \sum_{n=0}^{\infty} \frac{\sin (n + 1/2)\, \pi x/\delta}{(n + 1/2)\, \pi} \times \exp\left\{-[(n + 1/2)\, \pi/\delta]^2 \frac{D_{AB} z}{w_0}\right\}. \tag{5.42}$$

However, the assumption about the flat velocity profile is not well-founded. A more exact solution can be obtained for a steady-state laminar flow. In this case, the Navier-Stokes equation [see Eq. (3.40)] is reduced to the form

$$\rho g + \mu \frac{\partial^2 w_z}{\partial x^2} = 0. \tag{5.43}$$

Using the system of coordinates (Fig. 81) and considering that ρ and μ are constant quantities under the boundary conditions $w_z = 0$, $x = \delta$, and $\partial w_z/\partial x = 0$ for $x = 0$, we obtain after integrating

Eq. (5.43)

$$w_z(x) = \frac{\rho g \delta^2}{2\mu}\left[1 - \left(\frac{x}{\delta}\right)^2\right] = w_{\max}\left[1 - \left(\frac{x}{\delta}\right)^2\right], \qquad (5.44)$$

where $w_{\max}$ is the maximum velocity in the film (at the surface);

$$w_m = 2/3 w_{\max}. \qquad (5.45)$$

This leads to the following expression for the film thickness:

$$\delta = \sqrt[3]{\frac{3\mu\Gamma}{\rho^2 g}} = \sqrt[3]{\frac{3\mu^2 \mathrm{Re}}{4\rho^2 g}}, \qquad (5.46)$$

where $\mathrm{Re} = 4\Gamma/\mu$, $\Gamma = \rho w_m \delta$ is the mass velocity of flow in the z direction per unit width of the wetted wall in the x-direction.

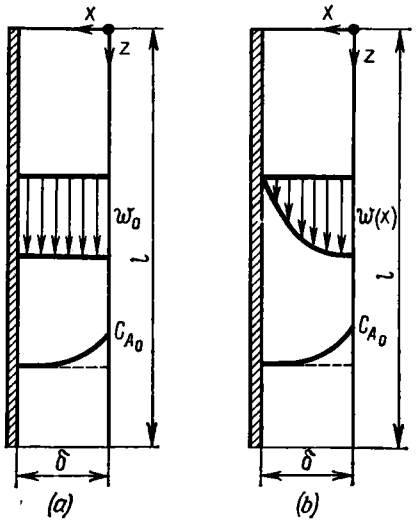

Fig. 81. To the derivation of the diffusion equation for a falling film:
a—flat profile; *b*—parabolic profile.

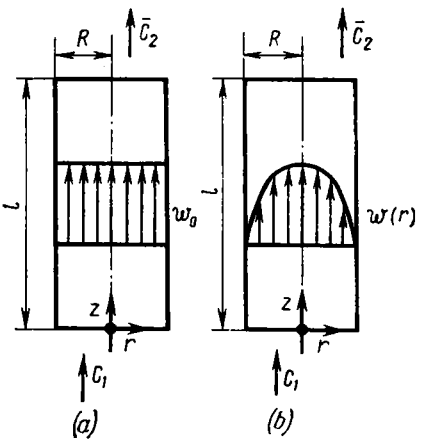

Fig. 82. To the derivation of diffusion equation for liquid flowing along the walls of a round pipe:
a—flat profile; *b*—parabolic profile.

Diffusion into a liquid moving along the walls of a round pipe. Let us consider a case when a gas moves with a flat and a parabolic velocity profile at the wetted walls (Fig. 82). If the velocity of liquid along the wall is constant over the entire tube cross section, and component A diffuses from the walls into the flow of component B, the diffusion equation can be represented in cylindrical coordinates:

$$w_0 \frac{\partial C_A}{\partial z} = D_{AB} \frac{1}{r} \frac{\partial}{\partial r}\left(r \frac{\partial C_A}{\partial r}\right), \qquad (5.47)$$

where r is the cylindrical coordinate equal to $r = \sqrt{x^2 + y^2}$.

The diffusion along the flow can be neglected in comparison with the convective component $w_0\,(\partial C_A/\partial z)$. Let us impose the following boundary conditions:

$$\begin{aligned} &\text{(a) } C_A = C_{A_1} \quad \text{at} \quad z = 0 \quad \text{for all } r, \text{ and} \\ &\text{(b) } C_A = C_{A_R} \quad \text{at} \quad z = R \quad \text{for all } r. \end{aligned} \tag{5.48}$$

The introduction of the Bessel functions I_0 and I_1 of the first kind leads to the expression

$$\frac{C_A - C_{A_1}}{C_{A_R} - C_{A_1}} = 1 - 2\sum_{n=1}^{\infty} \frac{1}{a_n} \frac{I_0(a_n r/R)}{I_1(a_n)} \exp\left(-\frac{D_{AB} a_n^2 z}{w_0 R^2}\right). \tag{5.49}$$

The average concentration $\overline{C}_{A_R}$ at the pipe exit for $z = l$ is given by

$$\frac{\overline{C}_{A_R} - C_{A_1}}{C_{A_R} - C_{A_1}} = 1 - 4\sum_{n=1}^{n} \frac{1}{a_n} \exp\left(-\frac{D_{AB} a_n^2 l}{w_0 R^2}\right), \tag{5.50}$$

where a_n is the radius for which $I_0(r) = 0$.

In accordance with the solution of the Navier-Stokes equation, we obtain for the parabolic velocity distribution (Fig. 82*b*)

$$w_{max}\left[1 - \left(\frac{r}{R}\right)^2\right] \frac{\partial C_A}{\partial z} = D_{AB} \frac{1}{r} \frac{\partial}{\partial r}\left(r \frac{\partial C_A}{\partial r}\right). \tag{5.51}$$

Taking the boundary conditions into account, we get

$$\frac{\overline{C}_{A_R} - C_{A_1}}{C_{A_R} - C_{A_1}} = 1 - 2\sum_{n=1}^{\infty} a_n \exp\left[-b_n \left(\frac{D_{AB}}{w_m R^3}\right) l\right], \tag{5.52}$$

where $w_m = (1/2)w_{max}$, and a_n and b_n are constants that assume the following values:

n	1	2	3
a_n	0.820	0.0972	0.0135
b_n	3.658	22.178	53.05

However, experimental results are in a better agreement with Eq. (5.49) than with Eq. (5.52), which is explained by the levelling out the velocity profile by convection. In actual practice, such diffusion is observed in apparatus with a fixed contact surface, as well as in those with wetted walls.

Diffusion from a point source to a moving medium. Let us consider diffusion of component A injected into a solvent B flowing in the z-direction at a constant velocity w_0. In this case, we must solve

the equation

$$w_0 \frac{\partial C_A}{\partial z} = D_{AB} \nabla^2 C_A \tag{5.53}$$

under the following boundary conditions: $C_A = 0$ as $r \to \infty$ and

$$-4\pi r^2 D_{AB} (\partial C_A / \partial r) = Q_A \text{ as } r \to 0,$$

where r is the distance from the source ($r^2 = x^2 + y^2 + z^2$); z is the distance along the flow from the source; and Q_A is the velocity with which component A enters the system. The solution of Eq. (5.53) leads to the dependence

$$C_A = \frac{Q_A}{4\pi r D_{AB}} e^{-\left(\frac{w_0}{2D_{AB}}\right)(r-z)}. \tag{5.54}$$

Diffusion from a point source is used for analyzing the concentration profile and for determining the eddy diffusion coefficients.

Diffusion in a single drop. Kronig and Bring investigated diffusion in a drop inside which circulation occurs with the circulation centre coinciding with the centre of a large sphere for Re < 1. They obtained the following equation:

$$\frac{C_0 - C_A}{C_0 - C_{A_i}} = 1 - \frac{3}{8} \sum_{n=1}^{\infty} A_n^2 \exp\left(1 - \frac{\varphi_n \times 64 D_m \tau}{d_p^2}\right)$$

$$= \left\{1 - \exp\left[\frac{-2.25 \times 4 D_m \pi \theta}{d_p^2}\right]\right\}^{0.8}, \tag{5.55}$$

where A_n and φ_n are the roots of the characteristic equation.

5.4. Mass Transfer in a Single-Phase Flow

In order to describe diffusion by using Eq. (5.29), we must integrate this equation together with the equation of motion and the continuity equation for given boundary conditions. However, the imposition of the boundary conditions for a turbulent flow is associated with unsurmountable difficulties, and hence the system of equations is replaced by an equation in dimensionless terms. Equation (5.29) for steady-state diffusion relative to a single axis x can be written in the form

$$w_x \frac{\partial C}{\partial x} = D_m \frac{\partial^2 C}{\partial x^2}. \tag{5.56}$$

In terms of finite differences, the left- and right-hand sides of this equation have the following form:

$$w_x \frac{\partial C}{\partial x} \sim w_x \frac{\Delta C}{l}, \tag{5.57}$$

$$D_{\text{m}} \frac{\partial^2 C}{\partial x^2} \sim D_{\text{m}} \frac{\Delta C}{l^2}. \tag{5.58}$$

Since Eq. (5.56) essentially expresses the concentration distribution on account of mass flux and molecular diffusion, the ratio of finite differences acquires the significance of a criterion. Dividing the finite differences (5.57) by (5.58), we obtain a dimensionless number, called the Peclet number, for molecular transport (if w_x is expressed in m/s and D_{m} in m^2/s):

$$\text{Pe}_{\text{m}} = \frac{wl}{D_{\text{m}}}. \tag{5.59}$$

The Peclet number is replaced by the so-called Prandtl diffusion number which is obtained by eliminating the convective term wl, dividing Eq. (5.59) by wl/ν. As a result of transformations, we obtain the Prandtl diffusion number in the following form:

$$\frac{wl/D_{\text{m}}}{wl/\nu} = \frac{\nu}{D_{\text{m}}} = \text{Pr}_{\text{D}}. \tag{5.60}$$

The Prandtl diffusion number not only expresses the ratio of physical constants, viz. molecular viscosity and molecular diffusion, but also has a deep physical meaning. The velocity distribution profile in a liquid flow is determined by the kinematic viscosity ν of the liquid: for a high viscosity it has the form of elongated parabola, while for fully developed turbulence it is flattened. Similarly, the concentration profile depends on the molecular diffusion coefficient D_{m}. Therefore, the value of the Prandtl number affects the relative distributions of velocity and concentration profiles in a liquid flow (Fig. 83).

The Prandtl number for gases is of the order of unity, while for dropping liquids it is of the order of 10^3. Hence, the velocity and concentration profiles in a single-phase gas flow coincide, while the effect of viscosity in a liquid is stronger than that of molecular diffusion, and therefore the concentration profile is more elongated.

The coincidence of velocity and concentration profiles (and for thermal processes the temperature profiles also) served as a basis for the development of methods of calculating heat- and mass-transfer according to friction coefficients in a single-phase gas flow bounded by rigid walls. For exam-

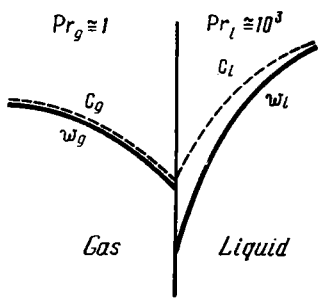

Fig. 83. Velocity profiles and concentration distribution as functions of the Prandtl number.

ple, by using this analogy and introducing the dimensionless j-factor, Colburn established the dependence

$$j_h = j_d = \frac{\xi}{2}, \tag{5.61}$$

where j_h is the convective heat transfer factor; j_a the mass-transfer factor; and ξ the friction coefficient. In this case,

$$j_h = \frac{\alpha}{c_p w \rho} \left(\frac{\nu}{a}\right)^{2/3}, \tag{5.62}$$

$$j_d = \frac{k_g p_m M}{w\rho} \left(\frac{\nu}{D_m}\right)^{2/3}, \tag{5.63}$$

where α is the coefficient of convective heat transfer from the gas to the walls; c_p the heat capacity of the gas; w the gas velocity; ρ the gas density (in kg/m³); a the thermal diffusivity of the gas ($a = \lambda/c_p\gamma$); k_g the mass-transfer coefficient for the gas flow; p_m the mean partial pressure of an inert gas; and M the mean molecular mass of the gas flux.

The analogy between friction and heat and mass transfer was observed for the processes of drying granulated solids, evaporation from a solid surface, from surfaces of cylinders made of solid volatile materials, and from the surfaces of industrial packings. This analogy is excluded for the processes associated with mass transfer of dropping liquids, since the velocity and concentration profiles do not coincide for large Prandtl numbers Pr_D. If we must take into account the effect of macrokinetic parameters, such as the magnitude of reverse agitation or eddy diffusion, on the concentration distribution, the coefficient of longitudinal mixing, D_L, or the turbulent diffusion coefficient D_t must be introduced into the denominator of the ratio (5.59):

$$\frac{wl}{D_L} = \frac{wl}{D_t} = \mathrm{Pe}. \tag{5.64}$$

The obtained dimensionless number is called the Peclet number for turbulent transfer.

If the mass-transfer coefficient k is the quantity to be determined in the process of mass transfer, it is introduced into the so-called Nusselt diffusion number Nu_D*, similar to the Nusselt thermal number. In this case, the following dimensionless relation is obtained:

$$Nu_D = \frac{kl}{D_m}. \tag{5.65}$$

Taking into account Eq. (5.21), we get

$$Nu_D \approx \frac{D_m + D_t}{D_m}.$$

* Instead of the Nusselt diffusion number Nu_D, its analogue, called the Sherwood number, is frequently used.

The general equation describing the mass transfer in a single-phase flow can be written in the following form:

$$\mathrm{Nu_D} = A\mathrm{Re}^m\mathrm{Pr}_\mathrm{D}^n. \quad (5.66)$$

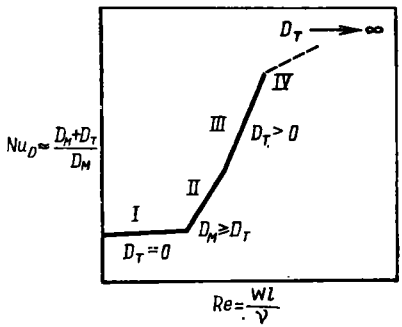

Fig. 84. To the mass-transfer mechanism in a single-phase flow.

Figure 84 shows the mass transfer conditions in a single-phase flow depending on its turbulence. For small values of Re, when the molecular viscous forces exceed the forces of inertia, the energy and mass transfer will be determined by molecular exchange coefficients (ν and D_m) which depend only on the nature of the substance and are independent of the flow velocities. As $D_\mathrm{t} \to 0$, the Nusselt number $\mathrm{Nu_D}$ tends to a constant value. Regime I (Fig. 84) can be defined as the *molecular (laminar) transfer regime.*

As turbulence is developed, the forces of inertia become comparable with the viscous forces, and hence the energy and mass transfer are accomplished not only through molecular, but also through turbulent exchange. As Re increases, the value of D_t must also increase, and hence the ratio $(D_\mathrm{m} + D_\mathrm{t})/D_\mathrm{m}$ increases as well. Accordingly, the value of $\mathrm{Nu_D}$ will also increase. In this case, two regimes are possible. The condition for the first regime is $D_\mathrm{m} \geqslant D_\mathrm{t} \geqslant 0$ and for the second, $D_\mathrm{t} > D_\mathrm{m}$. Taking into account the limits of variation of D_t, regime II can be defined as *the intermediate regime.*

When $D_\mathrm{t} > D_\mathrm{m}$, the conditions in which the coefficients of turbulent exchange dominate are created. Therefore, regime III can be defined as *the turbulent exchange regime.* The turbulence developed in this case is similar to the turbulence appearing at a solid boundary.

Regime IV, for which the turbulent viscosity and diffusion coefficients attain their maximum values corresponds to *self-modelling*, or *developed turbulence, regime.* In this regime the pressure drop in the flow is described by a quadratic law, and resistance does not depend on molecular viscosity. However, an increase in the turbulent viscosity coefficient during mass transfer leads to an intense longitudinal mixing and decreases the longitudinal concentration gradient. Hence, the mass transfer coefficient and the Nusselt number $\mathrm{Nu_D}$ cannot increase infinitely (dashed line).

5.5. Mass Transfer in Multicomponent Systems

In investigating the mass-transfer processes, we usually deal with multicomponent systems. At the present time, the problems associated with mass transfer in multicomponent systems are at the early stage of the investigation. The main difficulties are that no reliable models of the mass-transfer mechanism are available. On the basis of the theory of ideal gases an attempt has been made to create a thermodynamically substantiated model of the mass-transfer mechanism for multicomponent gas and vapour-liquid systems.

5.5.1. Diffusion in Multicomponent Gas Systems

Let us define the drift velocity v_i of each component of a mixture as the ratio of the number of molecules N_i of a substance passing through a given cross section per unit time to the number of molecules C_i in unit volume of the mixture in this cross section:

$$v_i = N_i/C_i. \tag{5.67}$$

In this case, the mean velocity of the flow for all molecules will be written as

$$v = \sum_{i=1}^{n} v_i y_i, \tag{5.68}$$

where $y_i = C_i/C$ is the mole fraction of the component and C the total number of molecules per unit volume of the cross section.

If we now define the relative drift velocity of the component as

$$u_i = v_i - v, \tag{5.69}$$

then, multiplying Eq. (5.69) by C_i, we get

$$u_i C_i = v_i C_i - v C_i. \tag{5.70}$$

Denoting by Φ_i the relative molar flux of the component, we can represent this equation in the form

$$N_i = \Phi_i + v C_i = \Phi_i + N y_i, \tag{5.71}$$

where N is the total number of molecules in the mixture passing through the given cross section per unit time. The last term in this equation determines the convective transport of the ith component, since it is associated with the general transport of mixture molecules for $N \neq 0$. The term Φ_i determines the excess rate of transport of the ith type of molecules relative to the general rate of transport of molecules of the mixture, and thus can be considered as a characteristic of diffusion transport of the component. For systems in equilibrium for which there is no diffusion transport of components, the following

equality is valid:

$$\Phi_i = 0, \tag{5.72}$$

and hence

$$N_i = Ny_i, \tag{5.73}$$

i.e. the transport of a component is determined only by the rate of convective transport. On the other hand, the summation of Eq. (5.71) over all mixture components allows us to obtain the following relation:

$$\sum_{i=1}^{N} \Phi_i = 0, \tag{5.74}$$

which indicates that there is no total diffusive mass transport in a flow. The quantity Φ_i is a function of equilibrium shift with respect to a given component, which is determined by the gradients of chemical potentials of all the components, i.e.

$$\Phi_i = \Phi_i (\nabla\mu_1, \nabla\mu_2, \ldots, \nabla\mu_n). \tag{5.75}$$

At a constant pressure and temperature, the chemical potential gradient $\nabla\mu_i$ for a component of an ideal gas mixture is proportional to ∇C_i, and hence expression (5.75) can be represented in the form

$$\Phi_i = \Phi_i (\nabla C_1, \nabla C_2, \ldots, \nabla C_n). \tag{5.76}$$

Expanding this expression into the Taylor series in ∇C_i to within the terms of first order of smallness, we get

$$\Phi_i = -\sum_{i=1}^{n} A_{ij}\nabla C_j, \tag{5.77}$$

where

$$A_{ij} = -\frac{\partial\Phi_i}{\partial(\nabla C_j)}.$$

Since $\sum_{j=1}^{n} \nabla C_j = 0$, Eq. (5.77) represents Fick's law for a binary mixture:

$$\Phi_1 = -(A_{11} - A_{12})\nabla C_1 = -D_{12}\nabla C_1. \tag{5.78}$$

For multicomponent systems, we have

$$\Phi_i = -\sum_{j=1}^{n-1} (A_{ij} - A_{in})\nabla C_j = -\sum_{j=1}^{n-1} D_{ij}\nabla C_j, \tag{5.79}$$

where D_{ij} are the diffusion coefficients in a multicomponent system, which in the general case depend on the concentrations of all the mixture components.

In relation (5.79), D_{ij} is the main diffusion coefficient of the ith component, which determines the transport of the component under

the action of its own concentration gradient and is always positive. The values of D_{ij} $(i \neq j)$ are the cross diffusion coefficients that determine the interaction between the ith component and other components of the mixture and can be positive or negative. Thus, Eq. (5.79) is a natural generalization of Fick's law, in which all diffusive flows of components depend on the concentration gradients with respect to all mixture components. Equation (5.79) is similar to the Maxwell-Stefan equation

$$-\nabla C_i = \sum_{j=1}^{n} \frac{N_i C_j - N_j C_i}{C D_{ij}}, \tag{5.80}$$

where D_{ij} are the binary diffusion coefficients, $D_{ij} = D_{ji}$.

Considering that $N_i = v_i C_i$, we can write Eq. (5.80) as follows:

$$-\nabla C_i = \sum_{j=1}^{n} (v_i - v_j) \frac{C_i C_j}{C D_{ij}}, \tag{5.81}$$

$$-\nabla C_1 = (v_1 - v_2) \frac{C_1 C_2}{C D_{12}} \tag{5.82}$$

for a binary mixture. Equation (5.82) is another form of Fick's law. Equations (5.79) and (5.82) describe the motion of mixture components relative to each other. The motion of the mixture as a whole is accounted for by the continuity equation for the ith component:

$$\frac{dC_i}{d\tau} + \nabla N_i = q_i. \tag{5.83}$$

Combining Eqs. (5.73), (5.79), and (5.83), we obtain

$$\frac{dC_i}{d\tau} + \nabla (vC_i) = \nabla \sum_{j=1}^{n-1} D_{ij} \nabla C_j + q_i, \quad i = 1, \ldots, n-1, \tag{5.84}$$

where q_i is the intensity of the source of the ith component in the flow. Equation (5.84) is the general description of diffusion in multicomponent systems.

The main features of diffusion in gas systems can be revealed in the analysis of steady-state diffusion through the interface in the absence of sources in the flow. It follows from Eq. (5.83) that

$$\frac{dN_i}{dz} = 0,$$

or

$$\frac{d \sum_{1}^{n} N_i}{dz} = \frac{dN}{dz} = \frac{d(vC)}{dz} = 0. \tag{5.85}$$

Suppose that $N = 0$ and $v = 0$ at the interface, corresponding to the equimolar diffusion through the interface. Then Eqs. (5.71) and (5.79) give

$$N_i = \sum_{j=1}^{n-1} D_{ij}\, dC_j/dz. \tag{5.86}$$

If we assume that $D_{ij} = \text{const}$, Eq. (5.86) can be written as

$$N_i = \sum_{j=1}^{n-1} \frac{D_{ij}}{z} [C_j(0) - C_j(z)] = \frac{C}{z} \sum_{j=1}^{n-1} D_{ij} \Delta y_j, \tag{5.87}$$

where

$$\Delta y_j = y_j(0) - y_j(z).$$

For a three-component system, Eq. (5.87) can be written in the form

$$\begin{aligned} N_1 &= (C/z)\,[D_{11}\Delta y_1 + D_{12}\Delta y_2], \\ N_2 &= (C/z)\,[D_{21}\Delta y_1 + D_{22}\Delta y_2]. \end{aligned} \tag{5.88}$$

For a binary mixture, Eq. (5.88) becomes

$$N_1 = \frac{D_{12}C}{z} \Delta y_1.$$

Analyzing Eq. (5.88), we can point out the following peculiarities of diffusion in ternary systems:

1. For $\Delta y_1 = 0$ and $\Delta y_2 = -\Delta y_3 \neq 0$, we have

$$N_1 = (C/z)\, D_{12}\Delta y_2.$$

Consequently, even in the absence of the concentration gradient with respect to the first component, this component is transported. This phenomenon is called *osmotic diffusion.*

2. For $D_{11}\Delta y_1 + D_{12}\Delta y_2 = 0$, there is no transport of the first component even in the presence of the concentration gradient for this component. This phenomenon is called *the diffusion barrier.*

3. If the quantity $D_{12}\Delta y_2$ has higher order of magnitude than $D_{11}\Delta y_1$ and is of opposite sign, the component will diffuse in the direction opposite to its gradient. This phenomenon is called *back diffusion.*

Thus, diffusion in binary and ternary systems differs both quantitatively and qualitatively. The effect of interaction will be still more pronounced if the coefficients D_{12} and D_{21} are relatively large in comparison with the coefficients D_{11} and D_{22}.

The multicomponent diffusion coefficients D_{ij} can be calculated for ideal gas mixtures from Maxwell-Stefan equations (5.80), permitting the expression of the coefficients D_{ij} through the binary diffusion coefficients D_{ij} and the mixture composition.

5.5.2. Diffusion in Multicomponent Liquid Systems

There are no equations similar to Maxwell-Stefan equations for liquids which cannot be treated as ideal mixtures. The drawbacks of the kinetic theory of liquids are more significant for multicomponent than for binary mixtures, since in the latter case we must know only one diffusion coefficient which can be measured or predicted by semi-empirical methods. In the case of multicomponent mixture, however, the number of diffusion coefficients to be determined considerably increases.

Just as for a gas mixture, we can suppose that the flow of a component of a liquid mixture in a relative coordinate system is a function of the chemical potential gradients at a constant pressure and temperature:

$$\Phi_i' = \Phi_i' (\nabla\mu_1, \nabla\mu_2, \ldots, \nabla\mu_n). \tag{5.89}$$

Assuming that the higher-order terms in the expansion of Eq. (5.89) into the Taylor series in $\nabla\mu_j$ are negligibly small, we obtain

$$\Phi_i' = -\sum_{j=1}^{n} \Omega_{ij}' \nabla\mu_j. \tag{5.90}$$

The Gibbs-Duhem equation

$$\sum_{1}^{n} C_i \nabla\mu_j = 0$$

permits the elimination of one of the gradients, say, $\nabla\mu_n$, from Eq. (5.90). On the other hand, at constant pressure and temperature, each gradient $\nabla\mu_j$ depends on $n - 1$ concentration gradients ∇C_k and can be represented in the form

$$\nabla\mu_j = \sum_{1}^{n-1} \frac{\partial\mu_j}{\partial C_k} \nabla C_k \tag{5.91}$$

to within the terms of the first order of smallness in ∇C_k. Thus, Eq. (5.90) can be written as

$$\Phi_i' = -\sum_{k=1}^{n-1} \left[\sum_{j=1}^{n-1} \left(\Omega_{ij} - \Omega_{in} \frac{C_i}{C_n} \right) \frac{\partial\mu_j}{\partial C_k} \right] \nabla C_k. \tag{5.92}$$

The terms in the brackets can be formally represented as the multicomponent diffusion coefficients, i.e.

$$\Phi_i' = -\sum_{k=1}^{n-1} D_{ik} \nabla C_k. \tag{5.93}$$

It was established experimentally that this equation satisfactorily describes diffusion in multicomponent liquid systems and can be used in engineering calculations. In this case, the diffusion coefficients appearing in this equation must be experimentally determined as functions of the composition. The cross-flow diffusion coefficients D_{ij} for multicomponent liquid mixtures are proportional to the difference between the corresponding binary coefficients, while the main diffusion coefficients D_{ii} are proportional to the mean binary coefficients. The binary diffusion coefficients for liquids vary within relatively narrow ranges. Consequently, the cross-flow diffusion coefficients for liquids are small in comparison with the main coefficients. The solution of Eq. (5.93) for diffusion through the interface in a steady state gives the results similar to those obtained for gas systems:

$$N_i = \frac{C}{z} \sum_{j=1}^{n-1} D_{ij} \Delta C_j \tag{5.94}$$

or

$$\begin{aligned} N_1 &= \frac{D_{11}}{z} \Delta C_1 + \frac{D_{12}}{z} \Delta C_2 \\ N_2 &= \frac{D_{21}}{z} \Delta C_1 + \frac{D_{22}}{z} \Delta C_2 \end{aligned} \tag{5.95}$$

for a ternary system.

The phenomena caused by the interaction between different mixture components (such as diffusion barrier, osmotic and back diffusion) are observed in liquid as well as gas mixtures. However, since the cross-flow diffusion coefficients D_{ij} for liquids are smaller than the main coefficients D_{ii}, these phenomena are considerably less pronounced in liquids, and multicomponent liquid mixtures are close to binary systems than gas mixtures in respect of diffusion properties.

5.5.3. Mass Transport in Multicomponent Vapour-Liquid Systems

Considering together the diffusion equations for gas and liquid systems and the material balance equations, we can obtain a mathematical description of mass transport in multicomponent two-phase systems. In this case, we must consider the state of the interface, determined by hydrodynamic conditions of interaction between the flows and by their physical properties. If we assume that laminar films exist on the interface and the core of the flows is in the regime of fully developed turbulence, the main resistance to mass transport will be due to the diffusive resistance of the liquid and gas films at the interface. Within the limits of each of these films, diffusive

mass transport can be described with the help of Eq. (5.87), (5.93) which define the diffusive transport of components of each phase.

Beyond the limits of boundary films, mass transport is due to turbulent diffusion which is much stronger than molecular diffusion. Hence we can assume that component concentrations are constant within the flows (with the exception of boundary films) and that concentrations vary only within the film thickness.

In the absence of sources in boundary films ($q_i = 0$), general mass-transfer equations (5.84) can be written in the form

$$\frac{dC_i}{d\tau} + \nabla(vC_i) = \sum_{j=1}^{n-1} D_{ij}\nabla^2 C_j, \quad i = 1, \ldots, n-1. \tag{5.96}$$

If we assume that the multicomponent diffusion coefficients D_{ij} vary within the boundary films insignificantly, the system of equations (5.96) can be transformed to a system similar to the diffusion equations for binary mixtures. For this purpose, the linear transformation

$$\psi_k = \sum_{i=1}^{n-1} s_{ik} C_j \tag{5.97}$$

is used, with the help of which system (5.96) is reduced to

$$\frac{d\psi_k}{d\tau} + \nabla(v\psi_k) = D_k^0 \nabla^2 \psi_k, \tag{5.98}$$

where the quantities ψ_k can be treated as concentrations of certain pseudocomponents for which binary diffusion equations (5.98) are valid. The diffusion coefficients D_k^0 for pseudocomponents are determined by solving the characteristic equation

$$| D_{ij} - D^0 \delta_{ij} | = 0. \tag{5.99}$$

The coefficients of linear transformation (5.97) can be found by solving the systems of linear equations

$$\sum_{i=1}^{n-1} s_{ik} D_{ij} = s_{jk} D_k^0, \quad j = 1, \ldots, n-1 \tag{5.100}$$

with different values of D_k^0 ($k = 1, \ldots, n-1$).

Binary relations of mass transfer are valid for pseudocomponents with the concentration ψ_k varying within boundary films in accordance with binary relations (5.98). In other words, we can write the following expression for the flux N_{ψ_k} of the kth pseudocomponent towards the interface:

$$N_{\psi_k} = k(D_k^0)\,\Delta\psi_k, \tag{5.101}$$

where $k(D_k^0)$ is the mass-transfer coefficient for a binary mixture, which is a known function of the diffusion coefficient D_k. The mass-transfer coefficient depends on the local hydrodynamic state of the interface.

There exists a reverse transformation which permits us to determine the initial mixture component fluxes in terms of pseudocomponent fluxes:

$$N_i = \sum_{i=1}^{n-1} k_{ij} \Delta C_i, \tag{5.102}$$

where k_{ij} are the multicomponent mass-transfer coefficients, forming the matrix of local mass-transfer coefficients.

Relations of the type (5.102) can be obtained for both phases, after which the matrix of general mass-transfer coefficients for the interface can be calculated by using the rule of additivity of phase resistances from the matrix formula

$$[K]^{-1} = [k_y]^{-1} + [m]\,[k_x]^{-1}, \tag{5.103}$$

where $[m]$ is the matrix of the slopes of the equilibrium dependence for a multicomponent mixture; $[k_y]$ and $[k_x]$ are the matrices of local mass-transfer coefficients which are determined for each phase.

Chapter Six

Kinetics of Interphase Transport

The main problem of the theory of mass transfer is to reveal the phenomena occurring on the interfacial surface. Not only must the type of the mechanism of mass transport through the interfacial area (i.e. molecular diffusion) or turbulent (eddy) diffusion be established, but the entire complex of interactions between micro- and marco-effects must also be elucidated.

Since the phenomena occurring simultaneously in two-phase systems are very complicated (see pp. 141-148), till now it has been impossible to work out a rigorous theory of mass transfer on the mobile interface having a stochastic and deterministic nature. For this reason, simplified model concepts are employed.

6.1. Two-Film Model of Mass Transfer

The two-film model of mass transfer, developed by Lewis and Whitman, was borrowed from the theory of solubility of solids put forward earlier by Nernst. The basic concepts of the Lewis-Whitman model are:

1. At the interface between two phases (gas-liquid, vapour-liquid, liquid-liquid) boundary films appear on the side of each phase (gas film, liquid film, etc.), which create the main resistance to mass transport from one phase to the other.

2. The conditions of dynamic equilibrium are created at the interface (and accordingly at the boundary between the films), i.e. steady-state mass transfer sets in.

3. Within the limits of each phase, the diffusion flux of a component is proportional to the difference in concentrations or in the partial pressure of the component in the bulk (C_l, p_g) and at the interface (C_i, p_i).

For desorption of ideal gases, the diffusion flux is

$$q = k_g (p_i - p_g) = k_l (C_l - C_i), \qquad (6.1)$$

where k_g and k_l are the proportionality factors, or *film coefficients of mass transfer*:

$$k_g = \frac{D_g}{RT\delta_g}, \tag{6.2}$$

$$k_l = \frac{D_l}{\delta_l}. \tag{6.3}$$

Here, D_g and D_l are the coefficients of molecular diffusion of the components through the gas and liquid films, and δ_g and δ_l are the thicknesses of the gas and liquid films.

The following equations are valid for diffusion of one component through a stationary layer:

$$k_g^0 = \frac{D_g P}{RT\delta_g p_m}, \tag{6.4}$$

$$k_l^0 = \frac{D_l \rho_m}{\delta_l C_m}, \tag{6.5}$$

where P is the total pressure; p_m is the logarithmic mean partial pressure of non-diffusing component; C_m is the logarithmic mean concentration of non-diffusing component; and ρ_m is the molar density of the liquid phase. Practically, $P/p_m = 1$ and $\rho_m/C_m = 1$, and hence $k_g^0 = k_g$ and $k_l^0 = k_l$.

It follows from Eqs. (6.2) and (6.3) that the film coefficients of mass transfer are proportional to the molecular diffusion coefficients.

Since it is impossible to measure the interfacial area in the industrial-scale apparatus, *volumetric coefficients* should be introduced into the mass-transfer equations: $k_g a$ for the gas film and $k_l a$ for the liquid film. Instead of equilibrium concentrations the concentrations at the interface are taken as limiting (subscripts "i"). The mass-transfer equations take the form

$$dG = k_g a\,(y_i - y)\,Pf\,dH, \tag{6.6}$$

$$dG = k_l a\,(x - x_i)\,\rho_m f\,dH. \tag{6.7}$$

The number of transport units N_g for the gas film and N_l for the liquid film are expressed by the equations

$$\frac{k_g a P H}{G} \int \frac{dy}{y_i - y} = N_g, \tag{6.8}$$

$$\frac{k_l a \rho_m H}{L} \int \frac{dx}{x - x_i} = N_l. \tag{6.9}$$

If one of the components diffuses through a stationary film, the equations for N_g and N_l become

$$\frac{k_g^0 a\,(1-y)_m\,P H}{G} \int \frac{(1-y)_m\,dy}{(1-y)\,(y_i - y)} = N_g, \tag{6.10}$$

$$\frac{k_l^0 a\,(1-x)_m\,\rho_m H}{L} \int \frac{(1-x)_m\,dx}{(1-x)\,(x - x_i)} = N_l, \tag{6.11}$$

where $(1 - y)_m$ and $(1 - x)_m$ are the logarithmic means of the differences $(1 - y)$ and $(1 - x)$.

4. Within the limits of each phase, mass transfer is considered independently, and the additivity of diffusive resistances is presumed. Hence, the total mass-transfer coefficients $K_{0y}a$ and $K_{0x}a$ are expressed in terms of the film coefficients in the following form:

$$\frac{1}{K_{0y}a} = \frac{1}{k_g a} + \frac{m\dfrac{P}{\rho_m}}{k_l a} = \frac{m\dfrac{P}{\rho_m}}{K_{0x}a}. \tag{6.12}$$

This relation directly follows from the assumed difference in concentrations:

$$y^* - y = y^* - y_i - y = \frac{dG}{K_{0y}aPf\,dH} = \frac{m\,dG}{k_l a\rho_m f\,dH} + \frac{dG}{k_g aPf\,dH} = m(x - x^*) = \frac{m\,dG}{K_{0x}a\rho_m f\,dH}, \tag{6.13}$$

where

$$y^* = mx + b, \tag{6.14}$$

and m is the slope of the equilibrium line.

For $P = 9.8 \times 10^4$ Pa (1 atm) and liquid concentration expressed in kg/kg, the relation between the coefficients is reduced to

$$\frac{1}{K_{0y}a} = \frac{1}{k_g a} + \frac{m}{k_l a} = \frac{m}{K_{0x}a}. \tag{6.15}$$

Accordingly, the relations for the transport units are

$$\frac{PH}{N_{0y}G} = \frac{PH}{N_g G} + \frac{mPH}{N_l L} = \frac{mPH}{N_{0x}L} \tag{6.16}$$

and

$$\frac{1}{N_{0y}} = \frac{1}{N_g} + \frac{1}{N_l}\frac{mG}{L} = \frac{mG}{LN_{0x}}. \tag{6.17}$$

If one component diffuses through a stationary film, we have

$$\frac{1}{N_{0y}} = \frac{1}{N_g} + \frac{1}{N_l}\cdot\frac{mG}{L}\cdot\frac{(1-x)_m}{(1-y)_m} = \frac{mG}{LN_{0x}}\cdot\frac{(1-x)_m}{(1-y)_m}. \tag{6.18}$$

For dilute solutions, the logarithmic mean of the difference in concentrations is close to unity. The predominant effect of the liquid or gas film resistance is determined in accordance with the solubility of the gas and liquid. If the gas dissolves well in the liquid the main resistance is offered by the gas film, while in the case of a poor gas solubility, the liquid film is the main source of resistance.

In the process of distillation, if m is small (mixture of components with close boiling points), the resistance of the vapour film plays the decisive role. The resistance offered by the gas film becomes

predominant in the following cases: (1) absorption or desorption of readily soluble gases; (2) distillation of mixtures of components with close boiling points, and (3) evaporation of pure liquids into a moving inert gas and condensation of liquids from the inert gas.

The resistance in the liquid film becomes predominant in the following cases: (1) absorption or desorption of difficultly soluble gases; (2) stripping of the volatile component from the still bottoms for large values of m, and (3) distillation of systems with a high viscosity of liquid.

In analyzing and treating experimental data with the help of the film model, the most difficult problem is to determine the concentrations y_i and x_i at the interface, which practically cannot be measured. For this reason, the driving force of a process is determined according to equilibrium concentrations, and overall coefficients rather than film coefficients of mass transfer are actually obtained.

However, several conventional methods were proposed in order to separate the total resistance into partial (film) resistances. The film model does not take into account the hydrodynamic interaction between phases, and essentially considers mass transfer in each phase separately. When the experimental results are generalized with the help of the film model, kinetic equations similar to those for a single-phase flow are obtained. For example, the following equations are obtained for the processes determined by the resistance in the gas phase:

$$\mathrm{Nu}_g = A\ \mathrm{Re}_g^a\ \mathrm{Pr}_g^b \tag{6.19}$$

or

$$\frac{k_g l}{D_g} = A \left(\frac{w_g l \rho_g}{\mu_g}\right)^a \left(\frac{\mu_g}{\rho_g D_g}\right)^b. \tag{6.20}$$

Accordingly, for the processes determined by the resistance in the liquid phase, we have

$$\mathrm{Nu}_l = A_1\ \mathrm{Re}_l^{a_1}\ \mathrm{Pr}_l^{b_1} \tag{6.21}$$

or

$$\frac{k_l l}{D_l} = A_1 \left(\frac{w_l l \rho_l}{\mu_l}\right)^{a_1} \left(\frac{\mu_l}{\rho_l D_l}\right)^{b_1}. \tag{6.22}$$

However, Eqs. (6.19) and (6.21) prove to be insufficient for the most important mass-transfer processes occurring in absorption and rectifying columns at high gas and liquid flow velocities and continuously deformed interface, since they do not take into account the interaction of phase flows.

6.2. The Model of Boundary Diffusion Layer

In order to explain the phenomena occurring at the interface, the concept of the diffusion boundary layer was introduced. The diffusion boundary layer is a thin layer of liquid adjoining the interface, in

which molecular diffusion occurs and an abrupt change in the concentration takes place. The effective thickness δ_l of this boundary layer is determined from the relation

$$\delta_l \approx D_m^{1/6} \nu^{1/6} \sqrt{\frac{z}{w}}, \tag{6.23}$$

where w is the flow velocity; D_m the molecular diffusion coefficient; z the distance from the point where the liquid flows over the body; and ν is the kinematic viscosity of the liquid.

Each substance with a given value of the diffusion coefficient has its own boundary layer. If several substances diffuse simultaneously under given mixing conditions, several boundary layers are formed. In contrast to ordinary films, the diffusion boundary layer takes into consideration the following circumstances: (1) motion of liquid and convective mass transfer; (2) molecular and convective diffusion in the transverse and tangential directions, and (3) the absence of pronounced boundary of the layer.

When a gas is absorbed by a liquid film in a turbulent flow, the coefficient of turbulent (eddy) diffusion is proportional to the squared distance from the free surface:

$$D_t \approx z^2 \frac{v_0}{\lambda}, \tag{6.24}$$

where v_0 is the characteristic fluctuation velocity determined through the skin friction drag $\tau = \rho g \delta = a \rho v_0^2$; δ is the thickness of the flowing-off film; a is a constant; ρ the density; and λ the size of the turbulence decay region at the free surface, defined by

$$\lambda = \frac{\sigma}{\rho v_0^2},$$

where σ is the surface tension.

In accordance with (6.24), the turbulent diffusion coefficient decreases in the direction to the surface, and is equal to the molecular diffusion coefficient for the boundary layer thickness δ_l:

$$\frac{v_0 \delta_l^2}{\lambda} = D_t = D_m \tag{6.25}$$

Thus, the flow is split into two regions: the region adjoining the interface of thickness δ_l (diffusion layer), where the turbulent diffusion coefficient is less than the molecular diffusion coefficient, and the region containing the remaining part of the flow where the turbulent diffusion coefficient is larger than the molecular diffusion coefficient. In the first region, turbulent diffusion is neglected in comparison with molecular diffusion, and the flow of substance passing through it is considered as a purely molecular flow. This assumption is valid in the presence of a rigid fixed interface.

6.3. Penetration and Surface Renewal Model

Higbie's penetration model. Assuming that the contact between the phases exists for a very short time and that diffusion is unsteady, Higbie solved the equation for a moving film, expressing the total number of moles of component A passing per unit time per unit cross-sectional area in the following form:

$$G = \frac{w_0}{l} \int_0^\infty (C_{A_0} - C_{A_\infty})_{z=l}\, dz = \sqrt{\frac{4D_{AB}w_0}{\pi l}}\,(C_{A_0} - C_{A_\infty}). \qquad (6.26)$$

Assuming the difference $C_{A_0} - C_{A\infty}$ to be the driving force, Higbie represented Eq. (6.26) in the form

$$G = \frac{w_0}{l} \int_0^\infty (C_{A_0} - C_{A_\infty})_{z=l}\, dz = k_l\,(C_{A_0} - C_{A_\infty}) \qquad (6.27)$$

and obtained the following expression for the mass-transfer coefficient for a liquid film:

$$k_l = \sqrt{\frac{4D_l w_0}{\pi l}} = \sqrt{\frac{4D_l}{\pi \tau_l}}, \qquad (6.28)$$

where τ_l is the time required for the liquid film to cover the distance l upon the change in the concentration from C_A to $C_{A\infty}$.

The main conclusion that can be drawn from the Higbie equation consists in that the mass-transfer coefficient is proportional to the molecular diffusion coefficient to the power of 1/2

$$k_g = \left(\frac{D_g}{\pi\tau}\right)^{1/2} \text{ and } k_l = \left(\frac{D_l}{\pi\tau}\right)^{1/2}. \qquad (6.29)$$

It follows from these relations that the ratio k_g/k_l does not depend on time. According to Higbie, the concentrations at the interface are also time-independent, and hence remain constant over the entire diffusion period.

Modified penetration and surface renewal models. Danckwerts and Kishenevskii have independently developed Higbie's penetration model by introducing the concept of renewal of gas-liquid interface. According to this theory, there are no boundary films or layers, and the interface is continuously renewed by fresh liquid. Mass transfer is accomplished not only due to molecular, but due to turbulent diffusion as well. The kinetic characteristic in this model is the effective diffusion coefficient D_{eff} equal to the sum of molecular (D_m) and turbulent (D_t) diffusion coefficients:

$$D_{eff} = D_m + D_t. \qquad (6.30)$$

It follows from this theory that the mass-transfer coefficient is proportional to the molecular diffusion coefficient to a power less than 1/2. This corresponds to the processes occurring in the presence of considerable turbulization.

In order to establish kinetic relations, we must take into account the age distribution of various surface elements. According to Danckwerts, the distribution function can be found from the assumption that the mean rate of surface renewal is constant in all regions and that the probability of the renewal of any surface element at a given moment of time does not depend on its age. Proceeding from this assumption, we obtain

$$\Phi = se^{-s\tau}, \tag{6.31}$$

where s is the frequency of renewal of surface element, which is constant over the entire interface, and τ is the age of the surface element under consideration.

The absorption rate is defined by the expression

$$q = \int_0^\infty \psi(\tau)\, se^{-s\tau}\, d\tau, \tag{6.32}$$

where $\psi(\tau)$ is the instantaneous absorption rate depending on time. In the case of physical absorption, we have

$$q = \int_0^\infty (C_{A_0} - C_{A_\infty}) \sqrt{\frac{D_{eff}}{\pi\tau}}\, se^{-s\tau}\, d\tau = \sqrt{D_{eff}s}\,(C_{A_0} - C_{A_\infty}) \tag{6.33}$$

since the instantaneous rate is

$$\psi(\tau) = (C_{A_0} - C_{A_\infty}) \sqrt{\frac{D_{eff}}{\pi\tau}}. \tag{6.34}$$

Thus, the absorption coefficient in the liquid phase is given by

$$k_l = \sqrt{D_{eff}s} \tag{6.35}$$

This expression is similar to that proposed by Higbie:

$$k_l = \sqrt{\frac{4D_{eff}}{\pi\tau_l}}, \tag{6.36}$$

since

$$\tau_l = \frac{1}{s} \text{ and } \sqrt{\frac{4}{\pi}} \sim 1.$$

The quantity s can be represented as the surface renewal factor. Introducing the effective diffusion coefficient D_{eff}, taking into account Eq. (6.36), and integrating Eq. (5.39), the equation for the

absorption rate was obtained in the following form:

$$q = \sqrt{\frac{4D_{\text{eff}}}{\pi\Delta\tau}}(C_{A_0} - C_{A_\infty}). \quad (6.37)$$

In order to determine the absorption rate with the help of this equation, we must know the value of $\Delta\tau$ (the time of surface renewal), which usually involves difficulties.

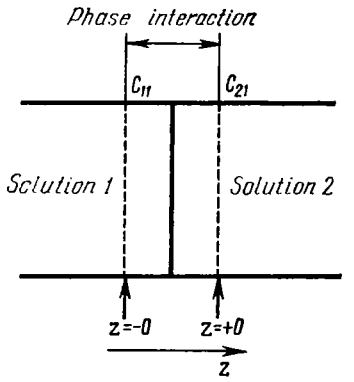

Fig. 85. Model of mass transport involving adsorption.

6.4. Mass-Transfer Model Involving Adsorption

While analyzing the process of mass transfer through an interface, it is assumed that the two concentrations at the interface are in equilibrium. This equilibrium is attained not instantaneously but takes a certain time. These assumptions form the basis of a model of mass transfer through the interface, taking into account the adsorption of the substance being distributed at the interface.

After the two phases come into contact, the substance being distributed is adsorbed at the interface. At the same time, the concentrations near the interface change so that the initial homogeneity of layers is violated. The adsorption rate decreases, and the amount of adsorbed substance becomes nearly constant. Usually, this state is attained very rapidly. The process of mass transfer can be divided into two stages. The first stage, when the adsorption rate is high, is called the adsorption stage. The second stage, when the adsorption rate is close to zero, is called the transient stage. The first stage terminates very quickly, while the second stage lasts till the equilibrium between the layers is attained. Adsorption (desorption) plays a leading role in the process of phase interaction.

The adsorption model is shown in Fig. 85. Mass transport in solutions 1 and 2 is accomplished in accordance with the diffusion equation. The boundary conditions determine the conditions of phase interaction and establish the relationship between C_{11} and C_{21}. The equation for the adsorption rate is represented in the form

$$\begin{aligned} \frac{d\Gamma_1}{d\tau} &= K_{a1}C_{11}(1-\theta)\,e^{r_1\theta} - K_{d1}\theta e^{-q_1\theta}, \\ \frac{d\Gamma_2}{d\tau} &= K_{a2}C_{21}(1-\theta)\,e^{r_2\theta} - K_{d2}\theta e^{-q_2\theta}, \end{aligned} \quad (6.38)$$

where Γ_1 and Γ_2 are the amounts of substance adsorbed by unit interfacial area from solutions 1 and 2 respectively; τ is the time;

K_{a1} and K_{a2} are the rate constants of adsorption on the interface from solutions 1 and 2 respectively; K_{d1} and K_{d2} are the rate constants of desorption from the interface to solutions 1 and 2 respectively; C_{11} and C_{21} are the concentrations of solutions 1 and 2 near the interface; θ is the fraction of interfacial surface covered by adsorbed molecules; and r_1, q_1, r_2, and q_2 are the constants taking into account the effect of interaction between adsorbed molecules. If we assume that $\Gamma = \text{const}$ (termination of the adsorption stage), we get

$$\frac{d\Gamma}{d\tau} = \frac{d\Gamma_1}{d\tau} + \frac{d\Gamma_2}{d\tau} = 0. \tag{6.39}$$

Equations (6.38) and (6.39) are used for establishing the relation between C_{11} and C_{21}:

$$C_{21} = \alpha C_{11} + \beta, \tag{6.40}$$

where $\alpha = -(K_{a1}/K_{a2}) \exp[(r_1 - r_2)\theta]$ is always negative and $\beta = \left(\frac{K_{d1}e^{-q_1\theta} + K_{d2}e^{-q_2\theta}}{K_{a2}e^{r_2\theta}}\right)\frac{\theta}{1-\theta}$ is always positive.

Thus, the system of equations describing the process with the boundary and initial conditions has the form

$$\begin{aligned} \frac{\partial C_1}{\partial \tau} &= D_1 \frac{\partial^2 C_1}{\partial z^2}, \quad z < 0, \\ \frac{\partial C_2}{\partial \tau} &= D_2 \frac{\partial^2 C_2}{\partial z^2}, \quad z > 0. \end{aligned} \tag{6.41}$$

The initial conditions are given by

$$\begin{aligned} C_1 &= C_{1,0}, \quad z < 0, \quad \tau = 0, \\ C_2 &= \xi e^{-\eta z}, \quad z > 0, \quad \tau = 0, \end{aligned} \tag{6.42}$$

where ξ and η are the adsorption constants. The boundary conditions are given by

$$\left.\begin{aligned} C_2 &= \alpha C_1 + \beta, \quad z = 0, \\ D_1 \frac{\partial C_1}{\partial z} &= D_2 \frac{\partial C_2}{\partial z}, \quad z = 0. \end{aligned}\right\} \tag{6.43}$$

Solving systems (6.41), (6.42), and (6.43), and determining the mass flux through the interface, we obtain

$$\begin{aligned} q_{11} &= -D_1 \left(\frac{\partial C_1}{\partial z}\right)_{z=0} \\ &= \left(\frac{D_1}{\pi\tau}\right)^{1/2} [\alpha C_{10} + \beta - \xi + \xi\eta (\pi D_2 \tau)^{1/2} e^{D_2\eta^2\tau} \, erf\, \eta (D_2\tau)^{1/2}]. \end{aligned} \tag{6.44}$$

Thus, the mass transfer rate is determined as a function of diffusion coefficients of the substance in the two phases and by the rate constants of adsorption and desorption of the substance being distributed over the interface. Experimental results are in better agreement for low-mobility layers.

6.5. Mass-Transfer Model Based on the Concept of Interfacial Turbulence

The mass-transfer equations taking into account the interaction between phase flows can be represented in the most general form by using the principles of system analysis (considered in Introduction) and, as a consequence, interfacial turbulence. Introducing the hydrodynamic state factor f of a two-phase system, the mass-transfer equations are given in the following form:

$$\mathrm{Nu}_{D_g} = A\,\mathrm{Re}_g^m\,\mathrm{Pr}_g^n\,(1+f),$$

$$\frac{K_{0y}l}{D_g} = A\left(\frac{w_g l\rho_g}{\mu_g}\right)^m\left(\frac{\mu_g}{\rho_g D_g}\right)^n(1+f) \qquad (6.45)$$

for the concentration difference in the gas phase, and

$$\mathrm{Nu}_{D_l} = A_1\,\mathrm{Re}_l^{m_1}\,\mathrm{Pr}_l^{n_1}\,(1+f),$$

$$\frac{K_{0l}l}{D_l} = A_1\left(\frac{w_l l\rho_l}{\mu_l}\right)^{m_1}\left(\frac{\mu_l}{\rho_l D_l}\right)^{n_1}(1+f) \qquad (6.46)$$

for the concentration difference in the liquid phase. Removing the parentheses in Eqs. (6.45) and (6.46), we obtain

$$\mathrm{Nu}_{D_g} = A\,\mathrm{Re}_g^m\,\mathrm{Pr}_g^n + A\,\mathrm{Re}_g^m\,\mathrm{Pr}_g^n f, \qquad (6.47)$$

$$\mathrm{Nu}_{D_l} = A_1\,\mathrm{Re}_l^{m_1}\,\mathrm{Pr}_l^{n_1} + A_1\,\mathrm{Re}_l^{m_1}\,\mathrm{Pr}_l^{n_1} f. \qquad (6.48)$$

The first terms in these equations determine the amount of substance transported within a given phase due to molecular and eddy diffusion, while the second terms correspond to the amount of substance transported due to the interaction between phase flows. For $f = 0$, Eqs. (6.47) and (6.48) are reduced to the mass transfer equations obtained in the film theory or, to be more precise, to the mass-transfer equations for a single-phase flow. Thus, Eqs. (6.47) and (6.48) are general equations for mass-transfer processes.

In accordance with the structure of mass-transfer equations (6.45) and (6.46), the amount of transported substance is determined from the mass transfer in the phase where the rate of the mass transfer is lower, i.e. which offers the main resistance. For example, if a gas is readily soluble in a liquid, Eq. (6.45) is used, and if it is difficultly soluble in liquid, Eq. (6.46) is employed. Accordingly, the mass-transfer coefficients in the Nusselt number are referred to the molecular diffusion coefficients of the phase in which the process occurs at

the lower rate. The Prandtl number of the phase which offers the main resistance is introduced in a similar way. But since the molecular diffusion coefficient appears in the denominators of the left- and right-hand sides of the equations, its resultant effect on the mass-transfer coefficient will depend on the exponent of the Prandtl number: the larger the exponent, the weaker the effect of molecular diffusion of the mass-transfer coefficient.

Since the Prandtl number characterizes the relationship between the velocity and concentration profiles, it should be expected that the effect of this relation on the process of mass transfer will change depending on the hydrodynamic pattern of the process, i.e. the exponent of the Prandtl number must change. In accordance with the structure of Eqs. (6.45) and (6.46), the exponent n should attain the maximum value equal to unity for the most uniform distribution of liquid and gas in a two-phase flow in the conditions of fully developed free turbulence. As turbulization of flows decreases, the exponent n of the Prandtl number must decrease, attaining zero in the limit when the motion ceases. In this case, the concept of the relationship between the velocity and concentration profiles becomes meaningless. Practically, according to normal hydrodynamic conditions in which diffusion processes occur, the exponent n of the Prandtl number must vary between 1/3 (laminar flow), if we conditionally assume that this term is applicable to a two-phase flow, and 1 (fully developed free turbulent flow). Thus, the form of Eqs. (6.45) may be modified for different hydrodynamic conditions.

Assuming the analogy between friction and mass transfer in a single-phase gas flow, we can determine the order of magnitude of the exponents m and n in Eqs. (6.45). The energy expended to overcome friction in a single-phase flow is determined by the shear stress [see Eq. (3.91)] proportional to the pressure drop:

$$\Delta P_g = -\rho\,(\nu + \varepsilon_p)\,\frac{dw_y}{dz},$$

where ρ is the gas density, and ν and ε_p are the coefficients of molecular and turbulent viscosity respectively. According to Eq. (5.18), the diffusion flux is determined as

$$q = -(D_m + D_t)\,\frac{dC}{dz}.$$

Considering the order of magnitude of the quantities appearing in them the last two dependences can be represented in the following form:

$$\Delta P_g = \rho\,(\nu + \varepsilon_p)\,\frac{w}{l}, \tag{6.49}$$

$$q = (D_m + D_t)\,\frac{\Delta C}{l}. \tag{6.50}$$

Dividing Eq. (6.50) by (6.49), assuming that the transport of mass and energy occurs over the same length l, and solving the result for $q/\Delta C$, we obtain

$$\frac{q}{\Delta C} = \frac{(D_m + D_t)\,\Delta P_g}{\rho\,(\nu + \varepsilon_p)\,w}. \tag{6.51}$$

But since $q/\Delta C = K$ (K is the overall mass-transfer coefficient) this equation can be written as

$$K = \frac{(D_m + D_t)\,\Delta P_g}{\rho\,(\nu + \varepsilon_p)\,w}. \tag{6.52}$$

For the same value of the dynamic state factor f of a two-phase system, the coefficients D_t and ε_p of the turbulent transport of mass and energy have the same order of magnitude. Consequently, the following relationship establishes the dependence between the mass-transfer coefficient K, pressure drop ΔP_g, and the flow velocity w:

$$K \propto \frac{\Delta P_g}{w}. \tag{6.53}$$

This relationship makes it possible to estimate the order of magnitude of the exponents in Eq. (6.45) for various hydrodynamic conditions.

Three kinds of the dependence between the pressure drop ΔP_g and the flow velocity w may exist: $\Delta P_g \propto w$ for a laminar flow, $\Delta P_g \propto w^{1.8}$ for a turbulent flow, and $\Delta P_g \propto w^2$ for a self-similar flow (fully developed turbulence). It is possible to determine the exponents of Re_g and Pr_g in generalized equation of mass transfer (6.45). For a laminar flow, $\Delta P_g \propto w$, and hence $K \propto w$; but since $\mathrm{Re}_g = wd_e/\nu$, $m = 0$ and $n = 1/3$. Thus, we obtain the following mass-transfer equation for a laminar flow:

$$\frac{Kd_e}{D_m} = A_0 \left(\frac{\nu}{D_m}\right)^{1/3} \cdot (1 + f_0) \tag{6.54}$$

whence

$$K \propto D_m^{2/3} \tag{6.55}$$

for a laminar flow. Since the factor f_0 is a small quantity (less than unity) for very small flow velocities, Eq. (6.54) can be reduced to

$$\mathrm{Nu}_D = \text{const}. \tag{6.56}$$

This equation expresses the conditions of molecular mass transfer and is a particular case of the more general equation (6.45).

For a turbulent flow, $\Delta P_g \propto w^{1.8}$ and hence $K \propto w^{0.8}$, $m = 0.8$, $n = 2/3$, and the mass-transfer equation assumes the form

$$\frac{Kd_e}{D_m} = A_1 \left(\frac{wd_e}{\nu}\right)^{0.8} \left(\frac{\nu}{D_m}\right)^{2/3} (1 + f_1). \tag{6.57}$$

It follows from this equation that

$$K \propto D_m^{1/3}. \tag{6.58}$$

For fully developed free turbulence, $\Delta P_g \propto w^2$, and hence $K \propto w$, $m = 1$, $n = 1$, and the mass-transfer equation becomes

$$\frac{Kd_e}{D_m} = A_2 \left(\frac{wd_e}{\nu}\right) \left(\frac{\nu}{D_m}\right) (1 + f_2). \tag{6.59}$$

It follows from this equation that

$$K \propto D_m^0, \tag{6.60}$$

i.e. mass transfer in the conditions of fully developed turbulence is practically independent of molecular diffusion and viscosity. Cancelling out the molecular characteristics on the left- and right-hand sides of Eq. (6.59), we obtain

$$K = A_2 w (1 + f_2) \tag{6.61}$$

or, in the dimensionless form,

$$\frac{K}{w} = A_2 \left[1 + \beta_2 \left(\frac{L}{G}\right)^{a_2} \left(\frac{\gamma_g}{\gamma_l}\right)^{b_2} \left(\frac{\mu_l}{\mu_g}\right)^{c_2} \left(\frac{\sigma_{1-2}}{\sigma_{1-a} + \sigma_{2-a}}\right)^x \left(\frac{l}{d_e}\right)^y\right]. \tag{6.62}$$

Since the factor f_2 may considerably exceed unity under the conditions of fully developed free turbulence, Eq. (6.62) becomes

$$\frac{K}{w} = A_3 \left(\frac{L}{G}\right)^{a_2} \left(\frac{\gamma_g}{\gamma_l}\right)^{b_2} \left(\frac{\mu_l}{\mu_g}\right)^{c_2} \left(\frac{\sigma_{1-2}}{\sigma_{1-a} + \sigma_{2-a}}\right)^x \left(\frac{l}{d_e}\right)^y. \tag{6.63}$$

Under these conditions, the molecular diffusion coefficients are eliminated from the mass-transfer equation, and the exponent c_2 has a small value close to zero. For fully developed turbulence, the ratio of mass-transfer coefficients for readily and difficultly soluble gases is determined by the ratio of the solubility coefficients for gases or, respectively, by the ratio of Henry's constants. Thus, the following relation is valid for fully developed turbulence:

$$\frac{K_1}{K_2} = \frac{m_1}{m_2}, \tag{6.64}$$

where K_1 and K_2 are the mass-transfer coefficients, and m_1 and m_2 are Henry's constants for processes in which the difference $\Delta P_{g-l} - \Delta P_g$ cannot be measured directly. The hydrodynamic state factor for a two-phase system can be determined independently. If follows from the analysis of hydrodynamics of a two-phase flow that the factor f is a function of the dimensionless group which expresses the relationship between basic quantities in the following form:

$$f = \psi \left[\left(\frac{L}{G}\right)^{2-m} \cdot \left(\frac{\gamma_g}{\gamma_l}\right) \left(\frac{\mu_l}{\mu_g}\right)^m\right]. \tag{6.65}$$

An analysis of the mechanism of mass transfer in a single-phase flow revealed that the analogy between friction, heat and mass transfer is possible only for $Pr_D = 1$, i.e. for gases. No such analogy can be observed for dropping liquids for which $Pr_D \sim 10^3$. Therefore, the exponents of Re_l and Pr_l cannot be predicted, and their values in Eq. (6.46) must be established experimentally. If an additional energy is supplied to the diffusion apparatus (agitated vessels, rotary apparatus, etc.), the factor f must contain a quantity taking into account this additional energy supply. The additional energy supply can be represented in terms of the work done on the liquid in a unit volume in the following form:

$$E = \frac{Ln_m^2 d^2}{gHD^2}, \tag{6.66}$$

where L is the amount of treated liquid, kg; n_m the working part speed, rps; d the characteristic dimension of the working part, m; H the height of the contact region, m; D the apparatus diameter, m; and g the acceleration due to gravity, m/s^2.

The hydrodynamic state factor for a two-phase system for the apparatus with additional energy supply can be calculated by the following equation:

$$f = \frac{\Delta P_{g-l} + E - \Delta P_g}{\Delta P_g}. \tag{6.67}$$

Chapter Seven

Methods of Expressing the Driving Force and Kinetics of Mass Transfer

Diffusion potential factor. When calculating mass-transfer processes, the dimensionless parameter $m/(L/G)$ is introduced. It shows the ratio of the slope m of the equilibrium line to the slope L/G of the operating line (i.e. the ratio of the flow rate L and G of the liquid and gas phases). Since the ratio of these slopes characterizes equilibrium conditions in a given system (the value of m) and the working conditions of the apparatus (the value of L/G), i.e. the potentialities of the apparatus, the parameter m (G/L) can be defined as the diffusion potential factor

$$\lambda = \frac{mG}{L}. \tag{7.1}$$

The diffusion potential factor is a determining criterion of mass-transfer processes. The value of G/L is specified by conditions under which a process occurs, while the value of m characterizes the equilibrium nature of the system. Since the average slope of the equilibrium curve is equal to the derivative $m = dy/dx$, the value of m in the general case can be determined by differentiating the equilibrium curve. For example, for distillation processes, the value of m can be determined to a sufficient degree of accuracy by differentiating Raoult's equation (1.13):

$$m = \frac{[y+\alpha(1-y)]^2}{\alpha} \tag{7.2}$$

or

$$m = \frac{\alpha}{[1+x(\alpha-1)]}. \tag{7.3}$$

If the relative volatility α of a mixture varies abruptly in some regions of the equilibrium curve, Eqs. (7.2) and (7.3) can be used as a first approximation for these regions, and then the entire curve can be reconstructed. The value of m can be approximately estimated by replacing the curve on individual sections, within specified concentration range, by an equivalent broken line, averaging by the

equation

$$m = \frac{m_1 + m_2 + m_3 + \ldots + m_n}{n}, \tag{7.4}$$

where n is the number of the broken line sections.

If the equilibrium line is a straight line, $dy/dx = m = \text{const}$. When determining the average slope m of the equilibrium curve for multicomponent vapour-liquid systems, it is assumed that the vapour phase obeys the laws of ideal gases, while the liquid phase belongs to non-ideal solutions. Then we can write

$$yP = \gamma x P_0, \tag{7.5}$$

where y is the content of a given component in the vapour; P the total pressure in the system; γ the coefficient of activity of the given component in the liquid; x the content of the given component in the liquid; and P_0 the vapour pressure of the pure component.

Let us consider a section of a column located between the nth and $(n + 1)$st plates and assume that on this section equilibrium is described by the straight line:

$$y = mx + b. \tag{7.6}$$

If we first write Eqs. (7.5) and (7.6) for x_n and then for x_{n+1} and eliminate y and b, we get

$$m = \frac{\gamma_n P_{0,\,n} x_n - \gamma_{n+1} P_{0,\,n+1} x_{n+1}}{P(x_n - x_{n+1})}. \tag{7.7}$$

In order to use this equation for calculations, we must know the liquid composition, temperature, and pressure.

While calculating mass-transfer processes, the driving force and kinetics of a process are usually expressed by one of three ways: (1) the driving force of the process is expressed in terms of the difference in concentrations, and kinetics, in terms of the mass-transfer coefficients; (2) the driving force of the process is expressed indirectly in terms of the number of transport units and parameter λ, while kinetics is expressed in terms of the transport unit height, and (3) the driving force of the process is expressed indirectly through the number of theoretical stages of contact (theoretical plates), while kinetics, through the efficiency or the height equivalent to the theoretical contact stage.

7.1. Expression of Driving Force in Terms of Difference in Concentrations, and Kinetics in Terms of Mass-Transfer Coefficients

Since for a two-phase flow the interfacial area cannot be determined directly, the process kinetics is expressed through the volumetric mass-transfer coefficient Ka, i.e. refers to the surface area a con-

tained in a unit volume of the gas and liquid in contact. In this case, the mass-transfer equations assume the form

$$dG = K_{0y}a\,(y - y^*)\,f\,dH = K_{0x}a\,(x^* - x)\,f\,dH, \qquad (7.8)$$

where G is the flow rate of transferred substance, kg-mole/hr; $K_{0y}a$ and $K_{0x}a$ are the volumetric mass-transfer coefficients in terms of the driving force in the liquid and gas phases, kg-mole/hr·m^3·unit driving force; $(y - y^*)$, $(x^* - x)$ are the driving forces of the process in the liquid and gas phases; f is the cross-sectional area of the apparatus, m^2; and H the length (height) of the contact region, m.

In accordance with the material-balance equation (2.1), we have

$$dG = -G\,dy = L\,dx. \qquad (7.9)$$

Solving Eqs. (7.8) and (7.9) together, we obtain

$$\frac{K_{0y}a \cdot f\,dH}{G} = \frac{dy}{y - y^*}, \qquad (7.10)$$

$$\frac{K_{0x}a \cdot f\,dH}{L} = \frac{dx}{x^* - x}. \qquad (7.11)$$

Assuming that $K_{0y}a/G$ and $K_{0x}a/L$ are constant, we obtain after integrating

$$\frac{K_{0y}a\,fH}{G} = \int \frac{dy}{y - y^*}, \qquad (7.12)$$

$$\frac{K_{0x}a\,fH}{L} = \int \frac{dx}{x^* - x}, \qquad (7.13)$$

whence the height of the contact region is

$$H = \frac{G}{K_{0y}af} \int \frac{dy}{y - y^*}, \qquad (7.14)$$

or

$$H = \frac{L}{K_{0x}af} \int \frac{dx}{x^* - x}. \qquad (7.15)$$

The limits of integration are determined by the given concentrations at the inlet and outlet of the apparatus. If the equilibrium and operating lines are straight, the driving force of the process is expressed as the logarithmic mean of the initial and final differences in concentrations:

$$\Delta y_m = \frac{\Delta y_{in} - \Delta y_{fin}}{2.3 \log \frac{\Delta y_{in}}{\Delta y_{fin}}}, \qquad (7.16)$$

$$\Delta x_m = \frac{\Delta x_{in} - \Delta x_{fin}}{2.3 \log \frac{\Delta x_{in}}{\Delta x_{fin}}}, \qquad (7.17)$$

where

$$\Delta y_{1n} = y_{1n} - y^*_{1n}, \quad \Delta y_{\text{fin}} = y_{\text{fin}} - y^*_{\text{fin}},$$
$$\Delta x_{1n} = x^*_{1n} - x_{1n}, \quad \Delta x_{\text{fin}} = x^*_{\text{fin}} - x_{\text{fin}}.$$

Taking into account Eq. (7.9), Eqs. (7.14) and (7.15) become

$$H = \frac{G}{K_{0y} a f \Delta y_m}, \tag{7.18}$$

$$H = \frac{L}{K_{0x} a f \Delta x_m}. \tag{7.19}$$

7.2. Expression of Driving Force in Terms of the Number of Transport Units and Parameter λ

It follows from Eqs. (7.12) and (7.13) that their right-hand sides are equal to a certain dimensionless number N determined by the driving force and the concentration range. Equations (7.14) and (7.15) show that the ratios $G/(K_{0y}af)$ and $L/(K_{0x}af)$ have the dimensions of height over which the mass is transported. These groups are called *the heights of transport units* and are denoted by $(\text{HTU})_{0y}$ and $(\text{HTU})_{0x}$ respectively:

$$H = (\text{HTU})_{0y} N_{0y}, \tag{7.20}$$

$$H = (\text{HTU})_{0x} N_{0x}. \tag{7.21}$$

The dimensionless quantities $N_{0y} = \int \frac{dy}{y - y^*}$ and $N_{0x} = \int \frac{dx}{x^* - x}$ are called *the numbers of transport units*; they can be calculated beforehand. The values of $(\text{HTU})_{0y}$ and $(\text{HTU})_{0x}$ are determined from experimental data and reflect the process kinetics. The numbers N_{0y} and N_{0x} of transport units are the results of joint solution of the equilibrium equation and the equation of the operating line of the process given by the initial and final concentrations which are limits of integration. The number of transport units in unidirectional diffusion (absorption, extraction) is defined by the following equation:

$$N_{0y} = \int_{y_2}^{y_1} \frac{(1-y)_f \, dy}{(1-y)(y-y^*)}, \tag{7.22}$$

where

$$(1-y)_f = \frac{(1-y)-(1-y^*)}{\ln \frac{(1-y)}{(1-y^*)}}. \tag{7.23}$$

If $(1 - y)_f$ can be replaced by the arithmetic mean, Eq. (7.22) is transformed to

$$N_{0y} = \int_{y_2}^{y_1} \frac{dy}{y - y^*} + 1.15 \ln \frac{(1-y_2)}{(1-y_1)}. \tag{7.24}$$

The second terms can often be neglected.

If diffusion occurs at the same rate in both directions, Eq. (7.22) is simplified by eliminating the ratio $(1 - y_2)/(1 - y_1)$ and reduced to

$$N_{0y} = \int_{y_2}^{y_1} \frac{dy}{y - y^*}. \tag{7.25}$$

Let us denote by y_1 the mole fraction of the component being distributed (solute) in the input flow and by y_2 its mole fraction in the output flow. Let y_a be some intermediate concentration of the component being distributed in the flow, equal to the geometrical mean of y_1 and y_2, i.e. $y_a = \sqrt{y_1 y_2}$. If y_2 is a very small quantity, y_a is also very small regardless of the value of y_1, and equilibrium and operating lines between y_a and y_2 can be assumed to be straight. Then

$$y^* = m_2 x, \tag{7.26}$$

$$y - y_2 = (x - x_2) \left(\frac{L}{G}\right)_2, \tag{7.27}$$

where m_2 is the Henry constant for dilute solutions, and $(L/G)_2$ is the ratio of flow rates at the apparatus outlet under strong dilution. Considering that $m_2/(L/G)_2 = \lambda_2$, we get

$$y - y^* = y - m_2 x = y - (y - y_2)\lambda_2 - m_2 x_2, \tag{7.28}$$

or

$$y - y^* = (y - m_2 x_2)(1 - \lambda_2) + (y_2 - m_2 x_2)\lambda_2. \tag{7.29}$$

Substituting (7.29) into (7.25), we obtain for strong dilution

$$\int_{y_2}^{y_a} \frac{dy}{y - y^*} = \int_{y_2}^{y_a} \frac{dy}{(y - m_2 x_2)(1 - \lambda_2) + (y_2 - m_2 x_2)\lambda_2}$$

$$= \frac{1}{1 - \lambda_2} \ln \left[(1 - \lambda_2) \frac{y_a - m_2 x_2}{y_2 - m_2 x_2} + \lambda_2 \right]. \tag{7.30}$$

Beyond the limits y_a and y_1, the operating and equilibrium lines may be curves. Then the expression $(y - y^*)$ is squared and the proportionality factor b is introduced. If the value of $(y_2 - m_2 x_2)$

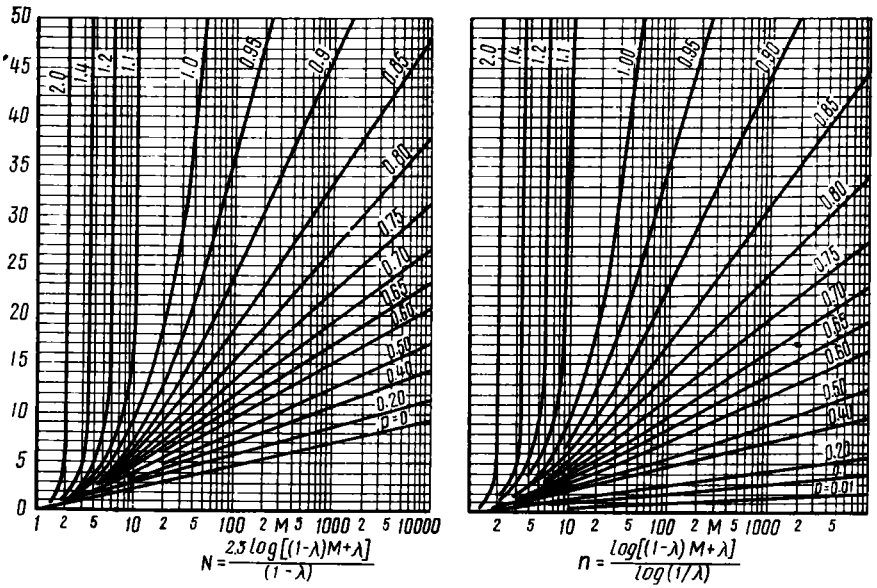

Fig. 86. Determination of the number N of transport units and the number n of theoretical plates.

is small in comparison with y, it can be omitted, i.e.

$$\int_{y_a}^{y_1} \frac{dy}{y-y^*} = \int_{y_a}^{y_1} \frac{dy}{(y-m_2x_2)(1-\lambda_2)+b(y-m_2x_2)^2}$$

$$= \frac{1}{1-\lambda_2} \ln \frac{(y_1-m_2x_2)[1-\lambda_2+b(y_a-m_2x_2)]}{(y_a-m_2x_2)[1-\lambda_2+b(y_1-m_2x_2)]}. \quad (7.31)$$

If $b(y_a - m_2x_2)$ is small in comparison with $(1 - \lambda_2)$, it can also be omitted. Then

$$[1-\lambda_2+b(y_1-m_2x_2)] = \frac{y_1-y^*}{y_1-m_2x_2},$$

or, if we neglect m_2x_2 in comparison with y_1 and introduce $(1 - y_1^*/y_1)$, Eq. (7.31) is reduced to

$$\int_{y_a}^{y_1} \frac{dy}{y-y^*} = \frac{1}{1-\lambda_2} \ln \frac{(y_1-m_2x_2)(1-\lambda_2)}{(y_a-m_2x_2)[1-y_1^*/y_1]}. \quad (7.32)$$

The required integral between y_2 and y_1 is now the sum of Eqs. (7.30) and (7.31):

$$\int_{y_2}^{y_1} \frac{dy}{y-y^*} = \frac{2.3}{1-\lambda_2} \ln \frac{(y_1-m_2x_2)(1-\lambda_2)}{(y_2-m_2x_2)(1-y_1^*/y_1)} + \lambda_2. \quad (7.33)$$

Table 5

Calculation Formulas for Mass-Transfer Processes

Process	Diffusion potential factor	N	λ	M
Absorption	$\frac{mG}{L}=\text{const}$	N_{0y}	$\frac{mG}{L}$	$\frac{y_1-mx_2}{y_2-mx_2}$
	$\frac{mG}{L}\neq\text{const}$ [1]	$N_{0y}-1.15\log\frac{1-y_2}{1-y_1}$	$\frac{m_2G_2}{L_2}$	$\left(\frac{y_1-m_2x_2}{y_2-m_2x_2}\right)\left(\frac{1-m_2G_2/L_2}{1-y_1^*/y_1}\right)$
		$N_{0y}+1.15\log\frac{1+\gamma_1}{1+\gamma_2}$	$\frac{m_2G_2}{L_2}$	$\left(\frac{\gamma_1-m_2x_2}{\gamma_2-m_2x_2}\right)\left(\frac{1-m_2G_2/L_2}{1-\gamma_1^*/\gamma_1}\right)$
Desorption	$\frac{L}{mG}=\text{const}$	N_{0x}	$\frac{L}{mG}$	$\frac{x_1-y_2/m}{x_2-y_2/m}$
	$\frac{L}{mG}\neq\text{const}$ [1]	$N_{0x}-1.15\log\frac{1-x_2}{1-x_1}$	$\frac{L_2}{m_2G_2}$	$\left(\frac{x_1-y_2/m_2}{x_2-y_2/m_2}\right)\left(\frac{1-L_2/m_2G_2}{1-x_1^*/x_1}\right)$
		$N_{0x}+1.15\log\frac{1+x_1}{1+x_2}$	$\frac{L_2}{m_2G_2}$	$\left(\frac{x_1-\gamma_2/m_2}{x_2-\gamma_2/m_2}\right)\left(\frac{1-L_2/m_2G_2}{1-x_1^*/x_1}\right)$
				$x=\frac{x}{1-x}\ ;\ y=\frac{y}{1-y}$
Distillation (rectification—enrichment) [2]	$\frac{mG}{L}=\text{const}$	N_{0y}	$\frac{mG}{L}$	$\frac{y_1-mx_2}{y_2-mx_2}$
	$\frac{mG}{L}\neq\text{const}$	N_{0y}	$\frac{m_2G_2}{L_2}$	$\left(\frac{y_1-m_2x_2}{y_2-m_2x_2}\right)\left(\frac{1-m_2G_2/L_2}{1-x_1^*/x_1}\right)$
		N_{0y} [3]	$\left(\frac{y^*}{x}\right)_m\frac{G}{L}$	$\frac{y_1-m_2x_2}{y_2-m_2x_2}$

Distillation (stripping, heating steam)[2]	$\frac{L}{mG} = \text{const}$	$N_{0x} + \frac{2.3 \log mG/L}{1 - L/mG}$	$\frac{L}{mG}$	$\frac{x_1 - x_2 m}{x_2 - x_2 m}$
	$\frac{L}{mG} \neq \text{const}$	$N_{0x} + \frac{2.3 \log m_2 G_2/L_2}{1 - L_2/m_2 G_2}$	$\frac{L_2}{m_2 G_2}$	$\left(\frac{x_1 - x_2/m_2}{x_2 - x_2/m_2}\right)\left(\frac{1 - L_2/m_2 G_2}{1 - x_1^*/x_1}\right)$
		$N_{0x} + \frac{2.3 \log m_2 G_2/L_2}{1 - L_2/m_2 G_2}$	$\left(\frac{y^*}{x}\right)_m \frac{G}{L}$	$\frac{x_1 - x_2/m_2}{x_2 - x_2 m_2}$
Distillation (stripping, live steam)	$\frac{L}{mG} = \text{const}$	N_{0x}	$\frac{L}{mG}$	$\frac{x_1}{x_2}$
	$\frac{L}{mG} \neq \text{const}$	N_{0x}	$\frac{L_2}{m_2 G_2}$	$\left(\frac{x_1}{x_2}\right)\frac{1 - L_2/m_2 G_2}{1 - x_1^*/x_1}$
Extraction (stripping)	$\frac{L}{mG} = \text{const}$	N_{0x}	$\frac{L_2}{mG}$	$\frac{\omega_1 - v_2/m}{\omega_2 - v_2/m}$[4]
	$\frac{L}{mG} \neq \text{const}$	$N_{0x} - \theta$[5]	$\frac{L_2}{m_2 G_2}$	$\left(\frac{\omega_1 - v_2/m}{\omega_2 - v_2/m}\right)\left(\frac{1 - L_2/m_2 G_2}{1 - \omega_1^*/\omega_1}\right)$
Extraction (enrichment)	$\frac{mG}{L} = \text{const}$	N_{0y}	$\frac{mG}{L}$	$\frac{v_1 - m\omega_2}{v_2 - m\omega_2}$
	$\frac{mG}{L} \neq \text{const}$	$N_{0y} - \theta'$[6]	$\frac{m_2 G_2}{L_2}$	$\left(\frac{v_1 - m\omega_2}{v_2 - m\omega_2}\right)\left(\frac{1 - m_2 G_2/L_2}{1 - v_1^*/v_1}\right)$

[1] The formulas for variables mG/L and L/mG are more accurate for $M > 120$.
[2] The concentrations x, y, and m are calculated for a high-boiling or a heavy key component.
[3] The concentrations x, y, and m are calculated for a low-boiling or a light key component.
[4] ω, v are the weight fractions of the solute in the solution and solvent, respectively.
[5] $\theta = 1.15 \log \frac{1 - \omega_2}{1 - \omega_1} - 1.15 (1 - r) \log \frac{1 - (1 - r)\omega_2}{1 - (1 - r)\omega_1}$.
[6] $\theta' = 1.15 \log \frac{1 - v_2}{1 - v_1} - 1.15 (1 - r) \log \frac{1 - (1 - r) v_2}{1 - (1 - r) v_1}$, where r is the ratio of molecular mass of the flow without the solute to the molecular mass of the solute.

The equations for rectification and extraction can be obtained in a similar way. Introducing the notation

$$\frac{y_1 - m_2 x_2}{(y_2 - m_2 x_2)\left(1 - \frac{y_1^*}{y_1}\right)} = M, \tag{7.34}$$

$N_{0y} = N$, Eq. (7.33) can be reduced to

$$N = \frac{2.3 \log [(1-\lambda_2) M + \lambda_2]}{(1-\lambda_2)}. \tag{7.35}$$

The following equation has been obtained for the number of theoretical plates:

$$n = \frac{\log [(1-\lambda_2) M + \lambda_2]}{\log (1/\lambda_2)}. \tag{7.36}$$

The ratio of the number N of transport units to the number n of theoretical plates is given by

$$\frac{N}{n} = \frac{2.3 \log 1/\lambda_2}{1-\lambda_2}. \tag{7.37}$$

Table 5 represents the equations for absorption, desorption, rectification, and extraction. Figure 86 shows a graphical solution of Eqs. (7.35) and (7.36).

7.3. Expression of Driving Force in Terms of the Number of Theoretical Contact Stages

The number of theoretical contact stages, or the number of theoretical plates, can be determined analytically or graphically by jointly solving the equations of equilibrium and operating lines of the process. One theoretical plate expresses a change Δy of the driving force with respect to the gas phase and a change Δx with respect to the liquid phase, the number of theoretical plates being inversely proportional to the driving force of the process. In other words, the larger the driving force (the larger the sections Δy and Δx), the smaller number of theoretical plates is required for a given separation. The actual number of plates which must be installed in an apparatus is determined by the efficiency. Three types of efficiency are distinguished: (1) local, or point efficiency η_0; (2) the plate efficiency η_p,* and (3) the column efficiency η.

The local efficiency η_0 is defined as the ratio of the change in the vapour or liquid composition at a given point of the plate to the

* The plate and local efficiencies are conventional concepts which are widely used for the description of diffusion processes. It would be more precisely to define them as the enrichment or relative extraction coefficients. However, since the former term is used in engineering more frequently, it will be used in further analysis.

change of the composition when the equilibrium concentration y^* (x^*) is attained (Fig. 87):

$$\eta_{oy} = \frac{y - y_{n+1}}{y^* - y_{n+1}}, \tag{7.38}$$

$$\eta_{ox} = \frac{x_{n-1} - x}{x_{n-1} - x^*}, \tag{7.39}$$

where y is the composition of the vapour rising at a given point from the nth plate; y_{n+1} the composition of the vapour coming to the nth plate at a given point; y^* the vapour composition in equilibrium

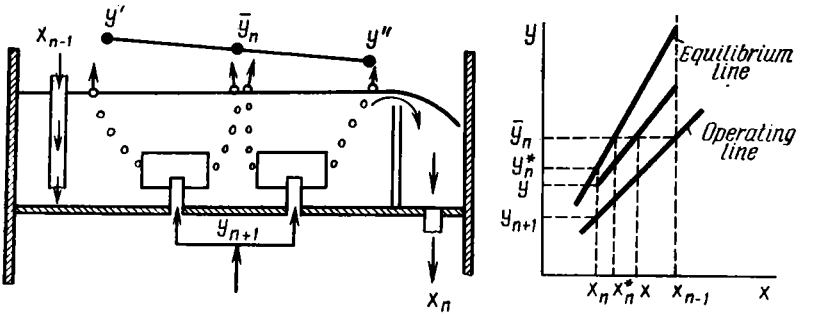

Fig. 87. To the determination of the plate efficiency and local efficiency.

with the liquid at a given point; x the liquid composition at a given point; x_{n-1} the composition of the liquid coming to the nth plate; and x^* the composition of liquid in equilibrium with the vapour rising from the nth plate at a given point.

The plate efficiency η_p, or the Murphree efficiency, is the ratio of the change in the mean composition of vapour or liquid on a plate to the change in the composition resulting in the equilibrium concentration (Fig. 87):

$$\eta_{p,\,y} = \frac{\bar{y}_n - \bar{y}_{n+1}}{y_n^* - \bar{y}_{n+1}}, \tag{7.40}$$

$$\eta_{p,\,x} = \frac{\bar{x}_{n-1} - \bar{x}_n}{\bar{x}_{n-1} - x_n^*}, \tag{7.41}$$

where $\bar{y}_n$ is the mean composition of the vapour rising from the nth plate; $\bar{y}_{n+1}$ the mean composition of the vapour coming to the nth plate; y_n^* the composition of the vapour which is in equilibrium with the liquid leaving the nth plate; $\bar{x}_{n-1}$ the composition of the liquid coming to the nth plate; $\bar{x}_n$ the composition of the liquid leaving the nth plate; and x_n^* the liquid composition in equilibrium with the mean composition of vapour rising from the nth plate.

The effectiveness of a plate is determined by the values of the local and Murphree (plate) efficiencies. The ratio of these efficiencies determines the degree of mixing of liquid on a plate. For complete mixing of liquid and vapour, the values of η_0 and η_p coincide for each phase.

The column efficiency η is the ratio of the number n of theoretical plates to the actual number n_a of plates required for mixture separation:

$$\eta = \frac{n}{n_a}. \tag{7.42}$$

The column efficiency, being a kinetic characteristic, depends on the ratio L/G of the flow rates of liquid and vapour, the ratio ρ_v/ρ_l of densities, the ratio μ_v/μ_l of viscosities, relative volatility α, and other parameters:

$$\eta = f\left(\frac{L}{G}, \frac{\rho_v}{\rho_l}, \frac{\mu_v}{\mu_l}, \alpha \ldots\right). \tag{7.43}$$

These parameters may vary over the column height, thus changing the conditions of mass transfer. Consequently, the column efficiency η is averaged over the entire column.

For packed columns, the ratio of the total packing height to the number of theoretical plates at this height is called *the height equivalent to the theoretical contact stage* (*theoretical plate*) HETP:

$$h_e = \frac{H}{n}, \tag{7.44}$$

where H is the total packing height, m; and n the number of theoretical plates. Thus, the height equivalent to a theoretical plate, or equivalent packing height, is a height of packing at which separation is the same as on a theoretical plate. The clarity and simplicity of the method of calculation of the equivalent height are also used for estimating the kinetics of other types of apparatus such as film-type columns.

7.4. Relations Between Efficiency, Mass-Transfer Coefficient, and Number of Transport Units

The relation between the vapour-phase efficiency, the mass-transfer coefficient $K_{0y}a$, and the number N_{0y} of transport units can be established by considering the model of flows.

Vapour bubbles in liquid in the vertical direction through the section filled by liquid having the composition x ranging between x_{n-1} and x_n. Suppose that x does not vary along the vertical. The vapour entering the section filled with liquid has the composition y_{n+1}, while the vapour leaving this section has the composition y_n. We assume that vapour rises vertically through the sections without

mixing. Applying Eq. (7.12) to the process of rectification, we obtain

$$\frac{K_{0y}afH}{G} = \int_{(y^*-y)_{n+1}}^{(y^*-y)_n} \frac{dy}{y^*-y} = N_{0y}. \tag{7.45}$$

Since x is constant along the vertical, y^* is also constant, and the integration yields

$$1 - \frac{y_n - y_{n+1}}{y^* - y_{n+1}} = e^{\frac{-K_{0y}afH}{G}} = e^{-N_{0y}}, \tag{7.46}$$

or, on the basis of (7.38), we get

$$1 - \eta_0 = e^{\frac{-K_{0y}afH}{G}} = e^{-N_{0y}}. \tag{7.47}$$

For complete mixing ($x = x_v$ and $\eta_0 = \eta_p$), Eq. (7.47) becomes

$$1 - \eta_p = e^{\frac{-K_{0y}afH}{G}} = e^{-N_{0y}}. \tag{7.48}$$

If there is no mixing or if the equilibrium line is straight, i.e. $y^* = mx + b$ for η_0, L and G = const, we can get

$$\eta_p = \frac{L}{mG}\left(e^{\frac{mG}{L}\eta_0} - 1\right). \tag{7.49}$$

It follows from this equation that η_p may exceed 100% if η_0 approaches unity.

In the absence of a concentration gradient in liquid along the vertical, for x = const, we obtain the following expression for the local efficiency $\eta_{0,l}$ of the liquid phase:

$$1 - \eta_{0,l} = e^{\frac{-K_{0x}afH}{L}} = e^{-N_{0x}}. \tag{7.50}$$

Since while deriving this equation it was assumed that the concentration gradient exists only along the plate in the direction of the liquid flow, we obtain the following relation:

$$\eta_{p,l} = \frac{e^{N_{0x}} - 1}{e^{N_{0x}}}. \tag{7.51}$$

In accordance with the material balance equation, for complete mixing of liquid on a plate we have

$$L(x_{n-1} - x_n) = K_{0x}a(x_n - x_n^*)fH, \tag{7.52}$$

whence

$$\frac{x_{n-1} - x_n}{x_n - x_n^*} = \frac{K_{0x}afH}{L} = N_{0x}. \tag{7.53}$$

Let us represent the plate efficiency in the form

$$\eta_{p,1} = \frac{x_{n-1} - x_n}{(x_n - x_n^*) + (x_{n-1} - x_n)}. \quad (7.54)$$

We divide the numerator and denominator of this expression by $x_n - x_n^*$:

$$\eta_{p,1} = \frac{\frac{x_{n-1} - x_n}{x_n - x_n^*}}{1 + \frac{x_{n-1} - x_n}{x_n - x_n^*}}. \quad (7.55)$$

Introducing N_{0x1} we can write (7.55) on the basis of Eq. (7.53) as follows:

$$\eta_{p,1} = \frac{N_{0x}}{1 + N_{0x}}. \quad (7.56)$$

The relation between the local gas-phase efficiency η_0 and the local liquid-phase efficiency $\eta_{0,1}$ can be found from the material balance equation:

$$\eta_0 = \frac{\eta_{0,1}}{\eta_{0,1} + \lambda(1 - \eta_{0,1})}. \quad (7.57)$$

A similar relationship can be applied to the plate efficiency if λ is constant over the plate:

$$\eta_p = \frac{\eta_{p,1}}{\eta_{p,1} + (1 - \eta_{p,1})}. \quad (7.58)$$

In the general case, η_p and η_0 are calculated from the vapour (gas) concentration, and for difficultly soluble gases, $\eta_{p,1}$ and $\eta_{0,1}$ are calculated.

7.5. Relations Between Mass-Transfer Coefficient, Equivalent Packing Height, and Height of Transport Unit

The mole fraction of a high-volatility component on the theoretical plate increases from y to y^* (see Fig. 87) so that the total amount of substance transferred is equal to $G(y^* - y)$. If the equilibrium on the section under consideration is described by a straight line, the driving force of the process can be expressed as the logarithmic mean of $(y^* - y)\, m\,(G/L)$ and $(y^* - y)$. Then, in accordance with Fig. 88, we have

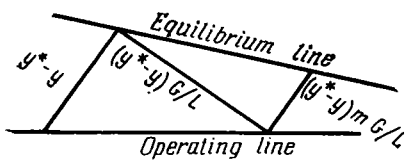

Fig. 88. To the derivation of Eq. (7.60).

$$G(y^* - y) = K_{0y} a h_e (y^* - y) \frac{\lambda - 1}{\log \lambda}, \quad (7.59)$$

whence

$$h_e = \frac{G}{K_{0y}a}\,\frac{\log\lambda}{\lambda-1} = \frac{G}{K_{0y}a}\,\frac{\log\frac{1}{\lambda}}{1-\lambda} = (\mathrm{HTU})_{0y}\,\frac{\log\frac{1}{\lambda}}{1-\lambda}. \qquad (7.60)$$

If the equilibrium line on the reference section is not straight, the following relation between h_e and $(\mathrm{HTU})_{0y}$ is observed for equimolar diffusion:

$$\frac{h_e}{(\mathrm{HTU})_{0y}} = \frac{N_{0y}}{n} = 1 + \frac{1}{12}\left[\frac{2.3\log\left(\frac{y_0-y_1}{y_n-y_{n+1}}\right)}{n}\right]^2 - \frac{1}{2}\left[\frac{2.3\log\left(\frac{y_0-y_1}{y_n-y_{n+1}}\right)}{n}\right], \qquad (7.61)$$

$$\frac{h_e}{(\mathrm{HTU})_{0x}} = \frac{N_{0x}}{n} = 1 + \frac{1}{12}\left[\frac{2.3\log\left(\frac{x_0-x_1}{x_n-x_{n+1}}\right)}{n}\right]^2 + \frac{1}{2}\left[\frac{2.3\log\left(\frac{x_0-x_1}{x_n-x_{n+1}}\right)}{n}\right]. \qquad (7.62)$$

If the equilibrium and operating lines are parallel, $mG/L = 1$, and

$$h_e = (\mathrm{HTU})_{0y} = (\mathrm{HTU})_{0x}. \qquad (7.63)$$

The relations between h_e and $(\mathrm{HTU})_{0y}$ can also be obtained directly from Eq. (7.37). Deriving an exact relation between the height equivalent to a theoretical plate and the height of transport units, we must consider the differential of the number of theoretical plates, corresponding to the differential of the packed column height. If the equilibrium and operating lines are straight, on the basis of Fig. 89 we have

$$\lambda = \frac{mG}{L} = \frac{x_1-a}{x_0-a} = \frac{x_2-a}{x_1-a} = \ldots = \frac{x_n-a}{x_{n-1}-a}, \qquad (7.64)$$

i.e.

$$\frac{x_n-a}{x_0-a} = \lambda^n, \qquad (7.65)$$

whence the value of n is determined from the relation

$$n = \frac{\ln\frac{x_n-a}{x_0-a}}{\ln\lambda} = \frac{\ln\frac{y_n^*-y_n}{y_0^*-y_0}}{\ln\lambda} = \frac{\ln\frac{x_n-x_n^*}{x_0-x_0^*}}{\ln\lambda}. \qquad (7.66)$$

This equation is valid for the general case when n is not an integer. Consequently, the differential of the number of theoretical plates, corresponding to the differential of the length of the operating line between the points (x, y) and $(x + dx, y + dy)$, can be obtained by

differentiating Eq. (7.66):

$$dn = \frac{\frac{dy^* - dy}{y^* - y}}{\ln \lambda} = \frac{\frac{dx - dx^*}{x - x^*}}{\ln \lambda}. \qquad (7.67)$$

Considering that the slope of the operating line is $dy/dx = L/G$ and the slope of the equilibrium line is $dy^*/dx = dy/dx^* = m$,

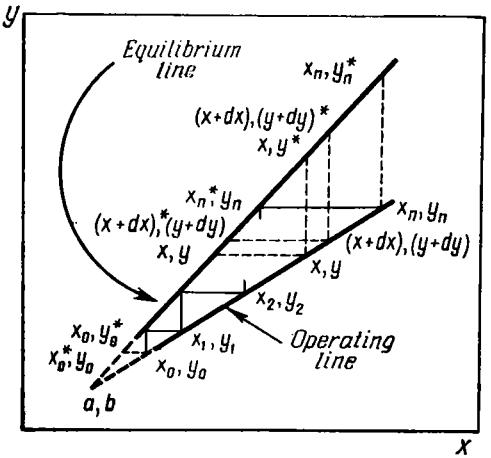

Fig. 89. To the determination of the number n of theoretical plates for a linear equilibrium dependence.

after the appropriate substitution into Eq. (7.67), we get

$$dn = \frac{\frac{1}{\lambda} - 1}{\ln \lambda} \cdot \frac{dy}{y^* - y}, \qquad (7.68)$$

or

$$dn = \frac{\frac{1}{\lambda} - 1}{\ln \lambda} \cdot \frac{dx}{x - x^*} \qquad (7.69)$$

Integrating Eq. (7.68), we obtain the well-known relation between the height of a transport unit and the height equivalent to a theoretical plate:

$$\frac{(\mathrm{HTU})_{oy}}{h_e} = \frac{n}{N_{oy}} = \frac{\lambda - 1}{\ln \lambda}. \qquad (7.70)$$

If the equilibrium line is a curve (Fig. 90), the quantities [Eqs. (7.68) and (7.69)] will differ since the values of m at the points (x, y^*) and (x^*, y) are different. If we denote by m_F the slope of the chord connecting the points (x, y^*) and (x^*, y) and substitute dy^*/dx and dy/dx^* into Eq. (7.67), expressions (7.68) and (7.69) will give

the equal values. It can be shown that the error introduced as a result of such a simplification is insignificant. Thus, integrating Eq. (7.68) with m_F instead of m and combining it with $(\mathrm{HTU})_{0y}$, we obtain

$$\frac{(\mathrm{HTU})_{0y}}{h_e} = \frac{n}{N_{0y}} = \frac{\int_{y_0}^{y_n} \frac{(m_F G/L)-1}{\ln (m_F G/L)} \cdot \frac{dy}{y^*-y}}{\int_{y_0}^{y_n} \frac{dy}{y^*-y}}. \quad (7.71)$$

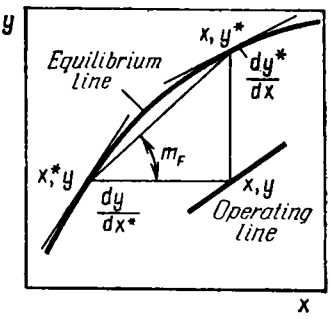

Fig. 90. To the determination of the number n of theoretical plates for a non-linear equilibrium dependence.

The expression $[(m_F G/L) - 1]/\ln (m_F G/L)$ can be replaced by the arithmetic mean of $m_F G/L$ and 1 with an error less than 4% if $0.5 \leqslant m_F G/L \leqslant 2.0$. As a result, we get

$$\frac{n}{N_{0y}} = \frac{\int_{y_0}^{y_n} \left(\frac{m_F G}{2L} + \frac{1}{2}\right) \frac{dy}{y^*-y}}{\int_{y_0}^{y_n} \frac{dy}{y^*-y}} = \frac{G/L}{2} \frac{\int_{y_0}^{y_n} \frac{m_F\, dy}{y^*-y}}{\int_{y_0}^{y_n} \frac{dy}{y^*-y}} + \frac{1}{2} \cdots . \quad (7.72)$$

If the equilibrium line has a large curvature, m_F considerably varies with concentration. The average slope $\bar{m}_F$ of the equilibrium line can be determined as follows:

$$\bar{m}_F = \frac{L}{G} \frac{N_{0x}}{N_{0y}} = \frac{L \int_{x_0}^{x_n} \frac{dx}{x-x^*}}{G \int_{y_0}^{y_n} \frac{dy}{y^*-y}}. \quad (7.73)$$

Considering that $dy/dx = L/G$, Eq. (7.73) can be represented in the form

$$\bar{m}_F = \frac{\int_{y_0}^{y_n} \frac{dy}{x-x^*}}{\int_{y_0}^{y_n} \frac{dy}{y^*-y}} = \frac{\int_{y_0}^{y_n} \frac{m_F\, dy}{y^*-y}}{\int_{y_0}^{y_n} \frac{dy}{y^*-y}}. \quad (7.74)$$

If the arithmetic mean is taken instead of the logarithmic mean [see Eq. (7.60)] Eqs. (7.74) and (7.73) can be used to obtain the following relation:

$$\frac{n}{N_{0y}} = \frac{(\mathrm{HTU})_{0y}}{h_e} \cong \frac{(\bar{m}_F G/L) - 1}{\ln (\bar{m}_F G/L)}. \tag{7.75}$$

However, this expression can hardly be used in practical calculations for determining n, since the estimates of N_{0y} and N_{0x} are required for calculating $\bar{m}_F$ in this case. The number of theoretical plates can be practically calculated by a conventional method with a small error introduced by the equilibrium line curvature. The following relation can be obtained from Eqs. (7.73) and (7.75):

$$n \cong (N_{0y} - N_{0x})/\ln (N_{0y}/N_{0x}). \tag{7.76}$$

When $0.5 \leqslant \bar{m}_F G/L \leqslant 2.0$, this relation can be approximated by the following equation with an error less than 4%:

$$n \cong \frac{1}{2}(N_{0y} + N_{0x}) \tag{7.77}$$

and hence

$$1/h_e \cong \frac{1}{2}\left(\frac{1}{(\mathrm{HTU})_{0y}} + \frac{1}{(\mathrm{HTU})_{0x}}\right). \tag{7.78}$$

Relation (7.78) is applicable for an analysis of the variation of HETP. It was established in an analysis of fractionation in packed columns with the help of the diffusion model that the higher the relative volatility, the stronger the dependence of HTU and HETP on the molar composition, this dependence being stronger for HTU than for HETP. The values of HTU and HETP vary along the column height. For this reason, it is better to calculate packed columns on the basis of HETP than of HTU.

Part Four

Modelling and Calculation of Diffusion Apparatus

Classification of Apparatus and Estimation of Efficiency

The basic characteristic of mass-transfer processes occurring in two-phase flows is the interaction between the phases which determines the area of the interfacial surface. Therefore, apparatus intended for mass-transfer processes must be designed in such a way that the interfaces are developed in them to the highest possible extent. Accordingly, the classification of diffusion apparatus is based on the principle of interfacial area formation. A large variety of diffusion apparatus can be conditionally classified into three basic groups.

I. Apparatus with a fixed interfacial area.

II. Apparatus with an interface formed during the flow of interacting phases.

III. Apparatus with an external power supply.

The classification involves both geometrical features of an apparatus and hydrodynamic conditions created in it. For example, in apparatus with a fixed interfacial area, such as film-type columns with wetted walls, the interfacial area is not fixed under conditions close to flooding. However, the main tendency in designing such apparatus (the creation of a thin film of liquid on the surface of the walls) continues to dominate.

According to this classification, the most typical apparatus widely used in industry are divided into groups as indicated in Table 6.

In calculating diffusion apparatus, the quantities being determined are (1) the diameter of the apparatus or its cross-sectional area which ensures the required capacity for the continuous phase. The apparatus diameter depends on the linear velocity of the continuous phase in the open area, which is determined by hydrodynamic conditions in the apparatus; (2) the total length of the contact zone of the apparatus, required for completing the separation process to preset final concentrations. The total length of the contact region is determined by hydrodynamic and kinetic characteristics and

Table 6

Classification of Diffusion Apparatus

Apparatus with fixed interfacial area	Apparatus with interface formed during flow of interacting phases	Apparatus with external power supply
Film-type wetted-wall columns	Bubble-cap plate columns	Apparatus with mechanical stirrers
Columns with vertical sheet packing	Sieve plate columns	Pulsed columns
	Plate columns with unidirectional flow of vapour and liquid	Rotational apparatus
Spray columns	Plate-grid or sieve columns without overflow devices (grid plate columns)	
	Packed columns	
	Columns with flooded packing	

usually depends on the number of plates for plate columns, the height of packing for packed columns, etc.

A correct and objective estimation of diffusion apparatus having a certain structure can be made only if hydrodynamic and diffusion characteristics of the apparatus are taken into account simultaneously.

Suppose that the volume of vapour (gas) passing per unit cross-sectional area of the apparatus per unit time is w ($m^3/m^2 \cdot s$), and the apparatus height at which the separation is equivalent to the separation at a theoretical contact stage (theoretical plate) is h (m). Then the ratio

$$I = \frac{w}{h}$$

expresses the volume of vapour (gas) consumed per unit time in 1 m^3 of the apparatus and determines the output from a unit apparatus volume. The velocity of vapour (gas) in the apparatus is chosen in accordance with a certain ratio of the gas and liquid flow rates, G and L, physical properties of vapour and liquid, their densities ρ_v and ρ_l, viscosities μ_v and μ_l, etc. Thus, the velocity of vapour or gas reflects the hydrodynamic conditions in the apparatus. The height h of the contact region characterizes the intensity of mass transfer: the smaller the height, the more effective the mass transfer. Thus, the above expression directly establishes the relation between hydrodynamics and mass transfer in a diffusion apparatus. It is taken as a criterion of comparative estimation of diffusion apparatus of different types. For packed columns, h corresponds to the equivalent packing height, while for plate-type columns $h = H_p/\eta$, where H_p is the separation between the plates, m, and η the efficiency of the column or plates.

For extraction apparatus, it is more convenient to represent the output coefficient in the form

$$I = \frac{w_0}{h} = \frac{1}{\tau_k},$$

where w_0 is the total velocity of flows of both phases, $m^3/m^2 \cdot s$; and τ_k is the time required for the mass transfer in the apparatus, s.

The value of τ_k can be calculated from the mean duration of stay of the disperse phase in the extractor, τ_m, according to the relation

$$\tau_k = \frac{\tau_m}{n},$$

where n is the number of theoretical contact stages.

The energy expenditures for a diffusion process in a given apparatus can be taken into account according to the pressure drop ΔP_{g-l} per theoretical contact stage:

$$E = \frac{\Delta P_{g-l}}{n}.$$

The energy parameter E has the maximum value for absorption and vacuum rectification. The effect of physical properties of gas (vapour) and liquid on the velocity w of the systems being compared can be estimated to a first approximation as

$$\frac{w}{w_c} = \sqrt{\frac{\rho_l \rho_{g,c}}{\rho_{l,c} \rho_g}},$$

where w and w_c are the velocities of gas (vapour) for the given system and the system being compared, m/s; ρ_l and $\rho_{l,c}$ are the densities of the given liquid and the liquid being compared, kg/m^3; ρ_g and $\rho_{g,c}$ are the densities of the gas (vapour) in the given system and the system being compared, kg/m^3.

While comparing plate-type columns separating different systems, the effect of physical properties of a system on its efficiency is described by the equation

$$\frac{\eta}{\eta_c} = \left(\frac{\mu_c \alpha_c}{\mu \alpha}\right)^{0.245},$$

where η is the efficiency of the given system; η_c is the efficiency of the system being compared; α and α_c are the relative volatilities of the components of the given and compared mixtures; and μ and μ_c are the molar viscosities (Pa·s) of the given and the compared systems, calculated from the equation

$$\mu = x_a \mu_a + x_b \mu_b,$$

where x_a and x_b are the concentrations of components in mixture, mole fractions; and μ_a and μ_b are the viscosities of the components.

While comparing apparatus, the factor $F_s = w\sqrt{\rho_g}$ is also used as a determining parameter. It is an analogue of the hydrodynamic state factor of a two-phase system.

Chapter Eight

Apparatus with a Fixed Phase-Contact Surface

8.1. Film-Type Columns with Wetted Walls

Film-type columns with wetted walls can be constructed either in the form of single tubes or as a system of tubes similar to the shell-and-tube type heat exchangers. At present, two trends can be distinguished in the applications of film columns: (1) a decrease in the thickness of the liquid film; (2) operation of film columns under emulsifying mode. A proper distribution of the liquid in the tubes is the main design requirement for thin-film wetted-wall columns.

Figure 91 shows the dependence of the pressure drop ΔP_{g-l} in a wetted-wall column (tube) on the liquid velocity under a constant velocity of the gas (air) in the countercurrent flow. The liquid velocity is expressed in terms of the Reynolds number of the moving liquid film:

$$\mathrm{Re}_l = \frac{4L'}{\mu_l},$$

where L' is the mass flow rate of the wetted perimeter per unit length; and μ_l is the viscosity of the liquid.

No waves are formed at point A and only skin friction exists at this point. The flow between points A and B is laminar and quite intense wave formation takes place in this case. A transition region exists between points B and C, the flow pattern changes from point C onwards and becomes turbulent. Point B corresponds to $\mathrm{Re}_l \simeq$ $\simeq$ 900-1000, and point C to $\mathrm{Re}_l \simeq$ 1300-1500. Turbulent flow sets in beyond point B which corresponds to the termination of the laminar flow. The large waves of the liquid formed during the laminar flow begin to break up, and the resulting small waves reduce the pressure drop until fully developed turbulence sets in at point C.

The dependence of the pressure drop on the mass flow rate of the gas G (kg/m^2·hr) for a constant liquid velocity is shown in Fig. 92. Point B corresponds to $\mathrm{Re}_{air} \simeq$ 1200-2000, and point C to $\mathrm{Re}_{air} \simeq$ $\simeq$ 1500-2300 (with respect to the liquid). The laminar flow of the gas (air) in this region facilitates the formation of large waves in the liquid, which increases the pressure drop with increasing gas velocity. Point C corresponds to the termination of the laminar region of air

flow. Segment *CD* corresponds to the transition region (here, the shape of the waves changes and hence the pressure drop decreases). A fully developed turbulence is observed in the flow beyond point *D*.

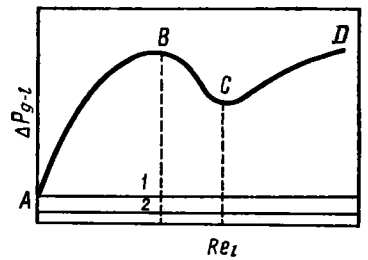

Fig. 91. $\Delta P_{g\text{-}l}$ vs. Re_l dependence for wetted-wall column at a constant gas (air) velocity:

1—wetted pipe in the presence of a surfactant; *2*—dry pipe.

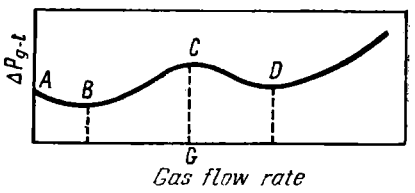

Fig. 92. Pressure drop as a function of the gas velocity at a constant velocity of liquid.

The anomalies observed in region *AB* for low air velocities are apparently explained by the edge effects due to the influence of the flowing liquid on the gas flow.

The mean velocity w_m and the maximum velocity w_{max} of the liquid film, as well as the film thickness σ for the laminar flow, are calculated with the help of the following equations:

$$w_m = \frac{w}{\rho_l \delta}, \tag{8.1}$$

$$\frac{w_{max}}{w_m} = \frac{3}{2}, \tag{8.2}$$

$$\delta = \left[\frac{3w\mu_l}{g\rho_l^2}\right]^{1/3}, \tag{8.3}$$

where w is the mass flow rate of the liquid per unit length of the wetted perimeter, kg/s·m; ρ_l is the density of the liquid, kg/m^3; δ is the film thickness, m; μ_l is the viscosity of the liquid, Pa·s; and g is the acceleration due to gravity, m/s^2.

When rectification is accomplished in tubes at low vapour velocities (up to 3-4 m/s in tubes of inner diameter 11 mm), the liquid flows down the tube surface as a thin film, forming a wavy surface. As the velocity at the bottom of the tube increases, individual liquid drops are picked up by the vapour, the flow of the liquid is somewhat slowed, and a vapour-liquid emulsion plug is formed at the bottom end of the tube. Subsequent insignificant increase in the vapour velocity leads to a gradual filling-up of the entire tube by an emulsion consisting of vapour bubbles of different sizes (from 0.5 to 10 mm in

diameter), moving in the liquid at a high speed. The whole emulsion mass performs large-amplitude oscillations along the tube, the amplitude ranging between 50 and 100 mm.

While testing a multitube column, it was established that the emulsifying regime appears and propagates in all the tubes simultaneously. The emulsion level in these tubes is controlled automatically in this case: as the emulsion level in a tube rises, the resistance offered to the vapour flow in it also increases. This reduces the vapour velocity in this tube, and a part of the liquid is dumped into the still. The velocity w_v at which a steady-state emulsifying regime sets in is given by the equation

$$\log\left(\frac{w_v^2}{gd_t}\,\frac{\rho_v}{\rho_l}\left(\frac{\mu_l}{\mu_w}\right)^{0.16}\right)=0.243-1.75\left(\frac{R}{R+1}\right)^{0.25}\left(\frac{\rho_v}{\rho_l}\right)^{0.125}, \quad (8.4)$$

where w_v is the vapour velocity in the empty-tube cross section, m/s; $g = 9.81$ m/s^2; d_t is the inner diameter of the tube, m; ρ_v and ρ_l are the densities of the vapour and the liquid, kg/m^3; μ_l is the viscosity of the liquid; R is the reflux ratio; and μ_w is the viscosity of water at 20°C.

The kinetic mass-transfer equations for wetted-wall tubes, as well as for all apparatus with a fixed phase-contact surface, are expressed in the form of dependences obtained from an analysis of diffusion in single-phase flows. This corresponds to Eqs. (6.47) and (6.48) in which the hydrodynamic state factor f for a two-phase system is close to zero.

The following equation is valid for calculating the mass-transfer coefficients during absorption with a fixed interface:

$$\mathrm{Nu_D}=\frac{k_x\delta}{D}=\text{const}\,\mathrm{Re}^n\,\mathrm{Pr_D^m}\left(\frac{d_t}{l}\right)^q. \quad (8.5)$$

For values of $\mathrm{Re_l}$ between 4 and 80, this equation assumes the form

$$\mathrm{Nu_D}=\frac{k_x\delta}{D}=0.0066\,\mathrm{Re_l}\,\mathrm{Pr_l^{0.5}}, \quad (8.6)$$

while for $\mathrm{Re_l} > 80$, we obtain

$$\mathrm{Nu_D}=\frac{k_x\delta}{D}=0.0286\,\mathrm{Re_l^{2/3}Pr_l^{0.5}}. \quad (8.7)$$

Four regimes are known to exist when rectification is carried out in hollow tubes: laminar, transient, turbulent, and emulsifying (Fig. 93). In the laminar and transient regimes, $\mathrm{Nu_D} = kd_t/D$ considerably depends on $\mathrm{Re_v} = wd_t/\mu_g$, as well as on the ratio l/d_t. No such dependence is observed in the turbulent region. Figure 94 shows the results of a comparison of rectification in single-tube columns under film-type and emulsifying regimes. It can be seen from this figure that the separation efficiency of these tubes sharply increases for $\mathrm{Re_v} > 4.3 \times 10^3$ ($d_t = 8$ mm) and for $\mathrm{Re_v} > 8 \times 10^3$

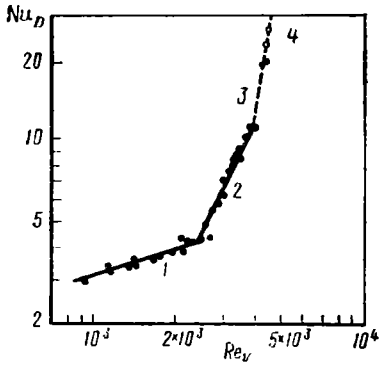

Fig. 93. Dependence of Nu_D on Re_v for the separation of ethyl alcohol-water mixture in a hollow pipe:

1—laminar flow; *2*—transient flow; *3*—turbulent flow; *4*—emulsifying flow.

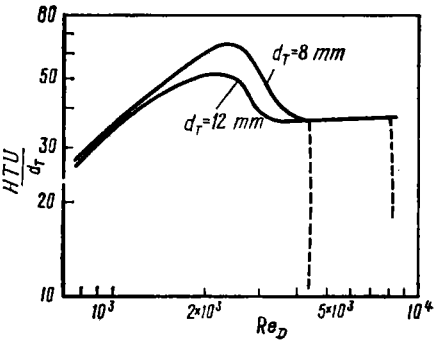

Fig. 94. The HTU/d_t vs. Re_v dependence for a single-pipe column during the separation of an ethyl alcohol-water mixture.

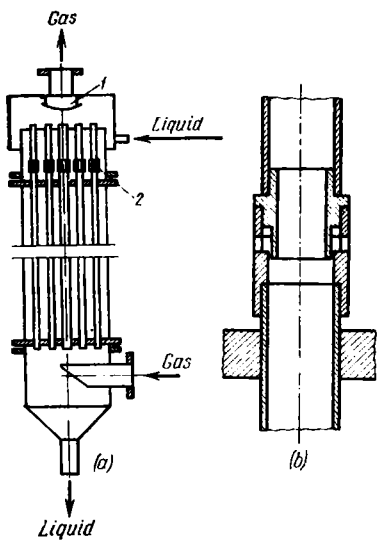

Fig. 95. Schematic diagram of a multitube film-type apparatus (*a*) and nozzles for the distribution of liquid (*b*)

1—baffle; *2*—irrigated packing.

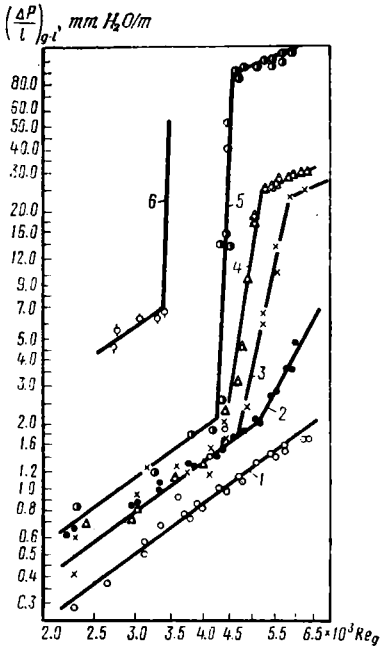

Fig. 96. Pressure drop in a multitube wetted-wall apparatus as a function of Re_g:

1—non-wetted apparatus $L = 0$; *2*—$L = 0.086$ m³/hr; *3*—$L = 0.259$ m³/hr; *4*—$L = 0.388$ m³/hr; *5*—$L = 0.518$ m³/hr; and *6*—$L = 0.700$ m³/hr.

(d_t = 12 mm), corresponding to emulsifying regime. The emulsifying regime has a considerable advantage in that no special devices are required for a uniform wetting of tubes in multitube columns operating in this regime. This eliminates the most serious technical obstacle encountered in the operation of a wetted-tube column.

Figure 95 shows the schematic diagram of a multitube apparatus and the packing for distribution of the liquid over the walls.

The dependence of the resistance of a multitube wetted apparatus (consisting of 19 tubes of diameter d_t = 19.4 mm) on the gas velocity and the reflux ratio is shown in Fig. 96.

8.2. Columns with Vertical Sheet Packing

The vertical sheet packing consists of rectangular blocks made of glass cloth or other materials and arranged vertically in the column. The liquid flows down the plane vertical walls of the block and covers them with a thin film, while the gas (vapour) is in the counterflow. The basic advantages of these apparatus are high gas velocities and relatively low friction losses. The pressure drop in a vertical sheet packing column is calculated by using the equation

$$\Delta P_g = \frac{2\xi_d l w^2}{g d_e F_v^2}, \tag{8.8}$$

where ξ_d is the drag coefficient of dry packing blocks; w is the gas velocity in the empty column, m/s; d_e is the equivalent packing diameter given by $d_e = 4F_v/a$, m; F_v is the fraction of voids in the packing, m^2/m^2; a is the specific packing area, m^2/m^3; and l is the height of the packing, m.

The drag coefficient of dry packing blocks can be calculated from the following formulas:
for vertical sheets,

for Re = 25-560 $\quad \xi_d = \frac{24}{Re}$,

for Re = 560-2500 $\quad \xi_d = \frac{2.62}{Re^{0.65}}$,

for Re > 2500 $\quad \xi_d = \frac{0.125}{Re^{0.26}}$,

for block packing,

for Re = 500-6000 $\quad \xi_d = \frac{1.65}{Re^{0.55}}$.

The maximum loads for wetted columns with vertical sheet packing can be calculated with the help of the graph shown in Fig. 97, where the usual two-phase flow criterion has been chosen as the characteristic group [see Eq. (4.47)]. Investigations of block packings of different

equivalent diameters (with clearances of 5, 10, 20, and 30 mm between plates) show that local mass-transfer coefficients can be determined from the following formulas:

for gases with a low solubility

$$\frac{k_x\delta}{D_l}=\mathrm{Nu_l}=0.011\,\mathrm{Re_l}\,\mathrm{Pr_l^{0.5}}, \qquad (8.9)$$

where δ is the thickness of the liquid film on the plates, D_l is the

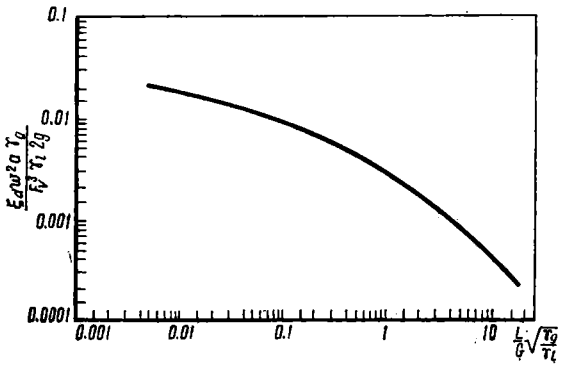

Fig. 97. To the calculation of limiting flow rates in columns with vertical sheet packing.

diffusion coefficient of the component being absorbed in liquid, k_x is the liquid-phase mass-transfer coefficient, and

$$\mathrm{Re_l}=\frac{w_l d_e}{\nu_l}; \quad \mathrm{Pr_l}=\frac{\nu_l}{D_l}.$$

For readily soluble gases,

$$\frac{k_y d_e}{D_g}=\mathrm{Nu_g}=0.013\left(\frac{b}{10}\right)^{0.45}\mathrm{Re_{rel}^{0.19}}\,\mathrm{Pr_g^{0.5}}, \qquad (8.10)$$

where b is the width of the channel, mm; k_y is the mass-transfer coefficient for the gas phase; $\mathrm{Re_{rel}}$ is calculated from the relative velocity of the gas; and $\mathrm{Pr_g}=\nu_g/D_g$.

Sheet packing blocks are more effective than individual wetted-wall tubes of the same equivalent diameter. This is explained by a large turbulization in the liquid and the boundary layers of the gas.

The height of a transport unit $(\mathrm{HTU})_{oy}$ for vertical sheet packing in rectification processes can be calculated with the help of formulas which are valid for an individual wetted-wall tube of the same equivalent diameter:

$$(\mathrm{HTU})_{oy}=0.069 d_e \mathrm{Re_g Pr_g} \qquad (8.11)$$

for laminar flow of vapour (up to $Re_g = 1000$), and

$$(HTU)_{0y} = 11.1 d_e^{0.64} Re_g^{0.23} Pr_g^{0.67} \quad (8.12)$$

for turbulent flow ($Re_g > 1000$), $(HTU)_{0y}$ and d_e being expressed in centimeters.

Wetted-wall film columns and columns with vertical sheet packing can be advantageously used in the following cases: (1) when a small pressure drop is required in the apparatus, a situation characteristic of operation under vacuum; and (2) when large amounts of liquid in the apparatus are not desirable because of explosion hazards or other reasons.

8.3. Spray Columns

Since the drops of the disperse phase usually retain their shape during mass transfer in a spray column, the phase-contact area (the surface of the drops) practically remains unchanged. A spray column is a typical device in which this condition is satisfied.

The spray column used for extraction (Fig. 98) is a hollow cylinder fitted with an atomizer. The design of the top and bottom parts of the spray column plays an important role in ensuring the most favourable hydrodynamic conditions for the flow of phases and their separation in the column. The column is flooded when the velocity of the drops attains a value equal to 75 percent of the free-fall velocity of particles in a stationary medium, calculated with the help of Stokes' law. The relative velocity of the drops is determined by the sum $w_s + w_c$, where w_s is the velocity of the drops relative to the column walls, m/s; and w_c is the velocity of the continuous phase, m/s. The disperse-phase holding capacity ($\varphi = w_d/w_s$) in a spray column varies from 0.1 to 0.35 m^3/m^3.

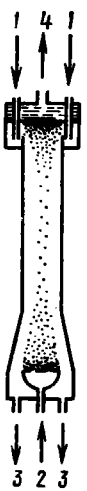

Fig. 98. Schematic diagram of a spray column:

1—heavy-liquid inlet; *2*—light-liquid inlet; *3*—heavy-liquid outlet; *4*—light-liquid outlet.

While designing the atomizer, it is necessary to take into account its wetting by the disperse phase. If the atomizer is wetted, it is constructed in the form of a disc with sharp nozzles which produce drops of the same size. If, on the other hand, the atomizer is not wetted, it is con-

structed in the form of a smooth perforated sphere or a plate. The efficiency of extraction in spray columns is usually calculated with the help of Kronig-Bring model (see p. 186).

The disadvantage of a spray column is that the drops in the column coalesce, thus reducing the phase-contact area and the recirculation of drops over the height of the column. The latter effect becomes prominent for large diameters of the column. Spray columns have low loading capacities, and the use of apparatus employing spray columns is recommended when a high degree of separation is not required, or when a chemical interaction between the reagents (chemisorption) takes place. Besides, spray columns have low friction losses.

Chapter Nine

Apparatus with Interfacial Area Formed in Flow

9.1. Plate Columns

9.1.1. Structural Features of Bubble-Cap Plate Columns and Their Hydraulics

The operation of a bubble-cap plate column is schematically shown in Fig. 99. Vapour (gas) rises in the column from bottom through vapour risers *3* and bubbles through the slots in caps *4* into the liquid. During rectification, the vapour condenses on the plate while the liquid evaporates from it at the same time, thus further turbulizing the flow.

A distinguishing feature of the bubble-cap plate columns is the existence of a crossflow between the liquid and the gas (vapour). The liquid moving along the plate from the feed pipe to the downcomer *6* is pierced by the gas rising from the lower plate to the upper plate. The required level of the liquid on the plates is maintained by fitting them with weirs *5*. In small-size columns, pipe *6* itself serves as the weir, and the height to which it projects over the plate determines the height of the liquid column over it.

Hydraulics of bubble-cap plate columns. The normal operation of a bubble-cap plate column is restricted by the conditions under which the plates themselves operate. The operating regimes of the plates are shown in Fig. 100. Normal operation of the plates is ensured when all caps are in the bubbling regime and nearly the same amount of vapour passes through each row of caps.

Regime *1* (low flow rate of the liquid): the caps are insufficiently immersed in the liquid, or the weir is not sufficiently high.

Regime *2* (low vapour flow rate): fluctuating passage of the vapour through the caps.

Regime *3* is characterized by a non-uniform distribution of vapour among different rows of caps; the operation of the plates is non-uniform.

Regime *4* (poor vapour distribution) is characterized by the flow of the liquid over the vapour risers and a distortion of the direction of flows.

Regime *5* (high liquid and vapour flow rates): the flooding of the column, characterized by an overfilling of the downcomers and reverse flow of the liquid on the plate. The flooding regime of a plate

column can be treated as the regime of maximum liquid and vapour flow rates.

Regime *6* (high vapour flow rate): an intensive entrainment of the liquid by the vapour to the upper plate.

Regime *7* is characterized by an inordinate vapour flow rate through the slots in the caps.

Regime *8* is observed when the duration of stay of the liquid on the plate is insufficient and an extremely large amount of the liquid flows over the weir.

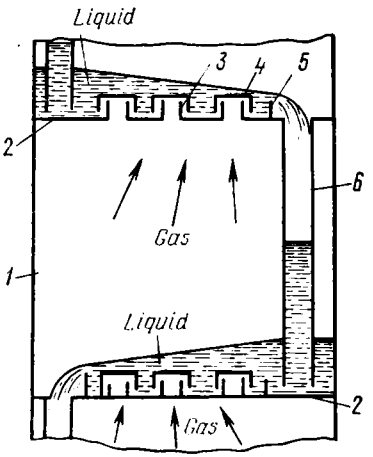

Fig. 99. Schematic diagram of a bubble-cap plate column:

1—column wall; *2*—plates; *3*—riser; *4*—cap; *5*—weir; *6*—downcomer.

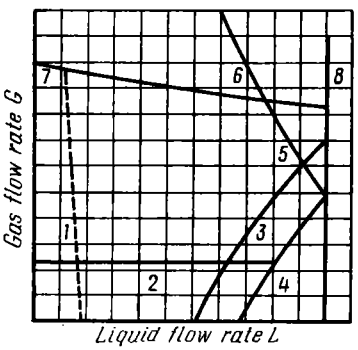

Fig. 100. Operating conditions of a bubble-cap column:

1—low liquid flow rate; *2*—vapour-phase fluctuation; *3*—non-uniform vapour distribution; *4*—seepage of liquid; *5*—flooding; *6*—intensive entrainment; *7*—overloading of slots; *8*—liquid throw-over across the weir.

The normal operation of a plate is determined by a correct distribution of the liquid and vapour flows. All the regimes considered above lie beyond the normal operating conditions of the plate.

Regulation of liquid flow on the plate. The following types of flow regulations can be attained with the help of weirs: crossflow, reverse flow, split (double pass) flow, and split (double pass) cascade flow. The first type of flow is the most characteristic one for bubble-cap plates.

On plates with a reverse flow, all downcomers are arranged on one side of the plates, the guide weir increases the liquid velocity on the plate and ensures that the caps near the downcomers are covered by the liquid. However, an increase in the path of the liquid on the plate increases the pressure gradient in the liquid. It is advisable to use plates with reverse flow only for low values of the ratio L/G [L is

the rate of flow of the liquid and G is the rate of flow of the vapour (gas) through the column].

On plates with a split flow, the liquid is divided into two parts, each part passing through half the plate. This type of flow ensures a high liquid-phase efficiency and an insignificant pressure gradient

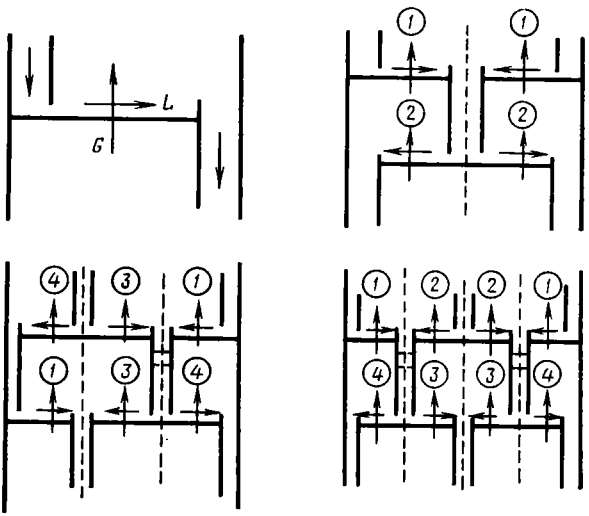

Fig. 101. Types of multiflow plates (numbers in circles denote the flow number).

in the liquid. Hence, it is expedient to use plates with split flow for large values of the ratio L/G or in large-diameter columns.

Plates with split cascade flow are fitted with intermediate weirs which ensure a uniform distribution of the pressure gradient in the liquid. Such plates should be used for significant values of L/G or in large-diameter columns.

Multiflow plates should be used when the flow rate of the liquid is high in comparison with the gas flow rate. The breaking up of a single liquid flow into several parts (Fig. 101) decreases the velocity of flow and the length of the path of the liquid on the plate. In turn, a decrease in the velocity and path of the liquid on the plate decreases the gradient of its level on the plate as well as the height of its layer over the weir. These effects are of great significance for plates with large diameters, where channel formation and a subsequent decrease in the efficiency of mass transfer may take place. While designing a multiflow plate, it is usually assumed that its efficiency is equal to the arithmetic mean of the efficiencies of individual flows which are calculated in the same way as for a plate with a single flow. This assumption is valid if a uniform distribution of flows in the liquid and vapour phases can be ensured. Actual design char-

acteristics of multiflow plates, however, do not always ensure such a uniform distribution. The real efficiency of a multiflow plate in operation is calculated with the help of a mathematical model taking into account the non-uniform distribution of phases over the flows in such a plate.

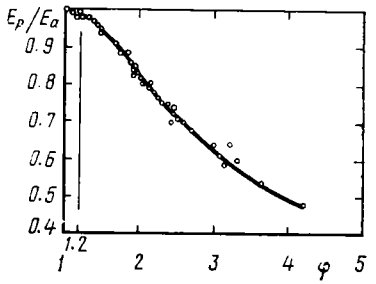

Fig. 102. Empirical correlations for efficiency of a multiflow plate.

It was found that the real efficiency of split-flow plates practically coincides with the arithmetic mean, since the possible non-uniformity in the distribution of flows is insignificant. Calculations for a four-fold flow on a plate were made for the following initial data: diameter of the sieve plate 10.7 m, fraction of the plate area occupied by each flow 0.25, area occupied by the overflows 6 percent of the flow area, total area of the perforations 10 percent of the active plate area, height of the overflow baffles 75 mm, their lengths being determined by the lengths of the corresponding chords of the plate contours. It was shown as a result of calculations that with decreasing ratio

$$\varphi = (L_p/V_p)_{\max} : (L_p/V_p)_{\min},$$

the real efficiency E_p^s of the plate increases, but remains less than the arithmetic mean E_a and attains this value as $\varphi \to 1$ (Fig. 102). It can be seen from Fig. 102 that for $\varphi \leqslant 1.2$, the efficiency of a four-fold flow plate can be considered as the arithmetic mean of the efficiencies of individual flows. Such a uniformity of distribution can be attained with the help of different design methods. In particular, the plate should be divided into parts of equal areas.

Empty-column vapour velocity. The diameter of a column is determined by the vapour velocity:

$$D = \sqrt{\frac{4v}{\pi w}}, \qquad (9.1)$$

where v is the volumetric velocity of the vapour (gas) passing through the column, m³/s; and w is the linear velocity of the vapour in the empty column, m/s. The permissible vapour velocity w (m/s) in the column is calculated from the equation

$$w = 0.305c \sqrt{\frac{\rho_l - \rho_v}{\rho_v}}, \qquad (9.2)$$

where ρ_l and ρ_v represent the density of the liquid and vapour respectively and c is a coefficient which depends on the spacing between the plates and the level of the liquid on the plate (Table 7).

Table 7

Values of Coefficient c in Eq. (9.2)

Plate spacing, mm	c for levels of clear liquid above upper edge of slots, mm			
	12.5	25	50	75
150	0.02-0.04	—	—	—
300	0.09-0.11	0.07-0.09	0.05-0.07	—
450	0.15	0.14	0.12	0.09
600	0.185	0.17	0.16	0.15
750	0.195	0.185	0.18	0.175
900	0.205	0.195	0.19	0.185

For operation under atmospheric pressure, the dependence of the vapour velocity in the column on the distance H_p (mm) between the plates and the bubbling depth h_b (mm) can be expressed in the form of the equation

$$w = \frac{0.305H_p}{60+0.05H_p} - 0.012h_b. \tag{9.3}$$

The maximum vapour velocity w (cm/s) can also be determined with the help of the equation

$$w = \frac{3.4}{d_{cap}^{2/3}} \sqrt{\frac{\rho_l}{\rho_v}}\,\Delta H, \tag{9.4}$$

where d_{cap} is the cap diameter, cm; and ΔH is the distance between the upper edge of the cap and the plate above it, cm.

The permissible vapour velocity w (m/s) in oil-refinery and gas-fractionating plant columns can be calculated by using the equation

$$w = 1.21 \times 10^{-3} \left(\frac{T}{MP}\right)^{0.5}, \tag{9.5}$$

where T is the vapour temperature, K, M is the molecular mass of the vapour and P is the column pressure, Pa.

As the vapour (gas) passes through the slots in the caps, the liquid covering the caps is displaced by the vapour and, depending on the vapour velocity, the slots become open to a certain height. The vapour flow rate v_m (m^3/s) required for complete opening of slots of height H_s can be calculated from the equation

$$v_m = 0.191 c_{sh} A_s \sqrt{H_s \frac{\rho_l - \rho_v}{\rho_v}}, \tag{9.6}$$

where A_s is the cross-sectional area of the slots, m^2; H_s is the total height of a slot, cm; and c_{sh} is a coefficient depending on the shape

of the slots, its value being equal to 0.63 for triangular slots, 0.74 for trapezoidal slots, and 0.79 for rectangular slots.

If the vapour flow rate is less than the value calculated from Eq. (9.6), a partial opening of the slots takes place and the height h_s to which they are opened is less than the height H_s. The ratio between the maximum vapour flow rate v_m for a full opening of the slots and the flow rate v for partially opened slots can be obtained from the following relations:

for rectangular slots

$$\frac{v}{v_m} = \left(\frac{h_s}{H_s}\right)^{3/2}, \tag{9.7}$$

for triangular slots

$$\frac{v}{v_m} = \left(\frac{h_s}{H_s}\right)^{5/2}, \tag{9.8}$$

for trapezoidal slots

$$\frac{v}{v_m} = 0.714\left(\frac{h_s}{H_s}\right)^{3/2} + 0.286\left(\frac{h_s}{H_s}\right)^{5/2}, \tag{9.9}$$

where H_s is the full height of a bubble-cap slot, cm; and h_s is the height of an open slot, cm.

The limiting relation between the shape coefficient c_{sh} and the height H_s of a slot is obtained on the basis of the permissible entrainment in the form $c_{sh} = \sqrt{H_s} = 1.44$. The value of H_s is usually less than 5 cm.

Pressure drop through a bubble-cap plate column. The resistance h_v to the passage of vapour through a plate or, in other words, the pressure drop through a plate is the sum of the pressure drop h_d through a dry plate and the pressure drop h_{em} through the vapour-liquid emulsion on the plate, i.e.

$$h_v = h_d + h_{em}. \tag{9.10}$$

The pressure drop for a dry plate is the sum of the pressure drop h_r through the risers (Fig. 103), the pressure drop $h_{c.c}$ in the space between risers and the caps, including the circular clearance, and the pressure drop h_s through the slots in the caps, which depends on the extent to which the slots are opened:

$$h_d = h_r + h_{c.c} + h_s. \tag{9.11}$$

The pressure drop through the risers (mm H_2O) can be obtained from the equation

$$h_r = k_u\left(\frac{v}{A_u}\right)^2 \frac{\gamma_v}{2g}, \tag{9.12}$$

where v is the volumetric velocity of the vapour, m^3/s; A_u is the total cross-sectional area of the risers on a plate, m^2; γ_v is the specific gravity of the vapour; and k_u is a coefficient which depends on the ratio of the total cross-sectional area A_u of the risers per plate to the

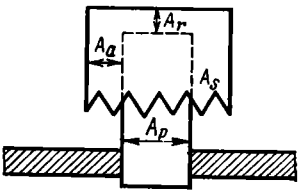

Fig. 103. To the calculation of the pressure drop across a dry bubble-cap plate.

cross-sectional area A_c of the column, i.e.

$$k_u = f\left(\frac{A_u}{A_c}\right). \quad (9.13)$$

The coefficient k_u is calculated from the equation

$$k_u = 1.5 - \frac{A_u}{A_c} - \left(\frac{A_u}{A_c}\right)^2. \quad (9.14)$$

The pressure drop in the space between a riser and a cap, including the circular clearance, is given by the equation

$$h_{c.c} = (k_{r_1} + k_{r_2} + k_{r_3})\left(\frac{v}{A_r}\right)^2 \frac{\gamma_v}{2g}, \quad (9.15)$$

where A_r is the total cross-sectional area between the cap and a riser per plate, m^2 (Fig. 103).

The coefficient k_{r_1} can be obtained from the equation

$$k_{r_1} = \frac{100}{\frac{A_{min}}{A_{max}}\left(1+\frac{A_a}{A_u}\right)+1.061} - 29.03, \quad (9.16)$$

where A_a is the total cross-sectional area of the annular clearance between the cap and the riser per plate, m^2; A_{min} is the minimum

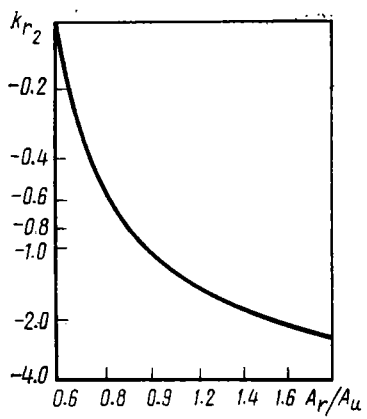

Fig. 104. k_{r_2} vs. A_r/A_u.

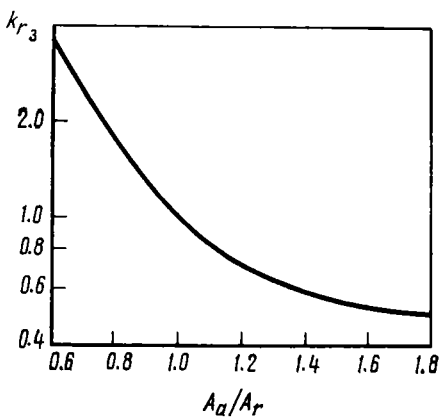

Fig. 105. k_{r_3} vs. A_a/A_r.

value of A_a; and A_{max} is its maximum value. The coefficients k_{r_2} and k_{r_3} can be determined graphically (Figs. 104 and 105).

The pressure drop (mm H_2O) during the passage of vapour through the slots of the cap, when the former are completely open, is

calculated from the equation

$$h_s = (k_{s_1} + k_{s_2}) \left(\frac{v}{A_s}\right)^2 \frac{\gamma_v}{2g}, \quad (9.17)$$

where A_s is the total area of the slots per plate, m^2.

The value of k_{s_1} depends on the ratio of areas A_s of the slots and A_c of the column, and is determined with the help of the equation

$$k_{s_1} = 2\left(\frac{A_s}{A_c}\right)^2 - 2\left(\frac{A_s}{A_c}\right) + 1. \quad (9.18)$$

The coefficient k_{s_2} depends on the ratio of the areas A_s of the slots and A_a of the annular clearances:

$$k_{s_2} = f(A_s/A_a).$$

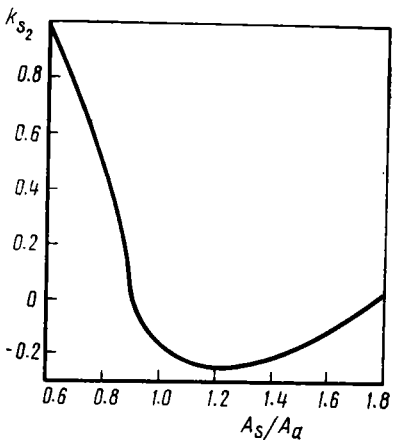

Fig. 106. k_{s_2} **vs.** A_s/A_a.

The coefficient k_{s_2} is determined graphically (Fig. 106). The area of slots for the passage of the vapour is calculated by the equation

$$A_s = 0.65\left(bnNv^2\frac{\rho_v}{\rho_l}\right)^{1/3}, \quad (9.19)$$

where b is the slot width at the bottom, m; n is the number of slots in a cap; N is the number of caps on a plate; v is the volumetric velocity of the vapour, m^3/s; and ρ_v and ρ_l are the densities of the vapour and the liquid, kg/m^3.

The pressure drop h_p through a wetted-wall plate depends on the hydraulic gradient Δ on the plate, the height h_0 of the static seal from the top edge of the slot to the top edge of the weir, the height h_1 of the layer above the weir, and the height h_2 from the upper edge of the slot to the liquid level on the plate (Fig. 107). In accordance with Bernoulli's equation, a hydraulic gradient Δ sets in in the layer of a liquid upon its passage through the plate. This gradient affects the pressure distribution as the vapour passes through the plate, especially for large column diameters. The maximum value of Δ is attained at the downcomer feeding the plate, while its value at the weir is equal to zero. Thus, Δ varies from its maximum value to zero over the length of the plate.

Assuming that the variation of the hydraulic gradient is almost linear, the pressure drop through the liquid layer covering the plate can be represented in the form of the sum

$$h_2 = h_0 + h_1 + 0.5\Delta, \quad (9.20)$$

where h_2 is a variable which depends on the operating conditions of the plate.

The following ranges for the variation of h_2 are recommended for different column pressures:

h_2, mm	12.5-38	25-50	50-100
Column pressure . .	50-200 mm Hg	1 atm	>1 atm

Since the plate is covered by a gas-liquid emulsion above the cap slots, the actual pressure drop through a wetted-wall plate will be

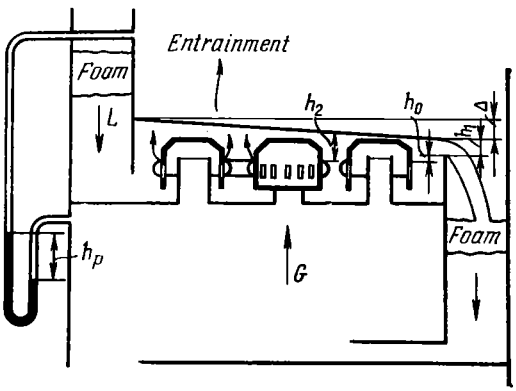

Fig. 107. Hydraulics of a refluxed plate.

lower than the value obtained from Eq. (9.20). Hence an additional factor, called the liquid aeration coefficient, φ, is introduced into Eq. (9.20). The pressure drop through the gas-liquid emulsion layer will then be given by

$$h_{em} = \varphi h_2 = \varphi\,(h_0 + h_1 + 0.5\Delta). \qquad (9.21)$$

For the water-air system, the aeration coefficient can be calculated from the equation

$$\varphi = 0.66 + \frac{16.2}{h_2} - \frac{0.85}{h_2^{0.8}}\,w^4\rho_v^2, \qquad (9.22)$$

where w is the velocity of the vapour in the empty column, m/s; and ρ_v is the density of the vapour, kg/m³.

Solving together Eqs. (9.21) and (9.22), we obtain the pressure drop in an aerated dynamic layer:

$$h_{em} = 16.2 + 0.66h_2 - 0.85h_2^{0.2}w^4\rho_v^2. \qquad (9.23)$$

The height h_0 of the static liquid seal must be of the order of 12.5 mm. The distance between the upper edge of the riser and the top edge of the slots must also be of the same order so as to prevent the liquid from penetrating into the riser.

The height of the liquid level h_1 (mm) over the weir is obtained from the equation

$$h_1 = 0.037 \left(\frac{L}{l_w}\right)^{2/3}, \quad (9.24)$$

where L is the flow rate of the liquid, kg/hr; and l_w is the length of the weir, m.

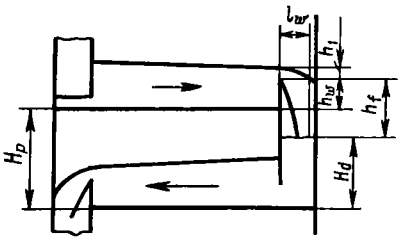

Fig. 108. To the calculation of the liquid overflow.

If the weir lies above a segment-shaped downcomer, the flow will contract and we must introduce into Eq. (9.24) a correction factor k_1 which depends on the ratio of the weir length l_w to the diameter D of the column. The values of k_1 lie between 1 and 1.24, increase with decreasing l_w/D, and the value $k_1 = 1.12$ is assumed for practical calculations. In this case, Eq. (9.24) becomes

$$h_1 = 0.037 k_1 \left(\frac{L}{l_w}\right)^{2/3}. \quad (9.25)$$

The height of the liquid layer above the weir must not be less than 6 mm if a uniform distribution of the liquid is to be ensured. The linear velocity (m/s) of the liquid above the weir is determined from the equation

$$w_{l.w} = 0.058\sqrt{h_1}, \quad (9.26)$$

where h_1 is the height of the liquid layer above the weir, mm.

The length of the jet over the weir is calculated from the formula

$$l_w' = 0.8\sqrt{h_1 h_f}, \quad (9.27)$$

where h_f is the free-fall height of a jet from the weir, mm (see Fig. 108):

$$h_f = H_p + h_w - H_d, \quad (9.28)$$

where H_p is the spacing between plates, mm; h_w is the height of the weir, mm; and H_d is the height of the clear liquid in the downcomer, mm.

Height of liquid in a downcomer. In order to prevent flooding, the level of the liquid in the downcomer should be below the upper level in the weir. The height of the clear liquid (in mm) in the downcomer is determined from the equation

$$H_d = h_w + h_1 + \Delta + h_t + h_d, \quad (9.29)$$

where Δ is the hydraulic gradient on a plate, mm; h_t is the total pressure drop through the plate, mm H_2O; and h_d is the pressure drop as a result of motion through the downcomer, mm H_2O.

The value of h_d (mm) is calculated with the help of the equation

$$h_d = 2.7 \times 10^{-13} \left(\frac{L}{A_d}\right)^2, \qquad (9.30)$$

where L is the flow rate of the liquid, kg/hr; and A_d is the area of the downcomer, m^2.

A layer of foam always lies on top of the liquid layer, and this must always be taken into consideration while making calculations for a downcomer. However, no computational methods are known for determining the height of the foam layer in the downcomer. Besides, the liquid in the downcomer is aerated, and this also increases the height of its layer as compared to the calculated value.

In practice, the maximum height of the clear liquid should be taken equal to half the spacing between plates, i.e.

$$H_d = 0.5H_p \qquad (9.31)$$

The hydraulic gradient Δ (m) for plates fitted with bubble caps of any design should be calculated with the help of the equation

$$\Delta = \lambda \frac{l_b}{r_h} \frac{w_{foam}^2}{2g}, \qquad (9.32)$$

where λ is a dimensionless coefficient; l_b is the length of the bubbling section, m; w_{foam} is the velocity of the foaming liquid, m/s; and r_h is the hydraulic radius, equal to the ratio of free cross-sectional area of the foaming liquid flow to the perimeter of the flow cross section in contact with the walls, m, i.e.

$$r_h = b_0 H_0/(b_0 + 2H_0). \qquad (9.33)$$

Here, b_0 is the averaged width of the foaming liquid flow, taken as the mean between the column diameter and the length of the front row of caps in the path of the liquid, m; and H_0 is the height of the flow (m), assumed to be equal to

$$H_0 = 2\,(h_w + h_1), \qquad (9.34)$$

where h_w and h_1 are expressed in meters.

In calculations for w_{foam} (m/s), the density of the foaming liquid is taken to be one-third the value for the liquid. Hence

$$w_{foam} = \frac{3v_l}{3600 H_0 b_0} = 0.000833 v_l / H_0 b_0,$$

where v_l is the volumetric velocity of the liquid on the plate, m^3/hr.

The dimensionless coefficient λ in Eq. (9.32) is calculated as follows:

$$\lambda = 14\,580 \left(\frac{h_s'}{h_w + h_1 + h_s'}\right)^{2/3} (\mathrm{Re}')^{-1.177}, \qquad (9.35)$$

where

$$\mathrm{Re}' = \frac{r_g w_{foam} \gamma_l}{\mu_l g} = 85 \times 10^{-6} v_l \gamma_l / \mu_l \, (b_0 + 2H_0) \qquad (9.36)$$

h_s' being the height of the upper edge of a cap slot above the plate, m.

The friction coefficient λ is inversely proportional to Re. Hence the hydraulic gradient Δ on a plate will be directly proportional to

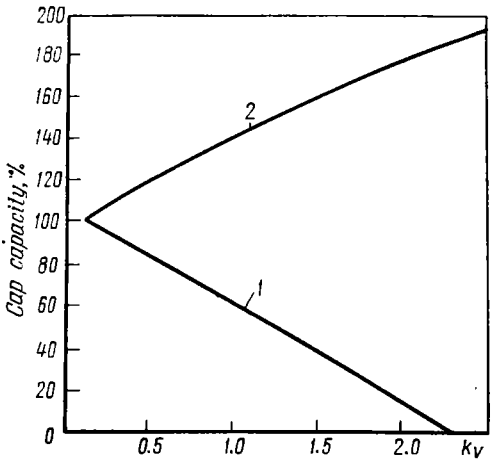

Fig. 109. Dependence of the flow rate through bubble caps on the vapour distribution coefficient:

1—the first row of caps at the liquid inlet to the plate; *2*—the last row of caps at the liquid outlet from the plate.

the viscosity of the liquid and its flow rate, as well as to the length of the bubbling section, and inversely proportional to the density of the liquid.

Vapour distribution coefficient. The distribution of the vapour over the rows of caps, and hence the normal operation of a plate, depends on the ratio of the height Δ of the liquid above a given row of caps to the pressure drop h_c across the caps. The ratio

$$\frac{\Delta}{h_c} = k_v \qquad (9.37)$$

is called *the coefficient of vapour distribution.* Figure 109 shows the dependence of the flow rate through the caps (expressed in percent of the slot capacity) on the vapour distribution coefficient. With increasing value of this coefficient, the operation of the first row of caps deteriorates. For $k_v = 2.3$, the capacity of the last row of caps attains the value 190 percent, while it is just 10 percent for the first row. A further increase in the value of k_v leads to the flow of

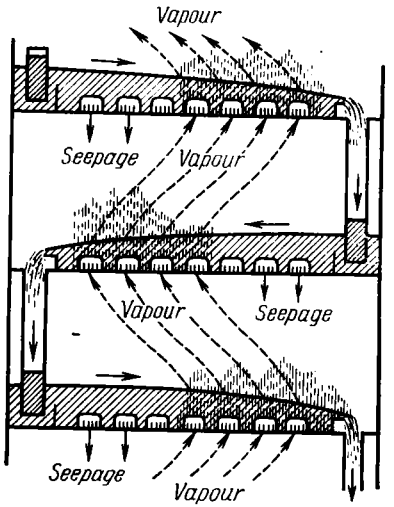

Fig. 110. Breakdown of column operation for large values of vapour distribution coefficient.

the liquid over the risers of the first row of caps. For large values of k_v, a crossflow of the vapour over the plate in countercurrent to the downflowing liquid is observed (Fig. 110). For small spacing between plates, the vapour counterflow may lead to a considerable friction between the vapour and the liquid, and increase the hydraulic gradient, thus further worsening the vapour distribution over the caps.

For normal operation of a plate, the coefficient of vapour distribution must not exceed 0.5. If a value of $k_v > 0.5$ is obtained as a result of calculations, we must assume some other distribution of the liquid over the plate.

Flooding of bubble-cap plates. The flooding of bubble-cap plates is characterized by an overfilling of the downcomers. For low flow rates, there is always some free space in the upper part of a downcomer (see Fig. 107). As the flow rate increases, the height of the aerated liquid in the downcomer also increases. When the liquid level in the downcomer reaches the top edge of the weir, maximum flow rate through the downcomer is ensured. A further increase in the flow rate through the column leads to a reverse flow of the liquid from plate to plate, and ultimately to a complete filling of the column by the liquid, i.e. flooding of the column. In this case, the pressure drop across the column sharply increases.

The vapour velocity corresponding to the state of flooding can be calculated from the equation

$$w_0\left(\frac{\rho_v}{\rho_l-\rho_v}\right)^{1/2}=f\left(\frac{L}{G}\right)\left(\frac{\rho_v}{\rho_l}\right)^{1/2}, \qquad (9.38)$$

where w_0 is the flooding velocity referred to an empty-column cross section, less the cross-sectional area of the downcomer, m/s.

Equation (9.38) can be solved with the help of the plot shown in Fig. 111. This plot has been obtained under the following assumptions: (1) there is no foaming of the liquid, (2) the height of the weir is less than 15 percent of the spacing between plates, and (3) the bubbling area is the predominant area between the weirs.

Entrainment of the liquid. The amount of entrained liquid can be calculated from the parameter characterizing the flooding of a

column, i.e. as a function of the dimensionless term

$$\left(\frac{L}{G}\right)\left(\frac{\rho_v}{\rho_l}\right)^{1/2}.$$

The dependence of the liquid entrainment on the operating conditions of a column is shown in Fig. 112.

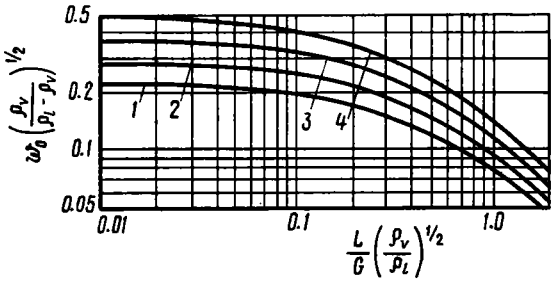

Fig. 111. To the calculation flooding velocity in a bubble-cap column for plate spacing:
1—H_p = 300 mm; *2*—H_p = 450 mm; *3*—H_p = 600 mm; *4*—H_p = 900 mm.

Effect of various factors on the interfacial area and the time of contact on bubble-cap plates. Special investigations have been carried out for bubbling out a gas through the cap slots and the formation of bubbles on the phase-contact surface, and measurements of the time of contact and local efficiency have been made. Experiments were carried out with a single cap and the following parameters were varied: the gas and liquid velocities, the weir height, the slot size, the static seal height, viscosity and surface tension of the liquid.

At the moment of their formation, bubbles emerging through the slots of the caps are paraboloids, the shape becoming ellipsoidal as a bubble is detached from the slot. Depending on the magnitude of the static seal h_0 two types of bubble motion are observed. For low values of h_0, the bubble growth period is very small and the bubbles arriving at

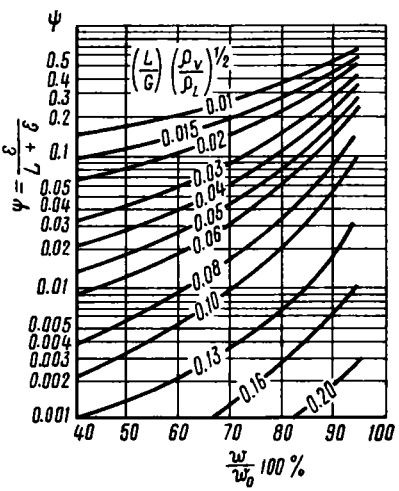

Fig. 112. To the calculation of liquid entrainment in bubble-cap plates:
w—vapour velocity; w_0—vapour velocity in the case of flooding; e—amount of entrained liquid, kg-mole/hr; L—liquid flow rate in the column, kg-mole/hr.

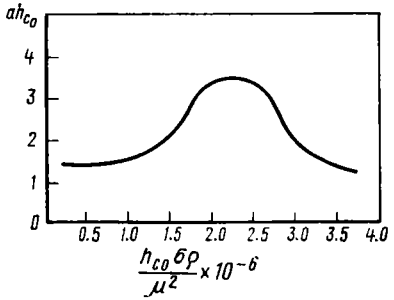

Fig. 113. To the calculation of the phase-contact area for the gas leaving the bubble cap.

the surface are comparatively small. No perceptible injecting action of the vapour is observed and the vapour dispersion takes place in the form of bubbles. The bubbles emerging from the slots increase in size as they reach the liquid surface. An increase in h_0 increases the bubble size.

For small values of h_0, the contact area between the vapour and the liquid is determined by the slot size and does not depend on the physical properties of the liquid and the gas. For large values of h_0, a link is formed between the bubble and the slot. In this case, the bubble continues to increase in size until the link becomes unstable and is ruptured. Large bubbles are formed, and the surface area per unit volume of the gas accordingly decreases. Upon a further increase in the height of the liquid seal (beyond 65 mm), the bubble size becomes independent of the height of the liquid seal.

The contact time increases with increasing height of the liquid seal. For large heights, the total contact time is the sum of two time periods: (a) the bubble formation period, when the velocity is quite low since energy has to be spent on the formation of a new surface, and (b) the free rise period. The latter is the decisive factor for large values of h_0. An increase in the vapour velocity in the slot and in the distances between the bottom of the plate and the lower edge of the cap (skirt clearance) decreases the contact time. For large values of h_0 (more than 65 mm) the phase contact area depends on the physical properties of the liquid, viz. viscosity, surface tension, and density, as well as on the distance s between the bottom of the cap and the lower edge of the cap. With decreasing surface tension and viscosity, the contact area attains its maximum value at $s = 6$ mm. For a liquid seal less than 65 mm, the phase-contact area is calculated from the equation

$$\frac{1}{0.305a - 12A_s^{0.3}} = A_s(418h_0 - 3580) + 0.00786h_0 + 0.40, \qquad (9.39)$$

where a is the phase-contact area per unit volume of the vapour, m^2/m^3; h_0 is the height of the static liquid seal, mm; and A_s is the total area of the slots, m^2.

The phase contact area is calculated with the help of the plot (Fig. 113) connecting two dimensionless terms:

$$ah_{c0} = f\left(\frac{h_{c0}\sigma\rho_l}{\mu_l^2}\right), \qquad (9.40)$$

where $h_{c0} = H_s + s$, (H_s is the height of the slot, m; s is the distance between the bottom of the plate and the lower edge of the cap, m); σ is the surface tension; ρ_l is the density of the liquid, and μ_l is its viscosity.

The total contact time τ_c (s) is determined from the equation

$$\tau_c = c_0 (h_0/h_{c0})^{0.27}, \qquad (9.41)$$

where c_0 is a coefficient depending on the slot height H_s and the distance s between the bottom of the plate and the lower edge of the

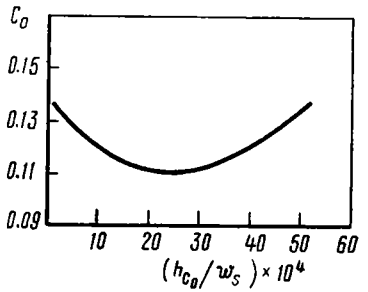

Fig. 114. To the calculation of the coefficient c_0.

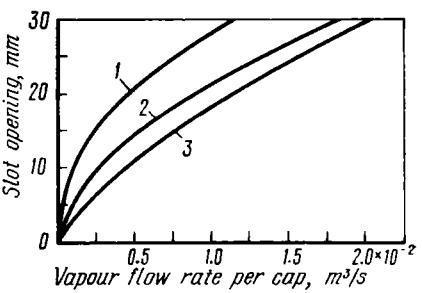

Fig. 115. Dependence of bubble-cap slot opening on the vapour flow rate:
1—triangular slots; *2*—trapezoidal slots; *3*—rectangular slots.

cap, as well as the velocity w_s of the gas flowing through the slot. The dependence of the coefficient c_0 (s) on h_{c0} (m) and w_s (m/s) is shown in Fig. 114.

Design features of bubble-cap plates. *Basic types and dimensions of caps.* A circular forged steel cap with rectangular or trapezoidal slots, and a tunnel cap are the ones encountered most frequently in practice. The diameter of the cap usually varies from 75 to 150 mm.

Depending on the column diameter, the following approximate cap sizes can be recommended, subject to the condition that the cap spacing is 25-75 mm, the skirt clearance is 12.5-38 mm, the minimum distance between the cap and the column wall is 38 mm, and the distance between the cap and the weir is 75 mm:

Column diameter, mm . . .	750-1200	1200-3000	3000-6000
Bubble cap diameter, mm . .	75	100	150

Shape and dimensions of slots. Rectangular, trapezoidal or triangular slots are the ones encountered most frequently. Figure 115 shows the dependence of the slot opening on the vapour flow rate through the cap. Triangular slots ensure a greater opening and,

consequently, a more stable operation under low flow rates. Rectangular slots open to a greater extent in the case of high flow rates. Trapezoidal slots are similar to rectangular ones. Since the triangular slots do not ensure high flow rates, their applicability is limited. The recommended slot width varies from 3 to 12.5 mm. A smaller slot width increases the phase-contact area. The optimal slot width is about 5.5 mm. The recommended slot height varies between 12.5 and 50 mm. Smaller values reduce the efficiency of the column, while larger values are restricted by the hydrodynamic factors concerning the operation of the plate. The optimal slot heights are:

Bubble cap diameter, mm . .	75	100	150
Height of slots, mm	25	32	38

Risers. The dimensions of the risers should be chosen after the cap sizes have been selected. Small diameters of the risers increase the pressure drop, decreasing it in the annular space between the riser and the bubble cap. Large diameters yield opposite results. Hence, the size of a riser is said to be optimal if the ratio of the cross-sectional area A_a of the annular space to the cross-sectional area A_u of the riser lies in the interval

$$A_a/A_u = 1.1\text{-}1.4. \tag{9.42}$$

The area of the risers is usually 8-16 percent of the cross-sectional area of the column for distillation columns, and 6-12 percent for the absorption columns. The are F_N (m^2) occupied by the bubble caps on a plate can be calculated from the equation

$$F_N = 125\left(\frac{a^2}{a^2-1}\right)\left(\frac{V_{max}}{c_{sh}}\right)\sqrt{\frac{1}{H_s}\frac{\rho_g}{\rho_l}}, \tag{9.43}$$

where

$$a = \sqrt{\frac{8}{d_c}H_s(x) + 1}$$

V_{max} is the maximum vapour flow rate through the column, m^3/s; H_s is the total height of the slot, cm; d_c is the outer diameter of a bubble cap, cm;

$$x = \frac{\Sigma b}{d_c}$$

Σb is the total width of the slots in a single cap, cm; and c_{sh} is the shape factor for the slots. The distance between slots is d_c $(a - 1)$.

The values of parameter a for a slot width $x = 0.5$ are given in Table 8.

The number of bubble caps is determined from the equation

$$N = \frac{132\,000 \cdot V_{max}}{c_{sh} d_c^2 (a^2 - 1)} \sqrt{\frac{1}{H_s} \cdot \frac{\rho_g}{\rho_l}}.$$

In order to prevent the liquid from falling into a riser, the distance between the top edge of the riser and the top edge of the slots should be of the order of 12.5 mm.

Weirs and overflow devices. The height of a weir in the form of a vertical plate varies between 25 and 50 mm.

Table 8

Values of Parameter a

H_s, cm	Parameter a at d_c (cm)		
	7.5	10.0	15
2.50	1.52	1.42	1.30
3.00	1.675	1.50	1.35
3.75	—	1.58	1.42

For low flow rates of the liquid, seals in the form of a recess (about 10 mm deep) must be provided at the spot where a downcomer to the next plate is introduced.

The most commonly used overflow devices are of segmental type (Fig. 116*a*). They are simple in construction and reliable in operation over a wide range of flow rates. Arc-shaped devices (Fig. 116*b*) are frequently used in columns of large diameters. The use of such devices helps increase the overflow perimeter as well as the operational area of the plate. The main overflow devices installed on multi-flow plates are usually of a rectangular profile (Fig. 116*c*). In order to increase the operational area of a single-flow plate, rectangular overflow devices are usually installed outside the column. Overflow

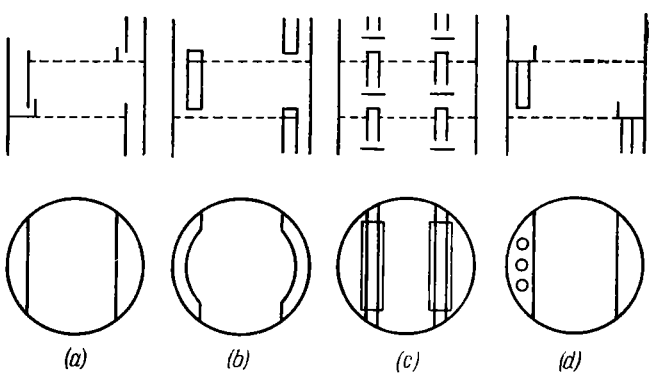

Fig. 116. Overflow devices with different types of channels.

devices having circular cross section (made of tubes) (Fig. 116*d*) are installed on plates operating at low flow rates of the liquid, since they have a narrow cross section and a small degassing space. Complex-shaped devices are characterized by an increased capacity. They ensure a collision-free and uniform introduction and removal of the liquid.

The maximum efficiency of a plate is attained when the gas-liquid (vapour-liquid) emulsion formed on the plate contains the smallest

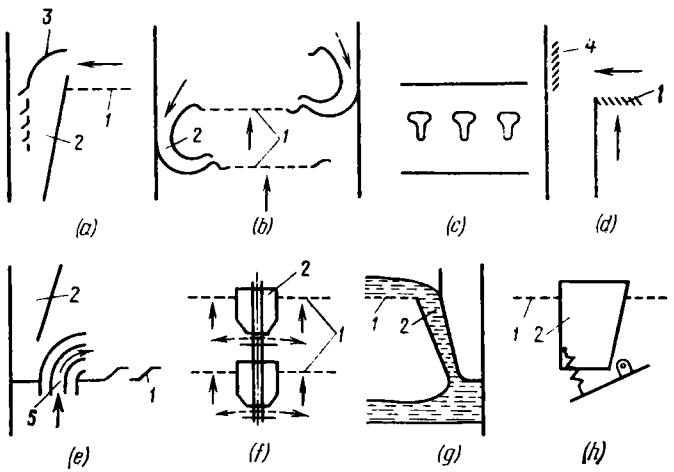

Fig. 117. Schematic diagrams of overflow devices:

1—base of a plate; *2*—overflow channel; *3*—perforated plate; *4*—baffle plate; *5*—liquid aerator.

amount of the clear liquid. In order to increase the plate efficiency and to improve the separation of a mixture, the process should be organized in such a way that the gas-liquid emulsion is retained on a plate and the clear liquid (free of the gas-liquid emulsion) flows down to the next plate. Besides, the existence of gas-liquid emulsion in the downspouts decreases the flooding limits of the column and increases the spacing between plates. The overflow devices must ensure a stable level of the gas-liquid emulsion on the plate and hence the stability of the hydrodynamic operation of the plates.

The methods used for separating a two-phase flow in an overflow device are based on the action of gravitational, inertial, centrifugal forces, forces of surface tension, or a joint action of these forces in different combinations. Figure 117*a* shows an overflow device in which the separation of a two-phase flow takes place under the action of gravitational and centrifugal forces. The application of any method of separation depends on the hydrodynamic operating conditions of

the plates, the tendency of the liquid toward foam formation, flow-rate parameters, and engineering and economical considerations.

Depending on the method of introduction of the liquid into the downcomer, overflow devices can be classified as setups with collision-free input or with a uniformly distributed input of the liquid. During a collision-free introduction of the liquid (Fig. 117), secondary foam formation of the liquid in the overflow device is prevented. Such devices are especially advantageous for a high flow rate of the liquid. A uniformly distributed input of the liquid is ensured in most cases by arranging the overflow plank strictly horizontally. Sometimes, planks with holes and cuts of different types are used (Fig. 117*c*), or complex-shaped planks are employed, which increases the range of stable and efficient operation of the overflow device and plates. For plates operating in the phase-inversion regime and usually not having any overflow planks, a uniformly distributed input of the liquid is ensured by installing special reflectors or baffles above the overflow device (Fig. 117*d*).

The design of a plate and the method of introduction of liquid into it have a considerable effect on the operation of an overflow device. Such devices may or may not contain an inlet pocket. The latter type of devices permit an increased operational area of the plate, and hence an increased gas flow rate. A uniform and collision-free introduction of the liquid ensures (Fig. 117*b*) a uniform flow distribution over the column cross section, which increases the productivity and efficiency of plates. Sometimes, the liquid arriving at the plate from the overflow device is aerated (Fig. 117*e*) to prevent its depression. This helps increase the stable operation range of the plate. In some cases, the introduction of liquid into the plate is accompanied by the formation of a second phase-contact region in the form of an umbrella (Fig. 117*f*), or as individual jets. Such an introduction of the liquid intensifies the mass transfer and allows an effective use of the separation space.

For stable operation of an overflow device and a plate, it is necessary to introduce a reliable hydraulic seal in the device to prevent the gas from escaping. Devices with a static or initial hydraulic seal are the ones most frequently encountered. Devices without inlet planks and with a dynamic hydraulic seal (Fig. 117*g*), facilitating an extension of the operating range of the device and a reduction in its resistance, have been recommended for plates with high liquid flow rates.

In recent years, several types of overflow devices with valve-type hydraulic seals have been constructed. One such device is shown in Fig. 117*h*. Its outlet cross section is automatically regulated, depending on the liquid flow rate. Such devices have a much wider range of stable operation.

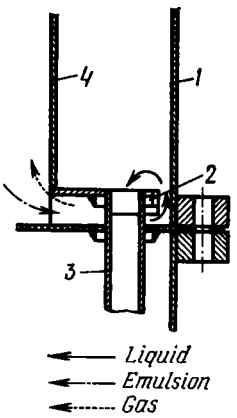

Fig. 118. Schematic diagram of a plate with a stable liquid level:
1—column wall; *2*—baffle; *3*—downcomer; *4*—standing weir.

Figure 118 shows the design of a plate on which a gas-liquid emulsion is maintained at a constant height over a wide range of gas and liquid flow rates, and only clear liquid without any emulsion flows through the downcomer. Such a process on the plate ensures maximum efficiency and a stable operation of plates over a wide range of variation of the gas and liquid flow rates. The constant level of the emulsion on the plate is ensured by standing weir *4*. The emulsion moves in the direction of baffle plate *2* and then to the downcomer *3*, passing under the segmental platform where the gas-liquid emulsion is separated. The vapour released from the emulsion is forced with the help of baffle plate *2* into the bubbling zone, while the liquid flows over the weir. Since only clear liquid flows through the downcomer, the latter has a small cross section and hence the plate area is used more effectively for bubbling.

9.1.2. Sieve-Plate Columns

In sieve-plate columns, the vapour (gas) passes through perforations in the plates, while the liquid is retained on them. The schematic diagram of a sieve-plate column is shown in Fig. 119. In order to reduce the hydraulic gradient along the plate and to decrease the effect of back mixing, the sieve plates are arranged in the form of a cascade, the liquid flowing down from plate to plate. The vapour or gas rises along a specially formed profile (Benturi profile) in the channel (Fig. 120).

Hydraulics of sieve-plate columns. The *pressure drop through dry sieve plates* is the sum of the pressure drop due to the contraction of the jet at the perforation inlet, the pressure drop due to friction at the perforations, and the losses in pressure due to expansion of the jet as it emerges through the perforation. The pressure drop through dry sieve plates can be calculated from the equation

$$h_d = k\left[0.4\left(0.125-\frac{f_0}{f_c}\right)+\lambda\left(\frac{\delta_p}{d_0}\right)+\left(1-\frac{f_0}{f_c}\right)^2\right]\frac{w_0^2}{2g}, \quad (9.44)$$

where h_d is the pressure drop through a dry plate, metres of gas column; f_0 is the total area of perforations, m^2; f_c is the cross-sectional area of a column, m^2; λ is the coefficient of skin friction in smooth

pipes; δ_p is the thickness of a plate, m; d_0 is the diameter of perforations, m; and w_0 is the mean velocity through the perforations, m/s.

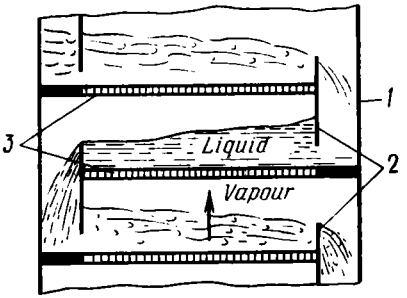

Fig. 119. Schematic diagram of a sieve-plate column:

1—column wall; *2*—downspouts; *3*—sieve plates.

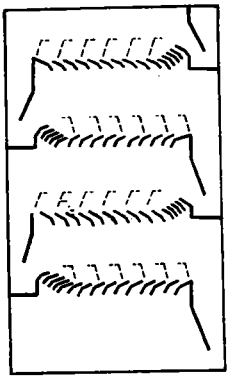

Fig. 120. Schematic diagram of a sieve-plate column with cascade-type plates.

The coefficient k, which is a function of the ratio δ_p/d_0, is determined from the plot shown in Fig. 121.

To a first approximation, the pressure drop through a dry plate without taking into account the thickness of the sieve is determined from the equation

$$\Delta P_d = \xi \frac{w_0^2}{2g} \gamma_g, \qquad (9.45)$$

where ξ is the drag coefficient which is practically independent of the dimensions and shape of the holes (cross section) as well as the

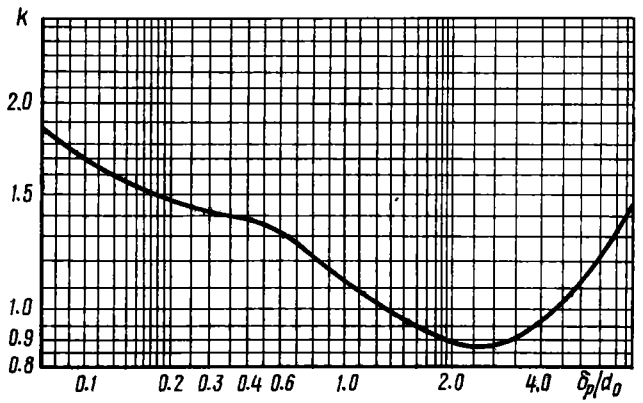

Fig. 121. k vs. δ_p/d_0 [Eq. (9.44)].

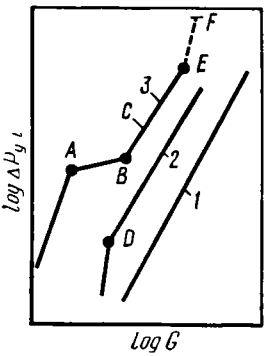

Fig. 122. Pressure drop across sieve plates vs. the mass flow rate of a gas:

1—dry plate; *2*—refluxed plate for low liquid flow rates; *3*—refluxed plate for moderate and high liquid flow rates.

way in which they are distributed on the plate; w_0 is the gas velocity in the hole, m/s; and γ_g is the specific gravity of the gas.

For conventional sieve plates with a fraction $f_0/f_c = a$ of the open area cross section of the holes, the drag coefficient ξ=1.95-2 for a = 3-5 percent for nozzle-spray plates, and ξ = 1.4-1.5 for a = 15-20 percent for perforated and grid plates.

Hydraulics of refluxed sieve plates. The hydrodynamics of sieve plates is determined not only by their geometry (the number and size of holes, the ratio of the plate thickness δ_p to the hole diameter d_0), but also by the gas and liquid flow rates of the plates and by their properties. The wettability of the plates is an important factor in the extraction processes.

Typical operating conditions for a sieve-plate column for a gas-liquid system are shown in Fig. 122. The pressure drop through a dry plate (straight line *1*) is approximately proportional to the square of the gas velocity $\Delta P_d \propto w_g^2$, which is in agreement with the self-modelling operation of single-phase flows. Curve *3* depicts the most typical refluxed sieve-plate. Below point *A* the liquid is in free flow over the plate and passes through the perforations, thus creating the so-called "shower" regime. Above point *A*, vapour bubbles through some holes in the plate, and this non-stationary operation of a sieve-plate column can be termed as the "seepage" regime, and point *B* can be called the "seepage" point. At this point, vapour bubbles through all the holes in the sieve plate and normal operation of the column is observed above this point. At the same time, a wave motion sets in at point *B*, and sometimes even at point *C* (for thin plates). In this case, the entire liquid and foam move back and forth in a direction perpendicular to the flow of the liquid. During the wave motion, a periodic dumping of the liquid takes place through the plate holes in the vicinity of the column walls on the same side on which the crest of the wave is located. The holes on this side of the plate instantaneously arrest the flow of vapour as the wave reaches its peak. Later, when the wave is on the wane, the liquid flows through the holes.

The reason behind the wave formation on the plate should be traced to the interaction between the foam, or the gas-liquid emulsion, and the liquid on the plate, as well as to the geometric conditions of

the fluid flow. The resulting complex hydrodynamic vapour-liquid system experiences a resistance from plates and column walls as it moves over a plate. The velocity, height and density of the gas-liquid emulsion vary upon passing through a circular plate. The presence of clear liquid on the plate, on the other hand, leads to wave formation in the same way as during the flow of a liquid in open conduits, where the vapour pressure is constant at the liquid surface along the conduit and the wave energy is transformed into vortices.

The intensity of wave formation depends on the two-phase flow parameter Φ:

$$\Phi = \left(\frac{L}{G}\right)^2 \left(\frac{\rho_l}{\rho_g}\right)$$

and can be expressed in the form of the dependence

$$I = k \frac{c}{2\pi} \left(\frac{L}{G}\right)^2 \left(\frac{\rho_l}{\rho_g}\right) \sqrt{\frac{f_0}{lV}}, \qquad (9.46)$$

where I is the pulsation frequency (cycles/s); c is the velocity of sound in gas (m/s); f_0 is the area of holes (m^2); l is the length of the system (m); V is the volume of the system (column and tubes) (m^3); and k is a proportionality factor equal to 2.5 ± 0.2.

Line EF (Fig. 122) characterizes the flooding of a sieve plate. This can occur due to several reasons: (1) reverse flow of the liquid from the downspout, (2) throwing over of the foam to the upper plate, (3) splashing of the liquid onto the upper plate as a result of the wave formation, (4) complete lifting of the liquid from the plate by gas (vapour), i.e. air lift, (5) transfer of the liquid to the plate as a result of entrainment, etc.

The first two types of flooding are typical of plate columns and are characterized by an almost vertical course of curve *3* when the flooding velocity is reached.

Depending on the plate spacing and the physical properties of a system, and especially on the nature of the foam being formed, flooding of the first two types can also occur between points A and E. The third type of flooding usually affects only a part of the plate. As soon as the point of wave formation is reached, any further increase in the gas velocity for a fixed velocity of the liquid increases turbulence and the wave amplitude. The entire liquid is suspended between plates in the fourth flooding regime. This type of flooding is unstable and easily passes into the fifth type. A further increase in the gas velocity inevitably leads to the fifth type of flooding, viz. an intensive entrainment. Several types of flooding are observed simultaneously in actual practice.

Curve *2* in Fig. 122 appears only at low velocities of the liquid (less than 1700 $kg/m^2 \cdot hr$) and only for some plates in a column. Below point D (seepage point), seepage of the liquid is observed and

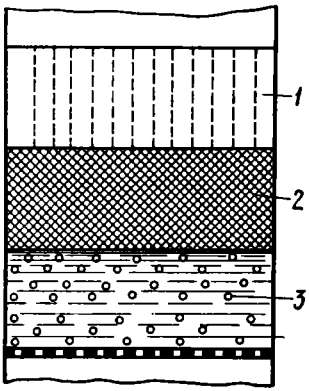

Fig. 123. Emergence of various zones on a sieve plate in a two-phase system

1—dispersion zone; *2*—foaming zone; *3*—bubbling zone.

there is no bubbling. At point *B*, the gas (vapour) begins to confine the liquid on the plate and bubbling occurs through some holes in the perforated plate. Other parts of the plate operate alternately under seepage and bubbling regimes. The seepage ceases only at high velocities of the gas flow.

Structure of a two-phase gas-liquid system on a sieve plate. The basic parameter determining the structure of a gas-liquid layer on a plate is the empty-column velocity w of the gas. The emergence of various zones in a two-phase gas-liquid system is shown in Fig. 123. At low values of w not exceeding the free rise velocity of bubbles of this gas in the given liquid, a typical dispersion (bubble) layer is formed. In other words, the gas bubbles under the action of buoyancy force freely rise to the surface of the liquid with a velocity of 0.1-0.4 m/s. Only in a thin layer of the liquid adjoining the perforated plate does the gas velocity approach the bubble velocity which ranges from several metres per second (after leaving a hole) to a few tenths of a metre per second in the bubbling layer. However, even for a typical bubbling regime, the bubbling zone containing the bulk of the liquid is usually topped by a foam zone, and then by a spray zone, the last two zones containing only an insignificant part of the liquid.

At low gas velocities, the formation of the foam zone is due to the fact that the kinetic energy of a rising bubble may not be sufficient to overcome the mechanical strength of the surface film, especially the adsorption layer of surfactants. Hence, a zone of slowly moving cellular cross-linked foam is formed over a typical bubbling layer.

The gas-liquid layer containing the liquid as the continuous phase is always topped by a spray zone of any concentration. The escape of bubbles through the liquid layer (foam) and the rupture of the film surface is always accompanied by a spray formation which is lifted by the gas flow to different heights above the liquid layer, depending on their dispersion and the velocity of the gas. As the gas velocity increases, the foam zone expands at the expense of the bubble zone. When the empty-column velocity reaches the value $w =$ $= 0.5$-0.7 m/s, the disperse system usually becomes foamy and only a typical bubbling layer of a few millimeters thickness remains at

the perforated plate. Besides, a spray zone containing an insignificant amount of liquid is also left behind.

Free rising of bubbles without an accumulation of gas in the liquid is possible only when the gas velocity in the empty column is less than $w_b\varphi_b$, where w_b is the velocity with which a bubble rises to the surface, and φ_b is the fraction of the cross-sectional area of the column occupied by bubbles. If the forced flow of the gas, introduced through the perforated plate, is higher than $w_b\varphi_b$, the free rising of the bubbles will not ensure the removal of the entire gas bubbling into the gas-liquid layer. Hence, for $w > w_b\varphi_b$, the formation of the cellular foam penetrating into the bulk of the liquid is accompanied by the accumulation of gas bubbles in the bulk of the liquid, thus leading to the formation of a mobile foam. A further increase in the gas velocity changes the height of the foam and its nature. A rupture of the cells of low-mobility foam in the liquid layer is observed together with the formation of the mobile foam. Thus, with increasing velocity, the bubbling regime is gradually replaced by the emulsifying regime. In the transient regime, the total height of the foam attains a maximum value, and then usually drops, especially in the case of liquids capable of forming stable colloidal foams. The predominance of the cellular cross-linked foam layer, observed in the transient regime between a bubbling system and a suspended layer of moving foam, occurs over a wide range of velocities between 0.5 and 1.0 m/s. In this interval, the foam becomes more mobile with increasing velocity w and is transformed into a strongly turbulized layer of movable foam at $w = 1.0$-1.3 m/s.

Calculations of sieve-plate hydraulics. The pressure drop through a sieve plate in the bubbling regime is defined as the sum

$$\Delta P_{g-l} = \Delta P_g + \Delta P_\sigma + \Delta P_l, \qquad (9.47)$$

where ΔP_g is the pressure drop through a dry plate; ΔP_σ is the pressure drop required to overcome the surface tension; and ΔP_l is the pressure drop required to overcome the weight of the liquid column on the plate.

At the instant a bubble is detached in a liquid, we have

$$\pi d_0\sigma = \frac{\pi d_0^2}{4} = \Delta P_\sigma \text{ or } \Delta P_\sigma = \frac{4\sigma}{d_0}, \qquad (9.48)$$

where d_0 is the diameter of the vapour outlet

The dependence (9.48) is applicable for hole diameters d_0 less than 1 mm. For larger diameters, ΔP_σ must be calculated from the formula

$$\Delta P_\sigma = \frac{4\sigma}{1.3d_0 + 0.08\,d_0^2}, \qquad (9.49)$$

where σ is the surface tension at the interface and d_0 is the diameter of the hole in the plate, m.

The term ΔP_1 for a sieve plate can be calculated from the equation

$$\Delta P_1 = 1.3\,(kh_w + \sqrt[3]{k\Delta h})\,\gamma_1, \tag{9.50}$$

where k is the ratio of the foam density on the plate to the density of the clear liquid; h_w is the height of the weir (m); and Δh is the head of the non-bubbling liquid layer at the weir (m), i.e.

$$\Delta h = \sqrt[3]{\left(\frac{L}{\alpha l}\right)^2}. \tag{9.51}$$

Here, L is the liquid flow rate (kg/hr); α is the flow coefficient over the weir (6400-10 000); and l is the length of the weir (m).

The height h_b of the bubbling layer is

$$h_b \cong \frac{h_1}{1-0.91\frac{w_0}{w_b}\left(\frac{d_0}{t}\right)^2}, \tag{9.52}$$

where w_0 is the velocity of gas flowing through a hole (m/s); w_b is the velocity with which a single bubble freely rises to the surface (m/s); and t is the spacing between holes.

The density ρ_e of the gas-liquid system formed in the bubbling layer is determined with the help of the formula

$$\rho_e = \left[1-0.91\frac{w_0}{w_b}\left(\frac{d_0}{t}\right)^2\right]\rho_1. \tag{9.53}$$

The critical velocity above which the bubbling regime is violated can be calculated from the equality

$$w_{cr} = \frac{2}{3}w_b\left(\frac{d_b}{d_0}\right), \tag{9.54}$$

where d_b is the bubble diameter. For $d_0 \leqslant 2.5$ mm, we get

$$d_b \cong \sqrt[3]{\frac{6\sigma d_0}{\gamma_1}}.$$

A sharp decrease in the relative density of the foam (gas emulsion) formed in the bubbling zone and the expulsion of a part of the liquid from this zone by the gas is accompanied by a drop in the static pressure, thus leading to a non-uniform performance of bubbling plates. The minimum velocity at which the entire area of a plate becomes operative is given by the equality

$$w_{min} = \frac{2}{3}\cdot\frac{f_0}{f_p}\sqrt{\frac{2g\Delta P_1}{\xi\gamma_g}}, \tag{9.55}$$

where f_0 and f_p are the cross-sectional areas of a hole and a plate respectively, and ξ is the dry plate friction coefficient.

Before the entire plate begins to operate, the static pressure at the region where bubbling takes place and the total pressure drop through

the plate vary insignificantly. For liquids which do not form a stable foam, the following equation can be used for evaluating the minimum specific gravity of the foam in the bubbling layer:

$$\gamma_{min} \cong A\left[\frac{\mu_l}{\sigma}(gh)^{0.5}\right]^{0.4}\gamma_l, \quad (9.56)$$

where A is a constant coefficient equal to 1.1.

In order to calculate the foam height on a plate, we can take $\gamma_e = 0.4\,\gamma_l$ to a first approximation. The gas concentration on a sieve plate can be expressed as

$$\varphi = \frac{\Delta P_{g-l} - \Delta P_g}{h\gamma_l}, \quad (9.57)$$

where $\Delta P_{g-l} - \Delta P_g$ is the difference in the pressure drops through a refluxed plate and a dry plate; h is the height of the liquid on a plate (m); and γ_l is the specific gravity of the liquid.

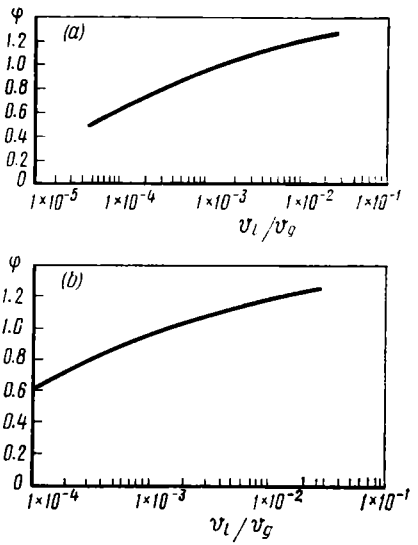

Fig. 124. Gas concentration φ vs. the ratio of liquid and gas volumetric velocities:

a—water-air and freon-water systems; *b*—nitrogen-ethanol, nitrogen-gas oil, and air-aqueous solutions of glycerol.

The dependence of the gas concentration φ on the volumetric velocities v_l and v_g of the liquid and the gas is shown in Fig. 124.

Entrainment of liquid. The entrainment of a liquid (kg liquid/kg vapour) from sieve plates for various vapour-liquid systems can be calculated from the equation

$$\varepsilon = 2.24 \times 10^4 \left(\frac{1}{\sigma}\right)\left(\frac{w}{H_e}\right)^{3.2}, \quad (9.58)$$

where σ is the surface tension (N/m); w is the vapour velocity in the empty column cross section (m/s); H_e is the effective distance (mm) between plates, which is equal to the distance between the foam layer and the upper plate, calculated for $\rho_{foam} = 0.4\,\rho_l$ by the equation

$$H_e = H_p - 2.5\,h_l. \quad (9.59)$$

Here H_p is the spacing between plates (mm) and h_l is the height of the clear liquid on the plate (mm).

Structural features of sieve plates. *Size and number of holes.* Table 9 shows the recommended hole diameters d_0 for sieve plates and their number for different values of the ratio f_0/f_c (f_0 is the cross-sectional area of a hole and f_c is the cross-sectional area of the column).

Usually, the holes are arranged in the form of an equilateral triangle with a spacing equal to $3d_0$. When holes of diameter d_0 are arranged at the corners of an equilateral triangle with a spacing equal to t, the following ratios are used between the area f_0 occupied by the holes and the area f_p covered by the perforations:

t/d_0	2.5	3.0	3 5	4.0	4.5
f_0/f_p	0.1450	0.10(7	0.0740	0.0566	0.0447

The non-perforated part of the plate near a downcomer is determined by the liquid flow rate and the column diameter. Depending on the column diameter D_c, the following distance b between the perforation and the downcomer is recommended:

for $D_c \geqslant 1.5$ m, $b = 100$ mm,

for $D_c \leqslant 1.5$ m, $b = 75$ mm.

Table 9

Hole Diameters and Their Number on Sieve Plate

Hole diameter d_0, mm	Number of holes per 1 m² of column cross-sectional area	(f_0/f_c) 100%
3	1000	9.15
4.5	450	8.0
6	250	6.9

The area f_p of the plate covered by the perforation is determined from the relation

$$f_p = f_c - \sum A_d - A_s - A_w, \quad (9.60)$$

where f_c is the cross-sectional area of the column; A_d is the cross-sectional area of the downspout; A_s is the area of the stabilization zone; and A_w is the cross-sectional area of the clearance between the column walls and the plate.

For ordinary plates with a single crossflow of the liquid, the area covered by perforations is calculated from the equation

$$f_p = f_c - 2A_d - A_s - A_w = 2\left(x\sqrt{r^2 - x^2} + r^2 \sin^{-1}\frac{x}{r}\right), \quad (9.61)$$

where

$$x = \frac{D_c}{2} - b_d + b_s, \quad (9.62)$$

$$r = \frac{D_c}{2} - b_w. \quad (9.63)$$

Here b_d is the width of a downcomer; b_s is the width of the stabilization zone; and b_w is the width of the clearance between the column wall and the plate. The thickness δ of the plates is taken equal to

$$\delta = (1/3\text{-}1/2)\, d_0.$$

Normal operation of sieve-plate columns is restricted by the stability and the flooding limits. The following relations should be satisfied for ensuring the normal operation of such a column:

1. In order to prevent flooding, the maximum height $h_{c.l}$ of the clear liquid in the downspout must not exceed half the sum of the spacing H_p between plates and the height h_w of the weir:

$$\frac{h_{c.l}}{H_p + h_w} \leqslant 1/2. \tag{9.64}$$

To ensure the separation of the vapour in the downspout, it is necessary to have

$$b_l = 0.6\ b_d, \tag{9.65}$$

where b_d is the width of the downspout and b_l is the width of the crest above the weir:

$$b_l = 0.8\sqrt{h_{0l}\,(H_p + h_w - h_{c.l})}. \tag{9.66}$$

Here, h_{0l} is the height of the liquid layer above the weir.

2. At maximum flow rates of the vapour and the liquid, the entrainment of the liquid must not exceed the optimal value. In other words, the following relation must be satisfied:

$$\frac{\varepsilon_{opt}}{\varepsilon} \geqslant 1,$$

where ε_{opt} is the optimal entrainment and ε is the entrainment defined by Eq. (9.58).

For a fixed vapour velocity and effective distance H_e, the entrainment from a sieve plate is less than from a bubble-cap plate. In industrial sieve-plate columns, flooding is observed before the onset of optimal entrainment regime.

3. In order to ensure a stable operation of sieve-plate columns, the following inequality must be satisfied:

$$\frac{h_m}{h_p} \geqslant 1. \tag{9.67}$$

where h_m is the pressure drop for a dry plate, corresponding to the minimum vapour velocity before the onset of dumping of the liquid, and h_p is the pressure drop calculated from the equation

$$h_p = 5.08 + 0.05\ h_{c.l}.$$

$h_{c\ l}$ being the height of the clear liquid in the plate (mm).

Foam apparatus. Sieve-plate columns can operate in a "mobile foam" or emulsifying ("foaming apparatus") regime. Figure 125 shows a schematic diagram of a sieve-plate column operating in the "foaming" regime. For such columns, the plate is in the form of a grid with an open area of about 15-25 percent (sometimes even 40 percent) and operates with a foam head created by a weir. The height of the mobile foam layer or the gas-liquid emulsion as well as the pressure drop across the layer are practically independent of the geometrical dimensions which are decisive for the bubbling regime.

If there is no leakage, the foam formation is independent of the diameter of the apparatus between 0.04 and 2.5 m, of the grid spacing H_g for $H_g > 400$ mm $> H_{foam}$, of the open area f_0 of the grid varying between 4 and 40 percent, and of the shape and size of openings within certain limits. The limits of the existence of a suspended layer of mobile foam and its height are determined by the gas

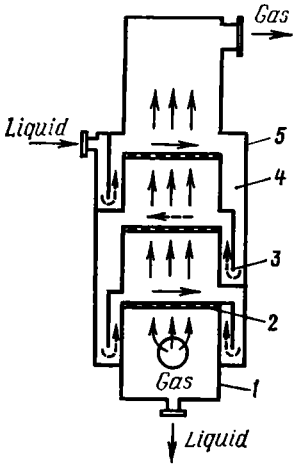

Fig. 125. Schematic diagram of a sieve-plate column operating in "foaming" regime:

1—apparatus shell; *2*—grids; *3*—hydraulic seal; *4*—overflow; *5*—weir.

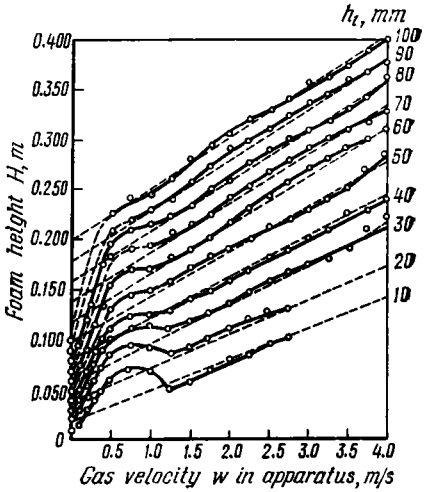

Fig. 126. Variation of the foam height H_{foam} with gas velocity w_g and the initial height h_l of the liquid in water-air system.

velocity in the apparatus and the height of the initial liquid layer. This dependence is shown in Fig. 126. In the region of gas velocities corresponding to the bubbling regime, the curves pass through a maximum. If there are foaming agents in the liquid, these maxima are several times higher and are displaced towards lower gas velocities. For high gas velocities, a stable foam layer appears beyond the maximum. The higher the initial liquid layer h_l, the wider the range of velocities for which a mobile foam layer is formed.

The height of the foam layer in the stable regime is proportional to the gas velocity and the height of the initial liquid layer (Fig. 126). The effect of the physical properties of the gas and the liquid on the height of the gas-liquid layer is less pronounced than in the case of bubbling. In industrial foam apparatus, the pressure drop through the grid usually ranges between 10 and 20 mm H_2O, the pressure drop across the grid being from 20 to 100 mm H_2O.

The processes of heat and mass transfer of highly soluble gases in a foam layer are self-modelling, i.e. the coefficients of heat and mass

transfer are independent of the size of the apparatus, grid characteristics and hole spacing over a wide range. The efficiency of a plate is almost independent of the gas velocity for a given height of the weir and a given liquid flow rate. For a constant height of the foamy layer, the efficiency linearly decreases with increasing gas velocity.

The following dimensions are recommended for designing foam apparatus: length of the grid in the direction of the liquid flow (diameter for cylindrical apparatus) not more than 3 m; grid spacing or the distance from the gas outlet between 400 and 700 mm; hole diameter between 2 and 8 mm; and weir height up to 300 mm.

9.1.3. Sieve-Plate Columns for Liquid-Liquid Systems

In sieve-plate columns, the disperse phase is alternately dispersed and collected in a continuous layer as it passes through the sieve plates. The continuous phase flows from the plate through the downcomers. For high flow rates for the continuous phase in the column, the plates are segmental in shape and have flanged edges. The hole size in the plates varies between 1.6 and 9.6 mm, and the total cross-sectional area covered by the perforations is about 10 percent of the column cross-sectional area. The plate spacing ranges from 0.15 to 0.6 mm.

In large-size columns with a large number of plates, used for refining petroleum products, the plates have a more intricate configuration with vertical sieve surfaces and special boxes with packing for phase separation. In columns of such a design, the interfacial area is arranged in the middle of the column, the light liquid disperses at the bottom of the column and the heavy liquid at the top. Several alternative versions have been proposed for the design of sieve-plate columns (Fig. 127). Some of these designs envisage the dispersion of both liquids on each plate.

The limiting flow rates in the columns are determined by the wettability of perforations by the disperse phase, the height of the disperse phase layer on a plate, the height of the disperse phase layer in the downspout, and the difference in the specific gravities of the liquids constituting the two phases. If wettability is not taken into account, the head required to force the disperse phase through the holes in the plate is determined by the equation

$$h_t = h_1 + h_2 + h_3 + h_\sigma \qquad (9.68)$$

where h_1 is the head expended on forcing the disperse phase through holes in the plate, m H_2O:

$$h_1 = \frac{\gamma_d}{\Delta\gamma} \cdot \frac{(1 - Nf_0/f_c)w_0^2}{2gc_0^2}, \qquad (9.69)$$

where f_0 is the cross-sectional area of a hole in the plate (m^2); f_c is the cross-sectional area of the column (m^2); w_0 is the velocity of the disperse phase flowing through the holes in the plate (m/s):

$$w_0 = w_d \frac{f_c}{N f_0}. \tag{9.70}$$

N being the number of holes; Nf_0 the total area of perforations (as-

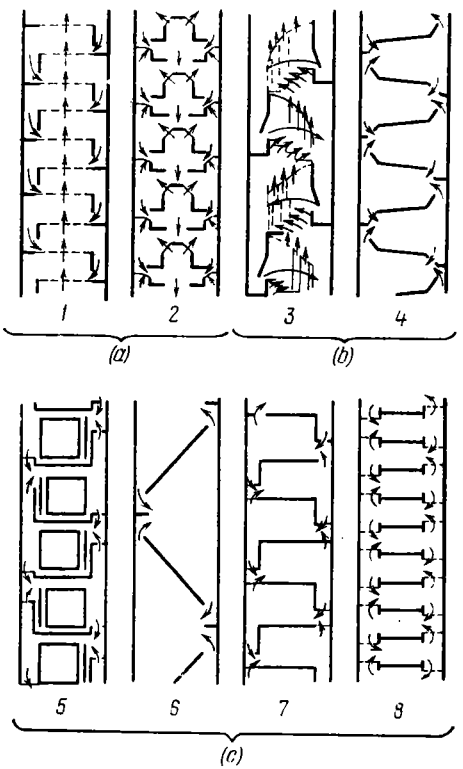

Fig. 127. Schematic diagrams of extraction columns and flows in them:

a—columns for dispersion of a light liquid; *1*—ordinary sieve-plate column; *2*—with spherical sieves; *b*—columns for dispersion of a heavy liquid; *3*—Benturi-type cascade; *4*—with inclined plates; *c*—columns for dispersion of light and heavy liquids; *5*—with baffles; *6*—with inclined plates; *7*—without perforations but with wire-mesh downcomers; *8*—without perforations and downcomers.

sumed to be 10 percent of f_c in actual practice); and c_0 is a coefficient which is calculated from the equation

$$c_0 = 1 - \frac{0.71}{\log \mathrm{Re}}. \tag{9.71}$$

In practical calculations, c_0 is assumed to be about 0.7, and h_2 is the pressure drop due to friction in the continuous phase in the downcomer (m H_2O):

$$h_2 = \frac{\Delta P_d}{\gamma_c} = \xi \frac{w_d^2}{2g}. \quad (9.72)$$

Here ΔP_d is the pressure drop in a downcomer; γ_c the specific gravity of the continuous phase; ξ the overall drag coefficient of the downcomer; w_d the velocity of the continuous phase in the downcomer (the cross-sectional area of the downcomers is usually about 5 percent of f_c), m/s; and h_3 the pressure drop due to friction of the disperse phase in the continuous phase (m H_2O):

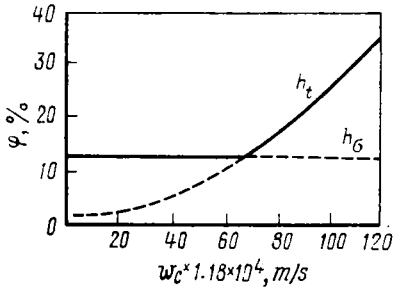

Fig. 128. φ vs. continuous-phase velocity in sieve-plate columns.

$$h_3 = \frac{\gamma_d}{\Delta\gamma}\left(\frac{1.5w_d^2}{2g}\right). \quad (9.73)$$

The loss of pressure incurred in order to overcome the interfacial tension forces is determined from the relation (m H_2O)

$$h_\sigma = \frac{4\sigma_{c,d}}{\Delta\gamma d_0} \quad (9.74)$$

This equation is true only for low velocities of the continuous phase. The surface tension effects become insignificant for large velocities of the continuous phase.

The holding capacity of the column with respect to one of the phases, say, the disperse phase, can serve as the hydrodynamic characteristic of the operation of a sieve-plate column. The holding capacity is directly linked with the head required to force the disperse phase through the plate. The relation between the holding capacity φ and the velocity of the continuous phase is shown in Fig. 128. For low continuous phase velocities, φ depends on h_σ. This dependence disappears at high velocities, the total pressure head h_t is independent of h_σ, and is determined entirely by the values of h_1, h_2, and h_3. The data on the effectiveness of sieve-plate extraction columns for some systems are given in Table 10.

9.1.4. Plates with a Unidirectional Phase Flow

Columns in which the vapour escapes through the slots in the direction of the flow of liquid on the plate are used in order to increase the plate efficiency by reducing the mixing on the plates. Besides, the kinetic energy of the vapour jet increases the velocity of the li-

Table 10

Extraction in Sieve-Plate Columns (Continuous Phase-Water)

Disperse phase	Extractable substance	Column diameter, mm	Plate spacing, mm	Hole diameter, mm	Holes area, % of column section	Downcomer area, % of column section	Linear velocity, m/s		Continuous-phase effectiveness equation $(HTU)_c$, m
							disperse phase w_d	continuous phase w_c	
Toluene	Benzoic acid	90	76	4.8	4.72	1.3	0.0008-0.0067	0.0013-0.0027	$(HTU)_c = 1.31 \left(\frac{w_c}{w_d}\right)^{0.91}$
		90	152	4.8	4.72	1.3	0.0026-0.0065	0.0019-0.0035	$(HTU)_c = 2.19 \left(\frac{w_c}{w_d}\right)^{0.91}$
		90	228	4.8	4.72	1.3	0.0030-0.0067	0.002-0.0033	$(HTU)_c = 2.47 \left(\frac{w_c}{w_d}\right)^{0.91}$
		222	152	3.2	9.48	1.43	0.001-0.004	0.001-0.00032	$(HTU_c) = 1.49 \left(\frac{w_c}{w_d}\right)^{1.03}$
		222	152	2.4	5.35	1.43	0.001-0.004	0.001-0.0032	$(HTU)_c = 1.31 \left(\frac{w_c}{w_d}\right)^{1.32}$
Kerosene	Benzoic acid	92	121	4.8	13.61	3.57	0.0033-0.0122	0.0031-0.0066	$(HTU)_c = 1.65 \left(\frac{w_c}{w_d}\right)^{0.94}$
		92	121	4.8	13.61	3.57	0.0029-0.0138	0.0021-0.0115	$(HTU)_c = 1.65 \left(\frac{w_c}{w_d}\right)^{0.94}$

Table 10 (continued)

Disperse phase	Extractable substance	Column diameter, mm	Plate spacing, mm	Hole diameter, mm	Holes area, % of column section	Downcomer area, % of column section	Linear velocity, m/s		Continuous-phase effectiveness equation $(HTU)_c$, m
							disperse phase w_d	continuous phase w_c	
Kerosene	Benzoic acid	95	76	3.2	3.0	2.25	0.0005-0.0013	0.0012-0.0057	$(HTU)_c = 0.44 \left(\frac{w_c}{w_d}\right)^{0.71}$
Gasoline	Methyl-ethylke-tone	95	152	3.2	3.0	2.25	0.0002-0.0014	0.0012-0.0042	$(HTU)_c = 0.956 \left(\frac{w_c}{w_d}\right)$
Ether	Acetic acid	219	117	2.8	3.34	—	0.0023-0.0062	0.001-0.0026	$(HTU)_c = 0.536 \left(\frac{w_c}{w_b}\right)$
		100	150	3.7	—	—	0.0053-0.00111*	0.0009-0.007	$(HTU)_c = 0.164 + 12.4 \left(\frac{w_c}{m^{**} w_d}\right)$
Toluene	Diethyl-amine	100	150	3.7	—	—	0.002-0.0057	0.0009-0.0063	$(HTU)_c = 35.3 \left(\frac{w_c}{m w_d}\right) - 0.33 w_c^{1.48}$

* Wire screens are placed underneath the plates.
** m is the slope of the equilibrium curve.

quid flow on the plate, thus increasing the flow rate of the liquid in the column. Entrainment in such columns is less than in ordinary bubble-cap columns. At present, various designs of columns operating on this principle are used in industry.

1. **Directional-slit plates (laminar or unidirectional jet plates)** (Fig. 129). Such plates carry staggered slots whose tongue-shaped tabs are bent at the same angle. The plate is fitted with conventional downcomers without any weir. The following dimensions are recommended

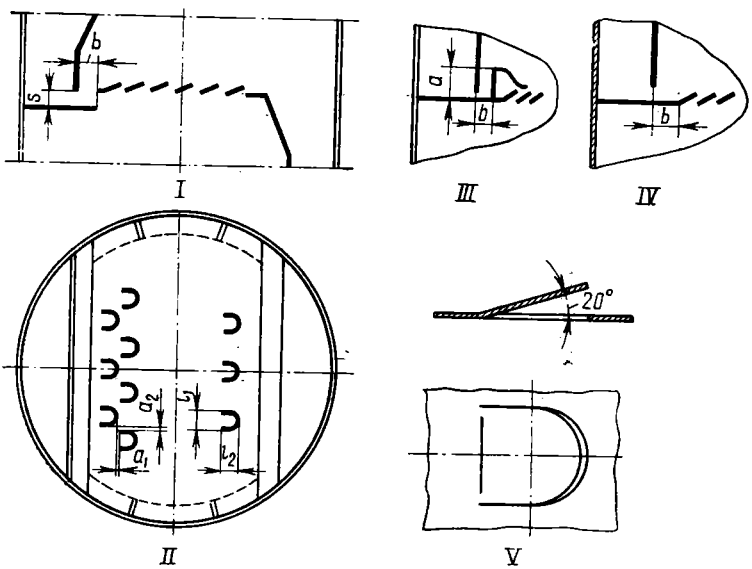

Fig. 129. Schematic diagram of a plate with directional slots and its components:

I—general view; *II*—plan view; *III*—downspout with a weir; *IV*—downspout without a weir; *V*—slot.

for the construction of such plates: for the tab $l_1 = l_2 = 50$ mm, the spacing between tabs $a_1 = 15$-20 mm, $a_2 = 20$-25 mm; the angle of inclination $= 20°$. For columns operating under pressure, it is advisable to use inclined downcomers covering an area of about 30 per cent of the column cross section. The first row of holes (in the direction of flow) is at a distance 30 mm from the downcomer, while the last row is 100-150 mm from the edge of the downcomer.

The following operating conditions are observed on directional-slit plates (Fig. 130). A uniform bubbling layer is formed by the liquid on the plate for low gas velocities. As the gas velocity increases, the motion of the liquid on the plate is accelerated on account of the velocity head and part of the liquid is carried away by the

gas. The height of the liquid at the downcomer reaches 200-250 mm. The liquid either flows quietly through the downcomer (Fig. 130*a*) or knocks against the column wall during its motion with the gas (Fig. 130*b*). In the latter case, a compaction zone for the gas-liquid flow is formed above the downcomer, thus serving as a source of intense liquid entrainment.

The separation of the gas from the liquid beyond the plate depends on the liquid flow rate. At low rates, when the layer is strongly dispersed, the gas is separated over the entire operating cross section

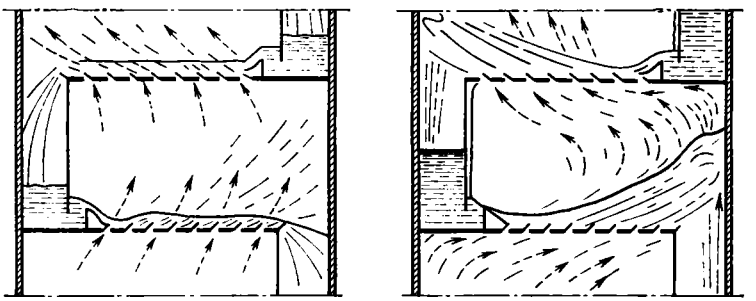

Fig. 130. Operation of a plate with directional slots for low gas flow rates (*a*) and high gas flow rates (*b*).

of the plate. As the flow rate of the liquid and the density of the layer increase, more and more gas is separated in the compaction zone above the downcomer. At the same time, aeration of the liquid in the downcomer increases, thus indicating an increased entrainment of the gas in the compaction zone. Besides ensuring an increased entrainment of the liquid to the upper plate, the existence of a compaction zone above the downcomer also leads to a weak degassing of the downflowing liquid, its accumulation on the plate and, for large flow rates of the gas, to flooding.

The following operating conditions are observed for the plate:

1. At small flow rates, the liquid appears at the plate in the form of a continuous film which is ruptured at increased velocities of the gas. A pulsating feeding of the liquid to the plate is observed upon a further increase in the gas velocity.

For moderate and large flow rates, the liquid is distributed nonuniformly along the downcomer, especially at low gas velocities. The bulk of the liquid flows through the centre of the downcomer, a part of it is directly thrown over the plate through the downcomer, thus increasing the dumping of the liquid through the slots. However, the liquid feed levels out with increasing gas velocities.

2. The beginning of plate operation coincides with the termination of the flow of liquid through the perforations.

3. The structure of the gas-liquid layer on the plate depends on the flow rates of both phases. Thus, for small values of the liquid flow rate, the layer is strongly dispersed, while the bubbling layer has a higher density for moderate flow rates. A cellular foam structure is observed at high flow rates of the liquid.

Pressure drop through the plates. The following equation is obtained from an analysis of the experimental data on the pressure drop through a dry plate:

$$\Delta P_g = 1.175 \frac{w^2 \gamma_g}{2gF_0^2} \tag{9.75}$$

where w is the empty-column velocity of the gas (vapour) (m/s); F_0 the open area of the plate (m^2/m^2); ΔP_g the pressure drop through a dry plate (mm H_2O); and γ_g the specific gravity of the gas (vapour) (kg/m^3).

The pressure drop through refluxed plates is determined from the equations

$$\Delta P_{g-l} = \Delta P_g \left[1 + 0.034 \left(\frac{L}{G}\right)^2\right], \tag{9.76}$$

$$\Delta P_{g-l} = \Delta P_l \left[1 + 2.7 \left(\frac{L}{G}\right)^2 \left(\frac{\rho_g}{\rho_l}\right)\right], \tag{9.77}$$

where L/G is the ratio of the mass flow rates of the liquid and the gas (vapour), and ρ_g and ρ_l represent the density of the gas and the liquid respectively.

The maximum and the minimum admissible gas (vapour) velocities are calculated from the equation

$$w = \frac{0.305}{3600} c \sqrt{\frac{\rho_l - \rho_g}{\rho_g}}, \tag{9.78}$$

where c is a constant. For the maximum admissible gas velocities $c = c_{max}$ and depends on the plate spacing and the liquid flow rate. For the minimum admissible gas velocities $c = c_{min}$ and depends on the empty-column cross section and the flow rate of the liquid. The coefficient c_{max} can be calculated with the help of the formula

$$c_{max} = k_1 c_1 - 5\,(L - 35), \tag{9.79}$$

where $k_1 = 1.2$ is the coefficient showing the increase in efficiency of a given plate in comparison with a bubble cap; L is the rate of flow of the liquid per unit length of the downcomer ($m^3/m \cdot hr$); and c_1 is a coefficient which is obtained from Fig. 131.

The following formula is used for determining c_{min}:

$$c_{min} = (5530 + 47.3L')\, F_0, \tag{9.80}$$

where L' is the liquid flow rate per unit length of the downcomer for the minimum gas flow rate ($m^3/m \cdot hr$).

The following relations must be satisfied under normal operation of the plates:

$$\delta = \frac{w_{max}}{w_{min}}, \quad c_{min} = \frac{c_{max}}{\delta}, \quad L' = \frac{L}{\delta},$$

whence

$$F_0 = \frac{c_{max}}{5530\delta + 47.3L}. \tag{9.81}$$

Stable operation of the plates is observed for δ varying between 2 and 3. Figure 132 should be used for determining the range of stable operation of the plates.

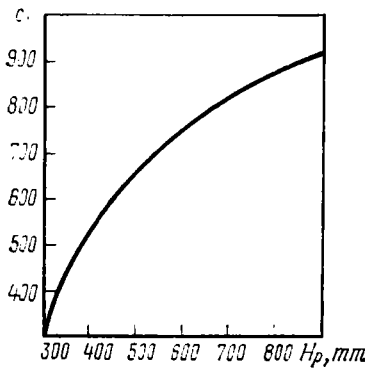

Fig. 131. Coefficient c_1 vs. the plate spacing H_p.

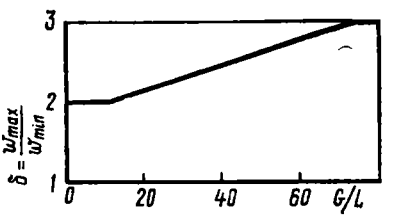

Fig. 132. To the calculation of the stability range of plate operation.

The basic dimensions for the column should be selected in the following order:

1. The plate spacing is first specified, and the maximum admissible gas velocity as well as the column diameter are determined with the help of Eqs. (9.78) and (9.79).
2. The relative length of the downcomer is specified, the liquid flow rate L is calculated and compared with the given rate.
3. The stable operation range is determined from Fig. 132 and the open cross section of the plates is determined by using Eq. (9.81).
4. The dimensions of the slots and their arrangement on the plate are specified and control calculations are carried out from the relation

$$F_0 \leqslant \frac{f_s \psi_{ef}}{2(l_1 + a_1)(l_2 + a_2)}, \tag{9.82}$$

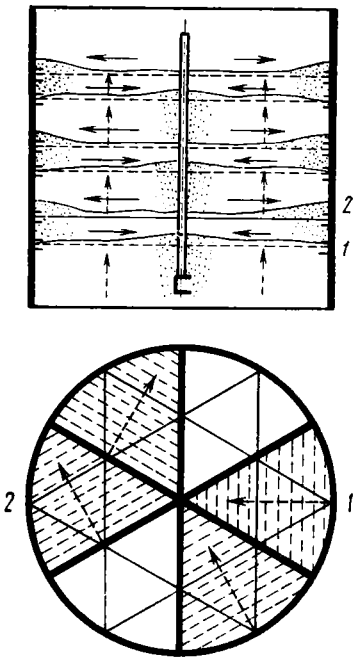

Fig. 133. Schematic diagram of the Kittel plate operation.

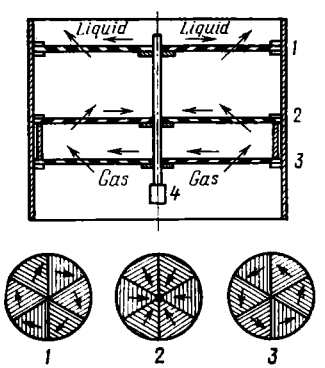

Fig. 134. Schematic diagram of a Kittel plate with spray grids:

1—upper grid; *2*—lower grid; *3*—spray grid; *4*—upright support.

where f_s is the total area of slots for the passage of the gas (mm²); and ψ_{ef} is a coefficient which takes into account the effective area of the plates, and usually varies from 0.7 to 0.9.

5. The pressure drop for a refluxed plate (ΔP_{g-l}, mm H_2O) is determined with the help of equations (9.76) and (9.77).

6. The plate spacing H_p (mm) is verified in accordance with Fig. 129 from the equation

$$\gamma_0 H_p > \left[a + 2.8\sqrt[3]{L^2} + \frac{\Delta P_{g-l}}{\gamma_l} + 200\left(\frac{L}{b \cdot 3600}\right)^2\right], \quad (9.83)$$

where γ_0 is the relative specific gravity of the frothed liquid in a downcomer, equal to 0.4 for columns under pressure and 0.5 for columns under normal pressure. If the inequality (9.83) is not satisfied, the plate spacing or the column diameter must be increased.

2. **The Kittel plate** (Fig. 133). This plate is usually made of a metal sheet and consists of two grids (upper grid *1* and lower grid *2*). Each grid is divided into six equal segments. The perforations in the metal sheet are at a certain angle to the plane of the sheet, thus creating a directional motion of the liquid on the plate (Fig. 134). The liquid is in a centrifugal flow on the upper grid and in a centripetal flow on the lower grid, thus ensuring a proper distribution of the liquid over the column cross section. Sometimes, a spray grid is placed on top of the upper grid. The former has larger perforations which impart a centrifugal motion to the vapour in the opposite di-

rection. As in the case of a sieve plate, there is a definite vapour velocity for the Kittel plate, below which the normal operation of the plate is violated due to dumping of the liquid. The total area of cross section of the perforations in these plates is about 20-25 per cent, and hence they have a lower pressure drop than a sieve plate. The spacing between Kittel plates (complete sets of grids) is 400 mm (for

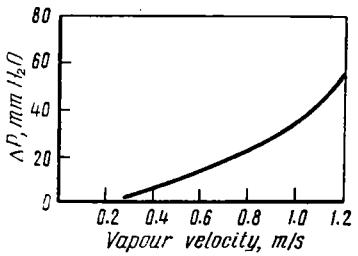

Fig. 135. Dependence of pressure drop across a Kittel plate on the empty-column vapour velocity.

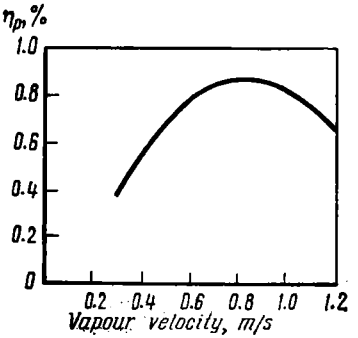

Fig. 136. The Kittel plate efficiency vs. vapour velocity.

vacuum distillation, this value is equal to 305 mm). Kittel plates usually have no downcomers and have the following advantages:

1 .A rapid and continuous renewal of the contact surface in the liquid.

2. A higher output owing to a comparatively large open area and the action of the centrifugal force which throws the liquid to the walls and not upwards.

3. A small height of the liquid on the plate and a large open area ensure a comparatively small pressure drop through the plates. This offers wide possibilities of their use in vacuum distillation.

4. The absence of a stagnation zone on the plates.

Figure 135 shows the dependence of the pressure drop across a Kittel plate (plate *2*, Fig. 133) on the vapour velocity in an empty column, while Fig. 136 shows the variation of the efficiency of a Kittel plate with the vapour velocity.

Hydraulic calculations for the refluxed Kittel plates can be made with the help of the following equations:

$$\frac{\Delta P_{g-lg}}{w^2\gamma} = 12\,\frac{w_g}{w_l}\left(\frac{L}{G}\right)^{0.5} \times \left(\frac{F_o}{F_p}\right)^{0.5}\left(\frac{1}{d_o}\right)^{0.66} \qquad (9.84)$$

for the pressure drop, and

$$\frac{gh}{w^2} = 0.0545\,\frac{w_g}{w_l}\left(\frac{L}{G}\right)^{0.5}\left(\frac{F_o}{F_p}\right)^{0.5}\left(\frac{1}{d_o}\right)^{0.66} \qquad (9.85)$$

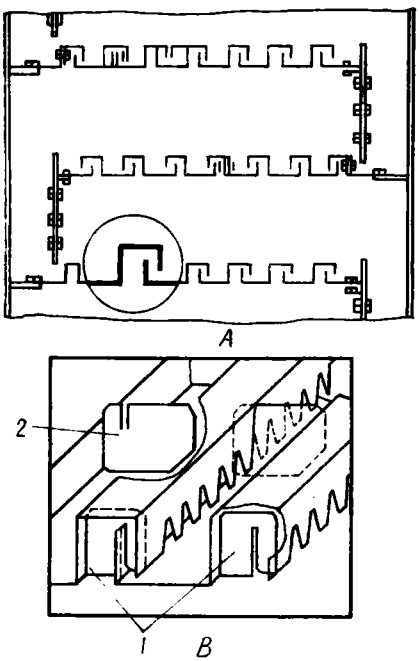

Fig. 137. General view of Uniflux plates (*A*) and construction of caps (*B*).

for the height of the foam layer, ΔP being the pressure drop across the plate; w_g the empty-column gas velocity; w_l the empty-column liquid velocity; F_o and F_p the cross-sectional areas of holes and plates; d_o the hole diameter; L and G the mass flow rates of the liquid and the gas respectively; and h the height of the foam layer on the plate.

Relations (9.84) and (9.85) are valid for the following range of variation of parameters: $w_g = 0.32\text{-}2.11$ m/s, $L/G = 0.26\text{-}4.41$, $F_o/F_p = 0.072\text{-}0.20$, and $1/d_o = 151\text{-}500$.

3. **Uniflux plates.** Of late, Uniflux plates have found wide applications in petrochemical and chemical industry. The construction of such a plate is shown in Fig. 137.

Uniflux plates are assembled from standard forged S-shaped elements provided with trapezoidal openings which are interconnected through the end strips *1* and intermediate strips *2* (Fig. 137). No intermediate support is required in columns of diameters up to 5 m. One intermediate support is fitted in columns of larger diameters. The cross-sectional area for the passage of vapour in a Uniflux plate is about 2-4 times higher than in bubble-cap plates of conventional design. The liquid flows over to the lower plate through the downcomer segments. The vapour passes through slits in the direction of the flow of liquid. This helps the motion of the latter, reduces the level difference on the plate, and decreases the resistance offered to the vapour flow. Just like plates of other types, Uniflux plates are available in single- and multisector designs. Single-sector plates are normally used in small-diameter columns, while columns of large diameters are fitted with multisector plates.

In order to determine the pressure drop through a refluxed plate, it is customary to consider the total pressure drop across a plate as the sum of the pressure drops through a dry plate ΔP_g, through the gas-(vapour) liquid emulsion layer (ΔP_e), and the pressure drops due to the motion of the liquid on the plate (ΔP_m) and the hydraulic

gradient (ΔP_h):

$$\Delta P_{g-l} = \Delta P_g + \Delta P_e + \Delta P_m + \Delta P_h. \quad (9.86)$$

The values of the individual terms in this equation, expressed in mm H_2O, can be calculated from the following equations:

pressure drop through a dry plate

$$\Delta P_g = 0.306\ w_0^2 \gamma_g, \quad (9.87)$$

where w_0 is the vapour velocity in the open cross section at the plate inlet (m/s); and γ_g is the specific gravity of the gas (vapour);

pressure drop through the layer of the gas-liquid emulsion

$$\Delta P_e = \varphi h_s, \quad (9.88)$$

where h_s is the open height of the slots in the S-shaped elements (mm); and φ is the aeration coefficient for the liquid.

The pressure drop ΔP_m through the refluxed plate is the sum of the static pressure h_{st} (static submerged depth can be taken equal to the height h_w of the weir) and the pressure drop due to the liquid layer h_1 above the weir:

$$\Delta P_m = h_w + h_1. \quad (9.89)$$

The height of the crest above the weir can be calculated from the equation

$$h_1 = 2.8 L_1^{2/3}, \quad (9.90)$$

where L_1 is the rate of flow of the liquid through the column per unit length of the weir ($m^3/hr \cdot m$).

The following equation was proposed to calculate the hydraulic gradient Δ on the plate:

$$\Delta^{1.5} + 16.4 L_1^{2/3} \Delta^{0.5} = \frac{L_1 N_r}{c_d}, \quad (9.91)$$

where N_r is the number of rows of S-shaped elements; c_d is the discharge coefficient which is a function of the liquid flow rate and the factor F_s; $F_s = w_v \gamma_g^{0.5}$. For $F_s = 6.57$, the discharge coefficient is determined with the help of the equation

$$c_d = L_1 N_r^{0.5} / (125 L_1^{2/3} \Delta^{0.5} + 2.21 \Delta^{3/2}). \quad (9.92)$$

The dependence of the coefficient c_d on the liquid flow rate is shown in Fig. 138. The pressure drop due to a gradient of the liquid level on the plate is calculated with the help of the equation

$$\Delta P_h = 0.5\Delta. \quad (9.93)$$

The working interval of variation of the gas (vapour) flow rate through the column is determined by the maximum and minimum admissible flow rates through the column. The maximum admissible flow

rate of the gas (vapour) through the column is determined from the equation

$$Q_{max} = 3600 f_p F_s \gamma_g^{-0.5}, \quad (9.94)$$

where f_p is the total plate area (m^2).

The admissible gas (vapour) velocity w_v in the empty column is calculated from the equation

$$w_v = F_s \gamma_g^{-0.5}.$$

Factor F_s is determined from a specified value of the plate spacing H_p (Fig. 139). While selecting a value for the plate spacing, it

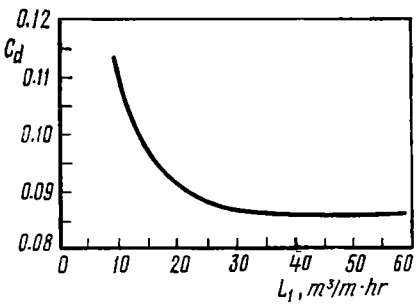

Fig. 138. Discharge coefficient c_d vs. the liquid flow rate through the column.

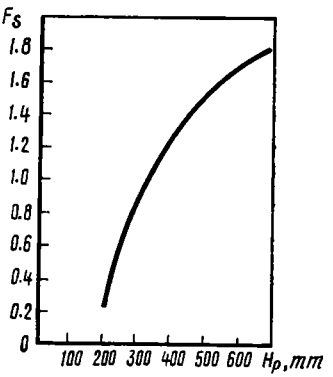

Fig. 139. Flow rate vs. the plate spacing.

must be noted that the hydrodynamic operation of the plate becomes unstable for $F_s < 0.5$. The minimum admissible flow rate (m^3/hr) for the gas (vapour) through the column is determined from the equation

$$V_{g\,min} = 1800\, f_p \gamma_g^{-0.5}. \quad (9.95)$$

The area of a plate can be estimated from a given flow rate of the gas (vapour) through the column and the maximum admissible gas (vapour) velocity in the empty-column cross section:

$$f_p = V_g/3600\, w_{v_s} \quad (9.96)$$

where V_g is the rate of flow of gas (vapour) through the column (m^3/hr).

The maximum flow rate over the plates is attained upon a sharp increase in the pressure drop in the vicinity of flooding, when the foam height attains a value higher than 2/3 of the plate spacing. In this case, the fluctuations on the plates sharply increases. The foam density on the plates varies between 0.4 and 0.8 of the liquid

density. The entrainment gradually increases from 1 to 10 percent, after which it registers a sudden rise. This abrupt increase in the entrainment corresponds to the onset of flooding.

9.1.5. Valve Plates

These are plates in which the flow area for the gas (vapour) varies with the gas flow rate in the column. Valves are caps of different types, covering the holes in the plates under their weight. As the flow

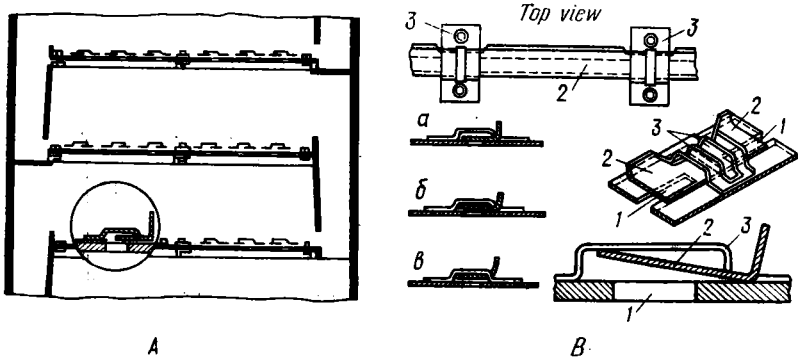

Fig. 140. General view (*A*) and parts (*B*) of a valve plate

rate of the gas (vapour) through the column increases, the valve is lifted and the open area for the gas flow increases. Let us consider some designs of valve plates.

One such construction is shown in Fig. 140. The plate has rectangular slots *1* which are covered by L-shaped strip valves *2* held in position by clamps *3*. In the idle position, valve *2* covers the slot under its own weight (Fig. 140*a*), while under operating conditions the flow of vapour or gas lifts the lighter part of valve *2* (Fig. 140*b*). In this case, the gas or vapour passes through the opening created in the valve and comes in contact with the liquid on the plate, injecting it in the direction of motion toward the downspout or segment. Upon a further increase in the gas (vapour) flow rate, valve *2* opens fully (Fig. 140*c*).

Figure 141 shows the cross-sectional view of a column fitted with free disc-type valves (plates of the type "Flexitray").

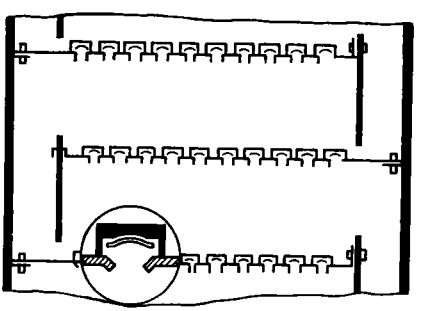

Fig. 141. Schematic diagram of a plate with free disc-type valves.

The construction of a disc-type valve with a limiter and the plate itself are shown in Fig. 142.

The schematic diagram of a "Glitsch" valve in the operating and idle conditions is shown in Fig. 143. The extent to which valves are opened depends on the vapour velocity as follows:

Valve opening, %	0	40	80	100
Vapour velocity (of maximum), %	10	25	50	100

The diameter of industrial columns fitted with valve plates of this type attains values up to 12 m. Depending on the diameter of

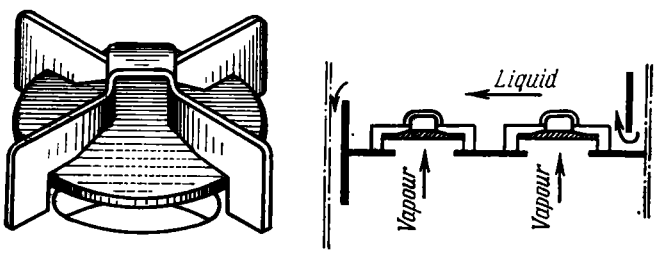

Fig. 142. Construction of a disc valve with a limiter (*a*) and schematic diagram of a plate (*b*).

the column, valve plates can have one, two or several sectors. Single-sector plates are recommended for use in columns whose diameter does not exceed 1800 mm, two-sector plates should be used for diameters between 1800 and 2700 mm, three-sector plates are best suited for diameters from 2700 to 3600 mm, while four-sector plates should be used for diameters exceeding 3600 mm. The design features of valve plates make it possible to maintain a high rate of mass transfer in almost the entire range of variation of flow rate through the column for an approximately constant pressure drop across the plates.

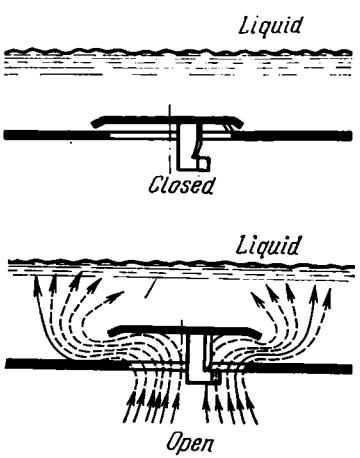

Fig. 143. Schematic operation of a plate with a Glitsch-type valve.

Mass-transfer apparatus fitted with valve plates are used as absorbers, stripping and fractionating columns. The efficiency of

valve plates is higher than that of conventional bubble-cap plates and has quite stable values. The output per unit volume of such columns is also much higher.

Hydraulic calculation of valve plates leads to the following results.

The total pressure drop across a plate is considered as the sum of the pressure drop through the dry plate (ΔP_g) and through the liquid (ΔP_l):

$$\Delta P_{g-l} = \Delta P_g + \Delta P_l. \tag{9.97}$$

The dependence of the pressure drop across dry and wet "Glitsch" plates on the gas- and liquid flow rates through the column is shown

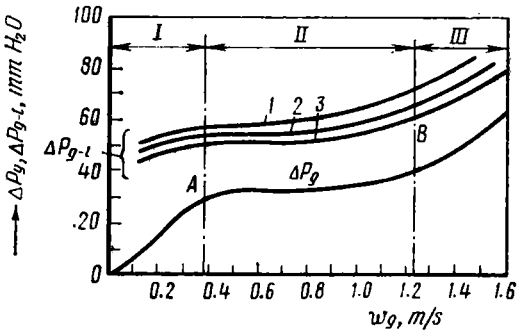

Fig. 144. Pressure drop across a valve plate vs. the gas and liquid flow rate through the column:

I—valve closed; *II*—valve partially open; *III*—valve completely open; *1*—L = 1.5 m³/hr; *2*—L = 3 m³/hr; *3*—L = 6 m³/hr.

in Fig. 144. The pressure drop curves for valve plates are flatter than the corresponding curves for other types of plates. It can be seen from Fig. 144 that the pressure drop across a dry plate varies nonuniformly with the gas flow rate through the column. Consequently, the dependence of the pressure drop of a dry plate on the gas velocity cannot be expressed by a single equation. The pressure drop curve can be divided into three parts: region *I* corresponding to the gas velocity up to point *A*, region *II* corresponding to the velocity variation from point *A* to point *B*, and region *III* corresponding to a variation in the gas velocity from point *B* to its maximum value. Different equations are used for calculating the pressure drop across a dry plate in each of these three regions. The lower limit of the gas velocity $w_{g_{I-II}}$ (m/s) corresponding to point *A* is determined from the equation

$$w_{g_{I-II}} = \sqrt{\frac{\xi_2}{\xi_1} \cdot \frac{m_v g}{\gamma_g f_0}}. \tag{9.98}$$

where m_v is the mass of the valve; f_0 is the cross-sectional area of the hole in the plate under the valve; ξ_1 and ξ_2 are the friction factors:

$$\xi_1 = 3500\,(A_{v0}/A_0)^{-1.2},$$

$$\xi_2 = 6.71\,(A_0/A_v)^{-2.49}e^{5.91\,(A_0/A_v)},$$

A_{v0} is the total flow area for the initial opening of all valves (m^2); A_0 is the total area of perforations in the plates (under the valves) (m^2); and A_v is the total flow area of all valves (m^2).

The upper limit of the gas velocity (m/s), corresponding to point B, is determined from the equation

$$w_{g_{II-III}} = 0.9\sqrt{\frac{\xi_2}{\xi_4-\xi_3}\cdot\frac{m_v g}{\gamma_g f_0}}, \tag{9.99}$$

where ξ_3 and ξ_4 are friction factors defined by the equations

$$\xi_3 = 920\,(A_{v_{max}}/A_0)^{-2,95}, \tag{9.100}$$

$$\xi_4 = 2160\,(A_{v_{max}}/A_0)^{-0,8}. \tag{9.101}$$

The upper and lower admissible gas velocities $w_{g_{max}}$ and $w_{g_{min}}$ in the plate holes can be determined from the equations:

$$w_{g_{max}} = 1.30\ w_{g_{II-III}} = 1.15\sqrt{\frac{\xi_2}{\xi_4-\xi_3}\cdot\frac{m_v g}{\gamma_g f_0}} \tag{9.102}$$

for the maximum admissible velocity (m/s), and

$$w_{g_{min}} = 0.9\ w_{g_{I-II}} = 0.9\sqrt{\frac{\xi_2}{\xi_1}\cdot\frac{m_v g}{\gamma_g f_0}} \tag{9.103}$$

for the minimum admissible velocity.

The pressure drop across a dry plate (mm H_2O) in the regions *I-III* can be calculated from the following equations:

region *I* (for closed valves)

$$\Delta P_{g_I} = \frac{\xi_1}{g}\left(\frac{\rho_g}{\rho_l}\right)\left(\frac{v_g}{3600A_0}\right)^2, \tag{9.104}$$

where ρ_l is the density of the liquid (kg/m^3) and v_g is the rate of flow of gas through the column (m^3/hr);

region *II* (for a partly open valve)

$$\Delta P_{g_{II}} = \xi_2\left(\frac{m_v}{f_0\gamma_l}\right) + \frac{\xi_2}{g}\left(\frac{\rho_g}{\rho_l}\right)\left(\frac{v_g}{3600A_0}\right) \tag{9.105}$$

region *III* (for a completely open valve)

$$\Delta P_{g_{III}} = \frac{\xi_4}{g}\left(\frac{\rho_g}{\rho_l}\right)\left(\frac{v_g}{3600A_0}\right). \tag{9.106}$$

The hydraulic pressure drop of the liquid on the plate (mm H_2O) is determined from the equations

$$\Delta P_l = 0.27\,(A_0/F_p)^{-0.25} h_w^{0.85} L_{ac}^{0.35} \qquad (9.107)$$

for regions *II-III*. Here, h_w is the weir height (mm); F_p is the plate area (m^2); L_{ac} is the rate of flow of the liquid through the plate referred to the active surface area of the plate (m/hr). The plate area A_{ac} occupied by valves placed at the corners of an equilateral triangle is determined from the equation

$$A_{ac} = 1.1\,(t/d_v)^2\,A_p \qquad (9.108)$$

where t is the distance between the centres of the valves; d_v is the valve diameter; A_p is the plate area between valves and between plate edges and the weir. The area of the plate is determined from the equation

$$F_p = 1.2\,(2A_d + A_{ac}), \qquad (9.109)$$

where A_d is the cross-sectional area of the downcomer segment.

The cross-sectional area of the downcomer segment is first determined roughly by specifying the admissible liquid velocity in the segment (of the order of 0.1 m/s), and is then refined by establishing the actual duration of stay of the liquid on the downcomer segment, which must not be less than 5 s. The plate spacing H_p is taken equal to twice the height of the gas-liquid emulsion layer in the downcomer segment H_d:

$$H_p = 2H_d.$$

The height of the gas-liquid emulsion layer in the downcomer segment is determined from the equation

$$H_d = (\Delta P_{g-l} + h_w + h_1 + \Delta)/c, \qquad (9.110)$$

where c is a coefficient which depends on the gas content in the gas-liquid emulsion and its foaming capacity. The value of c can be approximately taken from 0.5 to 0.8.

In order to take into account the influence of the gas flow through the column, the following empirical correction factor is introduced for region *I*:

$$\Delta P_{l_I} = 0.65 \times 1.2^{-w_0}\,(A_0/A_p)^{-0.25} h_w^{0.85} L_{ac}^{0.35} \qquad (9.111)$$

This equation can be used for approximate calculations only, since the hydrodynamic operation of the plate in region *I* is highly unstable and the pressure drop through it varies sharply. This, however, is not of great importance, since the valve plate columns do not operate in region *II*.

In most cases, the height of the weir can be taken equal to 50 mm. In the case of vacuum distillation, this height should be reduced

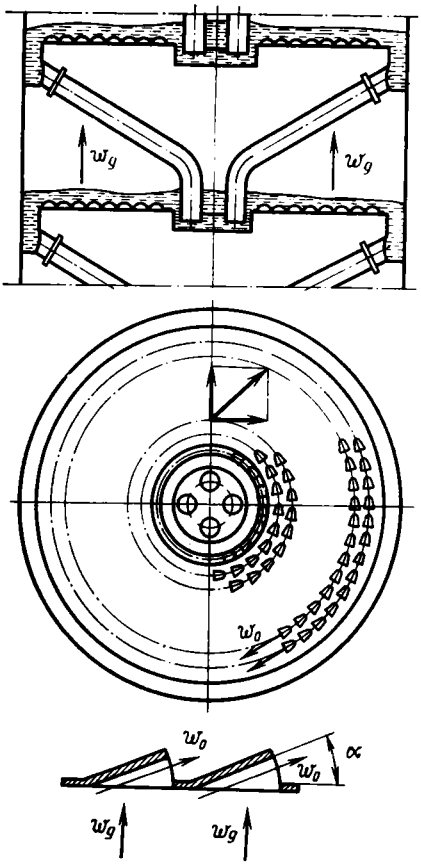

Fig. 145. Schematic diagram of phase flows on a jet-spray plate with a uniformly rotating flow.

to 12.5 mm, while for chemical processes (where the duration of stay must be long) it should be increased to 150 mm. The length of the weir for valve plates is determined in the same way as for bubble-cap plates. This length, however, must not be less than half the diameter of the plate or more than 0.85 times this value.

The valve plates have the following advantages: high relative velocities of gas and liquid ensuring a high intensity of mass transfer, a low pressure drop through the dry plate, and a stable operation over a wide range of variation of gas flow rates. (The maximum rate of gas flow is as much as eight times more than the minimum value.) Valve plates are widely used at present.

9.1.6. Regularly Rotating Two-Phase Flow in Contact Apparatus

In order to intensify the separation processes in plate columns, I.P. Slobodyanik recently proposed plates with regularly rotating two-phase flows. One of the versions of such a plate is shown in Fig. 145.

The gas (vapour), entering the plate at a velocity w_g, performs complex three-dimensional helical motion upwards. The liquid moves from centre to periphery, performing spiral motion in the horizontal plane. One of the simplest constructions is a jet plate in the form of a disc with forged arc-shaped slits and tangentially directed axes.

As the gas with velocity w_0 leaves the slits with tangentially directed axes at an angle α to horizontal, a rotating gas flow is generated at the plate. This flow entrains the liquid entering the central feed cup. A two-phase rotating motion is created as a result: the gas performs a helical upward motion under the upper plate, while

the liquid performs a spiral motion in the horizontal plane from centre to periphery, flows into the annular pocket and down to the centre of the lower plate through downcomers. Depending on the geometrical parameters of the plate, the properties of the phases and the ratio of their exchange velocities, three hydrodynamic plate operations are observed: bubbling regime, when the kinetic energy of the gas jets is insufficient for setting the liquid in rotation; the transient regime corresponding to the onset of rotation of the liquid; and the jet regime in which the gas-liquid layer undergoes a uniform rotational motion on the plate. In the field of centrifugal forces, the phases come in close contact and are separated clearly, the admissible phase velocities are increased in comparison with the bubbling regime, thus increasing the efficiency of the plate.

Under the conditions of a regular rotation of a two-phase flow on the plate, the gas serves as the continuous phase, while the liquid is the disperse phase. The liquid is expelled through the tangentially directed gas jets, receiving additional increase in the circular velocity from the gas during the entire course of its motion from centre to periphery. Since the liquid performs spiral motion in the horizontal plane, only the horizontal component of the velocity of gas jets, taking into account the angle of elevation α of the slit axis, has to be considered.

The ideal displacement model for both phases upon a thorough mixing of the liquid along the height of the gas-liquid layer quite accurately describes the real pattern of mass exchange on a plate under a regular rotation of the gas-liquid layer.

The efficiency of jet plates with a rotating flow is about 25 percent higher than that of the bubble-cap plates under identical conditions. The output is more than twice that in the case of bubble-cap plates, while the hydraulic pressure drop is two-to-three times less than for bubble-cap plates under similar conditions.

9.1.7. Flow Sectionalization in Contact Apparatus

Flow sectionalization on plates enables us to bring the plate model closer to the ideal displacement model with increasing number of zones, since each section functions as a cell of ideal displacement. A multiple-discharge plate with two phase-contact zones, proposed by O. S. Chekhov, is an example of such a device (Fig. 146). Plate *1* (sieve plate, bubble-cap plate, etc.) is divided into sections by partitions *4*. The partitions in the lower part are perforated or are mounted in such a way that there is a gap between them and the plate for ensuring a redistribution of the liquid between sections.

Downcomers *2* are mounted at the central zone of the sections. The lower part of the downcomers is equipped with baffle plates *3* in such a way that there is a gap between the two. The downcomers

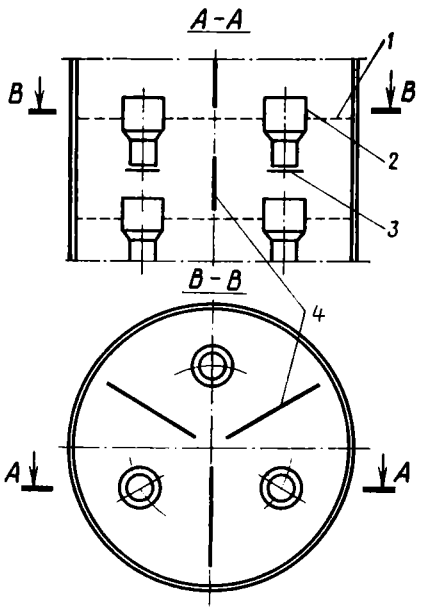

Fig. 146. A plate with two contact zones.

may have one or more slits. The dimensions of the circular slit may vary from 3 to 20 mm. The liquid flows from periphery to centre of an individual element over its plateau. Overflowing through the weir into the downcomer, the liquid flows out in the form of a plane circular jet under the action of the static head. This jet falls in the space between plates over the bubbling layer, thus creating an additional phase-contact zone. The creation of a two-slit downcomer considerably increased the range of stable operation of a plate and increased the efficiency of the plate as a whole. Such plates have a number of advantages:

(1) an increased efficiency owing to the creation of an additional phase-contact zone in the space between plates; (2) an increased relative working area of the plate due to the absence of an overflow pocket; (3) an increased length of the overflow plank, thus leading to much higher liquid flow rates; (4) reduced transverse inhomogeneities due to a sectionalization of the plate plateaus by partitions; (5) a quite high efficiency upon mounting the plateau of a plate with considerable departures from the horizontal position, attained by fixing the downcomers in one plane of the upper slot; and (6) increased flow rates of the gas (vapour) due to a high separating capacity of the additional (film-type) contact zone.

The design features mentioned above permit the construction of plates with a high liquid output up to 160 $m^3/m^2 \cdot hr$, although it is also possible to create plates capable of operating at a liquid flow rate of 8-10 $m^3/m^2 \cdot hr$. The hydraulic pressure drop of plates is of the same order as for the conventional plates, viz. sieve plates, bubble-cap plates, and can be somewhat reduced by creating plates with increased free cross-sectional area. This becomes possible owing to the high separation capacity of the second phase-contact zone. The hydraulic pressure drop for a film-type zone is not large, and amounts to just 1-4 mm H_2O. According to Murphree, the gas phase efficiency of the plates is approximately equal to unity, while for the predominant pressure drop in the liquid phase, the efficiency is between 0.85 and 0.9.

An interesting modification of plates has longitudinal-transverse sectionalization with several downcomers and collecting cups. This permits the creation of a cascade of films covering the cross section of the column.

9.1.8. Plates without Downcomers (Columns with Grid Plates)

Unlike sieve-plate or grid-tray columns, columns with grid plates have no downspouts (Fig. 147), and liquid flows down to the lower plate through the slots in the plate, in counterflow with the

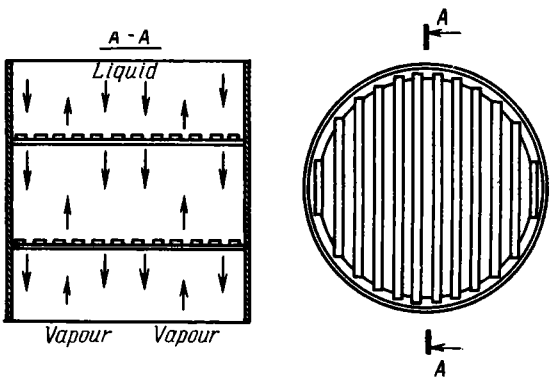

Fig. 147. Grid-plate column without downcomers.

rising vapour. The reflux at the plate distributed on it in the form of a layer whose height is related to the pressure drop of the vapour flow. The vapour flows continuously through the slots or holes in the plates, rising from the lower plate to the upper plate, while the liquid flows down from the upper plate to the lower plate. On the average, a dynamic equilibrium sets in on each part of the plate between the amount of liquid on it and the velocity of liquid and gaseous flows. Since there are no weirs on the plate, the height of the bubbling layer on different parts of the plate levels out in case of intensive bubbling. Plates having a diameter of about 400-500 mm can be made of one element, while plates of larger diameters are made of individual sections which are either fastened to the framework through gaskets or welded to it.

Circular holes are sometimes used instead of parallel slots. Slots can also be formed by arranging circular rods or tubes along a row or in the form of a spiral. In the latter case, heat can be supplied or removed during transfer between phases. A coolant or steam for heating can be circulated through the tubes. The plate spacing is

between 250 to 400 mm, and is usually equal to 300 mm. The advantages of this columns are a simple design and a high capacity.

Hydrodynamics of plates. Figure 148 shows the dependence of the pressure drop across a dry and wet grid plate on the gas veloc-

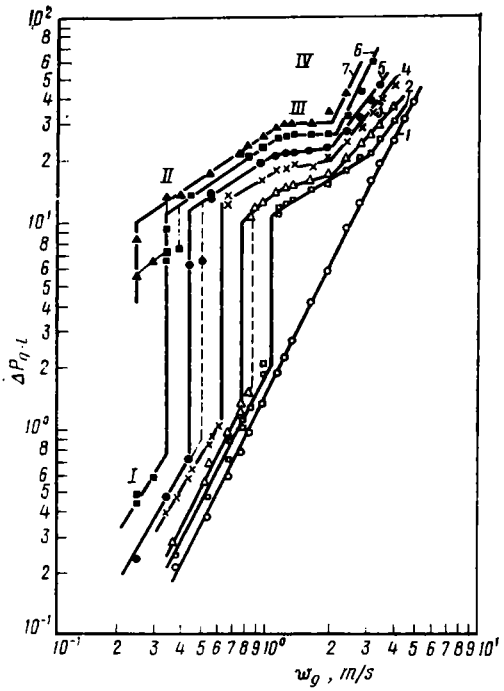

Fig. 148. Pressure drop across a dry and a refluxed grid plates with grid spacing 3 mm vs. the empty-column gas velocity:

1—dry plate; *2*—L = 1650 kg/m²·hr; *3*—L = 3780 kg/m²·hr; *4*—L = 8060 kg/m²·hr; *5*—L = 11 200 kg/m²·hr; *6*—L = 16 000 kg/m²·hr; *7*—L = 21 100 kg/m²·hr.

ity. Depending on the rate of flow of gas or liquid, various hydrodynamic regimes are observed on these plates.

The first regime I (Fig. 148) can be defined as the wetted-plate regime. It sets in at low velocities of the gas and the liquid. The liquid is in contact with the gas only at the film surface. For a constant reflux, the pressure drop across the plate varies approximately as the square of the gas velocity (Fig. 148). For a varying reflux, the pressure drop across a plate is represented in logarithmic coordinates as straight lines parallel to the dry plate pressure drop. The greater the reflux, the higher the lines on the plot.

In the wetted-plate regime, the amount of liquid on the plate is insignificant. This regime exists up to a certain critical velocity

of the gas at which the skin friction drag between the rising gas and the downflowing liquid becomes so large that a liquid layer is formed on the plate (loading). The velocity of the gas in this case depends on the geometry of the plate and the reflux. Critical points beyond which the loading of the liquid sets in are called loading points.

The second regime II (Fig. 148) of a grid plate, defined as the "bubbling" regime, sets in after the liquid loading point and is accompanied by an increased pressure drop across the plate. In this regime, the gas bubbles through the liquid layer formed on the plate, and it is possible to distinguish a zone of relatively clear liquid with bubbles passing through it as well as a foam zone formed above it. At a constant reflux, the first zone gradually decreases with increasing gas velocity until the entire liquid is transformed into a turbulized foam. The spots where the gas rises and the liquid flows through the slots keep on changing continuously but are distributed uniformly on the average over the entire cross-sectional area of the plate.

In the bubbling regime, the pressure drop across a plate, the height of the aerated liquid layer and its quantity increase with the gas velocity at a constant reflux. The value of these quantities also increases with increasing reflux. An increase in the quantity of gas decrease the open area for the liquid flow, the amount of liquid on the plates increases and the rate at which bubbles are formed increases. Gradually, the entire liquid on the plate is transformed into "foam".

In the case of loading of the liquid, a peculiar type of "hysteresis" is observed at the beginning of the bubbling regime. The liquid layer on the plate is formed at higher gas velocities than when this layer disappears ("dumping" of the liquid). In order to form a liquid layer on the plate, a higher energy of the gas flow is required than that required for holding an already formed layer on the plate. Therefore, if a liquid is at once delivered at the plate at a gas velocity lower than the loading velocity, a layer of this liquid may be formed on the plate. Hence, at velocities below the loading velocity, it is expedient to use distributing plate with a greater open area than the operating plate. In this case the liquid is loaded at higher gas velocities than during operation with identical distributing and operating plates (dotted lines in Fig. 148). The bubbling regime terminates when the entire liquid on the plate is transformed into a highly turbulized foam.

The third regime III (Fig. 148), called the aeration or emulsifying regime, sets in after the bubbling regime. The transition from the bubbling to emulsifying regime is characterized by the point of phase inversion. In this regime, the pressure drop across the plate

and the height of the aerated liquid layer increase only slightly with increasing gas velocity at a constant reflux. The quantity of the liquid on the plate is even reduced sometimes. In this case, the fraction of the slot area occupied by the liquid remains practically constant. This leads to a higher frequency of bubble formation or to larger bubbles.

The fourth regime IV (Fig. 148), called the spray regime, sets in after the aeration regime when the gas velocity in the slots increases to such an extent that individual bubbles begin to coalesce into jets. The gas jets, passing through different parts of the plate, impart oscillatory motion to the aerated liquid layer. In this regime, the pattern of liquid flow through the slots changes abruptly. While for low gas velocities the liquid flows on the average uniformly through all the slots in the form of "rain", the flow of the liquid after the wave formation occurs through different parts of the plate in portions, corresponding to the position of the moving wave trough. Besides, this regime is characterized by an intensive entrainment of the liquid drops to the upper plate.

At the end of wave motion of the liquid, the column is "flooded", the flow of the liquid through the slots ceases, an instantaneous increase in the amount of the liquid, the height of foam on the plate and the pressure drop through the plate is observed, and the liquid is expelled from the plate.

From the point of view of mass transfer, the optimal velocities should be the flow velocities corresponding to the point of phase inversion, since the interfacial area assumes its highest value at this point. The working regime should be taken as the interval of flow velocities covering the bubbling and emulsifying regimes.

It is, however, not always possible to clearly demarcate these regimes. Thus, a change in the amount of the reflux liquid strongly affects the loading velocity, leaving the inversion velocity practically unchanged. Hence, the absolute value of the loading velocity may turn out to be higher than the inversion velocity. In this case, the liquid layer formed during loading directly turns into a highly turbulized foam, by-passing the bubbling regime. The increase in the pressure drop across the plate with increasing gas velocity at a constant reflux is much sharper than during an ordinary aeration regime, and is expressed in logarithmic coordinates as a straight line right up to the column flooding rate $L = 1650$ kg/m^2·hr (Fig. 148)

The boundaries of regimes may also vary as a result of formation of waves in the liquid, which depend on the column dimensions. Below a certain critical diameter of the plate, the influence of the column walls is so insignificant that the results obtained in columns of diameters smaller than the critical diameter are not reproduced in large-diameter columns.

Hydraulic calculations for plates. The number of slots per plate can be calculated from the equation

$$X = \frac{0.785D^2F_0}{100lb} = \frac{1}{n}\left(\sqrt{n^2-1} + \ldots + \sqrt{n^2-(n^2-1)}\right), \qquad (9.112)$$

where D is the diameter of the column (m); F_0 is the open plate area (m^2); b is the slot width (m); l is the length of a slot along the column diameter (m); and n is the number of slots. The total length l_0 of all the slots is determined from the relation

$$l_0 = \frac{\pi D^2 F_0}{4b}. \qquad (9.113)$$

The distance between successive slots is calculated from the formula

$$\frac{l_0}{n} = c + b, \qquad (9.114)$$

where c is the distance between adjacent slots (m).

The solution of Eq. (9.112) for the number of slots is given in Table 11.

Table 11

Number of Slots for Grid Plates

n	X	n	X	n	X
1	0.000	11	8.042	21	15.915
2	0.866	12	8.832	22	16.713
3	1.688	13	9.620	23	17.500
4	2.498	14	10.411	24	18.287
5	3.296	15	11.200	25	19.074
6	4.093	16	11.982	26	19.860
7	4.887	17	12.776	27	20.648
8	5.679	18	13.564	28	21.432
9	6.471	19	14.352	29	22.219
10	7.257	20	15.138	30	23.005

When applied to grid plates, the pressure drop in the motion of a single-phase flow can be expressed as

$$\Delta P_g = \xi \frac{\delta_p}{d_e} \frac{w^2\gamma}{2g}, \qquad (9.115)$$

where ΔP_g is the pressure drop through a plate; ξ is the friction coefficient calculated for slots or holes; δ_p is the plate thickness (m); d_e is the equivalent diameter of the plate (m); w is the flow velocity in the slots of the plates (m/s), and γ is the specific gravity of the flow.

According to the definition of the factor f of hydrodynamic state of a two-phase system, the pressure drop across a refluxed grid plate is obtained from the dependence

$$\Delta P_{g-l} = \Delta P_g (1 + f). \tag{9.116}$$

The factor f is calculated in accordance with the operating conditions from one of the following equations:

$$f = 90 \left(\frac{\delta_p}{b}\right)^{1.5} \left(\frac{L}{G}\right)^{0.52} \left(\frac{\rho_g}{\rho_l}\right)^{0.26} \tag{9.117}$$

for the bubbling regime,

$$f = 2.5 \times 10^3 \left(\frac{L_{st}}{L}\right)^{1.7} \left(\frac{L}{G}\right)^2 \left(\frac{\rho_g}{\rho_l}\right); \quad L_{st} = 8060 \text{ kg/m}^2\cdot\text{hr} \tag{9.118}$$

for the emulsifying regime,

$$f = \frac{9}{F_0} \left(\frac{D_{st}}{D}\right)^{1.5} \left(\frac{L}{G}\right)^{0.82} \left(\frac{\rho_g}{\rho_l}\right)^{0.41}; \quad D_{st} = 100 \text{ mm} \tag{9.119}$$

for the spray regime,

$$f = 160 \left(\frac{a_{st}}{a}\right)^3 \left(\frac{L}{G}\right)^{0.82} \left(\frac{\rho_g}{\rho_l}\right)^{0.41}; \quad a_{st} = 3 \text{ mm} \tag{9.120}$$

for the point of loading (for plates of diameter smaller than 114 mm) at

$$\left(\frac{L}{G}\right)^2 \left(\frac{\rho_g}{\rho_l}\right) > 10^{-3},$$

and

$$f = 63 \left(\frac{a_{st}}{a}\right)^3 \left(\frac{L}{G}\right)^{0.52} \left(\frac{\rho_g}{\rho_l}\right)^{0.26} \tag{9.121}$$

for the inversion point.

The linear gas velocity at the point of loading for plates of diameter $\geqslant 120$ mm and for smaller-diameter plates at

$$\left(\frac{L}{G}\right)^2 \left(\frac{\rho_g}{\rho_l}\right) < 10^{-3}$$

is calculated from the equation

$$\log\left[\frac{w^2}{gF_0^2 b} \cdot \frac{\rho_g}{\rho_l} \left(\frac{\mu_l}{\mu_w}\right)\right]^{0.16} = 0.70 - 1.75 \left(\frac{L}{G}\right)^{1/4} \left(\frac{\rho_g}{\rho_l}\right)^{1/8}. \tag{9.122}$$

The following equation is used for other regimes:

$$\log\left[\frac{w^2}{gF_0^2 b} \cdot \frac{\rho_g}{\rho_l} \left(\frac{\mu_l}{\mu_w}\right)\right]^{0.16} = 1.0 - 2.45 \left(\frac{L}{G}\right)^{1/4} \left(\frac{\rho_g}{\rho_l}\right)^{1/8}, \tag{9.123}$$

where μ_w is the viscosity of water at 20 °C

9.2. Packed Columns

In their simplest design, packed columns consist of a tube with a supporting grid for packing which is randomly dumped into the column. The most common form of packing is rings whose outer diameter is equal to their height. Such a ratio of the dimensions ensures the most compact packing (maximum number of rings per cubic meter of the packing). The rings can be made of ceramic, porcelain, steel tubes, etc.

In packed columns, a gas, vapour or light liquid (for extraction) moves upwards in counterflow to the downflowing liquid. For small flow velocities, the main contact between the phases takes place on the wetted surface of the packing while for higher velocities the contact takes place in the voids in the packing. In the latter case, it is advisable to use emulsifying packed columns.

9.2.1. Pressure Drop Through Dry Packings

A packing is characterized by its linear dimensions, specific surface area, and the free volume (packing voids) F_v. The most typical packing is in the form of the so-called Raschig rings, which are hol-

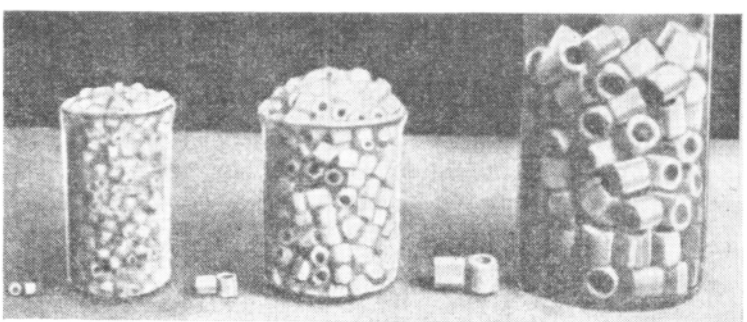

Fig. 149. Raschig ring packing.

low cylinders with a height equal to their outer diameter (Fig. 149). The most widely used Raschig rings have the following dimensions (mm): $8 \times 8 \times 1.5$, $10 \times 10 \times 1.5$, $15 \times 15 \times 2$, $25 \times 25 \times 3$, $35 \times 35 \times 4$, and $50 \times 50 \times 5$. The specific surface area a of a packing is the geometrical surface of the packing elements in 1 m^3 and is expressed in m^2/m^3. Thus, for example, $a = 195$ m^2/m^3 for rings of dimensions $25 \times 25 \times 3$.

The free volume of a packing F_v is the volume of voids in 1 m^3 and is accordingly expressed in m^3/m^3. The free packing volume is

numerically equal to the open area of the packing and can therefore be expressed in m^2/m^2. The free packing volume can be determined by filling a given packing volume with water. The ratio of the volume of water to the volume occupied by the packing will be the free volume. Thus, for example, the value of F_v for rings of size 25 × × 25 × 3 is equal to 0.75 m^3/m^3. The properties of packing rings are listed in Table 12.

Table 12

Physical Characteristic of Raschig Rings

Material	Size, mm	Specific surface a, m^2/m^3	Free volume F_v, m^3/m^3	Pieces per 1 m^3	Mass of packing, kg/m^3
Ceramics	5 × 5 × 1.0	1000	0.62	4000×10^3	900
	8 × 8 × 1.5	550	0.65	1280×10^3	850
	10 × 10 × 1.8	440	0.69	700×10^3	750
	12 × 12 × 1.8	360	0.67	390×10^3	800
	15 × 15 × 2.0	310	0.71	210×10^3	700
	20 × 20 × 2.2	240	0.73	95×10^3	650
	25 × 25 × 3.0	195	0.75	46×10^3	600
	30 × 30 × 3.5	165	0.76	25×10^3	570
	35 × 35 × 4.0	135	0.78	185×10^2	520
	50 × 50 × 5.0	95	0.79	58×10^2	500
	60 × 60 × 6.0	78	0.78	3350	520
	60 × 60 × 8.0	78	0.74	3300	630
	70 × 70 × 7.0	72	0.78	2100	530
	80 × 80 × 8.0	60	0.78	1530	535
	80 × 80 × 10	60	0.77	1530	560
	100 × 100 × 10	44	0.81	750	450
	120 × 120 × 12	35	0.82	450	420
Steel	8 × 8 × 0.3	630	0.90	1500×10^3	750
	10 × 10 × 0.5	500	0.88	770×10^3	950
	12 × 12 × 0.5	400	0.90	440×10^3	800
	15 × 15 × 0.5	350	0.92	230×10^3	660
	18 × 18 × 0.5	300	0.92	120×10^3	640
	25 × 25 × 0.3	220	0.97	52×10^3	240
	35 × 35 × 1.0	160	0.93	19×10^3	570
	50 × 50 × 1.0	100	0.94	6500	430
	50 × 50 × 1.2	100	0.93	6500	520
	70 × 70 × 1.5	75	0.94	2300	440
	80 × 80 × 1.5	65	0.96	1600	350
	100 × 100 × 1.5	48	0.96	750	310

Three different hydrodynamic regimes are observed as a gas (vapour) passes through a dry packing. The hydrodynamic regime of a single-phase flow is determined by the Reynolds number:

$$\mathrm{Re} = \frac{w_g d_e \gamma_g}{F_v \mu_g g} = \frac{4 w_g \gamma_g}{g a \mu_g}, \qquad (9.124)$$

where w_g is the gas velocity in the empty column (m/s).

The velocity, expressed as the ratio w_g/F_v, will characterize the velocity in the packing. Its value is always higher than the empty-column velocity.

The packing in a column causes turbulization to set in sooner than in smooth tubes, and hence the critical state is observed sooner for $Re \simeq 40$. For $Re < 40$, the gas and liquid flow past the packing is not accompanied by the vortex formation, while vortices are formed at $Re > 40$. The pressure drop across a packing layer is calculated from Eq. (3.144) for the pressure drop, in which d is replaced by the so-called equivalent packing diameter d_e (m) obtained from the ratio

$$d_e = \frac{4F_v}{a} \tag{9.125}$$

The generalized dependences between the friction coefficients of a dry packing and the Reynolds number have the following form:

for the region $Re < 80$

$$\xi_{fr} = \frac{400}{Re^{0.85}}; \tag{9.126}$$

for the region $80 < Re < 400$

$$\xi_{fr} = \frac{70}{Re^{0.45}}; \tag{9.127}$$

for the region $Re > 400$

$$\xi_{fr} = \frac{16.5}{Re^{0.2}} \tag{9.128}$$

For $Re > 400$, a joint solution of (3.144) and (9.128) for the turbulent flow of the gas, a situation which is typical of the packed columns, gives the following equation for calculating the pressure drop across a dry packing (mm H_2O):

$$\left(\frac{\Delta P}{l}\right)_g = 0.245 \frac{w_g^{1.8} \gamma_g^{0.8} a^{1.2} \mu_g^{0.2}}{F_v^3}, \tag{9.129}$$

where w_g is the gas velocity in the empty column (m/s).

9.2.2. Hydrodynamics of Two-Phase Systems in Packed Columns

Visual observations. Visual observations of flows in gas-liquid and liquid-liquid systems were carried out in coloured liquids. A transparent glass packing was used for investigating vapour-liquid systems, and no dye was required for visual observations in this case.

A comparison of the phenomena observed in transparent and opaque porcelain packings showed a complete identity of the ob-

served flow patterns, thus confirming that the photographs of flows present a true picture of the phenomena occurring in a packing.

Visual observations of flows in packed columns have shown that for low velocities of gas (vapour) and liquid flows, the downflowing liquid is accumulated at the points of contact of packing elements

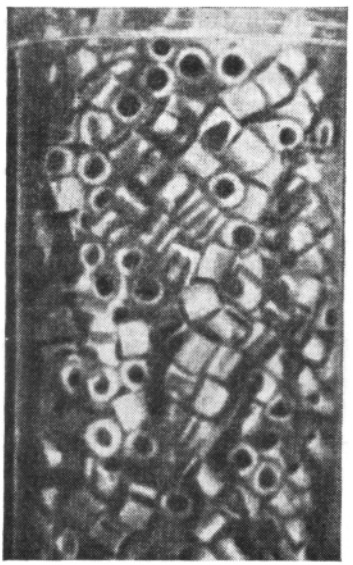

Fig. 150. Jet-film flow in a gas-liquid system. The packing consists of 8 × × 8 × 2-mm porcelain rings; L = = 1000 kg/m²·hr; G = 1300 kg/m²·hr.

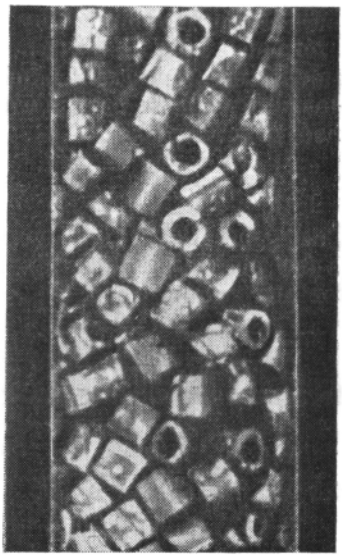

Fig. 151. Jet-film flow in water-benzene system. The packing consists of 8 × 8 × 2-mm porcelain rings; w_c = = 6 m³/m²·hr; w_d = 2 m³/m²·hr.

and on the lower surface of elements of the packing until the formation of drops. Upon attaining a certain size, the drops come in contact with the packing elements below and either flow over them or are detached and fall down. The rising gas or vapour does not cause any visible changes in the flow pattern for the liquid in this case.

As the flow rate in the column increases, the dropwise flow of the liquid is replaced by a jet-film flow. The liquid film wets some elements of the packing, but a considerable part of the surface remains dry. In this case also, the countercurrent flow of the gas or vapour does not alter the flow pattern of the liquid (Fig. 150). In this figure, the liquid film covering individual packing elements is darkened. A similar picture is observed when two immiscible liquids flow in countercurrent through the packing.

Figure 151 shows the photograph of flows when coloured water disperses in benzene. For a liquid-liquid system, the film is formed

by the liquid which has a greater "affinity" to the packing and hence wets it to a greater extent. This phenomenon is more pronounced in rough, unglazed packings. If an unglazed porcelain or ceramic packing is first wetted in water and then immersed in solvent, say, benzene, the water remains sticking to the packing elements. If,

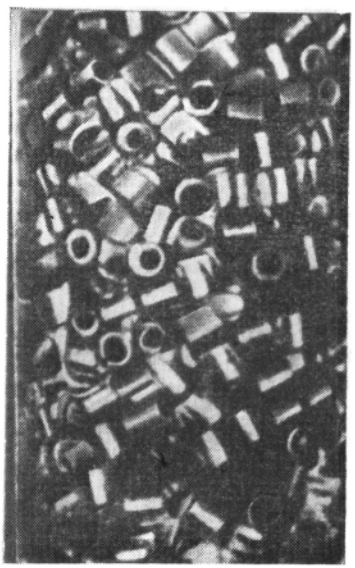

Fig. 152. Turbulent flow in a gas-liquid system. The packing consists of 8 × × 8 × 2-mm porcelain rings; L = = 5000 kg/m²·hr; G = 1300 kg/m²·hr; $(\Delta P/l)_{g-l}$ = 100 mm H_2O.

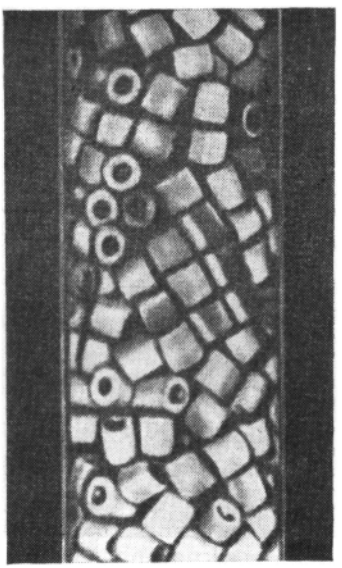

Fig. 153. Turbulent flow in a liquid-liquid system. The packing consists of 8 × 8 × 2-mm porcelain rings; w_c= =6 m³/m²·hr; w_d = 2.5 m³/m²·hr.

on the other hand, the packing is first wetted with benzene and then immersed in water, water rapidly displaces benzene and forms a film similar to the film formed in the first case.

If water is poured into a column with a wettable packing which has first been filled by benzene or some other organic solvent, the water will not flow in the form of drops, but will rather form a film which flows over the surface of the packing. All the voids between packings remain filled with benzene. On the other hand, if benzene (solvent) is introduced into a column filled with water, the solvent flows in the form of drops or a jet through the open cross section along winding paths.

The dark rings in Fig. 152 show the jet-film nature of the disperse-phase flow. As in the case of a gas-liquid system, not all the pack-

ing surface serves as the contact surface. The contact between phases takes place on individual packing elements and no appreciable flow turbulization is observed on the liquid film surface. Upon a further increase in the rate of flow through the column, more and more surface of the packing is covered by a liquid film. An interac-

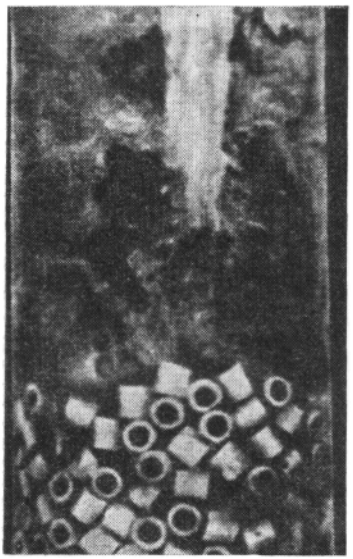

Fig. 154. Emulsifying regime in a gas-liquid system. The packing consists of 8 × 8 × 2-mm porcelain rings; L = = 9500 kg/m²·hr; G = 1300 kg/m²·hr; $(\Delta P/l)_{g-l}$ = 200 mm H_2O.

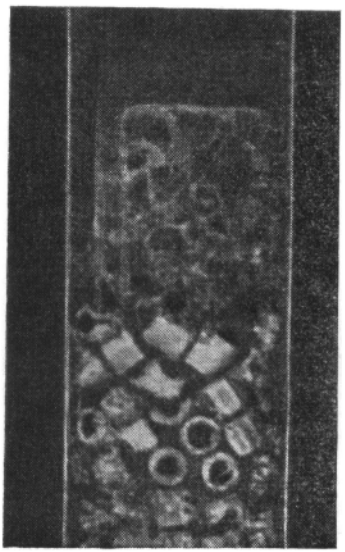

Fig. 155. Emulsifying regime in a liquid-liquid system. The packing consists of 8 × 8 × 2-mm porcelain rings; w_c = 6 m³/m²·hr; w_d = 3 m³/m²·hr.

tion between flows is observed in this case. The film begins to break and its fluctuation and vorticity become noticeable. A considerable part of the packing surface serves as the phase contact area. The photographs of flows shown in Figs. 152 and 153 give an idea of such a regime.

As the flow rate through the column increases, the turbulization of the liquid film becomes more appreciable and an increase in the turbulized liquid is observed in the packing. This liquid then fills the entire free volume of the packing. The liquid filling the packing is in the form of an emulsion, the emulsification is carried out by the flow of gas (vapour) and extends right up to the top of the packing. In the liquid-liquid system, the liquid is emulsified by the disperse phase (Figs. 154 and 155). In the emulsifying regime, the properties of the disperse phase do not affect the flow pattern: iden-

tical pictures are observed for dispersion of water into benzene and vice versa.

Emulsification of the liquid takes place in the narrowest cross section of the packing. For a given packing, the boundary of the emulsified layer is not strictly fixed and may move along the height of the packing depending on the position where the narrowest cross section was formed when the packing was charged into the column. The boundary of the emulsifying layer can be displaced toward the supporting grid by artificially creating a constriction in its vicinity.

For certain constant flow rates through the column, at which the packing begins to be filled by the emulsified liquid, a complete flooding of the column may not occur. The emulsified liquid fills the free packing volume only up to a certain height. In this case, the pressure drop across the packing also becomes constant after attaining a certain value. The regime gets stabilized and equal amounts of liquid enter and leave the packing. An increase in the gas (vapour) velocity leads to an increase in the height of the emulsified layer of the liquid and, if the gas (vapour) is supplied at a constant rate, the regime may become stabilized once again. This phenomenon can be explained by the fact that the accumulation of liquid in the packing increases the absolute pressure in the column and decreases the linear velocity of the gas (vapour).

A decrease in the linear velocity of the gas (vapour) decreases the skin friction drag at the interface, and the ratio of the gravitational force of the downflowing liquid to the force of friction between the gas and the liquid remains constant, corresponding to a definite height of the emulsified liquid column. Thus, the height of the emulsified liquid layer increases until the linear velocity of the gas (vapour) decreases to such an extent that the gravitational force of the downflowing liquid balances the friction force of the gas. Upon an increase in the height of the emulsified liquid layer in the packing, the linear velocity of the gas (vapour) remains constant in spite of an increase in the rate of evaporation or in the gas feed rate. The emulsifying regime for a liquid in a packing, during which the continuous flow of a gas (vapour) becomes discontinuous, is similar to the emulsifying regime of flow in smooth pipes.

When the emulsifying regime sets in over the entire height of the packed column, a further increase in the flow rate of one or both phases in the column leads to an accumulation of the liquid on top of the packing. The height of the liquid layer may attain such a value that a liquid seal, disturbing the normal operation of the packed column, appears on top of the packing. The insignificant increase in the flow velocity in the latter case leads to a rapid increase in the height of the layer and its subsequent expulsion from the column. Thus, four characteristic types of flows can be observed

in packed columns under a countercurrent flow of the phases through the packing (see Fig. 156):

(1) a dropwise flow of the liquid from element to element of the packing, observed for low reflux ratios and low gas velocities; the phases interact at individual points of contact between different packing elements;

(2) a jet-film flow of the liquid, when the liquid covers the packing in the form of a thin film, and a considerable part of the pack-

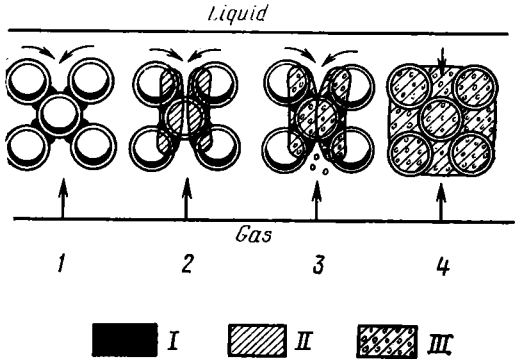

Fig. 156. Flow patterns in a packed column:

1—film regime for a drop-film flow of the liquid; *2*—intermediate regime for jet-film flow; *3*—regime for jet-film flow and turbulization of the liquid; *4*—emulsifying regime; *I*—liquid contact; *II*—liquid film; *III*—liquid film turbulization.

ing surface remains dry; the interaction between phases takes place at the film contact surface and at the points of contact between the liquid and individual elements of the packing;

(3) the liquid flows over the packing in the form of a film, but the fraction of the wetted surface increases considerably and the liquid film itself turbulizes; vortices are sort of impregnated in the film and the phases interact at the surface of the turbulized liquid film;

(4) the liquid occupies the entire free volume in the packing and is whirled; the gas phase is dispersed in the liquid in the form of tiny bubbles which emulsify the liquid.

Pressure drop in two-phase systems. Visual observations and quantitative measurements of the pressure drop in two-phase systems in packed columns have led to the determination of the hydrodynamic regimes and characteristic transition points in a packing (Fig. 157). At small reflux ratios and low gas velocities a film flow pattern sets in during which the liquid flows from one element of the packing to another in the form of drops and films. The interaction between phases takes place on the surface of the wetted packing elements. This regime may terminate at the first point of inflection, called *the gas deceleration point*, when the gas velocity decreases due to a

relatively high velocity of the liquid flowing in countercurrent. The larger the reflux ratio, the higher the position of this point. However, this point is not always observed distinctly. *An intermediate regime* sets in beyond this point, and the liquid flows in the form of a jet-film. The liquid covers the packing in the form of a thin downflowing film and individual jets of liquid. The interaction between phases occurs at the surface of films and the liquid jets (streams), as well as at the points of contact between the liquid and individual packing elements. The film and jets of the liquid decelerate the gas flow and individual vortices are formed in the flow.

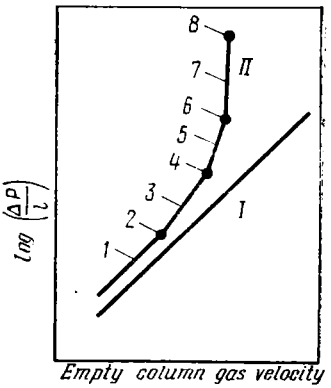

Fig. 157. Hydrodynamic regimes and transition points in packed columns:

I — for dry packing; *II*—for refluxed packing; *1*—film regime; *2*—stagnation point; *3*—intermediate regime; *4*—loading point; *5*—turbulization regime for a two-phase system; *6*—phase-inversion point; *7*—emulsifying regime; *8*—flooding point.

A further increase in the gas velocity causes the loading of the liquid in the packing (*point of loading*), when more and more liquid is held by the gas flowing in the opposite direction. The phases interact at the surface of the turbulized liquid film. Hence, the hydrodynamic regime may be defined as *the regime of turbulization of a two-phase system at the packing surface.*

As the liquid is further accumulated in the packing, the interaction between flows and at the wetted packing surface is transferred to its volume. This is characterized by the appearance of a new hydrodynamic regime, viz. *the emulsifying regime.* This regime corresponds to the region of fully developed turbulence and arises in packed columns beyond *the phase inversion point.* As a result of the development of turbulence in each phase in the packing volume, the interfacial surface also participates in turbulent fluctuations. The concept of continuous and disperse phases loses its meaning in this case, since the phase inversion occurs continuously and the liquid and the gas become disperse or continuous phases at random. In this case, the phases are penetrated by an infinite number of minutest vortices. Under these conditions, there exists a stable hydrodynamic system of "emulsified" liquid. Gaseous vortices which are continuously generated and displaced penetrate the whirled liquid in which the liquid vortices also appear and move continuously. Unlike the first two points (gas deceleration point and the liquid loading point), the point of inversion always manifests itself sharply and can be observed distinctly.

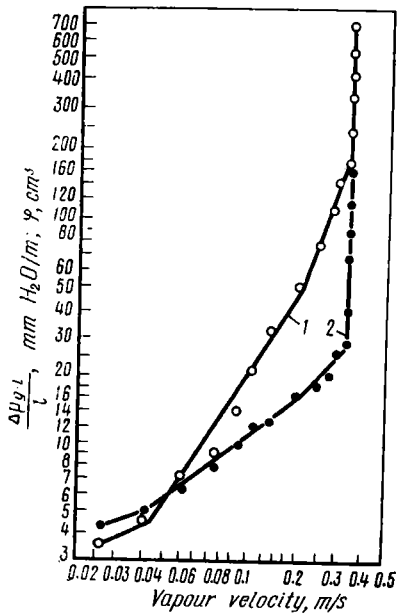

Fig. 158. Holding capacity φ of packing and pressure drop vs. the linear vapour velocity for $L/G = 1$. The packing consists of 5.7 × 5.9 × 0.6-mm ceramic rings; carbon tetrachloride-benzene system:

1—pressure drop; *2*—holding capacity of packing.

The flooding point corresponds to the conditions when the height of the gas-liquid (vapour-liquid) emulsion layer exceeds the height of the packing layer and a liquid layer which is a bubbling layer undergoing intensive mixing is accumulated over the packing.

Holding capacity of the packing. Under conditions close to the flooding of the column, the pressure drop sharply increases due to a rapid accumulation of the reflux in the packing. The efficiency of packed columns is closely related to the amount of the liquid held in the packing. The velocity of a gas does not significantly affect the holding capacity of the packing up to the phase inversion point. Beyond this point, the holding capacity rises sharply. Figure 158 shows the dependence of the pressure drop (curve *1*) and the holding capacity of the packing (curve *2*) on the linear velocity of the vapour. As the point of inversion is reached, a sharp increase in the pressure drop and holding capacity is observed. This corresponds to the vertical straight lines depicting the emulsifying regime. The appearance of characteristic points on the two straight lines for the same vapour velocities indicates that the pressure drop (energy transport) is directly linked to the quantity of the liquid held in the packing.

The analogy between the straight lines ΔP_{g-l} and the holding capacity is observed only beyond the point of inversion and is then preserved during the entire emulsifying regime. This is explained by the fact that during the emulsification of wetted packings, the energy transfer is mainly determined by the quantity of the liquid held in the packing and its state. The holding capacity of a packed column is assumed to consist of two parts: (1) static holding capacity and (2) dynamic holding capacity.

By *static holding capacity* we mean the quantity of the liquid required for wetting the packing. *The dynamic holding capacity* is defined as the difference between the total quantity of the liquid

in the column and the quantity of the liquid spent on wetting the packing. Such a division of the total volume of the liquid in the packing into components is not equivalent to the division of the system into a moving part and a stagnant part, since stagnant zones in a packing can be of different types and cannot be restricted to just one film surrounding a packing element.

Hydrodynamic characteristics of the inversion points for different phase systems. The inversion points are the most characteristic for describing the hydrodynamics of packed columns. As the point of inversion is reached, the mass exchange sharply increases, thus intensifying the mass-transfer processes. Since the creation of a hydrodynamic regime depends on the pressure drop through the packing or on its holding capacity, while the rate of flow through the column is determined by the velocity of the continuous phase, the value of each of these quantities can uniquely define the point of inversion.

The pressure drop for a gas-liquid system and a vapour-liquid system is calculated in accordance with (4.33) with the help of the following equations:

for gas-liquid systems at

$$\Phi = \left(\frac{L}{G}\right)^{1.8} \left(\frac{\rho_g}{\rho_l}\right) \left(\frac{\mu_l}{\mu_g}\right)^{0.2} < 0.5$$

$$\left(\frac{\Delta P}{l}\right)_{g-l} = \left(\frac{\Delta P}{l}\right)_g \left[1 + 8.4 \left(\frac{L}{G}\right)^{0.405} \left(\frac{\rho_g}{\rho_l}\right)^{0.225} \left(\frac{\mu_l}{\mu_g}\right)^{0.045}\right]; \tag{9.130}$$

at $\Phi > 0.5$

$$\left(\frac{\Delta P}{l}\right)_{g-l} = \left(\frac{\Delta P}{l}\right)_g \left[1 + 10 \left(\frac{L}{G}\right)^{0.945} \left(\frac{\rho_g}{\rho_l}\right)^{0.525} \left(\frac{\mu_l}{\mu_g}\right)^{0.105}\right]; \tag{9.131}$$

for vapour-liquid systems

$$\left(\frac{\Delta P}{l}\right)_{g-l} = \left(\frac{\Delta P}{l}\right)_g \left[1 + 5.15 \left(\frac{L}{G}\right)^{0.342} \left(\frac{\rho_g}{\rho_l}\right)^{0.19} \left(\frac{\mu_l}{\mu_g}\right)^{0.038}\right]; \tag{9.132}$$

where $(\Delta P/l)_{g-l}$ and $(\Delta P/l)_g$ are the pressure drops in a two-phase and a single-phase systems at the same gas velocity corresponding to the phase inversion point. The small exponents of the molecular viscosity coefficients in Eqs. (9.130)-(9.132) indicate that the molecular nature of the exchange does not play a significant role.

Above the point of inversion, when the entire packing is filled with the gas-liquid or the vapour-liquid emulsion, the pressure drop can be calculated with the help of the equation

$$\Delta P_e = \Delta P_{inv} + H\gamma_e, \tag{9.133}$$

where ΔP_{inv} is the pressure drop at the point of inversion, defined by Eqs. (9.130)-(9.132); H is the height of the packing layer coinciding with the height of the gas-liquid emulsion layer (m); and γ_e is the fictitious specific gravity of the gas-liquid or the vapour-liquid emulsion, defined by the relation

$$\frac{\gamma_e-\gamma_g}{\gamma_l-\gamma_g}=0.43\left(\frac{L}{G}\right)^{0.325}\left(\frac{\gamma_g}{\gamma_l}\right)^{0.18}\left(\frac{\mu_l}{\mu_g}\right)^{0.0362}, \quad (9.134)$$

where γ_l is the specific gravity of the liquid and γ_g is the specific gravity of the gas.

In packed absorption and rectification columns, *the linear velocity of the gas or vapour flow in a two-phase system* at the point of inversion can be calculated from the equation

$$\log\left[\frac{w_g^2 a}{gF_v^3}\cdot\frac{\gamma_g}{\gamma_l}\left(\frac{\mu_l}{\mu_w}\right)^{0.16}\right]=A-1.75\left(\frac{L}{G}\right)^{1/4}\left(\frac{\gamma_g}{\gamma_l}\right)^{1/8}, \quad (9.135)$$

where w_g is the linear velocity of the gas (vapour), referred to the empty column (m/s); γ_g and γ_l are the specific gravity of the gas and the liquid respectively; μ_l and μ_w are the viscosities of the liquid and water; L and G are the rates of flow of the liquid and the gas respectively (kg/m^2·hr); a is the specific surface area of the packing, m^2/m^3; F_v is the free volume in the packing, m^3/m^2; and $A = 0.022$ for gas-liquid systems and -0.125 for vapour-liquid systems.

The linear velocity of the liquid (continuous phase) in the packed extraction columns at the point of inversion can be calculated from the equation

$$\log\left[\frac{w_c^2 a}{gF_v^2}\cdot\frac{\rho_c}{\Delta\rho}\left(\frac{\mu_c}{\mu_w}\right)^{0.16}\left(\frac{\sigma_{c.d}}{\sigma_{c.a}+\sigma_{d.a}}\right)^{0.2}\right]$$
$$=-0.474-1.75\left(\frac{v_d}{v_c}\right)^{1/4}\left(\frac{\rho_c}{\rho_d}\right)^{1/8}, \quad (9.136)$$

where w_c is the empty-column linear velocity of the continuous-phase liquid (m/s); ρ_c is the density of the liquid constituting the continuous phase, kg/m^3; $\Delta\rho$ is the difference in the densities of the liquids, kg/m^3; μ_c is the viscosity of the liquid constituting the continuous phase; μ_w is the viscosity of water at 20 °C; $\sigma_{c.d}$ is the surface tension at the interface between the continuous and the disperse phases, dyne/cm; $\sigma_{c.a}$ and $\sigma_{d.a}$ are the surface tensions at the continuous phase-air and disperse phase-air interfaces respectively; and v_d and v_c are the volumetric velocities of the disperse and continuous phase respectively, m^3/hr.

For a gas-liquid system, the complex

$$\frac{\sigma_{c.d}}{\sigma_{c.a}+\sigma_{d.a}}$$

is equal to unity and Eq. (9.136) is transformed into Eq. (9.135).

The straight lines corresponding to Eqs. (9.130)-(9.132) and (9.136) for absorption, rectification and extraction columns are compared in Fig. 159. Phase inversion occurs first in a liquid-liquid system, then in a vapour-liquid system and finally in a gas-liquid system. All the three straight lines are parallel, which indicates the validity of the general law governing the phase inversion. Accordingly, Eqs. (9.135) and (9.136) can be reduced to the form

$$y = 1.2e^{-4x}, \tag{9.137}$$

where

$$x = \left(\frac{L}{G}\right)^{1/4}\left(\frac{\rho_l}{\Delta\rho}\right)^{1/8},$$

$$y = \frac{w_l^2 a}{gF_v^2}\cdot\frac{\rho_l}{\Delta\rho}\left(\frac{\mu}{\mu_w}\right)^{0.16}\left(\frac{\sigma_{c.d}}{\sigma_{c.a}+\sigma_{d.a}}\right)^{0.2},$$

w_l is the empty-column linear velocity of the light phase, m/s; ρ_l is the density of the light phase, kg/m³; $\Delta\rho$ is the difference in the densities of the heavy and light phases, kg/m³; μ is the viscosity of the liquid (viscosity of the continuous phase in the case of extraction); μ_w is the viscosity of water at 20 °C; L is the velocity of the heavy phase for gas-liquid and vapour-liquid systems (mass velocity, kg/m²·hr); and for liquid-liquid system (volumetric velocity, m³/m²·hr); and G is the velocity of the lighter phase, kg/m²·hr (m³/m²·hr for extraction).

Since the point of inversion characterizes the instability of the interfaces, it is impossible to establish as to which phase in the packing will be continuous and which one will be disperse. Hence, while calculating the velocities at the inversion point, it is sufficient to determine the linear velocity of one of the phases. The linear velocity of the other phase can be calculated on the basis of the ratio of the flow velocities:

$$w_c = w_l\frac{L}{G}.$$

Effect of pressure on the vapour (gas) velocity at the point of inversion. In accordance with Eq. (9.135), and neglecting the viscosity of the liquid and the ratio

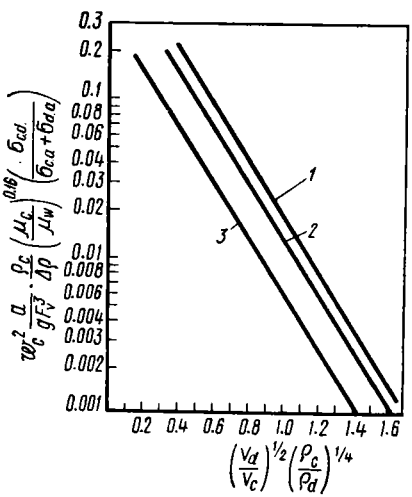

Fig. 159. Comparison of straight lines corresponding to Eqs. (9.130)-(9.132) and (9.136):

1—gas-liquid, Eq. (9.130); *2*—vapour-liquid, Eq. (9.132); *3*—liquid-liquid, Eq. (9.136).

ρ_g/ρ_l in view of their small exponents, we can write

$$\left(\frac{w_g^2}{2g}\right)\frac{\rho_g}{\rho_l} = H_p, \tag{9.138}$$

where H_p is a constant for the given packing.

Denoting $(2gH_p)^{0.5}$ by k_p, we obtain

$$w_g = k_p \sqrt{\frac{\rho_l}{\rho_g}}, \tag{9.139}$$

while for the mass velocity, we get

$$G = w_g\rho_g = k_p\sqrt{\rho_l\rho_g}. \tag{9.140}$$

For pressures P_1 and P_2, we get

$$\frac{w_{1g}}{w_{2l}} = \sqrt{\frac{\rho_{g2}\rho_{l1}}{\rho_{g1}\rho_{l2}}}, \tag{9.141}$$

$$\frac{G_1}{G_2} = \sqrt{\frac{\rho_{g1}\rho_{l1}}{\rho_{g2}\rho_{l2}}}. \tag{9.142}$$

Assuming that the vapour (gas) obeys the law of gaseous state $\rho_g = M_gP/R_gT$, we get

$$w_1 = w_2\left(\frac{P_2}{P_1}\right)^{0.5}\left(\frac{\rho_{l1}}{\rho_{l2}}\right)^{0.5}\left(\frac{T_1}{T_2}\right)^{0.5}\left(\frac{M_{g2}}{M_{g1}}\right)^{0.5}, \tag{9.143}$$

$$G_1 = G_2\left(\frac{P_1}{P_2}\right)^{0.5}\left(\frac{\rho_{l1}}{\rho_{l2}}\right)^{0.5}\left(\frac{T_2}{T_1}\right)^{0.5}\left(\frac{M_{g1}}{M_{g2}}\right)^{0.5}. \tag{9.144}$$

Hence, to a first approximation, it can be assumed that Eqs. (9.143) and (9.144) will be valid for plate columns.

The amount of liquid held in the packing (φ_l, m^3/m^3) for gas-liquid and vapour-liquid systems at the inversion point can be calculated

Table 13

Values of Constants in Eq. (9.145)

System	Constants			
	A_2	m_1	n_1	c_1
Gas-liquid				
at $\left(\frac{L}{G}\right)^{1.8}\left(\frac{\rho_g}{\rho_l}\right)\left(\frac{\mu_l}{\mu_g}\right) < 0.5$	2.03	0.465	0.258	0.0516
at $\left(\frac{L}{G}\right)^{1.8}\left(\frac{\rho_g}{\rho_l}\right)\left(\frac{\mu_l}{\mu_g}\right) > 0.5$	2.15	0.285	0.159	0.0317
Vapour-liquid	1.73	0.486	0.270	0.0540

from the equation

$$\varphi_1 = \frac{F_v}{1 + A_2 \left(\frac{G}{L}\right)^{m_1} \left(\frac{\rho_l}{\rho_g}\right)^{n_1} \left(\frac{\mu_g}{\mu_l}\right)^{c_1}}. \quad (9.145)$$

The values of the constants A_2, m_1, n_1, and c_1 are given in Table 13.

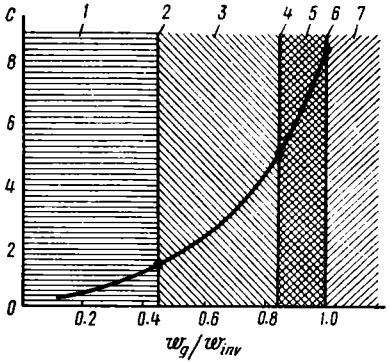

Fig. 160. Variation of coefficient c with $w_g/w_{g_{inv}}$ for different hydrodynamic regimes:

1—film regime; *2*—stagnation point; *3*—intermediate regime; *4*—loading point; *5*—turbulent regime; *6*—inversion point; *7*—emulsifying regime.

Quantitative hydrodynamic characteristics of packed columns below the inversion point. The most important parameters of the hydrodynamic structure of flows in a packed column below the point of inversion are the pressure drop in the packing, the ratio of the gas (vapour) velocity to the velocity at the point of inversion, the duration of stay of flows in the apparatus, the fraction of the effectively used volume of the system, the extent of the longitudinal displacement in the column, the nature and intensity of the exchange processes in the liquid and gas (vapour) phases, etc.

In order to determine the pressure drop in a two-phase flow in a packed column below the inversion point, the following general equation is used:

$$\left(\frac{\Delta P}{l}\right)_{g\text{-}l} = \left(\frac{\Delta P}{l}\right)_g \left[1 + c \left(\frac{L}{G}\right)^{0.405} \left(\frac{\rho_g}{\rho_l}\right)^{0.225} \left(\frac{\mu_l}{\mu_g}\right)^{0.045}\right] \quad (9.146)$$

for $0.13 < L/G < 15$, where $c = 8.4$ is the point of inversion, $c = 8.4\text{-}5.1$ corresponds to the turbulization regime; $c = 5.1$ is the loading point; $c = 5.1\text{-}1.81$ corresponds to the intermediate regime; $c = 1.81$ is the stagnation point; and $c < 1.81$ defines the film-flow regime. For each regime, the coefficient c can be determined from Fig. 160 or the equations at

$$\left(\frac{L}{G}\right)^{1.8} \left(\frac{\rho_g}{\rho_l}\right) \left(\frac{\mu_l}{\mu_g}\right)^{0.2} < 0.5$$

$$\left(\frac{\Delta P}{l}\right)_{g\text{-}l} = \left(\frac{\Delta P}{l}\right)_g \left[1 + c_1 \left(\frac{L}{G}\right)^{0.405} \left(\frac{\rho_g}{\rho_l}\right)^{0.225} \left(\frac{\mu_l}{\mu_g}\right)^{0.045}\right],$$

where $c_1 = \exp\left[3.0 \frac{w_g}{w_{g_{inv}}} - 0.853\right] - 0.175;$ (9.147)

$$\text{at } \left(\frac{L}{G}\right)^{1.8}\left(\frac{\rho_g}{\rho_l}\right)\left(\frac{\mu_l}{\mu_g}\right)^{0.2} > 0.5$$

$$\left(\frac{\Delta P}{l}\right)_{g\text{-}l} = \left(\frac{\Delta P}{l}\right)_g\left[1 + c_2\left(\frac{L}{G}\right)^{0.945}\left(\frac{\rho_g}{\rho_l}\right)^{0.525}\left(\frac{\mu_l}{\mu_g}\right)^{0.105}\right],$$

where $c_2 = \exp\left[3.0\frac{w_g}{w_{g_{inv}}} - 0.853\right] + 1.39.$

Accordingly, we get the following values for the hydrodynamic factor of state for a two-phase system:

$$f = \frac{\left(\frac{\Delta P}{l}\right)_{g\text{-}l} - \left(\frac{\Delta P}{l}\right)_g}{\left(\frac{\Delta P}{l}\right)_g} = c\left(\frac{L}{G}\right)^{0.405}\left(\frac{\rho_g}{\rho_l}\right)^{0.225}\left(\frac{\mu_l}{\mu_g}\right)^{0.045}. \quad (9.148)$$

If for the reference velocity we take the velocity at the point of inversion ($w_{g_{inv}}$) which can be uniquely determined for a gas-liquid system from the equation

$$\log\left[w^2_{g_{inv}}\frac{a}{gF_v^3}\cdot\frac{\rho_g}{\rho_l}\left(\frac{\mu_l}{\mu_w}\right)^{0.16}\right] = 0.022 - 1.75\left(\frac{G}{L}\right)^{1/4}\left(\frac{\rho_g}{\rho_l}\right)^{1/8}, \quad (9.149)$$

we obtain the following equations for various column regimes on the basis of the law of corresponding states and in accordance with Fig. 160:

for the turbulence regime

$$\frac{w_g}{w_{g_{inv}}} = 1 - 0.85, \quad (9.150)$$

for the point of loading

$$\frac{w_g}{w_{g_{inv}}} = 0.85, \quad (9.151)$$

for the intermediate regime

$$\frac{w_g}{w_{g_{inv}}} = 0.85 - 0.45, \quad (9.152)$$

for the deceleration point

$$\frac{w_g}{w_{g_{inv}}} = 0.45, \text{ and} \quad (9.153)$$

for the film-flow regime

$$\frac{w_g}{w_{g_{inv}}} < 0.45. \quad (9.154)$$

Having calculated $w_{g_{inv}}$ from Eq. (9.149), we can determine the value of w_g from Eqs. (9.150)-(9.154) and hence the regime under which a given column is operating.

The dependence of static holding capacity on the hydrodynamic regimes in the apparatus is extremal in nature (Fig. 161).

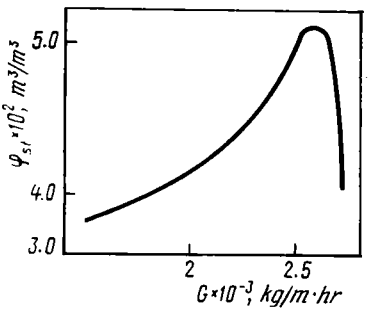

Fig. 161. Static holding capacity φ vs. the gas flow rate through the column.

Static holding capacity is calculated from the equations:

for $0.3 < w_g/w_{g_{inv}} < 0.85$

$$\varphi_{st} = 6.44 \times 10^{-2} \left(\frac{w_g - 0.3 w_{g_{inv}}}{w_{g_{inv}}} \right) + \frac{0.185}{d_e G^{1.042}}, \quad (9.155)$$

for $w_g/w_{g_{inv}} > 0.85$

$$\varphi_{st} = \frac{0.258 \times 10^{-3}}{d_e} - 0.17 \left(\frac{w_g - 0.82 w_{g_{inv}}}{w_{g_{inv}}} \right). \quad (9.156)$$

The dynamic holding capacity φ_{dyn} for a two-phase system can be calculated from the following equations:

for $w_g/w_{g_{inv}} < 0.85$,

$$\frac{\Delta\varphi_{dyn}}{\varphi_{dyn_0}} = 13.2 \left(\frac{\Delta P}{\gamma_l l} \right)^{1.92}; \quad (9.157)$$

for $w_g/w_{g_{inv}} > 0.85$,

$$\frac{\Delta\varphi_{dyn}}{\varphi_{dyn_0}} = 7.12 \times 10^3 \left(\frac{\Delta P}{\gamma_l l} \right)^{6.35}, \quad (9.158)$$

where φ_{dyn_0} is the dynamic holding capacity with no gas flow ($G = 0$), and can be calculated from the equations:

for Gallileo number $Ga = \frac{d_p^3 g \rho^2}{\mu^2} \leqslant 4 \times 10^4$,

$$\varphi_{dyn_0} = 0.183 \left(\frac{d_p L \rho}{\mu} \right)^{0.74} \left(\frac{d_p^3 g \rho^2}{\mu^2} \right)^{-0.256} a d_p; \quad (9.159)$$

for $Ga = \frac{d_p^3 g \rho^2}{\mu^2} \geqslant 4 \times 10^4$,

$$\varphi_{dyn_0} = 3 \left(\frac{d_p L \rho}{\mu} \right)^{0.74} \left(\frac{d_p^3 g \rho^2}{\mu^2} \right)^{-0.52} a d_p, \quad (9.160)$$

Table 14

Holding Capacity of Extraction Packed Columns

Relationship	Note
$\varphi = \dfrac{w_d}{F_v w_0 - w_c/(1-\varphi)}$	For $\varphi < 0.15$
$w_d + \dfrac{\varphi}{1-\varphi} w_c = F_v w_0 \varphi (1-\varphi)$	For φ below the inversion point
The value of w_0 in the first two equations is	Approximate relationship
$\dfrac{w_0 \mu_c}{\sigma} = c \left(\dfrac{\Delta\rho\sigma^3}{\mu_c^4 g}\right)\left(\dfrac{\rho_c}{\Delta\rho}\right)^{-0.6}$ $\times \left[\dfrac{a}{F_v}\left(\dfrac{\sigma}{\Delta\rho g}\right)^{1/2}\right]^{-0.65}\left[\dfrac{1}{D}\left(\dfrac{\sigma}{\Delta\rho g}\right)^{1/2}\right]^{0.26}$	
$15\left[\left(\dfrac{\sigma}{\Delta\rho g}\right)^{1/2}\left(\dfrac{w_0\rho_c}{\mu_c}\right)\right]^{-1/2} + c\left[\left(\dfrac{\sigma}{\Delta\rho g}\right)^{1/2}\dfrac{a}{F_v}\right]^2$ $\times \left[1 - e^{-0.65\left(\frac{aD}{4F_v} - 1\right)}\right] = \dfrac{(\sigma/\Delta\rho g)^{1/2}}{\rho_c w_0^2}$	Relationship based on the additivity of pressure drops
$\left(\dfrac{\rho_d w_t w_0}{\Delta\rho g}\right)\left(\dfrac{w_0}{w_t}\right)^{1.35} + 0.22\left(\dfrac{\sigma}{\Delta\rho g}\right)^{1/2} = 0.239 c d_e^n$	Relationship based on the collision theory
$\dfrac{\varphi^3}{w_d^{1.5}} = A' \dfrac{w_c^n}{w_d^{1.5}}\left(\dfrac{\varphi}{1-\varphi}\right)^3 + B'$	For φ below the inversion point (A', B', n are constants)
$\left[\left(\dfrac{w_d}{w_c}\right) + \dfrac{\varphi}{1-\varphi}\right]\left(\dfrac{w_c^2 a}{g F_v^3} \cdot \dfrac{\rho_c}{\Delta\rho}\right)^{1/2} = 0.683\varphi(1-\varphi)$	For φ below the inversion point, Raschig rings, Lessing rings, Berl saddles
$\left[\left(\dfrac{w_d}{w_c}\right) + \dfrac{\varphi}{1-\varphi}\right]\left(\dfrac{w_c^2 a}{g F_v^3} \cdot \dfrac{\rho_c}{\Delta\rho}\right)^{1/2} = 0.973\varphi(1-\varphi)$	For φ below the inversion point. Packing made up of spherical particles
$\varphi_f = 0.753\left(\dfrac{w_d^2 a}{g F_v^3} \cdot \dfrac{\rho_d}{\Delta\rho}\right)^{0.111}$	For φ at the inversion point, Raschig rings, Lessing rings, Berl saddles and spherical particles
$\varphi_f \sqrt{1-\varphi_f} = c\left(\dfrac{w_d^2 a}{g F_v^3} \cdot \dfrac{\rho_c}{\Delta\rho}\right)^n$	For φ at the inversion point

Table 14 (continued)

Relationship	Note
$\left(\frac{w_d}{w_c}+\frac{\varphi}{1-\varphi}\right)\left(\frac{w_c^2 a}{gF_v^3}\cdot\frac{\rho_c}{\Delta\rho}\right)^{1/2}=0.683\varphi(1-\varphi)$	For φ below the inversion point, mutually saturated binary systems in the absence of mass transfer
$\left(\frac{w_d}{w_c}+\frac{\varphi}{1-\varphi}\right)\left(\frac{w_c^2 a}{gF_v^3}\cdot\frac{\rho_c}{\Delta\rho}\right)^{1/2}=0.574\varphi(1-\varphi)$	For φ below the inversion point, mutually saturated systems with mass transfer from the continuous phase into the disperse one
$\left(\frac{w_d}{w_c}+\frac{\varphi}{1-\varphi}\right)\left(\frac{w_c^2 a}{gF_v^3}\cdot\frac{\rho_c}{\Delta\rho}\right)^{1/2}=0.791\varphi(1-\varphi)$	For φ below the inversion point, mutually saturated systems with mass transfer from the disperse phase into the continuous one

Constants in Equations

Packing	c	n
Raschig rings	0.520	0.083
Lessing rings	0.466	0.074
Berl saddles	0.540	0.092
Balls	0.464	0.076

Notation

D is the apparatus diameter, cm; d_e is the equivalent packing diameter, cm; w_0 the characteristic droplet velocity, cm/s; and w_t the free rising velocity of droplets, cm/s.

where d_p is the packing diameter, m; ρ is the density; μ the viscosity; L is the reflux rate, $m^3/m^2 \cdot s$; and a is the free surface of the packing, m^{-1}.

The holding capacity for liquid-liquid systems in packed columns is given in Table 14.

9.2.3. Axial Dispersion in a Packing

The axial dispersion in single-phase flows is characterized by the following: (1) the longitudinal diffusion coefficient in gas systems is lower than in liquid systems; (2) the axial dispersion in a packing exceeds the radial dispersion; (3) the lower the velocity of the li-

quid, the stronger the axial dispersion in a liquid phase; and (4) the axial dispersion coefficient is independent of viscosity.

The axial dispersion of the gas flow in a two-phase system can be described by the following equation:

$$Pe_G = 2.4\,(Re_G)^{-0.2} \times 10^{-\left(0.013-0.88\frac{d}{D}\right)Re_L}, \qquad (9.161)$$

$$Pe_G = 3.4\,(Re_G)^{-0.67} \times 10^{-0.0026\,Re_L}, \qquad (9.162)$$

where d is the diameter of the Raschig rings; D is the diameter of the column; Re_L and Re_G are the Reynolds numbers for liquid and gas phases, respectively.

Equation (9.161) is valid for $D = 100$ mm and for values of d between 6 and 12 mm, while Eq. (9.162) holds for $D = 100$ mm and $d = 12$ mm, and for Berl saddles of diameter 12 mm.

The following empirical relations have been proposed for determining the coefficient D_L of axial dispersion in the liquid phase of a two-phase system:

$$\frac{D_L}{\nu} = 0.527\left(\frac{dw_l}{\nu}\right)\left(\frac{d^3g}{\nu^2}\right)^{1/3}, \qquad (9.163)$$

$$Pe_L = 1.425\,Ga^{-0.333}\,Re_L^{0.777}, \qquad (9.164)$$

$$Pe_L = 7.58 \times 10^{-3}\left(\frac{dL}{\mu}\right)^{0.703}, \qquad (9.165)$$

where ν is the kinematic viscosity; d is the packing diameter; w_l is the average flow velocity of the liquid, and

$$Ga = \frac{d^3g\rho^2}{\mu^2}.$$

The following empirical dependences have been obtained for determining the axial dispersion in a liquid for a vapour-liquid system

for $w_g/w_{g_{inv}} \leqslant 0.45$:

$$Pe_L = 16.8\,(dL)^{0.561}, \qquad (9.166)$$

for $w_g/w_{g_{inv}} \geqslant 0.45$

$$Pe_L = 26.5\,(dL)^{0.561}\left(\frac{w_g}{w_{g_{inv}} - w_g}\right)^{0.436}. \qquad (9.167)$$

Calculations for axial dispersion taking into account the effective and stagnation zones, carried out by using source- and -sink model and with the help of the direct hydrodynamic method for determining the response curves, have shown that the axial dispersion coefficient increases with the liquid flow rate and decreases with an increasing gas flow rate. The flow rate profiles level out in intensive hydrodynamic regimes, thus decreasing the axial disper-

sion coefficient. A similar dependence is also observed for the liquid flow rate. The Peclet number decreases with an increase in the gas and liquid flow rates. In the flow-through zones of the apparatus, the dependence of the Peclet number on the gas flow rate and the reflux rate in the column assumes an extremal character. The axial dispersion coefficients determined by the indicator method are much higher (several times more in some flow regimes) than the values obtained directly. The difference between the values of the coefficients vanishes in the emulsifying regime owing to the absence of stagnation zones.

The Peclet numbers for the liquid phase increase with the density of the liquid, and decrease with increasing viscosity of the liquid. An analysis of the experimental data give the following dependences for the Peclet number in the flow-through zone of the apparatus:

$$\text{at } 0.86\left(\frac{w_g}{w_{g_{inv}}}\right)\left(\frac{d_p L\rho}{\mu}\right)^{0.107} \leqslant 0.85$$

$$Pe_L = 4.75\left(\frac{w_g}{w_{g_{inv}}}\right)^{1.4}\left(\frac{d_p L\rho}{\mu}\right)^{0.15}\left(\frac{d_p^3 g\rho^2}{\mu^2}\right)^{-0.17}; \quad (9.168)$$

$$\text{at } 0.86\left(\frac{w_g}{w_{g_{inv}}}\right)\left(\frac{d_p L\rho}{\mu}\right)^{0.107} \geqslant 0.85$$

$$Pe_L = 2.25 \times 10^{-3}\left(\frac{w_g}{w_{g_{inv}}}\right)^{-3.3}\left(\frac{d_p L\rho}{\mu}\right)^{-0.353}\left(\frac{d_p^3 g\rho^2}{\mu^2}\right)^{0.29}; \quad (9.169)$$

where

$$Pe_L = \frac{w_l d_p}{D_L}$$

and d_p is the diameter of a packing element.

9.2.4. Scaling of Packed Columns

Since at the point of inversion the distribution of the vapour and the liquid over the column cross section is the most uniform and unique, and the structure of flows corresponds to the plug-flow model, it becomes possible to scale a packed column. The variation of the holding capacity with respect to the liquid, the pressure drop, and HETP is the same in the region of the inversion point. The entire height of the packed column is sort of broken into individual cells in which ideal mixing takes place, but between which there is no mixing.

In the analysis of the same systems in a model and in a large-scale equipment for the same slope of the equilibrium curve, the scaling of packed columns at the point of inversion involves the fulfilment

of the following conditions:

$$\frac{h_1}{h_2} = \left(\frac{a_2}{a_1}\right)^{1.3} \left(\frac{F_{v_1}}{F_{v_2}}\right)^{1.3} \tag{9.170}$$

for the height of the packing layer,

$$\frac{D_1}{D_2} = \left(\frac{a_1}{a_2}\right)^{0.25} \left(\frac{F_{v_2}}{F_{v_1}}\right)^{0.75} \tag{9.171}$$

for the diameters of the columns, and

$$\frac{\Delta P_1}{\Delta P_2} = \left(\frac{a_1}{a_2}\right)^{0.3} \left(\frac{F_{v_2}}{F_{v_1}}\right)^{0.3} \tag{9.172}$$

for the pressure drop.

Table 15 shows the relation between the equivalent heights of the packing, column diameters and the pressure drop for different randomly dumped ceramic rings.

Table 15

Scaling of Packed Columns*

Raschig rings size, mm	Specific surface a, m^2/m^3	Free volume F_v, m^3/m^3	Equivalent height ratio h_1/h_2, 25×25	Diameter ratio D_1/D_2, 25×25	Pressure drop ratio $\Delta P_1/\Delta P_2$, 25×25
10×10×1.5	440	0.70	0.316	1.265	1.280
15×15×2	330	0.70	0.503	1.135	1.180
25×25×3	200	0.74	1.000	1.000	1.000
35×35×4	140	0.78	1.740	0.872	0.835
50×50×5	90	0.785	3.100	0.770	0.775

* The comparison is made with 25×25×3-mm Raschig rings.

9.2.5. Columns with Flooded Packing (Emulsifying Columns)

One of the main reasons behind the low efficiency of packed columns operating under ordinary hydrodynamic conditions is the non-uniform distribution of the liquid phase over the surface of the packing. The liquid flowing down forms channels which cause a sharp decrease in the interfacial area, the thickness of the layer of liquid flowing down increases and the heat- and mass-transfer deteriorate. A uniform distribution of the liquid over the packing becomes especially difficult with increasing column diameter. Consequently, the performance of large-diameter packed columns below the point of inversion is worse than that of small-diameter

columns, and their height equivalent to one theoretical plate is also small.

The emulsifying regime, which is the most favourable regime for the operation of packed columns, exists in a comparatively narrow range of vapour- and liquid-flow velocities. The upper limit is set by the flooding of the column, i.e. by an accumulation of the liquid above the packing, while the disappearance of the gas-liquid emulsion serves as the lower limit. Since the HETP of a column increases abruptly as a result of a transition to the emulsifying regime, the conventional packed columns operate in this regime under one constant velocity of the flows. Therefore, the emulsifying regime must be stabilized.

A transition from the liquid phase into a continuous phase and a vapour (gas) phase into a disperse phase, as well as the creation of emulsifying regime in packed columns is also possible by filling the free volume of the packing and by organizing the process in such a way that the amount of liquid extracted in a unit time from the lower part of the column is exactly equal to the amount of reflux being supplied to its upper part. In this case, the gas flow in the packing is broken into jets which penetrate the liquid. Figures 162 and 163 show schematic lay-outs of such a system. The extraction of the liquid through the lower part of the column is possible only through a U-shaped overflow tube which, together with the column, serves as the communicating vessel. The overflow tube is fitted with valves used to maintain the level of the gas-liquid mixture at the same height as the packing layer under all operating conditions. Such an organization of the column operation ensures a distribution of the gas and liquid phases identical to the distribution of flows in an ordinary packed column operating in emulsifying regime. In columns with flooded packing, the liquid is retained in the packing

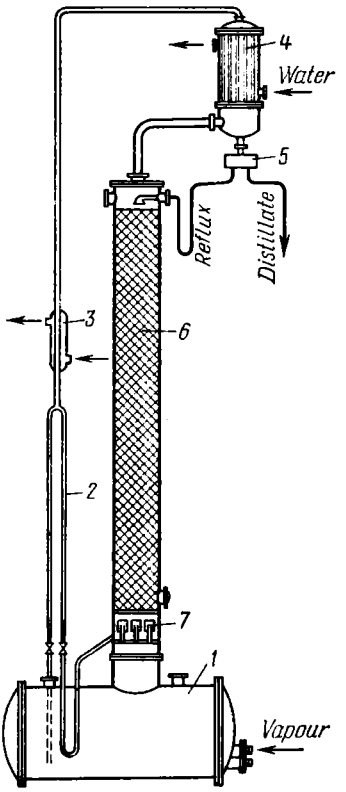

Fig. 162. Schematic diagram of a batch-type emulsifying column:

1—still; *2*—overflow pipe; *3*—cooler; *4*—condenser; *5*—regulator; *6*—packed column; *7*—vapour distributor.

for different vapour velocities varying from the lowest to the maximum admissible values.

It is not necessary to construct devices for the redistribution of the liquid and the gas in view of the fact that in the emulsifying regime the phases are automatically distributed uniformly over the column

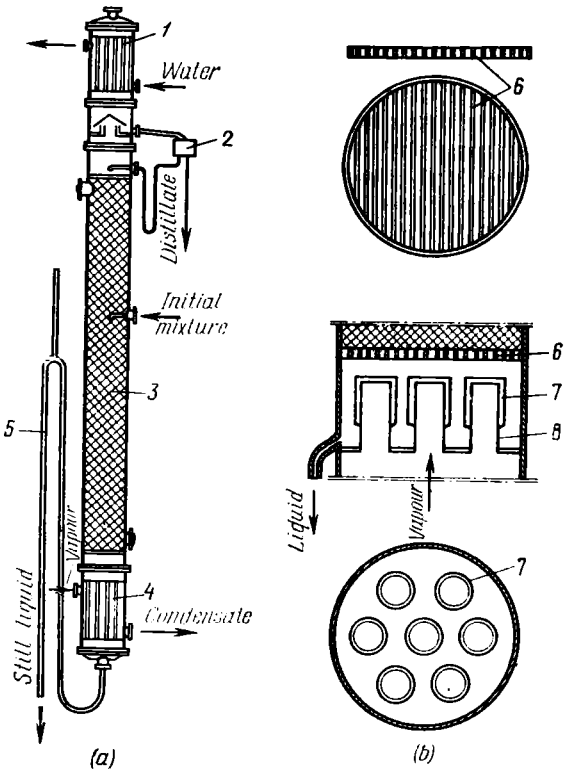

Fig. 163. Continuous-action emulsifying column (*a*) and its parts (*b*):

1—condenser; *2*—reflux regulator; *3*—packed column; *4*—boiler; *5*—overflow pipe; *6*—support grid plate for packing; *7*—caps; *8*—risers.

cross section. The division of the packing into layers with a separating volume between them is not allowed from columns operating in the emulsifying regime. During operation, the separating volume gets filled with the liquid which then mixes with the vapour, the circulation flows cover the boundary layers of the packing and liquids of different concentrations mix, thus violating the separation operation of the packing at a certain stage.

A large open area, equal to or greater than the open area of the packing, is the requirement imposed on the supporting grid in columns with flooded packing. This is necessary because these columns

must operate at maximum flow rates of the liquid and vapour, and an insufficient open area of the supporting grid may hamper the normal operation of the column. Hence, it is inadvisable to use supporting grids obtained by drilling holes in flat plates. It is expedient to use grid bars for this purpose. An inlet for the vapour and an outlet for the liquid should be provided below the supporting grid in the column. In large-diameter columns, vapour is introduced into the column through several bubble-caps in order to ensure a uniform distribution of the vapour as it enters the column packing.

The removal of the liquid from the column and its supply to the still are ensured by using a U-shaped overflow tube fitted with a hydraulic seal at the lower part and a device for preventing the formation of a siphon in the upper part. For columns operating at atmospheric pressure, the upper part of the overflow tube may be in contact with the surroundings. The tube connecting the overflowing liquid with the atmosphere is provided with a small cooler since the liquid in the overflow tube is at the boiling point of the still liquid. For operation under vacuum, the upper part of the overflow tube must be in contact with a region where the pressure is equal to that in the upper part of the column.

Hydrodynamic regularities. No abrupt transitions to various hydrodynamic regimes are possible in columns with flooded packing (Figs. 164 and 165). The pressure drop and the volumetric rate of the gas flow vary smoothly. The open area of the column occupied by the liquid is practically independent of the liquid flow rate. The velocity of the gas bubbles rising through the column is about three orders of magnitude higher than the linear velocity of the descending liquid. The ascending gas causes the circulation of the liquid in the column, as a result of which the descending flow actually exceeds the liquid fed into the column. If the packing is wetted, the ascending and descending liquid flows occur in different ways: the liquid descends along the column walls and ascends through the voids in the packing. The pressure drop due to the liquid column decreases in view of the fact that the skin friction drag of the descending liquid is directed upwards. For high flow rates of the liquid, the pressure drop through the column may be smaller than the weight of the liquid retained in the column.

Thus, the pressure drop ΔP_{g-l} in a column with flooded packing can be calculated from the equation

$$\frac{\Delta P_{g\text{-}l}}{l} = \frac{\Delta P^*_{fr}}{l} - \frac{\Delta P_{fr.l}}{l} + (1-\varphi)\,\gamma_l, \qquad (9.173)$$

where $\Delta P_{fr.l}/l$ are the friction losses due to the descending liquid flow (this quantity is equal to zero in a batch-type column); $\Delta P^*_{fr}/l$ is the friction loss in a batch-type column; and φ is the gas-content of the layer.

At a constant reflux, the pressure drop through a column can depend on the gas flow rate in three different ways (Fig. 166*a*). For columns filled with a coarse packing the third term in Eq. (9.173) determines the pressure drop (Fig. 166*a*). For columns with a fine

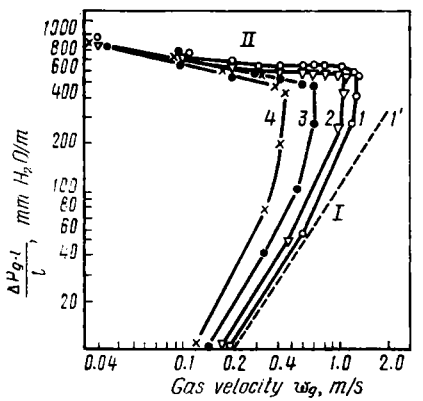

Fig. 164. Pressure drop across unflooded (*I*) and flooded (*II*) packed columns. The packing consists of 10 × × 10-mm porcelain Raschig rings:

1'—dry packing; *1*—L = 1.04 m³/m²·hr; *2*—L = 1.875 m³/m²·hr; *3*—L=7.08 m³/m²·hr; *4*—L = 16.25 m³/m²·hr.

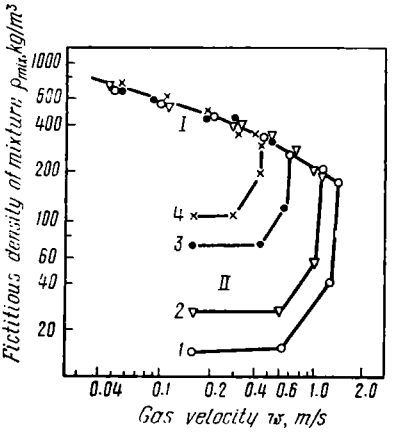

Fig. 165. Holding capacity of flooded (*I*) and unflooded (*II*) columns. The packing consists of 10 × 10-mm porcelain Raschig rings:

1-4 the same as in Fig. 164.

packing and for low liquid flow rates, the friction losses ΔP^*_{fr} in a batch-type column sharply rise with increasing gas flow rates

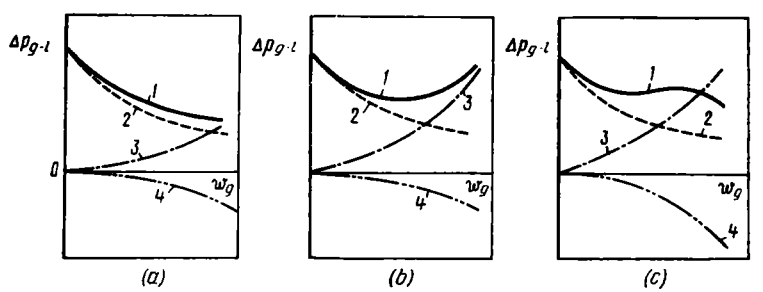

Fig. 166. The pressure drop through a column vs. the gas velocity:

1—ΔP_{g-} ; *2*—$(1-\varphi)\gamma_l$; *3*—ΔP^*_{fr}; *4*—$\Delta P_{fr.l}$.

(the overall pressure ΔP_{g-l} passes through a minimum, see Fig. 166*b*). An increase in the liquid flow rate under these conditions gives two extremal points (curve *1* in Fig. 166*c*).

The following is the sequence of hydrodynamic calculations for a column with flooded packing: (a) the fraction of the column cross section occupied by the liquid is calculated from the equation

$$1-\varphi = 0.766 \cdot A \exp\left(36.3 d_e - 1.38 w_g e^{-54.5 d_e}\right), \qquad (9.174)$$

where

$$A = \left(\frac{\gamma_l}{\gamma_g}\right)^{-0.094} \left(\frac{\mu_l}{\mu_g}\right)^{0.072} (\mathrm{We}^{0.058}),$$

We $= \sigma/(\gamma_l - \gamma_g)\, d_e^2$ being the Weber number.

(b) The velocity $w^*_{g_{inv}}$ at the point of inversion is calculated for $(L/G) = 0$ (batch-type column) and for a given value of L/G from the equation

$$\log\left[\frac{w^2_{g_{inv}} a \gamma_g}{F_v^2 g \gamma_l} \mu_l^{0.16}\right] = 0.022 - 1.75 \left(\frac{L}{G}\right)^{1/4} \left(\frac{\gamma_g}{\gamma_l}\right)^{1/8}. \qquad (9.175)$$

(c) The friction losses ΔP^*_{fr} in a batch-type column are calculated

$$\Delta P^*_{fr} = 0.814 w_g^{0.28} d_e^{-0.62} \mu_l^{0.05} \rho_l^{0.75} l \qquad (9.176)$$

for $(w_g/w^*_{g_{inv}}) \leqslant 0.25$,

$$\Delta P^*_{fr} = 0.286 w_g^{0.75} d_e^{-1.00} \mu_l^{0.05} \rho_l^{0.69} l \qquad (9.177)$$

for $(w_g/w^*_{g_{inv}}) > 0.25$.

(d) The friction losses due to the descending liquid $\Delta P_{fr.l}$ are calculated:

$$\Delta P_{fr.l} = 45.2 w_l d_e^{-1} (1-\varphi)^{-1} \rho_l^{2/3} \mu_l^{1/3} l \qquad (9.178)$$

for $(w_g/w_{g_{inv}}) \leqslant 0.75$,

$$\Delta P_{fr.l} = 0.022 w_l^{0.96} w_g^{1.75} d_e^{-2.85} (1-\varphi)^{-1} \rho_l^{1/3} \mu_l^{1/6} l \qquad (9.179)$$

for $(w_g/w_{g_{inv}}) > 0.75$.

(e) The total hydrodynamic pressure drop in the column is calculated with the help of Eq. (9.173).

Relaxation self-oscillations may set in in columns with flooded packing. Such a situation arises when the gas bubbles rising to the surface due to the difference in densities cannot ensure the passage of the required quantity of gas. The gas is held up in the lower part of the column and, together with small gas bubbles, forms large gas aggregates which do not break up in the packing and rise through the column with a velocity exceeding the velocity with which small bubbles rise to the surface. The formation of the gas aggregates and their discharge from the foam layer leads to fluctuations and the liquid is thrown above the packing layer. The fluctuation frequencies and amplitudes depend but weakly on

the physical properties of the liquids. The fluctuation amplitude is the larger, the higher the packing layer. Moreover, their dependence on the liquid flow rate is quite weak. The frequency and amplitude of fluctuations decrease with increasing size of the packing elements. The self-oscillations generated by the column are filtered by the column overflow and the low frequency passes into the still in the form of discharge fluctuations. Induced oscillations through thermal channels are created in the case of rectification. The amplitude of fluctuations attains its maximum value at the overflow where the self-oscillations in the column are in resonance with the eigenfrequency of overflow.

As the gas flow rate increases, self-oscillations appear in the column after the motion of the gas bubbles due to a difference in specific gravities ceases and the amplitude of these oscillations attains its maximum value at a relative velocity $w_g/w_{g_{inv}} \simeq 0.6\text{-}0.8$. As the velocity approaches the value corresponding to the point of inversion, the oscillations are completely damped.

The following empirical relations can be used for determining the axial dispersion coefficient in columns with flooded packing

$$Pe_L = 180 \left(\frac{F_v}{F_0}\right)^{5.7} \left(\frac{L}{L_{st}}\right)^{0.5} \left(\frac{w_g}{w_g^*}\right)^{2.8} \qquad (9.180)$$

for $0.5 < \frac{w_g}{w_{g_{inv}}} < 0.75$,

$$Pe_L = 248 \left(\frac{F_v}{F_0}\right)^{5.7} \left(\frac{L}{L_{st}}\right)^{0.5} \left(\frac{w_g}{w_{g_{inv}}}\right)^{4.0} \qquad (9.181)$$

for $\frac{w_g}{w_{g_{inv}}} > 0.75$,

where $Pe_L = (w_l l/D_L)$; w_l is the linear velocity of the liquid phase, m/hr; D_L is the axial dispersion coefficient, m^2/hr; l is the height of the packing; F_v/F_0 is the free volume in the packing, referred to the free volume in 15 × 15-mm packing; L/L_{st} is reflux rate referred to the standard flow rate for the liquid, taken equal to 1000 $kg/m^2 \cdot hr$; and $w_g/w_{g_{inv}}$ is the linear gas velocity referred to the velocity at the phase inversion point.

The axial dispersion coefficient is independent of the liquid flow rate and decreases with increasing gas velocity due to an equalization of the velocity field over the column cross section and a decrease in the fraction of stagnation zones.

Mass transfer in columns with flooded packing. A comparison between the height equivalent to one theoretical plate (HETP) of a column with flooded packing and the HETP of a conventional column shows that for vapour velocities corresponding to the point of inversion, the two values are identical (Fig. 167). The HETP for columns with flooded packing increases uniformly with the vapour velocity.

The efficiency of flooded-packing rectifying columns for various binary systems and Raschig rings of diameter 6-25 mm can be calculated from the equation

$$\mathrm{HTU}_{0y} = (5.6 + 8.5d_e)\,(w_v/w_{v_{inv}})^{-0.88}\,\mathrm{Pr}_v^{0.66}, \qquad (9.182)$$

where $(\mathrm{HTU})_{0y}$ is the height-transfer unit for the vapour phase cm;

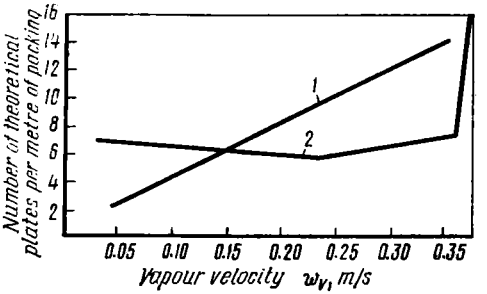

Fig. 167. HETP of rectifying columns with flooded packing (*1*) and conventional columns (*2*) vs. the vapour velocity. Benzene-carbon tetrachloride system. The packing consists of 8 × 8 × 2-mm Raschig rings.

d_e is the equivalent packing diameter, cm; $w_v/w_{v_{inv}}$ is the relative velocity of the vapour; and Pr_v is the Prandtl number for the vapour phase.

Since mass transfer in flooded-packing columns takes place on free phase surfaces, its intensity can be assumed to be proportional to the component ΔP^*_{fr} (see Eqs. (9.176), (9.177) as well as Fig. 168). The utilization factor for a column with flooded packing (the ratio of the volumetric mass-transfer coefficient, taking into account the axial dispersion, to the volumetric mass-transfer coefficient for a plug-flow model) attains the value ~75 percent in the case of absorption. At velocities close to those at the inversion point, however, the coefficient reaches 100 percent owing to a decrease in the axial dispersion. In rectifying columns with flooded packing, the

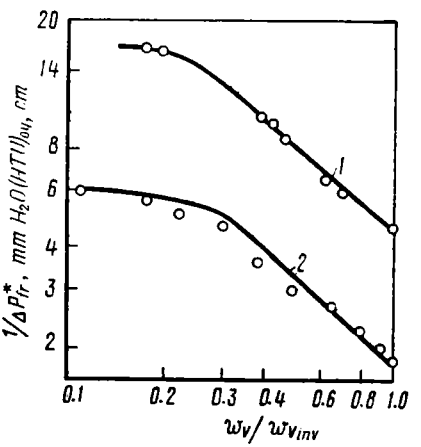

Fig. 168. Dependence of the efficiency (*1*) and pressure drop (*2*) in a flooded rectifying column with 6 × 6-mm Raschig ring packing on the relative velocity of vapour for an ethyl alcohol-water system.

axial dispersion at $w_v/w_{v_{inv}} > 0.5$ has no appreciable effect on the driving force of the process. Since in columns with flooded packing the maximum efficiency is attained at limiting vapour velocities, corresponding to the point of inversion, the efficiency of these columns should be compared at the inversion-point velocities. The free packing volume in flooded-packing columns, just as in ordinary columns, affects the output of the apparatus, since it determines the mean open cross-sectional area. The specific area of packing also influences the limiting vapour velocity and, consequently, is also connected with the output of the apparatus. When rectification is carried out with different packings for systems with similar physical and chemical properties, we obtain from Eq. (9.175).

$$\frac{(w_1^*)^2 a_1}{F_{v_1}^3 g} = \frac{(w_2^*)^2 a_2}{F_{v_2}^3 g}.$$

In other words, the limiting vapour velocity (maximum output) is determined uniquely, for identical physical and chemical properties of the systems, by the complex $\sqrt{F_v^3 g/a}$ which characterizes the maximum efficiency of a packed column and has the dimensions of velocity. When physical and chemical properties of solutions are taken into account, the efficiency is equal to $(HTU)_{0y}/Pr_v^{0.66} = 5.6 + 8.5d_e$ and is a constant for a given packing. The relative efficiency ε can then be expressed in the following form:

$$\varepsilon = \frac{\sqrt{F_v^3 g/a}}{(5.6 + 8.5d_e)\,10^{-2}}, \qquad (9.183)$$

where $d_e = 400\ F_v/a$ (cm).

This equation characterizes the yield of the apparatus per unit volume. The relative efficiency of some packings is shown in Table 16.

Table 16

Relative Efficiency of Some Packings

Packing shape	Material	Packing size, mm	$5.6 + 8.5d_e$, m	$\sqrt{F_V^3 g/a} \times 10^{-2}$, m/s	ε
Raschig rings	Steel	10.1×10.0×0.5	11.3	11.3	1.00
Wire spirals	Nichrome	4.4× 4.9×0.40	7.7	6.6	0.86
Raschig rings	Porcelain	25.9×25.7×3.1	16.5	13.0	0.79
—Do—	—Do—	15.8×15.0×3.1	11.7	7.8	0.66
10-Turn trihedral wire prizms	Stainless steel	2.0× 0.15	6.3	3.7	0.59
Raschig rings	Porcelain	10.2× 9.9×2.4	9.5	5.6	0.59
—Do—	—Do—	7.8 7.8×2.1	8.0	4.1	0.51
—Do—	—Do—	6.1× 6.3×1.7	7.4	3.7	0.50

It can be seen from Table 16 that Raschig rings and spiral packing have the highest efficiency. This is due to a large free volume in these packings. In order to increase the efficiency of flooded-packing columns, it is preferable to use packings with large values of the free volume. Thin-walled Raschig steel rings belong to this category. Packings made of steel rings of size 10 × 10 × 0.5 and 15 × × 15 × 0.5 mm in flooded columns provide the highest yield per unit volume of the apparatus.

One of the main advantages of flooded-packing columns is that their HETP varies only slightly with increasing column diameter. Packed rectifying columns of diameters above 1000 mm are rarely used due to their low efficiency, while absorption units of higher diameters almost always consist of a cascade of columns operating in series. Columns with flooded packing remain quite efficient for all column diameters, and are therefore quite suitable for construction of high-capacity apparatus. Flooded-packing columns can be used most effectively for separation of mixtures whose components have close boiling points. The height equivalent of an apparatus of moderate size in this case can be about 80-100 theoretical plates.

Chapter 10

Modelling and Design Calculations of Apparatus with Interfacial Surface Formed in Flows

10.1. Principles of Modelling the Processes of Separation of Multicomponent Systems

Modern trends to intensify production and create processes and aggregates with a high unit power require the development and introduction of the separation processes having appropriately high output. The design of new separation processes with the help of so-called safety factors (which are often inordinately exaggerated) may sometimes be unprofitable since it may lead to over-expenditures of construction materials and energy during operation. On the other hand, even using the safety factors, we cannot alwasy guarantee that a new process will satisfy the imposed technological requirements since the choice of safety factors is subjective in most cases. This explains a considerable attention which has of late been devoted to the creation of more precise methods of calculation of various technological equipment, including mass-transfer apparatus, which are based on the mathematical models of processes of various degree of complexity.

The creation of more precise design methods for rectification processes requires the application of the concept of real separation stage, i.e. the development of methods which are based not on the theoretical separation stage presuming the equilibrium between vapour and liquid at the contact stages, but on the real stage with a separation capacity determined by taking into account the finite rate of mass-transfer processes occurring under the conditions of concrete motion of interacting vapour and liquid flows. The application of the concept of the real separation stage makes it possible to improve the calculation accuracy considerably, but requires a much greater information for constructing the mathematical model of a process. This calls for a deeper study of such vague features of rectification process as hydrodynamics of interaction between vapour and liquid in columns and kinetics of mass transfer in multicomponent systems.

In chemical and petrochemical industries, rectification stages in multicomponent systems are often made in the form of a number of columns (plate or packed) combined into a single complex by

intermediate flows of semiproducts of separation. If the columns of a complex are connected in parallel or series-parallels, the calculation of all the columns can be carried out consecutively, in accordance with the construction of the separation circuit. If, however, there are recirculating flows among those connecting the columns, the columns involved in recycling cannot be calculated independently, since the recirculating flow compositions are unknown at the moment when calculation begins. In this case, the complex of columns should be treated as a single rectification system. When creating and investigating rectification systems for multicomponent systems, we must know the algorithms of modelling both separate columns and their complexes of an arbitrary complexity, which allows us to select the most expedient methods of separating mixtures and to determine the optimal operating conditions for each column, taking into account the interaction of all the columns of the complex.

From the point of view of mathematical modelling, the analysis of any rectifying setup permits its division into separate elements such as boilers, condensers, plates, and packed sections. In the general separation complex, each such element has a certain separation capacity with respect to the compositions of flows coming to it.

In order to analyze the separation capacity of each element, it is necessary to investigate the peculiarities of hydrodynamics of interaction between vapour and liquid flows, kinetics of mass transfer as well as the conditions of vapour-liquid equilibrium, which in total determines the precision of describing the effectiveness of element operation.

Thus, from the point of view of constructing a mathematical model, a rectifying setup can be considered as a large system consisting of a number of subsystems, viz. the elements of the setup whose individual properties are determined by subsystems of the next level, i.e. by hydrodynamics, equilibrium, and kinetics of mass transfer. In this case, the construction of a mathematical model must begin with the description of subsystems from the lower levels, whose modelling also requires the development of corresponding algorithms. Combining subsequently these descriptions into a single system of equations (using the general relations of material and energy balance), we obtain a mathematical description of individual elements and the rectifying system as a whole.

Consequently, the initial stage of constructing the mathematical model of a rectifying system involves the development of a mathematical description consisting of interconnected descriptions of mass-transfer kinetics, flow hydrodynamics, equilibrium relations, and equations of thermal and material balance of elements of the system. In this description, hydrodynamics of vapour and liquid flows has a dual effect on the HETP of individual elements. On the

one hand, the effect of hydrodynamics is manifested through the general structure of interacting vapour and liquid flows (macrolevel). On the other hand, the hydrodynamics affects the characteristics of the intensity of a local mass transfer between vapour and liquid flows in contact. It was the complexity of such a dual effect of hydrodynamic conditions of interaction between contacting flows on the intensity of mass transfer in rectifying systems that led to a wide use of the concept of theoretical separation stage. Another reason is considerable difficulties in the theoretical description of interfacial mass transfer in multicomponent systems, and especially during rectification of mixtures of components with different physical and chemical properties.

One of the important stages in the solution of the general problem of mathematical modelling is the estimation of the degrees of freedom of a process model, i.e. the determination of the variables whose values must be given numerically before solving the system of equations of the mathematical description. In the general case, the parameters used for describing various internal mechanisms of rectification should be taken into consideration.

The basic external variables which determine the separation regime in a rectifying system are (1) the characteristics of initial flows of raw materials; (2) the characteristics which determine the operation of reflux condensers and boilers; (3) controlling influences determining the regimes of extraction of intermediate fractions, and (4) pressures in the columns. In actual practice, there exist such indeterminate external variables as heat losses, unknown and immeasurable oscillations in the parameters of heat agent, and so on. Such phenomena as heat losses from fractionating system to the surrounding medium affect the results of modelling insignificantly. Besides, certain structural parameters such as the number of plates in a column or its diameter, as well as the structural parameters of the plates, can be treated as the degrees of freedom.

Considering only the variables that are taken into account in mathematical models, we can define the total number of degrees of freedom of rectifying setup as follows:

$$r = \sum_{i=1}^{n_f} r_f^{(i)} + \sum_{i+1}^{n_w} r_w^{(i)} + \sum_{i=1}^{n_B} r_B^{(i)} + \sum_{i=1}^{n_D} r_p^{(i)} + r_A + N_p,$$

where n_f and n_w are the numbers of flows of initial raw materials and distilled fractions; n_B and n_D the numbers of boilers and dephlegmators in the system; $r_f^{(i)}$ is the number of parameters characterizing the state of the ith flow of raw material; $r_w^{(i)}$ the number of parameters characterizing the ith distillation of a fraction; $r_B^{(i)}$ and $r_p^{(i)}$ the numbers of parameters determining the operation of the

ith boiler and the ith dephlegmator; r_A is the total number of structural parameters of the system, included into the mathematical description; and N_p the number of points in the system, at which the pressure is maintained at a given level.

The parameters determining the state of the raw material flow are usually the amount F of raw material, the composition x_{fj} ($j = 1, \ldots, k$) for liquid phase and y_{fj} ($j = 1, \ldots, k$) for vapour phase, the enthalpy h_f or H_f for liquid- or vapour-phase feed. Sometimes, the feed temperature T_f and its state of aggregation are given instead of enthalpy. With such characteristics of raw material flows it is assumed that only single-phase flows feed the system. Otherwise (if the feed is a vapour-liquid mixture), the feed can be treated as a combination of two single-phase flows.

Only one characteristic, viz. the amount of extracted fraction with the state of aggregation of the fraction being extracted, is usually chosen as a parameter determining extraction of fractions. As to the pressure in the fractionating system, it is usually assumed that it is maintained at given levels at a number of points of the system with the help of special techniques.

In designing rectification processes, three versions of the formulation of the problem are possible:

1. Determination of the values of some external variables of the process for given values of some internal variables.

2. Determination of the values of some external variables at which the discrepancy (in accordance with the defined criterion) between given and calculated values of certain internal variables is minimum.

3. The same as in item 2, but with additional restrictions imposed on the values of certain variables (internal or external), in the form of inequalities.

In design problems, it is always necessary to determine a set of variables which are external both with respect to the model and to the object of modelling. They usually include structural parameters of the system. Thus, in design problems, the parameters determining the degrees of freedom of a mathematical model must be found. The necessary condition for the solvability of a design problem consists in concerted account of the degree of freedom of the mathematical model. For example, for the first version of the formulation of such a problem, the following condition must be observed:

$$r_1 \leqslant r_0,$$

where r_1 is the number of internal fixed values of variables, and r_0 is the number of external variables being determined.

This condition is necessary but not sufficient. The reason behind this consists in the following. For direct modelling, when the values

of internal variables of the model are determined for a given set of values of external variables determining the number of degrees of freedom, a solution of the system of equations for the mathematical description always exists. On the other hand, in design problems with the formulation corresponding to the first version, the "inverse" problem of modelling is essentially solved, when certain operation conditions for a system are given and external conditions corresponding to this regime have to be determined. An *a priori* given regime can be realized in a mathematical model not in all cases. For this reason, the solution of a design problem for the first version of formulation is usually possible if one or at the most two values of concentrations of the components in separation products are given.

In the case of the second and third formulations of a design problem, no limitations are required either on the number or on the values of internal variables. The determining of the required set of the values of external variables in this case is reduced to the problem of minimization of a given criterion, whose solution can be obtained with the help of non-linear programming methods.

While solving a design problem or analyzing the existing system, the estimates (if possible, objective) of the effectiveness of its operation must be available. Various optimization criteria are used for obtaining such estimates, most of which are formed with calculation of expenditures or gain, which makes it possible to compare different operation regimes of a setup in accordance with the adopted criterion and find the optimal operation conditions among them.

Any model allows us to only approximately reproduce certain properties of the prototype. It is practically impossible to create a model which would absolutely correspond to its prototype. Thus, approximate models have to be used in each specific case, which to a certain extent satisfactorily describe the properties of the object which are of interest to us.

A sufficiently large number of mathematical models of rectification process are developed today. A general feature of all models is that they use various assumptions. Each model is characterized by parameters whose values are determined empirically by the relations obtained in the course of modelling of a concrete rectification system. For example, the mathematical models with a constant value of the plate effectiveness were widely used and are still being used now. It is this value which is often treated as the one being corrected.

This assumption can be admitted only in a very limited number of cases such as the modelling of rectification of binary mixture. However, it is only a rough approximation for modelling the rectification in multicomponent systems. The development of more refined

mathematical models required the introduction of the variables determining the hydrodynamic structure of interaction between the flows of phases in contact at the separation stages, as well as the variables characterizing the local parameters of mass transfer in the contact region of vapour and liquid flows. The first group of variables may often be determined with a sufficient accuracy from an analysis of plate structure or on the basis of experimental data on the flow structure, while the determination of local characteristics of mass transfer is usually possible only at the correction stage of a mathematical model.

The correction of a mathematical model for rectification process is carried out on the basis of experimental results for the process being modelled. The distribution of concentration of mixture components over the height of the column in the vapour and liquid phases, the values of temperature at the separation stages, and also the compositions of the products of separation are frequently used for this purpose. The adequacy of the model and the prototype is judged from a comparison of calculated and experimental results. This comparison provides the correction which must be applied to the mathematical model. In many cases, it is difficult to obtain sufficiently complete experimental information, and this may serve as a source of error unless special measures are taken in order to verify its correctness.

For verifying the adequacy and for correcting a mathematical model, functional dependencies between the values of the adequacy criterion and mismatching of calculated and experimental results are normally used. For this purpose, the criteria in the form of buadratic mismatch estimates are often employed:

$$\varphi = \sum \left(\frac{x_{ij}^{\text{exp}} - x_{ij}^{\text{cal}}}{x_{ij}^{\text{cal}}} \right)^2 .$$

Besides, the criterion of the form

$$\varphi = \sum (x_{ij}^{\text{exp}} - x_{ij}^{\text{cal}}) \left(\frac{x_{ij}^{\text{exp}} - x_{ij}^{\text{cal}}}{x_{ij}^{\text{cal}}} \right)^2 ,$$

which ensures a better matching between the experimental and calculated concentration profiles during its minimization than the first of the above criteria is also used.

The problem of model correction is formulated as the problem of minimizaton of the criterion in the admitted form for the allowed range of variation of the parameters of a process being modelled. For this purpose, the method of successive approximations is normally used. Any other method of minimization is also applicable. It is desirable that model correction should be carried out under the

conditions of excessive information and that models should contain the smallest possible number of parameters requiring correction. The latter condition should not be treated as a recommendation to use simplified models, except for the cases when such models correspond to the formulated problem of modelling.

It is impossible to solve the problems of optimum design and optimization of the processes of separation of multicomponent mixtures by rectification without using the results of mathematical modelling. The main task of mathematical modelling of rectifying columns is to predict their HETP under different operation conditions, including possible variation of apparatus design and separation regimes.

A rectifying system is a combination of several apparatus: the column, boiler, and dephlegmator. During operation, these apparatus are interconnected by common liquid and vapour flows. An insufficiently complete reflection of any property of these apparatus in a model may lead to errors. Thus, different mathematical models of rectifying columns have separate groups of equations that describe similar features of the process being modelled. The models may differ in the degree of completeness of the description of these features, which mainly determines the fields of their application in each case.

In mathematical modelling, the block principle of constructing a model is used, and mathematical description of individual blocks is given. One of the main subsystems of the general algorithm of the synthesis of separation circuits for multicomponent mixtures is the subsystem of analysis of their physical and chemical properties which include the dependences describing the vapour-liquid equilibrium. It should be borne in mind that the main contribution to the error in the results of modelling is made by the errors in the description of equilibrium dependences.

As to the application of various models of hydrodynamics in modelling rectifying setups, we can state that the use of simple models is quite justified at the design stage for qualitative analysis of various separation circuits, since it gives a certain margin for the separation capacity and saves the computation time. For a refined modelling hydrodynamic models based on the cellular structure of flows are preferable from the point of view of computation, since the application of diffusion models, especially for multicomponent rectification, is fraught with serious computational difficulties. These difficulties are associated with the necessity of solving a two-point boundary value problem for a system of differential equations. The error in the estimation of the parameters of hydrodynamic models affects the accuracy of the results of modelling to a smaller extent in comparison with the errors in determining kinetic parameters and the parameters of equations describing vapour-liquid equilibrium.

When hydrodynamic models of contact apparatus are employed, the calculation of HETP of the apparatus is usually performed on the basis of the assumption about the constancy of the local effectiveness of the contact in the bulk where mass transfer takes place with respect to all the components of the mixture being separated. Such an approach in calculating the rectification processes in multicomponent mixtures may lead to significant errors. As a result of many experimental and theoretical investigations and calculations it was shown that the effectiveness of plates in multicomponent rectification for different components of the mixture being separated may differ significantly. In this case, the effectiveness of a plate for some mixture component may be less than zero or greater than unity, which is typical of multicomponent mixtures.

It follows from a general analysis of mass-transfer theories that mass-transfer coefficients are functions of two groups of parameters, viz. the parameters that determine diffusive mass transport to the interface and the parameters that characterize the hydrodynamic state of the interface. If in a process of multicomponent mass transfer hydrodynamic parameters produce the same effect on the mass-transfer coefficients as in the case of binary mixtures, the diffusive transport processes in multicomponent mixtures have peculiar properties in comparison with those in binary mixtures, which include above all the osmotic and reversive diffusion processes.

10.2. Modelling Algorithms and Mathematical Models of Rectifying Columns

After a certain mathematical description has been adopted, the process of modelling consists in solving the system of equations of the mathematical model for a given set of environmental conditions. These conditions usually are (a) the column feed taking into account quantitative and qualitative characteristics; (b) the quantity of heat supplied to the boiler, and (c) the quantity of heat removed from the condenser. The last condition is often replaced by specifying the reflux characteristics. Environmental conditions may be connected with each other or with the internal parameters of the process through additional relations which are included in the model equations for an analysis of the control system.

Formally, the mathematical problem of calculating the column regime for a given set of external conditions consists in solving the system of non-linear equations of a high order. Direct methods of its solution, known from numerical analysis, lead to cumbersome calculations which can be carried out only on high-power computers. For this reason, the methods which make use of the specific structure of the system of equations of mathematical description are normally employed. If the heat flows are ignored, the material balance is de-

scribed by the linear equations in the known compositions (see Part One):

$$L(x_{i+1,k} - x_{i,k}) = V(y_{i,k} - y_{i-1,k}).$$

If heat balances for separation stages are introduced into the mathematical model, the flow rates cannot be treated as given known quantities. Their values are connected with the heat contents of the liquid and vapour. Hence, the balance equations become essentially non-linear:

$$L_{i+1}x_{i+1,k} - L_i x_{i,k} = V_{i,k}y_{i,k} - V_{i-1}y_{i-1,k}.$$

The most widespread method of solving the system of equations of a mathematical model, taking into consideration heat balances at separation stages consists in a successive refinement of the values of mass flows and compositions. First, the compositions for all separation stages are calculated in accordance with the approximately adopted values of flows. Then the initially adopted values of vapour and liquid flows are corrected, after which the compositions are calculated again, and so on.

The solution algorithm of the systems of equations for a mathematical model constructed by taking into account the heat balances in a column may be considered as the sum of two algorithms, one of which ensures the calculation of compositions for separation stages, while the other is used for correcting the values of vapour and liquid flow rates in a column. This makes it possible to avoid to a considerable extent the difficulties associated with the solution of non-linear systems of equations, since at each calculation stage most of equations are linear. A computational algorithm for calculating the compositions for given values of vapour and liquid flow rates can be realized by using various techniques which are mainly based on specific properties of the system of equations describing the distribution of compositions over separation stages.

One of such techniques is the widely known method of "plate-to-plate count". The disadvantage of this method is the instabilities that may appear in the count, and especially during the calculation of separation of components considerably differing in volatilities. In order to eliminate this shortcoming, various modifications of the method were proposed, most of which are based on different directions of counting. For example, it was suggested that calculation should be performed for heavy components in the direction from the still to the condenser, while for light components, in the opposite direction. The countercount method is also used, according to which the stripping part of the column is calculated in the direction from the still to the feed-plate cross section, while the rectifying part, from the condenser to the feed plate. The disagreement between the results obtained for the feed-plate cross section serves as a criterion for correcting the composition of the end products.

While using a mathematical model based on theoretical plates it is assumed that vapour has an equilibrium composition with respect to the composition of the liquid on the plate, i.e.

$$y_{i,l} = k_l(T)\, x_{i,k}.$$

The system of balance equations for the values of temperatures given for the plates becomes linear in compositions. Consequently, in order to calculate the compositions for separation stages, matrix methods of the solution of systems of linear equations with a subsequent correction of temperature distribution can be used.

In modelling a rectification process by using the mass-transfer mechanism, the only practically used method is the plate-to-plate method of calculation in the direction from the still to the condenser over the entire column. The reverse count requires the solution of a system of transcendental equations for each plate, which is due to the structure of equations describing mass transfer on a plate. In order to ensure the stability of count in one direction, effective algorithms have been developed, which do not require a significant increase in the computer memory and in some cases even reduce the total time of solution.

Let us consider several examples of mathematical modelling of rectifying columns.

Model 1. The mathematical description of a rectifying plate column, which is used in this model, involves the following assumptions: (1) the initial binary mixture is fed to the column at the boiling point; (2) the liquid on the column plates is at the boiling point, while the vapour is at the dew point (saturated vapour); (3) the vapour and liquid flow rates are constant over the column height; (4) the pressure is constant over the column height; (5) the reflux is supplied at the boiling point; (6) the column has a complete condenser; (7) the column still operates as a partial evaporator; (8) mass transfer on the column plates is equimolar, and (9) ideal mixing of liquid and ideal displacement of vapour take place in the mass-transfer region on a column plate.

The following equations for mathematical description are used:

the equation for calculating the composition of vapour disposed from the ith plate:

$$y_i = y_{i-1} + \left[1 - \exp\left\{-\frac{K_{oyi}}{G}\right\}\right](y_i^* - y_{i-1}), \quad i = 1, \ldots, N, \qquad (10.1)$$

where y_i^* is the concentration of vapour in equilibrium with the liquid on the plate, defined by the given analytical expression

$$y_i^* = \varphi(x_i); \qquad (10.2)$$

the equation for calculating the volumetric mass-transfer coefficient K_{0yi} with the local mass-transfer coefficients k_y and k_x:

$$K_{0yi} = \frac{1}{1/k_{yi} + m_i/k_{xi}}, \tag{10.3}$$

where m_i is the slope of the tangent to the equilibrium dependence

$$m_i = \left(\frac{d\varphi}{dx}\right)_{x=x_i}; \tag{10.4}$$

the material-balance equations for the components in the stripping part of the column:

$$(L + F)\, x_{i+1} - Gy_i - Wx_w = 0, \quad i = 1, \ldots, f - 1; \tag{10.5}$$

the material-balance equations for the components in the rectifying part of the column:

$$Lx_{i+1} - Gy_i - Wx_w + Fx_f = 0, \quad i = f, \ldots, N; \tag{10.6}$$

the equation for the total condenser:

$$x_p = x_{N+1} = y_N; \tag{10.7}$$

the material-balance equation for the components in the column still:

$$(L + F)\, x_i + Gy_w^* - Wx_w = 0; \tag{10.8}$$

the total material-balance equation for the column:

$$Fx_f - Wx_w - Dx_p = 0. \tag{10.9}$$

The initial data for solving the system of equations of the mathematical description are: the number of plates N in a column, the number f of the feed plate, the feed rate F, the feed composition x_f, the flow rate $D = G_p$ of the distillate being removed and the reflux rate $L = \Phi = G_pR$. The flow rates are given in kilogram-moles and the compositions in mole fractions. The vapour flow rate G is calculated by the equation

$$G = L + D = G_p\,(R + 1). \tag{10.10}$$

The system of equations of the mathematical description is solved by using the plate-to-plate count method in the direction from the column still to the condenser in the following sequence (see Part One):

1. The initial value x_w of the component concentration in the still is taken, for example, equal to the feed composition x_f.
2. The composition y_w^* of vapour leaving the column still is calculated by formula (10.2).
3. The liquid composition on the first plate of the stripping part of the column is calculated by Eq. (10.8).

4. The composition of vapour leaving the plate is determined by formula (10.1).

5. The liquid composition on the upper plate is determined from Eq. (10.5) for the stripping or Eq. (10.6) for the rectifying part of the column.

6. The distillate composition x_p is determined, after which the calculations of items 4 and 5 are repeated.

7. The total material balance is verified for the components of the column for the given value of x_w and calculated value of x_p:

$$\Pi = Wx_w + Dx_p - Fx_f. \tag{10.11}$$

If $|\Pi| > \varepsilon$, where ε is the required accuracy of the total component balance, the adopted value of a volatile component x_w in the still is changed, and the calculation is repeated starting from item 2. If $|\Pi| < \varepsilon$, the calculation is terminated. In order to refine the value of x_w, the half-division method is used.

As a result of solving the system of equations of the mathematical description, the compositions x_p and x_w of separation products are determined as well as the liquid and vapour compositions for all the plates of the column. If we include the relation

$$T = f(x), \tag{10.12}$$

which defines the boiling temperature of the liquid as a function of the composition, into the system of equations of mathematical description, the temperatures of all the plates can be calculated.

The mathematical model can be used for investigating various regimes of separation as well as for calculating static characteristics of the column for different channels, for instance, for the "feed flow rate—separation product composition", "feed composition—separation product composition", or "reflux flow rate—separation product composition" channels. If the dependence (10.12) of temperature on composition is known, the model considered above can be used for determining the position of the check plate in the column. The regime of separation is controlled in accordance with the temperature on the check plate.

Model 2. The mathematical description of model 2 takes into account thermal interaction between the vapour and liquid flows along the column height as well as the non-ideal mixing of the liquid on the plates. The following assumptions are made in constructing the mathematical description of the model.

1. The liquid on the plates is at the boiling point, while vapour is at the dew point.

2. Mass transfer is equimolar on the column plates.

3. The non-ideality of mixing liquid is taken into account by the cellular model.

4. The flow of vapour in the mass-transfer region of the plate is described by the ideal displacement model.

5. Vapour is perfectly dispersed in the space between the plates.

6. The column still operates as a total or partial evaporator.

7. The column reflux is formed either in a total or partial condenser.

8. The plate operates under adiabatic conditions, i.e. there are no heat losses.

9. The enthalpies of the vapour and liquid phases are calculated following the additivity law in terms of the enthalpies of pure components.

Under these assumptions, the following equations of the mathematical description can be written:

the equation for calculating the composition of the vapour leaving a plate:

$$y_i = \frac{G_{i-1}}{G_i}\left[y_{i-1} + E_i\left(y_i^* - y_{i-1}\right)\right] + \Omega_i, \tag{10.13}$$

where

$$E_i = \frac{L_i}{G_i m_i}\left[\left(1 + \frac{G_i}{L_i}\frac{m_i\eta_i}{s}\right)^s - 1\right]; \tag{10.14}$$

Ω_i is the correction for a change in the vapour flow, defined as

$$\Omega_i = \begin{cases} y_i^*\left(G_i - G_{i-1}\right)/G_i & G_i > G_{i-1} \\ x_{i-1}^*\left(G_i - G_{i-1}\right)/G_i & G_i < G_{i-1}; \end{cases} \tag{10.15}$$

s is the number of cells in the model of liquid flow, and η_i is the efficiency of a mixing cell:

$$\eta_i = 1 - \exp\left(-N_{0yi}\right); \tag{10.16}$$

y_i^* is the vapour concentration in equilibrium with liquid:

$$y_i^* = \frac{\left(a + bx_i\right)x_i}{1 + \left(c + dx_i\right)x_i}; \tag{10.17}$$

x_{i-1}^* is the liquid concentration in equilibrium with vapour supplied to the plate, N_{0yi} the total number of transport units:

$$N_{0yi} = 1\Big/\left(\frac{1}{N_{yi}} + m_i\frac{G_i}{L_i}\frac{1}{N_{xi}}\right); \tag{10.18}$$

N_{yi} is the vapour-phase number of transport units:

$$N_{yi} = \left(\frac{D_{yi}\gamma_{yi}}{\mu_{yi}}\right)^{0.5} \times \left(0.776 + 4.57h_{wi} - 0.24V_{si}\sqrt{\gamma_{yi}} + 0.029\frac{L_{si}}{l_i}\right); \tag{10.19}$$

N_{xi} is the liquid-phase number of transport units;

$$N_{xi} = 5.15 \times 10^4\left(D_{xi}\right)^{0.5}\left(0.213V_{si}\sqrt{\gamma_{yi}} + 0.15\right)\tau_{L_i}; \tag{10.20}$$

τ_{L_i} is the mean duration of stay of liquid on the plate, hr:

$$\tau_{L_i} = \frac{h_{L_i} z_{L_i} l_i}{L_{si}}; \qquad (10.21)$$

h_{L_i} is the height of the liquid layer on a plate, m:

$$h_{L_i} = 0.042 + 0.19 h_{wi} - 0.5 V_{si} \sqrt{\gamma_{yi}} + 0.0135 \frac{L_{si}}{l_i}; \qquad (10.22)$$

h_{wi} is the height of weir, m; V_{si} the volumetric flow rate of vapour in empty column, $m^3/m^2 \cdot hr$; γ_{yi} is the specific gravity of vapour; L_{si} is the volumetric flow rate of liquid, m/hr; l_i is the mean width of the liquid flow on a plate, m; z_{Li} is the liquid path on a plate, m; D_{yi} is the molecular diffusion coefficient in vapour, m^2/hr; D_{xi} the molecular diffusion coefficient in liquid, m^2/hr; and μ_{yi} is the viscosity of the vapour;

the material-balance equations for the components in the stripping part of the column:

$$L_{i+1} x_{i+1} - G_i y_i - W x_w = 0, \quad i = 1, \ldots, f-1; \qquad (10.23)$$

the material-balance equations for the components in the rectifying part of the column:

$$L_{i+1} x_{i+1} - G_i y_i - W x_w + F x_f = 0, \quad i = f, \ldots, N; \qquad (10.24)$$

the equation for the condenser

$$x_p = y_{N+1} = y_N + E_D (y^*_{N+1} - y_N), \qquad (10.25)$$

where E_D is the dephlegmator efficiency.

For a total condenser, $E_D = 0$ and for a partial condenser $E_D = 1$. For a partial reflux condenser (dephlegmator), the composition of liquid fed as the reflux is in equilibrium with the distillate composition y_{N+1};

the equation for the material balance of the components in the column still:

$$L_1 x_1 - G_0 [x_w + E_w (y^*_w - x_w)] - W x_w = 0; \qquad (10.26)$$

where $E_w = 0$ for a total evaporator and $E_w = 1$ for a partial evaporator;

the total material-balance equation for the stripping part:

$$L_{i+1} - G_i - W = 0, \quad i = 1, \ldots, f-1; \qquad (10.27)$$

the total material-balance equation for the rectifying part:

$$L_{i+1} - G_i - W + F = 0, \quad i = f, \ldots, N; \qquad (10.28)$$

the heat-balance equation for the stripping part:

$$L_{i+1} h_{i+1} - G_i H_i - W h_w + Q_w = 0, \quad i = 1, \ldots, f-1; \qquad (10.29)$$

the heat-balance equation for the rectifying part:

$$L_{i+1}h_{i+1} - G_iH_i - Wh_w + Q_w + \overline{Fh_f} = 0, \quad i = f, \ldots, N; \tag{10.30}$$

the expression for calculating the liquid enthalpy:

$$h_i = [c_{L_1}x_i + c_{L_2}(1 - x_i)]\, T_{xi}; \tag{10.31}$$

the expression for calculating the vapour enthalpy:

$$H_i = [c_{v_1}y_i + c_{v_2}(1 - y_i)]\, T_{y_i} + r_1y_1 + r_2(1 - y_i), \tag{10.32}$$

where c_{Lj} and c_{vj} are the specific heat capacities of liquid and vapour; r_j is the heat of evaporation for the jth component;

the equation for calculating the temperature of vapour condensation:

$$T_{yi} = \sum_{p=0}^{k} a_p y_i^p, \tag{10.33}$$

where a_p is the constant of the approximating polynomial;

the total material-balance equation for the column:

$$F - W - D = 0; \tag{10.34}$$

the total heat-balance equation for the column (without the condenser):

$$L_{N+1}\bar{h}_{N+1} + F\bar{h}_f + Q_w - G_NH_N - Wh_w = 0, \tag{10.35}$$

where Q_w is the amount of heat supplied to the still; $\bar{h}_{N+1}$ is the enthalpy of the supplied reflux; and $\bar{h}_f$ the enthalpy of feed.

Since the reflux enthalpy may differ from the enthalpy corresponding to its boiling point, the reflux temperature must be given in the initial data. The feed enthalpy is determined considering its phase state. The feed is supplied either in the liquid phase at the boiling point or cooling temperature, or in the vapour phase, or in the form of a vapour-liquid mixture. In the last two cases, when calculating the composition of vapour leaving the feed plate, the value of y_f is corrected by the following formula, taking into account Eq. (10.13):

$$y_f = [(G_f - G_F)\, y_f + G_Fy_F]/G_f, \tag{10.36}$$

where G_f is the flow rate of the vapour phase supplied to the plate above the feed plate; G_F is the flow rate of the vapour phase in the feed; and y_F is the feed vapour-phase composition.

The initial data for solving the system of equations of the mathematical description are: the number N of plates in the column, the number f of the feed plate, the number F of feed plates, the vapour-phase flow rate G_F in the feed, the feed composition x_F, the feed va-

pour-phase composition y_F, the total feed enthalpy $\bar{h}_F$, the temperature $T_{x,N+1}$ or enthalpy $\bar{h}_{N+1}$ of the reflux, the amount of heat Q_W supplied to the column still, the reflux rate L_{N+1}, the specific heat capacities c_{Lj} and c_{vj} and heats of evaporation r_j of components, the structural parameters of the column and physical properties of the components.

The system of equations of the mathematical description is solved by the iterative method, which consists in a successive refinement of the values of concentrations and flow rates for the column plates. The sequence of calculation is as follows.

1. The initial distribution of vapour- and liquid-phase composition is given for the column plates. For example, it is assumed that the compositions of liquid and vapour on the plates are the same as the feed composition.

2. The values of G_N and W are determined by the joint solution of Eqs. (10.34) and (10.35), after which the flow rates G_i and L_i are calculated with the help of balance equations (10.27)-(10.30) for all the column plates.

3. The vapour- and liquid-phase compositions are calculated for the plates (the sequence of calculating compositions is the same as in Model 1).

The calculations by items 2 and 3 are repeated until the values of concentrations and flow rates for two successive iterations coincide. For a more rapid convergence in calculation of the value of W, the Wegstein iterative method is used. As a result of solving the system of equations of the mathematical description, the composition of separation products, the composition and temperature for all the column plates, as well as the vapour and liquid flow rates on the plates are determined. The mathematical model can be used for investigating various separation regimes and for calculating various static characteristics of rectifying columns for separating binary mixtures of components with sharply differing boiling points.

Model 3. This model, which is the most widely used for design calculations, is based on the concept of the theoretical separation stage. Numerous modifications of this model do not differ much in principle. The basic assumption used in this model is that the vapour leaving a separation stage is in equilibrium with the liquid leaving this stage. Thus, there is no need to consider the mass-transfer process in multicomponent mixtures, which considerably simplifies the solution of the system of equations of mathematical description. The mathematical description of rectification of a multicomponent mixture includes the following equations:

the equations for calculating the composition of vapour in equilibrium with liquid:

$$y_{ij}^* = f_j(T_i, P_i, x_{i,1}, x_{i,2}, \ldots, x_{i,n}), \quad j = 1, \ldots, n \quad (10.37)$$

Introducing the concept of coefficients of activity γ_j and fugacity φ_j we can write

$$y_{ij}^{*} = \frac{1}{\varphi_{ij}} \gamma_{ij} P^{0}(T_i)\, x_{ij} = K_{ij}(T_i)\, x_{ij}, \qquad (10.38)$$

where $P^0(T_i)$ is the vapour pressure of the pure component, which is a function of temperature.

The activity coefficients γ_j and fugacity φ_j in general depend on the concentrations of all the components as well as on temperature and pressure, which is taken into account by the corresponding relations preset for them:

$$\gamma_{ij} = \gamma_j(T_i,\ P_i,\ x_{i,1},\ x_{i,2},\ \ldots,\ x_{i,n}), \qquad (10.39)$$

$$\varphi_{ij} = \varphi_j(T_i,\ P_i,\ y_{i,1},\ y_{i,2},\ \ldots,\ y_{i,n}); \qquad (10.40)$$

the component-wise material-balance equation at the separation stages:

$$L_{f_i} x_{f_i j} + G_{f_i} y_{f_i j} + L_{i+1} x_{i+1,j} \quad j + G_{i-1},\ y_{i-1,j} - L_{w_i} x_{ij} - G_{w_i} y_{ij} - L_i x_{ij} - G_i y_{ij} = 0, \quad f = 1, \ldots, n, \quad i = 0, \ldots, N+1, \qquad (10.41)$$

where L_{f_i} is the flow rate of liquid feed supplied to the ith stage; G_{f_i} is the flow rate of vapour feed supplied to the ith stage; L_{w_i} is the flow rate of liquid fraction removed from the ith stage; and G_{w_i} the flow rate of the vapour fraction removed at the ith stage.

In the case of a vapour-phase feed, the composition of the vapour leaving the ith stage is determined by the equation

$$y_{ij} = [(G_i - G_{f_i})\, y_{ij}^{*} + G_{f_i} y_{f_i j}]/G_i; \qquad (10.42)$$

the total material-balance equation for stages is

$$L_{f_i} + G_{f_i} + L_{i+1} + G_{i-1} - L_{w_i} - G_{w_i} - L_i - G_i = 0, \quad i = 0, \ldots, N+1; \qquad (10.43)$$

the total heat-balance equation for the stages is

$$q_i + L_{f_i} h_{f_i} + G_{f_i} H_{f_i} + L_{i+1} h_{i+1} + G_{i-1} H_{i-1} - L_{w_i} h_i - G_{w_i}^{*} H_i - L_i h_i - G_i H_i = 0, \quad i = 0, \ldots, N+1, \qquad (10.44)$$

where q_i is the amount of heat supplied to the ith stage from outside.

The temperature at the ith stage is defined by the equation

$$\Pi(T_i) = \sum_{j=1}^{n} K_{ij}(T_i)\, x_{ij} - 1 = 0. \qquad (10.45)$$

For solving this equation, the column still ($i = 0$) is considered either as a partial evaporator, whose HETP is equal to that of the theoretical stage, or as a total evaporator for which the vapour composition is assumed to be equal to the liquid composition in the still. Similarly, for a total condenser the composition of the liquid supplied for reflux into the column is assumed to be the same as the distillate composition. For a partial reflux condenser (dephlegmator), the composition of the distillate removed in the vapour phase is assumed to be in equilibrium with the reflux liquid, i.e. the dephlegmator is treated as the theoretical separation stage.

The equations of the mathematical description are solved by using the iterative method of consecutive refinement of the values of concentrations and vapour and liquid flow rates. At each iteration step, the temperature distribution over separation stages is assumed to be constant and dependent on the component's concentration calculated at the preceding iteration. Under this assumption, the system of equations (10.41) turns out to be linear.

The iterations are terminated when the conditions

$$\left|\sum_{j=1}^{n} x_{ij} - 1\right| < \varepsilon, \quad i = 0, \ldots, N+1 \tag{10.46}$$

are fulfilled. These conditions must be satisfied for all separation stages with a preset accuracy ε. In the process of calculating the compositions for separation stages, the compositions must be corrected so that the following relations hold when temperatures are calculated:

$$\sum_{j} x_{ij} = 1, \quad i = 0, \ldots, N+1. \tag{10.47}$$

The simplest method of such a correction is the normalization of concentrations, when the correct values are determined by the formula

$$x_{ij} = \frac{x_{ij}}{\sum\limits_{j} x_{ij}}, \quad \begin{matrix} j = 1, \ldots, n \\ i = 0, \ldots, N+1. \end{matrix} \tag{10.48}$$

With such a correction method, however, the total material balance for the components in the entire column is violated, which significantly affects the convergence rate of the iterative method. In order to eliminate this contradiction and to increase the convergence rate of the solution, the θ-method of correction of the concentration in a column is used.

For a column in which M extractions of fractions are performed, including the extraction of distillate and excluding the still bottom, M quantities θ_s are introduced, which are used for correcting the

where α_j are the relative volatilities of the components, which are assumed to be temperature independent.

4. The column has a total condenser whose inertia is determined by the amount of liquid in the reflux tank.

5. The effectiveness E of the plates is constant over the column height and is the same for all the components.

6. The vapour and liquid flows are constant in the column cross sections.

The systems of equations for the mathematical description of non-stationary regimes includes:

the equation for the plates of the stripping part:

$$v_{L_i}\frac{dx_{ij}}{d\tau} = (L+F)(x_{i+1,\,j}-x_{ij})+G(y_{i-1,\,j}-y_{ij}),$$
$$j=1,\ \ldots,\ n,\quad i=1,\ \ldots,\ f-1; \tag{10.56}$$

the equation for the plates of the rectifying section:

$$v_{L_i}\frac{dx_{ij}}{d\tau} = L(x_{i+1,\,j}-x_{ij})+G(y_{i-1,\,j}-y_{ij}),$$
$$j=1,\ \ldots,\ n,\quad i=f+1,\ \ldots,\ N; \tag{10.57}$$

the equation for the feed plate:

$$v_{L_i}\frac{dx_{fi}}{d\tau} = Lx_{f+1,\,j}-(L+F)x_{fj}+G(y_{f-1,\,j}-y_{fj})+Fx_{fj},$$
$$j=1,\ \ldots,\ n; \tag{10.58}$$

the equation for the column still:

$$v_{L_W}\frac{dx_{Wj}}{d\tau} = (L+F)x_{1,\,j}-Gy^*_{Wj}-Wx_{Wj},$$
$$j=1,\ \ldots,\ n; \tag{10.59}$$

the equation for the column dephlegmator:

$$v_{L_D}=\frac{dx_{Dj}}{d\tau} = Gy_{Wj}-(L+D)x_{Dj},\quad j=1,\ \ldots,\ n, \tag{10.60}$$

where v_{Li}, v_{Lw}, and v_{L_D} are the holding capacities with respect to liquid on a plate, in the still, and in the reflux tank.

The equation for calculating the composition of the vapour leaving a plate in the non-stationary regime has the form

$$y_{ij} = y_{i-1,\,j}+\eta(y^*_{ij}-y_{i-1,\,j}). \tag{10.61}$$

The initial data for calculating a non-stationary process in a rectifying column are the initial values of the vapour- and liquid-phase concentrations, corresponding to an unperturbed regime of column operation, as well as the parameters of the regime, which correspond

to a perturbation appearing due to a variation in the flow rate of the feed, its composition, the reflux flow rate L or the vapour flow rate G. Perturbations can be applied either simultaneously via several channels or in a certain sequence. The initial concentrations for the initial unperturbed regime are determined with the help of a stationary or non-stationary model. For this purpose, the equations of the mathematical description are integrated under arbitrary initial conditions with the parameters corresponding to the required stationary regime. System of equations (10.56)-(10.61) is integrated by using the Euler method with a constant step. The magnitude of the step is determined from the condition

$$\Delta\tau = (0\ 01\text{-}0.1)\ \tau_{min}, \tag{10.62}$$

where τ_{min} is the smallest time constant among the time constants τ_{ij} of the equations, which are calculated by the formula

$$\tau_{ij} = \frac{v_{L_i}}{L_i + m_{ij}\eta G_i}, \tag{10.63}$$

where

$$m_{ij} = \frac{\partial y^*_{ij}}{\partial x_{ij}}. \tag{10.64}$$

The above model of the dynamics of plate columns can be used for calculating the start-up regimes of columns and for investigating transient processes under operating conditions, including the transition of a column from one regime to another.

Model 6. This model involves the linearization of differential equations describing the variation of the concentration on the column plates. The slightly changing complexes are singled out. The values of these complexes can be predicted to a sufficient degree of accuracy in the course of integration by the extrapolation method. For this purpose, the equations describing the time variation of the concentration on the column plates,

$$v_{L_i}\frac{dx_{ij}}{d\tau} = L_{i+1}x_{i+1,\,j} - L_i x_{ij} + G_{i-1}y_{i-1,\,j} - G_i y_{ij}, \tag{10.65}$$

are written in the form

$$v_{L_i}\frac{dx_{ij}}{d\tau} = L_{i+1}x_{i+1,\,j} - \left(L_i + G_i\frac{y_{ij}}{x_{ij}}\right)x_{ij} + \left(G_{i-1}\frac{y_{i-1}}{x_{i-1,\,j}}\right)x_{i-1,\,j}, \tag{10.66}$$

or

$$\frac{dx_{ij}}{d\tau} = A_{ij}x_{i-1,\,j} + B_{ij}x_{ij} + C_{ij}x_{i+1,\,j}. \tag{10.67}$$

The equations for the still are represented in a similar way:

$$\frac{dx_{wj}}{d\tau} = B_{wj}x_{wj} + C_{wj}x_{1,\,j}; \tag{10.68}$$

the equation for the condenser is

$$\frac{dx_{pj}}{d\tau} = A_{pj}x_{Nj} + B_{pj}x_{pj}, \tag{10.69}$$

where

$$A_{ij} = G_{i-1}\frac{y_{i-1,\,j}}{x_{i-1,\,j}} \cdot \frac{1}{v_{L_i}}; \quad A_{pj} = G_N \frac{y_{Nj}}{x_{Nj}} \cdot \frac{1}{v_{Lp}}; \tag{10.70}$$

$$B_{ij} = -\left(L_i + G_j \frac{y_{ij}}{x_{ij}}\right) \frac{1}{v_{L_i}};$$

$$B_{wj} = -\left(W + G_w \frac{y_{wj}}{x_{wj}}\right) \frac{1}{v_{LN}}; \tag{10.71}$$

$$B = -(L + D) \frac{1}{v_{L_p}};$$

$$C_{ij} = L_{i+1}/v_{L_i}; \quad G_{wj} = L_1/v_{L_w}. \tag{10.72}$$

The composition y_{ij} of vapour leaving a plate can be calculated by using any method of description of equilibrium and of HETP of plates. The ratios y_{ij}/x_{ij} appearing in (10.70) and (10.71) change to a smaller extent than the concentration on the column plates. This allows us to consider expressions (10.70)-(10.72) as slightly varying complexes in Eqs. (10.66)-(10.69), and instead of calculating their value at every integration step, we can use extrapolated dependences which can be constructed from the results of previous steps.

This algorithm uses the Euler integration method with a constant step chosen by taking into account condition (10.62), in which the minimum value τ_{min} of the time constant is determined as the smallest among the time constants for all the plates:

$$\tau_{ij} = \frac{v_{L_i}}{L_i + G_i y_{ij}/x_{ij}} \tag{10.73}$$

While integrating with the extrapolated values of A_{ij}, B_{ij}, and C_{ij}, the validity of the condition

$$\left| \sum_{j=1}^{n} x_{ij} - 1 \right| < \varepsilon \tag{10.74}$$

is verified. The violation of this condition indicates that the extrapolation step should be decreased. The process is returned to the beginning of the last extrapolation interval, and integration is repeated with a decreased extrapolation step.

This algorithm of integration with the extrapolation of slightly varying terms in the differential equations turns out to be more rapid while calculating transient processes in rectifying columns, and especially for modelling start-up regimes. Besides, the algorithms under consideration can be used for modelling the transient processes occurring upon a stepwise transition of a column from one regime to another, since the magnitude of the extrapolation step in these cases may become significant by the end of the transient process.

10.3. Effect of the Flow Structure on Efficiency of Plate Columns

The general regularities of the structure of flows on plates are observed for plate columns which form the major group of apparatus with an interface formed in the course of flow. In turn, the efficiency of plate columns depends on hydrodynamic structure of flows, which determines the degree of mixing on the plates. In the course of mass transfer, the liquid concentration on a plate varies from the region where the liquid enters the plate to the region where it leaves it. The best conditions of separation would be attained if no mixing of liquids with different compositions occurred on the plate. In order to get an idea of the mixing mechanism for liquids, let us consider three modes of motion of liquid and vapour:

(1) the liquid is not mixed on the plate, while vapour is perfectly mixed in the space between the plates;

(2) the liquid and vapour flow without mixing, the direction of liquid flows coinciding on adjacent plates;

(3) the liquid and vapour flow without mixing, but liquid flows in opposite directions on the adjacent plates.

The unidirectional motion of liquid on adjacent plates is the most effective, and the mixing of liquid on a plate and vapour in the space between the plates is undesirable. The material-balance equation for the first mode of motion for an elementary volume of a constant-width layer on a plate is

$$L\,dx = G\,\frac{dz}{l_p}(y - \bar{y}_{n+1}), \tag{10.75}$$

where L is the liquid flow rate, kg-mole/hr; G the vapour flow rate, kg-mole/hr; l_p the length of the operating part of a plate, m; x and y are the liquid- and vapour-phase concentrations of the volatile component, mole fractions.

We assume that the equilibrium dependence within a plate is linear and can be represented in the form

$$y^* = mx + b,$$

where m is the slope of the equilibrium curve. Introducing the dimensionless coordinate $Z = z/l_p$, where l_p is the length of the oper-

ating part of the plate and z is the running coordinate of a point, measured from the end of the operating part of the plate, we transform Eq. (10.75) as follows:

$$\frac{L}{m}\, dy^* = G\, dZ\, (y - \bar{y}_{n+1}). \tag{10.76}$$

Since the diffusion potential factor λ is equal to the ratio of the slope of the equilibrium and operating lines (mG/L), expression (10.76) can be written in the form

$$dy^* = \lambda\, (y - \bar{y}_{n+1})\, dZ, \tag{10.77}$$

or

$$\frac{dy^*}{y - \bar{y}_{n+1}} = \lambda\, dZ \tag{10.78}$$

and since $\bar{y}_{n+1} = \text{const}$, we have

$$\frac{d\,(y^* - \bar{y}_{n+1})}{y - \bar{y}_{n+1}} = \lambda\, dZ. \tag{10.79}$$

According to Eq. (7.38), we get

$$\eta_{oy} = \frac{y - \bar{y}_{n+1}}{y^* - \bar{y}_{n+1}} \tag{10.80}$$

and

$$y^* - \bar{y}_{n+1} = \frac{1}{\eta_{oy}}\, (y - \bar{y}_{n+1}). \tag{10.81}$$

Assuming that $\eta_{oy} = \text{const}$ and differentiating, we obtain

$$d\,(y^* - \bar{y}_{n+1})\, \frac{d\,(y - \bar{y}_{n+1})}{\eta_{oy}}. \tag{10.82}$$

Substituting into this equation the value of $d\,(y^* - \bar{y}_{n+1})$ from Eq. (10.79), we get

$$\frac{d\,(y - \bar{y}_{n+1})}{y - \bar{y}_{n+1}} = \eta_{oy} \lambda\, dZ. \tag{10.83}$$

Integrating this equation between 0 and Z, we get

$$\ln \frac{y - \bar{y}_{n+1}}{y_n - \bar{y}_{n+1}} = \eta_{oy}\, \lambda Z \tag{10.84}$$

or

$$y = e^{\eta_{oy} \lambda Z}\, (y_n - \bar{y}_{n+1}) + \bar{y}_{n+1}. \tag{10.85}$$

The mean composition of vapour rising from a plate can be determined from Eq. (10.85):

$$\bar{y}_n = \int_0^1 y\,dZ = \int_0^1 [e^{\eta_{0y}\lambda Z}(y_n - \bar{y}_{n+1}) + \bar{y}_{n+1}]\,dZ$$

$$= \frac{1}{\eta_{0y}\lambda}(y - \bar{y}_{n+1})(e^{\eta_{0y}\lambda} - 1) + \bar{y}_{n+1}. \qquad (10.86)$$

Substituting $\bar{y}_n$ from Eq. (10.86) into (10.80), we can determine the gas-phase efficiency of the plate:

$$\eta_{py} = \frac{\frac{1}{\eta_{0y}\lambda}(y - \bar{y}_{n+1})(e^{\eta_{0y}\lambda} - 1) + \bar{y}_{n+1} - \bar{y}_{n+1}}{y^* - \bar{y}_{n+1}} = \frac{1}{\lambda}(e^{\eta_{0y}\lambda} - 1). \qquad (10.87)$$

Figure 169 shows the dependence of the plate efficiency on the local efficiency and the diffusion potential factor in the case of cross-flow of gas and liquid in the apparatus. The efficiency η_{py} attains its maximum value in the absence of gas mixing for a unidirectional liquid flow on all the plates (direct-flow plates). The plates with a complete mixing of gas in the space between the plates come next, followed by the plates with the counterflow of liquid (without gas mixing). The last place is occupied by the plates with a complete mixing of liquid and gas. However, a noticeable difference in the efficiencies is observed only for sufficiently high values of the local efficiency (above 0.7-0.8) and for large values of the diffusion potential factor (above 0.5).

The gas-phase efficiency of a plate, determined in the absence of gas mixing in the space between the plates, should be assumed exaggerated for direct-flow plates and underrated for counterflow plates, since under real conditions the motion of gas in the space between the plates without mixing is hardly possible. The effect of mixing of liquid on the column plates, which affects the ratio between η_0 and η_p can be estimated with the help of different methods.

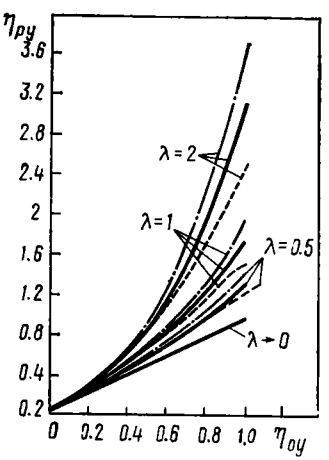

Fig. 169. Plate efficiency η_{py} vs. the local efficiency η_{0y} for a cross current flow:

——— gas is mixed between plates; – – – liquid on neighbouring plates moves in counterflow (gas between plates is not mixed); -·-·- liquid on neighbouring plates moves in the same direction (gas between plates is not mixed).

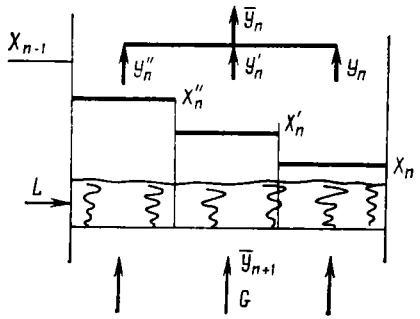

Fig. 170. Structural diagram of the mass-transfer process on a plate.

Cellular model. The following idea about the process of mixing on plates has found the widest recognition. A plate is divided into a number n of sections (cells) along the liquid flow. In each section, perfect mixing takes place but there is no mixing between the sections. It is assumed that (1) the vapour- and liquid-flow rates are constant within each cell; (2) the vapour has the same composition at the entrance of each cell; (3) the equilibrium dependence is linear, and (4) the local efficiency is constant over the entire area of the plate.

The structural diagrams of mass transfer, corresponding to the cellular model, are shown in Figs. 170 and 171. The material balance

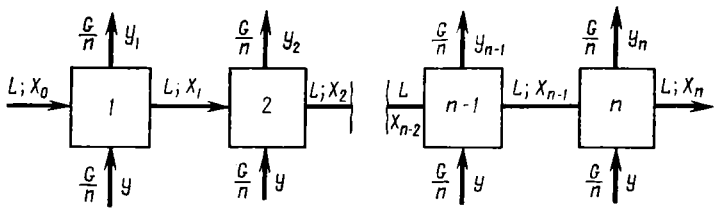

Fig. 171. Cellular model of the mass-transfer process on a plate.

equation for region *I* (Fig. 171) can be written in the form

$$Lx_0 + \frac{G}{n} y = Lx_1 + \frac{G}{n} y_1. \tag{10.88}$$

In accordance with the definition of the local efficiency, we have

$$\eta_{0y} = \frac{y_1 - y}{mx_1 - y + b}. \tag{10.89}$$

It follows from this expression that

$$y_1 = \eta_{0y} m x_1 - \eta_{0y} y + y + \eta_{0y} b. \tag{10.90}$$

Combining (10.88) and (10.90), we can write

$$x_1 = \frac{x_0}{1+B} + \frac{y'B}{m}\left(\frac{1}{1+B}\right), \tag{10.91}$$

where

$$B = \frac{\eta_{0y} m G}{nL}; \quad y' = y - b.$$

Similarly, we can write the expression for x_2:

$$x_2 = \frac{x_0}{(1+B)^2} + \frac{y'B}{m}\left[\frac{1}{1+B} + \frac{1}{(1+B)^2}\right] \tag{10.92}$$

and, in general,

$$x_n = \frac{x_0}{(1+B)^n} + \frac{y'B}{m}\left[\frac{1}{1+B} + \frac{1}{(1+B)^2} + \ldots + \frac{1}{(1+B)^n}\right]. \tag{10.93}$$

The number of terms of a geometrical progression is given by

$$\frac{1}{B}\left[1 - \frac{1}{(1+B)^n}\right]. \tag{10.94}$$

Consequently,

$$x_n = \frac{x_0}{(1+B)^n} + \frac{y'}{m}\left[1 - \frac{1}{(1+B)^n}\right]. \tag{10.95}$$

We determine the mean vapour concentration $\bar{y}$ above the plate:

$$\bar{y} = \frac{1}{G}\left[\frac{G}{n}y_1 + \frac{G}{n}y_2 + \ldots + \frac{G}{n}y_n\right] = \frac{\Sigma y}{n}. \tag{10.96}$$

Combining (10.90) and (10.96), we obtain

$$\bar{y} = \frac{\eta_{0y}m}{n}(\Sigma X) - \eta_{0y}y + y + \eta_{0y}b. \tag{10.97}$$

The quantity ΣX can be determined from the relation

$$x_1 + x_2 = x_0\left[\frac{1}{1+B} + \frac{1}{(1+B)^2}\right] + \frac{y'B}{m}\left[\frac{1}{(1+B)^2} + \frac{2}{1+B}\right] \tag{10.98}$$

and, generalizing the result, we obtain

$$\sum X = x_0\left[\frac{1}{1+B} + \frac{1}{(1+B)^2} + \ldots + \frac{1}{(1+B)^n}\right] + \frac{y'B}{m}\left[\frac{1}{(1+B)^n} + \frac{2}{(1+B)^{n-1}} + \ldots + \frac{n}{(1+B)}\right]. \tag{10.99}$$

The sum of the terms of geometrical and arithmetic progression, which follow $y'B/m$, is given by

$$\frac{(1+B)^n(Bn-1)+1}{B^2(1+B)^n}. \tag{10.100}$$

Substituting (10.94) and (10.100) into (10.99) and combining (10.99) and (10.97), we obtain

$$\bar{y} = \frac{\eta_{0y}mx_0}{nB}\left\{1 - \frac{1}{(1+B)^n} + \frac{\eta_{0y}my'B}{nm} \times \left[\frac{(1+B)^n(Bn-1)+1}{B^2(1+B)^n}\right]\right\} - \eta_{0y}y' + y. \tag{10.101}$$

Considering that the plate efficiency is

$$\eta_{py} = \frac{\bar{y} - y}{y_n^* - y}, \qquad (10.102)$$

obtain by substituting x_n from (10.95) into (10.100) and simplifying

$$y_n^* - y = \frac{mx_0 - y'}{(1+B)^n}. \qquad (10.103)$$

Substituting $\bar{y}$ from (10.101) into (10.102) and simplifying the result, we get

$$\bar{y} - y = \frac{\eta_{oy}}{nB}(mx_0 - y')\left[\frac{(1+B)^n - 1}{(1+B)^n}\right]. \qquad (10.104)$$

Substituting (10.97) and (10.98) into Eq. (10.103), we obtain

$$\eta_{py} = \frac{1}{\lambda}\left[\left(1 + \frac{\lambda\eta_{oy}}{n}\right) - 1\right]. \qquad (10.105)$$

For a practical application of this equation, the local efficiency and the number n of cells must be determined beforehand. For complete mixing of the liquid on a plate, $n = 1$. There is no mixing on the plate for $n \to \infty$. The number of cells as a function of the path of liquid on a plate can be approximately determined by using the plot in Fig. 172.

When using the cellular model for analyzing the intensity of mixing on plates it should be borne in mind that (1) the number of cells for perfect mixing depends on the liquid path: the longer the path, the weaker the mixing, and hence the larger the number of cells; (2) the number of cells depends on the velocity of liquid (increases with it); (3) the number of cells is determined by the construction of a plate; (4) the number of cells depends on the vapour velocity; (5) the effect of mixing of liquid is stronger for higher local efficiencies; and (6) for a constant number of cells, the plate efficiency increases with the diffusion potential factor.

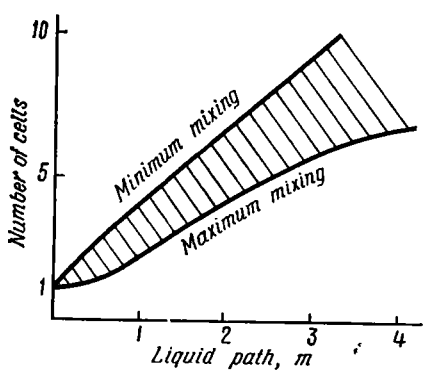

Fig. 172. The number of cells vs. the path covered by the liquid on the operating part of the plate.

The presence of a liquid-phase concentration gradient on a plate can be taken into account with the help of the coefficient ε of deviation of the actual mass-transfer driving force from the driving force in the case of perfect mixing:

$$\varepsilon = \frac{\Delta y_a}{\Delta y_m}. \qquad (10.106)$$

The value of ε is connected with the number of cells of complete mixing through the following relation:

$$\varepsilon = \frac{1}{n}\frac{y_n - y_{n+1}}{y^* - y_{n+1}} \cdot \frac{1}{\sqrt[n]{\frac{y_n^* - y_{n+1}}{y_n^* - y_n}} - 1}. \qquad (10.107)$$

In order to determine the number of perfect-mixing cells on a bubble-cap plate, the following equation can be used:

$$n = 0.915 \times 10^{-2}\,\mathrm{Re}_l^{0.6}\left(\frac{D}{h_w}\right)^{1.2}, \qquad (10.108)$$

where $\mathrm{Re}_l = Lh_L/\nu_L$; D is the column diameter, m; L the liquid flow rate, $m^3/m^2 \cdot s$; h_L the conditional height of clear liquid on a plate, m; h_w the weir height, m; and ν_L the kinematic viscosity, m^2/s.

The number of perfect-mixing cells into which a plate can be conventionally divided depends only on the hydrodynamic conditions. The velocity of the gas phase in the range from 0.4 to 0.97 m/s does not produce any noticeable effect on the intensity of liquid-phase mixing. The intensity of liquid-phase mixing is most strongly affected by the liquid flow rate and the weir height; mixing attenuates with increasing flow rate and is intensified with increasing weir height. The number of complete-mixing cells for sieve plate can be calculated by the equation

$$n = 0.45 + l_p\,(8.4 - 0.036h_w) - 0.0028\frac{G}{L}. \qquad (10.109)$$

Recirculation model. The effect of liquid-phase mixing on a plate can also be taken into account by the following considerations. Assuming that a part of liquid recirculates instantaneously from the weir to the plate inlet and that liquid flows under ideal displacement conditions, the plate efficiency can be calculated by the equation

$$\frac{\eta_{py}}{\eta_{oy}} = \frac{c\left[e^{\frac{\lambda\eta_{oy}}{c}} - 1\right]}{\lambda\eta_{oy}}, \qquad (10.110)$$

where

$$c = \frac{x_{n-1} - x_n}{x_1 - x_n}, \qquad (10.111)$$

x_{n-1} is the composition of liquid entering the plate; x_1 the liquid composition at the weir; and x_n the composition of liquid leaving the plate.

For $c = 1$ there is no mixing, while complete mixing is observed when $c = \infty$. However, for practical calculations the following expression is convenient:

$$\eta_{py} = \frac{e^{\lambda\eta_{oy}(1-I)} - 1}{\lambda(1-I)}, \qquad (10.112)$$

where I is the mixing factor. In the absence of mixing, $I = 0$ and η_{py} attains its maximum value given by

$$\eta_{py} = \frac{1}{\lambda}(e^{\lambda\eta_{0y}} - 1). \qquad (10.113)$$

For complete mixing, $I = 1$, and η_{py} attains its minimum value equal to $\eta_{py} = \eta_{0y}$. Practically, the values of the mixing factor lie between 0.25 and 0.75.

By-passing model. According to this model, a part A of liquid and B of gas pass through a plate in by-passing regimes. Such an idea about the structure of flows leads to the following relation:

$$\eta_{py} = \frac{(1-B)\,\eta_{0y}}{1+\frac{A(1+B)}{1-A}}. \qquad (10.114)$$

Diffusion model. A model of mixing on plates can be developed on the basis of turbulent diffusion concept. The degree of mixing is characterized by the dimensionless number Pe equal to the ratio of the path l_l covered by the liquid to the mixing length D_L/w_l where D_L is the turbulent diffusion coefficient and w_l the linear velocity of aerated liquid flowing through the plate. Thus, the number Pe is expressed in the form

$$\mathrm{Pe} = \frac{w_l l_l}{D_L} = \frac{l_l^2}{D_L \tau}, \qquad (10.115)$$

where τ is the duration of stay of liquid on a plate, equal to $\tau = \gamma_l h_L / L$; γ_l is the specific molar density of liquid, kg-mole/m^3; h_L the height of clear liquid, m; and L the liquid flow rate, kg-mole/m^2.

The higher the degree of mixing, the greater the value of D_L and the smaller the value of Pe. An increase in Pe indicates a decrease in the degree of mixing.

According to the diffusion model, it is assumed that the mixing rate for a component is proportional to the concentration gradient, and the transported mass is described by equations similar to the molecular-diffusion equations. The basic equation of the one-parametric diffusion model is obtained from the material balance equation written for an elementary foam layer on a plate (Fig. 173) and is written in the form

$$D_L \frac{d^2x}{dz^2} - \frac{L}{F_{c.l}\rho_l} \cdot \frac{dx}{dz} + \frac{y_1 - y_2}{F_{c.l}\rho_l} \frac{G}{l_p} = 0, \qquad (10.116)$$

where $F_{c.l.}$ is the cross-sectional area of the clear-liquid flow, m^2. If the local efficiency is constant over the length of a plate and the equilibrium dependence is linear, Eq. (10.116) can be written in the

form

$$\frac{1}{\mathrm{Pe}}\frac{d^2x}{dZ^2}-\frac{dx}{dZ}-\lambda\eta_{0y}(x-x_1^*)=0, \qquad (10.117)$$

where

$$\mathrm{Pe}=\frac{Ll_\mathrm{p}}{D_\mathrm{L}F_{\mathrm{c.l.}}\rho_\mathrm{l}}=\frac{w_\mathrm{l}l_\mathrm{p}}{D_\mathrm{L}},$$

L is the liquid flow rate, kg-mole/s; w_l is the velocity of liquid on a plate, m/s; $\lambda = mG/L$ is the diffusion potential factor; x_1^* is the equi-

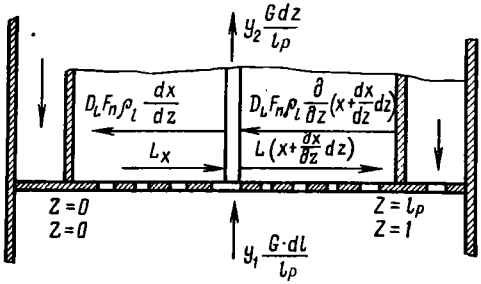

Fig. 173. To the derivation of the equation of the diffusion model.

librium concentration at the plate outlet; and $Z = z/l_\mathrm{p}$ is the dimensionless coordinate.

Using the boundary conditions

$$x=x_1 \text{ and } \frac{dx}{dZ}=0 \quad \text{for } Z=1, \qquad (10.118)$$

we obtain the following solution of Eq. (10.117):

$$\frac{x-x_1^*}{x_1-x_1^*}=\frac{e^{(\alpha+\mathrm{Pe})(Z-1)}}{1+\frac{\alpha+\mathrm{Pe}}{\alpha}}+\frac{e^{\alpha(1-Z)}}{1+\frac{\alpha}{\alpha+\mathrm{Pe}}}, \qquad (10.119)$$

where

$$\alpha=\frac{\mathrm{Pe}}{2}\left[\sqrt{1+\frac{4\lambda\eta_{0y}}{\mathrm{Pe}}}-1\right]. \qquad (10.120)$$

Equation (10.119) describes the variation of liquid concentration on a plate provided that vapour of constant composition is supplied to the plate. Let us determine the plate efficiency $\eta_{\mathrm{p}y}$ as a function of the degree of mixing of the liquid and of the local efficiency η_{0y}. For this purpose, we write the expression for the local efficiency in the form

$$\eta_{0y}=\frac{y-y_{n+1}}{y^*-y_{n+1}}=\frac{y-y_{n+1}}{m(x-x_{n+1}^*)} \qquad (10.121)$$

or

$$y-y_{n+1}=m(x-x_{n+1}^*)\,\eta_{0y}. \qquad (10.122)$$

In the absence of complete mixing, the composition of liquid, and, hence, of vapour, varies over the plate length. For a constant velocity of vapour (gas) over the entire plate cross section and in the absence of a concentration gradient of liquid in the direction perpendicular to the liquid flow, the following relation is valid:

$$\bar{y}_n - \bar{y}_{n+1} = m\eta_{0y} \int_0^1 (x - x^*_{n+1})\, dZ, \qquad (10.123)$$

where $\bar{y}_n$ and $\bar{y}_{n+1}$ are the mean composition of vapour entering and leaving a plate; Z is the dimensionless coordinate of the cross section where the liquid concentration is x. This coordinate is equal to the ratio of the distance between the cross section and the beginning of the active region to the entire length of the gas bubbling region.

Using Eq. (10.87) and assuming that $y^*_n = mx_n + b$, we obtain the following expression for determining the gas-phase plate efficiency:

$$\eta_{py} = \frac{\bar{y}_n - \bar{y}_{n+1}}{m(x_n - x^*_{n+1})}. \qquad (10.124)$$

Assuming that the composition of supplied vapour is constant over the plate cross section, i.e. $x^*_{n+1} = \text{const}$, this equation can be written in the form

$$\frac{\eta_{py}}{\eta_{0y}} = \int_0^1 \frac{x - x^*_{n+1}}{x_n - x^*_{n+1}}\, dZ. \qquad (10.125)$$

While deriving this equation, no assumptions were made about the nature of mixing. It shows that for $\eta_{0y} = \text{const}$, the liquid concentration profile on the plate unambiguously determines the mean composition of the vapour leaving the plate.

Substituting Eq. (10.119) into (10.125) and integrating, we get

$$\frac{\eta_{py}}{\eta_{0y}} = \frac{1 - e^{-(\alpha+\mathrm{Pe})}}{(\alpha+\mathrm{Pe})\left(1+\dfrac{\alpha+\mathrm{Pe}}{\alpha}\right)} + \frac{e^{\alpha}-1}{\alpha\left(1+\dfrac{\alpha}{\alpha+\mathrm{Pe}}\right)}, \qquad (10.126)$$

$$\alpha = \frac{\mathrm{Pe}}{2}\left(\sqrt{1 + \frac{4\dfrac{mG}{L}\eta_0}{\mathrm{Pe}}} - 1\right),$$

where L and G are liquid and gas flow rates, kg-mole/s.

Using for the solution of Eq. (10.117) the boundary conditions

$$\frac{dx}{dz} = \frac{L}{F_{\mathrm{c.l.}}\rho_l D_{\mathrm{L}}}(x - x_{l_p}) \quad \text{for } z = 0, \qquad (10.127)$$

$$\frac{dx}{dz} = 0 \quad \text{for } z = l_p,$$

and the material-balance equation for the entire plate

$$\bar{y}_n = \bar{y}_{n+1} + \frac{L}{G}(x - x_{l_p}), \tag{10.128}$$

we obtain the following ratio of η_{py} to η_{oy}:

$$\frac{\eta_{py}}{\eta_{oy}} = \frac{1}{4p\lambda\eta_{oy}}\{(1+p)^2 \exp[-z(1-p)] - (1-p)^2 \times \exp[-z(1+p)] - 4p\}, \tag{10.129}$$

where

$$p = \left(1 + \frac{4\lambda}{\mathrm{Pe}}\eta_{oy}\right)^{1/2}. \tag{10.130}$$

A graphic solution of Eq. (10.129) is shown in Fig. 174. As $D_L \to 0$, this equation is reduced to the form

$$\frac{\eta_{py}}{\eta_{oy}} = \frac{\exp \lambda_{oy} - 1}{\lambda\eta_{oy}}. \tag{10.131}$$

As $D_L \to \infty$, $\eta_{py}/\eta_{oy} = 1$.

Using the main assumptions of the diffusion model, we can obtain the following equation for calculating the local efficiency:

$$\eta_{oy} = 1 - \frac{4p \exp(2M_g)}{(1+p)^2 \exp[M_g(1+p)] - (1-p)^2 \exp[M_g(1-p)]} = N_{oy}\alpha = \frac{N_{ox}\alpha}{\lambda}, \tag{10.132}$$

where $p = (1 + 2N_{oy}/M_g)^{1/2}$; $\alpha = \eta_{oy}/N_{oy}$; λ is the diffusion potential factor; $N_{ox} = K_l a\,(l_p/w_l)$ the total number of transport units referred to the liquid phase; $N_{oy} = K_g a\,(h_f/w_g)$ the total number of transport units referred to the gas phase; w_l and w_g are the velocities of the liquid and gas phases, m/s; $M_g = h_f w_g/(2D_G)$ is the parameter characterizing gas mixing; $K_{ox}a$ and $K_{oy}a$ are the mass-transfer coefficients for liquid and gas phases, kg-mole/m^3·s; and h_f is the foam height, m.

It follows from this equation that the local efficiency depends on the phase contact time, mass-transfer coefficient and gas-phase mixing and does not depend on the position of a point under consideration on the plate. For perfect-gas mixing over the foam

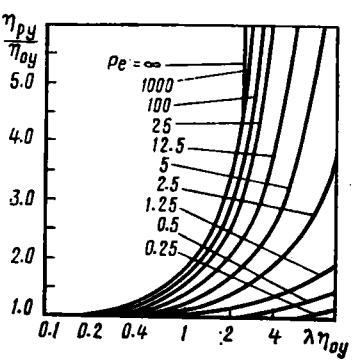

Fig. 174. Graphic solution of Eq. (10.129).

height ($M_g = 0$), η_{0y} tends to its limiting value defined by the equation

$$\eta_{0y} = \frac{N_{0y}}{1+N_{0y}} = \frac{N_{0x}}{\lambda\left(1-\frac{N_{0x}}{\lambda}\right)}, \qquad (10.133)$$

while in the absence of mixing over the foam height ($M_g \to \infty$), we have

$$\eta_{0y} = 1-\exp(-N_{0y}) = 1-\exp\left(-\frac{N_{0x}}{\lambda}\right). \qquad (10.134)$$

Figure 175 shows the variation of η_{0y} depending on N_{0y} and N_{0x} for different values of M_g.

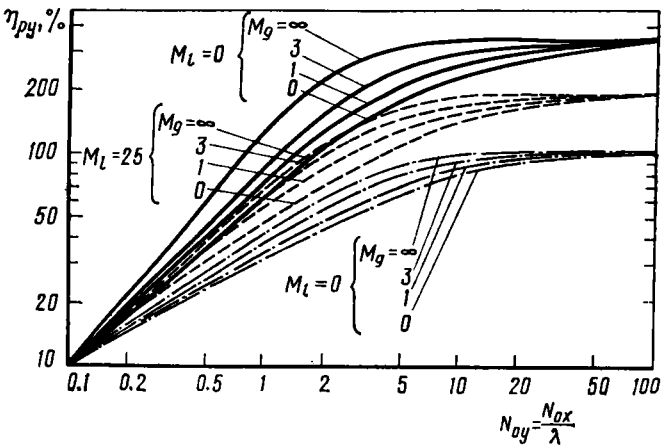

Fig. 175. The plate efficiency vs. the degree of mixing of liquid and gas and the number of transfer units.

The gas-phase plate efficiency can be calculated by the equation

$$\eta_{py} = \frac{1}{\lambda}\left[\frac{(1+q)^2\exp[M_1(1+q)]-(1-q)^2\exp[M_1(1-q)]}{4q\exp(2M_1)} - 1\right], \qquad (10.135)$$

where $M_1 = l_p w_f h_f/(2D_L h_L)$ is the parameter characterizing the mixing of liquid:

$$q = \left(1+\frac{2\lambda\eta_{0y}}{M_1}\right)^{1/2}; \qquad (10.136)$$

w_f is the linear velocity of liquid, calculated for the foam layer cross section, m/s; $\varphi = 1 - (h_L/h_f)$ is the gas content of the bubbling layer, m^3/m^3; and D_L is the turbulent diffusion coefficient for liquid on a plate, m^2/s.

Figure 176 shows the variation of the plate efficiency depending on M_l, M_g, N_{0y}, or N_{0x}, calculated by formula (10.136). The plate efficiency rapidly grows with N_{0y} or N_{0x} and decreases with increasing intensity of liquid- and gas-phase mixing. The effect of liquid-phase mixing on the plate efficiency is stronger than that of gas-phase mixing in the foam layer, the difference becoming especially noticeable with increasing N_{0y} or N_{0x}. An analysis of the dependence

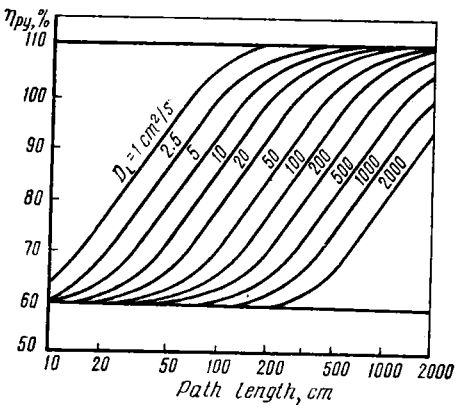

Fig. 176. The effect of the path covered by the liquid on the plate efficiency.

of plate efficiency for perfect gas mixing on the total number of transport units for the gas phase indicates that the effect of gas mixing is limited to the range of N_{0y} from 0.5 to 20. For $N_{0y} < 0.5$ and $N_{0y} > 20$, the variation of η_{py} upon a change in M_g from infinity to zero does not exceed 10 percent, and the maximum value of $\eta_{py}/(\eta_{py})\, M_{g=0}$ is attained for $N_{0y} = 2.5$-3.

Figure 176 represents the influence of the path l_p covered by the liquid on the plate efficiency for different values of the longitudinal mixing coefficients. For a constant turbulent diffusion coefficient D_L, the plate efficiency increases with the column diameter. The gas-phase plate efficiency in the case of cross-current gas and liquid flows can be calculated by the following equation:

$$\eta_{py} = \frac{1}{\lambda}\left[\left(\lambda\eta_{0y} + \frac{\mathrm{Pe}}{2}\right)\varepsilon^{-1}\sinh\exp\left(-\frac{\mathrm{Pe}}{2}\right) + \cosh\varepsilon\exp\left(-\frac{\mathrm{Pe}}{2}\right) - 1\right], \quad (10.137)$$

where

$$\varepsilon = \left(\lambda\eta_{0y}\,\mathrm{Pe} + \frac{\mathrm{Pe}^2}{4}\right)^{1/2}.$$

For determining the turbulent diffusion coefficient, the following empirical equations can be used:

1. For a bubble-cap plate with round caps of 75-mm diameter, arranged at the corners of an equilateral triangle with side 115 mm, as well as for a sieve plate,

$$D_L^{0.5} = 0.00378 + 0.0171w_g' + 0.0614L' + 0.18h_w. \quad (10.138)$$

2. For a plate with caps of diameter 165 mm, arranged at the corners of an equilateral triangle with side 222 mm, we have

$$D_L^{0.5} = 1.154\,(0.00378 + 0.0171w_g' + 0.0614L' + 0.18h_w), \quad (10.139)$$

where D_L is the turbulent diffusion coefficient, m^2/s; w_g' the gas velocity referred to dispersion area, m/s; L' the volumetric flow rate of liquid per unit weir width, m^3/s; and h_w the weir height, m.

It was established experimentally that such physical properties as viscosity, density, and surface tension do not considerably affect the degree of mixing of liquid on bubble-cap plates. The weir height, the density of bubbling gas (column pressure), and liquid- and gas-phase velocity do produce a noticeable effect.

The turbulent diffusion coefficient for a sieve plate can also be calculated from the empirical equation:

$$D_L = 24\left(\frac{G}{F'}\right)^{1.3}\left(\frac{L}{b'}\right)^{0.3} h_w^{0.6} B^{-0.4}, \quad (10.140)$$

where F' is the dispersion area, cm^2; L the liquid flow rate, kg/min; b' the weir width, m; h_w the weir height, m; and B the fraction of the plate open area, %.

Hybrid model. An analysis of the concentration profile for an indicator on sieve- and bubble-cap plates of diameter 700 mm has shown that there are zones with different mixing intensities on the plates. In the part of a sieve plate adjoining the disengaging zone at the inlet weir, gas flames are deflected by the liquid flow to the plate at the lower part of the foam layer and to the receiver weir at the upper part. Intensive foam circulation is observed at the column walls. The structure of liquid flow on plates is described by a hybrid model consisting of series-connected zones of complete mixing, viz. the zones described by the diffusion model and the zones of complete mixing.

The sizes of complete mixing zones on a sieve plate were: at the receiving weir the region is from 100 to 150 mm long, and at the downcomer, from 0 to 50 mm. The size of the zones changed only slightly upon a change in the gas and liquid flow rate and in the weir height. The heights of the weirs were 25, 50, 75, and 100 mm. The

reflux density changed from 0.5 to 3.5 $m^3/hr \cdot m$. The gas velocity calculated for the open-column area changed from 0.5 to 1.35 m/s. A transverse non-uniformity in the flow structure was also observed. The values of Pe for the diffusion zones at the centre of the plate were several times larger than the value of Pe at the column walls. The

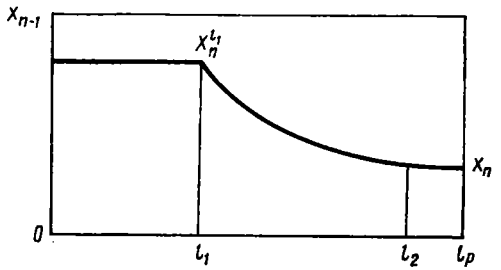

Fig. 177. Variation of the liquid concentration on a plate (hybrid model)

following dependence was proposed for determining the turbulent diffusion coefficient averaged over cross section in the zone described by the diffusion model:

$$D_{L_m} = 7.08 \times 10^{-2} \left(\frac{w_g}{w_l}\right)^{-0.47} h_w^{0.33} w_g^{1.25}, \qquad (10.141)$$

where D_{L_m} is the mean turbulent diffusion coefficient, m^2/s; w_g the gas velocity calculated for the column open area, m/s; w_l the mean velocity of liquid, m/s; and h_w the weir height, m.

Figure 177 represents the variation of liquid-phase concentration over the length of the operating part of a plate. The region from 0 to l_1 is a complete mixing cell. In the interval from l_1 to l_2 the change in the concentration is described by the equation of the diffusion model. Finally, the region from l_2 to l_p corresponds to a complete mixing cell. In order to determine the plate efficiency with the help of the hybrid model, we write Eq. (10.125) in the form

$$\frac{\eta_{py}}{\eta_{oy}} = \int_0^{Z_1} \frac{x - x_{n+1}^*}{x_n - x_{n+1}^*} dZ + \int_{Z_1}^{Z_2} \frac{x - x_{n+1}^*}{x_n - x_{n+1}^*} dZ + \int_{Z_2}^{1} \frac{x - x_{n+1}^*}{x_n - x_{n+1}^*} dZ. \qquad (10.142)$$

The liquid concentration in the complete mixing region at the weir is constant ($x = x_n$). For this region, we have

$$Z/Z_2 = \frac{l_p - l_2}{l_p}. \qquad (10.143)$$

In order to determine the second integral in (10.142), let us introduce the dimensionless coordinate Z' which is the ratio of the distance between the cross section and the beginning of the zone de-

scribed by the equation of the diffusion model to the entire length of this zone. Then, changing the limits of integration for the second term in (10.142), we can write

$$\int_{Z_1}^{Z_2} \frac{x-x^*_{n+1}}{x_n-x^*_{n+1}}dZ = \frac{l_2-l_1}{l_p}\int_0^1 \frac{x-x^*_{n+1}}{x_n-x^*_{n+1}}dZ'. \qquad (10.144)$$

For the diffusive mechanism of mixing and boundary conditions (10.118), the integrand is given by

$$\frac{x-x^*_{n+1}}{x_n-x^*_{n+1}} = \frac{e^{(\alpha+\mathrm{Pe})(Z'-1)}}{1+\dfrac{\alpha+\mathrm{Pe}}{\alpha}} + \frac{e^{\alpha(1-Z')}}{1+\dfrac{\alpha}{\alpha+\mathrm{Pe}}}, \qquad (10.145)$$

where

$$\alpha = \frac{\mathrm{Pe}}{2}\left(\sqrt{1+\frac{4\eta_{0y}\lambda_D}{\mathrm{Pe}}}-1\right),$$

$$\mathrm{Pe} = \frac{w(l_2-l_1)}{D_m}, \quad \lambda_D = \frac{mG(l_2-l_1)}{Ll_p}.$$

Substituting Eq. (10.145) into the integrand of Eq. (10.144), we obtain

$$\int_{Z_1}^{Z_2} \frac{x-x^*_{n+1}}{x_n-x^*_{n+1}}dZ = \frac{l_2-l_1}{l_p}\left[\frac{1-e^{-(\alpha+\mathrm{Pe})}}{(\alpha+\mathrm{Pe})\left(1+\dfrac{\alpha+\mathrm{Pe}}{\alpha}\right)} + \frac{e^{\alpha}-1}{\alpha\left(1+\dfrac{\alpha}{\alpha+\mathrm{Pe}}\right)}\right]. \qquad (10.146)$$

While calculating the first zone, we use Eq. (10.145) for determining x for $Z' = 0$. As a result, we obtain

$$\int_0^{Z_1} \frac{x-x^*_{n+1}}{x_n-x^*_{n+1}}dZ = \frac{l_1}{l_p}\left[\frac{e^{-(\alpha+\mathrm{Pe})}}{1+\dfrac{\alpha+\mathrm{Pe}}{\alpha}} + \frac{e^{\alpha}}{1+\dfrac{\alpha}{\alpha+\mathrm{Pe}}}\right]. \qquad (10.147)$$

Substituting the values of three terms, (10.143), (10.144), and (10.147) into Eq. (10.142), we obtain the ratio of the plate efficiency to the local efficiency for the entire operating part of the plate:

$$\frac{\eta_{py}}{\eta_{0y}} = \frac{l_1}{p}\left[\frac{e^{-(\alpha+\mathrm{Pe})}}{1+\dfrac{\alpha+\mathrm{Pe}}{\alpha}} + \frac{e^{\alpha}}{1+\dfrac{\alpha}{\alpha+\mathrm{Pe}}}\right]$$

$$+\frac{l_2-l_1}{l_p}\left[\frac{1-e^{-(\alpha+\mathrm{Pe})}}{(\alpha+\mathrm{Pe})\left(1+\dfrac{\alpha+\mathrm{Pe}}{\alpha}\right)} + \frac{e^{\alpha}-1}{\alpha\left(1+\dfrac{\alpha}{\alpha+\mathrm{Pe}}\right)}\right] + \frac{l_p-l_2}{l_p}. \qquad (10.148)$$

For a more accurate calculation η_{py}/η_{oy}, the ratio of the linear dimensions can be replaced by the ratio of areas.

Figure 178 represents the block diagram of a hybrid model of the liquid-phase flow structure. Assuming that the equilibrium dependence corresponds to the linear equilibrium dependence $y^* = mx$ within the limits of concentration variation on a plate, the local

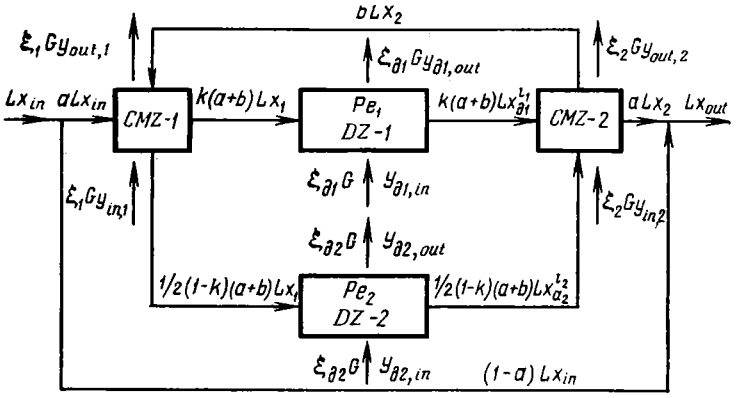

Fig. 178. Block diagram for the hybrid model of the structure of the liquid-phase flow on a bubbling plate.

efficiency is constant over the entire dispersion area; the volumetric flow rates of the liquid and gas phases are constant over the entire cross section of the operating part of the plate, and the entrainment of liquid between plates is ignored. The system of equations for calculating the material balance and kinetics of the mass-transfer process, determined by the local efficiency η_{oy}, was solved by using the finite difference method. This system has the form

$$ax_{1n} + bx_2 - (a+b)\,x_1 = \eta_{oy}\lambda\xi_1 x_1 - \eta_{oy}\frac{G\xi_1}{LZ_1}\int_0^{Z_1} y_{1n,\,1}(Z)\,dZ, \quad (10.149)$$

$$y_{out,\,1}(Z) - y_{1n,\,1}(Z) = \eta_{oy}\,[mx_1 - y_{1n,\,1}(Z)], \quad (10.150)$$

$$\frac{d^2x_{\partial 1}}{dZ_{\partial 1}^2} - \mathrm{Pe}_1\frac{dx_{\partial 1}}{dZ_{\partial 1}} = \eta_{oy}\,\mathrm{Pe}_1\frac{\lambda\xi_{\partial 1}}{Z_{\partial 1}}\int_{Z_1}^{Z_{\partial 1}} x_{\partial 1}(Z)\,dZ$$

$$-\eta_{oy}\,\mathrm{Pe}_1\frac{G\xi_{\partial 1}}{LZ_{\partial 1}}\int_{Z_1}^{Z_{\partial 1}} y_{\partial 1,\,in}(Z)\,dZ, \quad (10.151)$$

$$y_{\partial 1,\,out}(Z) - y_{\partial 1,\,in}(Z) = \eta_{oy}\,[mx_{\partial 1}(Z) - y_{\partial 1,\,in}(Z)], \quad (10.152)$$

$$\frac{d^2x_{\partial 2}}{dZ_{\partial 2}^2} - \mathrm{Pe}_2 \frac{dx_{\partial 2}}{dZ_{\partial 2}} = \eta_{0y}\,\mathrm{Pe}_2 \frac{\lambda\xi_{\partial 2}}{Z_{\partial 2}} \int_{Z_2}^{Z_{\partial 2}} x_{\partial 2}(Z)\,dZ$$

$$- \eta_{0y}\,\mathrm{Pe}_2 \frac{G\xi_{\partial 2}}{LZ_{\partial 2}} \int_{Z_2}^{Z_{\partial 2}} y_{\partial 2,\,\mathrm{in}}(Z)\,dZ, \quad (10.153)$$

$$y_{\partial 2,\,\mathrm{out}}(Z) - y_{\partial 2,\,\mathrm{in}}(Z) = \eta_{0y}\,[mx_{\partial 2}(Z) - y_{\partial 2,\,\mathrm{in}}(Z)], \quad (10.154)$$

$$k(a+b)\,x_{\partial 1}^{Z_1} + (1-k)(a+b)\,x_{\partial 2}^{Z_{\partial 2}} - (a+b)\,x_2$$

$$= \eta_{0y}\lambda\xi_2 x_2 - \eta_{0y}\frac{G\xi_2}{LZ_2} \int_{Z_1}^{1} y_{\mathrm{in},\,2}(Z)\,dZ, \quad (10.155)$$

$$y_{\mathrm{out},\,2}(Z) - y_{\mathrm{in},\,2}(Z) = \eta_{0y}\,[mx_2 - y_{\mathrm{in},\,2}(Z)], \quad (10.156)$$

$$ax_2 + (1-a)\,x_{\mathrm{in}} = x_{\mathrm{out}}. \quad (10.157)$$

The boundary conditions are

$$Z_{\partial 1} = Z_{\partial 2} = 0; \quad \frac{dx_{\partial 1}}{dZ_{\partial 1}} = \mathrm{Pe}_1\,(x_{\partial 1} - x_1); \quad \frac{dx_{\partial 2}}{dZ_{\partial 2}} = \mathrm{Pe}_2\,(x_{\partial 2} - x_2), \quad (10.158)$$

$$Z_{\partial 1} = Z_{\partial 2} = 1, \quad \frac{dx_{\partial 1}}{dZ_1} = \frac{dx_{\partial 2}}{dZ_{\partial 2}} = 0. \quad (10.159)$$

While calculating the lower part of the column, it was assumed that

$$y_{\mathrm{in},\,1} = y_{\partial 1,\,\mathrm{in}} = y_{\partial 2,\,\mathrm{in}} = y_{\mathrm{in},\,2} = y_0^* = mx_{\mathrm{w}}, \quad (10.160)$$

$$Lx_{\mathrm{out},\,1} = Gy_0^* + Wx_{\mathrm{w}}, \quad (10.161)$$

where L is the liquid-phase flow rate; G the gas-phase flow rate; W the still waste; x_{w} the liquid-phase composition in the column still; y_0^* the vapour composition is in equilibrium with that of liquid in the still; $\lambda = mG/L$ the diffusion potential factor; m the equilibrium constant; η_{0y} the local efficiency; ξ_1, ξ_2, $\xi_{\partial 1}$, $\xi_{\partial 2}$ are the volume fractions of corresponding zones of the plate; a is the fraction of liquid flow taking part in dispersion; $(1-a)$ the fraction of by-passing flow; b the fraction of the recirculating flow; k the fraction of liquid passing through the average section of the plate; Pe_1, Pe_2 are the Peclet numbers of the corresponding zones of the plate; $Z = l/l_{\mathrm{p}}$ is the dimensionless length of the operating part of the plate; l_{p} the length of the operating part of the plate; 1, 2, $\partial 1$, $\partial 2$ are the indices of the variables Z, x, y indicating that they respectively belong to the complete mixing zone at the plate inlet (CMZ-1, Fig. 178); the mixing zone at the plate outlet (CMZ-2, Fig. 178); the central

diffusion zone (DZ-1, Fig. 178); and to the side diffusion zone (DZ-2, Fig. 178); in and out are the indices denoting the compositions x and y of liquid and vapour entering the plate or a corresponding zone of the plate and leaving the corresponding zones of the plate or the plate on the whole.

Figure 179 represents the dependences of the number n of separation stages on the values of η_{0y} and λ, which show that the efficiency abruptly increases with η_{0y} and λ, while the number of separation stages correspondingly decreases. The ranges of η_{0y} and λ were chosen on the basis of experimental results obtained on industrial rectifying setups.

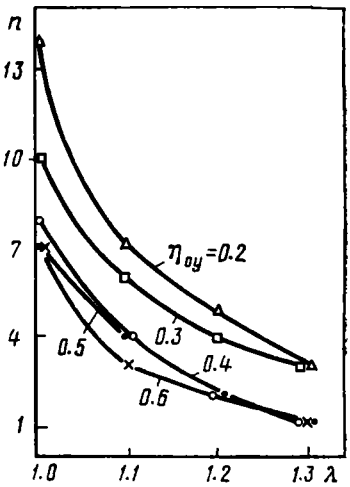

Fig. 179. The number n of separation stages vs. η_{0y} and λ for a given HETP.

In the ranges $\eta_{0y} = 0.2\text{-}0.6$ and $\lambda = 1.0\text{-}1.3$ in which we are interested, for a given degree of separation, a change in the structure of the vapour-phase flow practically does not affect the efficiency and height of mass-transfer apparatus. Indeed, the number of separation stages remains unchanged, if the actual structure of the vapour-phase flow is idealized by the complete mixing model. This permits the assumption about complete vapour mixing in the space between the plates and the calculation of mass-transfer apparatus according to the dependences which determine the plate efficiency.

An analysis of the variation of the liquid- and vapour-phase concentrations upon a plate-to-plate transition revealed that for $\eta_{0y} = 0.6\text{-}1.0$ and $\lambda < 1$, we must take into account the actual structure of the flow not only of liquid but the vapour phase as well.

In addition to the effect of the vapour-phase flow structure, the dependence of the efficiency of mass-transfer apparatus on the direction of liquid flows on adjacent plates was also investigated. The results of calculations show that if the actual vapour- and liquid-phase flow structure is taken into account, the direct and countercurrent flows of liquid ensure practically the same degree of separation for the same number of phase contacts. This makes it possible to considerably simplify the structure of column-type mass-transfer apparatus.

Besides the calculations described above, the effect of deformation of the hybrid model on the mass transfer efficiency was also studied. A change in the size of complete mixing zones at the plate inlet and

outlet ($\xi_1 = \xi_2 = 0.14$) led to a two-fold decrease in the efficiency, while an additional increase in the degree of recirculation to 0.5 decreases the efficiency by a factor of 4.6.

In order to compare the results obtained with the help of the hybrid model, the number of separation stages was calculated for the vapour- and liquid-phase flow structure described by the following models: (1) ideal vapour-phase displacement and ideal liquid-phase displacement; (2) complete vapour-phase mixing and ideal liquid-phase displacement.

The results of calculation testify that it is necessary to take into account the effect of actual flow structure on the efficiency of mass-transfer apparatus. An unsubstantiated idealization of the liquid-phase flow by the models of ideal displacement or complete mixing may lead to an incorrect results of calculation of the height of mass-transfer apparatus with a reduced number of contact units which, in turn, will not allow to attain in them the required degree of separation. In this case, the error in the dependence of η_{0y} on the model type may reach 40 percent for $\eta_{0y} = 0.6$ and 10-70 percent for $\eta_{0y} = 0.2$. The analysis has shown that the actual structure of liquid- and vapour-phase flows must be taken into consideration while calculating the plate columns for diffusion processes.

10.4. Estimation of the Efficiency of Mass Transfer on Plates for Separating Multicomponent Mixtures

In separating multicomponent mixtures, the efficiency of the same plate with respect to different components of a mixture being separated, calculated by formula (7.40), may differ considerably. Let us analyze the variation of the plate efficiency for different components of the mixture. We consider a three-component mixture and a rectifying column operating with total reflux. In the conditions of total reflux, for each plate we have

$$x_{i+1,k} = y_{i,k} \quad (k = 1, 2, 3). \tag{10.162}$$

When relation (7.40) is used for determining the plate efficiency with respect to any of the components being separated, the composition of the vapour phase leaving the ith plate can be calculated from the equation

$$y_{i,k} = (1 - \eta_p)\, y_{i-1,k} + \eta_p y^*_{i,k} \quad (k = 1, 2, 3). \tag{10.163}$$

Not all quantities η_p in this equation are independent, since $y_{i,k}$ must satisfy the condition

$$\sum_{k=1}^{3} y_{i,k} = 1. \tag{10.164}$$

Let us suppose that the relative volatilities of the mixture components being separated are temperature independent. Then, determining the relative volatilities a_k with respect to the lightest component ($k = 1$), we obtain the following relation:

$$a_1 > a_2 > a_3 \quad (a_1 = 1). \tag{10.165}$$

Then the vapour-phase composition which is in equilibrium with the liquid on the ith plate can be calculated by the formula

$$y_{i,\,k} = \frac{a_k x_{i,\,k}}{\sum\limits_{k=1}^{3} a_k x_{i,\,k}}. \tag{10.166}$$

Taking (10.162) into consideration, this formula can be written as

$$y^*_{i,\,k} = \frac{a_k y_{i-1,\,k}}{\sum\limits_{k=1}^{3} a_k y_{i-1,\,k}}. \tag{10.167}$$

Expression (10.163) can be written in the form

$$y_{i,\,k} = y_{i-1,\,k}\left[1 - \eta_p + \frac{a_k \eta_p}{\sum\limits_{k=1}^{3} a_k y_{i-1,\,k}}\right]. \tag{10.168}$$

An identical expression can be written for the $(i + 1)$th column plate:

$$y_{i+1,\,k} = y_{i,\,k}\left[1 - \eta_p + \frac{a_k \eta_p}{\sum\limits_{k=1}^{3} a_k y_{i,\,k}}\right]. \tag{10.169}$$

If we know the composition of vapour entering the $(i - 1)$th plate, it is possible to determine the composition of the vapour phase leaving the $(i + 1)$th plate. For this purpose, we substitute into Eq. (10.169) the values of $y_{i,k}$ calculated from (10.168). Suppose that the required separation product is the lightest component, and the plate efficiency η_{p1} with respect to this component is a known constant quantity.

Let us consider the effect of plate efficiencies η_{p2} and η_{p3} with respect to heavy components on the separation capacity of the two plates. For estimating the HETP, we shall use the difference in concentrations

$$\Delta y_1 = y_{i+1,1} - y_{i-1,1}, \tag{10.170}$$

which is equal to the amount of the light component extracted from the liquid on the two plates. For this purpose, it is sufficient to investigate the signs of the derivatives $\partial \Delta y_1 / \partial \eta_{p2}$ and $\partial \Delta y_1 / \partial \eta_{p3}$.

Since η_{p1} is a given constant quantity, and all the values of η_p are interrelated through the condition (10.164), it is sufficient to in-

vestigate the sign of only one derivative, taking into account the relation between η_{p2} and η_{p3}. Substituting into (10.170) the values of y_{i+1} from (10.169) and differentiating with respect to λ_{p3}, we obtain

$$\frac{\partial \Delta y_1}{\partial \eta_{p3}} = \frac{\partial y_{i,1}}{\partial \eta_{p3}} \left[1 - \eta_{p1} + \frac{a_1 \eta_{p1}}{\sum_{k=1}^{3} a_k y_{i,k}} \right] - y_{i,k} \frac{a_k \eta_{p1}}{\left(\sum_{k=1}^{3} a_k y_{i,k} \right)^2} \sum_{k=1}^{3} a_k \frac{\partial y_{i,k}}{\partial \eta_{p3}}. \quad (10.171)$$

Since $\eta_{p1} = \text{const}$, we obtain

$$\frac{\partial \eta_{p1}}{\partial \eta_{p3}} = 0, \quad \frac{\partial y_{i,1}}{\partial \eta_{p3}} = 0. \quad (10.172)$$

Differentiating relation (10.164) taking into account (10.172), we obtain

$$\frac{\partial y_{i,2}}{\partial \eta_{p3}} = -\frac{\partial y_{i,3}}{\partial \eta_{p3}}. \quad (10.173)$$

Besides, it follows from (10.168) that

$$\frac{\partial y_{i,3}}{\partial \eta_{p3}} = y_{i-1,3} \left(\frac{a_3}{\sum_{k=1}^{3} a_k y_{i-1,k}} - 1 \right). \quad (10.174)$$

Considering (10.172)-(10.174), expression (10.171) assumes the form

$$\frac{\partial \Delta y_1}{\partial \eta_{p3}} = \frac{a_1 y_{i,1} \eta_{p1}}{\left(\sum_{k=1}^{3} a_k y_{i,k} \right)^2} y_{i-1,3} \left(1 - \frac{a_3}{\sum_{k=1}^{3} a_k y_{i-1,k}} \right) (a_3 - a_2), \quad (10.175)$$

In this equation, the term

$$1 - \frac{a_3}{\sum_{k=1}^{3} a_k y_{i-1,k}}$$

is a positive quantity:

$$1 - \frac{a_3}{\sum_{k=1}^{3} a_k y_{i-1,k}} = \frac{\sum_{k=1}^{3} a_k y_{i-1,k} - a_3 \sum_{k=1}^{3} y_{i-1,k}}{\sum_{k=1}^{3} a_k y_{i-1,k}} = \frac{\sum_{k=1}^{3} (a_k - a_3) y_{i-1,k}}{\sum_{k=1}^{3} a_k y_{i-1,k}} > 0,$$

since, in accordance with (10.165), $a_k - a_3 \geqslant 0$ for any value of k. The difference $a_3 - a_2$ is a negative quantity, while all the remaining terms of Eq. (10.175) are positive. Consequently,

$$\frac{\partial \Delta y_1}{\partial \eta_{p3}} < 0. \tag{10.176}$$

The same result can be obtained by assuming that the relative volatilities of the components are temperature dependent. It follows from inequality (10.176) that for a constant plate efficiency η_{p1} for the lightest component, the HETP of a group of plates for this component increases with decreasing η_{p2}. Hence, the HETP of plates for the light component is higher for plates with a lower value of efficiency calculated for the heavy component.

While determining the number of actual plates in rectifying columns intended for separating multicomponent mixtures, use should be made of the calculation methods that take into account a possible difference in plate efficiencies with respect to all the components of the mixture being separated. The interfacial mass transfer for multicomponent systems is determined by the matrix of the overall mass-transfer coefficients $[K_{0y}]$, which is calculated through the matrices of local mass-transfer coefficients by the formula (see Part One)

$$[K_{0y}]^{-1} = [k_y]^{-2} + [m]\ [k_x]^{-1}. \tag{10.177}$$

The vector of the numbers of components transferred from the liquid to the vapour phase is then defined by the following expression:

$$N = [K_{0y}]\ (y^* - y), \tag{10.178}$$

where $y^* = \begin{pmatrix} y_1^* \\ \vdots \\ y_{n-1}^* \end{pmatrix}$ is the vector of the vapour phase composition in equilibrium with the liquid phase; $y = \begin{pmatrix} y_1 \\ \vdots \\ y_{n-1} \end{pmatrix}$ the vapour-phase composition vector; and $N = \begin{pmatrix} N_1 \\ \vdots \\ N_{n-1} \end{pmatrix}$ the vector of component flows through unit interfacial area of mass transfer.

It follows from formula (10.178) that if the matrix of overall mass-transfer coefficients $[K_{0y}]$ is non-diagonal, the amount of a component transferred from one phase to another will depend not only on the driving force of this component but also on driving forces of other mixture components. If the components being separated are close in physical properties and we can assume that the local mass-transfer coefficients are the same for each phase with respect to all the components, i.e. the matrices of the local mass-transfer coefficients

are diagonal, the matrix $[K_{0y}]$ of the overall mass-transfer coefficients may be non-diagonal, since the matrix $[m]$ of the slopes of the tangents to equilibrium dependences is non-diagonal in the general case.

In the ideal displacement model, the equation describing the variation of component concentrations over the height of the mass-transfer space has the form

$$G\frac{dy}{dh} = aN \tag{10.179}$$

or, taking into account expression (10.178) for the vector N,

$$G\frac{dy}{dh} = a[K_{0y}](y^* - y), \tag{10.180}$$

where a is the interfacial area per unit height of the mass-transfer space.

If we suppose that the liquid is perfectly mixed over the height of the mass-transfer space and the matrix of the overall mass-transfer coefficients $[K_{0y}]$ and the interfacial area a are constant, the analytical solution of Eq. (10.180) has the form

$$y = y^* + \exp\{-[N]\}(y - y^*), \tag{10.181}$$

where $\{N\}$ denotes the matrix of the number of transport units, defined as

$$[N] = \frac{ah}{G}[K_{0y}]. \tag{10.182}$$

In order to use formula (10.180) for determining the composition of vapour leaving a plate, we must calculate the exponential function of the matrix of transport units. For this purpose, we can use the relation

$$\exp\{-[N]\} = \sum_{l=1}^{n-1} \exp\{-N_l^0\}[Z(N_l^0)], \tag{10.183}$$

where

$$[Z(N_l^0)] = \frac{\prod_{j\neq l}^{n=1}(N_l^0[I] - [N])}{\prod_{j\neq l}^{n=1}(N_j^0 - N_l^0)}, \tag{10.184}$$

$N_l^0[I]$ is the unit matrix, and $[N]$ are the eigenvalues of the transport unit matrix.

Relation (10.183) is used for calculating the function of the matrix only when all the eigenvalues N_l^0 are different. The function of the matrix, defined by (10.183), is also a matrix which is non-diagonal in the general case. This matrix can be employed for deter-

mining the local efficiency matrix by the formula

$$[\eta] = [I] - \exp\{-[N]\}. \quad (10.185)$$

Using the local efficiency matrix in this form, expression (10.181) defining the composition of the vapour leaving the plate can be written in the form

$$y = y_0 + [\eta]\,(y^* - y_0) \quad (10.186)$$

or, in the conventional form,

$$y_j = y_{0j} + \sum_{l=1}^{n-1} \eta_{jl}\,(y_l^* - y_{0l}), \quad j = 1, \ldots, n-1. \quad (10.187)$$

In accordance with the definition, the local vapour-phase contact efficiency is expressed as

$$\eta_j = \frac{y_j - y_{0j}}{y_j^* - y_{0j}}. \quad (10.188)$$

Formula (10.187) makes it possible to establish the relation between the local efficiency η_j and elements of the matrix of local efficiency in the following form:

$$\eta_j = \frac{\sum_{l=1}^{n-1} \eta_{jl}\,(y_l^* - y_{0l})}{y_j^* - y_{0j}}. \quad (10.189)$$

It follows from this expression that the local efficiency of contact depends not only on the local conditions of mass transfer, which are accounted for by the local efficiency matrix $[\eta]$, but also on the driving forces of the mixture components being separated. The local efficiency defined by formula (10.189) can be greater than unity or negative for a multicomponent mixture. Thus, the concept of local efficiency of contact for a multicomponent mixture loses its physical meaning and can be used only for formally expressing the observed HETP.

The matrix $[\eta]$ of local efficiencies of a contact can also be calculated directly through the matrix of the number of transport units $[N]$ by using the following formula:

$$[\eta] = \sum_{l=1}^{n-1} (1 - \exp\{-N_l^0\})\,[Z\,(N_l^0)] \quad (10.190)$$

which can be obtained by substituting (10.183) into (10.185).

For calculating the matrix of overall mass-transfer coefficients K_{0y}, through which the matrix $[N]$ (10.182) of transport units can be determined, use should be made of the matrix $[m]$ of slopes of the tangents to equilibrium dependences. The slope matrix is determined as the matrix of the linear approximation of equilibrium equa-

tions

$$y^* = y_0^* + [m]\,(x - x_0). \tag{10.191}$$

Since the concentrations of only $(n-1)$ components of a multicomponent mixture are linearly independent, formula (10.177) may only contain the matrices that determine the mass-transfer conditions for $(n-1)$ components. The same applies to the matrix $[m]$. If the equilibrium dependence is known, we obtain

$$y_i^* = K_i\,(T,\ P,\ x_1,\ x_2,\ \ldots,\ x_n)\,x_i, \quad i = 1,\ \ldots,\ n. \tag{10.192}$$

The linear approximation of the equilibrium dependence for the jth mixture component is represented in the form

$$y_i^* = y_{0i}^* + \sum_{j=1}^{n} \frac{\partial y_i^*}{\partial x_j}\,(x_j - x_{0j}). \tag{10.193}$$

In order to exclude from this expression the liquid-phase concentration of one component, say, the nth component, we can use the relation

$$\sum_{l=1}^{n-1} (x_j - x_{0j}) = 0, \tag{10.194}$$

from which it follows that

$$x_n - x_{0n} = -\sum_{l=1}^{n-1} (x_j - x_{0j}). \tag{10.195}$$

Substituting the value of $x_n - x_{0n}$ from this equation into (10.193) we obtain

$$y_i^* = y_{0i}^* + \sum_{l=1}^{n-1} \left(\frac{\partial y_i^*}{\partial x_l} - \frac{\partial y_i^*}{\partial x_n}\right)(x_l - x_{0l}), \tag{10.196}$$

whence

$$m_{ij} = \frac{\partial y_i^*}{\partial x_j} - \frac{\partial y_i^*}{\partial x_n}. \tag{10.197}$$

Thus, the matrix elements of $[m]$ are determined by the partial derivatives of the equilibrium expressions (10.192). For small deviations in concentrations, for which the error of the linear approximation (10.191) is insignificant, we can assume that the relative volatilities of the components are constant, and equilibrium relations can be represented in the form

$$y_i^* = \frac{\alpha_{il} x_i}{\sum_{s=1}^{n} \alpha_{sl} x_s}, \tag{10.198}$$

where

$$\alpha_{sl} = \frac{K_s}{K_l} = \text{const}, \tag{10.199}$$

K_s and K_l are equilibrium constants.

Differentiating (10.198) with respect to x_j, we can obtain the following formula for the derivative:

$$\frac{\partial y_i^*}{\partial x_j} = \begin{cases} -y_i^* \dfrac{y_j^*}{x_j} & i \neq j \\ (1 - y_i^*) \dfrac{y_i^*}{x_i} & i = j, \end{cases} \tag{10.200}$$

or

$$\frac{\partial y_i^*}{\partial x_j} = (\delta_{ij} - y_i^*) \frac{y_j^*}{x_j}. \tag{10.201}$$

Substituting the obtained value of the derivative (10.201) into (10.197), we obtain the required expression for the matrix elements of $[m]$:

$$m_{ij} = (\delta_{ij} - y_i^*) \frac{y_j^*}{x_j} + y_i^* \frac{y_n^*}{x_n}. \tag{10.202}$$

10.5. Modelling and Calculation of Packed Columns

10.5.1. Mass Transfer in Packed Columns

Figure 180 represents the height of an equivalent theoretical plate for a packed rectifying column (HETP) as a function of the vapour velocity referred to the total column cross section for different ring diameters. It follows from the figure that the nature of the dependence of HETP on the vapour velocity is the same for different packings and remains the same for different mixtures. For all packings, regimes corresponding to definite hydrodynamic conditions are different. For a comparatively low flow rates through a column, an increase in the vapour velocity in the column decreases the HETP for the packing. The hydrodynamic investigation carried out under these conditions has shown that liquid flows without eddy formation. The time of phase contact,

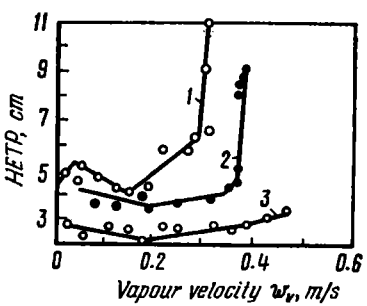

Fig. 180. HETP of a packed rectifying column vs. the vapour velocity in a carbon tetrachloride-benzene system: *1*—5.7 × 5.9 × 0.6-mm rings; *2*—8 × 8 × ×2-mm rings; *3*—10.9 × 11.5 × 2-mm rings.

which can be expressed through the duration of stay of the liquid in the packing under these conditions, decreases with increasing vapour velocity, since the ratio of the holding capacity of a packing to the amount of liquid flowing down per unit time decreases. The total interfacial area in this regime remains unchanged since the liquid flows down without whirling, and an increase in the amount of flowing-down liquid only increases the thickness of the flowing-down liquid film. The interfacial area per unit volume of the flowing-down liquid decreases with increasing amount of liquid. An increase in the liquid-film thickness slows down the levelling out of concentration and temperature in the bulk of liquid, which diminishes the driving force of the process at the interface. An increase in flow rates in the column leads to the turbulization of the liquid flowing down the packing, thus improving mass transfer. The increasing vapour velocity increases the HETP of the packing. Since the holding capacity of the packing rapidly increases, the phase contact time increases. The interfacial area increases due to eddy formation. The driving force of the process also increases due to a faster levelling of concentration and temperature in whirled liquid.

As the vapour velocity attains the value corresponding to the point of phase inversion, the HETP of the packed column abruptly increases, the efficiency curve running almost vertically. The hydrodynamic characteristics of the column operation, viz. the holding capacity (φ) of packing for liquid and the pressure drop ΔP_{g-l}, also sharply increase at the inversion point, and the nature of variation of the three parameters becomes the same (Fig. 181). Since in this case the amount of liquid in the packing exceeds many times the amount of liquid flowing down per unit time, the phase-contact time also abruptly increases. All liquid in the packing is pierced by vapour bubbles and is emulsified by them. Mass transfer takes place in the free volume filled by vapour-liquid emulsion rather than on the surface of the liquid film covering the packing. The concentrations are levelled out very quickly. Besides, an increase in the pressure drop leads to an increase in the temperature drop per unit packing height, thus improving the conditions of heat and mass transfer. At the phase inversion point, the vapour is no longer a continuous phase. It disperses in the bulk of whirled liquid. The regime of filling the packing by a vapour-liquid emulsion is an emulsifying regime.

In the emulsifying regime, the packing breaks vapour streams into a large number of tiny bubbles piercing the liquid, distributes them over the entire column cross section, and increases the path, and hence the time of contact with the liquid. An increase in the evaporation intensity in this regime does not change the linear velocity of vapour bubbles, increasing only their number, interfacial area, and mass transfer. The large number of vapour bubbles reduces the open area for liquid, thus increasing its linear velocity.

Below the phase inversion point, the vapour is a continuous phase. An increase in the evaporation intensity increases the linear velocity of vapour without producing a noticeable effect on the linear velocity of liquid. On the other hand, in the emulsifying regime an increase in the evaporation rate increases the linear velocity of liquid without affecting the linear velocity of vapour. The upper limiting point on the vertical emulsification line can be defined as

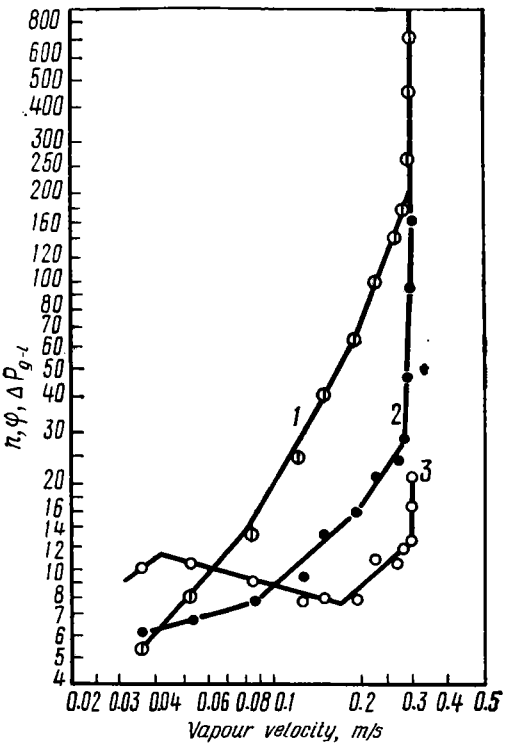

Fig. 181. Variation of basic parameters characterizing the operation of a packed rectifying column; packing is 5.7 × 5.9 × 0.6-mm rings:

1—pressure drop, mm H_2O; *2*—holding capacity of packing, cm^3; *3*—number of theoretical plates.

the point of flooding of a packed column, since beyond this point the vapour-liquid emulsion accumulates above the packing and is intensely mixed in this zone, thus violating the normal course of the process.

Emulsifying regime is realized for limiting flow velocities and ensures the maximum output of the apparatus. Considering that the maximum HETP is attained in this case, this regime can be defined

as the optimal regime for operation of packed columns. The pressure drop per theoretical plate is the same as under normal conditions (25-35 mm H_2O). The heat-transfer coefficients in the emulsifying

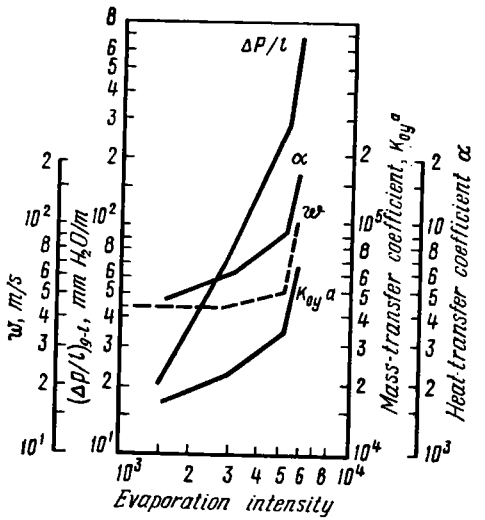

Fig. 182. Variation of basic parameters characterizing the operation of a packed column in emulsifying regime.

regime vary in the same way as the HETP of the column (Fig. 182). The absorption coefficients for readily and difficultly soluble gases are calculated by the equation

$$\mathrm{Nu}_{g(l)} = \beta \frac{d_e}{d_{e.s}} \mathrm{Re}_{g(l)}^{0.8} \mathrm{Pr}_{g(l)}^{2/3} (1+f), \qquad (10.203)$$

where

$$\mathrm{Nu}_{g(l)} = \frac{K_{0y} a d_e}{a D_g},$$

$$\mathrm{Re}_{g(l)} = \frac{w_g d_e \rho_g}{F_v \mu_g},$$

$$\mathrm{Pr}_{g(l)} = \frac{360 \mu_g}{\rho_g D_g},$$

$K_{0y}a$ is the mass-transfer coefficient, kg/m³·hr·kg/m³; $d_{e.s}$ the equivalent diameter of standard packing of the size 25 × 25 × 3 mm; w_g the gas velocity in empty column, m/s; f the factor of the hydrodynamic state of the system; and β the proportionality factor determined experimentally and depending on hydrodynamic conditions of the absorber operation.

At the inversion point $\Delta P \simeq w_g^2$, $m = 1$, and Eq. (6.59) establishes the proportionality between $K_{0y}a$ and w_g. Since the mass-transfer coefficients at the inversion point do not depend on the molecular-kinetic characteristics, and the gas solubility remains different, the experimental results for gases with different solubilities can be generalized in the form of a single equation by introducing the ratio m_1/m_2 of solubility coefficients. The following equations were obtained for calculating the overall mass-transfer coefficients at the inversion point:

$$K_{0y}a = 10.4a\left(\frac{d_e}{d_{e.s}}\right)^{0.66}\left(\frac{m_1}{m_2}\right)w_g(1+f),$$

or

$$K_{0y}a = 10.4a\left(\frac{d_e}{d_{e.s}}\right)^{0.66}\left(\frac{m_1}{m_2}\right)w_g \times\left[1+8.4\left(\frac{L}{G}\right)^{0.405}\times\left(\frac{\rho_g}{\rho_l}\right)^{0.225}\left(\frac{\mu_l}{\mu_g}\right)^{0.045}\right], \quad (10.204)$$

where $d_{e.s}$ is the equivalent diameter of standard packing, for which the diameter $d_{e.s}$ of 25 × 25-mm rings is taken, and m_1 is the solubility coefficient for NH_3.

For calculating the equivalent packing height h_{1nv} at the inversion point (m) for rectification processes, the following equation was obtained:

$$h_{1nv} = 28w_v^{0.2}\rho_v^{0.2}\mu_v^{-0.2}a^{1.2}F_v\left(\frac{G}{L}\right)^{0.342} \times\left(\frac{\rho_l}{\rho_v}\right)^{0.19}\left(\frac{\mu_v}{\mu_l}\right)^{0.038}\frac{\log(L/mG)}{1-(mG/L)} \quad (10.205)$$

or, in the dimensionless form, we obtain by rounding off the exponents:

$$\frac{h_{1nv}}{d_e} = 5.2\mathrm{Re}_v^{0.2}\left(\frac{G}{L}\right)^{0.35}\left(\frac{\rho_l}{\rho_v}\right)^{0.2}\frac{\log(L/mG)}{1-(mG/L)}, \quad (10.206)$$

where d_e is the equivalent diameter of packing, equal to $d_e = 4F_v/a$, m; F_v is the free packing volume, m^3/m^3; a the specific surface area of packing, m^2/m^3; Re_v the Reynolds number for vapour, equal to $\mathrm{Re}_v = w_v d_e \rho_v/(F_v\mu_v)$; w_v the vapour velocity referred to the total column cross section, m/s; ρ_v the vapour density, kg/m^3; μ_v the vapour viscosity; $G/L = (R+1)/R$ for the upper part and $G/L = (R+1)/(R+F)$ for the lower part of the column; R the reflux number; F the feed number; and m the slope of the equilibrium curve.

The equivalent packing height depends on the relative volatilities of the mixture components being separated (on the slope m of the equilibrium curve) and on the ratio of the reflux rate to the vapour rate, i.e. on the diffusion potential $mG/L = \lambda$ (Fig. 183).

The equivalent packing height decreases with increasing slope of the equilibrium curve. For example, for a methyl alcohol-water

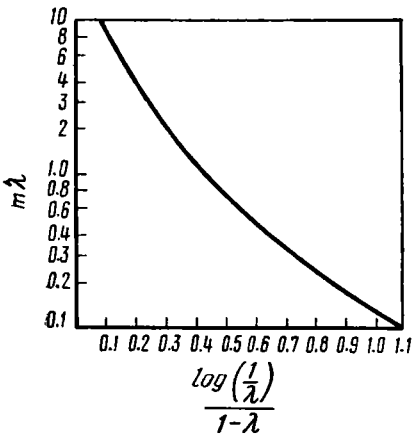

Fig. 183. Effect of diffusion potential on the variation of equivalent packing height.

mixture, the slope of the equilibrium curve is about 2 for the 50 per cent volatile content in vapour, and about 1 for an ethyl alcohol-water mixture of the same concentration. Consequently, other conditions being equal, we should expect lower values of equivalent packing heights for the methyl alcohol-water mixture. The equivalent packing height h_e (mm) in extraction columns can be determined from the empirical equation

$$h_e = \frac{(25.4)^{h-1} c \mu_c d_r^h w_c^{0.5}}{\Delta\gamma w_d^{0.5}}, \qquad (10.207)$$

where d_r is the diameter of the packing ring, mm; c and h are constants determined from Fig. 184 and from the mutual solubilities of

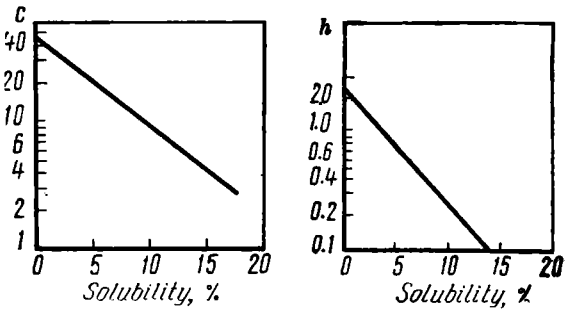

Fig. 184. To the calculation of constants c and h in Eq. (10.207).

liquids constituting the continuous and disperse phases; w_c and w_d are the velocities of the continuous and disperse phases; μ_c is the viscosity of the continuous phase; and $\Delta\gamma$ the difference in the specific gravities, g/cm^3.

For practically immiscible liquids (with mutual solubility below 1 per cent), Eq. (10.207) is reduced to

$$h_e = 1.6 \frac{d_r^2 \mu_c w_c^{0.5}}{\Delta\gamma w_d^{0.5}}. \qquad (10.208)$$

For a mutual solubility of more than 10 per cent, the height of the equivalent theoretical plate is almost independent of the ring

diameter. It is expedient to use Eqs. (10.207) and (10.208) for calculating extraction from aqueous solutions. In order to determine the minimum equivalent packing height h_{min} for extraction columns in a regime close to flooding, the following equation can be used for approximate calculations:

$$\frac{h_{min}}{d_e} = 24 \left(\frac{w_l^2}{g d_e} \right)^{-0.2}, \qquad (10.209)$$

where h_{min} is the minimum equivalent packing height, m; d_e the equivalent packing diameter, m; $d_e = 4F_v/a$ (where F_v is the free packing volume, m^3/m^3; a_e the specific surface area of packing, m^2/m^3); and w_l the maximum linear velocity of the light phase, m/s. The equivalent packing height below the inversion point can be approximately determined from the relation $h_e = (1.5 \text{ to } 2)\, h_{min}$.

10.5.2. Modelling and Calculation of Packed Absorption Columns

For the optimal designing and control, it is expedient to divide the mathematical models of absorption process into two groups: (1) mathematical models disregarding the longitudinal mixing and (2) mathematical models where longitudinal mixing is taken into account. The first group of models (Table 17) presumes the complete displacement regime in the column with respect to interacting phases. Mass-transfer process in non-stationary regime is described in the general case by the system of non-linear differential equations in partial derivatives:

$$\begin{aligned} L \frac{\partial x}{\partial z} + K_{0x} a\,(L,\ G)\,\Delta c &= \varphi_L (L,\ G) \frac{\partial x}{\partial \tau}, \\ G \frac{\partial y}{\partial z} + K_{0y} a\,(L,\ G)\,\Delta c &= -\varphi_G\,(L,\ G) \frac{\partial y}{\partial \tau}. \end{aligned} \qquad (10.210)$$

where G and L are the empty column gas and liquid flow rates, $kg/m^2 \cdot hr$; x and y are the component concentrations in the liquid and gas phase respectively, kg/kg (or %); Δc is the driving force of the process, kg/kg (or %); $K_{0y}a$ the volumetric mass-transfer coefficient, $kg/m^3 \cdot hr \cdot kg/kg$; φ_L and φ_G are the liquid- and gas-phase holding capacities, kg/m^3; τ the time, hr; and z the packing height, m.

The non-linear properties of the equation are determined by the dependence of the coefficients on the magnitude of perturbing action. An analytical solution of such a system is fraught with considerable difficulties and can be obtained only with certain simplifying assumptions. Considering the behaviour of the process at small deviations from the stationary state, we can assume that the coefficients in the equations of the mathematical model are constant. A further simplification is attained by the averaging of the driving force of the process over the column height. Then the initial system of equations in

Table 17

Mathematical Models of Packed Absorption Columns

Model No.	Model	Equations
	Without accounting for longitudinal mixing	
1	With concentrated parameters (arithmetic mean driving force)	$G(y_{in}-y_{out})+\Delta G(y^0_{in}-y^0_{out})-L(x_{out}-x_{in})=\frac{\varphi_L}{2}x^0_{out}\frac{dx_{out}}{d\tau}+\frac{\varphi_L}{2}x^0_{in}\frac{dx_{in}}{d\tau}+\frac{\varphi_G}{2}y^0_{out}\frac{dy_{out}}{d\tau}+\frac{\varphi_G}{2}y^0_{in}\frac{dy_{in}}{d\tau}$
		$G(y_{in}-y_{out})+\Delta G(y^0_{in}-y^0_{out})-\frac{\varphi_G}{2}y^0_{in}\frac{dy_{in}}{d\tau}-\frac{\varphi_G}{2}y^0_{out}\frac{dy_{out}}{d\tau}=\frac{K_{0y}Z}{2}(y_{in}-mx_{out}+y_{out}-mx_{in})$
2	For separation stages	$G(y_{n-1}-y_n)+L(x_{n+1}-x_n)=\varphi_L\frac{dx_n}{d\tau}+\varphi_G\frac{dy_n}{d\tau}$
3	Multistage representation of a process (linearization of the driving force by stages)	$G(y_{n-1}-y_n)+\Delta G(y^0_{n-1}-y^0_n)-L(x_n-x_{n+1})=\frac{\varphi_L}{2N}x^0_n\frac{dx_n}{d\tau}+\frac{\varphi_L}{2N}x^0_{n+1}\frac{dx_{n+1}}{d\tau}+\frac{\varphi_G}{2N}y^0_{n-1}\frac{dy_{n-1}}{d\tau},$
		$G(y_{n-1}-y_n)+\Delta G(y^0_{n-1}-y^0_n)-\frac{\varphi_G}{2N}y^0_{n-1}\frac{dy_{n-1}}{d\tau}-\frac{\varphi_G}{2N}y^0_n\frac{dy_n}{d\tau}=\frac{K_{0y}Z}{2N}(y_{n-1}-mx_n+y_n-mx_{n+1})$
4	With distributed parameters (logarithmical mean driving force)	$L\frac{\partial x}{\partial z}+K_{0y}a(y-y^*)=\varphi_L\frac{\partial x}{\partial \tau},$
		$G\frac{\partial y}{\partial z}+K_{0y}a(y-y^*)=-\varphi_G\frac{\partial y}{\partial \tau}$

Table 17 (continued)

Model No.	Model	Equations
		With account taken of longitudinal mixing
5	Fully asymmetrical model	$G\frac{\partial y}{\partial z}+K_{0y}a\,(y-y^*)=-\varphi_G\frac{\partial y}{\partial \tau}$, $L\bar{x}+K_{0y}a\,(y-y^*)=\varphi_L\frac{d\bar{x}}{d\tau}$, $\bar{x}=\frac{1}{z}\int_0^z x\,dz$
6	Asymmetrical model	$L\,(x_{n,\,k+1}-x_{n,\,k})+\frac{K_{0y}az}{N}(y_n-mx_{n,\,k})=\varphi_L\frac{dx_{n,\,k}}{d\tau}$, $G\,(y_{n-1}-y_n)-\frac{K_{0x}az}{N}\left(ay_n-m\sum^{a}x_{n,k}\right)=\varphi_G\frac{dy_n}{d\tau}$
7	Symmetrical model	$L\,(x_{n+1}-x_n)+\frac{K_{0x}az}{N}(x_n^*-x_n)=\varphi_L\frac{dx_n}{d\tau}$, $G\,(y_{n-1}-y_n)-\frac{K_{0y}az}{N}(x_n^*-x_n)=\varphi_G\frac{dy_n}{d\tau}$
		Plug flow
8	Full symmetry	$L\frac{\partial x}{\partial z}+K_{0y}a\,(y-y^*)=\varphi_L\frac{\partial x}{\partial \tau}$, $G\frac{\partial y}{\partial z}+K_{0y}a\,(y-y^*)=-\varphi_G\frac{\partial y}{\partial \tau}$
		Complete mixing
		$G\,(y_{1n}-y_{out})-K_{0y}az\,(y_{out}-y^*_{out})=\varphi_G\frac{dy_{out}}{d\tau}$, $L\,(x_{1n}-x_{out})+K_{0y}az\,(y_{out}-y^*_{out})=\varphi_{L.}\frac{dx_{out}}{d\tau}$

partial derivatives is transformed to the system of ordinary differential equations. To a first approximation, the change in the phase concentration along the column height is approximated by a linear dependence, and the mean concentrations are expressed as arithmetic means of their initial and final values (model 1). However, while calculating non-stationary regimes of the process under conditions when the driving force changes more than twice, such a simplification may lead to considerable deviations from the exact solution, especially on the initial part of the time characteristic. In this case, the logarithmic mean of the driving force must be used.

Another method of analysis of distributed systems used for solving the differential equations in partial derivatives on computers is based on the representation of a continuous process by a multistage process with the parameters concentrated in each stage. Depending on the assumptions about the mechanism of mass-transfer process in a stage, and also on the way of representation of the driving force, several modifications of mathematical models are possible (see Table 17, models 2 and 3). The simplest mathematical model is that discarding the kinetics of the absorption process. A packed absorber is considered to be a plate-type apparatus with plate efficiency equal to 1 (model 2). The number of plates is taken equal to the number of stages equivalent to one theoretical plate. An analysis of dynamic characteristics with the help of this model has shown that the delay section of the time characteristic of the process is represented inadequately in the case of a small number of separation stages. Besides, the stationary regimes can be calculated only to a certain approximation since the number of stages cannot be fractional.

The material-balance equation for this model is satisfied by taking into account the process kinetics. The number of stages into which the height of the packing in the apparatus is conventionally divided is larger than the number of stages for complete separation. Model 3 cannot be used for describing non-stationary properties of a real process.

All the models considered above presume complete displacement with respect to interacting phases. The models differ from each other in the ways of approximating the driving force whose distribution along the column height in the limit tends to the logarithmic mean. For example, according to multistage model, the mathematical description is the more exact the larger the value of n, i.e. the closer the model approaches the plug flow model. At the same time, the plug flow regime is simplified in actual apparatus, and the degree of approximation depends on the hydrodynamic conditions under which a packed absorber operates. In a real apparatus, the flow elements are distributed non-uniformly over the time of stay due to non-uniformity of velocity profiles, molecular diffusion, and flow turbulization.

In constructing mathematical models of packed columns as apparatus with distributed parameters, taking into account longitudinal mixing, two approaches are possible: the description of the process with the help of second-order differential equations in partial derivatives (diffusion model) or the approximate representation of a continuous process in the form of a multistage process with parameters concentrated at each stage (cellular model).

Before considering these models, let us introduce the concept of axial symmetry of flows in an apparatus. We shall call the flows with the same degree of axial dispersion of phases symmetric flows. The degree of axial dispersion can be estimated by the number n of cells of complete mixing and the coefficient D_L of axial dispersion. Then the mathematical models of absorption process in a packed apparatus can be classified as follows:

symmetrical model $n_L = n_G = N$,

asymmetrical model $n_L \neq n_G$, $n_L = N_L$, $n_G = N_G$,

fully symmetrical model $n_L = n_G = \infty$ or 1,

fully asymmetrical model $n_L \neq n_G$, $n_L = 1$, $n_G = \infty$ or $n_L = \infty$, $n_G = 1$.

The construction of a mathematical model taking into account the hydrodynamic structure of interacting phases makes it possible to obtain a more precise mathematical description of the process in a two-phase system.

In the cellular model, a packed absorber is treated as an object consisting of two consecutive complete mixing cells between which mass transfer takes place. The number of cells per phase is determined by the degree of axial dispersion of these phases. Two limiting cases are possible here: complete mixing in the liquid phase and the plug flow in the gas phase, and vice versa, complete mixing in the gas phase and the plug flow in the liquid phase. The first case is the most important for packed absorbers. The cellular model is described by a system of differential-difference equations which can be easily solved with the help of digital computers.

The block structure of the model permits us to use block algebra for an analysis of the column model, and hence is convenient for modelling on analogue computers. Besides, for the symmetrical and completely asymmetrical models, transfer functions employed for the analysis and synthesis of automatic control systems for packed columns can be obtained analytically. The mathematical description of a packed absorption column on the basis of the cellular symmetric model includes the following equations:

$$\begin{aligned} L(x_{n+1} - x_n) + K_{0x} a H \Delta C &= \varphi_L H \frac{dx_n}{d\tau}, \\ G(y_{n-1} - y_n) - K_{0y} a H \Delta C &= \varphi_G H \frac{dy_n}{d\tau}, \end{aligned} \tag{10.211}$$

where H is the height of complete-mixing cell, m; x_n and y_n are the component concentrations in the liquid and gas phases of the nth cell, kg/kg (or %).

In order to determine the degree of axial dispersion, pulse method is normally used. Calculating the moments of the distribution function over the duration of stay of indicator elements in the column and using the relation between the number of cells and the axial dispersion coefficient,

$$n = \frac{zw}{2D_L}, \tag{10.212}$$

where z is the packing height, m; n the number of complete-mixing cells; w the mean velocity of a phase, m/hr; and D_L the longitudinal mixing coefficient, m²/hr. We can determine the values of n for different hydrodynamic conditions.

The kinetics of absorption is usually calculated under the assumption of the plug flow regime. When kinetic data are used for calculating stationary regimes on the basis of a mathematical model taking into account axial dispersion, the results of calculation differ considerably from the actual values of the compositions of exit flows in a real apparatus. The cellular model with stagnation zones gives better agreement with experiment. The equations of this model are

$$\begin{aligned} L(x_{n+1} - x_n) + K_{0x}aH\Delta C &= \varphi_L H \frac{dx_n}{d\tau}, \\ G(y_{n-1} - y'_n) - K_{0y}aH\Delta C &= \varphi_G H \frac{dy'_n}{d\tau}, \\ G(y'_n - y_n) &= \varphi_{s,z} H \frac{dx^*_n}{d\tau}. \end{aligned} \tag{10.213}$$

where $\varphi_{s,z}$ is the volume of liquid in the stagnation zone (static holding capacity), kg/m³; and y'_n the component concentration in the gas phase at the entrance of the stagnation zone, kg/kg (or %).

The driving force of the process in the nth cell for readily soluble gases is given by

$$\Delta C_n = y_n - y^*_n,$$

and

$$\Delta C_n = x^*_n - x_n.$$

for difficultly soluble gases, where y^* and x^* are the equilibrium concentrations of gas and liquid.

The relation between the equilibrium concentrations are approximated by the linear dependence

$$y^* = mx,$$

where m is the equilibrium constant.

While solving the equations of the mathematical model, it is assumed that the deviations in the flow concentrations before a per-

turbation is applied are equal to zero, i.e. for $\tau = 0$, $\Delta y\,(0) = 0$, and $\Delta x\,(0) = 0$. Figure 185 shows the dependence of the variation of the mass-transfer coefficient K_{0y} and the packing height z on the

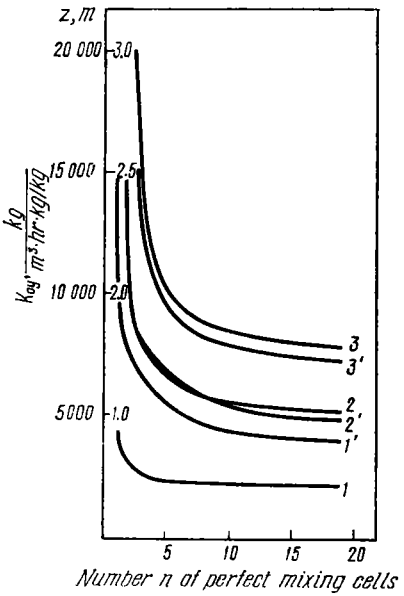

Fig. 185. The mass-transfer coefficient and the packing height vs. the degree of axial dispersion for a water-ammonia system. The packing consists of 15 × 15-mm Raschig rings; *1*, *2*, and *3* correspond to z vs. n dependence; *1'*, *2'*, and *3'*, to K_{0y} vs. n dependence:

1, *1'*—L=1900 kg/m²·hr; G=3020 kg/m²·hr;
2, *2'*—L=3423 kg/m²·hr; G=3820 kg/m²·hr;
3, *3'*—L=4358 kg/m²·hr; G=3020 kg/m²·hr.

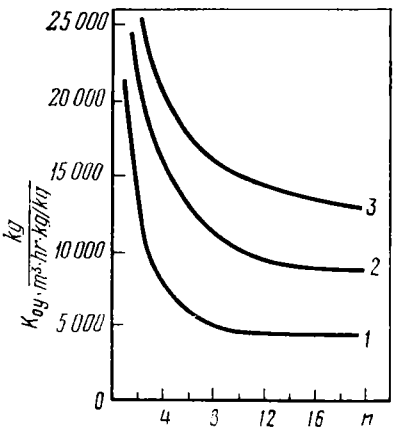

Fig. 186. The mass-transfer coefficient vs. the number of cells:

1—film regime; *2*—intermediate regime; *3*—turbulent regime.

degree of longitudinal mixing. A noticeable change in the mass-transfer coefficient K_{0y} (more than 10 percent) takes place at a high degree of mixing ($n < 5$). Figure 186 represents the dependence of the mass-transfer coefficient on hydrodynamic conditions in packed absorption columns and on the intensity of mixing in the packing.

10.5.3. Modelling and Calculation of Packed Extraction Columns

The flow of continuous and disperse phases in packed extraction columns is usually described by plug-flow models. However, these models fail to explain many phenomena. First of all this applies to

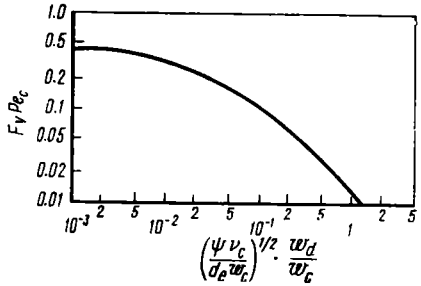

Fig. 187. To calculation of Pe_c number in extraction columns.

the process of coalescence and the existence of static holding capacity, which affect the function of distribution over the duration of stay in the apparatus and hence must be taken into account in the analysis and calculation of hydrodynamics of extraction in a packed column. The continuous-phase flow is satisfactorily described by the diffusion model.

The Pecklet numbers increase with the flow rates of both phases, the effect being stronger if the disperse phase wets the packing. Approximate values of numbers Pe_c for the continuous phase in a two-phase flow can be determined with the help of Fig. 187 which represents the dependence of $F_v\ Pe_c$ on the dimensionless group:

$$F_v Pe_c = f\left[\left(\frac{\psi \nu_c}{d_e w_c}\right)^{1/2} \frac{w_d}{w_c}\right],$$

where F_v is the free volume of packing; ν_c the kinematic viscosity of the continuous phase; d_c the equivalent diameter of packing; and ψ dimensionless coefficient given by

$$\psi = [\Lambda + (\Lambda f_x + f_y)]/(1 - \Lambda),$$

where Λ is the ratio of counterflows taking into account the distribution coefficient; f_x and f_y are the fractions of back flows for refined oil and solvent, respectively. The above dependence was obtained for comparatively small column diameters (the maximum diameter was 148 mm). The structure of disperse phase flow considerably differs from that described by the diffusion model. The mechanism of the disperse-phase flow is directly related to the packing size. Free motion of disperse-phase drops is observed if the packing size exceeds the critical value. In this case the drops freely pass through the packing elements and only an insignificant part of drops may be held by the packing. The volume of the disperse phase held by the packing is comparatively small, and the entire effect of velocity distribution can be attributed to the flow-through part of the disperse-phase flow.

If the packing size is below critical, a considerable volume of the disperse phase is retained in the packing of the apparatus. Moreover, the collisions between the moving droplets of the disperse phase and the drops retained in the packing increase the probability of coalescence. The effect of this type of interactions make it impossible to use the diffusion model in its conventional form for describing the disperse-phase flow.

Model with stagnation zone. In order to construct the mathematical model of phase flows in a packed column, we make the following assumptions.

1. The total volume of the disperse phase in the column can be divided into the static and dynamic components. The static component is the volume of the disperse phase whose velocity is equal to zero. The dynamic component is the volume of the disperse phase whose velocity differs from zero.
2. The motion of the dynamic component is described by the diffusion model.
3. Mass transfer takes place between the static and dynamic components due to coalescence.
4. Equal volumes of the static and dynamic components take part in coalescence.
5. Ideal mixing is observed in the volume of liquid appearing as a result of coalescence.
6. Coalescence is followed by redispersion.

The volume dV_c of the disperse phase formed as a result of coalescence during time $d\tau$ in the volume element dV is equal to

$$dV_c = \omega\varphi_{st}\varphi_d \, dV \, d\tau, \tag{10.214}$$

where ω is the constant coalescence rate, hr^{-1}; and φ_{st}, φ_d are the static and dynamic holding capacities of packing, m^3/m^3.

Let us calculate the amount of substance transferred as a result of coalescence and redispersion from the dynamic to static component. Taking into account assumptions 4 and 5, we can write

$$Q_c = \frac{1}{2} dV_c y - \frac{1}{2} dV_c \frac{y+y_1}{2} = \frac{1}{2} dV_c \frac{1}{2} (y - y_1), \tag{10.215}$$

where $(1/2)\, dV_c y$ is the amount of substance taking part in coalescence on the side of dynamic component and $(1/2)\, dV_c\, (y + y_1)/2$ the amount of substance after redispersion with the dynamic component.

Substituting (10.214) into (10.215), we obtain

$$Q_c = \frac{1}{4} \omega\varphi_{st}\varphi_d \, (y - y_1) \, dV \, d\tau. \tag{10.216}$$

Let us introduce the concept of the total holding capacity

$$\varphi = \varphi_{st} + \varphi_d \tag{10.217}$$

and denote $\alpha = \varphi_d/\varphi$. Then $(1 - \alpha) = \varphi_{st}/\varphi$. Equation (10.216) can now be represented in the form

$$Q_c = \frac{1}{4} \omega\varphi^2\alpha \, (1 - \alpha) \, (y - y_1) \, dV \, d\tau. \tag{10.218}$$

Let us construct the tracer material-balance equation for the disperse phase in the column element of height dz. The structure of

mass flows is depicted in Fig. 188. The material-balance equations have the form

$$-L\frac{\partial y}{\partial z}+D_G\frac{\partial^2 y}{\partial z^2}-\frac{1}{4}\omega\varphi^2\alpha(1-\alpha)F(y-y_1)=F_v\varphi_d\frac{\partial y}{\partial\tau}, \quad (10.219)$$

$$\frac{1}{4}\omega\varphi^2\alpha(1-\alpha)F(y-y_1)=F_v\varphi_{st}\frac{\partial y_1}{\partial\tau} \quad (10.220)$$

These equations describe the disperse-phase flow in a packed extraction column. Introducing the dimensionless coordinates $\theta = \tau/\bar{\tau}_{disp}$

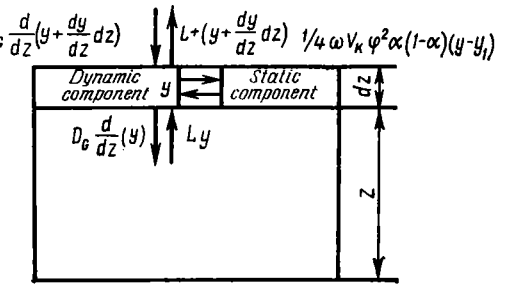

Fig. 188. Flow structure in a packed extraction column.

and $Z = z/H$ and the quantity $N_c = (1/4)\,\omega FH/L$ which characterizes the mass-transfer rate between the flow-through and stagnation zones, we obtain

$$\frac{\partial y}{\partial Z}+\frac{1}{Pe_D}\cdot\frac{\partial^2 y}{\partial Z^2}-N_c\varphi^2\alpha(1-\alpha)(y-y_1)=\alpha\frac{\partial y}{\partial\theta},$$

$$N_c\varphi^2\alpha(1-\alpha)(y-y_1)=(1-\alpha)\frac{\partial y_1}{\partial\theta}. \quad (10.221)$$

Suppose that coalescence at the ends of the column is insignificant. Then the boundary conditions of the diffusion model, viz.

$$Z=0:-\frac{1}{Pe_D}\cdot\frac{\partial y}{\partial Z}=y_{in}-y,$$

$$Z=1:\frac{\partial y}{\partial Z}=0 \quad (10.222)$$

can be taken as the boundary conditions for model (10.221).

Solving Eq. (10.221) with boundary conditions (10.222), we obtain the transfer function

$$W(p)=\frac{y_{out}(p)}{y_{in}(p)},$$

where p is the Laplace operator.

The structure of the transfer function for model (10.221) is similar to that of the transfer function for the diffusion model:

$$W(p) = \frac{4e^{\frac{Pe_D}{2}a}}{(1+a)^2 e^{\frac{Pe_D}{2}a} - (1-a)^2 e^{-\frac{Pe_D}{2}a}} \tag{10.223}$$

the only difference being in the value of the parameter a, which for model (10.221) is given by

$$a = \sqrt{1 + \frac{4}{Pe_D}\left[\frac{N_c\varphi^2\alpha(1-\alpha)p}{N_c\varphi^2\alpha + p} + \alpha p\right]}. \tag{10.224}$$

Transfer function (10.223) was obtained for zero initial conditions. Solving Eqs. (10.221), we get

$$y(\theta) = \sum_{k=1}^{\infty} \frac{A(p_c)}{B'(p_c)} e^{p_k\theta}, \tag{10.225}$$

where

$$A(p_c) = 4e^{\frac{Pe_D}{2}a}(p_c), \tag{10.226}$$

$$B'(p_c) = \frac{d}{dp}\left[(1+\alpha)^2 e^{\frac{Pe_D}{2}a} - (1-\alpha)^2 e^{-\frac{Pe_D}{2}a}\right]_{p\to p_c}. \tag{10.227}$$

As a result, we have

$$y(\theta) = \sum_{k=1}^{\infty}\sum_{i=1}^{2} \frac{2\lambda_c^2 e^{\left[\frac{Pe_D}{2} + p_{c,i}\theta\right]}}{E(p_{c,i})\left\{\lambda_c\left(1+\frac{Pe_D}{2}\right)\sin 2\lambda_c - \left[\frac{Pe_D}{4} + \left(\frac{Pe_D}{4}\right)^2 - \lambda_c^2\right]\cos 2\lambda_c\right\}}, \tag{10.228}$$

where λ_c can be determined from the following equation:

$$\tan 2\lambda_c = \frac{\frac{Pe_D}{2}\lambda_c}{\lambda_c^2 - \left(\frac{Pe_D}{4}\right)^2}, \tag{10.229}$$

$$p_c(1, 2) = -\frac{C}{2}\left(1 \pm \sqrt{1 - \frac{4D}{C^2}}\right), \tag{10.230}$$

$$C = \frac{1}{\alpha}\cdot\frac{4}{Pe_D}\left[\left(\frac{4}{Pe_D}\right)^2 + \lambda_c^2\right] + N_c\varphi^2, \tag{10.231}$$

$$D = \frac{4}{Pe_D}\left[\left(\frac{4}{Pe_D}\right)^2 + \lambda_c^2\right] N_c\varphi^2, \tag{10.232}$$

$$E(p_{c,i}) = \frac{N_c^2\varphi^4\alpha^2(1-\alpha)}{[N_c\varphi^2\alpha + p_{c,i}]^2} + \alpha. \tag{10.233}$$

The solution for the diffusion model disregarding coalescence and stagnation zones has the form

$$y(\theta)=\sum_{k=1}^{\infty}\frac{2\lambda_c^2\, e^{\left[\frac{Pe_D}{2}-\frac{Pe_D}{4}\theta-\lambda_c^2\frac{4}{Pe_D}\theta\right]}}{\lambda_c\left(1+\frac{Pe_D}{2}\right)\sin 2\lambda_c-\left[\frac{Pe_D}{4}+\left(\frac{Pe_D}{4}\right)^2-\lambda_c^2\right]\cos 2\lambda_c}. \tag{10.234}$$

Let us consider the numerical characteristics of the model, for which we usually employ the first two moments of the particle distribution function over the duration of stay. A moment of an arbitrary order can be calculated by the formula

$$M_i=(-1)^i\left[\frac{d^iW(p)}{dp^i}\right]_{p\to 0}. \tag{10.235}$$

Let us consider the basic model parameters determining the numerical characteristics.

1. The volume of the stagnation zone is zero. Since $(1-\alpha)=0$, we obtain the diffusion model in its conventional form. For this model, we have

$$M_1=1, \tag{10.236}$$

$$M_2=1+\frac{2}{Pe_D}-\frac{2}{Pe_D^2}(1-e^{-Pe_D}), \tag{10.237}$$

i.e. the second moment is a function of only Pe_D.

2. The coalescence rate constant is equal to zero, i.e. $N_c=0$. From the physical point of view this means that there is no mass transfer between the static and dynamic components. Consequently, the duration of stay distribution function is not affected by the part of volume corresponding to the static component. Then

$$M_1=\alpha, \tag{10.238}$$

$$M_2=\alpha^2\left[1+\frac{2}{Pe_D}-\frac{2}{Pe_D^2}(1-e^{-Pe_D})\right]. \tag{10.239}$$

Thus, the values of moments depend on the volume of the stagnation zone.

3. The coalescence rate constant is high. Then we obtain the expressions for the first two moments which exactly coincide with (10.236) and (10.237). Thus, for a considerable coalescence rate constant, the entire disperse phase is the dynamic component.

4. The coalescence rate constant ω and the volume of the flow-through zone have finite values differing from zero. Apparently, this case is typical of real apparatus. The first and second moments

have the form

$$M_1 = 1, \tag{10.240}$$

$$M_2 = \frac{2(1-\alpha)}{N_c\beta^2\alpha} + \left[1 + \frac{2}{Pe_D} - \frac{2}{Pe_D^2}(1 - e^{-Pe_D})\right]. \tag{10.241}$$

The first moment is equal to unity and is independent of the volume of the stagnation zone. The second moment may assume large values depending on the magnitude of N_c and α. Figures 189-191 show the M_2 vs. α, φ, and N_c dependences for different values of Pe_D.

As the coalescence rate decreases, the second moment abruptly increases, but as the value $N_c = 0$ is attained, the function M_2 (N_c) undergoes a discontinuity, and the value of M_2 turns out to be less than unity (Fig. 189). This can be explained by the fact that upon a decrease in the coalescence rate, the washingout of the tracer lasts for a very long time and essentially determines the value of the second moment. For $N_c = 0$, the volume corresponding to the stagnation zone is excluded from the process. In this case, the second moment depends only on the magnitude of Pe_D (for α = const). This model of the disperse-phase flow in a packed column reflects the processes occurring in the column to the fullest extent.

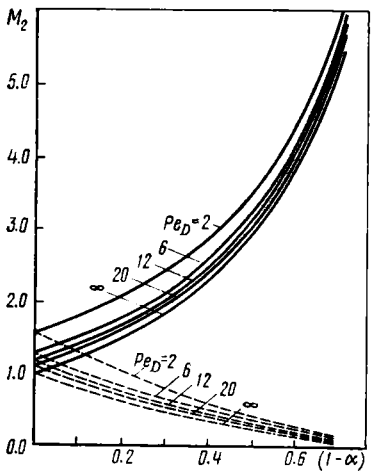

Fig. 189. Effect of the volume of the stagnation zone on the value of the second moment for different values of N_c and Pe_D:

———— $N_c = 2.5$; $\varphi = 0.2$;
- - - - $N_c = 0$, $\varphi = 0.2$.

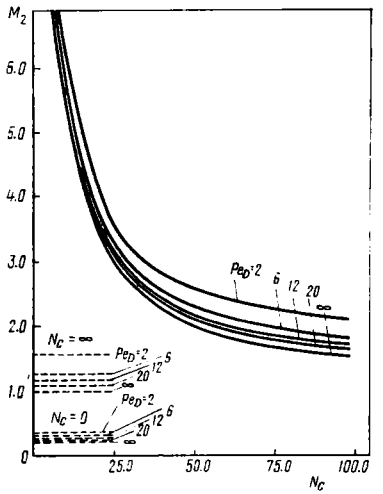

Fig. 190. The effect of the coalescence rate on the value of the second moment for different values of Pe_D (α = 0.5; φ = 0.2).

Cellular model with backmixing between cells. In this case, a column is considered as a sequence of sections with concentrated parameters, each section being equivalent to a perfect-mixing stage. The flow structure of the model is shown in Fig. 192. The magnitudes of the recirculation flow rates f_L and f_G characterize the intensity of mass transport in the directions opposite to the main flows L and G.

The system of equations for the cellular model involving backmixing during mass transfer between phases (Fig. 192) denoted by $P(C)$ can be written in the form

$$\left.\begin{aligned}
&-C_0^L+(1+f_L)\,C_1^L+\lambda\varphi\psi\,(C_1^L)-\lambda\varphi C_1^G-C_2^L f_L\\
&\quad=P_1\,(C_1^L,\ C_1^G,\ C_2^L)=0,\\
&-\lambda\psi\,(C_1^L)+(1+f_G+\lambda)\,C_1^G-(1+f_G)\,C_2^G\\
&\quad=P_2\,(C_1^L,\ C_1^G,\ C_2^G)=0,\\
&\cdots\cdots\cdots\cdots\cdots\cdots\cdots\cdots\cdots\cdots\\
&-(1+f_L)\,C_{j-1}^L+\lambda\varphi\psi\,(C_j^L)+(1+2f_L)\,C_j^L\\
&-\lambda\varphi C_j^G-f_L C_{j+1}^L=P_{2j-1}\,(C_{j-1}^L,\ C_j^L,\ C_j^G,\ C_{j+1}^L)=0,\\
&-f_G C_{j-1}^G-\lambda\psi\,(C_j^L)+(1+2f_L+\lambda)\,C_j^G-(1+f_G)\,C_{j+1}^G\\
&\quad=P_{2j}\,(C_{j-1}^G,\ C_j^L,\ C_j^G,\ C_{j+1}^G)=0\\
&\cdots\cdots\cdots\cdots\cdots\cdots\cdots\cdots\cdots\cdots\\
&-(1+f_L)\,C_{n-1}^L+(1+f_L)\,C_n^L+\lambda\varphi\psi\,(C_n^L)-\lambda\varphi C_n^G\\
&\quad=P_{2n-1}\,(C_{n-1}^L,\ C_n^L,\ C_n^G)=0\\
&-f_G C_{n-1}^G-\lambda\psi\,(C_n^L)+(1+f_G+\lambda)\,C_n^G-C_{n+1}^G\\
&\quad=P_{2n}\,(C_{n-1}^G,\ C_n^L,\ C_n^G,\ C_{n+1}^G)=0
\end{aligned}\right\}\ P(c)\quad(10.242)$$

In this system $P(C)$, the column vector

$$[C]=\begin{vmatrix} C_1^L\\ C_1^G\\ \vdots\\ C_j^L\\ C_j^G\\ \vdots\\ C_n^L\\ C_n^G \end{vmatrix}\qquad(10.243)$$

determines the set of quantities characterizing the concentration distribution over the extractor height in both phases.

For a system of equations of an arbitrary order, the Newton algorithm can be represented in the generalized form:

$$P(C_k) + P'(C_k)\,(C_{k+1} - C_k) = 0, \qquad (10.244)$$

where $P'(C_k)$ is the Jacobi matrix of the functions P_1, P_2, .

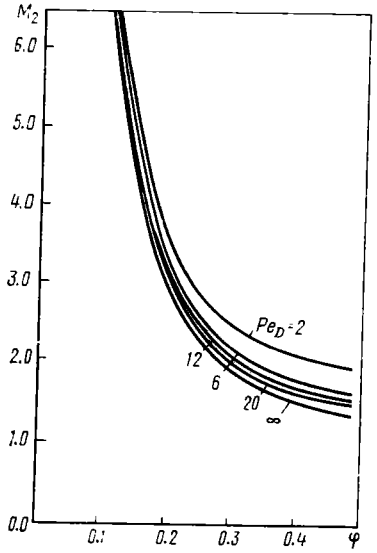

Fig. 191. The effect of the total holding capacity on the value of the second moment for different values of Pe_D ($N_c = 2.5$; $\varphi = 0.5$).

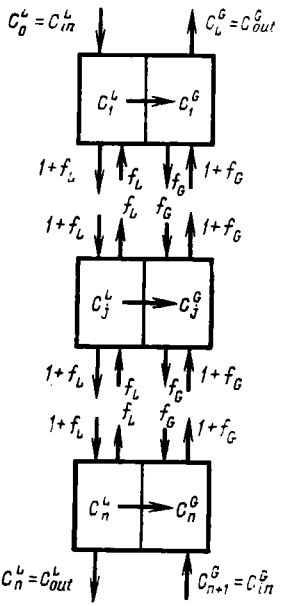

Fig. 192. Cellular model with back flows.

. . ., P_{2j-1}, P_{2j}, . . ., P_{2n-1}, P_{2n} of the system (10.242). The meaning of the Jacobi matrix is in conformity with the following operations

$$P'(C) = \begin{vmatrix} \frac{\partial P_1}{\partial C_1^L} \frac{\partial P_1}{\partial C_1^G} & \cdots & \frac{\partial P_1}{\partial C_j^L} \frac{\partial P_1}{\partial C_j^G} & \cdots & \frac{\partial P_1}{\partial C_n^L} \frac{\partial P_1}{\partial C_n^G} \\ \cdots\cdots\cdots\

After carrying out transformations (10.245) for a system of equations (10.222), we obtain the theoretical dependences for calculating the concentration distribution over the apparatus height at the kth step of the approximation. This dependence has the form of the block matrix

$$\underbrace{\begin{vmatrix} [B_1] & [D_1] & 0 & 0 & \dots & 0 & 0 & 0 & 0 & 0 \\ [A_2] & [B_2] & [D_2] & 0 & \dots & 0 & 0 & 0 & 0 & 0 \\ 0 & [A_3] & [B_3] & [D_3] & \dots & 0 & 0 & 0 & 0 & 0 \\ \dots & \dots & \dots & \dots & \dots & \dots & \dots & \dots & \dots & \dots \\ 0 & 0 & 0 & 0 & \dots & 0 & [A_{n-2}] & [B_{n-2}] & [D_{n-2}] & 0 \\ 0 & 0 & 0 & 0 & \dots & 0 & 0 & [A_{n-1}] & [B_{n-1}] & [D_{n-1}] \\ 0 & 0 & 0 & 0 & \dots & 0 & 0 & 0 & [A_n] & [B_n] \end{vmatrix}}_{[F]}$$

$$\times \begin{vmatrix} [C_1]_k \\ [C_2]_k \\ [C_3]_k \\ \vdots \\ [C_{n-2}]_k \\ [C_{n-1}]_k \\ [C_n]_k \end{vmatrix} = \begin{vmatrix} [A_1] \\ 0 \\ 0 \\ \vdots \\ 0 \\ 0 \\ 0 \end{vmatrix} \times [C_0] + \begin{vmatrix} 0 \\ 0 \\ 0 \\ \vdots \\ 0 \\ 0 \\ [D_n] \end{vmatrix} \times [C_{n-1}] + \begin{vmatrix} [T_1] \\ [T_2] \\ [T_3] \\ \vdots \\ [T_{n-2}] \\ [T_{n-1}] \\ [T_n] \end{vmatrix} \times [V] \quad (10.246)$$

$$[A_j] = \begin{vmatrix} -(1+\delta_j f_L) & 0 \\ 0 & -\delta_j f_G \end{vmatrix},$$

where $\delta_j = \begin{cases} 0 & \text{for } j=1, \\ 1 & \text{for } 2 \leqslant j \leqslant n, \end{cases}$

$$[B_j] = \begin{vmatrix} \{1+(1+\bar{\delta}_j) f_L + \lambda\varphi\psi' [(C_j^L)_k]\} & 0 \\ 0 & \{1+(1+\bar{\delta}_j) f_G + \lambda\} \end{vmatrix},$$

$$[C_j]_k = \begin{vmatrix} (C_j^L)_k \\ (C_j^G)_k \end{vmatrix},$$

where $\bar{\delta}_j = \begin{cases} 0 & \text{for } j=1,\ n, \\ 1 & \text{for } 2 \leqslant j \leqslant n-1, \end{cases}$

$$[D_j] = \begin{vmatrix} -\delta_j^* f_L & 0 \\ 0 & -(1+\delta_j^*) f_L \end{vmatrix},$$

$$[T_j] = \begin{vmatrix} -\{\psi [(C_j^L)_{k-1}] - \psi' [(C_j^L)_{k-1}] (C_j^L)_{k-1}\} & \times \\ 0 & \\ 0 & \\ \times \{\psi [(C_j^L)_{k-1}] - \psi' [(C_j^L)_{k-1}] (C_j^L)_{k-1}\} & \end{vmatrix},$$

$$\text{where } \delta_j^* = \begin{cases} 0 & \text{for } j = n, \\ 1 & \text{for } 1 \leqslant j \leqslant n-1, \end{cases}$$

$$[V] = \begin{vmatrix} \lambda\varphi \\ \lambda \end{vmatrix}.$$

Matrix system (10.246) is solved by the method of diagonalization of the block Jacobi matrix (matrix F). The uniqueness of the solution is guaranteed by the non-degeneracy of the matrix F whose determinant is always non-zero if the equilibrium dependence is not

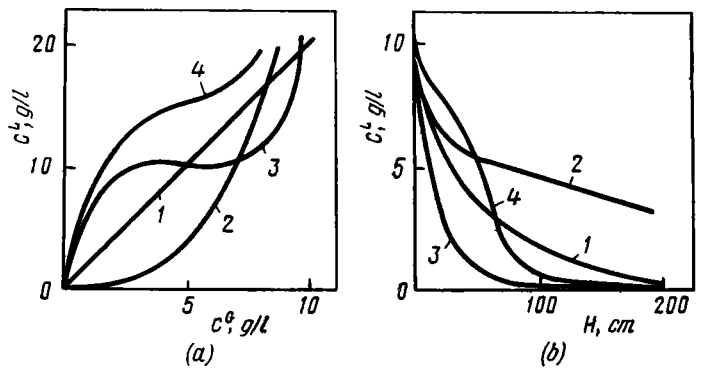

Fig. 193. The effect of the type of equilibrium dependence (*a*) on the concentration distribution over the column height (*b*):

1—linear dependence; *2*—exponential dependence; *3*—curve with an extremum; *4*—curve with an inflection.

extremal. For the initial approximation the concentration distribution calculated for the linear equilibrium dependence with a constant distribution coefficient $m = \psi'(0)$ is normally used. For this case, $[T_1] = \ldots = [T_j] = \ldots = [T_n] = 0$. Calculations made on a digital computer showed that the concentration distribution over the extractor height (Fig. 193) is determined by the form of the equilibrium dependence.

The practical application of the cellular model with back mixing between stages involves the determination of theoretical dependences of the model parameters on the numerical characteristics of the distribution function. In order to solve this problem, a one-phase model discarding mass transfer is analyzed theoretically and constraint equations for determining hydrodynamic parameters of the model are thus obtained. The results of the solution of constraint equations are used for constructing generalized nomograms connecting the magnitudes of the second M_2 (Fig. 194) and third M_3 (Fig. 195)

initial moments with the model parameters: the number n of mixing cells and countercurrent flow rate f.

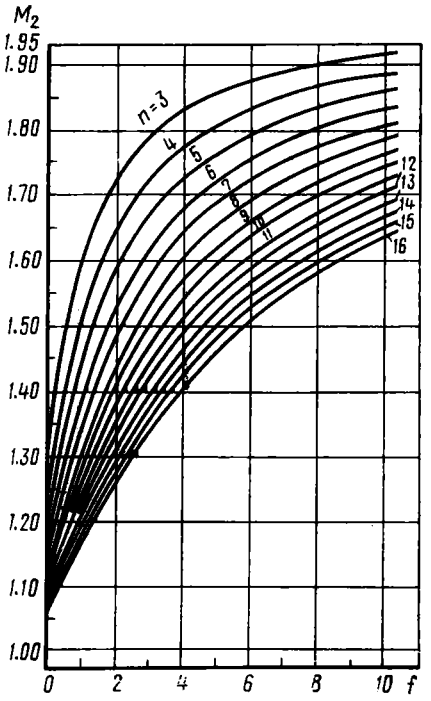

Fig. 194. Nomogram for determining the set of values f and n from M_2.

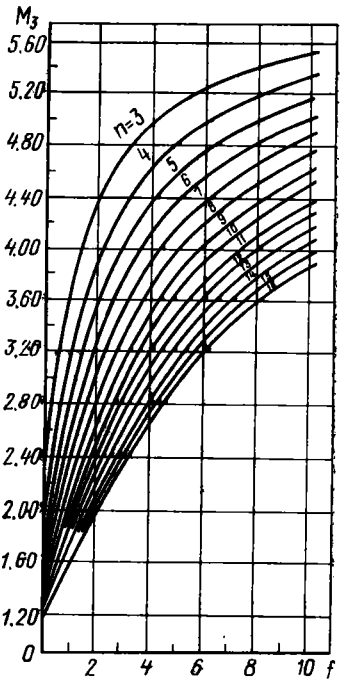

Fig. 195. Nomogram for determining the set of values f and n from M_3.

Diffusion model. In order to take into account the axial dispersion in extraction columns, we use a diffusion model (Fig. 196). The balance equation for the element dz is

$$D_L \frac{d^2x}{dz^2} - w_L \frac{dx}{dz} = K_x a\,(x - x^*), \qquad (10.247)$$

where D_L is the axial dispersion coefficient for the stripped phase, m²/hr; x is the stripped-phase concentration, kg/m³; w_L is the fictitious velocity of the stripped phase, m/hr; z is the coordinate, m; and $K_x a$ is the volumetric mass-transfer coefficient, 1/hr.

The material-balance equation for the bottom part of the column to the point z is written in the form

$$L_f x_f + Gy = Gy_E + Lx - D_G \frac{dy}{dz} - D_L \frac{dx}{dz}, \qquad (10.248)$$

where G is the fictitious flow rate of enriched phase, m/hr; y is the concentration in the enriched phase, kg/m³; and D_G is the axial dispersion coefficient in the enriched phase, m²/hr.

Equations (10.247) and (10.248) can be reduced to

$$\frac{dX}{dz} = -\frac{K_x a}{L}(x - x^*), \quad (10.249)$$

$$Px_p = LX - GY,$$

where

$$X = x - \frac{D_L}{L} \cdot \frac{dx}{dz}, \quad (10.250)$$

$$Y = y - \frac{D_G}{G} \cdot \frac{dy}{dz}, \quad (10.251)$$

$$Px_p = L_f x_f - Gy_E. \quad (10.252)$$

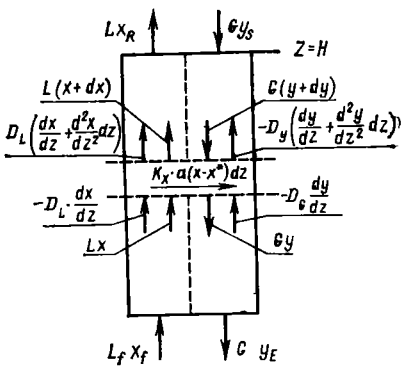

Fig. 196. Diffusion model of an extraction column.

For solving system (10.249)-(10.252), the boundary conditions must be formulated in the form

$$\begin{aligned} &\text{for } z = 0 \quad X_0 = x_f; \quad Y_0 = y_E, \\ &\text{for } z = H \quad X_H = x_R; \quad Y_H = y_s. \end{aligned} \quad (10.253)$$

In order to construct the operating line, system (10.249)-(10.252) is written in terms of finite differences:

$$\Delta X_i = -\frac{K_x a}{L}\Delta z\,(x_i - x_i^*), \quad (10.254)$$

$$Y_{i+1} = \frac{L}{G}X_{i+1} - \frac{Px_p}{G}, \quad (10.255)$$

$$\Delta x_i = -\frac{L}{D_L}\Delta z\,(X_i - x_i), \quad (10.256)$$

$$\Delta y_i = -\frac{y_i - Y_{i+1}}{1 + \frac{D_G}{G\Delta z}}. \quad (10.257)$$

The schematic diagram of flows in the finite-difference approximation is shown in Fig. 197. Let us consider the sequence of calculation of axial mixing in the stripped and enriched phases.

1. The construction of the operating line taking into account the axial dispersion in the enriched phase (Fig. 198). In this case $D_L = 0$, then $X = x$, and system (10.254)-(10.257) assumes the form

$$\Delta x_i = -\frac{K_x a}{L}\Delta z\,(x_i - x_i^*), \quad (10.258)$$

$$Y_{i+1} = \frac{L}{G}X_{i+1} - \frac{Px_p}{G}, \quad (10.259)$$

$$\Delta y_i = -\frac{y_i - Y_{i+1}}{1 + D_G/G\Delta z}. \quad (10.260)$$

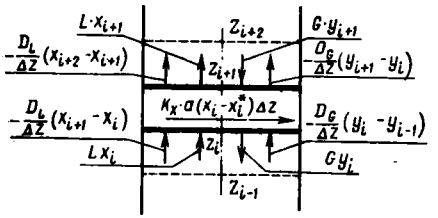

Fig. 197. Flow diagram in the finite-difference approximation.

In the figure, OED is the equilibrium line and $A'B'$ is the operating line. According to Eqs. (10.258)-(10.260), the concentrations in $(i + 1)$st cross section can be expressed in terms of concentrations in the ith section. This corresponds to the point $B\ (x_{i+1},\ y_{i+1})$ for a given position of the point $A\ (x_i,\ y_i)$. In accordance with the relation

$$\frac{AC}{AD} = \frac{K_x a}{L} \Delta z,$$

obtained from Eq. (10.258), we plot the point $C\ (x_{i+1},\ y_i)$ lying on the line AD. The step Δz is chosen arbitrarily. It follows from

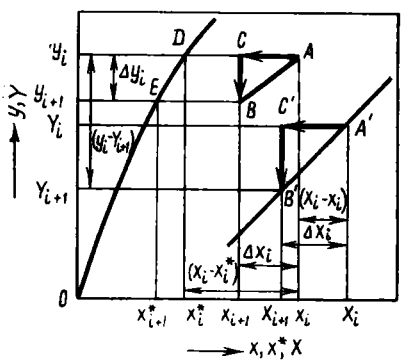

Fig. 198. Construction of the operating line, taking into account axial dispersion in the enriched phase.

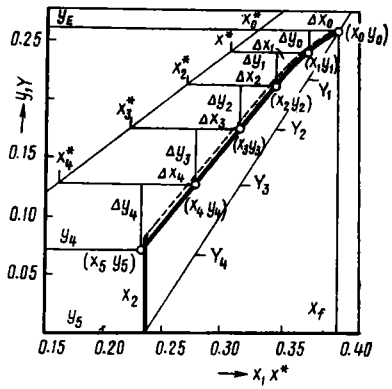

Fig. 199. Construction of the operating line and determination of the number of contact stages, taking into account axial dispersion.

Eq. (10.259) that the point B must lie on the operating line. Then the position of the point B on the line CB is determined from the relation

$$\frac{CB}{CB'} = \frac{1}{1 + \frac{D_G}{G\Delta z}}.$$

The line AB is the operating line element corresponding to the step Δz.

The construction of the operating line and determination of the number of separation stages is carried out under the following conditions: $m = 0.8$, $L = 16$, $G = 10$, $x_f = 0.4$, $y_s = 0.0$, $y_F = 0.265$, $K_x a = 3.2$, $D_G = 25$, $D_L = 0$, $\Delta z = 2$, and is shown in Fig. 199.

The construction starts from the point with the coordinates $x_f = x_0$, $y_s = y_0$. As a result of calculations, it was obtained that $n = 4.9$ separation stages and accordingly, the column height $H = n\,\Delta z = 4.9 \times 2 = 9.8$.

2. The construction of the operating line by taking into account the axial dispersion in the stripped phase. In this case, the construction starts from the point with the coordinates $x_0 = X_0 = x_R$ and $y_0 = y_s$. The following relations are used for determining the increments Δx_i and Δy_i:

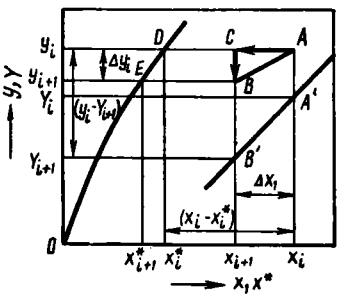

Fig. 200. Construction of the operation line taking into account axial dispersion in enriched and depleted phases.

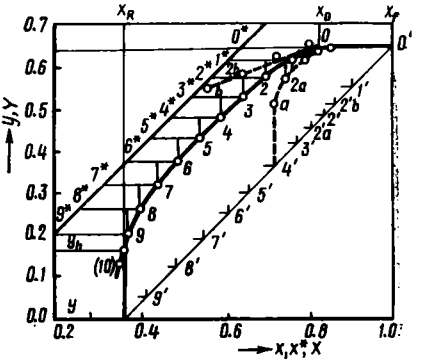

Fig. 201. Construction of the operating line and determination of the number of contact stages in the enriched and depleted phases, taking into account axial dispersion.

$$\Delta y_i = \frac{K_{0y}a}{G}\,\Delta z\,(y_i^* - y_i), \tag{10.261}$$

$$X_{i+1} = \frac{G}{L}\,y_{i+1} + \frac{Px_P}{L}, \tag{10.262}$$

$$\Delta x_i = \frac{1}{1 + \dfrac{D_L}{L\Delta z}}\,(X_{i+1} - x_i). \tag{10.263}$$

The number of separation stages is calculated until the point with the coordinate y_E is attained.

3. The construction of the operating line by taking into account the axial dispersion in the two phases. This is the most complicated case, since it requires the employment of the trial-and-error method. For constructing the operating line, the system of equations (10.254)-(10.257) is used. Figure 200 shows the graphic determination of x_{i+1}, y_{i+1} through x_i, y_i.

The point A (x_i, y_i) lies on the operating line, while the point A' (x_i, y_i) lies on the operating line taking mixing into account. The

position of the point $B\,(x_{i+1},\ y_{i+1})$ is determined as follows. The point $C'\ (x_{i+1},\ y_i)$ is found with the help of the relation

$$\frac{A'C'}{AD} = \frac{K_{0x}a}{L}\,\Delta z \text{ by } \Delta X_i .$$

The point $B'\ (X_{i+1},\ Y_{i+1})$ lies on the operating line taking mixing into account. The second point $C\,(x_{i+1},\ y_i)$ is determined from Eq. (10.256), and then the point $B\,(x_{i+1},\ y_{i+1})$ is found from Eq. (10.257). The construction of the operating line and determination of the number of theoretical plates for $m = 1$, $L = 10$, $V = 10$, $x_f = 1$, $x_R = 0.36$, $K_{0xi}a = 5.0$, $D_L = 25$, $D_G = 25$, and $\Delta z = 1$ is shown in Fig. 201.

Starting from the point 0′ with the coordinates $X_0 = x_f$, $y_0 = y_E$ and the arbitrarily assumed position of the point 0 $(x_0,\ y_E)$, the positions of the points 1, 1′, 2, 2′, etc. are calculated.

Chapter 11

Apparatus with External Energy Supply

Apparatus with external supply of energy are frequently used for treatment of liquid-liquid systems with a small difference in specific gravities and with a small relative velocity of their motion. At the interface between such liquids, friction is insignificant. Consequently, external energy supply to the flows is required for the development of phase-contact surface and turbulization. The apparatus with external energy supply are also used for gas-liquid systems.

11.1. Apparatus with Mechanical Stirrers (Rabbles)

11.1.1. Modelling of Apparatus with Rabbles

Various mathematical models, starting with the simplest (perfect mixing) and finishing with complicated hybrid and multicircuit circulation models are used for describing diffusion processes occurring in apparatus with rabbles. Besides, cellular and diffusion models are used for the description of non-ideal mixing. The indeterministic and stochastic nature of mixing processes made it possible to apply probability and statistical methods for their description. This led to the appearance of stochastic models.

The residence-time distribution of particles in an apparatus is essentially non-uniform due to flow turbulization by the stirrer, spurting, by-passing of a part of flows and the presence of stagnation zones, molecular diffusion as well as the non-uniformity of velocity profiles and their deformation. Taking into account various phenomena and introducing into the model the characterizing parameters, it is possible to obtain a description of the process of mixing which is in conformity with the actual process.

Hybrid models. This type of models is the one most frequently used for describing processes of mixing in apparatus with stirrers. Practically, such models consist of similar perfect-mixing and displacement cells connected by exchange flows, which also include by-passing, recycling, and stagnation zones whose presence determines

the non-uniformity of mixing in the bulk and thus affects the efficiency of mass-transfer processes.

Stagnation zones appearing in the flow passing through the apparatus deteriorate heat and mass transfer. Since it is not always possible to eliminate stagnation zones and by-passing completely, they must be taken into consideration while designing the apparatus. Figures 202*a-c* show stagnation zones (hatched regions) in an apparatus with poor stirring, and Fig. 202*d* shows stagnation zones with by-passing (see p. 393).

In order to quantitatively describe apparatus with inperfect mixing, the models (Table 18) which take into account a large

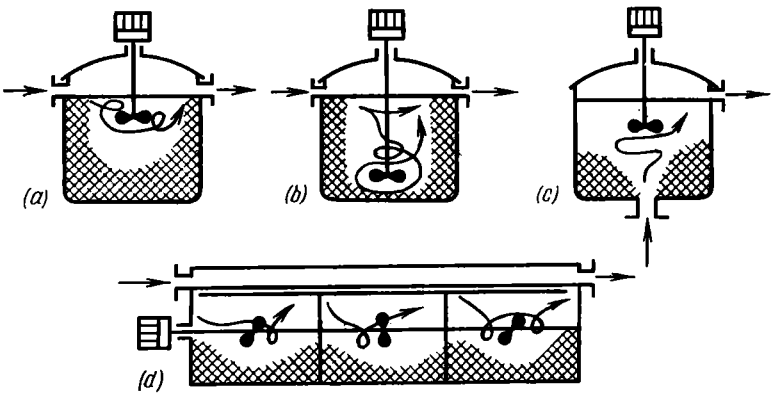

Fig. 202. Emergence of stagnation zones in flow-through apparatus with stirrers.

number of physical phenomena and are comparatively simple for calculations are employed. In a simplified form, the systems can be described by a model consisting of two perfect-mixing zones. The particles continuously supplied to the system may, in principle, get into any of these zones and remain there until they leave the system and go over to the other zone. Thus, the model under consideration is a three-parametric model. Its parameters are: the fraction of volume d of one zone, the fraction of flow j passing through one of the zones, and the flow i that takes into account the exchange between the zones. In this case, the by-passing can be represented as one of the mixing zones with a small mean duration of stay dV_a/jV or $(1-d)\,V_a/(1-j)\,V$, where V is the total volume and V_a the volume of the apparatus. The second zone is the stagnation zone.

The perfect mixing volume is obtained for two boundary conditions: (a) for $i \to \infty$ for any d and j, (b) for $d = j$ for any i.

Table 18

Properties of Two-Zone Models

Name of the model	Model	Distribution functions for residence time
Two-parametric model with parallel flows	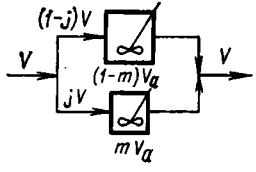	$\tau f(t)=\frac{j^2}{m}\exp\left[-\frac{j}{m}\frac{t}{\tau}\right]+\frac{(1-j)^2}{1-m}\exp\left[-\frac{1-j}{1-m}\frac{t}{\tau}\right]$ (1) $F(t)=1-\left\{j\exp\left[-\frac{j}{m}\frac{t}{\tau}\right]+(1-j)\exp\left[-\frac{1-j}{1-m}\frac{t}{\tau}\right]\right\}$ (2) $\tau\lambda(t)=\frac{\frac{j^2}{m}\exp\left[-\frac{j}{m}\frac{t}{\tau}\right]+\frac{(1-j)^2}{1-m}\exp\left[-\frac{1-j}{1-m}\frac{t}{\tau}\right]}{j\exp\left[-\frac{j}{m}\frac{t}{\tau}\right]+(1-j)\exp\left[-\frac{1-j}{1-m}\frac{t}{\tau}\right]}$ (3)
One-parametric model with parallel flows	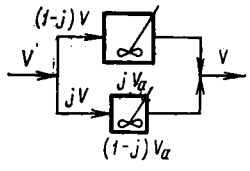	$\tau f(t)=\frac{j^2}{1-j}\exp\left[-\frac{j}{1-j}\frac{t}{\tau}\right]+\frac{(1-j)^2}{j}\exp\left[-\frac{1-j}{j}\frac{t}{\tau}\right]$ (4) $F(t)=1-\left\{j\exp\left[-\frac{j}{1-j}\frac{t}{\tau}\right]+(1-j)\exp\left[-\frac{1-j}{j}\frac{t}{\tau}\right]\right\}$ (5) $\tau\lambda(t)=\frac{\frac{j^2}{1-j}\exp\left[-\frac{j}{1-j}\frac{t}{\tau}\right]+\frac{(1-j)^2}{j}\exp\left[-\frac{1-j}{j}\frac{t}{\tau}\right]}{j\exp\left[-\frac{j}{1-j}\frac{t}{\tau}\right]+(1-j)\exp\left[-\frac{1-j}{j}\frac{t}{\tau}\right]}$ (6)

Table 18 (continued)

Name of the model	Model	Distribution functions for residence time
One-parametric model with a by-pass	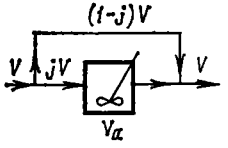	$\tau f(t)=\begin{cases}\infty & t=0\\ j^2\exp\left[-j\frac{t}{\tau}\right] & t>0\end{cases}$ (7) $F(t)=1-j\exp\left[-j\frac{t}{\tau}\right]$ (8) $\tau\lambda(t)=\begin{cases}\infty & t=0\\ j & t>0\end{cases}$ (9)
Two-parametric exchange model	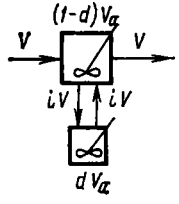	$\tau f(t)=\frac{a+b}{2a(1-d)}\exp\left[-\frac{i+d-a}{2d(1-d)\tau}\frac{t}{\tau}\right]+\frac{a-b}{2a(1-d)}\exp\left[-\frac{i+d+a}{2d(1-d)}\frac{t}{\tau}\right]$ (10) $F(t)=1-\left\{\frac{d(a+b)}{a(i+d-a)}\exp\left[-\frac{i+d-a}{2d(1-d)\tau}\right]+\frac{d(a-b)}{a(i+d-a)}\exp\left[-\frac{i+d+a}{2d(1-d)}\frac{t}{\tau}\right]\right\}$ (11) $\tau\lambda(t)=\frac{\frac{a+b}{2(1-d)}\exp\left[\frac{a}{2d(1-d)}\frac{t}{\tau}\right]+\frac{a-b}{2d(1-d)}\exp\left[-\frac{a}{2d(1-d)}\frac{t}{\tau}\right]}{\frac{d(a+b)}{i+d-a}\exp\left[+\frac{a}{2d(1-d)}\frac{t}{\tau}\right]+\frac{d(a-b)}{1+d+a}\exp\left[-\frac{a}{2d(1-d)}\frac{t}{\tau}\right]}$ (12)

Table 18 (continued)

Name of the model	Model	Distribution functions for residence time
		$a=\sqrt{i^2-2id+4id^2+d^2}$ $\quad b=i-2id-d$
One-parametric exchange model	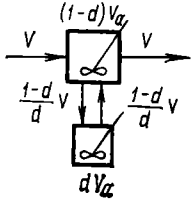	$\tau f(t)=\frac{a+b}{2a(1-d)}\exp\left[\frac{1-d+d^2-ad}{2d^2(1-d)}\frac{t}{\tau}\right]+\frac{a-b}{2a(1-d)}\exp\left[-\frac{1-d+d^2+ad}{2d^2(1-d)}\frac{t}{\tau}\right]$ (13) $F(t)=1-\frac{a^2(a+b)}{a(1-d+d^2-ad)}\exp\left[-\frac{1-d+d^2-ad}{2d^2(1-d)}\frac{t}{\tau}\right]+\frac{d^2(a-b)}{a(1-d+d^2+ad)}\exp\left[-\frac{1-d+d^2+ad}{2d^2(1-d)}\frac{t}{\tau}\right]$ (14) $\tau\lambda(t)=\frac{\frac{a+b}{2(1-d)}\exp\left[+\frac{a}{2d(1-d)}\frac{t}{\tau}\right]}{\frac{d^2(a+b)}{1-d+d^2-ad}\exp\left[+\frac{a}{2d(1-d)}\frac{t}{\tau}\right]}$ $\frac{+\frac{a-b}{2(1-d)}\exp\left[-\frac{a}{2d(1-d)}\frac{t}{\tau}\right]}{+\frac{d^2(a-b)}{1-d+d^2+ad}\exp\left[-\frac{a}{2d(1-d)}\frac{t}{\tau}\right]}$ (15) $a=\sqrt{1-2d-d^2+6d^3-3d^4}/d$ $\quad b=(1-3d+d^2)/d$

Table 18 (continued)

Name of the model	Model	Distribution functions for residence time
One-parametric model with a stagnation zone	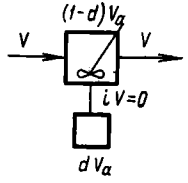	$\tau f(t) = \frac{1}{1-d} \exp\left[-\frac{1}{1-d}\frac{t}{\tau}\right]$ (16) $F(t) = 1 - \exp\left[-\frac{1}{1-d}\frac{t}{\tau}\right]$ (17) $\tau\lambda(t) = \frac{1}{1-d}$ (18)
Two-parametric model	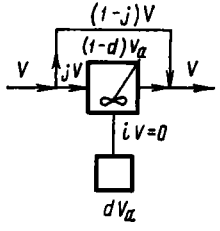	$\tau f(t) = \begin{cases} \infty & t=0 \\ \frac{j^2}{1-d} \exp\left[\frac{j}{1-d}\frac{t}{\tau}\right] & t>0 \end{cases}$ (19) $F(t) = 1 - j \exp\left[-\frac{j}{1-d}\frac{t}{\tau}\right]$ (20) $\tau\lambda(t) = \begin{cases} \infty & t=0 \\ \frac{j}{1-d} & t>0 \end{cases}$ (21)

Since an increase in the parameter i and a decrease in the difference between d and j affect the deformation of the model in the same way, it is assumed that either $i = 0$ or $j = 0$. Then the model is reduced to two two-parametric models: (1) the model with parallel flows (Table 18) ($i = 0$) and (2) the exchange model (Table 18) in which the stagnation zone is not connected directly with the inlet and outlet flows ($j = 0$).

The model with parallel flows. The parameters of this model are the fraction j of the flow and the fraction m of the volume.

The duration of stay distribution function is described by Eqs. (1)-(9) of Table 18.

This model gives the duration of stay distributions which correspond to the duration of stay in an imperfect-mixing apparatus. The model describes the region from perfect mixing ($j = m$) to by-pass ($j = 1$, $m = 0$). The deviation from the perfect mixing is the larger, the greater the difference between the parameters j and m for the two zones. The fact that different combinations of model parameters give similar distribution curves allows us to combine these parameters and reduce the model to a one-parametric model with parallel flows for $m = 1 - j$. The model with by-pass corresponds to the value of $m = 1$.

The exchange model. The parameters of this model are the volume d of the stagnation zone and the exchange flow i between the zones. The duration of stay distribution function for such a model is described by Eqs. (10)-(21) (Table 18). As in the case of the preceding model, the perfect-mixing model is the limiting case $i \to \infty$; another limiting case $i \to 0$ (one-parametric model in Table 18) is identical to the limiting case $j \to 0$ or $(1 - j) \to 0$ for the model with parallel flows. Combining the model parameters $i = (1 - d)/d$ (Table 18), we arrive at the perfect-mixing model ($d = 0$) and by-pass ($d = 1$).

Recirculation models. Recirculation flows appear in agitated vessels, therefore a special class of models called the recirculation models has been created. An advantage of these models is that they consist of single-type elements, viz. the perfect-mixing cells. The uniformity of elements having an exponential law for the duration of stay distribution made it possible to apply the mathematical apparatus of the Markov processes for obtaining the duration of stay distribution functions. Let us introduce the concept of the degree of recirculation $R = q/Q$, which will be assumed equal to the ratio of the flow created by the stirrer (the pumping capacity q of the stirrer) to the main flow Q entering the apparatus. The pumping capacity of the stirrer is a basic characteristic of an agitated vessel. It was this parameter with which the first studies of hydrodynamic processes occurring in such apparatus began. Experimental and theoretical investigations in this field confirmed the formula proposed by Van de

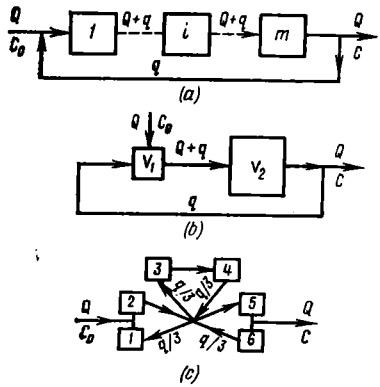

Fig. 203. Hybrid models with recirculation contours.

Vusse for the impeller and turbine-type mixers:

$$q = K_m n d_s^2 b, \qquad (11.1)$$

where K_m is the proportionality factor depending on the type of mixer, arrangement and the number of blades; n the stirrer speed, rps; d_s the stirrer diameter, m; and b the blade width, m.

The simplest recirculation model is the cellular model with recycle: the material returns to the initial flow (Fig. 203*a*). This is a one-parametric model (the number n of cells, and its transfer function (the Laplace operator p) reflects the entire spectrum of the duration of stay distribution functions between the perfect-mixing and plug-flow regimes:

$$W(p) = \frac{1}{\left(\frac{V}{q(R+1)n}p+1\right)^n - R}. \qquad (11.2)$$

The entire apparatus volume is divided into two zones: the perfect-mixing zone around the stirrer and the zone of a single mixing cell (the remaining volume of the apparatus). The two zones are connected by a recirculation loop (Fig. 203*b*). The transfer function of this model has the form

$$W(p) = \frac{1}{\left(\frac{V_1}{q(R+1)}p+1\right) - \frac{R}{\left(\frac{V_2}{q(R+1)}p+1\right)}}. \qquad (11.3)$$

However, single-loop models do not fully reflect the actual hydrodynamic processes in agitated vessels where at least two recirculation loops are present.

In the three-loop recirculation model (Fig. 203*c*), each half of the loop volume before and after the stirrer consists of n consecutive mixing cells. After certain simplifications, for low degrees of recirculation, the model is reduced to the single-loop model:

$$W(p) = \frac{1}{(1+R)\left(\frac{3V}{q(R+1)^n}p+1\right)^n - R}. \qquad (11.4)$$

This model was used for calculating the apparatus with one and two stirrers.

In the four-loop recirculation model, the entire apparatus volume is divided into four zones depending on the position and the diameter of the stirrer (Fig. 204*a*). Each zone can be represented in the form of a perfect mixing cell and is connected with the neighbouring

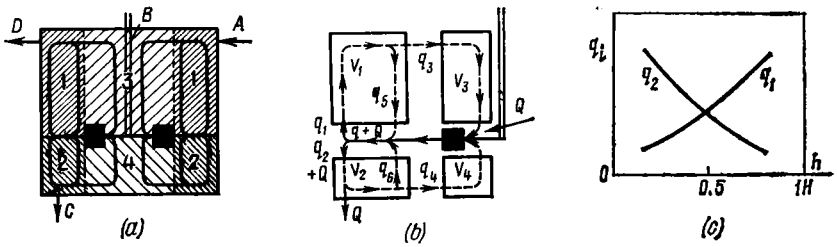

Fig. 204. Four-loop recirculation model (*a*, *b*) and the dependence of recirculation flows q_1 and q_2 on the height h of the stirrer (*c*).

cells by recirculation flows. The trajectory of the feed flow depends on the position of the inlet and the outlet of the apparatus and coincides with the recirculation flow. The block diagram of the model is shown in Fig. 204*b*. Figure 204*c* represents the dependences of the

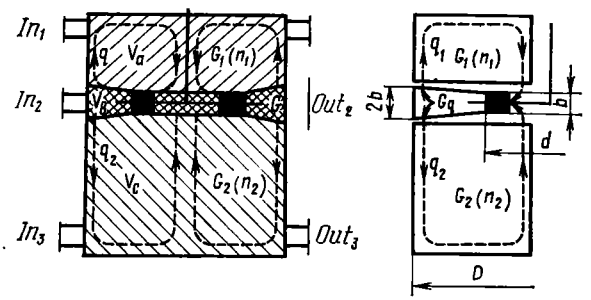

Fig. 205. Recirculation model with a varying structure.

recirculation flows q_1 and q_2, which form the upper and lower recirculation loops, on the height H of the layer of liquid in the apparatus and on the height h of the stirrer location.

The recirculation model with a varying structure consists of two recirculation loops with a varying number $G(n)$ of perfect-mixing cells in each, which are connected in the mixing zone that is a perfect-mixing cell (Fig. 205). The model parameter is the trajectory of the inlet flow in the apparatus, which coincides with recirculation flow and is determined by the mutual arrangement of the inlet and outlet. The volume of the zones in each loop depends on the position

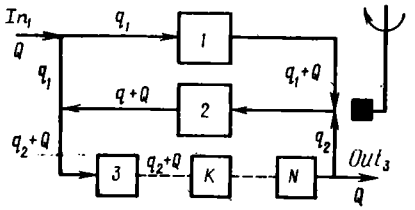

Fig. 206. Structure of flows in a recirculation model with a varying number of cells.

of the stirrer and can be calculated from the formulas

$$V_a = \frac{\pi D^2}{4}(H-h) - \frac{V_b}{2}, \quad (11.5)$$

$$V_c = \frac{\pi D^2}{4} h - \frac{V_b}{2}, \quad (11.6)$$

where D is the apparatus diameter, m; H the height of the level of liquid in the apparatus, m; and h the height at which the stirrer is located, m.

The volume of the perfect-mixing zone near the stirrer is determined by the equation

$$V_b = \frac{\pi b}{12}(5D^2 + d_s^2 - Dd_s), \quad (11.7)$$

where d_s is the stirrer diameter, m; and b is the blade width, m.

The number of cells in the upper and lower zones can be calculated from the ratio

$$\Delta = \frac{n_{max}}{n_{min}}, \quad (11.8)$$

the smaller zone being always represented by a single cell ($n_{min} = 1$).

The change in the stirrer position deforms the model:

$$n_a = n_{min} = 1; \quad n_c = n_{max} = \Delta \quad \text{for} \quad h/H > 0.5,$$
$$n_a = n_c = 1; \quad \text{for} \quad h/H = 0.5,$$
$$n_a = n_{max} = \Delta; \quad n_c = m_{min} = 1 \quad \text{for} \quad h/H < 0.5.$$

The main flow q is calculated by formula (11.1), while the ratio of flows in the upper and lower loops, from the relation

$$\frac{q_1}{q_2} = \frac{h}{H-h}. \quad (11.9)$$

The inlet and outlet of the apparatus are diametrically opposite pipes. A two-loop recirculation model with a varying structure is shown in Fig. 206.

Power consumption for mixing. The amount of energy consumed by rabbles in geometrically similar apparatus is determined from the relation

$$Eu_s = cRe_s^m, \quad (11.10)$$

where $Eu_s = N/(n^3 d_s^5 \rho)$ is the Euler number for stirrers; $Re_s = nd_s^2\rho/\mu$ is the Reynolds number for stirrers; N is the power consumed for mixing, n the speed of rotation of the stirrer, rps; d_s is the stirrer diameter, m; ρ the density of the medium being mixed;

μ the viscosity of this medium; c a constant depending on the shape of the mixer blades; and m a constant depending on hydrodynamic conditions.

In the turbulent region ($Re_s = nd_s^2\rho_l/\mu_l > 10^4$), in the presence of baffles, $m = 0$, Eq. (11.10) assumes the form

$$Eu_s = \frac{N}{n^3 d_s^5 \rho} = \text{const}, \qquad (11.11)$$

or

$$N = \text{const}\, n^3 d_s^5 \rho. \qquad (11.12)$$

11.1.2. Mixing in Gas-Liquid Systems

When mass-transfer processes occur in gas-liquid systems in apparatus with rabbles, the gas is usually fed through a perforated steam sprayer (Fig. 207), and baffles for suppressing the eddies are

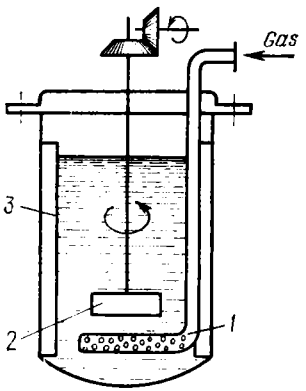

Fig. 207. Schematic diagram of a perforated sprayer with a stirrer:
1—prayer; *2*—stirrer; *3*—baffles.

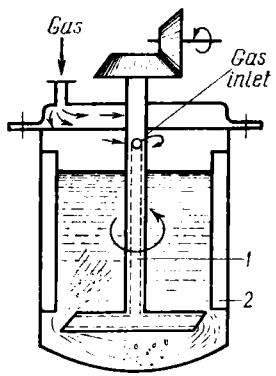

Fig. 208. Suction stirrer:
1—tube-stirrer; *2*—baffles.

mounted at the apparatus walls. Rabbles operating without bubblers have found wide application. Suction stirrer is an example of this type of rabbles. It consists of a hollow tube with a nozzle through which the gas is ejected. This nozzle surves as the stirrer blade (Fig. 208).

Perforated steam sprayers divided into compartments along their height, which contain stirrers between the compartments and in which the gas is supplied at the bottom of the apparatus are also frequently used (Fig. 209). The introduction of the gas into the liquid phase changes the density of the medium interacting with the stirrer.

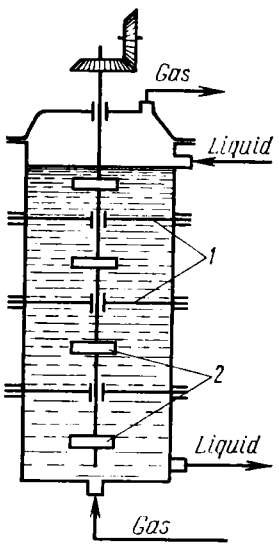

Fig. 209. Perforated sprayer compartmented along its height:
1—partitions; *2*—stirrers.

Since the volumetric output of the stirrer is proportional to nd_s^3, and the amount of gas in the medium being mixed is a function of the amount of gas V_g (m^3/s) delivered under the stirrer, the fraction of gas φ_g in the volume of the medium being mixed can be represented in the following form:

$$\varphi_g = f\left(\frac{V_g}{nd_s^3}\right). \quad (11.13)$$

When a gas-liquid mixture is stirred by a six-blade turbine-type stirrer in a vessel with baffles of width $b = 0.08D$, this dependence assumes the form

$$\varphi_g = cA^m k_1 k_2 k_3, \quad (11.14)$$

where A and c are coefficients; k_1 is a coefficient taking into account the viscosity of the working liquid; k_2 is a coefficient that takes into consideration the diameters D and d_s of the vessel and the stirrer; and k_3 is a coefficient that takes into account the height at which the stirrer is mounted relative to the bottom of the vessel:

$$A = \left(\frac{V_g \rho_l n}{\sigma}\right)^{0,21n\sqrt{d_s}} \left(\frac{H}{D}\right)^{0.4},$$

$$k_1 = 10^{0.003(1-\mu/\mu_w)}, \quad k_2 = 0.413\left(5.43 - \frac{D}{d_s}\right); \quad k_3 = f\left(\frac{h}{D}\right),$$

where μ_w is the viscosity of water at 20 °C. The values of c, m, and k_3 are given in Table 19.

Table 19

The Values of Coefficients c, m, and k_3 in Eq. (11.14)

Number of baffles	Applicability range of Eq. (11.14)	c	m	k_3
3	$A \leqslant 30$	0.425	0.42	$1.16\,(h/D)^{-0.15}$
3	$A > 30$	1.50	0.26	$(h/D)^{-0.32}$
4	$A \leqslant 30$	0.83	0.61	$0.76\,(h/D)^{-0.566}$
4	$A > 30$	1.50	0.26	$(h/D)^{-0.385}$

The power consumption in the gas-liquid system can be determined from the power consumed for mixing liquid containing no gas:

$$\frac{N_g}{N_0} = f\left(\frac{V_g}{nd_s^3}\right), \quad (11.15)$$

where N_0 is the power consumed for mixing liquid without gas.

The dependence of N_g/N_0 on $V_g/(nd_s^3) \times 10^2$ for perforated steam sprayers with six blades is shown in Fig. 210.

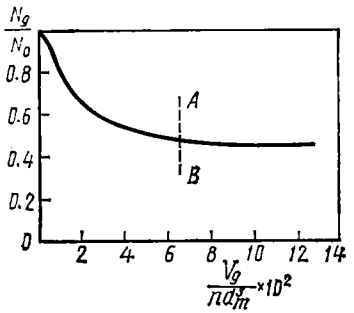

Fig. 210. Dependence of a relative power on V_g/nd_s^3.

The excess of gas delivered under a stirrer may cause flooding. In this case, the gas is neither dispersed nor sprayed by the stirrer into surrounding medium. As it flows past the stirrer, the gas rises along the shaft. This regime is described by the horizontal section of the curve in Fig. 210. The range of $V_g/(nd_s^3) \times 10^2$ for which flooding regime usually sets in is marked in Fig. 210 by the line AB and lies to the right of it. For this regime, the approximate equality $N_g/N_0 \approx$ const is valid, i.e. the power consumption is a function of dimensions and speed of the stirrer and is practically independent on the amount of gas delivered under it. For all types of stirrers there exists a linear dependence of $\log (N_g/N_0)$ on $\log (V_g/(nd_s^3) \times 10^2$, and hence

$$\frac{N_g}{N_0} = c\left(\frac{V_g}{nd_s^3} \times 10^2\right)^p, \quad (11.16)$$

where c and p are constants having different values for different stirrers. The values of c and p are given in Table 20.

In scaling up geometrically similar stirrers for gas-liquid system, it is necessary to take into account the fact that the equality of power consumption per unit volume of liquid being mixed must be conserved as well as the equality of dimensionless ratios $V_{g_1}/(n_1 d_{s_1}^3) = V_{g_2}/(n_2 d_{s_2}^2)$.

When gases are dispersed in the liquid in an apparatus with a rabble, the size of gas bubbles is determined by the balance between the surface tension forces and the forces of turbulent fluctuations. In the case of coalescence, the bubble size depends on their merging which is impeded by turbulent flow. The bubble diameter d_b is proportional to $N^{-1/4}$, or $d_b \propto n^{-3/4}$. In the absence of coalescence, $d_b \propto n^{-1/2}$. The presence of finest impurities and foreign admixtures prevents the coalescence of bubbles. In this case, $d_b \propto n^{0.76-1.5}$. If we discard coalescence, the mean bubble size can be determined from

Table 20

Values of Constants c and p in Eq. (11.16) $\left(\text{for } \frac{nd_s^2\rho_l}{\mu_l} > 10^4\right)$

Type of stirrer	Eu_s for $v_g = 0$	$\frac{D}{d_s}$	$\frac{b}{d_s}$	$\frac{H}{d_s}$	$\frac{h}{d_s}$	n, rpm	$\frac{g}{nd_s^3}\times 10^2$	c	p	Remarks
Flat-bladed stirrers with two blades	2.07	3	0.2	3	1	470-780	0.7-3.5	0.81	—0.54	Four baffles
Flat-bladed stirrers with four blades	2.52	3	0.2	3	1		0.6-7.0			
	1.61	3	0.133	3	1	485-1180				
	3.70	3-4.5	0.3	3-4.5	1		0.6-7.5	0.87	—0.32	—Do—
	4.96	3-4.5	0.4	3-4.5	1		0.6-8.0			
Two-bladed stirrers of the "hollow tube" type	1.3	3	0.2	3	1	470-790	0.7-2.9	0.79	—0.53	—Do—
	0.67		0.133	3	1					
Four-bladed stirrers of the "hollow tube" type	2.16		0.2							
	1.50	3	0.133	3	1	470-970	0.7-6.5	0.85	—0.376	—Do—
Six-bladed turbines	2.34	3-4.5	0.1	3-4.5	1	477-1160	0.6-6.5	0.82	—0.310	—Do—
	4.8	3-4.5	0.2	3-4.5	1	490-790	1.0-8.5	0.88	—0.330	—Do—
Sixteen-bladed turbines, d = = 9.58 cm	3.0	2.45	0.1	2.45	1	173-598	0.7-8.0	0.89	—0.255	—Do—
Pitched-blade turbines with six blades, d = 10.2 cm	4.47					423-854	3.3-12.0	1.05	—0.53	Three baffles
	3.86	3.13	0.218		0.815-1.55					

the following relation:

$$\bar{d}_b = 4.15\left[\frac{\sigma^{0.6}}{(N_e/V)^{0.4}\rho_c^{0.2}}\right]\varphi_g^{0.5} + 0.0009, \qquad (11.17)$$

where N_e/V is the total power supply

$$N_e/V = N_g/V + c_1 N_g/V,$$

N_g is the power delivered with the gas,

$$N_g/V = \frac{V_g\rho_g}{V}\left\{\frac{\eta w_0^2}{2} + \frac{RT}{M}\ln\left(\frac{P_0}{P}\right)\right\},$$

$\eta = 0.06$ is the fraction of the gas energy transferred to the liquid; w_0 is the gas velocity in perforations of the gas distributor, m/s; P_0 is the pressure in the gas distributor, N/m^2; R is the gas constant; T is the absolute temperature; and M is the molecular mass of the gas.

The mean bubble diameter in a bubbler with a rabble is connected with the gas content through the following linear dependence:

$$d_{b_\varphi}/d_{b_{0.1}} \simeq 2.5\varphi + 0.75, \qquad (11.18)$$

where $d_{b_{0.1}}$ is the mean bubble diameter for a gas content equal to $\varphi = 0.1$, d_{b_φ} is the mean bubble diameter for a gas content equal to φ.

The following relations were obtained for the mean bubble diameter (cm) of the air supplied to electrolyte solutions (sodium chloride, sulphate and phosphate):

$$\bar{d}_b = 2.25 c_1 \varphi_g^{0.4}(\mu_\alpha/\mu_m)^{0.4}, \qquad (11.19)$$

and to aqueous solutions of alcohols (cm)

$$\bar{d}_b = 1.9 c_1 \varphi_g^{0.65}(\mu_\alpha/\mu_m)^{0.25}, \qquad (11.20)$$

where μ_α is the viscosity of water and μ_m the viscosity of the medium.

The interfacial area a_0 can be determined from the relation

$$a_0 = 1.44\left[\frac{(N/V)^{0.4}\rho_m^{0.2}}{\sigma^{0.6}}\right]\left(\frac{w_g}{w_0}\right)^{1/2}, \qquad (11.21)$$

where w_0 is the final velocity of a freely rising gas bubble and ρ_m is the density of the medium.

A positive deviation from Eq. (11.21) is observed for large values of Re_s, which is due to bubble recirculation. Equation (11.21) is valid when

$$Re_s^{0.7}\left(\frac{nd_s}{w_g}\right)^{0.3} < 20\,000, \text{ where } Re_s = nd_s^2\rho_m/\mu_m.$$

For large values of Re_s, the interfacial area a_{ph} can be calculated from the relation

$$2.3 \log \frac{a_{ph}}{a_0} = 1.95 \times 10^{-5} Re_s^{0.7} \left(\frac{nd_s}{w_g}\right)^{0.3}. \qquad (11.22)$$

The presence of even insignificant amounts of dissolved hydrophilic substances in aerated mixtures increases the interfacial area. This can be explained by the fact that such dissolved substances (for example, alcohol) prevent gas bubbles from coalescing. The gas content of liquid is determined from the relation

$$\varphi = \left(\frac{w_g \varphi}{w_0}\right)^{1/2} + 0.0216 \left[\frac{(N/V)^{0.4} \rho_m^{0.2}}{\sigma^{0.6}}\right] \left(\frac{w_g}{w_0}\right)^{1/2} \qquad (11.23)$$

For low gas flow rates, an increase in the power consumed for mixing increases the gas content. As the speed n increases (up to 3000 rpm), the gas content varies insignificantly and tends to the upper limit (~40 per cent). With increasing gas flow rate, the dependence of the gas content on the stirrer speed becomes less pronounced and vanishes at high gas flow rates. In this case, axial dispersion remains practically independent of the stirrer speed of rotation. An increase in intensity of mechanical mixing improves axial dispersion of the gas phase. However, in compartmented bubblers, the intensity of mixing does not affect axial dispersion.

11.1.3. Mixing in Liquid-Liquid Systems

Disperse liquid-liquid systems, as well as gas-liquid systems, are characterized by such parameters as the holding capacity, and the size of disperse-phase drops. While the value of the holding capacity of batch apparatus is determined by the ratio of volumes of the liquids in it, the fraction of the disperse phase in a flow-through apparatus may differ significantly from its fraction in the feed. At certain values of power, which are determined by the properties of phases, the holding capacity becomes equal to the fraction of the disperse phase in the feed.

The magnitude of the holding capacity for flow-through apparatus with baffles, in which two-row impeller mixers are used, is virtually equal to the fraction of the disperse phase in the feed if the following inequality is satisfied:

$$\left(q_c + q_d + 0.01 \frac{nd_s}{\omega_r}\right) > 3,$$

where q_c and q_d are the specific flow rates of continuous- and disperse-phase in the apparatus, and ω_r is the velocity at which the drops in the disperse-phase rise (sink). This velocity can be calculated with

the help of the Hadamard-Rybchinskii equation

$$\omega_r = \frac{\Delta\rho g d_c}{18\mu_c}\left(\frac{1+\mu_d/\mu_c}{2/3+\mu_d/\mu_c}\right).$$

The quantity in front of the parentheses is the velocity of a descending spherical particle obeying the Stokes law. The parentheses contain the correction that takes into account the effect of internal circulation in a drop on the velocity of its motion. The Hadamard-Rybchinskii and Stokes equations are applicable for small values of the Reynolds numbers for the drop (Re < 1). For large values of the Reynolds number, the velocity of ascending (descending) drops is calculated with the help of empirical equations.

The magnitude of the holding capacity is usually determined from empirical equations obtained with the aid of the dimensionality theory:

$$N_\varphi = CN_{PV}^a N_F^b N_\rho^c N_G^d N_\mu^e,$$

$$N_{PV} = \frac{NQ_d\mu_c^2}{V_R\sigma^3}, \quad N_F = \frac{Q_d\rho_c\sigma}{\mu_c^3}, \quad (11.24)$$

$$N_\rho = \frac{\Delta\rho}{\rho_c}, \quad N_G = \frac{\mu_c^4 g}{\rho_c\sigma^3}, \quad N_\mu = \frac{\mu_d}{\mu_c},$$

$N_\varphi = \bar{\varphi}/x_F$ is the dimensionless holding capacity; C is the dimensionless constant; P is the stirrer power; Q is the volumetric flow rate; x_F is the fraction of the disperse phase in the inlet flow; $x_F = Q_d/(Q_c + Q_d)$; μ is the viscosity; φ is the mean holding capacity; and ρ is the density.

Relations (11.24) for an apparatus with baffles is different for the cases when the continuous phase is lighter and heavier than the disperse phase:

$$\rho_d < \rho_c, \quad N_\varphi = 10^{0.53} N_{PV}^{0.247} N_F^{-0.247} N_\rho^{-0.43} N_G^{-0.401} N_\mu^{0.0987},$$

$$\rho_d > \rho_c, \quad N_\varphi = 10^{0.703} N_{PV}^{-0.131} N_F^{0.0752} N_\rho^{0.0677} N_G^{0.0299} N_\mu^{0.0949}.$$

The following relation was obtained for an apparatus with baffles for calculating the mean holding capacity:

$$N_\varphi = 10^{-0.117} N_{PV}^{0.3} N_F^{-0.178} N_\rho^{-0.0741} N_G^{-0.276} N_\mu^{0.136}.$$

At present, not only mean but also the local values of the holding capacity of heterogeneous systems serve as their characteristics. Three zones determined by different states of disperse-phase particles can be distinguished in an apparatus with a stirrer and baffles (Fig. 211): (1) zone *I* characterized by a small diameter of particles and a high holding capacity; (2) zone *II* with an intermediate size of particles and the mean value of the holding capacity; and (3) zone *III* with a large size of particles and a small value of the holding capacity.

An analysis of the disperse system at different points of the apparatus, with the exception of the zone adjacent to the stirrer, shows that the magnitude of the local holding capacity and the local drop size does not depend on the radial position and is determined by the vertical distance from the stirrer (Fig. 212). The non-uniformity in the disperse phase distribution along the apparatus height is

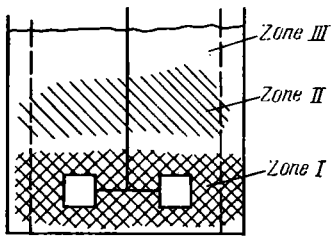

Fig. 211. Schematic diagram of apparatus with mixing in a two-phase system.

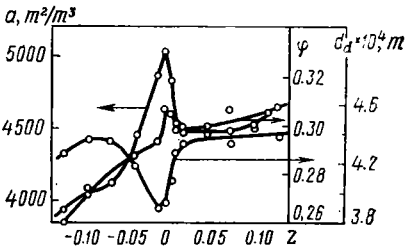

Fig. 212. Dependence of the holding capacity, interfacial area, and drop size on the vertical distance from the stirrer in an octanol-water system; $D = 0.245$ m, $d_s = 0.076$ m, $n = 6.67$ rps.

determined by the ratio of densities ρ_c and ρ_d of the continuous and disperse phases. Thus, the holding capacity is higher in the top part of the apparatus for $\rho_d < \rho_c$ and in the bottom part for $\rho_d > \rho_c$. As the stirrer speed increases and as it is displaced to the apparatus bottom, the distribution of the disperse phase over the height levels out.

One of the parameters characterizing the state of a two-phase system is the size of disperse-phase drops, which stabilizes as a result of mixing. The disperse-phase particles continuously take part in the fragmentation and coalescence. These two processes determine microscopic mixing of the disperse phase. The presence of the turbulent velocity field and recirculating flow of the continuous phase during mixing causes macroscopic mixing of disperse-phase particles. Macroscopic and microscopic mixing considerably depends on the physical properties of the two phases, regime of mixing, and geometry of the stirrer and the apparatus.

The size of a disperse-phase particle and the distribution of particles over the size are determined by the mechanism of interaction of disperse-phase particles. The main type of interaction in the disperse phase of a liquid-liquid two-phase system in a mixer is coalescence and fragmentation of particles of volume V_1 and V_2 and concentration c_1 and c_2. When two drops coalesce, the energy liberated in the process is sufficiently high for complete mixing in

the formed drop. Therefore, upon splitting of the formed drop, the concentrations in both drops are identical and equal to

$$c_1' = c_2' (V_1c_1 + V_2c_2)/(V_1 + V_2).$$

If we assume that the size of the drops is the same, the final concentration in the drops will be (1/2) $(c_1 + c_2)$. For a uniform distribution of drops over size, the coalescence rate must be equal to the rate of fragmentation. The coalescence rate ω_c, defined as the fraction of the total volume of the disperse phase taking part in coalescence per unit time can be taken as the rate of interaction.

The mean drop size and dispersion decrease with time and with increasing intensity of mixing. The distribution of drops over size corresponds to the Pierson β-distribution. However, the deviation from the Gauss normal distribution is insignificant. In fragmentation, ternary and quaternary disintegrations dominate, i.e. 3-4 drops are formed. The half-life of drops noticeably varies depending on the drop size. The size of the disperse-phase drops and the distribution of drops over size, as well as the holding capacity, considerably change from zone to zone of the apparatus.

11.1.4. Extraction Columns with Stirrers

This type of apparatus includes the so-called rotating-disc extractors. Figure 213 shows a rotating-disc extractor proposed for the first time by Reman. This extractor is a continuously operating vertical apparatus with a central shaft on which horizontal circular discs are fixed. The extraction zone of the apparatus consists of a number of sections formed by stationary discs between which the mixer discs are rotated. The power consumption per disc for a given regime is calculated from the equation

$$N = \text{const } n^3 d_s^5 \rho_{mix}$$

The power consumed per unit mass is calculated as follows:

$$\frac{N}{\pi D^2 H \rho_{mix}} = \text{const} \frac{n^3 d_s^5}{HD^2},$$

where D is the apparatus diameter, m; and H is the apparatus height, m.

The parameter $n^3 d_s^5/HD^2$ can be used for determining the limiting

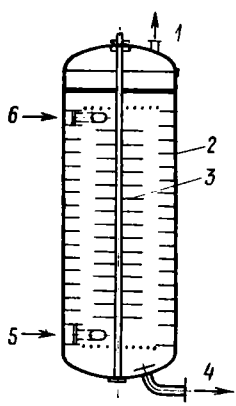

Fig. 213. Schematic diagram of a rotating-disc extractor:

1—light-liquid outlet; *2*—fixed discs; *3*—discs rotating with the shaft; *4*—heavy-liquid outlet; *5*—light-liquid inlet; *6*—heavy-liquid inlet.

flow rates w_c and w_d for continuous and disperse phases of a rotating-disc extractor. Figure 214 represents the dependence of the limiting flow rates in the apparatus on the parameters $n^3d_s^5/HD^2$ and $c_R = (D^2 - d_s^2)/D^2$ for the apparatus of diameters 82, 640, and 2200 mm for $w_c:w_d = 3:4$.

Figure 215 depicts the efficiency of rotating disc extractors with diameters 50 and 400 mm, which is expressed by the ratio of the number n_p of theoretical stages of contact to the column height H,

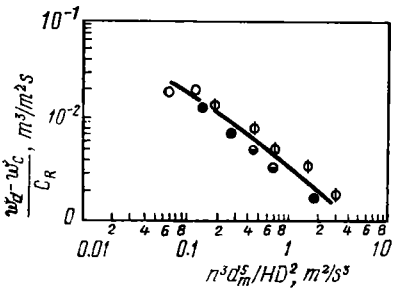

Fig. 214. Limiting flow rates in a rotating-disc extractor.

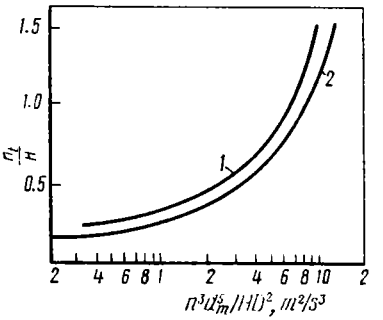

Fig. 215. Efficiency of a rotating-disc extractor for different ratios of flow rates and apparatus diameters (100 and 400 mm):

1—$w_d/w_c = 0.64$; $w_d = 4.4\times10^{-3}$ m³/m²·s;
2—$w_d/w_c = 0.32$; $w_d = 2.2\times10^{-3}$ m³/m²·s.

as a function of the parameter $n^3d_s^5/HD^2$. The efficiency of a rotating-disc extractor increases under the following conditions (1) when the speed of the rotor increases; sometimes the efficiency passes through the maximum due to the effect of axial dispersion in extraction zones; (2) the diameter of rotating discs increases; (3) the diameter of the annular gap between the rotor and stator decreases; (4) with increasing unit load; and (5) with an increase in the disperse-phase flow rate at a constant velocity of the continuous phase.

If we consider a rotating-disc extractor as an apparatus with a series of n perfect-mixing cells with phases in counterflow and neglect the holding capacity and entrainment, its efficiency can be expressed by the following relation:

$$\frac{n}{H} \simeq \frac{6K}{d_d} \cdot \frac{\varphi}{w_d} \lambda^{0.5}, \qquad (11.25)$$

where K is the mass-transfer coefficient, kg-mole/m²·s·kg-mole/m³; φ is the disperse-phase holding capacity; d_d is the diameter of drops, m; w_d is the linear velocity of the disperse phase in the empty column, m/s; and λ is the diffusion potential factor, equal to the product of the

distribution coefficient and the ratio of the solvent and raffinate flows.

Approximate scaling can be carried out when the following relations are observed:

$$\frac{n}{H} \simeq D^{0.15} \quad \text{for} \quad \frac{n^3 d_s^5}{HD^2} \leqslant 0.1. \tag{11.26}$$

The average relative velocity of the disperse phase in a liquid-liquid system, taking into account the dispersion of drops over size can be calculated by the following equation:

$$\bar{V} = \int_0^{d_{d_{max}}} V(d_d) H(d_d) d(d_d),$$

where $d_{d_{max}}$ is the maximum drop diameter; $H(d_d)$ is the distribution function for drop size; $V(d_d)$ is the velocity of motion of drops, m/s. The drop-size distribution function is defined as

$$H(d_d) = \frac{d_d^3}{6\alpha^4} \exp(-d_d/\alpha),$$

where α is an experimentally determined parameter.

The relative velocity of drops in the zone of turbulent flows is determined from the equation

$$V(d_d) = \sqrt{\frac{4/3 \Delta\rho g d_d}{c_W \rho_c}},$$

where c_W is the drag coefficient which depends on the Reynolds number:

$$c_W = 24/\mathrm{Re} + 4/\sqrt{\mathrm{Re}} + 0.4,$$
$$\mathrm{Re}(d_d) = V(d_d) d_d \rho_c / \mu_c.$$

In order to calculate $\bar{V}$, it is convenient to use numerical methods, in particular, the iterative method.

Axial mixing in rotating-disc extractors is estimated with the help of two models: the diffusion model and the cellular model with back mixing. The axial dispersion coefficient in the diffusion model is considered to be the overall coefficient taking into account two effects, viz. the non-uniformity of the velocity profile over the apparatus cross section and turbulent diffusion. Accordingly, the axial dispersion coefficient can be calculated by the following formulas:

$$\frac{(1-\varphi) D_c}{w_c H} = 0.5 + 0.09 (1-\varphi) \frac{d_s n}{w_c} \left(\frac{d_s}{D}\right)^2 \left[\left(\frac{d_{st}}{D}\right)^2 - \left(\frac{d_s}{D}\right)^2\right] \tag{11.27}$$

for the continuous phase D_c and

$$\frac{\varphi D_d}{w_d H} = 0.5 + 0.09\varphi \frac{d_s n}{w_d} \left(\frac{d_s}{D}\right)^2 \left[\left(\frac{d_{st}}{D}\right)^2 - \left(\frac{d_s}{D}\right)^2\right] \quad (11.28)$$

for the disperse phase D_d, where d_{st} is the stator diameter.

When the cellular model with backmixing is employed, the number of perfect-mixing cells connected in series is taken equal to the number of rotor discs, and the fraction of the counterflow between the cells Δ_c and Δ_d is determined by the following equations:

$$\Delta_c = 0.09(1-\varphi) \frac{d_s n}{w_c} \left(\frac{d_s}{D}\right)^2 \left[\left(\frac{d_{st}}{D}\right)^2 - \left(\frac{d_s}{D}\right)^2\right] \quad (11.29)$$

for the continuous phase and

$$\Delta_d = 0.09\varphi \frac{d_s n}{w_d} \left[\left(\frac{d_s}{D}\right)^2 - \left(\frac{d_s}{D}\right)^2\right] \quad (11.30)$$

for the disperse phase.

11.2. Pulsed Columns

In systems characterized by a small difference in specific gravities and high viscosity (liquid-liquid systems), the interaction between phases can be intensified by applying to the flows fluctuations which give rise to additional interfacial friction and hence increase the dispersion and turbulization of phase flows. This principle is widely used for extraction in sieve-type columns without downcomers and sometimes in packed columns.

The main advantages of the fluctuation method are the uniform energy supply to the apparatus cross section and the absence of moving parts. In order to create the reciprocal motion of liquid, various types of pulsors with mechanical, hydraulic, or pneumatic drives are used (Fig. 216). In the mechanical drive, it is difficult to control the fluctuation frequency. Besides, such drives have a rigid construction, which leads to cavitation and hydraulic shocks in the column. The hydraulic drive is characterized by a smooth control of the fluctuation frequency and amplitude over a wide range. However, hydraulic shocks appear in this case due to incompressibility of liquid, especially at a high fluctuation frequency. The pneumatic drive, which provides a smooth control of the parameters over a wide range like the hydraulic drive, has good shock-absorbing properties. When this type of drive is employed, the height of the column is not limited by cavitation in the pulsation line since the gas volume play the role of a buffer. Pneumatic method of pulsations has several advantages over the mechanical and hydraulic drives. However, it is less economic from the point of view of energy expenditures than the mechanical drive where the pulse is transferred directly to

the liquid through the piston, membrane, or bellows. With increasing size of the apparatus, the energy spent for generating fluctuations abruptly increases, this increase being the sharper the higher the fluctuation frequency. This can be explained by an increase in the energy consumption for decelerating the liquid column upon velocity reversal. An analysis of power expenditures for generating

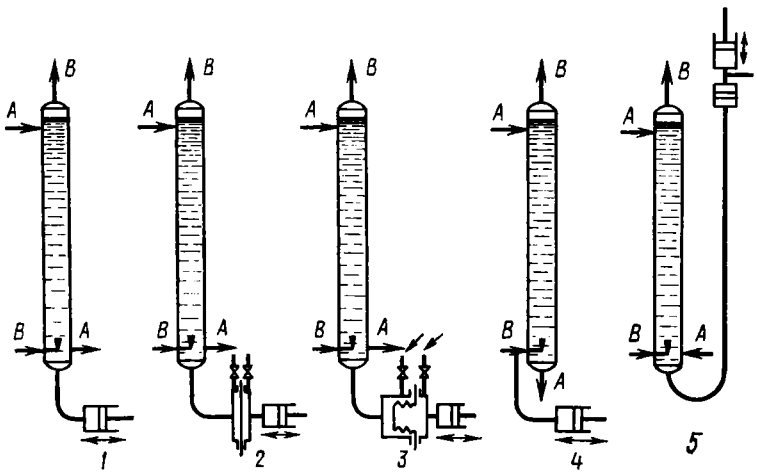

Fig. 216. Different methods of applying fluctuations:

1—direct contact between a pulser and treated liquids; *2*—contact through a separating diaphragm; *3*—through a siphon; *4*—through an auxiliary flow; *5*—through an air cushion; *A*—heavy phase; *B*—light phase.

pulsations reveals that overall expenditures can be divided into three components: gravitational component associated with the weight of the liquid column in an apparatus; inertial component connected with deceleration and acceleration of the liquid column upon the velocity reversal, and the component associated with overcoming the friction losses in the apparatus. The latter component includes energy expenditures useful from the point of view of the mass-transfer process. The first two components must be reduced to the smallest possible values by improving the apparatus structure and the connection of the apparatus with the pulsor.

Hence, pneumatic-drive apparatus were being recently improved in order to completely use the energy of compressed air and flowing liquid.

Power consumptions for generating pulsations can be considerably reduced if fluctuations are created on the natural frequency of the system. The resonance frequency of liquid pulsations in the column with a hydraulic drive can be calculated from the following equation

$$\omega = 2\pi f = \sqrt{\gamma^p P_G/\rho_L H_L H_G + 2g/H_L - K^2}, \qquad (11.31)$$

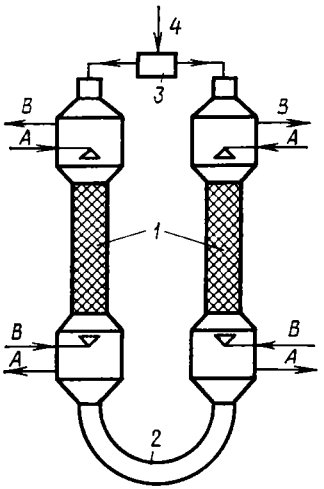

Fig. 217. Schematic diagram of a U-shaped apparatus pulsating at the resonance frequency:

A—heavy phase; *B*—light phase.

where ω is the angular velocity; f is the fluctuation frequency; γ^p is the ratio of specific heat capacities of the gas, $\gamma^p = c_p/c_v$; ρ_L is the density of liquid; P_G is the gas pressure; H_L is the equivalent height of the liquid column; H_G is the equivalent height of the gas volume; and K is the damping factor. This equation is derived on the basis of the balance of forces in an oscillating system.

It follows from Eq. (11.31) that with increasing apparatus size, the natural frequency of oscillations considerably decreases. Therefore, the resonance frequency of large-scale industrial extractors is much lower than in laboratory apparatus. On the other hand, for each process there exists the fluctuation intensity optimal from the point of separation efficiency. Since the pulsation amplitude in extractors is usually of the order of several centimeters, the optimal intensity of pulsations will correspond to a much higher frequency than the resonance frequency for a given apparatus, which is optimal from the point of view of energy expenditures for pulsation. The choice of operating conditions for pulsation can be made on the basis of economic criterion taking into account both the production cost and energy expenditures. For this reason, it is interesting to analyze the methods of calculating an apparatus with pulsations at a given frequency.

Another way to reduce energy consumptions for generating pulsations is associated with a reduction of the gravitational component. This can be achieved by constructing systems in static equilibrium. An example of an apparatus with static compensation is the U-shaped pulsed column where compressed air is supplied to both arms of the apparatus.

The apparatus (Fig. 217) consists of two identical packed or plate columns (*1*) connected by the U-shaped tube (*2*). Compressed air is supplied to the pulsation chambers through the sleeve-valve gear (*3*) which alternately connects each pulsation chamber to compressed air supply line (*4*) and to the surroundings.

The system described above is a full-period one in contrast to commonly used half-period systems in which the liquid column moves

under the action of external force only upwards, performing the downward motion under its own weight. The power consumption for generating pulsations in full-period systems are somewhat higher as compared to half-period systems. The advantage of the full-period system is that the same forces, which only change their direction act on the liquid column in the upward and downward motion. This ensures the same duration of both parts of the cycle and the symmetry of oscillations. The U-shaped pulsed apparatus is a pneumohydraulic system.

The differential equation of the oscillatory motion of the liquid column in the apparatus can be constructed on the basis of energy balance of a moving system. The surface of liquid in a pulsation chamber is acted upon by an alternating force reduced to the pulsation chamber area and varying according to a periodic law $p_{p.f}(t)$. Under the action of the perturbing force, the liquid in the pulsation chamber is displaced by a certain distance $x_{p.c}$. The work done by the perturbing force is spent to change the kinetic and potential energy of the system and to overcome pressure losses.

Considering the entire system (Fig. 217) consisting of n sections with various flow areas, lengths, hydraulic diameters, drag coefficients, and specific gravities, and using the continuity equation for the flow in order to reduce the displacements in all parts of the apparatus to the displacement in the operating section, we obtain an equation which describes the displacement of liquid under the action of external force $p_{p.f}$:

$$\frac{2F_c}{g}\sum_{i=1}^{n}\gamma_i L_i\frac{1}{F_i}\frac{d^2x_c}{dt^2}+\frac{F_c^2\omega x_c^{max}}{2g}$$

$$\times\sum_{i=1}^{n}\gamma_i\frac{1}{F_i}\left(\xi_i+\lambda_i\frac{L_i}{D_i}\right)\frac{dx_c}{dt}+2\gamma_{p.c}\frac{F_c}{F_{p.c}}x_c=p_{p.f} \qquad (11.32)$$

where F_c is the open area of the column; $F_{p.c}$ is the cross-sectional area of the pulsation chamber; F_i is the cross-sectional area of the ith section of the column; x_c is the displacement of liquid in the operating compartment of the column; γ_i is the specific gravity of liquid in the ith section of the column; $\gamma_{p.c}$ is the specific gravity of liquid in the pulsation chamber; L_i is the length of the ith section; ξ_i is the local drag coefficient on the ith section; x_c^{max} is the maximum amplitude of pulsation in the working section; ω is the angular frequency of pulsation; λ_i is the friction coefficient on the ith section; D is the hydraulic diameter of the ith section; t is the time; and $\rho_{p.f}=p_{p.c}^{II}-p_{p.c}^{I}$.

It was assumed in deriving Eq. (11.32) that the local drag coefficients are equal to the arithmetic means of their values in the upward and downward motion. The second term on the right-hand side of Eq. (11.32), taking into account the pressure losses, is linearized with respect to the velocity of liquid. Such a simplification is possible due to gradually rising friction losses in plate and packed columns with the flow velocity.

The equations describing the behaviour of air in pulsation chambers can be obtained from an analysis of relations connecting the air flow rate through the sliding valve, the pressure in the pulsation chamber, and the slide-valve resistance:

$$G_{sl} = \frac{p_f - p_{p.c}(t)}{R_{sl}^{si}(t)}, \tag{11.33}$$

$$G_{so} = \frac{p_{p.c}(t)}{R_{sl}^{so}(t)}, \tag{11.34}$$

where p_f is the pressure of the compressed air in a slide-valve gear; $p_{p.c}$ (t) is the running value of the pressure in the pulsation chamber; and R_{sl}^{so} and R_{sl}^{si} denote the resistance of the slide valve at the source and sink, respectively.

Equations (11.33) and (11.34) are used for calculating the amount of air in the pulsation chamber at any instant of time. The variables in these equations are represented in the form of increments, assuming that the resistance at the source and sink lines at the instant t_0 are equal in magnitude but opposite in sign:

$$\frac{d(\Delta Q)}{dt} = -\frac{2\Delta p_{p.c}}{R_{sl}^0} + \frac{p_f}{(R_{sl}^0)^2}\Delta R_{sl}^{si} = -\frac{2\Delta p_{p.c}}{R_{sl}^0} - \frac{p_f}{(R_{sl}^0)^2}\Delta R_{sl}^{si}, \tag{11.35}$$

where ΔQ is the increment in the amount of air in the pulsation chamber; $\Delta p_{p.c}$ is the increment in pressure in the pulsation chamber; R_{sl}^0 is the mean resistance of the slide-valve gear; and ΔR_{sl}^{so} and ΔR_{sl}^{si} denote the increment in the resistance of the slide valve at the source and sink, respectively.

Next, using Eq. (11.35) for each arm of the apparatus, we integrate with respect to t the obtained equations in which the relation between the pressure, volume and amount of air is described by Clapeyron-Mendeleev equation. After transformations we obtain equations connecting the change in the air pressure in the pulsation chambers for both arms of the apparatus with the displacement of the liquid and the resistance of the slide valve. In the Laplace transformation

region, these equations have the form

$$\Delta\bar{p}^{\mathrm{I}}_{\mathrm{p.c}} = \frac{\frac{\mu p_{\mathrm{f}} F_{\mathrm{c}} K_{\mathrm{s}}}{2RT}\Delta\bar{x}_{\mathrm{c}} - \frac{p_{\mathrm{f}}}{p\,(R^0_{\mathrm{sl}})^2}\Delta\bar{R}_{\mathrm{sl}}}{\frac{\mu F_{\mathrm{c}} x_{\mathrm{c}}^{\max} K_{\mathrm{s}}}{RT} + \frac{2}{pR^0_{\mathrm{sl}}}}, \qquad (11.36)$$

$$\Delta\bar{p}^{\mathrm{II}}_{\mathrm{p.c}} = \frac{-\frac{\mu p_{\mathrm{f}} F_{\mathrm{c}} K_{\mathrm{s}}}{2RT}\Delta\bar{x}_{\mathrm{c}} - \frac{p_{\mathrm{f}}}{p\,(R^0_{\mathrm{sl}})^2}\Delta\bar{R}_{\mathrm{sl}}}{\frac{\mu F_{\mathrm{c}} x_{\mathrm{c}}^{\max} K_{\mathrm{s}}}{RT} + \frac{2}{pR^0_{\mathrm{sl}}}}, \qquad (11.37)$$

where μ is the molecular weight of air; R is the gas constant; T is the absolute temperature; p is the Laplace operator; $\Delta\bar{p}_{\mathrm{p.c}}$, $\Delta\bar{x}_{\mathrm{c}}$ and $\Delta\bar{R}_{\mathrm{sl}}$ are the Laplace transforms of the corresponding functions; K_{s} is the safety factor which determines the dimensions of the pulsation chamber.

Substituting Eqs. (11.36) and (11.37) into Eq. (11.32) expressed in terms of increments and subjected to Laplace transformation, we obtain the transfer function of the system for the channel slide-valve resistance-displacement of the liquid in the column. The corresponding frequency response has the form

$$A_{\mathrm{x}}(\omega) = \frac{\varkappa}{\sqrt{[1-(I\varepsilon-\eta)\,\omega^2]^2 + \{[I\,(1+\varkappa)+\varepsilon]\,\omega - I\eta\omega^3\}^2}}, \qquad (11.38)$$

where

$$I = \frac{\mu R^0_{\mathrm{sl}} V_{\mathrm{p.c}} K_{\mathrm{s}}}{2RT}; \quad \varkappa = \frac{p_{\mathrm{f}} F_{\mathrm{p.c}}}{2\gamma_{\mathrm{p.c}} V_{\mathrm{p.c}}},$$

$$\varepsilon = \frac{\omega V_{\mathrm{p.c}} F_{\mathrm{p.c}}}{4g\gamma_{\mathrm{p.c}}} \sum_{i=1}^{n} \frac{\gamma_i}{F_i}\left(\xi_i + \lambda_i \frac{L_i}{D_i}\right); \quad \eta = \frac{F_{\mathrm{p.c}}}{g\gamma_{\mathrm{p.c}}} \sum_{i=1}^{n} \frac{\gamma_i}{F_i} L_i.$$

The combinations of the pulsation system parameters characterize various properties of the system. The complex I takes into account the properties and volume of the gas in the pulsation chamber and the mean resistance on the air feed and discharge lines; ε is the friction loss; $\varkappa$ is a factor describing the effect of the pressure of the compressed air supplied to the system; and η describes the inertial properties of the liquid column in the apparatus.

Equation (11.38) can be used to estimate the effect of various properties of the system on the pulsation amplitude for a given pulsation frequency, and to determine the air pressure required at the input of the slide valve in order to ensure a given pulsation regime in the column. Figure 218 shows the dependence of the pulsation intensity in the apparatus on frequency upon a variation of packing resistance for a column with working sections of height 5 m,

diameter 0.2 m of each arm of the apparatus, and the diameter 0.1 m of the U-shaped connecting pipe filled with the two-phase system dichloroethane-water.

The well-known fact that the pulsation amplitude decreases sharply with increasing frequency is confirmed by calculations. Since the intensity of pulsations is the product of the amplitude

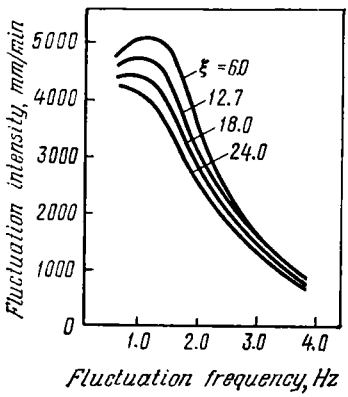

Fig. 218. Dependence of the pulsation intensity on pulsation frequency for different packing resistances in the operating section of a column.

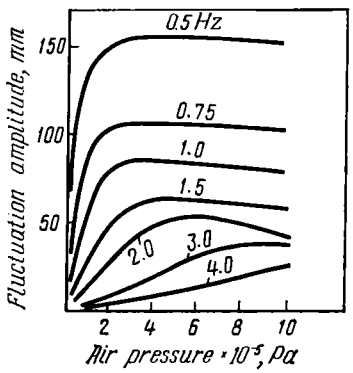

Fig. 219. Dependence of pulsation amplitude on air pressure for different pulsation frequencies.

and frequency, i.e. the product of a linearly increasing function and a decreasing function, the dependence of intensity on frequency is of an extremal nature, the extremum shifting towards higher frequencies with increasing air pressure, decreasing packing resistance and the resistance of the piston-type selector valve. The dependence of the pulsation amplitude on the compressed-air pressure in a column for different frequencies is shown in Fig. 219. This figure can be used as a nomogram for selecting the pressure necessary for ensuring the required pulsation intensity at a given frequency.

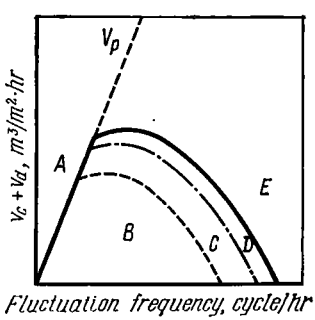

Fig. 220. Dependence of total volumetric velocity on pulsation frequency at constant amplitude in a pulsed sieve-plate column.

Hydrodynamic regimes and mass transfer in pulsed sieve-plate columns. The hydrodynamic regimes are observed in sieve-plate columns without downcomers (Fig. 220): at a low pulse

frequency, the column is flooded (regime *A*) since the flow through the column perforations cannot occur in this case. As the pulse frequency increases, the operation of the column becomes normal: the phases are mixed and separated in the space between plates (regime *B*). A further increase in the pulse frequency leads to emulsification which is characterized by a homogeneous dispersion and a slight change in the phase dispersivity during a pulse period (regime *C*). This is followed by a transient regime characterized by local flooding and inhomogeneous dispersion under conditions close to flooding (regime *D*). An inordinate increase in the pulse frequency leads to flooding of the column (regime *E*).

The column output at low frequencies is equal to the product of the amplitude and frequency, or to the volumetric pulsating velocity:

$$V_p = fV,$$

where f is the pulse frequency, cycles/min; and V is the pulsating volume (volume of the liquid displaced during one pulse cycle), cm³/cycle. At low frequencies, the flooding curve is a straight line starting at the origin. With increasing frequency, the flooding curve deviates from the volumetric pulsation velocity, passes through a maximum, and then drops. Finally, a limiting frequency (or the product of frequency and amplitude) sets in, beyond which there is no countercurrent flow through the column. For the first flooding regime, the ratios of the volumetric flow velocities and the volumetric pulsation velocity have the form

$$\pi V_l/V_h + \pi/2 = (\cos\theta)\,\theta \ldots, \qquad (11.39)$$

$$\theta = V_h/\pi V_p \ldots, \qquad (11.40)$$

where V_l is the volumetric velocity of the light phase, cm³/min; and V_h is the volumetric velocity of the heavy phase, cm³/min. The left-hand side of Eq. (11.39) is a function of only the ratio of volumetric flow velocities whose values are usually given. The value of θ can be determined from the ratio V_l/V_h, whence the minimum required value of volumetric velocity of fluctuation for a given value of V_h can be obtained with the help of Eq. (11.40). If the left-hand side of Eq. (11.39) is greater than the right-hand side, the column gets flooded due to insufficient fluctuation. Otherwise, the column operates normally. The fluctuation frequency can be determined from the volumetric velocity of fluctuations.

The ratio of volumetric flow velocities in case of flooding as a result of excessive fluctuation (regime *E*, Fig. 220) can be calculated from the equation

$$\frac{(w_c+w_d)\,\mu_c}{\sigma} = b_0\left(\frac{w_c}{w_d}\right)^{b_1}\left(\frac{\Delta\gamma}{\Delta\gamma_c}\right)^{b_2}\left(\frac{\psi\mu_c^5 g}{\gamma_c\sigma^4 3600^3}\right)^{b_3}\left(\frac{d_0\sigma\gamma_c}{\mu_c^2 g}\right)^{b_4} \times\left(\frac{D}{d_0}\right)^{b_5}\left(\frac{g^2\mu_c^4}{\gamma_c\sigma^3}\right)^{b_6}\left(\frac{\mu_d}{\mu_c}\right)^{b_7}, \qquad (11.41)$$

where ψ is the maximum power consumed by a unit mass of the liquid, m^2/hr:

$$\psi = \frac{\pi^2 (1-\varepsilon^2)(fa)^3}{2\varepsilon^2 c_0^2 H_p}, \qquad (11.42)$$

w_c and w_d are the linear velocities of the continuous and disperse phase, $m^3/m^2 \cdot hr$; σ is the interfacial tension, kg/m; d_0 is the plate perforation diameter, m; ε is the open cross-sectional area of a plate; f is the fluctuation frequency, cycle/hr; a is the fluctuation amplitude, m/cycle; H_p is the spacing between plates, m; and $c_0 = 0.60$ is the perforation discharge factor. The constant b_0 and the exponents appearing in Eq. (11.41) have the following values: $b_0 = 0.527$, $b_1 = -0.014$, $b_2 = 0.63$, $b_3 = -0.207$, $b_4 = 0.458$, $b_5 = 0$, $b_6 = 0.81$, and $b_7 = -0.20$.

The overall flooding velocity $w_c + w_d$ is independent of the ratio of the column diameter to the plate perforation diameter ($b_5 = 0$). The standard deviation of the experimental data from the data obtained theoretically from Eq. (11.41) is 19.6%.

The diameter D of a pulsed sieve-plate column is calculated from the equation

$$D = \sqrt{\frac{4w_c}{\pi\Phi(w_c + w_d)}}, \qquad (11.43)$$

where w_c is the overall output of the column over both phases, m^3/hr; $(w_c + w_d)$ is the total flooding rate calculated from Eq. (11.41); and Φ is a fraction of the flooding rate, given by

$$\Phi = \frac{(w_c + w_d)_{op}}{(w_c + w_d)_{fl}}.$$

The height of a transfer unit in the continuous phase $(HTU)_{tc}$ can be calculated by using the equation

$$\frac{(HTU)_{tc}}{H_p} = c_0 \left(\frac{V_0 d_0 \gamma_d}{g\mu_d}\right)^{c_1} \left(\frac{\Delta\gamma}{\gamma_d}\right)^{c_2} \left(\frac{\mu_d g}{\gamma_d D_d}\right)^{c_3} \times \left(\frac{\sigma 3600}{\mu_c w_c}\right)^{c_4} \left(\frac{w_d}{w_c}\right)^{c_5} \left(\frac{D}{H_p}\right)^{c_6} \left(\frac{\mu_c}{\mu_d}\right)^{c_7}, \qquad (11.44)$$

where $V_0 = fa/\varepsilon$; f is the fluctuation frequency, cycles/s; a is the fluctuation amplitude, m/cycle; and D_d is the coefficient of diffusion into the disperse phase, m^2/s. The constants appearing in Eq. (11.44) have the following values:

$c_0 = 0.20$; $c_1 = -0.434$; $c_2 = 1.04$; $c_3 = 0.865$; $c_4 = 0.096$;

$c_5 = -0.636$; $c_6 = 0.37$; $c_7 = 4.57$.

The standard deviation of the experimental data from the values obtained theoretically with the help of Eq. (11.44) is 16.4%. Equation (11.44) is applicable when the extraction takes place from the

disperse phase into the continuous aqueous phase, and the resistance to the flow is mainly offered by the disperse phase.

The height of a pulsed sieve-plate column can be calculated by using the equation

$$H = (\mathrm{HTU})_{tc} N_{tc},$$

where N_{tc} is the total number of transfer units calculated for the continuous phase.

For pulsed sieve-plate extractors with downcomers, the following three states of a two-phase system are observed, depending on the flow velocities and the extent of fluctuation (Fig. 221).

Regime I. The continuous phase flow is similar to that in columns without fluctuations. The disperse phase coalesces to form a con-

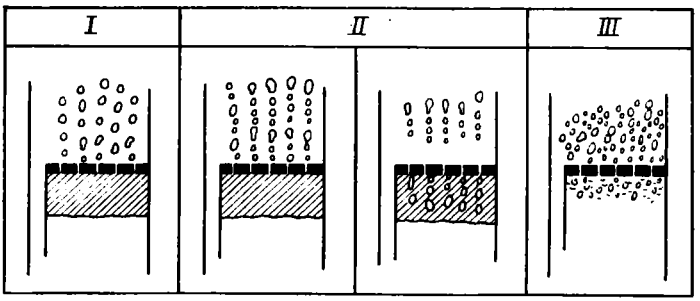

Fig. 221. State of a two-phase liquid-liquid system in a pulsed sieve-plate column with downspouts.

tinuous layer below the plate and passes through it without being subjected to any pulsation. On account of the disperse phase layer under the plate, the resistance to the flow increases due to fluctuation.

Regime II. The continuous phase flow is subjected to fluctuations. As a result, a part of the liquid flows through the downcomer, and another part through the perforation. Neither phase is continuous, since each phase is dispersed in the other by alternating fluctuation cycles. Nevertheless, the lighter liquid coalesces under the plate and the height of this layer depends on the extent of fluctuation and the phase flow velocity. The drops are of different sizes, larger drops being formed at the beginning of fluctuations, and small ones as a result of collisions between the reciprocal injection and upward or downward impact.

Regime III. The liquid coalesces under the plate for a short time. The product of frequency and amplitude is large. The drops formed from the lighter liquid are of different sizes and smaller than in the first two regimes. Turbulence increases in the regions below and above the plate, thus increasing the holding capacity with respect

to the lighter liquid. A significant increase in fluctuation results in localized flooding and the operating regime of the column resembles the emulsifying regime.

The flooding limit for the sieve-plate columns with downcomers is higher than for the corresponding columns without downcomers. For minimum HTU or HETP, there exists an optimal fluctuation amplitude which is defined by the equation

$$f = \alpha + \beta \log a_f, \tag{11.45}$$

where f is the fluctuation frequency, cycle/min; a_f is the optimal fluctuation amplitude corresponding to the minimum HTU for a given frequency, mm; and α and β are coefficients depending on the system properties, flow velocities, and the type of packing.

The fluctuation frequency, amplitude and HTU are connected through the relation

$$f = g\,(r - \mathrm{HTU}) + s \log a, \tag{11.46}$$

where g, r and s are coefficients depending on the system properties, the flow velocities and the type of packing. Theoretically, f and a are equal if $\mathrm{HTU} = (\mathrm{HTU})_{wf}$, where $(\mathrm{HTU})_{wf}$ is HTU without fluctuation.

The following equation (linear dimensions in metres) can be used for scaling pulsed extractors:

$$(\mathrm{HTU})_l = (\mathrm{HTU})_s\, e^{\frac{D_s - D_l}{0.61}}, \tag{11.47}$$

where the indices l and s refer to large and small columns respectively.

In order to maintain the intensity of mass transfer with increasing diameter of the pulsed extractor, it is necessary to use redistributors for the continuous phase. The efficiency of a pulsed packed column is compared with that of an ordinary packed column in Fig. 222. The maximum efficiency of a pulsed packed column is attained at a fluctuation frequency of 250 cycles/min and an amplitude of 1 mm.

Axial dispersion in pulsed columns. In order to evaluate axial dispersion in pulsed sieve-plate columns, diffusion and cellular models with backflow are employed. The axial dispersion coefficient attains its maximum value for the minimum holding capacity of the column and at a fluctuation frequency f_H given by the equation

$$f_H = 40\,(0.3 + 9 \times 10^{-8}\mu_d\gamma_d\Delta j - \ln a). \tag{11.48}$$

For the mixing-settling regime (fluctuation frequency below f_H), the equation for the calculating the axial dispersion coefficient in

the continuous phase has the form

$$D_c = 4.18 - 1.64 \times 10^{-5} w_c^3 (f - f_H)^2 + 0.190\,\Delta\gamma, \quad (11.49)$$

while for the emulsifying regime (fluctuation frequency above f_H), we have

$$D_c = 6.97 - 9.08 \times 10^{-9} w_c^3 (f - f_H) + 0.166\,\Delta\gamma - 4.8a + 2.49a^2. \quad (11.50)$$

Thus, the influence of fluctuation amplitude becomes significant in the emulsifying regime.

Three modes of operation have been established for pulsed packed columns: the mixing-settling regime, the transient regime, and the

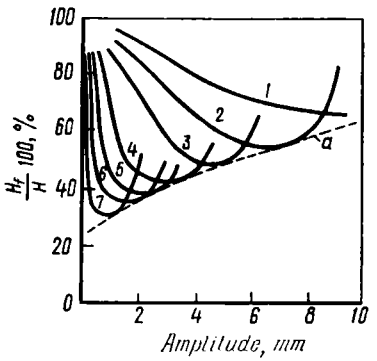

Fig. 222. Comparison of efficiencies of a packed column with and without flow pulsations:

a—optimal regime; *1*—25 cycles/min; 2—50 cycles/min; *3*—75 cycles/min; *4*—100 cycles/min; 5—150 cycles/min; 6—200 cycles/min; *7*—250 cycles/min.

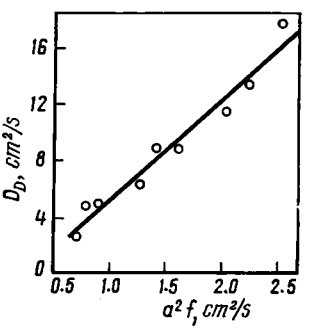

Fig. 223. Dependence of the disperse phase turbulent diffusion coefficient on $a^2 f$ in emulsifying regime.

emulsifying regime. The axial dispersion coefficient D_c for the continuous phase in emulsifying regime can be calculated from the relation

$$\frac{D_c}{a^2 f} = 0.64 \left(\frac{v_c + v_d}{a^2 J} \right)^{0.5}. \quad (11.51)$$

where v_c and v_d are the respective flow rates of the phases, cm³/s; and $J = af$ is the fluctuation intensity, cm/s.

This equation was obtained for an apparatus with diameter 148 mm packed with Raschig rings of size 15 × 15 mm. The coefficients D_d of turbulent diffusion in the disperse phase were found to be weakly correlated with the flow rates and depend only on the fluctuation parameters. The empirical dependence for the emulsifying regime is shown in Fig. 223.

11.3. Columns with Flow Vibrations

Turbulization and development of the interfacial surface in vibrating-flow columns occur as a result of the reciprocal motion of a vibrator placed in the path of the liquid flow. One such column is shown in Fig. 224. Perforated plates are fixed to the central shaft of a column with diameter 58, 76 mm and height 915 mm. The shaft with perforated plates is mounted to the roof of the column with the help of a crank-and-connecting rod mechanism and performs reciprocal motion. The height of the operating extraction zone is about 500-610 mm, while the separating zones are about 150-200 mm in height. The plates are 1 mm thick, the diameter of perforations is 15.9 mm, and the total cross-sectional area of the perforations is 62.8% of the total plate area. The spacing between plates and the inner walls of the column is up to 3 mm.

Experiments were carried out on systems methylisobutyl ketone-acetic acid-water and *o*-xylene-acetic acid-water. The dependences of HETP on the frequency of vibration were obtained for a vibration amplitude 12.7 mm, the overall specific flow rates 1.15 $m^3/hr \cdot m^2$ and a plate spacing 25.4 mm. These dependences have a minimum, the minimum HETP and the corresponding vibration amplitudes being functions of the column diameter. The ratio of the minimum HETP to the column diameter has the form

$$(HETP)_{D2}/(HETP)_{D_1}=(D_2/D_1)^{0.38}.$$

The values f of the vibration frequencies (cycles/min) are connected through the relation

$$f_{D_1}/f_{D2}= (D_1/D_2)^{0.14}.$$

These ratios can be used for scaling vibration columns with diameters up to 180 cm. Baffles should be mounted in columns of larger diameters in order to decrease the axial dispersion. The above relations are then found to be valid even for columns of large diameters. The plate spacing, the number of steps per minute and the duration of each step can be taken the same as the ones obtained experimentally under optimal functioning of the apparatus.

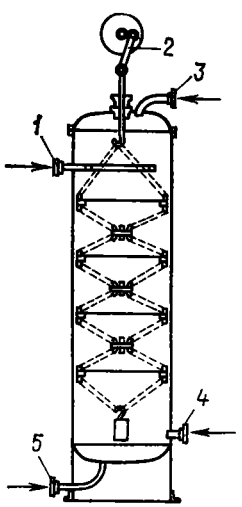

Fig. 224. Column with vibrating plates:

1—heavy-liquid inlet; *2*—crank- and connecting rod mechanism of the vibrator; *3*—light-liquid outlet; *4*—light-liquid inlet; *5*—heavy-liquid outlet.

The plate spacing plays an important role in columns with a large number of theoretical stages. Since the concentration of the substance dissolved in phases is different in different parts of the column, the plate spacing also must vary along the height of the column. The plate spacing is reduced in the zone with low concentration of the dissolved substance in order to obtain a uniform mixing over the entire column height. This ensures the maximum number of theoretical stages in a column of a given height. Besides, as the concentration of the dissolved substance increases, the interfacial tension rapidly falls in most liquid-liquid systems and the power consumed for dispersion of one of the phases is also reduced. In order to avoid a premature flooding of the column during reciprocating motion of plates, the plate spacing must be increased in the region with a high concentration of the dissolved substance. The ultimate plate spacing in different parts of the column must be established experimentally.

11.4. Rotational Apparatus

Classification and construction of rotational apparatus. Each design of a rotational apparatus mainly determines the state of the interfacial surface in it. Depending on the way in which an interfacial surface is formed in a centrifugal force field, rotational apparatus can be of three different types: (1) apparatus with a fixed interfacial surface (film-type apparatus); (2) apparatus in which the interfacial surface is formed in the empty apparatus volume; and (3) apparatus in which the interfacial surface is fixed and is formed in the empty volume of the apparatus.

Apparatus with fixed interfacial area (film-type apparatus). Figure 225 shows different versions of centrifugal apparatus with a film-type regime of the liquid flow. The mass-transfer process in such apparatus is intensified on account of a rapid, continuous and forced renewal of the interfacial surface in the field of centrifugal forces. Apparatus with inner block packing, spirals and various cylinders, etc. are the ones most widely used. Figure 226 shows a Podbel'nyak centrifugal extractor. The main part of the extractor is the rotor which is mounted on a shaft and rotates together with it at a speed of 2000-5000 revolutions per minute. The rotor is in the form of a spiral and mass transfer takes place in its channels. A light and a heavy liquid are continuously pumped into the apparatus, the lighter liquid being supplied at the periphery, and the heavier near the axis of the rotor. As the rotor rotates under the action of the resulting centrifugal force, the heavier liquid is thrown toward the periphery, encountering the lighter liquid on its way. The spiral walls may have perforations. The supply and removal of the liquids in the extractor is usually carried out through a hollow shaft.

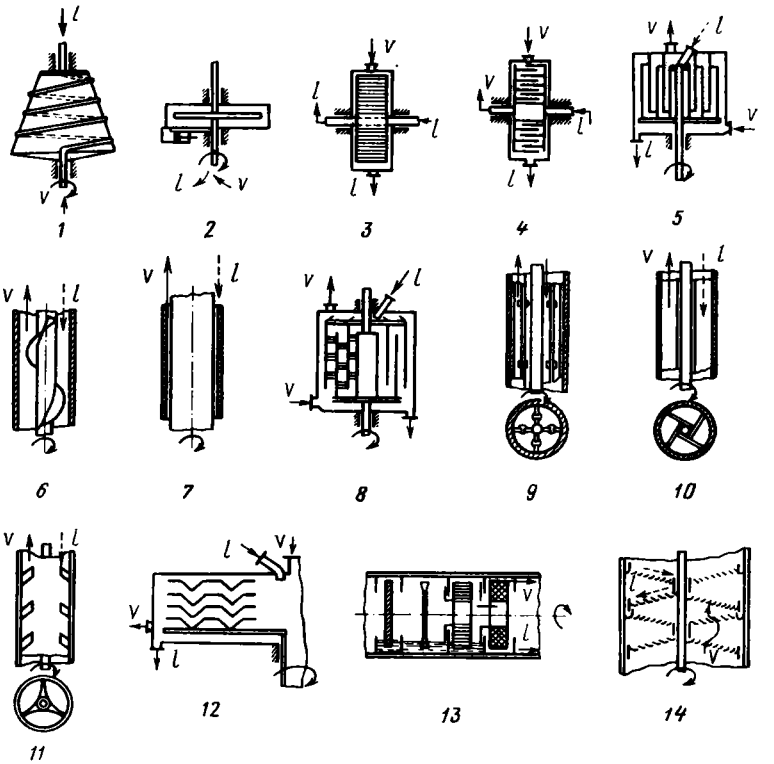

Fig. 225. Designs of centrifugal apparatus involving film-type liquid flow:

1—apparatus with a rotating spiral loop around a conical rotor; *2*—apparatus with a loop rotating in a horizontal plane; *3*—apparatus with a spiral cassette (Podbel'nyak extractor); *4*—apparatus with coaxial cylinders; *5*—vertical rotary apparatus; *6*—apparatus with a ribbon-like rotor; *7*—apparatus with a tubular rotor; *8*—multicylinder column with oppositely rotating coaxial cylinders; *9*—rotary apparatus with turbulizers; *10*—apparatus with articulated rotating blades; *11*—apparatus with a vertical rotor and inner plates and troughs; *12*—rotary apparatus with corrugated plates; *13*—different packings used in a rotary apparatus; *14*—apparatus with rotating and fixed perforated plates.

Due to a relatively small difference in the specific gravities of liquids and a large frictional force between layers, the wave formation destroys the laminar flow at relatively low velocities of the liquids. Since the laminar counterflow of liquids in the extractor channels is impossible, the spiral must have holes in it. In this case, the liquids in the extractor flow not only through the channels formed by the spiral, but also in the radial direction from channel to channel. The liquid channels become laminar, the velocity of each layer relative to the channel walls depending on the ratio of the rates of flow of components. For relatively small amounts of the lighter extractant, the heavier liquid entrains the lighter liquid during

its motion from the axis to the periphery of the drum, and both layers move relative to the channel walls in a direction opposite to the rotation of the drum. The friction at the walls turbulizes the flow and intensifies the mass transfer. Figure 227 shows the motion of liquids in channels of a drum rotating in the clockwise direction.

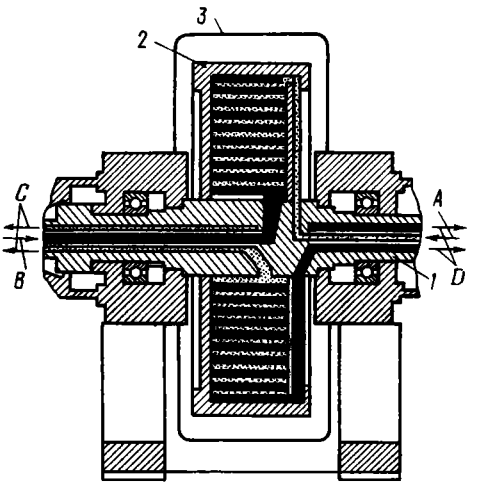

Fig. 226. Centrifugal Podbel'nyak extractor:

1—hollow shaft; *2*—rotor; *3*—enclosure; *A*—light-liquid inlet; *B*—heavy-liquid inlet; *C*—light-liquid outlet; *D*—heavy-liquid outlet.

The heavy liquid flows from channel *A* into channel *B* and then to channel *C*, while the lighter liquid flows in the opposite direction. Both layers move in channels in a direction opposite to the rotation of the drum.

Optimal operating conditions can be created for a definite relation between the amount of the lighter liquid passing through the extractor, and its pressure at the output of the extractor. A decrease in the pressure of the lighter liquid at the output under a constant flow rate may result in flooding of the extractor: heavier liquid appears in the line through which the lighter liquid is withdrawn from the extractor. The highest extraction efficiency is observed during operation in the regime close to flooding of the return line for the lighter liquid. An increase in the pressure of the lighter liquid at the output may cause flooding of

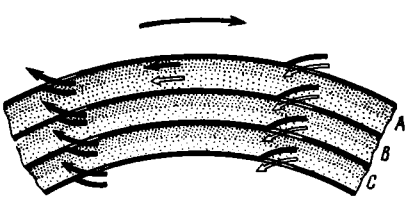

Fig. 227. Motion of a liquid in channels of a centrifugal extractor drum.

the extractor, which is characterized by the appearance of the lighter liquid in the line through which the heavier liquid is withdrawn from the extractor. The maximum pressure at the lighter liquid output corresponding to flooding is called the limiting pressure. The maximum number of revolutions of the rotor is defined by the equation

$$\Delta P_{l.ph'} = 2\Delta\gamma\omega^2 r^2 g, \qquad (11.52)$$

where $\Delta P_{l.ph}$ is the pressure of the light phase at the output; $\Delta\gamma$ is the difference in the specific gravities of the liquids; ω is the angular velocity of the rotors, s^{-1}; and r is the rotor radius, m.

The flooding of the extractor takes place under the condition

$$\Delta P_{l.ph.f} = 2\Delta\gamma\omega^2 (r^2 - V_c/\pi b) g_s \qquad (11.53)$$

where $\Delta P_{l.ph.f}$ is the pressure of the light phase upon flooding; V_c is the continuous phase capacity of the rotor, m^3; and b is the rotor width, m.

The overall efficiency of commercial extractors for the light and heavy liquids is up to 9 m^3/hr, and the number of theoretical stages of separation in this case is about seven or eight. Podbel'nyak extractor should be used for systems in which a rapid extraction is required. The applications of such extractors are restricted on account of an intricate construction, servicing problems, and a relatively high power consumption.

Film-type rotational apparatus with vertical and coaxial mobile and fixed cylinders are also commonly used. The liquid is supplied to the inner cavity of the first rotating cylinder and moves against the vapour flow in the form of a thin film, alternately along the mobile and fixed cylinders in the radial direction. Such an apparatus works at large tip speeds of the rotor and requires a high precision of construction of the rotating parts. Columns with rotors in the form of a spiral are used in small-scale equipment. The operating part of the apparatus consists of a vertical tube and a rotating thin plate which is rolled in a single loop along the length of the apparatus. Such an apparatus has low friction losses and ensures a highly turbulent flow of the vapour. A multicylinder column with coaxial cylinders which rotate in opposite directions and have turbulizers permits a proper turbulization of a two-phase flow for a small number of rotations and considerably increases the column capacity for both phases under low friction losses.

In centrifugal rectifying apparatus, the reflux is supplied to the inner terminal of the spiral and is extracted from the outer terminal. The liquid flows in the form of a film over the surface of the spiral, and the vapour flows in the opposite direction. Since the specific gravities of the gas and the vapour differ considerably and the force of friction between them is relatively small, the liquid continues its stable flow even when the vapour flow in the opposite direction

attains velocities of 10 m/s and higher. When two liquids flow in opposite directions, the interaction between them is stronger than for the motion of a liquid and a vapour.

Rotational apparatus have relatively low friction losses and are effectively used in industry for conducting processes under vacuum. These apparatus can be employed for non-adiabatic fractionation

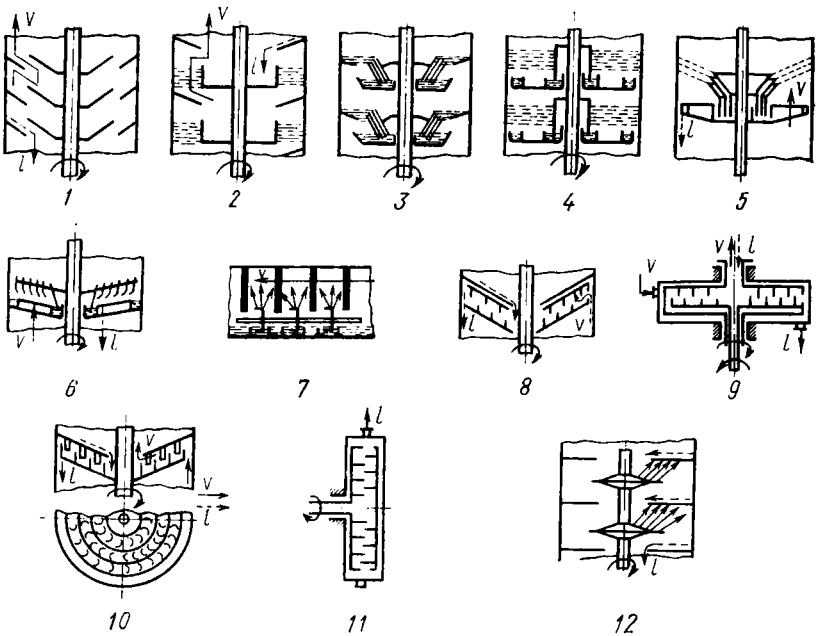

Fig. 228. Different types of apparatus with an interfacial area formed in free volume:

1—apparatus with rotating and fixed partitions; *2*—with rotating baskets and fixed partitions; *3*—with a moving rotor and multiple dispersion; *4*—with rotating plates; *5*—with rotating packet plates; *6*—with cassettes of concentric rings; *7*—with rotating stirrers; *8*—vertical apparatus with a twin rotor; *9*—vertical apparatus with rotating and fixed rings; *10*—with concentric rings arranged on a cone; *11*—with a horizontal rotor; *12*—with rotating discs.

during which the still and the shell of the apparatus are simultaneously heated while the rotor is cooled. Such a fractionation leads to the thermal diffusion effect which improves the mass-transfer process. A drawback of such an apparatus is that the mass-transfer area varies with increasing diameter in direct proportion to the diameter and not to the squared diameter. This decreases the efficiency per unit volume of large apparatus.

Apparatus with interfacial area formed in the free volume. The schematic diagram of an apparatus in which the liquid is sprayed by the rotating parts is shown in Fig. 228. Mass transfer in such an

apparatus is considerably improved owing to a highly developed interfacial area which is rapidly renewed, the existence of the shock effect and fragmentation of drops.

Basically, the apparatus of this type consist of a vertical shaft fitted with cones which are separated by fixed partitions (baffles). The combination of these elements forms a sort of labyrinth channel along the height of the column. The liquid from a baffle flows on to the upper rotating cone from which it is sprayed and flows down to the lower cone along the walls of the apparatus. The liquid comes in contact with the vapour passing through the annular space between the rotating cones and fixed baffles.

Apparatus with a fixed interfacial area and an interfacial area formed in the free volume. Film-type as well as drop-type interfa-

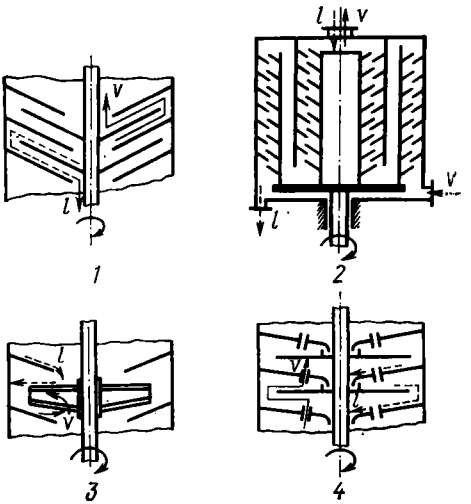

Fig. 229. Different types of apparatus with a fixed interfacial area formed in the free volume:

1—apparatus with alternating rotating and fixed inverted cones; *2*—with a system of mobile and fixed cylinders; *3*—vertical apparatus with a centrifugal fan; *4*—compartment of an apparatus with rotating flat discs.

cial surfaces are formed in such apparatus (Fig. 229) under the action of a centrifugal field. Most apparatus of this type consist of rotating or fixed and inverted cones arranged alternately at close intervals. Under the action of gravity, the liquid flows from a fixed cone to a rotating one. Under the action of a centrifugal field, the liquid flows in the form of a film toward the periphery and is sprayed in the annular space. While passing through the annular space, the vapour encounters the liquid flowing in the opposite direction. The separating capacity of such an apparatus is quite high, although its output is low.

One such apparatus consists of a system of mobile and fixed cylinders (Fig. 230) to which cones are fastened. The liquid supplied at the centre of the apparatus is repeatedly dispersed during its downward motion by cones attached to the central cylinder. Upon reaching the bottom of the cylinder, the liquid flows to the next clearance between the cylinders, rises in the form of a film under the action of centrifugal force, is sprayed by the upper cut to the next annular

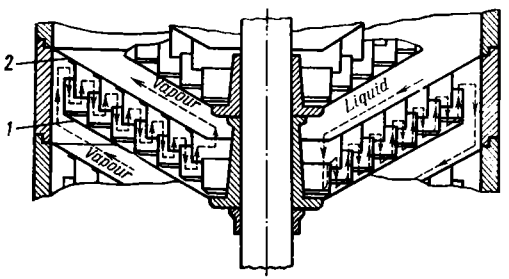

Fig. 230. Apparatus with a multiple dispersion of the liquid involving a rupture of the formed surface upon impact with the barrier.

space with cones, and so on. The vapour moves in counterflow to the liquid. Such an apparatus requires high peripheral velocities of the cylinders.

Vertical apparatus have been constructed in which, besides the use of a drop-film contact surface, the vapour is circulated at each contact stage and is sucked in order to reduce the pressure drop. The operating units of such an apparatus are centrifugal fans with ports in the lower part for suction of vapour.

Figure 229 shows the section of an apparatus with rotating flat discs. The fixed plates in such an apparatus are fitted with connecting pipes permitting the separation of vapour- and liquid phases into independent flows upon passing through the narrow cross section of the apparatus, thus increasing the capacity of the apparatus. This type of apparatus is recommended for rectification processes.

Calculation of rotary apparatus. It is expedient to develop and use designs of apparatus in which multiple dispersion of liquid take place and the droplet-jet surface formed breaks up as a result of an impact with the barrier. By way of an illustration, let us consider one of the designs of such an apparatus (Fig. 230).

The operating part of this apparatus is a device consisting of a rotating cone *1* and a fixed cone *2* with rings forming labyrinth channels which narrow down toward the centre. The rotor and stator rings overlap each other over about 3-5 mm. The liquid is introduced into the cavity of the first rotor ring and is sprayed by the edge of the ring. Passing through the annular channel, the drops and jets

strike the stator ring and the liquid flows into the cavity between the first and second rotor rings, and so on. The vapour flowing in countercurrent to the liquid in the apparatus repeatedly passes through the zone in which the liquid is dispersed. The phases interact in the labyrinth-type annular channels. The vapour changes its velocity and direction as it passes through these channels. The pressure drop ΔP_v through a dry apparatus with a revolving rotor can be expressed in the following form in the general case:

$$\Delta P_v = \Delta P_0 + \Delta P_r, \tag{11.54}$$

where ΔP_0 is the pressure drop through a dry apparatus with a stationary rotor; and ΔP_r is the increment in the pressure drop due to the appearance of a peripheral component of the vapour velocity.

The pressure drop ΔP_0 during the flow of vapour through stationary channels are proportional to the square of the vapour velocity and are mainly composed of the pressure drops due to repeated changes in the direction and velocity of flow. Considering such pressure drops as the sum of local pressure drops ΔP_i, we can write

$$\Delta P_0 = \sum_{i=1}^{m} \xi_i \frac{\rho w_i^2}{2}, \tag{11.55}$$

where m is the number of rings in a section; ξ_i is the drag coefficient upon passage through the ith channel; and w_i is the vapour velocity in this channel, m/s.

To a fairly high degree of accuracy, the above equation can be reduced to the form

$$\Delta P_0 = Ac'_m m' \frac{\rho_v w^2}{2}, \tag{11.56}$$

where c'_m is a coefficient taking into account the factors affecting the state of vapour flowing through the middle of the channel; and m' is the number of rings in the apparatus. The values $A \cong 1.07$ and $c'_m \cong 1.85$ are usually assumed.

The motion of the rotor results in the appearance of a peripheral component of vapour velocity, which considerably affects the hydrodynamic conditions in the apparatus.

The pressure drop ΔP_r due to whirling of the vapour flow by the rotor in a reflux apparatus is described by the equation

$$\Delta P_r = 0.29 \Delta P_0 \left(\frac{n d_m}{w_v}\right)^{1.54} \frac{d_e}{d_m}, \tag{11.57}$$

where n_r is the rotational frequency of the rotor, rev/s; d_m is the mean diameter of the first channel from the centre, m; $d_e = \frac{2}{m}(d_r - d)$ is the equivalent diameter, m; d is the diameter of

the first moving ring, m; m is the number of rings in a section; and d_r is the diameter of the rotor, m.

Usually, for $w_v = 0.2\text{-}8$ m/s, we have

$$\frac{nd_m}{w_v} = 0.1 + 11.2, \quad d_e/d_m = 0.215 + 0.5.$$

An analysis of the component ΔP_r of the pressure drop through the apparatus permits a more precise evaluation of the hydrodynamic conditions for calculating the mass-transfer process. There exists a definite limit of the flow rate in the case of a countercurrent flow. For certain velocities of the vapour flow, the liquid is accumulated in the neck of the stationary cone. This is accompanied by a sharp increase in the pressure drop through the apparatus. Upon a further increase in the accumulated liquid, the rotor gets filled ("flooded"). The maximum admissible vapour velocity is defined by the equation

$$\log\left[\frac{w_0^2}{gd}\frac{\rho_v}{\rho_l}\left(\frac{\mu_l}{\mu_w}\right)^{0.16}\right] = -1.05 - 7.73\left(\frac{R}{R+1}\right)^{0.25}\left(\frac{\rho_v}{\rho_l}\right)^{0.125}\left(\frac{v_l}{nd^3}\right)^{0.3}, \quad (11.58)$$

where w_0 is the maximum vapour velocity in the smaller annular channel, m/s; μ_l is the viscosity of the liquid; μ_w is the viscosity of water at 20 °C; R is the reflux ratio; d is the diameter of the smaller rotor ring, m; v_l is the liquid flow rate, m³/s; and n is the angular velocity of the rotor, rev/s.

Equation (11.58) is applicable within the following limits of variation of the parameters:

$R/(R+1) = 0.18 + 1.0$, $\rho_v/\rho_l = 0.62 \times 10^{-3}$ to 3.4×10^{-3},

$\mu_l/\mu_w = 0.2$ to 1.0, $v_l/nd^3 = 0.3 \times 10^{-3}$ to 3×10^{-3}.

The factor f of the hydrodynamic state of a two-phase system for a rotary apparatus with labyrinth-type channels is defined by the equation

$$f = \frac{\Delta P_{v\text{-}l} - (\Delta P_0 + \Delta P_r)}{\Delta P_0 - \Delta P_r} + \frac{\Delta k}{\Delta P_0 + \Delta P_r}, \quad (11.59)$$

where Δk is the kinetic energy imparted to the liquid:

$$\Delta k = 0.384\frac{Ln^2\sum_{i=1}^{m} d_i^2}{(D^2 - d^2)Hg}, \quad (11.60)$$

L is the weight of the liquid, kg; D is the inner diameter of apparatus, m; and H is the height of a section, m.

When the rotor is not in motion, ΔP_r and Δk are equal to zero. In this case, the bubbling regime is observed in the apparatus and

Eq. (11.59) assumes the following familiar form:

$$f = \frac{\Delta P_{v-1} - \Delta P_0}{\Delta P_0}.$$

The numerator of the first term in (11.59) is small, i.e. only a small part of the kinetic energy of the vapour flow is spent in a rotary apparatus on the creation of the interfacial surface. In practical calculations, the first term in Eq. (11.59) can be neglected. This gives

$$f = 0.384 \frac{Ln^2 \sum_{i=1}^{m} d_i^2}{\Delta P_0 \left[1 + 0.29 \left(\frac{nd_m}{w_v}\right)^{1.54} \frac{d_e}{d_m}\right] (D^2 - d^2) H}. \quad (11.61)$$

The following dependence is used for calculating the mass-transfer coefficient:

$$\mathrm{Nu}' = 0.032 \mathrm{Re}_v^{0.89} \mathrm{Pr}_v^{0.6} (1 + f), \quad (11.62)$$

where $\mathrm{Nu}' = \frac{22.4 K_v d_e^2}{3600 D_v}$ is Nusselt's diffusion number; $\mathrm{Pr}_v = \frac{\mu_v}{\rho_v D_v}$ is Prandtl's diffusion number; and D_v is the vapour-phase molecular diffusion coefficient, m^2/s.

The rotor speed is selected in such a way that the peripheral velocity of the inner ring of the rotor must be between 5 and 7 m/s.

The vapour velocity w_v is taken equal to $0.9w_0$ and the diameter of the smallest stator ring is calculated from the relation $d_2 = \sqrt{\frac{G}{0.785 w_v + d_1^2}}$ and the separation between the rings is $\delta = \frac{d_2 - d_1}{2}$.

The gap between the outer ring of the rotor and the shell of the apparatus is 1.5δ. The number of rings in a rotor usually varies between 5 and 9. The distance between movable and fixed cones (mm) is determined from the formula

$$h = 2.4 (d_2 - d_1),$$

the height of the ring $h_r = \frac{(6 \text{ to } 10) + h}{2}$,

the height of the section $H = (2.5 \text{ to } 3) h_c$.

The performance of diffusion apparatus can be improved by turbulizing the flow of the phases, a continuous renewal of the interfacial area, operation in the inversion point regime or regimes close to the phase inversion point, as well as by creating pulsed and cyclic regimes. The mass-transfer process in the apparatus should be organized in such a way as to minimize the effect of axial dispersion. In practice, this is achieved by using a finer packing, by operating in

the phase inversion regime, by creating a unidirectional flow of gas and liquid in specially designed plate columns, and by producing gas-liquid emulsions on plates.

Modern methods of calculating diffusion processes must be based on the application of systems analysis and mathematical modelling. Block-simulation principle should be applied for mathematical modelling. Any mathematical model is unable to describe a complicated physical or chemical system with absolute precision and gives only an approximate description to a certain degree. However, a mathematical model should endeavour to describe the essence of the phenomena occurring in the system to the maximum possible extent. At the same time the mathematical description must not be complicated, and should be simple enough without distorting the physical and chemical meaning of the process under consideration.

A separate analysis of each phase in heterogeneous systems is allowed only for velocities below the phase inversion velocity. For sufficiently high phase velocities, the relative velocity of their motion must be taken into account, or the flow interaction factor should be introduced. It should be noted that a change in the hydrodynamic conditions of the system may change the form of the models, in other words, the model may be deformed.

Subject Index

Absorptivity, 42
apparatus,
  bubbling, 173
    sectioning, 175
  column, 290f
  diffusion, 10, 229ff, 450
  extraction, 231
  film-type, 441
  with fixed interfacial area, 446
  with fixed phase-contact surface, 232ff
  foam, 269
  with interfacial surface area, 240ff, 330ff
  with mechanical stirrers, 230, 407
  with multiple dispersion, 447
  pneumatic-driven, 429
  rotary, 447
  rotational, 230, 441ff, 445
atomizer, 238

Berl saddles, 316ff
boundary layer, 102, 202
Brownian movement, 176

Coefficient(s),
  absorption, 204
  activity, 20ff, 26f, 29f, 37
  aeration, 248
  diffusion,
    binary, 192
    effective, 203f
    molecular, 123ff, 142, 177, 202, 208
    multicomponent, 194
    turbulent, 138, 179, 203, 364, 439
  distribution, 37
  drag, 116, 131, 161, 236
  film, 200
    of mass transfer, 199
  friction,
    dry plate, 266
    external, 133
  lift, 115
  longitudinal mixing, 173f
  mass transfer, 155f, 197, 222, 337, 391
    liquid-phase, 237
    local, 375
    overall, 200, 209, 383
    volumetric, 213, 340
  of resistance, 171
  selectivity, 37, 79
  turbulent exchange, 144
  vapour distribution, 251
  virial,
    second, 23ff
    third, 23
  volatility, 22, 23ff
  volumetric, 199
  vortex viscosity, 121
column(s),
  absorption, 88
  batch-type, 325
  cyclic countercurrent plate, 82
  cyclic distillation, 88
  emulsifying, 320
    batch-type, 321
    continuous-action, 322
  column(s),
  extraction, 272
    with stirrers, 425
  film-type, 232ff
    wetted-wall, 230
  flooded-packing, 320, 329
  with flow vibrations, 440
  fractionating, 72
  grid-plate, 293
  packed, 230, 299, 301, 313, 324, 330, 379
    absorption, 385
    emulsifying, 132, 137
    extraction, 391
    scaling, 319
    vertical-sheet, 230
  plate, 80, 240ff, 330
    bubble-cap, 230, 240, 245
  plate-grid, 230
  pulsed, 230, 428
  rectifying, 337
  sieve-plate, 230, 260f, 270f, 274, 293
  spray, 230, 238
  stripping, 71, 81
  vertical-sheet packing, 236
  wetted-tube, 236, 238
condition(s),
  minimizing, 31
  periodicity, 82, 85, 87f
  stability, 113
conode, 36
constant
  Boltzmann, 179
  equilibrium association, 25
  Henry, 14, 210, 216
  molar gas, 15
contact time, 255

Degree,
  of circulation, 174
  of dispersion, 390
  of mixing, 364
  of segregation, 141
  of separation, 87
density, 142
diffusion
  back, 193
  barrier, 193
  eddy (turbulent), 179
  through falling film, 182
  in multicomponent system, 190, 194
  osmotic, 193
  from a point source to a moving medium, 185
  in a single drop, 186
  in a single-phase stagnant medium, 181
  steady-state, in a moving medium, 182
dipole moment, 25
dimensional analysis, 129
dimension, characteristic geometrical, 125, 133
dispersion, axial, 317, 404f, 422
  in pulsed columns, 438
dynamic head, 133

Effective thickness, 202
efficiency,
column, 82, 220, 222
estimation, 229
gas-phase, of plate, 355
local, 220, 224, 355, 361, 368
of mass transfer, 372
of packed columns, 439
plate (Murphree), 43, 220ff, 224, 258, 364f, 368
of plate column, 80, 353
of rotating disc extractor, 426
enthalpy, 142
equation(s),
absorption, 218, 220
balance, 14ff
basic, of hydrodynamics, 101
Bernoulli, 99ff, 103, 247
Clapeyron, 15
constant flow-rate, 95
continuity, 95, 107
differential, for steady-state flow, 97
desorption, 218, 220
differential, fluid-flow, 97, 105f
with friction, 100
diffusion, 183
of diffusion kinetics, 10
of drag, 164, 168
Einstein, diffusion, 123
equilibrium, 14ff, 39f
of extraction, 220
Fenske, 56
Gibbs-Duham, 26, 194
Gromeka, 106, 119
Hadamard-Rybchinskii, 423
Hayle, NRTR, 32
heat-balance, 11, 39ff, 343f, 346
Higbie, 203
Kármán-Howarth, 123
kinetic mass-transfer, 234
Margules, 27
mass transfer, 199, 209f
material balance, 10f, 39ff, 56, 58, 63, 72, 76, 81, 86, 214, 223f, 340, 343f, 346, 353, 399, 402
component-wise, 348
Maxwell-Stefan, 193
of motion, 98
Euler's differential, 98ff
of a fluid, 106
Newton's, 100
Navier-Stokes, 101, 183, 185
for operating line, 47, 82
Raoult, 49, 212
of rectification, 218ff
Redlich-Kister, third-order, 28
Scatchard-Hammer, 27
single-stage, 73
Stokes-Einstein, 179
tracer material-balance, 393
Trouton, 15
Underwood, 54
van "Laar, 27
virial, 23f
Wilson, 29f, 32
Wohl's, 26, 29
third-order, 27
Zhukovskii, 113
quilibrium diameter, 95
experiments, Prandtl's 116
extraction,
countercurrent, 76ff
with two solvents, 79f
extractor,
Podbel'nyak centrifugal, 441, 443f
rotating disc, 426

Factor,
diffusion potential, 212, 370, 429
dynamic state, 209
hydrodynamic state, 163f, 207, 210f
surface renewal, 204
flow,
core-type, 166
drop, 166
dropwise, 306
film-emulsion, 166
jet-film, 302, 306
laminar, 117, 134, 162, 232
linear velocity of, 137
plug, 136
semi-annular, 166
single-phase, 92ff, 133f, 141
steady, 93f
turbulent, 134, 162, 232, 303
two-phase, 144f, 161, 290
unidirectional, 165f
unsteady, 93f
foam, 152
force,
Archimedean, 142
centrifugal, 101
drag, 115, 129f, 142f
driving, 10, 40, 49, 52, 212ff, 215
friction, 127
gravity, 126
inertial, 127, 142
lift, 114f
pressure, 127
Zhukovskii, 144, 150
formula, Simpson's, 59, 61
fractionation, batch, 55f, 62
free cross-sectional area, 94
free surface, 141
fugacity, 21f
function, Hamiltonian, 64

Gibbs' excess free energy, 29
Gilliland plot, 53
gradient, surface tension, 154f

Heat capacity, 142
heat, latent, of evaporation, 15
height,
equivalent packing, 384
equivalent to theoretical contact stage (theoretical plate) (HETP) 225, 228, 319, 326, 329, 331, 336f, 347, 349, 373, 377, 379f, 382, 438, 440
of transport units (HTU), 215, 225, 227f, 237, 327, 436ff
holding capacity, 58, 167, 273, 316, 381, 393, 424
dimensionless, 423
dynamic, 308, 315
mean, 423
static, 308, 315
hydraulic gradient, 283
hydraulic radius, 94

Interfacial surface tension, 148

Laplace operator, 394
Laplace transformation, 432f
law(s),
Dalton's, 17
diffusion, 176ff

law(s),
Fick's, 192
first, 177f
second, 180f
Henry's, 14, 34
of macrokinetics, 92
of microkinetics, 92
Newton's, 100
Raoult's, 16, 19, 44
resistance, 133
Stokes, 116, 171, 238
settling, 134
of vortex motion, 105f
layer, bubbling, 171
gas content of, 172
Lessing rings, 316f

Matrix,
local efficiency, 377
Jacobi, 399
block, 401
of mass transfer coefficients, 377
slope, 377
method(s),
diagonalization, 401
Euler integration, 352
finite difference, 369
graphic, 67
iterative secants, 35
least-square, 131
mathematical modelling, 72
of minimization, 335
"plate-to-plate", 58
secants, 59
Stefan, 182
of successive approximations, 31, 42, 335
trial-and-error, 88
Underwood's, 54
Wegstein's iterative, 345
mixing
axial (longitudinal), 138, 173, 175, 427
radial, 138
mixing length, 119ff, 122
mobility, 178
model(s),
asymmetric, 387, 389
boundary diffusion, 201
cellular, 136f, 356
with backmixing, 398
diffusion, 136, 138, 360f, 363, 367, 395f, 402
one-parametric, 138
two-parametric, 138
dynamic plate column, 351
exchange, 413
four-loop recirculation, 415
fully symmetric, 387, 389
Higbie penetration, 203
hybrid, 139, 366, 369, 407, 414
ideal displacement, 136, 376
ideal mixing, 136
Kronig-Bring, 239
mass transfer,
with absorption, 205
based on interfacial turbulence, 207f
with parallel flows, 413
parameters of, 136
penetration and surface diffusion, 203
modified, 203
physical, 132
Prandtl turbulence, 121
recirculation, 359, 413, 415f
scale of, 125
with stagnation zone, 393
symmetric, 387, 389
model(s),
Taylor turbulence, 117, 121
two-parametric, 409
two-zone,
one-parametric, 409ff
two-parametric, 409ff
Wilson, 29
motion,
vortex, of fluid, 101
vortex-free, 101

Newtonian shear stress, 119
number,
Euler, 128, 131, 416
feed, 46f
Froude, 127, 131, 164
for mixtures, 167
Gallileo, 315
Nusselt's, 207
diffusion, 188, 450
thermal, 188
Peclet's, 138, 187, 319, 370, 392
Prandtl's, 208
diffusion, 187f, 450
Reynolds, 116, 122ff, 128, 131, 134, 161f, 168, 232, 300f, 416
still, 46
of theoretical plates, 39, 41, 44f, 51, 65, 67f, 90f, 217, 220, 227f, 231, 381
of transport units, 215, 217, 220, 222
Weber, 149

Operating line, 39
operator, Laplace, 414, 433
overflow devices, 257

Packing,
flooded, 326
parachor, 148
parameter(s), hydrodynamic, 169
plate(s),
bubble-cap, 246, 291, 366
flooding of, 252f, 255
bubbling, 369
cascade-type, 261
directional-slip, 276f
without downcomers, 293
feed, 89
jet-spray, 290
Kittel, 280f
multiflow, 242
reflux, 248
refluxed grid, 294
sieve, 268
refluxed, 262
with two contact zones, 292
with unidirectional phase flow, 273
uniflux, 282
valve, 285
wetted-wall, 247
point(s),
boiling, 22
gas deceleration, 306, 314
holding, 308
inversion, 147, 163, 288, 383
loading, 314
phase-inversion, 307, 309ff, 313
seepage, 263
potential,
diffusion, 383f
Gibbs chemical, 21
pressure,
partial, 14
saturation, 24

pressure drop, 245, 278, 287, 309, 313, 324, 381
  hydraulic, 289, 299
  in two-phase flow, 161, 167ff
principle(s),
  of conservation of vortices, 110
  of corresponding states, 121, 147, 163
  hydrodynamic, 92ff
  of interfacial area formation, 228
  of isomorphism, 128
  Pontryagin maximal, 62
  similarity, 125, 132
process,
  cyclic, 80
  distillation, 20

Raschig rings, 299ff, 316ff 324, 327, 439
rate(s),
  extraction, 57
  flow, 39f, 95
  fluctuation, 124
  mass flow, 165
reflux ratio, 39, 46f, 49, 52f 55, 57f, 61f, 64, 306
regime(s),
  annular, 166
  bubbling, 166f, 266, 269, 295, 298
  emulsifying, 166, 295, 298, 304f, 321, 382, 439
  intermediate, 189, 307, 314
  molecular (laminar) transfer, 189
  plug, 166f
  self-modelling (developed turbulence), 189
  self-similar, 134
  spray, 296, 298
  turbulence, 314
  turbulent exchange, 189
  turbulization, 307
relative volatility, 15f, 51, 54
risers, 256
rule, phase 10, 14

Scale, 120
scaling, 12
segregation, 142
separation in multicomponent systems, 68ff
separation surface, 102
similarity
  complete, 125
  geometrical, 125
    invariants of, 126, 133
  partial, 125f
  physical, 125
    invariants of, 128
stirrer(s), 417ff
Stokes resistance, 179
stream filament, 94
streamline, 94
stream tube, 94, 107
surface-active substance (surfactant), 143, 154
surface, elasticity, 158
system(s),
  azeotropic, 20
  batch-type, 173
  gas-liquid, 14f, 304
  ideal, 16f
  liquid-liquid, 35f
    three-component, 35
  multicomponent, 69ff, 190ff
  non-ideal, 19f
    three-component, 19
    two-component, 19
  ternary, Redlich-Kister, 28
  two-component, azeotropic, 22
  two-phase, 165
  vapour-liquid, 14ff

Temperature,
  critical, 149
  reduced, 24
tension, interfacial, 150
theorem,
  Bernoulli, 114
  Bjerknes, 103
  π-, 129f
  Stokes, 110
  Thomson, 110
  Zhukovskii, 113ff, 133
theoretical contact stage (theoretical plate), 40
theory,
  of adjoint vortices, 115
  Kolmogorov's, of isotropic turbulence, 122
thermal conductivity, 142
turbulence,
  evolution of, 121f
  free, 121f
  fully developed, free, 151
  interfacial, 150, 153, 156ff
  isotropic, 120, 123
  scale of, 124
turbulent fluctuations, 122
turbulent mixing, 117
turbulent shear stress, 121
transport,
  molecular, 117
  vorticity, 117

Valve
  disc-type, 285ff
  Glitsch, 286
vapour velocity, empty-column, 243
velocity, vortex, 108
viscosity, 101, 142, 169
  kinematic, 124, 144
volatile component, 15
vortex components, 104
vortex couple, 112
vortex line, 107f
vortex surface, 108
vortex tube, 107f
  strength, 108

Weir(s), 257
wetted perimeter, 94